FLASH PYROLYSIS OF BIOMASS FOR THE PRODUCTION OF RENEWABLE CHEMICALS

A thesis submitted in partial fulfilment of the requirements for the Degree

of Doctor of Philosophy in Chemical and Process Engineering

at the University of Canterbury

by G.Dedual

University of Canterbury

2018

For My Mother

Je tiendrai toujours le temps que nous avons partagé pendant que

j'écrivais cette thèse très près de mon cœur.

Table of Contents

Table of Figures

Table of Tables

Acknowledgments

I would like to express my deepest gratefulness to my associate supervisor, Dr. Brendon Miller, who always went above and beyond to help me through my P.h.D journey. The interest he had for the project and depth of knowledge he has, stimulated my interest throughout the last four years and was invaluable when guiding me through the journey. The contact and level of support helped me enormously and the research would have never gotten as far as I did without him.

I would also like to thank my principal supervisor, Professor Shusheng Pang, for the administrative and technical support throughout the project. As well as providing me with funding throughout the project to make it all possible.

I am very appreciative of the work from all technical staff in the Department of Chemical and Process Engineering; Frank Weerts, Graham Mitchell, Stephen Beuzenberg, Time Moore, Leigh Richardson, Michael Sandridge, Glenn Wilson and Stephen Hood, who all completed the work in some of the most testing situations. A special thanks to Frank Weerts for your continual support and quality craftsmanship throughout the reactor design and build.

The reactor build, commissioning and analysis of results required input from a wide range of people throughout the University. I would like to extend my thanks to Rob McGregor in the Chemistry Department for his help and phenomenal craftsmanship throughout the quartz fabrications, which without, I would have never been able to complete as much research as I would have liked. Thank you to Dr. Matthew Polson from the Chemistry Department for the analytical expertise. From the Forestry Engineering Department: Nigel Pink, for all the help throughout the characterisation of the biomass.

I would also like to thoroughly thank the Lake Taupo Hospice and Turangi Community Health, for which I would have never been able to complete the writing of this thesis. I would like to thank my family which supported me throughout the project and were an unlimited source of encouragement throughout the difficulties encountered. Lastly, I would like to thank my partner Francesca Reynolds, whose understanding, love and patience made this journey much more enjoyable.

Abstract

To investigate the methanolysis of biomass, a fluidised bed reactor system was designed, constructed, commissioned and operated to investigate the product distribution during operation up to temperatures of 1000 °C and pressures of 1010 kPa. The system was designed to operate with a maximum methane flowrate of 1 kg/hr and 2 kg/hr biomass, at 1000 °C and 101 kPa. The focus of the investigation of the methanolysis process was to optimize the production of carbon monoxide (CO), ethylene and benzene from pinus radiata chips, as a potential source of renewable chemicals for a range of different industries. A modular and portable reactor system was successfully constructed, which allowed for numerous experiments to be conducted. Significant variations in the biomass feed flowability was experienced between different chip sources. It was determined that the initial preparation of the chip highly influential on the flow characteristics of the final sawdust. A new methodology for the preparation of feedstocks from logs was devised and was shown to perform well, allowing for adequate feeding by gravity in a 30° hopper system.

Due to the high operating temperatures, extensive methane thermal degradation (MTD) occurred, introducing significant biomass – hydrogen interactions into the reaction zone. The extent of degradation was significantly decreased by the removal of suspected catalytic surfaces and subsequent retrofitting with quartz fabrications. During reactor operation MTD was inevitable, and the concentration of hydrogen and methane was analysed throughout experiments to aid in characterisation of the products formed during methanolysis. In contrast to dropper tube reactors, the utilization of the fluidised bed reactor was observed to significantly increase the yield of target species, due to enhanced heat transfer to the gas from the fluidising sand. However, it was also noted that the increased heat transfer led to increased MTD, in turn, increasing the consumption of methane in the system.

The system was optimized with the use of 710-1000 µm chips, operated at 988 °C, with a residence time of 1.5 s (0.66 s reaction zone), operating pressure of 380 kPa and a methane to biomass ratios above 4. By use of the described conditions, the CO, ethylene and benzene biomass carbon conversion yields were 46 ± 3 %, 19 ± 3 % and 8.2 ± 0.5 %. Further increases in conversion to particular species were obtained with differing operating conditions. In general the concentration of CO_2 and ethane remained relatively low throughout all experiments, with average biomass carbon conversion values of 8 - 5 % and 2 - 5 %, respectively. Toluene and naphthalene were the other major tar species, with styrene, phenol, indene and biphenyl measured in low concentrations, quantification of the solids product through mass balances were also attempted.

At high operating temperatures cracking of hydrocarbons is suspected to be the main cause of reduced ethylene and benzene yield; whilst, at lower temperatures the energy is not sufficient to promote

hydrocarbon formation reactions. As the degradation of methane was also heavily influenced by temperature, the maximization of target species yield was likely heavily influenced by the characteristics of MTD. At residence times of approximately 1.5 s, the yield of ethylene and benzene was reduced. Likely due to insufficient time at temperature for methyl radicals formed during MTD with the species devolatilized from biomass pyrolysis. At higher residence times of 2.5 s, benzene production increased from, 11 ± 2 % to 21 ± 3 % carbon conversion, which was assumed to be due increases in the HACA (H abstraction C_2H_2 reaction pathway) aromatic reaction pathway, which reduced the ethylene yield due to dehydrogenation of ethylene to form acetylene.

At methane to biomass ratios (M/B ratio) of < 4, decreased yields of target species were obtained. For an M/B ratio of 1.29; CO, ethylene and benzene yields decreased to 9 ± 1 %, 32 ± 2 % and 3.5 ± 0.4 %. Higher target product yields were obtained at higher M/B ratios due to a greater residence time due to a reduction in the volume of devolatilized species released at the lower biomass feed rate. This was thought to be due to the significant reduction in hydrocarbon production with decreasing M/B ratio; which was similar to observations with decreasing residence time. Stable ethylene production was observed within the operating pressures of 275-380 kPa, whereas, increases or decreases in the operating pressure led to decreased ethylene yields. This was likely due to the increased stability of ethylene in the pressure region, as a local maximum equilibrium exists within 300-450 kPa, as identified by Gibbs energy modelling. However, higher pressure led to significant aromatic tar increases, primarily benzene, where an overall increase from 9 ± 2 % to 16 ± 3 % carbon conversion was recorded for pressures of 380 kPa and 480 kPa, respectively. Higher operating pressures were suspected of increasing the aromatic tar production due to enhancement of the HACA pathway, allowing for increase aromatization reactions.

Decreased chip size led to increased tar yield, whilst gas product and solids production decreased. However, larger particles were suspected of resisting the flow of volatiles from the centre core of the particle due to the larger overall pore length. It was suspected the lack of interactions of the devolatilized species resulted in a decreased ethylene and benzene production for the larger chips. The effective degradation of methane was enhanced with smaller chips, resulting in the 710-1000 µm chip being desirable for methanolysis applications. Lower yields of all target species was obtained with the use of Douglas fir, possibly due to the high mineral content of this biomass sample enhancing hydrocarbon cracking. This was suggested due to the apparent effect of mineral accumulation, ash, within the system after specific trials. The use of moist wood (atmospheric moisture), led to significant increases in the hydrogen and CO yields probably due to steam reforming of the methane feed, and highlighted the importance of ensuring the biomass feed stock was completely dry.

From comparative nitrogen and methane trials the yields of ethylene, CO and benzene increased from 5 %, 26 ± 2 % and 7 ± 1 %, to, 16 ± 1 %, 56 ± 3% and 11 ± 2 %, respectively. By use of methane as

the fluidising gas, it was suspected that through a series of complex pathways, the interactions with radicals may be a pathway for the production of the target species. The particular importance of methyl radicals is highlighted by the recombination reaction to form ethane, which can subsequently be dehydrogenated to ethylene and acetylene, indicating the pathway for the beginning of the HACA pathways. Tar production was also likely to originate from fragmentation of the biomass constituents during methanolysis, especially the highly aromatized lignin fraction.

Overall, the conversion of biomass to products during methanolysis was difficult to quantify due to variations in MTD characteristics throughout methanolysis experiments. MTD was also determined to vary with elapsed time, indicating a possibility for a conditioning effect within the reactor, varying the product distribution until equilibrium was obtained. However, production of hydrogen via MTD in the fluidised gas stream was also suspected of facilitating desirable hydrogenation reactions as a result. Further work in the characterising of the MTD behaviour during methanolysis is required, with an emphasis on the control of the extent of degradation is highly recommended.

Glossary

Symbol	Description	Units
C_p	Heat Capacity	*J/kg.°K*
$\dot{Q}$	Volumetric Flowrate	m^3/hr
V_{SF}	Superficial velocity	*m/s*
$\dot{m}$	Mass flowrate	*kg/hr*
c	Amount of volatiles released	mg
E	Energy	*J*
h	Height	*m*
m	Mass	*kg*
Γ	Metal linear expansion coefficient	*m/m°C*
β	Maximum operating extent of fluidisation	-
λ	Heating rate	*°C/min*
A	Area	m^2
A, B, C, D	Constants	-
Ar	Archimedes Number	-
Cd	Coefficient of Drag	-
F	Force	*N*
I	Current	*A*
L	Characteristic Length	*m*
M	Number of fractions in biomass	-
MW	Molecular weight	*g/mol*
Nu	Nusselt Number	-
P	Pressure	*kPa*
Pr	Prandtl Number	-
Pw	Power	*W*
Q	Heat transfer	
R	Resistance	Ω

Symbol	Description	Units
Re	Reynolds Number	-
S	Sum	-
T	Temperature	$°K$
U	Overall Heat transfer coefficient	
V	Voltage	V
X	Fraction of biomass constituent	-
d	Diameter	m
g	Gravity	m/s^2
k	Thermal conduction	$W/m.°K$
n	Number of perforations	-
q	Heat flux	W/m^2
t	Time	s
u	Velocity	m/s
z	Bed Height	m
Ψ	Sphericitiy	-
α	Bubble wake volume to bubble volume ratio	-
γ	Bed physical property constant	-
δ	Bubble occupied fraction	-
ε	Bed porosity	-
η	$g(\rho_p - \rho_F)$	kg/s^2m^2
μ	Viscosity	$Pa.s$
ξ	Emissivity	-
ρ	Density	kg/m^3
σ	Stefan Boltzmann Constant	$W/m.K^4$
ϑ	Deviation of model value	-

Subscripts	Description
0	Initial
$Calc$	Calculated Value
D	Drag
F	Fluid
G	Gravity
Obs	Observed Value
SF	Superficial
a	Activation
$a1, a2$	Reference temperatures
b	Bubble
bf	Bulk fluid
d	Fluidisation disc
f	Final
g	Gas
i	Initial
j	Species
$loss$	Loss
mf	Minimum Fluidisation
p	Particle
pm	Fraction of bed occupied by particles at the fluidisation threshold
req	Required
s	Slugging
std	Standard conditions (25 °C, 101 kPa)
t	Terminal
w	Wall

Acronym	Description
M/B	Methane to Biomass ratio
MTD	Methane Thermal Degradation
TGA	Thermogravimetric Analysis
FBR	Fluidised Bed Reactor
PID	Piping and Instrumentation Diagram
HAZOP	Hazard and operability study
NCG	Non-condensable gas
LEL	Lower explosion limit
MC	Moisture content
VSD	Variable speed drive
RPM	Revolutions per minute
GHSV	Gas hour space velocity
SPE	Solid phase extraction
RS	Red Stag timber chip
SRS	SRS Rolleston Chip
L/W	Length to width ratio
FAME	Fatty acid methyl esters
BTX	Benzene, Toluene, Xylene
PAH	Poly Aromatic Hydrocarbons

1 Introduction

Today, fossil fuel resources are extensively utilized for the production of electricity, heat, transportation fuels and the vast majority of chemicals required by contemporary society. Fossil resources are also used to produce about 95 % of all the carbon containing chemicals required to sustain modern lifestyles [1]. The majority of chemicals can be traced back to seven basic building blocks of the chemicals industry; CO/H_2 Syngas, ethylene, propene, butadiene, benzene, toluene and xylene [2]. The production of CO is also favoured for the potential production of an array of products via Fischer Tropsch reactions with hydrogen. The value chain shown in Figure 1-1, displays the derivation of some of these chemicals is somewhat more valuable than transportation fuels.

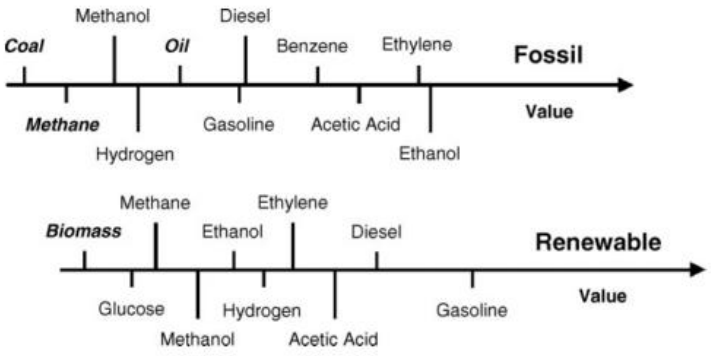

Figure 1-1: Indication of the relative price for a range of chemicals produced from fossil fuel or biomass sources. Raw materials identified in italics with typically one or more steps to form the produced chemicals, [3].

During the 20th century, continual scientific and technological advancements led to ongoing refinements in these areas, resulting in greatly optimized and proficient utilization of fossil fuel resources [4]. Throughout this period fossil resources were abundantly available at relatively low costs, which in turn, resulted in the existing industrial processes being very competitive when compared to new emerging technologies. Herein, significant efforts are required to develop such alternatives into commercially viable solutions, where utilizing biomass is an attractive alternative to fossil resources as a feedstock for the chemical industry. This is due primarily to the negative effects of greenhouse gas emissions on global warming by using fossil fuels, and the dwindling stocks of the fossil fuels worldwide [5], [6].

In relative terms, the production of some chemicals is streamlined by fewer processing steps by the use of biomass as a feedstock in comparison to fossil fuels, whilst, other chemicals require additional steps for production [3]. Rass-Hansen et al. [3], determined that although biomass as a feedstock is not necessarily an equivalent starting point, in regards to fossil fuel, the relative price for a range of chemicals produced varies, as shown in Figure 1-1. Significant effort has been placed on the production of liquid fuels from biomass due to the advantages of using a renewable feedstock which

is low in nitrogen and sulphur, in comparison to fossil fuels. Complications in the production of liquid fuels for the automotive industry include high water content in product liquid, high amounts of oxygenated species, high ash content and instability during storage [7]–[10]. These are all issues which are receiving significant attention by researchers; however, the production of specialty chemicals from lignocellulosic biomass is a relatively new scientific region experiencing increased consideration. This is due to the higher value of the end product, with the produced species being able to be utilized extensively throughout different chemical industries.

In New Zealand biomass resources are abundant due to the excellent growing climate and fertile landscapes throughout the length of New Zealand. As of April 2015, it was calculated that 1.7m ha of plantation forest is currently active in New Zealand, which consists of approximately 90 % *Pinus radiata*, 6 % Douglas fir and the remaining ~4 % including cypress and eucalyptus species [11]. Forestry and wood processing industries are New Zealand's 3rd largest export owner which contributed $4.3 billion in product exports in 2013, with an increase to $12 billion by 2022 envisaged by the wood council of New Zealand (Woodco) [12]. In 2015 a total of 46,000 ha of plantation forest was cleared, producing an estimated roundwood volume of 30,258,000 m^3 [11]. Significant increases in forestry are predicted with the incoming change of government as of 2017, with the announcement that the government is planning on planting another 100 million trees each year for ten years [13]. The government has also announced reestablishment of the forestry services within New Zealand, with a focus on the development of the industry. This is also accompanied by a recent announcement of the governments Zero Carbon Act, which is aiming to reduce the greenhouse gas emissions to net zero by 2050 [14], [15]. It is believed that New Zealand is in an advantageous position to capitalise on the abundance of biomass resources for the production of speciality chemicals from biomass. In 2008, Wakelin and Hock [16], estimated that the total energy from biomass which was not currently utilized equated to 18.3 PJ from forest residues and 8.8 PJ from wood residues. With the foresight of the government, and stated intentions for the future it is very likely that forestry will be a significant contributor to achieving the targets.

Methanolysis is a term which was initial utilized by Steinberg et al [17]–[19] to describe pyrolysis occurring in a methane environment. Initially Steinberg et al. [20], investigated the methanolysis of coal, which rendered higher concentrations of ethylene than when other inert gases, such as helium and nitrogen, were used. Subsequently, biomass was trialled as the feed during methanolysis and the yields of ethylene, benzene and CO were found to significantly increase, thus, stimulating interest in this area of research [19], [21]. High yields of ethylene, benzene and CO were obtained when operating the system at 1000 °C and 3.5 Bar when using sugar pine wood in a drop tube reactor. The work was conducted in the aftermath of the oil crises of the 1970's, for which, after the resolution, interest in production of chemicals from renewable resources subdued.

Methanolysis of biomass is an interesting alternative compared to other biomass thermochemical conversion technologies and since the work of Steinberg et al [17]–[19], [21] was conducted no new publications regarding methanolysis have been found. Methanolysis is unique, as unlike conventional pyrolysis, which is conducted in an inert atmosphere, methanolysis allows for interactions between the volatised products formed, and the methane feed. These interactions are suggested to be due to the production of radicals formed at high temperature [17]. This provides an encouraging opportunity to investigate the possibility of ethylene, benzene and CO production from renewable resources for applications in the chemical industry. No superior technology has emerged for the production of these target chemicals from biomass, and with the high carbon conversions[I] obtained by Steinberg et al. [17], [18], [21], 27.4 %, 24.6 % and 38.7 %, for ethylene, benzene and CO, respectively, the utilization of flash methanolysis seems promising. It is believed that with applications of new technologies which have been developed since the pioneering methanolysis work, the thermochemical process can be better understood to increase yields of ethylene, benzene and CO, and is the focus of this thesis.

1.1 Thesis Scope and Outline

The objective of this thesis was to investigate the production characteristics of ethylene, CO and benzene during methanolysis of biomass in a fluidised bed reactor. By understanding the characteristics of the reactions, it was hoped that the process could be optimized to produce the target species.

Chapter 1; covers the introduction and thesis outline of the thesis.

Chapter 2; includes the literature review of pyrolysis, the flash pyrolysis of biomass and methane thermal degradation. The literature review for pyrolysis includes a brief summary of the characteristics of slow and fast pyrolysis with an overarching review of the general issues accounted by the technologies, and the target products. The flash pyrolysis of biomass literature review is an extensive review of high temperature pyrolysis (> 800 °C). The different reactors used in the pyrolysis (fast and flash) were also briefly summarized, with a focus on the previous arrangements utilized. The methane degradation literature review investigates the effects of pressure, temperature, residence time and potential catalytic influences.

Chapter 3; details the design, construction and commissioning of the fluidised bed reactor. The section extensively details the commissioning experiments which led to an evolution of the reactor system and the derivation of the system characteristics.

[I] Carbon conversion based on the carbon introduced from the biomass feed.

Chapter 4; describes the methods used for the quantification of the results measured and the models which were produced.

Chapter 5; investigates the biomass preparation effects in regards to the flowability of the particles through the system. The biomass feed is also characterised by using a thermogravimetric analyser (TGA), which allowed for an investigation into the kinetics of the biomass constituents during pyrolysis.

Chapter 6; this chapter covers an extensive review of the methane degradation characteristics. As the thermal degradation of methane led to subsequent redesign of the reactor system, the methane degradation characteristics are documented throughout the commissioning phase, and highlight the reasoning behind the system modifications. A complete review of the optimized reactor, compared to another highly inert system for reference, is also provided.

Chapter 7; investigates the influence of reactor operation conditions on the end product during methanolysis, namely regarding the production of ethylene, benzene and CO. This chapter investigates the effects of operation temperature, pressure, methane to biomass ratio, particle size and residence time on the product yields and composition. Trials were also conducted using nitrogen as the fluidising gas. An investigation into the production of the target species was also conducted for alternative feeds of; Douglas fir, moist (room moisture content) pine wood, pine bark and charcoal. The operation of the reactor was also investigated by changing the reactor configuration to simulate the product characteristics from a drop tube reactor and a packed bed reactor, for comparison to the fluidised bed arrangement. The characteristics of the system are investigated throughout all the variations, with gases and tars collected from the trial and analysed. The oxygen and carbon balances are utilized to investigate the overall distribution and conversion of the inlet biomass species. The effective efficiency of the methanolysis process is documented as carbon conversion, relating to the carbonaceous products which are formed on a basis of the carbon from the feed biomass.

Chapter 8; concludes the thesis, with an overview of the key results and recommendations for future research. Additional information can also be found in the appropriate section of the appendix

1.2 References

[1] J. Rass-Hansen, H. Falsig, B. Jorgensen, and C. H. Christensen, "Perspective Bioethanol: fuel or feedstock?," *J. Chem. Technol. Biotechnol.*, vol. 82, no. May, pp. 329–333, 2007.

[2] E. S. Lipinsky, "Chemicals from biomass: petrochemical substitution options," *Science (80-.).*, vol. 212, no. 4502, pp. 1465–1471, 1981.

[3] N. Kosaric *et al.*, "Ethanol," *Ullmann's Encycl. Ind. Chem.*, 2001.

[4] C. H. Christensen, J. Rass-Hansen, C. C. Marsden, E. Taarning, and K. Egeblad, "The renewable chemicals industry," *ChemSusChem*, vol. 1, no. 4, pp. 283–289, 2008.

[5] K. Zeng, D. Gauthier, J. Soria, G. Mazza, and G. Flamant, "Solar pyrolysis of carbonaceous feedstocks: A review," *Sol. Energy*, vol. 156, pp. 73–92, 2017.

[6] B. J. Vreugdenhil and R. W. R. Zwart, "Tar formation in pyrolysis and gasification," 2009.

[7] Xiaoquan Wang, * Sascha R. A. Kersten, Wolter Prins, and and Wim P. M. van Swaaij, "Biomass Pyrolysis in a Fluidized Bed Reactor. Part 2: Experimental Validation of Model Results," *Ind. Eng. Chem. Res.*, vol. 44, no. 23, pp. 8786–8795, 2005.

[8] J. P. Diebold, "A Review of the Chemical and Physical Mechanisms of the Storage Stability of Fast Pyrolysis Bio-oils," *Natl. Renew. Energy Lab.*, no. January, p. 59, 2000.

[9] R. Fahmi, A. V. Bridgwater, I. Donnison, N. Yates, and J. M. Jones, "The effect of lignin and inorganic species in biomass on pyrolysis oil yields, quality and stability," *Fuel*, vol. 87, no. 7, pp. 1230–1240, 2008.

[10] G. Brem and E. A. Bramer, "PyRos : a new flash pyrolysis technology for the production of bio-oil from biomass residues," *Proc. Int. Conf. Exhib. bioenergy outlook*, no. January, pp. 1–14, 2007.

[11] Forest Owners Association, "Facts & Figures 2015/2016," *New Zeal. J. For.*, vol. 46, no. 2, p. 13, 2001.

[12] A. Bartley *et al.*, *Situation and Outlook for Primary Industries 2013*. 2013.

[13] J. Arden, "Speech from the Throne," *Speech from the Throne,Delivered by Her Excellency The Rt Hon Dame Patsy Reddy, GNZM, QSO, Governor-General of New Zealand, on the occasion of the State Opening of Parliament, Wednesday 8 November 2017.*, 2017. .

[14] J. Shaw, "First Important Step towards the Zero Carbon Act," *Beehive Announcement*, 2017. [Online]. Available: https://www.beehive.govt.nz/release/first-important-step-towards-zero-carbon-act.

[15] New Zealand Green Party, "Climate Protection Plan," 2017.

[16] S. J. Wakelin and B. Hock, “Bioenergy options for New Zealand,” *Wood Availab. from New Zealand’s For.,* 2007.

[17] M. Steinberg, P. T. Fallon, and M. S. Sundaram, “The Flash Pyrolysis and Methanolysis of Biomass (Wood) for Production of Ethylene, Benzene and Methanol,” 1990.

[18] and M. S. S. M. Steinberg, P.T. Fallon, “Flash Pyrolysis of Biomass with Reactive and Non-Reactive Gases,” Richland, Washington, 1984.

[19] M. Steinberg, “Flash Pyrolsyis of Biomass with Reactive and Non-Reactive Gases,” 1984.

[20] M. S. Sundaram, M. Steinberg, and P. T. Fallon, “Enhanced Ethylene Production via Flash Methanolysis of Coal,” 1985.

[21] M. Steinberg, P. T. Fallon, and M. S. Sundaram, “Flash pyrolysis of biomass with reactive and non-reactive gas,” *Biomass*, vol. 9, no. 4, pp. 293–315, 1986.

2 Literature Review

This section contains an extensive literature review which investigates the characteristics of flash pyrolysis and methane thermal degradation, as well as, a review of the forestry industry nationally and internationally. Due to the limited research which has been conducted on the flash methanolysis of biomass, the amount of literature on this process is limited. As well, the conditions under which methanolysis is of interest has received little investigation by pyrolysis researchers. For the sake of consistency, biomass refers to woody biomass, *lignocellulosic*, which was the main biomass source investigated.

2.1 Introduction

As mankind's dependence on fossil fuels increase and the stocks of available fuel decreases, new technology utilizing renewable resources must be developed to satisfy the needs of the world. By utilization of renewable resources such as biomass, ongoing production of fossil fuel derived chemicals can continue with reduced environmental impact. Research in the flash methanolysis of biomass was first conducted by Steinberg et al, [1]–[3] where production of benzene, CO and ethylene was the focus. Methanolysis was a term coined by Steinberg et al [1], [3], during their work, which was defined as pyrolysis in the presence of methane. Interest in the flash methanolysis of biomass originates from the 1973 oil crisis, which stimulated research into alternative feed stocks for traditionally oil derived chemical products. After the oil crisis, the chemical production industry returned to similar operation as before the crisis, which in turn may be the reason for the scarce follow-up work conducted in the area of flash methanolysis. It is envisaged that with the technological improvements of pyrolysis and reactor technology since the 1980's, the application of newly investigated systems can be applied to the flash methanolysis system. In this literature review, an overview of pyrolysis is given with emphasis on high temperature and pressurized systems, where the production of gas products and aromatic tars are of interest.

2.2 Biomass Chemical Compounds and Reaction Pathways

Woody biomass is a useful waste stream from industrial activities; such as, milling and, pulp and paper processing. In theory, biomass from any source can be utilized in pyrolysis systems. This has been proved by numerous experiments which have investigated the pyrolysis of maize stalks, rice husk, apricot stones and palm kernels [4]–[6]. It is also envisaged for the future, that waste biomass from the construction industry and domestic households can be used as feedstocks for pyrolysis. In general, biomass is largely comprised of C, O, H, N, S, (in descending wt %), where the composition of the biomass varies significantly between sources [7]. Other important chemical species within biomass include K, Fe, Zn, Mn and Cu which are commonly required for growth in plantations and

are often supplied through fertilisation of the soil during growth [8]. The structure of biomass species contains varying concentrations of three main chemical species; cellulose, hemicellulose and lignin. Other minor components such as organic acids, tannins, proteins and secondary metabolites of differing intrinsic value, are also present within the cell wall of lignocellulosic plant material. The variability in these minor components is pronounced between hardwoods and softwoods, whereas, softwoods are generally attributed to higher tannin and organic acid concentrations [9]. Variations in concentration of all major and minor species occur throughout a tree, which makes the selection and development of efficient process methods difficult [10]. The behaviour of these species during pyrolysis is of interest due to the significantly varied product selectivity throughout pyrolysis. A review of the characteristics of each species is provided below. Lv and Wu [11], investigated the product distribution of each biomass constituent and found strong relationships between the produced species and the biomass constituent pyrolysed, as shown in Figure 2-1.

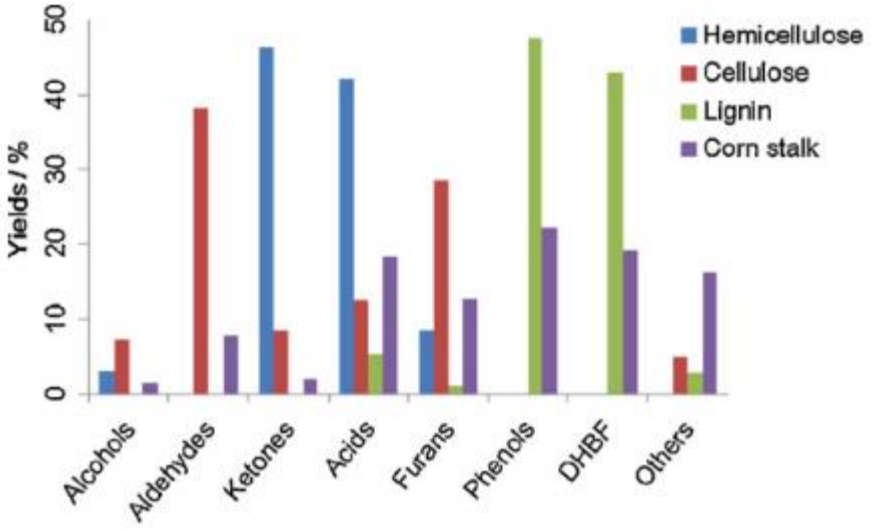

Figure 2-1: Yields of major identified products from the main structural components of biomass and a comparative run with whole corn stalk, [11].

2.2.1 Cellulose

Cellulose is the most abundant organic compound in the world, containing a simple chemical structure based on D-glucose linked through β-1→4 linkage in a linear configuration [12]. Cellulose accounts for approximately 45 % of woody biomass composition, with different biomass sources able to higher cellulose concentrations up to 80-95 % [13]. As defined by Habibi et al. [14], cellulose crystals can be characterised by the linkage of two anhydroglucose molecules rotated about the helical axis by 180°, therefore, cellobiose rather than glucose is the basic unit of the cellulose polymer. Cellulose is often denoted as $(C_6H_{10}O_6)_n$, where n indicates the extent of polymerisation which varies with biomass source as well as variations throughout biomass. Typically woody biomass has a polymerisation level

of approximately n=4000, Pinus Radiata is observed to have a slightly lower degree of polymerization at n=3063 [15]. Due to the weak nature of the glycosidic bonds within cellulose, the cleavage of the glucose bonds occurs at relatively low temperatures and generally degrades shortly after the initial degradation of hemicellulose during pyrolysis. The degradation of the glycosidic bonds can also be facilitated by the use of acid and has been used extensively as a pre-treatment technique to decrease the degree of polymerisation within biomass [16]. In the optimization of levoglucosan production through pyrolysis of biomass, the degree of polymerisation has been determined as a key influential parameter [17], [18].

Methanolysis work conducted by Steinberg et al [3], suggested that the production of hydrocarbons were primarily attributed to the methanolysis of cellulose. This was determined by the comparison of trials conducted with pine chip and pine derived lignin, where at 900 °C and 345 kPa 15.7 % and 5.1 % of C_2H_4 carbon conversion was recorded [1]. High temperature cellulose pyrolysis (1150-1700 °C) was also conducted by Ozturk and Merklin [19], who investigated the influence of gases with the addition of 1 % and 5 % H_2 in argon gas on product distribution. From this work it was observed that with increasing temperature, the ethylene and methane formation decreased; whilst, CO, CO_2 and C_2H_2 product yields increased, Table 2-1. At lower temperatures (500 °C), the degradation of cellulose was also observed to be influential on formation of non-condensable gases (NCG). From pyrolysis trials conducted with three separate biomass sources (spruce bark, wheat straw and rape straw), the non-condensable fraction of gas produced was increased by use of high cellulose content biomass [20]. Overall, gas production reached 20 wt% in the high cellulose biomass feed, as opposed to 16 wt% in the low cellulose feed.

Table 2-1: Cellulose pyrolysis in a reactive environment at high temperatures, computed from data collected from Burhenne et al. [20], and recalculated for carbon conversion.

1% H_2 99 % Ar

Temperature	**CO**	**CO_2**	**CH_4**	**C_2H_4**	**C_2H_2**
1150 °C	47%	3%	13%	19%	17%
1350 °C	46%	4%	13%	6%	30%
1550 °C	49%	4%	9%	1%	37%
1700 °C	52%	5%	3%	1%	39%

5 % H_2 95% Ar

Temperature	**CO**	**CO_2**	**CH_4**	**C_2H_4**	**C_2H_2**
1150 °C	46%	2%	19%	24%	11%
1350 °C	45%	2%	18%	12%	24%
1550 °C	46%	2%	16%	4%	32%
1700 °C	51%	1%	11%	3%	33%

In an inert atmosphere the products of the thermal degradation of cellulose peak at ~500 °C, with CO and CO_2 the main products. With further increases in temperature the production of CO and CO_2 decreases with hydrogen becoming the most abundant product gas.

2.2.2 Hemicellulose

Hemicellulose is comprised of various heteropolysaccahrides such as; xylose, mannose and glucose. The structure of hemicellulose is random, causing the structure of the molecule to be non-uniform and amorphous in structure. Due to the random branching of the molecule, the thermal stability of hemicellulose is generally less than that of cellulose, causing the hemicellulose fraction of biomass gas to pyrolyse initially [21]. As a result of the relative fragility of hemicellulose, the extraction of the fraction from biomass has been extensively investigated, but no procedure able to adequately extract

the fraction without chemical alteration of functional groups has been developed. Because of this difficulty in extraction, research has focused on the model compounds and the altered hemicellulose structures after extraction. Generally, alkali extraction is the most favoured extraction method with the degree of polymerisation remaining high after extraction [22]. When investigating the use of hemicellulose extracted via alkali extraction, it was observed that the thermal degradation of the extract resulted in high yields of char [22]. Other significant products include hydroxyacetone and acetic acid, of which, the latter is likely to be underestimated as alkali extraction decreases the acetyl groups of natural hemicellulose.

2.2.3 Lignin

In contrast to the carbohydrate structure of hemicellulose and cellulose, lignin is composed of an aromatic matrix structure which adds strength to the biomass structure. Lignin is a macromolecule consisting of alkyl-phenols in a complex three dimensional structure full of aromatic rings [23]. The structure of lignin can be described as an amorphous tridimensional polymer which mainly comprises of p-hydroxyphenyl (H), syringyl (S) and guaiacyl (G) units. All three units share the same core structure with the units varying primarily with the addition of methoxyl groups attached to the aromatic structure, Figure 2-2. Lignin consists of a complex arrangement of lignin unit bonds, where the bondage between the different lignin units can be classified as; ester, ether and carbon bonds. Softwood is dominated by the ester forming bond of β-O-4 which accounts for approximately 50 % of the linkage bonds of lignin. Additionally, carbon-carbon bonds 5-5 are also present in larger numbers with 10-25 % reported within softwoods. In contrary hardwoods exhibit a higher content of β-O-4 linkage bonds, 50-65 %, and lower 5-5 lignin linkages [24]. Other common bonds within the lignin structure include β-5, α-O-4, 4-O-5 and β-1 linkages. The chemistry of the lignin chemistry is very diverse and complex, excellent detailed reviews of the chemistry have been made by Changzhi and Wang, [22], [24].

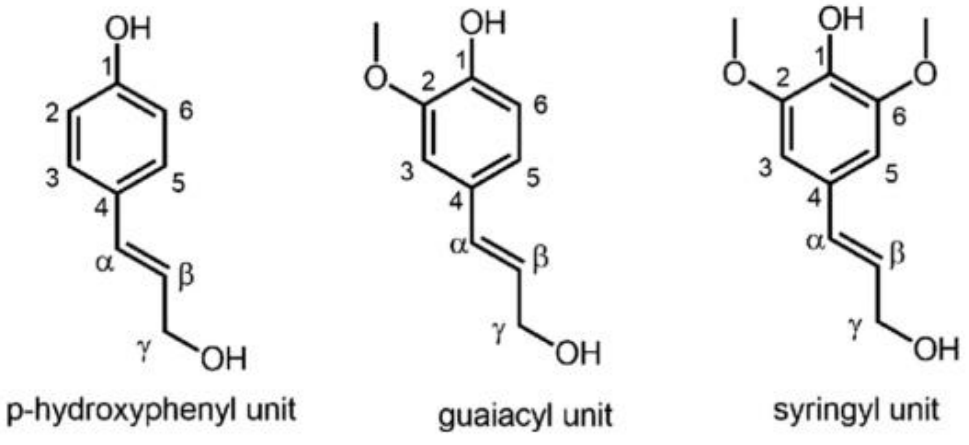

Figure 2-2: Structures of H, G and S lignin units found within biomass, [22].

The relative content of the different basic units of lignin within the biomass differs depending on the source. Softwoods are characterised with high concentration of G-units and low concentrations of S and H units. Hardwoods tend to have complementary concentrations of both S and G type units, whilst other sources such as grass lignin can have a large variation of all units [24], Table 2-2. Due to the large amounts of aromatic rings which branch form the molecule, degradation of lignin occurs in a wide temperature range (100-900 °C) [21].

Table 2-2: Relative difference of lignin units for different biomass sources, data retrieved from [24].

Basic Unit	Softwood Lignin	Hardwood Lignin	Grass Lignin
Syringyl Unit (S)	0-1 %	50-75 %	25-50 %
Guaiacyl Unit (G)	90-95 %	25-50 %	25-50 %
p-hydroxyphenyl Unit	0.5-3.4 %	Trace	10-25 %

The concentration of the different lignin units has been investigated as a possible explanation of the variation in differing product distributions during pyrolysis. Due to the assortment of different bond types throughout the lignin structure the pyrolising temperature of lignin varies. This leads to larger temperature differences required to thermally cleave the weak bonds of β-O-4, (200-250 °C) [25], [26] in comparison to the stronger carbon-carbon bonds, which are dependent on positioning and require temperatures of 240-550 °C before cleavage of the bonds occurs [11].

In addition to the varied lignin units are a number of different oxygenated functional groups which exist in the lignin matrix. The functional groups include methoxyl, hydroxyl, carboxyl and carbonyl groups, all of which significantly affect the reactivity of lignin [22]. Generally, the abundance of methoxyl groups is higher in hardwoods in comparison to softwoods, due to higher concentration of syringyl lignin units in hardwoods [22]. The concentration of methoxyl units can be correlated to the formation of char due to the location of the methoxyl groups. This pathway has been suggested as the methoxyl groups decompose into smaller molecular radicals which further stabilize the lignin molecular fragment and prevents polymerization [22]. Ultimately, the increased methoxyl concentration has been associated with decreased char production during pyrolysis. The decomposition of methoxyl groups from lignin has also been suggested as possible pathways for the production of methane [27]. Hydroxyl functional groups have also been of interest due to the range of different phenol products which are formed during pyrolysis. A vast range of phenol variations were

reported by Gaojin and Wu [11], investigating the tar products produced during the thermal degradation of lignin, of which 2-methoxy-4-vinylphenol represented approximately 10 % of the product. Carbonyl and carboxyl functional groups have been reported to decompose during pyrolysis to form CO_2, CO and water [28]. In the gas phase, lignin pyrolysis is observed to undergo two main stages; with the evolution of CO_2, H_2 and CH_4 occurring at approximately 500 °C, whilst, higher temperatures of 800 °C leads to increased CO yield with decreased CO_2 and CH_4 production [21].

2.3 Biomass Overview

Prior to the industrial revolution, biomass energy was the primary energy source for the world [29]. But since 2000, biomass represents only ~7 % of the worlds primary energy needs, which is roughly a third of the energy sourced from non-fossil fuel derived energy [29], [30]. The utilization of biomass throughout the world varies extensively, where 2 % of world biomass energy is consumed for automotive fuel; whilst, in Brazil over 30 % of automotive fuel is derived from biomass [31], [32]. Parikka [33], concluded that only in Asia, the current use of biomass exceeds the available potential, highlighting the opportunity throughout the world to increase the proportion of biomass derived energy [33]. However, the production of automotive fuels has drawn criticism due to the competition with land traditionally used for food production. Field et al [34], concluded that the area with the greatest potential of yielding biomass energy, that reduces greenhouse gas (GHG) effects and does not comprise food security, is land that was previously used in agriculture which has not been converted to forest or urban areas.

Benefits of using woody biomass as the feed for renewable energy and chemical production, is the relatively high energy density of wood compared to other biomass sources. The production of chemicals from biomass is also desired, as, the growth of trees actively sequesters carbon. This allows for the release of carbon to be offset by the carbon consumed during photosynthesis. Therefore, with good management of the plantation forest, the biomass source can be operated in a renewable manner.

Throughout the world, forestry and agricultural residues are treated as wastes and are usually left to decompose on site, or, are inefficiently burnt. In Nigeria up to 50% of the raw log is wasted in the processing phase, where the waste biomass is dumped in the river, causing significant ecological issues surrounding milling operations [35]. The applications of pyrolysis systems have great potential for developing countries to solve this waste issues as well as electrical demand. Along with an excess of biomass found in developing countries, European countries, such as, Germany face economic incentives to determine alternative methods of biomass disposal. Due to the high costs of disposing wood waste, Table 2-3, many alternative sources for alternative wood waste are being actively investigated [36].

Table 2-3: Average disposal costs for wood wastes in Germany [36].

Material	Cost
Untreated wood	€ 47
Fruit boxes	€ 35
Used furniture	€ 86
Mixed woods	€ 85
Painted wood	€ 96
Demolition wood	€ 68
Impregnated wood	€ 237
Windows with glass	€ 146

It is difficult to estimate the total amount of biomass waste which is present in the world, as dumping of the waste materials are generally not well documented. In North America, it has been reported that the extent of recycling of pulp and paper products has steadily increased in the past years, and recovery rates of 63% and 66% have been reported in America and Canada, respectively, Figure 2-3. Due to the large demand for recycled paper from China, recycled paper from the Americas is frequently exported for the production of tissue [37]. The planting of sugarcane for the production of ethanol has been a pathway to utilize biomass energy which has shown promise, with a net energy balance ratio of 8 to 10, achieved by combusting the stalks to meet thermal requirements [32]. Whereas, biodiesel from soy typically has a net energy balance of 1.3 to 1.9[II] [38] .

[II] (Energy Out/Energy In)

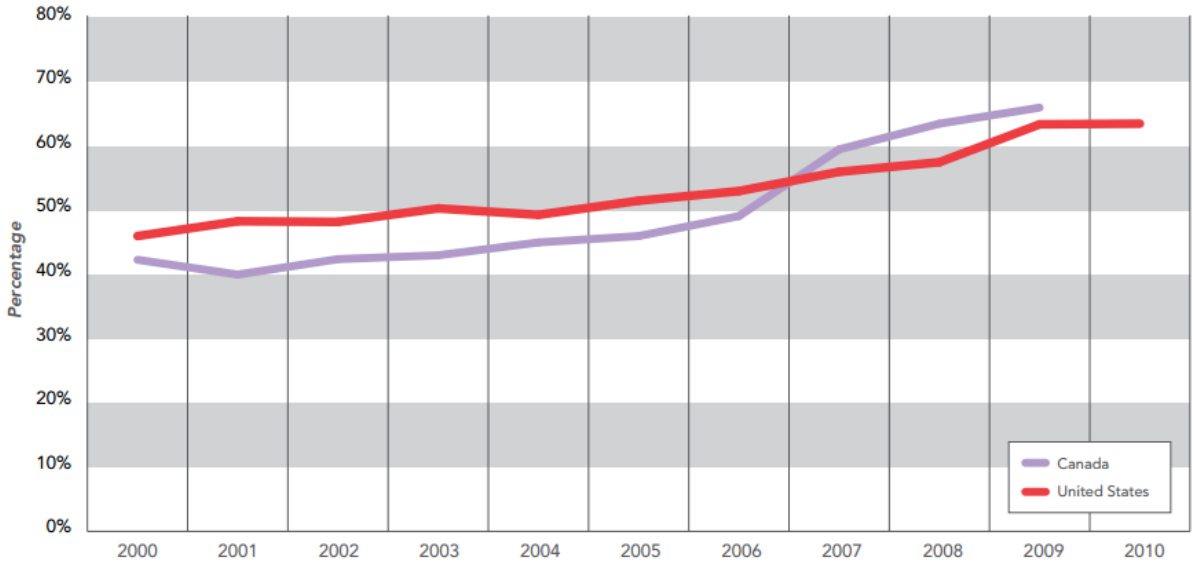

Figure 2-3: Recycling trend in North America of paper and Pulp derived products [37].

2.3.1 Forestry

A plantation is defined as *'a forest crop or stand raised artificially, either by sowing or planting'*, as proposed by Ford-Robertson [39]. An overview into the status of plantation forests and the availability of woody biomass from these plantations nationally and internationally is discussed below.

2.3.1.1 World Forestry Overview

When classifying the forests of the world two extremes are encountered; harvested plantations and managed conserved forests. Of the 3.5 billion ha of forests in the world, about 650 million ha are either plantations or actively managed for the production of goods and services [40]. The majority of wood harvested from plantations is used in the production of timber and paper, which have reported efficiencies of approximately 56% [41]. The wood waste produced during processing, is usually combusted to provide fuel for the process, sent to pulp and paper industries or disposed of in landfills. Due to the large volumes of biomass waste which are produced from industrial applications, a large waste biomass stock is available worldwide [42]. This large inventory of biomass is also complemented by decreasing demand for print paper worldwide, which has arisen interest in the utilization of woody biomass which is not suitable for timber production [43].

Forestry is also an admirable biomass feedstock, due to the expected increases in tree plantations to meet the world's needs. As highlighted by Fox [44], with the increasing population, an increase in demand for forest products is coupled against decreasing amounts of forests in the world. Which can possibility lead to further increases in the volumes of waste which are produced from the forestry industry worldwide.

2.3.1.2 Forestry in New Zealand

In 2014 the forestry industry in New Zealand employed approximately 25, 830 people [45], contributing approximately 1.6 % of GDP, with an overall export value of $4.8 billion. Overall the forestry sector is comprised of approximately 1.76 million hectares, of which the majority is privately owned *Pinus Radiata* plantations. *Pinus Radiata*, is the most abundantly planted forestry accounting for 90 % of plantations; where, Douglas fir, Cypress, Eucalyptus account for an additional 8 % [46]. The remaining planted forests are various hard and soft woods which are usually slower growing species used to satisfy niche markets. Other competitive land use activities include dairy production and agriculture which utilize a substantial proportion of pastureland in New Zealand, Table 2-4.

Table 2-4: Export Value comparisons, data from NZ Forest Owners Association 2015/2016 [45].

Product Activity	**Area Famed (Ha)**	**Export Earnings 2011-2015 Average (Billion NZD)**	**Export Earnings (Per hectare)**
Red Meat and Wool	5,397,855	$7.93	$1,470
Dairy Products	2,110,569	$13.36	$6,328
Forestry	1,684,209	$4.75	$2,819

In the year to June 2013, the forestry sector within New Zealand experienced record log exports, driven by the larger demand for unsawn logs leaving for the China market, following the free trade agreement (signed in 2008). It has been reported from media that New Zealand wood has been exported as an unsawn log and returned as milled timber, much to the disapproval of many New Zealanders [47]. In China the milling activity is labour intensive and costs are equivalent to $\$15/m^3$ as opposed to $\$65/m^3$ in New Zealand, due primarily to lower labouring costs [48]. The decreases in exports from New Zealand, Figure 2-4, and the increase in offshore milling of New Zealand pine expose a large opportunity loss. Whereas, the potential of creating value added products, as well as, the collection of the biomass residues from the wood processing industry is lost. Of particular

importance is the advantage which the milling activity poses on the preparation of chip which is envisaged as a potential early adopter for pyrolysis processing. It is hoped that with successful experimental research on the flash pyrolysis of Pinus Radiata, the milling of New Zealand logs can be conducted in New Zealand to recover the useful waste products from the milling industry; whilst, providing value added products for export.

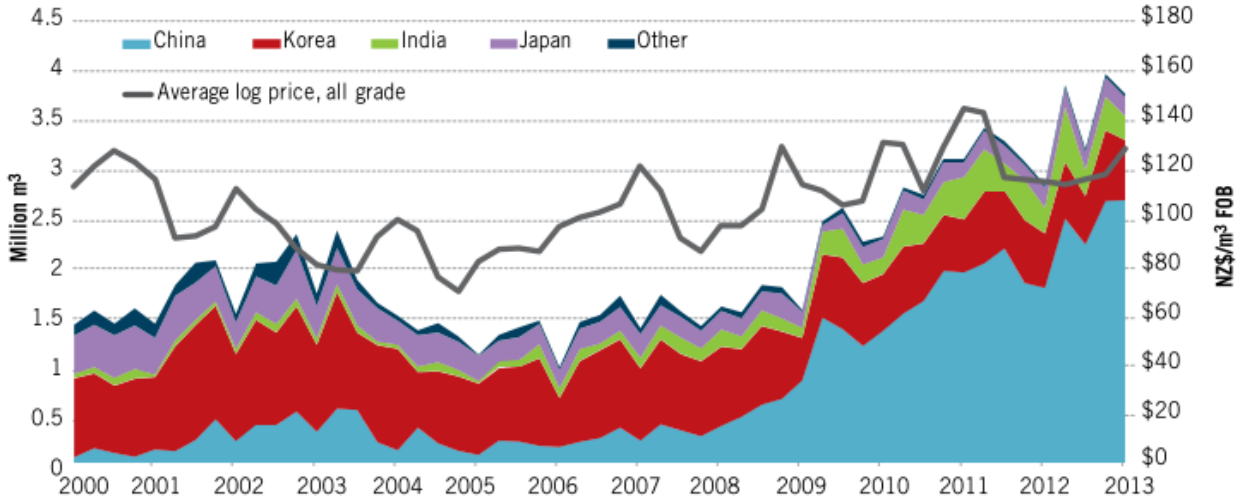

Figure 2-4: New Zealand exports to China, (Free trade agreement signed in 2008), Extracted from, 'Situation and Outlook for Primary Industries 2013 Report' [49].

New Zealand is in a favourable position for the application of pyrolysis, due to the stocks of pine wood which are expected to emerge in the coming decades. Estimates of 69.6 million m^3 of wood are expected to mature in the year of 2023, with a six year average of 58 million m^3 available to harvest from 2022-2027 [45]. New Zealand has the potential to capitalize on this large inventory that can be harvested in the foreseeable future. The large influx of maturing logs can rejuvenate employment in an industry which has experienced severe job losses in the past years. By use of the pyrolysis technology it is envisioned that the milling of logs becomes economically viable. By milling the logs in New Zealand, the residues from the process can be collected and used in the pyrolysis process, whilst, the timber can then be exported at a competitive price, as the value of logs can effectively increase. This can provide stimulation to the industry within New Zealand, and increase exports throughout the world; whilst, increasing the number of available jobs within New Zealand and reinforcing the countries clean green image.

Along with the already considerable reserves of plantation forests which exist within New Zealand, reports show that New Zealand has from 3-5 million ha of land suitable for exotic reforestation [50]. This highlights the capability of New Zealand to increase the biomass output from the country to meet demand. Research has also been conducted into the effects of plantations on the surrounding

indigenous forests. It was concluded that with in-depth investigation into the indigenous species in the forest and the characteristics of the plantation forests, an ecological integrity can be preserved. By careful operation of plantations forest management should be able to integrate productive and protective uses in the same landscape [51].

2.3.1.3 Future of Forestry in New Zealand

Over the past 10 years the forestry sector has experienced a downturn in growth in the forestry sector. This has been observed by significant deforestation which has occurred since the new millennium. 112 002 ha of pre-1990 planted forest and 24 657 ha of post 1989 planted forest was deforested between 1990 and 2014, with the most notable conversion to dairy farms [52]. This has been observed by a decrease of ~ 20 % employment in the forestry sector from 2006 [45].

Although significant changes have occurred in the forestry sector over the past decade, recent announcements on the future of New Zealand climate change legislation, and subsequently forestry, have reinvigorated the market. Most notably with the recent change in government in October 2017, it has been announced that the government is committed to planting 100 million trees per year to reach a billion more trees in 10 years. To compliment this future goal it was also announced that the New Zealand Forestry Services would be re-established, to strengthen rural New Zealand [53]. Complementary to the announcements made, the government has also announced that the target of a Net Zero Carbon Emissions Economy by 2050, where legally binding emission targets have been implemented [53]. This announcement strengthens the agreements which were made in 2015 to decrease emissions by 30 % below 2005 levels by 2030 [54].

In 2014 agriculture and particularly dairy, accounted for 49 % New Zealand's greenhouse gas emissions with the majority of emissions comprising of CH_4 and N_2O [55]. With strengthening of the regulations and limits of emissions from farming practises it has been suspected that this will result in extensive land use changes throughout New Zealand. This is in accordance with the objective of increasing plantations throughout New Zealand, where the extra plantations are to be allocated to marginal land which has poor efficiency in terms of agriculture [53]. Further pressure on the agriculture industry arises from omitting that overall current dairy farming practises in New Zealand are unsustainable [56]. This has been exemplified by the current attention which freshwater has received over the past few years. With a significant proportion of pollution arising from excess nutrients discharge through intensive nitrogen use as well as effluent contamination of streams. This has resulted in heighted E.coli and nitrogen concentrations through a significant amount of New Zealand's waterways, resulting in 62 % of the length of all rivers exceeding (ministry of health) MOH safe limits for swimming [57].

With the increased environmental consciousness and low carbon practises it is believed that forestry has high future growth potential, primarily due to the relatively low environmental effects from correctly managed plantation forests. Attention must be placed on the environmental issues of soil degradation and erosion which have been identified as significant environmental burdens from forestry [44], [52], [58]. It has been speculated that in order for New Zealand to reach the desired carbon targets converting land from intensive agriculture to forestry is required. Other interesting prospects for the forestry industry have been discussed with the potential for native long term forestry to be established for niche timber production [59].

2.4 Methane Thermal Degradation (MTD)

Similar to the methanolysis of biomass, methane thermal decomposition (MTD) is a process which received considerable attention since the 1973 oil crisis. Ever since, the target chemicals from the degradation of methane have varied with interest in; hydrogen, ethylene, ethane, acetylene and benzene reported [60], [61]. In literature, the thermal degradation process is sometimes referred to as methane cracking, methane pyrolysis and methane thermal decomposition. For this review, MTD applies to the use of a heated reactor system fed with methane only. Other MTD like experiments which have been conducted include; gasification, hydropyrolysis and hydrogenation, all of which are found in literature and at times terminology conflicts add to confusion.

MTD employs the direct decomposition of methane in a heated environment and can be summarised by the carbon and hydrogen forming reaction, equation (2.4.1). The majority of the work which was conducted on investigating the characteristics of MTD focused on the production of hydrogen. This is due to the majority of hydrogen which is formed currently produced by methane steam reforming, equation (2.4.2).

$$CH_4 \rightarrow C + 2H_2 \;\; \Delta H_f^0 = 75\ kJ/mol \qquad (2.4.1)$$

$$CH_4 + H_2O \rightarrow CO + 3H_2 \; \Delta H_f^0 = 206.4\ kJ/mol \qquad (2.4.2)$$

With an increase emphasis on decreasing environmental effects of chemical processes, MTD has been explored in the production of hydrogen due to the absence of CO_2 production, which arises from the utilization of CO in (2.4.2). As opposed to methane steam reforming, the carbon in MTD is formed in a solid state and CO_2 emissions can be mitigated if the solids are collected. The solids can possibly be used in the formation of carbon fibre and as filler in construction materials [62]. Presently, carbon is typically combusted to provide the energy requirements of the process, which in turn removes the advantage of carbon sequestration in solid form. Methane steam reforming is a well research chemical

process and is used extensively in industry, where, the process is advantageous as the efficiency of hydrogen production per mol of methane is double that of MTD. However, the enthalpy of the methane steam reforming process is much higher, resulting in higher relative energy consumption. MTD has also been of interest in the production of acetylene, with the earliest reports of successful acetylene production from 1940, from the Huels process using a DC arc reactor [63]. Similar reactors were subsequently commercialized, with DuPont operating a 9 MW plant between 1963 and 1968, for the production of acetylene to supply neoprene plants [64].

Currently 96% of hydrogen produced globally originates from fossil fuel feedstocks. Electrolysis of water is widely regarded as the ideal production pathway for hydrogen production, however, there is still significant research needed in the field to allow the process to compete with conventional processes. At the moment, the costs of electrolysis are uneconomic with production costs at 6.3 NZD/kg, compared to methane steam reforming costing 1.3 NZD/kg. It is believed that the process of methane degradation could allow as a useful transition technology for the production of H_2 whilst reducing CO_2 release.

Considerable work has also been conducted on the investigation and intermediate productions of reaction (2.4.1). The extent of the intermediate production is vast and has been documented by a number of different researches in time. A radical pathway has been suggested by a number of different authors and has been commonly accepted. Equation (2.4.1) is generally regarded as a comprehensive reaction to summarize the completion of the reaction. Acetylene, ethane, ethylene, propane and butane have all been documented as significant intermediates in the production of hydrogen, of which will be discussed in depth below.

2.4.1 MTD Reaction Pathways

Since the interest for the production of hydrogen from methane, the pathways for the decomposition have received extensive attention. This is primarily due to the large array of C_2+ hydrocarbons which are found in the degradation product, highlighting the complexity of the MTD reaction summarized in (2.4.1). It has been concluded from a number of publications that MTD mechanism is a complicated series of multi-stage radical reactions that are strongly influenced by temperature, residence time and pressure. The leading initiation reaction for MTD Reaction (2.4.3) is shown below with important parameters listed in Table 2-5.

$$CH_4 \rightarrow CH_3 + H \qquad (2.4.3)$$

Table 2-5: Arrhenius parameters and rate constants for MTD, ΔH0 = + 431.78 kJ/mol.

Reaction	log(A)	E_a (kJ/mol)	Ref
$CH_4 \rightarrow CH_3 + H$	17.34	377	*[65]*
	17.42	375	*[66]*
	17.00	359	*[67]*

The reaction is initiated by the breaking of the C-H bonds within methane at high temperatures. For larger hydrocarbons (C_2+), the enthalpy of formation is significantly lower due to the presence of a lower strength C-C bond which is broken. Resulting in, rapid degradation of the products which are formed during degradation, as the radical reactions from methane are at elevated temperatures which suffice to break the C-C bond.

It is well documented that during MTD, gaseous hydrocarbons with increasing carbon length are formed. The range of products which are able to form is vast due to the extensive amount of radical interactions possible, for the overview the production of C_1 and C_2 hydrocarbon species and benzene will be focused on.

2.4.1.1 Methane (CH_4) Pyrolysis

Due to the relatively high strength of the C-H bond by comparison to higher molecular weight hydrocarbons, the degradation mechanism is dominated with terminating reactions. As a result the majority of the products which are formed from MTD are C_2 hydrocarbons. Overall it has been concluded that the rate determining step of the process is the initial formation of the methyl radicals, with Reaction (2.4.3) more dominant than Reaction (2.4.4):

$$CH_4 + H \rightarrow CH_3 + H_2 \quad (2.4.4)$$

$$2CH_3 \rightarrow C_2H_6 \quad (2.4.5)$$

$$CH_4 + H \rightarrow CH_3 + H_2 \quad (2.4.6)$$

$$CH_3 + C_2H_6 \rightarrow CH_4 + C_2H_5 \quad (2.4.7)$$

$$C_2H_5 \rightleftarrows H + C_2H_4 \quad (2.4.8)$$

$$CH_3 + C_2H_4 \rightleftarrows 1 - C_3H_7 \quad (2.4.9)$$

$$1 - C_3H_7 \rightarrow H + 1 - C_3H_6 \quad (2.4.10)$$

$$C_2H_4 + H \rightarrow C_2H_3 + H_2 \quad (2.4.11)$$

$$C_2H_3 \rightarrow C_2H_2 + H \quad (2.4.12)$$

2.4.1.2 Ethane (C_2H_6) Pyrolysis

Ethane decomposition occurs at lower temperatures in comparison to that of methane, with the free energy allowing for conversion into carbon and hydrogen at temperatures slightly higher than 200 °C. The initiating reaction of ethane degradation, to form methyl radicals, has a significantly lower enthalpy of reaction, ΔH^0 = + 366.19 kJ/mol. The overall pyrolytic decomposition reactions are as follows:

$$C_2H_6 \rightarrow 2CH_3 \quad (2.4.13)$$

$$C_2H_6 + CH_3 \rightarrow CH_4 + C_2H_5 \quad (2.4.14)$$

$$C_2H_5 \rightarrow C_2H_4 + H \quad (2.4.15)$$

$$H + C_2H_6 \rightarrow C_2H_5 + H_2 \quad (2.4.16)$$

$$2C_2H_5 \rightarrow C_4H_{10} \quad (2.4.17)$$

$$2C_2H_5 \rightarrow C_2H_4 + C_2H_6 \quad (2.4.18)$$

2.4.1.3 Ethylene (C_2H_4) Pyrolysis

The pyrolysis of ethylene is considerably more complicated with an extensive array of possible products. This is largely due to the presence of the double bonded carbon atoms, allowing for a wide range of larger hydrocarbon products to be formed. The degradation of ethylene is also a key pathway which has been identified for the production of aromatic hydrocarbons, which is suggested to form through the dehydrogenation of the products formed in reaction (2.4.24) [68]. Westbrook et al [68], suggested a vast reaction mechanism with 93 elementary reactions defined between 26 species for the pyrolysis of ethylene [68]. The initiating reaction of the process has been suggested as a bimolecular process with the production of vinyl radical;

$$2C_2H_4 \rightarrow C_2H_3 + C_2H_5 \quad (2.4.19)$$

With the following propagation and termination reactions (given up to C_4 hydrocarbons);

$$2C_2H_5 \rightarrow C_4H_{10} \quad (2.4.20)$$

$$2C_2H_5 \rightarrow C_2H_4 + C_2H_6 \quad (2.4.21)$$

$$C_2H_5 + C_2H_4 \rightarrow C_2H_6 + C_2H_3 \quad (2.4.22)$$

$$C_2H_5 + C_2H_4 \rightarrow C_4H_9 \quad (2.4.23)$$

$$C_4H_9 + C_2H_4 \rightarrow 1 - C_6H_{13} \quad (2.4.24)$$

The propagation and termination reactions continue with a number of saturated and unsaturated $C_{3\text{-}6}$ hydrocarbons formed. Given that the decomposition of ethylene is not believed to be excessive in the process an investigation into higher molecular weight hydrocarbons will not be conducted. An excellent review on the pyrolytic decomposition is given by Hucknall [69].

2.4.1.4 Acetylene (C_2H_2) Pyrolysis

The pyrolysis of acetylene has been of interest because of the production of acetylene in a number of hydrocarbon pyrolysis processes. There has been renewed interest in the production of acetylene as a large quantity of newly discovered natural gas reserves exist in remote parts of the world. In New Zealand, acetylene is generally formed by the more common process using calcium carbide and water

[70]. The degradation of acetylene is of particular interest as it is well known to have an influence on the polyaromatic hydrocarbon yields, especially that of benzene [71], [72]. The degradation of acetylene has been investigated at very high temperatures, largely due to the decreasing trend of free energy with temperature, which is unlike other C_2 hydrocarbons.

The thermal degradation of acetylene has been observed to be highly influential on temperature. From literature the thermal conversion of acetylene is low at temperatures of ~1200 °K. Back [71], suggested the following initiating reaction:

$$2C_2H_2 \rightarrow C_2H + C_2H_3 \quad (2.4.25)$$

With terminating and propagating reactions of:

$$C_2H_3 \rightarrow C_2H_2 + H \quad (2.4.26)$$

$$C_2H_2 \rightarrow C_2H + C_4H_3 \quad (2.4.27)$$

Following from the initiating reactions, Back [71], proposed a framework of subsequent reactions, with the low temperature acetylene degradation pathways characterised mostly by the reactions:

$$C_6H_7 + C_2H_2 \rightarrow C_8H_9 \quad (2.4.28)$$

$$C_nH_{n+1} + C_2H_2 \rightarrow C_{n+2}H_{n+3} \quad (2.4.29)$$

With other important butenynyl radicals identified as:

$$C_4H_3 + C_2H_2 \rightarrow C_6H_5 \quad (2.4.30)$$

$$C_4H_5 + C_2H_2 \rightarrow C_6H_6 + H \quad (2.4.31)$$

From the low temperature pathway the possibility of aromatic tar formation is apparent with the phenyl radicals attributed to aromatic production.

2.4.1.5 Benzene (C_6H_6) pyrolysis

The pyrolysis of benzene has been investigated for the potential of production of upgraded products and investigating the soot forming characteristics of the degradation. Soot formation is attributed to the degradation of polyaromatic hydrocarbons (PAH). Although benzene is not polyaromatic, the reaction pathway tends to produce PAH's from the benzene structure through a series of propagating reactions. Benzene and acetylene coupled degradation has been conducted to investigate these characteristics throughout the system, where acetylene aids in the propagation of the polycyclic nature of the products. A number of publications have had issues with system blockages and high tar productions which may be attributed to this pathway [73]. As with the previous description of the products formed from C_2 pyrolysis, the amount of products is vast and a huge variety of potential products exist.

A number of different proposals are given for the initiating step of the reaction, with the production of phenyl radicals being widely suggested and supported by Kern and Wu [74];

$$C_6H_6 \rightarrow C_6H_5 + H \tag{2.4.32}$$

$$C_6H_5 \rightarrow C_4H_3 + C_2H_2 \tag{2.4.33}$$

With the overall rate of decomposition occurring through the ring rupturing reaction;

$$C_6H_6 \rightarrow C_2H_2 + C_4H_4 \tag{2.4.34}$$

Hou and Palmer [75], have also suggested a simple bimolecular homogeneous reaction which occurs on reactor walls to produce biphenyl as;

$$2C_6H_6 \rightarrow C_{12}H_{10} + H_2 \tag{2.4.35}$$

A lot of in-depth and extensive work has been conducted by H. Böhm [76], in the field of benzene pyrolysis. Extensive work has been conducted on the investigation of PAH growth throughout the process highlighting possible pathways which were investigated using acetylene/benzene mixtures. Given the tendency for acetylene production from the degradation of methane, benzene interaction with acetylene is expected in the system and is a probable pathway which explains sooting within the system and aromatic production. A summary of reaction pathways is given below, Figure 2-5.

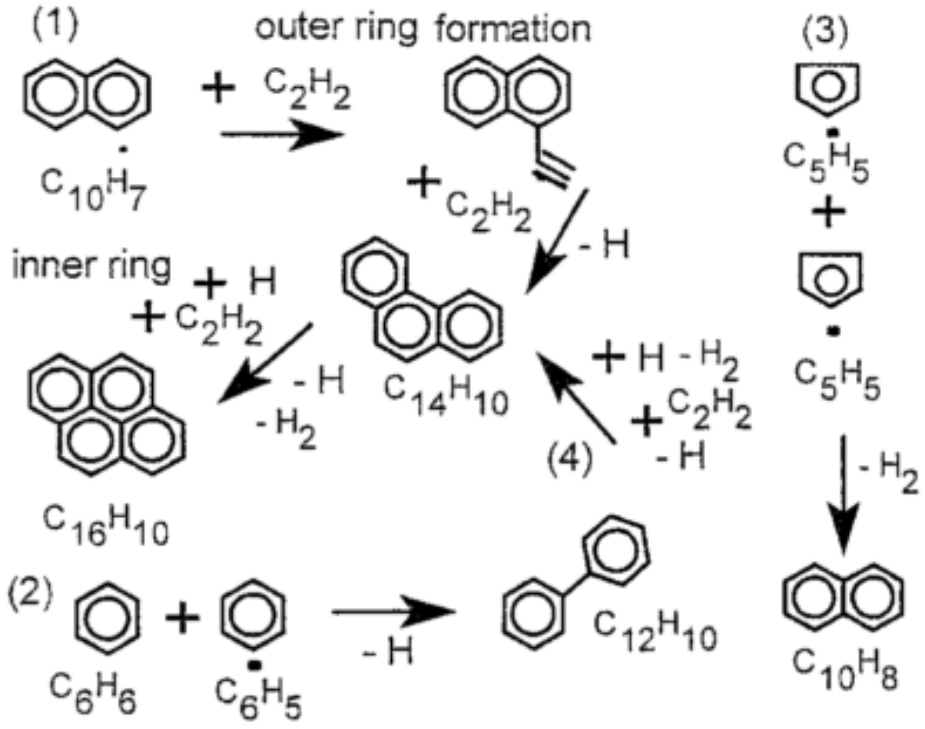

Figure 2-5: PAH growth and soot formation from the pyrolysis of acetylene and benzene, with possible highlighted pathways up to 4 aromatic rings [77].

2.4.1.6 Coke, Soot and Carbon formation

Another important pathway in the pyrolytic reaction pathway is the formation of solid carbon, sometimes referred interchangeably to 'coke', 'soot', 'carbon black', 'carbon'. Although the terminology is not accurately used in a number of publications, the product is dominated largely by the carbon fraction and is of most importance when determining the MTD overall efficiency. Carbon production from methane becomes thermodynamically possible at 527 °C. Interest of soot formation arose from the production of fine particles in facilitating radiant heat transfer in boiler and furnace flames [69]. More recently, research into the carbon/soot deposition have been focussed on the effects on catalysts. Soot and carbon formation is detrimental to catalyst efficiency and at times can cause significant decreases in catalytic conversion [69]. Various differences in maximum temperature before significant carbon deposition occurs are reported, with some estimates of temperatures as high as 1100 °C [78].

Carbon formed by hydrocarbon pyrolysis has been reported to occur heterogeneously, in the gas phase. The leading factors in coke formation have been reported as temperature, fuel, reactor construction material and residence time, it has been suggested that coke formation occurs through a number of propagation and termination reactions [79], [80];

- Production of unsaturated hydrocarbons in the gas phase
- Polymerisation and condensation reactions which form larger and heavier hydrocarbons, aromatic structures are very common with the production of PAHs.
- Condensation of the tar species which have been formed adhering onto the side of the reactor walls.
- Extended exposure leading to the decomposition of the liquid to form carbon/tars/coke and hydrogen.

Another pathway for soot formation has been proposed where the direct reaction of free radical and small species (usually termed as species with a molecular weight lower than 100) reacting directly with the coke. As a result the carbon grows due to a number of dehydrogenation reactions [81]. This leads to continual thickening and elongation of carbon filaments, Figure 2-6. The characteristic filament structure of carbon is common in experimental practise [73], [82]–[84].

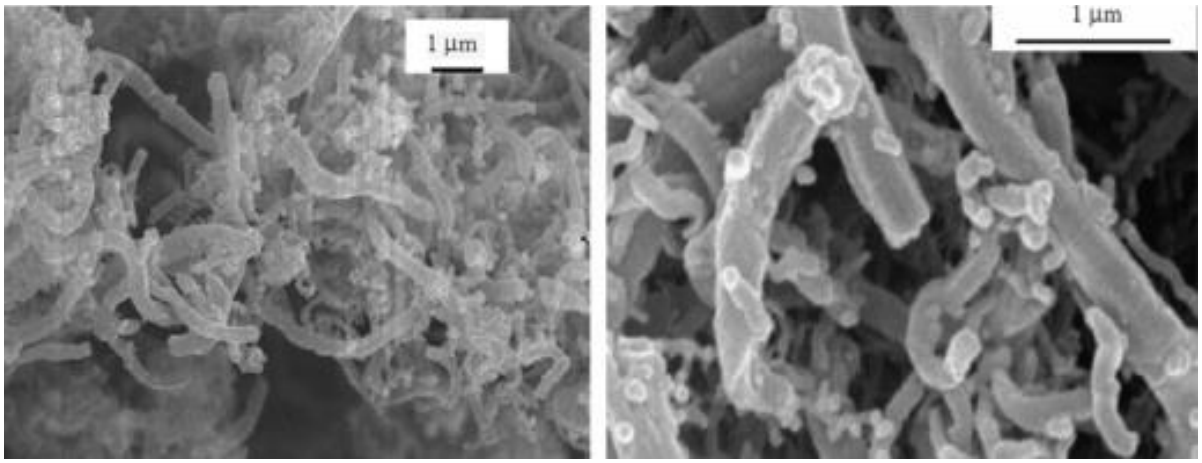

Figure 2-6: SEM images of a catalyst surface (Nu:Cu:Al-78:6:16) after a 16 hr run, left image, 8000x, right, 20200x. Image retrieved from [84].

Böhm and Jander [76], conducted extensive work in modelling the PAH growth characteristics using benzene/pyrene and acetylene as model compounds. The effect of small radical molecules was investigated on the influence of sooting pathways. By subsequent H abstraction and C_2H_2 addition (HACA) the composition and structure of the PAH's vast. The model also includes the addition reaction of other small aliphatic hydrocarbons which are formed in the pyrolysis and have bearings on the end products. An overview of the proposed pathways is given below:

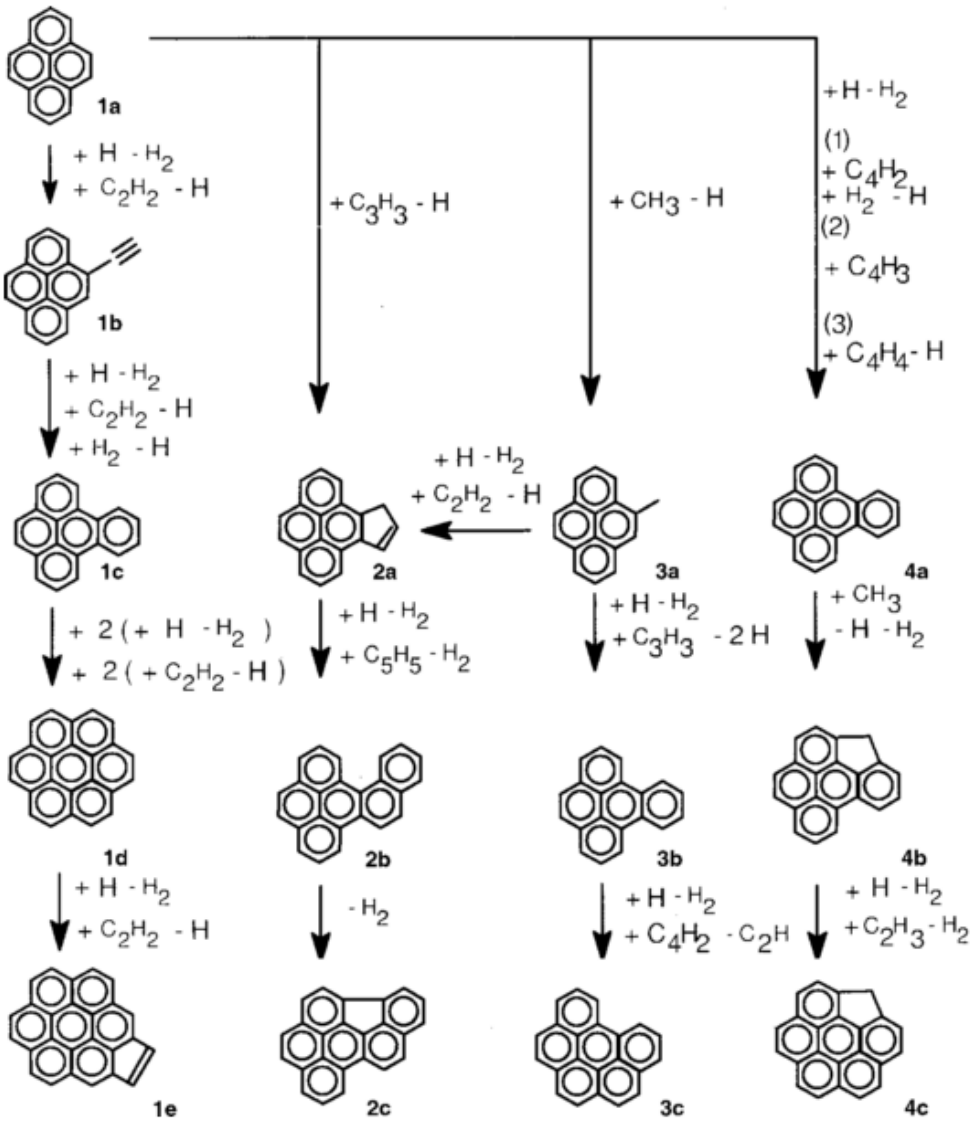

Figure 2-7: Possible pathways for the growth of poly-aromatic hydrocarbons by small aliphatic hydrocarbons, retrieved from [76].

Another characteristic of carbon deposition is the 'carbon black mirroring' which has been found to occur in numerous experiments. This phenomenon is observed as a near silver mirror finish on tube interiors Figure 2-8. This is typical of a quartz tube based reactor system and seems to have different carbon producing characteristics than other metallic based reactor configurations. The surface of the system is observed to have a significant effect on the carbon production, with increased surface area and roughness attributed to higher carbon productions.

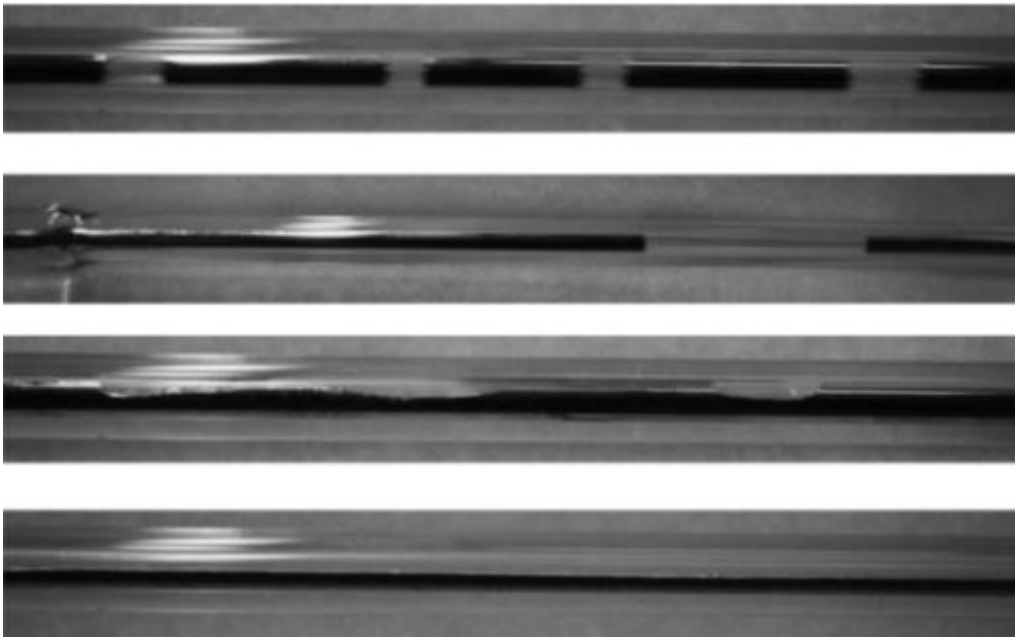

Figure 2-8: Mirror finish on the inside of a quartz liner tube, [78].

For MTD, the formation of soot is due to the consecutive formation of ethylene and acetylene as the soot forming pathway. In turn, the theoretical measurements of methane consumption are best approximated with acetylene and ethylene formation, this arises uncertainties in the rate coefficients of methane pyrolysis [79]. Generally, hydrocarbons are regarded as unstable at all temperatures, due to their high free energy. Methane is generally stable with respect to its elements up to temperatures of 573 °C. At higher temperatures, the free energy of the gas is raised and the formation of carbon and hydrogen are preferred, with increasing kinetic favourability from large residence times and high temperatures [85].

Soot formation from the growth of PAH molecules is a widely accepted theory for the production of soot. Experiments have indicated that soot is formed by the growth of PAH during combustion until the vapour pressure is low enough to facilitate the condensation of the tar species. This mechanism is in accordance with a number of experiments which have been conducted. A. Dunker et al [73], found numerous tar species in deposited carbon in the distribution of pyrene > benzo(ghl)perylene > benzo(a)pyrene = benzo(e)pyrene > phenanthracene. Numerous other species were detected at lower concentrations, and it is suspected that a number of species were undetected due to the large range of aromatic structures possible. From the same experiment it was also shown that the addition of a MTD catalyst decreased PAH production, as opposed to reactions with no catalyst (albeit, catalysed by the carbon formed in the process).

The production of carbon is also an interesting area of research, due to the autocatalytic and catalytic processes evident throughout MTD. The production of carbon has been reported to further catalyse

MTD [86]. The carbon has been described as having a large surface area and causing severe blocking within systems which are susceptible to carbon build up. The carbon has been reported to adhere to most of the reactor surfaces and also have significantly different characteristics arising from reactor operation. In some cases, with a catalyst present, the characteristics of the formed carbon can change drastically to increase carbon density by a magnitude of 10 [73]. Due to the high surface area and the efficiency of the carbon activing as a catalyst, some researchers have reported activation energies lower than expected [86]. Interestingly it has also been observed that coke created from a metallic reactor contains the same metal particles in the coke. Analysis by SEM of coke has determined that coking occurred on the reactor walls and in a heterogeneous reaction metal particles are present in the coke [87].

The formation of carbon is also extensively influenced by the residence time of the system. Where, increasing residence times result in increased hydrogen and carbon yield, due to increased nucleation sites on the surface of reactor walls and allows for increased soot deposit. Increased residence times allow for interactions between molecules to become more frequent and also facilitates the increase potential of PAH aromatic ring growth.

To limit the effect of carbon accumulation in the system, carbon is usually combusted to ensure there is not compounding effect between trials during experiments. Carbon build-up is problematic for reactor operation as it leads to a significant proportion of the reactor walls being covered in carbon and has a tendency to agglomerate at the smallest orifices. This can cause experimental malfunctions and large pressure drops, as experienced in nozzle fed, fluidised bed and drop tube reactors [73], [86], [88]. A reactor which has been successful in mitigating many of the physical issues is a molten metal reactor which, due to density differences, accumulates carbon at the top of the molten metal which can easily be removed [78]. For trials with catalysts, a characteristic high conversion of methane usually last for the first few minutes, then a region of constant methane/hydrogen concentration occurs, with a tailing of hydrogen concentration and increase in methane concentration. Dunker et al [73], experienced over the 6-12 hours of sampling for each experiment, deposition of carbon eliminated over 93 % of the micropore structures in carbon catalyst; whilst, the concentration of mesopores was increased overall. The increase was due to the depositing of carbon onto the catalyst. It was ultimately concluded that the reduction of micropores led to the decrease in MTD efficiency, whilst the mesopores are no believed to have a significant influence in the soot formation. It was also reported that the carbon which was deposited from the reaction has a less catalytic effect than the carbon black catalyst.

2.4.2 Effect of Hydrogen Addition in Pyrolysis Atmosphere

A number of different additional gases have been investigated for their effect in the pyrolytic reaction of methane. This has stemmed from two areas of interest; firstly, the large production of hydrogen and the effect of additional hydrogen in reaction pathways, secondly, the addition of other longer chain hydrocarbons > C_2 as these species are commonly found in natural gas. In general the addition of large chain hydrocarbons leads to increased carbon formation as the introduction of C_2 hydrocarbons adds species that are more prone to carbon deposition than methane. Although this is a general conclusion from the work conducted, the results from hydrogen seem more influential. Hydrogen addition has been shown to successfully reduce carbon deposition rates in systems operating up to 2000 °C and very short residence times < $6.8x10^{-2}$ s [89]. Gueret and Billaud [90], modelled the production of production gas species and concluded that increased dilution of hydrogen the conversion of methane was decreased whilst coke yields decreased [60], [90] It is suggested that the decrease in coke production may be due to the reduction in methyl radicals due to the shifting equilibrium of equation (2.4.4). Considerable dilution of the gas stream with hydrogen is also believed to reduce the coke formation, where, it was also reported that ethylene and acetylene selectivity increased, with a significant decrease of benzene [90]. It is suggested that the reduced coke is possibly due to the hydrogen inhibiting the aromatic forming Reactions (2.4.30), (2.4.31).

2.4.3 Thermodynamics of Methane Thermal Degradation

From the reaction enthalpies it is observed that there is a considerable amount of heat required for the reaction to proceed. The formation of hydrocarbons from the elements may be written per C atom as:

$$C + \frac{1}{n}\frac{m}{2}H_2 \rightarrow \frac{1}{n}C_nH_m \qquad (2.4.36)$$

The decomposition of methane is observed to begin at temperatures of approximately 527 °C. From the standard free energy data given in Figure 2-9, the free energy formation shows significant variation with increasing temperature. At temperatures below 527 °C the free energy of methane and ethane are relatively high in respect to the other species. With an increase in temperature the stability of methane decreases significantly. At temperatures above 1027 °K the standard free energy of methane is higher than that of benzene, causing methane to be unstable and favour the production of benzene. Upon further increasing of the temperature the free energy of both ethylene and acetylene become lower than that of methane. However, at these elevated temperatures the stability of the hydrocarbon molecules is significantly lower than that of carbon and hydrogen. Interestingly, it is observed that the free energy of acetylene decreases throughout the temperature range with elevated temperatures >1727 °K considerably more favourable to acetylene than other hydrocarbon species.

However, at these temperatures the kinetics of the system is so high that the deposition of carbon is extremely quick and hydrogen is expected to be the primary product. From this analysis it is observed that with increasing temperature, the thermodynamic standpoint for hydrocarbon production with increasing temperature is in order of; benzene, acetylene and ethylene. Although ethane is more stable throughout the process, the free energy increases in a similar fashion to that of methane and is ~ 25 kJ/C-atom larger throughout the temperature range of. This concludes that at the higher temperature the production of ethane is significantly decreased and unsaturated hydrocarbons are thermodynamically preferred. Overall the free energy of olefinic molecules is observed to increase with temperature significantly slower than paraffinic molecules.

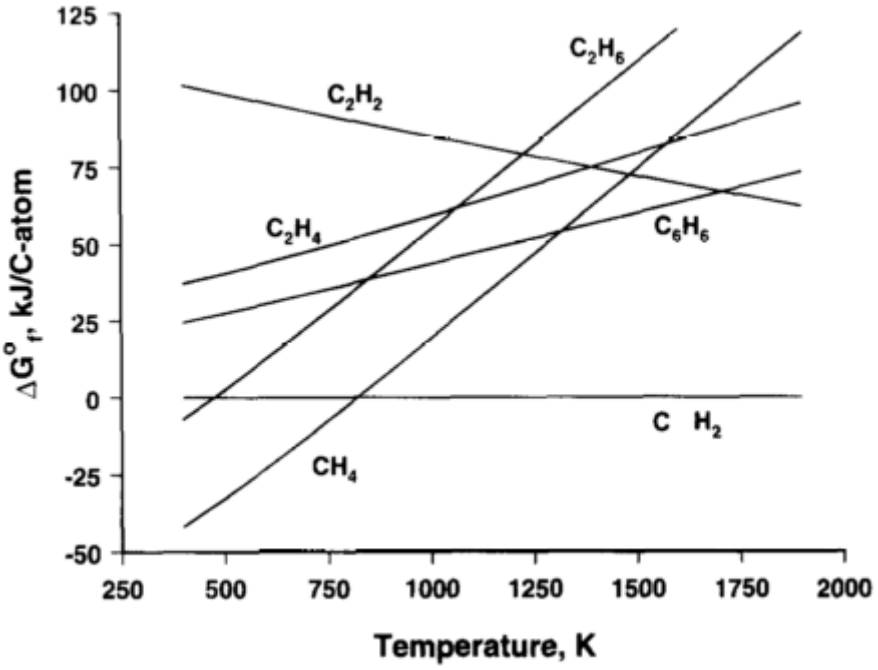

Figure 2-9: Standard free energy of formation (del G(f)) of some of the important hydrocarbons produced in MTD, [91].

Carbon formation has been documented to be influential in the derivation of products from methane degradation. In the work from Chen et al. [92], a reactor was allowed to completely pyrolyse methane for a few hours, and then a degradation experiment was run. Chen et al [92], concluded that there was a strong relationship with erratic and faster than normal reaction systems, with carbon coated reactor systems. Catalytic pathways have been reported from a number of different authors, as sources of uncertainty for the measurement of reaction kinetics from the system. Although the effect of the degradation has been concluded form a number of different sources, the pathways have been disputed between literatures. Naphtha formation and the subsequent formation of increasing molecular weight aromatic molecules have been suggested as a route for carbon deposition onto reactor walls. Another pathway which has been disputed is the dehydrogenation pathway of ethane:

$$2CH_4 \rightarrow C_2H_6 \rightarrow C_2H_4 \rightarrow C_2H_2 \rightarrow 2C \quad (2.4.37)$$
$$+H_2 \quad +H_2 \quad +H_2 \quad +H_2$$

It is speculated that the carbon is formed from dehydrogenation of ethane as the primary product, leading to the eventual formation of carbon [91]. However, conflicting reasoning has been associated with the pathway with some disagreeing on condensation reaction pathways. This is primarily due to the dissociation pathway reactions of methyl reactions being unfavoured by the high enthalpy of the radical species [92].

$$C_2H \rightarrow C_2 + H \quad \Delta H = 837\ kJ/mol^{III} \quad (2.4.38)$$

$$C_2H \rightarrow C + CH \quad \Delta H = 582\ kJ/mol^{III} \quad (2.4.39)$$

High temperature and pressure have been observed to increases the rate of carbon formation during MTD. The increase in temperature allows the enthalpy requirements of the reaction system to be reached in substantially shorter times and fulfils the energy requirements for the system. The kinetics of the reaction is also greatly enhanced by the increasing temperature. It is important to distinguish the differences between that of coke and carbon in describing the pathways for MTD. The formation of coke is attributed to the forming of carbonaceous solid products which usually contain hydrogen. This allows for an insight into the possible pathways in the production of the coke product. Analyses have shown that, from the coke formed in MTD the inclusion of a number of different molecular weight aromatic hydrocarbons were present [60]. From SEM imaging, Blekkan et al [60], observed coke depositions on the reactor wall in cobble like forms, indicating a strong potential for tar adhesion to the reactor wall. Coke deposition has been observed as a mixture of gas phase coke suspension and deposition onto surfaces [60]. Multiple explanations for the formation of coke have been suggested from literature with a number of different pathways put forward. In comparing all of the sources of the sources of possible pathways for coke formation it is found that acetylene is a fundamental species. As summarized by Holmen et al [91], two main mechanisms for coke or carbon formation are thought to be;

1. Aromatic trimerization of acetylene; the production of polynuclear aromatics which are formed from the sequential dehydrogenation reactions, as shown in equation (2.4.31). From this creation of polynuclear aromatics, droplets are then condensed on the reactor wall and then deposited. It is however noted that other possible acetylenic compounds may provide another route to the aromatic product, however not with significant yields.

[III] Based on D(HCC-H) = 469 kJ/mol

2. Lahaye and Prado [93], also proposed another mechanism which suggested that small species/radical reactions were responsible for the production of aromatic structures on coke surfaces. It was suggested that the radicals of interest were small species such as mono/di-olefins or small acetylene species. This mechanism explains the growth of the long filament like structure of the carbon.

The important reaction which initiates the MTD reaction is the initial dehydrogenation reaction (2.4.3), which is the primary initiating reaction, coupled with the hydrogen radical consuming reaction, equation (2.4.4). The stability of the radicals which are formed in reaction, equation (2.4.3) is strongly dependent on temperature. With increasing temperature the stability greatly increases with respect to the end products of hydrogen gas and solid carbon. Overall a higher reaction temperature favours the production of the methyl radicals.

2.4.4 Reaction Kinetics during Methane Thermal Degradation

2.4.4.1 Temperature effect

MTD temperatures over 1127 °C are required to make the conversion of methane to C_2 products viable. At these temperatures, the products which formed are unstable and require removal and/or quenching, whereas, if the reaction is allowed to carry on further carbon and hydrogen will largely be produced [91]. To increase C_2 hydrocarbon yields, short residence times and high temperatures are favoured, due to a range of different intermediate steps between the degradation of methane to hydrogen and carbon. With known system kinetics and thermodynamics the process can be modified to specifically produce target molecules in the reaction mechanisms described above. However, due to the range of different reaction kinetics some of the species such as acetylene are easier to target than ethane. Most research in the production of C_2 species from MTD have focussed about acetylene [89], [94]. With large power consumption and product contamination some of the key issues which were encountered when targeting other species such as ethane and ethylene.

Accurate kinetic data is difficult to determine due to the high temperatures of reaction which are needed to initiate MTD. Due to the high temperature requirements, reactors are more susceptible to temperature variations. This has been attributed to disparities in derived data and literature on a number of occasions [89]. A commonly used reactor in the derivation of reaction kinetics is the shock tube reactor, which allows the reaction to proceed with uniform temperature and solely with homogeneous gas interactions. The systems are generally regarded as ‘wall less’ due to the apparent surface free reaction environment which reduces the possibility of catalytic heterogeneous reactions effecting product distribution.

Many of the kinetic investigations have been focused on the acetylene production route, Holmen et al [89],were pioneers in the field and investigated the kinetics of ethane, ethylene and acetylene formation from methane. The reaction scheme is associated with that of Reaction (2.4.37), with the associated rate constants k_1 [s^{-1}], k_3 [s^{-1}], k_4 [L/mol.s] and $k_2 >> k_1$ [89];

$$\begin{matrix} 2CH_4 \overset{k_1}{\rightarrow} C_2H_6 \overset{k_2}{\rightarrow} C_2H_4 \overset{k_3}{\rightarrow} C_2H_2 \overset{k_4}{\rightarrow} 2C + H_2 \\ + H_2 \quad + H_2 \quad + H_2 \end{matrix} \tag{2.4.40}$$

$$k_1 = 4.5\ x\ 10^{13} exp(-\frac{91000}{RT}) \tag{2.4.41}$$

$$k_3 = 2.58\ x\ 10^{8} exp(-\frac{40000}{RT}) \tag{2.4.42}$$

$$k_4 = 10^{11} exp(-\frac{44370}{RT}) \tag{2.4.43}$$

It is assumed that the first three reactions $k_{1\text{-}3}$ are all irreversible first order reactions, whilst the final reaction is irreversible homogenous second order reaction [89] . From the kinetic equations shown a low ethane concentrations are expected, due to the high reaction constant of the process, where the high activation energy also highlights the large energy requirements. The production of acetylene is favoured due to the lowest activation energy of the entire reaction scheme. However, with the large activation energy of the initiating reaction, the subsequent activation energies are all in excess. After the initiating reaction the ethane is readily consumed and reacted to ethylene given that $K_2 >> k_1$. In the temperature range of interest, 850-1050 °K the rate constants are relatively stable and are well defined by the associated pre-exponential factors. Careful consideration of the residence time value is required, and by reaction kinetics an optimisation of the process can be achieved. A discussion on the residence time effect will be given below.

Another important MTD reaction that has received considerable attention is that of the methyl radical formation, Reaction (2.4.3). Numerous researchers have investigated the kinetics of the base reaction to better control the reaction products. A summary of the findings are given in Table 2-6.

Table 2-6: Reaction kinetics for initial methane dehydrogenation Reaction (2.4.3): $CH_4 \rightarrow CH_3 + H$.

Pre-exponential Factor (A)	**Temperature Order (n)**	**Activation Energy (Ea)**	***Ref.***
[cm^3/mol.s]	[-]	[kJ/mol]	*[-]*
3.00x10^{16}	0	339	*[95]*
3.51 x10^{15}	0	435	*[96]*
4.24 x10^{16}	0	373	*[97]*
8.47 x10^{16}	0	366	*[98]*

2.5 Case Study - A. Kobayashi and M. Steinberg (1992) [99].

Given that the only previous work which was conducted on the flash methanolysis of biomass was conducted by M. Steinberg [1], [2], an investigation and comparison of the MTD results obtained by Kobayashi and Steinberg [99], was conducted. This is to ensure that the MTD characteristics are similar to that reported by literature. This allows for an insight into possible catalytic effects; as, if there are any variations due to construction material that alter the MTD characteristics, there is a high chance that the properties from the methanolysis will be different. This is most interesting as the degradation work from Kobayashi and Steinberg [99], was conducted in the same reactor as the flash methanolysis trials [1], [2], [100].

The methane degradation trials

were conducted in the temperature range 700-900 °C and pressures from 28.2-56.1 atm. The trials were conducted in a 1" diameter, 2.4 m heated zone reactor. The reactor was constructed from Inconel 617. The system consisted of a preheater section followed by the hot reaction zone in quick succession. The activation energy and rate constants were derived using Arrhenius plots and back calculation for the rate constants. A comparison of the data collected from A. Kobayashi and M. Steinberg is given below, Table 2-7 .Unfortunately no data was collected from A. Kobayashi and M. Steinberg at pressures lower than 28.2 bar; however, it was concluded that there was little variation in rate constant with varying pressure.

Table 2-7: Comparison of activation energy and rate constants for the MTD.

Author	**Temperature**	**Pressure**	**Rate constant**	**Activation Energy**	**Ref.**
[-]	*[°C]*	*[Bar]*	*[1/s]*	*[kJ/mol]*	*[-]*
A. Kobayashi and M. Steinberg	700	56.1	5.76×10^{-4}	131	*[99]*
A. Kobayashi and M. Steinberg	800	56.1	1.75×10^{-3}	131	*[99]*
A. Kobayashi and M. Steinberg	900	56.1	9.31×10^{-3}	131	*[99]*
G. Skinner and R. Ruehrwein[IV]	700	5	3.45×10^{-4}	423	*[101]*
G. Skinner and R. Ruehrwein[IV]	800	5	2.86×10^{-3}	423	*[101]*
G. Skinner and R. Ruehrwein[IV]	900	5	1.65×10^{-2}	423	*[101]*
H. Palmer et al.[V]	700	1	2.00×10^{-4}	431	*[93]*
H. Palmer et al.[V]	800	1	1.71×10^{-3}	431	*[93]*
H. Palmer et al.[V]	900	1	1.02×10^{-2}	431	*[93]*

From the comparison collated in the Table 2-7, it is apparent that the rate constants between the trials are relatively constant between the temperature ranges. However, there is a clear discrepancy between the work of Kobayashi and Steinberg in regards to the activation energy. It is apparent that the activation energy of MTD is approximately 427 kJ/mol. Kobayashi and Steinberg have reported activation energy over three times smaller than previous reports [99]. This large difference leads to different conclusions which are drawn from the results. This is primarily due to the consideration that activation energy values below 125 kJ/mol are usually considered to be controlled by diffusion. Activation energies greater than 210 kJ/mol have been attributed to chemical reaction controlled processes [99]. Indicating that the results obtained by A. Kobayashi and M. Steinberg [99] are possibly influenced by external sources.

[IV] Rate constant calculated from expression in publication [$\log(k) = 14.71 - \frac{22070}{T}$]

[V] Rate constant calculated from expression in publication [$\log(k) = 14.6 - \frac{22500}{T}$]

It is speculated that the considerable variation in activation energies could be due to catalysis from the reactor wall and/or carbon which is formed in the process. Carbon is a known autocatalyst and has been attributed to higher ethane concentrations than expected from homogeneous reactions, by models and may lead to discrepancies [102]. Unfortunately due to the absence of C_2 hydrocarbon formation from the data, a comparison and investigation of the potential is unavailable. Another possible influence for the end activation energy and product streams could be attributed to the construction material of the reactor, which could possibly facilitate a heterogeneous catalytic gas phase reaction. Table 2-8 shows the chemical composition of Inconel 617, the high concentration of nickel, cobalt and molybdenum has significant scope of being a catalyst in the system. However, due to the high chromium content a chromium surface layer suspected to form on the inside of the reactor. Although literature about the effect of chromium catalysts directly for MTD is scarce, thermal degradation of other hydrocarbons in the presence of chromium catalysts has been investigated. Chromium supported on Al_2O_3 has been proven as a useful catalyst in the dehydrogenation of alkanes [103]. This could possibly explain the lower than expected activation energy derived from Kobayashi and Steinberg [99].

Table 2-8: Chemical composition of Inconel 617.

Element	Chemical Composition
Nickel	44.5 % min
Chromium	20-24 %
Cobalt	10-15 %
Molybdenum	8-10 %
Aluminium	0.8-1.5 %
Carbon	0.05-0.15 %

2.6 Overview of Pyrolysis

Pyrolysis is a thermochemical process which occurs by heating materials in the absence of oxygen to produce a mixture of solid, liquid and gaseous products [104]. Generally pyrolysis is split into two categories; slow pyrolysis and fast pyrolysis. Slow pyrolysis is used primarily in the production of biochar due to the high residence time and low operating temperature, whilst, fast pyrolysis has traditionally been investigated for the production of bio-oil. Flash pyrolysis is a term which has also been utilized throughout literature as well, which has generally related to high heating rates of the

particles. Steinberg et al [1], [3], utilized the term flash pyrolysis to describe the pyrolysis process at high temperatures and low residence times for various fluidising gases. Due to the lack of research focusing on the production of gases from pyrolysis, no universal name has been given to the production of bio-gas. In general the production of biogas utilizes higher temperatures, lower residence times and higher heating rates than that of bio-oil production. For the purpose of this report pyrolysis targeting the production of bio-gas (T >800 °C, residence time <2 s and heating rates >1000°C/s), the term flash pyrolysis will be utilized. As opposed to fast pyrolysis (defined for bio-oil focused), as from the range of literature there is no distinct definition between processes which targets bio-oil as opposed to one which targets gases. A brief overview of slow and fast pyrolysis will be give below, with a review of methanolysis from Steinberg et al [1], [3], [99], [100].

2.6.1 Pyrolysis Kinetics

The kinetics of biomass during pyrolysis is a region of research which has received much attention due to the desire of understanding the formation characteristics of the product species. Although there are extensive amounts of research attempting to understand the kinetics of the pyrolysis reactions, the overall reaction pathways of pyrolysis are not well understood. This is primarily due to the large array of reactions which are possible during the process, as the product of pyrolysis can lead to over species.

Due to the varying composition of biomass feedstocks, it is of interest to develop kinetic models which can correctly predict product selectivity during pyrolysis. When investigating the kinetics of the system the same approach is taken as the derivation of the thermodynamic characteristics of the system. The kinetics of the pyrolysis of biomass is divided into the separate constituents of biomass and the product prediction is determined in regards to the operating conditions.

Due to the array of reactions and high reaction kinetics derivation of the product distribution during pyrolysis is difficult, a lumped kinetic model approach has been adopted many researchers. These models assume that the products are formed in single-step and/or multistep reaction pathways for the production of; tars, char and gases. These models do not include information about the reaction pathways and generally do not require characterisation of the inlet biomass feed. The application of a lumped kinetic model for the pyrolysis of cellulose has been extensively utilized with the Broido-Shafizadeh (B-S) model commonly used to describe cellulose pyrolysis [105]. The model assumes that cellulose first decomposes into active cellulose, then, through competitive pathways tar formation and char and gas formation occurs, Figure 2-10. Other models have been developed which are based on the active cellulose intermediate and consider the formation of secondary tars, secondary gases and water to increase model accuracy [106], [107]. Diebold [108], proposed a model which incorporates these other product pathways which has also been extensively utilized by other researchers, as shown

in Figure 2-11. Other models have not used the activated cellulose step, however, in general the use of the active cellulose intermediate leads to improved accuracy in the model [109].

Figure 2-10: Broido-Shafizadeh cellulose pyrolysis model.

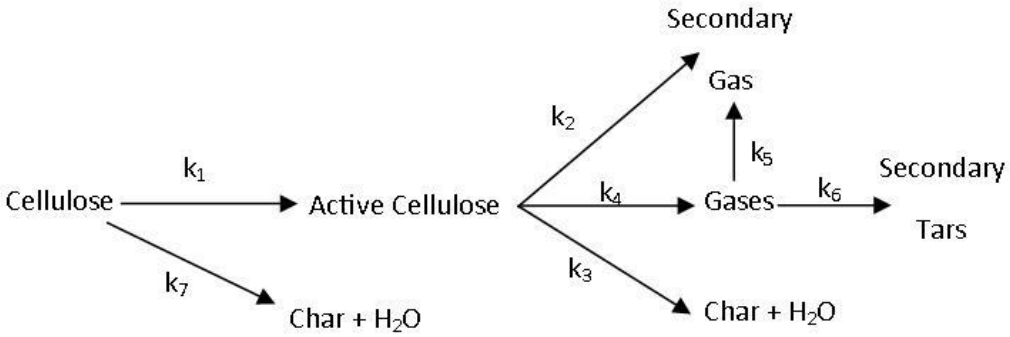

Figure 2-11: Diebold model reaction pathways for cellulose pyrolysis.

For the modelling of the pyrolysis of hemicellulose and lignin the proposed kinetic pathways are similar to that of the B-S model. The number of lumped kinetic models describing hemicellulose and lignin are sparse, due to the much more complicated structures and pyrolysis pathways. Miller et al [107], suggested a modular model which could be utilized for all the biomass constituents, Figure 2-12. The model contained a competitive step for tar and char, whilst, also assuming additional gas was produced through the cracking of tars:

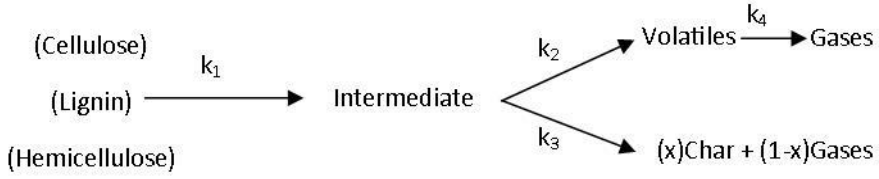

Figure 2-12: Miller et al [107], proposed kinetic pathway during the pyrolysis of biomass constituents.

Other models have also been implemented as a way of describing the production of desired species of the process directly. Ranzi et al [110], developed a model which looked at the production of

levoglucosan directly, and deemed all other products as decomposition products from competitive reaction with active cellulose.

Expansive kinetic schemes exist for the pyrolysis of hemicellulose, cellulose and lignin which have been used in an attempt to determine the rate constant of the reactions within the models shown in Figure 2-10, Figure 2-11 and Figure 2-12. In the work from Ranzi et al [110] a detailed lump kinetic model was successfully applied to characterised biomass structures. The model focused on biomass devolatilisation process and secondary gas phase reactions of the released gases and tars during pyrolysis. The model takes into the reaction steps and accounts for the structural bonds within the biomass constituents, and the lignin structures, LIG-C, LIG-O and LIG-H are all considered through different steps in the kinetics of the reaction. The initial kinetic rate expressions for the major biomass constituents from the modelling of Ranzi et al [110], is shown in Figure 2-9.

Table 2-9: Initial reactions of core biomass constituents used within the model proposed by Ranzi et al. [110], Where Cell= Cellulose, HCE= Hemicellulose, LIG (C,H,O)= Lignin structures, LIG(OH) and LIG(CC) = Intermediate species.

Reaction	Rate Expression	Units
$Cellulose \rightarrow Active\ Cellulose$	$k = 8x10^{13}\exp(-46000/RT)$	$[s^{-1}]$
$Cellulose \rightarrow 5H_2O + 6\ Char$	$k = 8x10^{7}\exp(-32000/RT)$	$[s^{-1}]$
$HCE \rightarrow 0.4\ HCE_1 + 0.6\ HCE_2$	$k = 1x10^{10}\exp(-31000/RT)$	$[s^{-1}]$
$LIG(C) \rightarrow 0.35LIG_{CC} + 0.1pCoumaryl + 0.08Phenol + 1.49\ H_2 + H_2O + 1.32G\{COH_2\} + 7.05Char$	$k = 4x10^{15}\exp(-48500/RT)$	$[s^{-1}]$
$LIG(H) \rightarrow LIG_{OH} + C_3H_6O$	$k = 2x10^{13}\exp(-37500/RT)$	$[s^{-1}]$
$LIG(O) \rightarrow LIG_{OH} + CO_2$	$k = 2x10^{13}\exp(-37500/RT)$	$[s^{-1}]$

2.6.1.1 Hydrocarbon Production within Hydrocarbon Flames

Investigations into the products of combustion in different hydrocarbon flames are proposed as a possible source of literature to explain the production distribution during methanolysis. This is due to the large amount of research which has been conducted to determine the combustion reaction pathways, which may have similarities in methanolysis when regarding some species interactions.

Flames of methane [111], [112], acetylene [113]–[115], ethylene [111], [113], [115], benzene [113] and ethane [115] have all been investigated for their combustion characteristics; to mainly decrease soot production, increase combustion efficiency and better understand PAH formation [112].

Slavinskaya and Frank [111] attempted to model the aromatic to soot precursor formation in methane and ethylene flames, the model was developed with 93 species and 729 reactions highlighting the complex nature of the aromatic to soot formation pathway. Slavinskaya and Frank determined that at temperatures of < 1500 °K, the HACA sequence is highly influential in the distribution of aromatic products, as shown in Figure 2-13.

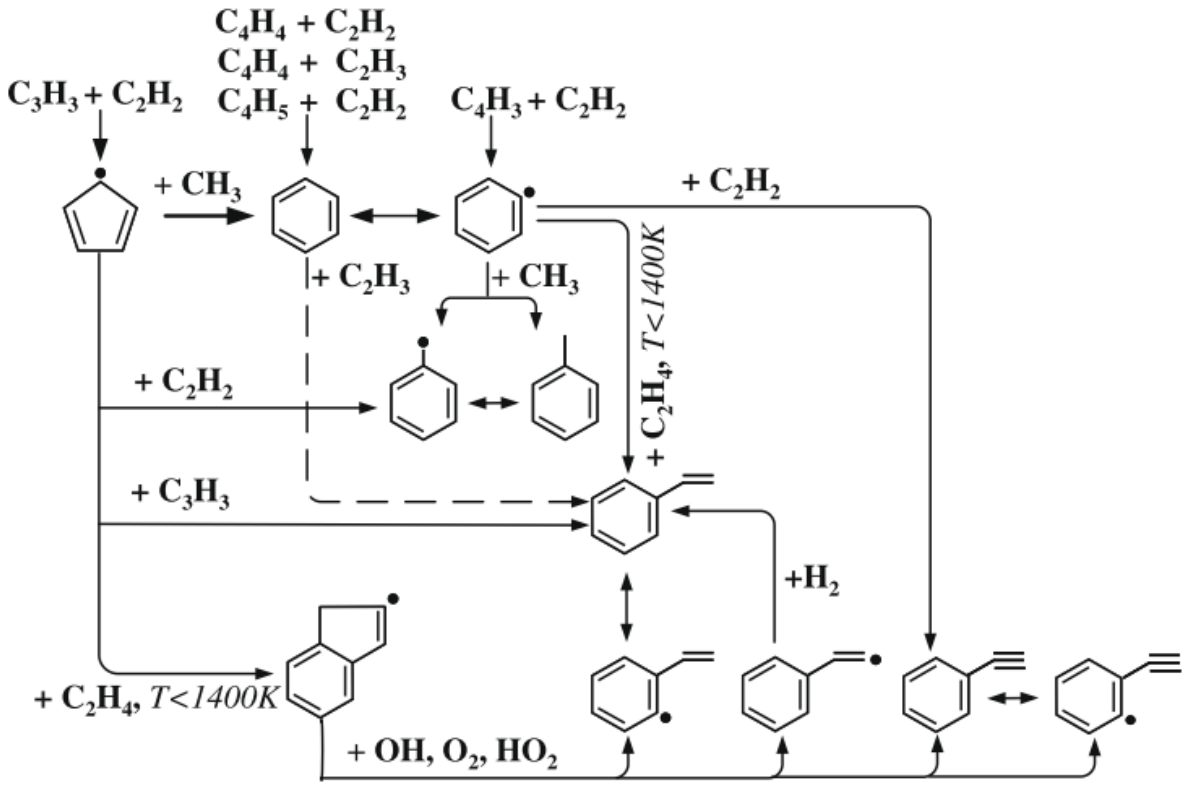

Figure 2-13: The main reaction pathway for the formation of single aromatic ring formation at T< 1550 °K, as deduced for the CH_4 and C_2H_4. Retrieved from [111].

Where it was described that the key reaction for the production of aromatic rings was the formation of cyclopentadienyl radicals, which were suggested to be predominantly formed by the recombination reaction of acetylene and propargyl radicals:

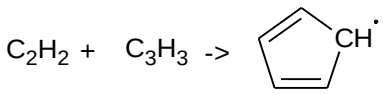

(2.6.1)

Where Olsvik and Billaud [116] proposed that propene production could occur via dehydrogenation of n-C_3H_7, C_3H_6 and C_3H_5 which are formed through methyl radical pathways with ethylene, ethyl radicals and acetylene, respectively:

$$CH_3 + C_2H_4 \rightarrow n - C_3H_7 \tag{2.6.2}$$

$$CH_3 + C_2H_3 \rightarrow C_3H_6 \tag{2.6.3}$$

$$CH_3 + C_2H_2 \rightarrow C_3H_5 \tag{2.6.4}$$

$$\underset{-\,H^{\cdot}}{nC_3H_7} + \underset{-\,H^{\cdot}}{C_3H_6} + \underset{-\,H^{\cdot}}{C_3H_5} + C_3H_4 \tag{2.6.5}$$

Where the hydrogen radical acts as a catalyst throughout the process and forms the propargyl radical:

$$C_3H_4 \rightarrow C_3H_3 + H \tag{2.6.6}$$

Senkan and Castadli [117] used three separate flames of propane, ethane and methane to investigate the extent of PAH production with different gases. It was determined that when using methane, the production of benzene, acetylene and naphthalene all occurred later[VI] than when the other hydrocarbon fuel sources were used. Overall it was concluded that the methane flame was the least sooting and the production of PAH was significantly higher than that of ethane, but about the same as when propane was used [117]. As a result, It was suspected that the PAH formation was enhanced with the presence of odd numbered hydrocarbon species, which is in agreement with Equation (2.6.1).

Marinov et al [118], also identified that the formation of PAH is also strongly influenced by methylallenyl radicals which can be formed by hydrogen catalysed radical stabilisation, as shown in Equation (2.6.7) [119], [120] The methylallenyl radicals formed are then suspected of interacting with propargyl radicals to form benzyl radicals, which can then be stabilized to form benzene, toluene, indene, anthracene and phenanthrene [118].

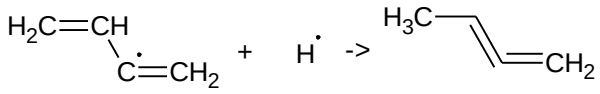

(2.6.7)

[VI] Where later in production refers to greater distance above the burner surface.

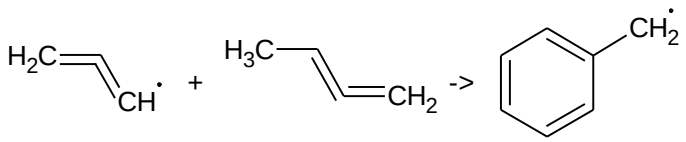

(2.6.8)

The pathways of the combustion process for relatively simple hydrocarbon species highlights the complexity of the combustion process and the extent, and array of multiple reactions which could concentrated to PAH production. As many of the pathways for the production of aromatics are not oxidation reactions, it is interesting to investigate the potential reactions which are possibly also observed during methanolysis. The extent of influence which methane can have on the products is shown in Figure 2-14, where significant contribution of methyl, benzyl and cyclopentadienyl radicals with the products of methanolysis can produce a range of different product species, and possibly influences the product distribution during methanolysis.

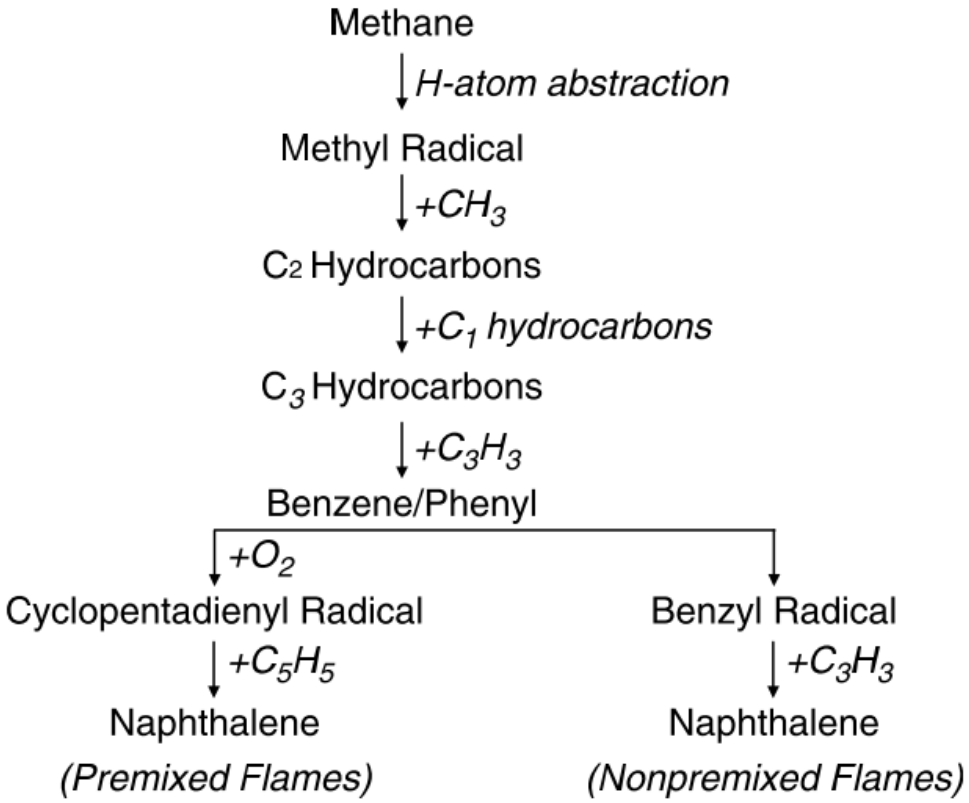

Figure 2-14: Extent of methane decomposition and aromatic formation pathways for methane [121].

2.6.2 Pyrolysis Thermodynamics

Although pyrolysis is widely regarded as an endothermic process, an exact value for the total heat of reaction is not available in literature, as many reactions are involved. Reported energy requirements

vary from slightly exothermic to endothermic 1 MJ/kg [122], [123]. For the application of methanolysis it is likely that the process will remain, if not, increase in endothermicity due to the methane degradation reaction, (2.4.1). However, the exothermic nature of the methane steam reforming reaction, (2.4.2) may alter the overall heat requirements dependent on the extent of water formation. The addition of the MTD occurrence during methanolysis makes the overall energy requirements difficult to determine for the individual processes, and is an overall energy balance which has not received much attention.

Due to the variation in between biomass feedstocks, the thermodynamics of pyrolysis are usually considered in relations to the cellulose, lignin and hemicellulose concentration within the system. As the key to understanding the complex phenomena which occur during pyrolysis, is to better understand the primary devolatilisation phase released products secondary and successive gas phase reactions of the gas phase reactions, investigations into the behaviour of cellulose, hemicellulose and lignin are conducted [110]. For conventional fast pyrolysis (reaction temperature of 500-600 °C), the utilization of an equilibrium model has been deemed not accurate enough due to the common underestimation of CO_2 , CH_4 and heavier species; whilst, CO and H_2 are frequently overestimated [124]. Zhang et al [125], applied equilibrium models for the prediction of pyrolysis products at 1000 °C, which resulted in an overall product yield of over 70 % for CO and under 10 % for hydrogen, relative to the initial sawdust mass. From this model the production of CO and H_2 are dominant above 600 °C, with CH_4, H_2O and CO_2 not predicted above this temperature range.

Of interest in understanding the chemical composition of the product stream is the utilization of reactions of major gas species, which have been used frequently. This allows for a model to be produced determining the gas phase distribution, an approach which has been extensively utilized in gasification predication. Important reactions for the consideration of the thermodynamic characteristics of the system suggested by Zhang et al [125], are provided in Table 2-10.

Table 2-10: Main gas phase reactions of C, H_2, CO, CO_2, H_2O and CH_4, used for the modelling of the gas phase product composition from Zhang et al [125].

Reaction	ΔH^0_{298}
$3H_2 + CO \leftrightarrow CH_4 + H_2O$	*-206 kJ/mol*
$4H_2 + CO_2 \leftrightarrow CH_4 + 2H_2O$	*-165 kJ/mol*
$H_2O + CO \leftrightarrow CO_2 + H_2$	*-41 kJ/mol*
$C + 2H_2 \leftrightarrow CH_4$	*-75 kJ/mol*
$C + CO_2 \leftrightarrow 2CO_2$	*+168 kJ/mol*
$C + H_2O \leftrightarrow CO + H_2$	*+175 kJ/mol*

2.6.3 Slow Pyrolysis

Slow pyrolysis is a technology which has been used for several thousands of years with evidence of charcoal production found in ice age cave paintings [126]. This is largely due to the creation of charcoal via pyrolysis by using an open fire. The popularity of charcoal production by pyrolysis expanded in the 1900's with the production of kilns which produced charcoal throughout Europe for several years [126]. Slow pyrolysis is characterized by low heating rates of the particles (<100 °K/min) with low end temperature values [126]. The production of bio-char from slow pyrolysis is favoured by the use of low temperatures and heating rates with large residence times. Char yields of 60.8 % were obtained for the slow pyrolysis of biomass where, the heating rate was constant at 80 °C/min with a final temperature of 300 °C [126]. The liquids formed by this process are very complex due to long residence times forming long chain, heavy molecular weight hydrocarbons. As a result, the oils undergo a number of secondary and tertiary reactions as described by the Diels-Alder-type reaction mechanism [126]. The non-condensable gas fraction from slow pyrolysis, which are suitable to provide the upper energy limits for bio-char production. This results in the potential for a self-sufficient system, which is fuelled by the non-condensable gas fraction [127].

Slow pyrolysis is a desirable process as it produces medium to high energy density materials (HHV~ 18 MJ/kg), from a low energy density product [128]. Bio-char produced through the slow and fast pyrolysis processes are usually used as fuel for industrial heaters or upgraded to produce activated carbon [126]. Research has also been conducted for novel uses of the bio-char product. The bio-char produced has been seen to have the ability to be used as an effective fertilizer. With correct evaluation

of the bio-char type and soil properties, soil fertility was seen to increase significantly with CEC (cation exchange capacity) levels more than doubling with the presence of biochars [129].

2.6.4 Fast Pyrolysis

Of all of the pyrolysis processes, fast pyrolysis has received the most attention, with rapid interest growing throughout the world in the last few decades [104]. The application of fast pyrolysis is desirable for the production of bio-oil, where the produced liquid can be used as fuel, upgraded and stored. A foremost advantage of bio-oil production is the application of the fuel in present technology. Interest in fast pyrolysis stems from the oil crisis of 1973, initiating research throughout the world for renewable energy sources for fuels [104], [130], [131]. In the past few decades the technology has become industrialized and plants with nominal capacities of 200 t/day have been operated by DynaMotive in Vancouver, Canada. The rate of production increase has been substantial with increases from a 10 t/day operation to a 200 t/day operation occurring within the years of 2004-2006 [104]. Ensyn and Premium (Wilmington U.S.A) have also reported that over 10,400 t/day of biomass feedstock could be required in the produced rapid thermal processing plants (RTP) in Malaysia by 2015, with an equal number possible for Indonesia. This high demand for processing plants in the stated areas is due to the high density of palm plantations, which is a biomass feed that has received extensive research due to the profusion of waste from processing [4], [5], [132].

Fast pyrolysis of biomass for the production of oil is of particular interest due to the ease of transport, renewability, high energy density and ease of application into existing technology [133], [134]. Currently the bio oil which is produced is only suitable for the application in boilers and other static heating applications. Issues with the use of bio-oil include; high viscosity, poor aging characteristics, poor combustion behaviour, inadequate energy density, high oxygen and water content, high acidity, high ash content and complex mixtures of hundreds of different molecules [104], [131], [135]. To upgrade the bio oil for applications in the transportation sector, research has been conducted into catalytic upgrading, tar elimination and multistage processes [136]–[138]. With the large amount of interest in the production of oils from biomass, it is believed that this technology will continue to advance. However, further breakthroughs for the upgrading of the oil are required for application in the automotive industry.

2.6.5 Flash Pyrolysis

Flash pyrolysis is differentiated from the previous pyrolysis processes discussed due to the very short residence times and high operating temperatures. The process is characterised with very fast particle heat-up rates from 10^3-10^6 °C/s and residence times of < 2 seconds [3]. Flash pyrolysis and fast pyrolysis have been used as interchangeable words in the past. However, for the purpose of this report

the term flash pyrolysis is used for a process conducted at temperatures of 850-1050 °C and a residence time of < 2 s. Temperatures of the system are usually above 800 °C, to ensure that the volatilisation of the organic components occurs instantaneously [3], [139], [140]. High operating temperature pyrolysis literature is sparse with operating temperatures up to 1400 °C the highest reported [141]. Short residence times of the product volatiles are essential to reduce the extent of secondary reactions within the system. Dependent on the reactor used during pyrolysis, different pyrolysis gases cause differing process characteristics, numerous different pyrolysis gases have been trialled, including; CO, H_2, CO_2, CH_4, H_2O, Ne, He, Ar [2], [3], [86], [142]. A wide range of reactor configurations have been investigated with fluidized bed and drop tubes, which the latter is the most reported. Large literature gaps for flash pyrolysis using biomass exist due to the majority of experiments being conducted with coal as the feed stream. From the literature reviewed it is difficult to directly compare data from biomass and coal feed systems due to the significant difference in the structure of the feeds. The desired products from the flash pyrolysis of biomass can be divided into; the production of valuable gases, such as; ethylene, ethane and methane [3], [140], [143] or, the production of a fuel gas to power boilers and turbines [144].

Pyrolysis is a complex process during which several reactions occur simultaneously [143]. Due to the complexity of the reaction scheme, generic reactions have been derived to describe the gas evolution during flash pyrolysis, Equation (2.6.9) [144];

$$Biomass \xrightarrow{\Delta} Char + tar + H_2 + CO + CO_2 + CH_4 + C_2 \quad \Delta H^{\circ}_{298} > 0 \tag{2.6.9}$$

It has been widely hypothesised that the water gas shift (Equation (2.6.10) and methane reforming (Equation (2.6.11) reactions are highly influential in the chemical equilibrium of the process [144];

$$CO + H_2O \leftrightarrow CO_2 + H_2 \quad \Delta H^{\circ}_{298} = -41.5\ kJ/mol \tag{2.6.10}$$

$$CH_4 + H_2O \leftrightarrow CO + 3H_2 \quad \Delta H^{\circ}_{298} = 208.2\ kJ/mol \tag{2.6.11}$$

Equations (2.6.10) and (2.6.11) highlight key reactions which are believed to occur during the flash pyrolysis process which determine the composition of oxygenated species during methanolysis. Reactor temperature, pressure, residence time, particle size, feed gas, product and feed composition and the use of catalysts all significantly affect the reaction mechanisms. An overview of the

influences of each parameter during flash pyrolysis is given below, whereas there are large knowledge gaps due to the lack of research conducted in the area.

2.6.5.1 The Effect of Temperature and Pressure during Flash Pyrolysis

S.Septien et.al [141], investigated the temperature effect of flash pyrolysis from 1000-1400 °C for biomass in an alumina drop tube furnace. For the experiments, nitrogen gas was used as the fluidizing agent. At 1000°C product yields of 85% gas, 10 % tar and 5 % char were obtained. Of the biomass fed into the system, a total of 25 %wt of the initial feedstock was converted into hydrocarbons. It was reported that with increasing temperature the yield of hydrocarbons in the gas phase drastically decreased by 75 % and 95 % when the temperature of the system was increased to 1200 °C and 1400°C, respectively [141]. It was observed that the overall gas yield did not vary significantly with increasing temperature. It is proposed that an explanation for the decrease in hydrocarbon yield can be described by the steam reforming (Equation (2.6.12), carbon dioxide reforming (Equation (2.6.13) and polymerization of hydrocarbon (Equation (2.6.14) reactions;

$$C_nH_m + nH_2O \rightarrow \left(n + \frac{m}{2}\right) H_2 + nCO \qquad (2.6.12)$$

$$C_nH_m + nCO_2 \rightarrow \left(\frac{m}{2}\right) H_2 + nC_{soot} \qquad (2.6.13)$$

$$C_nH_m \rightarrow \left(\frac{m}{2}\right) H_2 + nC_{soot} \qquad (2.6.14)$$

At temperatures above 1000°C the yield of hydrogen and carbon monoxide increased, along with significant soot yield increases (which were negligible at 1000 °C). The large soot yield increase is reported to be due to Equation (2.6.14), whilst Equations (2.6.12) and (2.6.13) are believed to be less influential with only moderate CO yield increases as the carbon dioxide and water yields decrease. It is noted however, that the decrease in yields cannot be taken figuratively as the permanent gases are susceptible to be modified via Equation (2.6.10) [141].

2.6.5.2 Effect of Pressure during Flash Pyrolysis

The effect of pressure on the products produced is highly influenced by the composition of the gas feed. The overall percentage of carbon converted with respect to initial biomass, is seen to decrease when the pressure is increased when nitrogen, methane and helium are used as the sweeping gas [1], [3], [140]. In contrast the total conversion of carbon increases with increasing pressure during

hydrogenation [3], [100]. When regarding the hydrogenation of biomass, the yield of methane is seen to increase from 22 % to 78 % with an increase in system pressure from 3.4-34.4 bar. With increasing pressure the concentration of CO was also observed to decrease from 58 % to 17 %. Overall the total carbon converted increases from 82 % to 91 % [1]. When methane is used as the sweeping gas a product yield peak is observed at 3.4 bar. At this pressure the total carbon conversion is ~80 % where ethylene, carbon monoxide and BTX produced yields of 20 %, 45 % and 10 % respectively [140]. Increasing the pressure over 3.4 bar causes a decrease in total carbon converted; whilst, the total yield of carbon monoxide and BTX remain constant. Sundaram [143] used a free fall reactor feeding coal with hydrogen as the sweeping gas, and determined that at a pressure of 13.8 bar the yield of ethylene is negligible, decreasing from 4 % carbon conversion at atmospheric pressure. When nitrogen was used as the carry gas, the overall carbon conversion is seen to decrease at a similar rate to the ethylene yield. The BTX and methane yields are relatively constant between pressures of 3.4-34 bar. The work from Sundaram et al [143], does not describe if the liquid or solid products increase in yield as pressure increases, whereas, If the yield of liquids is increased, the molecules are likely to be long chain hydrocarbons with a molecular weight larger than xylene.

2.6.5.3 Effect of Particle Size during Pyrolysis

Particle size has been identified as a crucial design characteristic and process characteristic which requires investigation, primarily due to the poor thermal conductivity of biomass. Short residence times, high operating temperatures and small particle sizes are favoured for complete pyrolysis of biomass during pyrolysis. However, a balance must be determined to optimize the yield whilst minimizing crushing costs if the process is ever to become industrialized.

Li et al [6], utilized a drop tube furnace feeding legume straw and apricot stone operating at 800°C with nitrogen as the carrier gas. It was determined that the gas yield increased from 50 % to 75 % when feeding particles within the range of 0.30-0.45 mm, as opposed to particles in the size of 0.45-0.9 mm. When operating with particles in the size bracket 0.90-2.00 mm the gas yield was significantly hindered and decreased by 75 % to 15 %, consequently, the liquid and char yields increased by 50 % and 80 %, respectively. It was also determined carbon dioxide yields decreased by half when decreasing the particle size from the 0.90-2.00 mm bracket, to the 0.30-0.45 mm bracket. No significant increase in gas yield and product composition was determined between the particle sizes of 0.30-0.45 mm and 0.20-0.30 mm. This led to the belief that the heating rate experienced by the 0.30-0.45 mm range particle sizes was sufficient for flash pyrolysis, thus the use of 0.20-0.30 mm particles became obsolete [6]. At higher temperatures of 1000 °C, Septien et al. discovered that there was no significant effect between chip sizes of 0.35 mm and 0.80 mm. It was also discovered that the product yield of gas, tar, char and soot was independent of feeding chip size at temperatures above 800 °C [141].

The selectivity of gas species formed in the pyrolysis process is also observed to vary with differing particle feed sizes. R. Zanzi et al., showed that variation in product distribution at 800 °C in a free fall reactor with Birch wood used as the feed stock. It was reported that with 0.5-0.8 mm and 0.8-1.0 mm feed the relative hydrogen concentrations of the product were 17.3 vol% and 12.8 vol% , respectively [145]. From the results it was speculated that the decrease in particle size led to higher hydrogen concentrations as the primary produced gas is able to leave the biomass particle sooner than larger biomass particles. This leads to the retention time of the gas outside of the biomass to be larger and favour cracking of the formed species, revealing a pseudo-retention time cracking potential of product gases.

2.6.5.4 Effect of Residence Time during Pyrolysis

Due to the effect of methane degradation within the system, it is likely that the residence time affects both MTD characteristics and the extent of methanolysis. The effect of residence time in fast pyrolysis systems is relatively well understood, whereas, gaps in literature emerge when considering the residence time of vapours at elevated temperatures [146]. From the work of Steinberg et al, the effect of residence time during methanolysis did not receive significant attention, where residence times between 0.9 s and 2.8 s were graphed on the same x-axis (which investigated the operating pressure). Direct comparisons of reactions with varying residence times and constant reaction conditions should be done with caution due to the possibility of secondary reactions. From drop tube experiments conducted with hydrogen, Steinberg et al [3] suggested that residence times greater than 1 s were reported to induce secondary reactions. For fast pyrolysis at 400 °C, Bridgwater et al [146] has reported high liquid yields when operating at residence times below 5 s. With the added complexity due to MTD, and limited literature on secondary reactions, the investigation into the effect of residence time on product selectivity should be conducted with care. Increased particle residence time has also been associated with decreased hydrocarbon yields [3][2]. Further research is required in this region of the reactor conditions, as the interaction of methane with volatiles formed at these temperatures is not well understood.

2.6.5.5 Effect of different Feed Gas during Pyrolysis

As opposed to the particle residence time and particle size, the gas which is fed into the reactors has received significant research. Sweeping and fluidizing gases are used in drop tube and fluidized bed reactors, respectively, these feed gases can be divided into two groups, reactive; CO, H_2, CH_4 and non-reactive; Ne, He, Ar. From literature the terms hydropyrolysis and methanolysis are used to distinguish between the use of hydrogen and methane as the reacting gas, respectively.

Due to the low costs of nitrogen as opposed to other inert gases, the use of nitrogen as the fluidising medium gas has been well documented. Other non-reactive gases have been reported in literature to determine the influence of heat transfer rates between the gases. Steinberg et al [140], determined that the effective heat-up rates of coal in a 1000 °C reactor follow the order of He>N_2>Ar. When coal was used as the feed stock at 900°C total carbon conversions were 21 %, 20 % and 15 % for helium nitrogen and argon, respectively [140]. At identical reaction conditions experiments were conducted with the use of reactive gases carbon monoxide, methane and hydrogen, which produced carbon conversions of 18 %, 30 % and 38 %, respectively. Although carbon monoxide is a reactive gas, no significant increase in carbon conversion was noticed. The differences in total carbon conversion between the reactive and non-reactive gases was suggested to be due to the effect of the heat capacity and effect on heat transfer coefficient of the different gases [143]. Similar results were obtained by Steinberg et al [1], which determined that with the use of biomass, the ethylene yield was significantly greater with methanolysis as opposed to the use of helium, nitrogen and hydrogen. In total a 7.5 fold increase in ethylene production was reported for the methanolysis of sugar pine wood in comparison to the use of helium gas [1]. The significantly increased yield of ethylene was explained by Steinberg et al as a free radical reaction where CH_2 and CH_3 radicals are formed during flash heating, which are stabilized by high partial pressures of methane, equation (2.6.15). The radicals are subsequently reacted with the methane, equation (2.6.16), to form ethylene and benzene [1]. The identification of radical formation has also been documented by Gao et al [147], who concluded that the presence of radicals stabilized volatile hydrocarbons formed during the pyrolysis reaction as well:

$$biomass \xrightarrow{\Delta} HC\ Free\ Radicals + CO + H_2O \qquad (2.6.15)$$

$$HC\ Free\ Radicals + CH_4 \rightarrow C_2H_4 + C_6H_6 \qquad (2.6.16)$$

Whilst the use of methane has been associated with high ethylene yields, increased char production is also reported. In an experiment conducted with coal as the feed material and a mixture of N_2, O_2, H_2, CO and CH_4 increased tar yields were experienced with increased concentration of methane [148]. The same report also states that increasing the methane content also causes a slight increase in C_2 hydrocarbon production.

From the above results it is easy to see that the use of reactive gases for flash pyrolysis is desired. When comparing the effectiveness of hydrolysis and methanolysis interesting conclusions have been reported. In a report by Sundaram [140], it is reported that the overall carbon conversion is higher for hydropyrolysis, where overall carbon conversions of coal were 30 % and 38 % for methane and hydrogen feed gases, respectively. During flash hydropyrolysis the products produced are largely methane and carbon monoxide, carbon dioxide is not produced at pressures above 3.5 MPa. Overall

liquid yields of the process are reported to be less than 2%. The yield of methane is seen to increase with increasing pressure, at low pressures carbon monoxide formation is favoured whilst, at pressures above 2 MPa the methane is favoured [1]. It is suggested that the higher pressures favour both the hydrogenation of the wood carbon and the methanation reaction:

$$CH_4 + H_2O \rightarrow CO + 3H_2 \quad (2.6.17)$$

Flash methanolysis of wood has the advantage of producing gases which are more valuable than methane. Methanolysis of biomass produces carbon monoxide, ethylene, BTX and small amounts of ethane. By the use of methane as the reacting gas, the production of ethylene is significantly higher than any other carrier gases which have been experimented with. The use of methanolysis for pyrolysis of biomass is also favourable due to a much higher yield of ethylene when biomass is used instead of coal [140], [143].

2.6.6 Effect of Biomass during Pyrolysis

Biomass stocks which have been used in flash pyrolysis systems include; legume straw, apricot stone, pine wood and fir wood. Steinberg et al [1], [2] , conducted flash pyrolysis with Sugar pine (*Pinus lambertiana),* and Douglas fir biomass stocks, from the experiments the yields of hydrocarbons from flash methanolysis of pine wood was 23 to 43 % higher than that of Douglas fir. The difference in elemental composition of the two woods was deemed negligible, and the differences in product yields were attributed to the chemical structure of the biomass. As Douglas fir contains less cellulose and higher lignin concentrations within the biomass structure, the production of hydrocarbons from methanolysis was suggested to be influence by the cellulose concentrations. Whereas, high concentrations of lignin have been attributed to increased yields of aromatic liquids such as benzene, derived from the aromatic structure of lignin [2]. Reports from Li et al [6], have also investigated the differences when feeding apricot stone and legume straw into the flash pyrolysis reactor. Legume straw is significantly higher in concentration of cellulose/hemicellulose and resulted in larger yields of NCG components, as opposed to apricot stone pyrolysis in nitrogen at 800 °C [6]. A component analysis was not conducted on the gases produced, however it was concluded that cellulose and hemicellulose produce more hydrogen-rich gas than lignin [6]. Apricot stone was comprised of significantly more lignin, resulting in decreased gas yields and increased char and tar yields. Zanzi et al [149], investigated pyrolysis products from the use for; Birch wood, White quebracho, straw pellets and bagasse at 800 °C, and concluded that lignin concentrations, low H/C ratios and low oxygen concentrations, were associated with high char production. From the same study, it was also concluded that lower ash content facilitated the prediction of product distribution from the composition of the biomass feed [149].

2.6.7 Effect of Catalysts in Pyrolysis

The use of catalysts in the flash pyrolysis of biomass at the temperatures of interest, has received relatively little research. The use of catalysts has the possibility of increasing product yields and allowing for increased product selectivity during the flash pyrolysis process. Few catalyst trials have been conducted for the use in flash pyrolysis to produce gaseous products. Calcium oxide has been reported to show desirable characteristics during pyrolysis. With increased mass ratios of calcium oxide to sawdust (Ca/S), increased yields of hydrogen and methane were obtained. The levels of carbon monoxide and carbon dioxide were decreased as a consequence. It was determined that at a ratio of 0.65 Ca/S, the optimal operating conditions were determined to produce a heat fuel gas (energy density of 16 MJ/nm^3) [144]. The increase in concentration of hydrogen is believed to be due to the following reaction:

$$Tar \xrightarrow{CaO} H_2 + CO + CO_2 + CH_4 + C_2 + C \quad \Delta H^{\circ}_{298} > 0 \tag{2.6.18}$$

$$CaO + CO_2 \leftrightarrow CaCO_3 \quad \Delta H^{\circ}_{298} = -178.2\ kJ/mol \tag{2.6.19}$$

B. Zhao et al [144], reported that calcium oxide catalyses the cracking of long chain hydrocarbons which are formed, equation (2.6.18). This reaction is irreversible and increases the total yield on non-condensable gases. With large Ca/S values the equilibrium is believed to be shifted towards reduction of the carbon dioxide, equation (2.6.19). This is then suggested to increase the production due to the WGS reaction, equation (2.6.10).

Another catalyst of interest is char. Char is formed as a by-product from the incomplete pyrolysis of the feed biomass. Char is a very effective catalyst due to the highly porous structure created as volatiles are rapidly released during pyrolysis, producing a porous structure in the process [141]. During the process of fast pyrolysis, char is an unwanted by product as the char has a tendency to decrease the overall liquid yield of the product [131]. It is worth noting that to ensure that results obtained are generally not affected by the presence of char, all char must be removed from the system during pyrolysis. This is generally achieved by use of a tar trap at the bottom of a fluidized bed, where the reactor can be operated to entrain the formed char for collection.

2.6.8 By-products Production during Pyrolysis

Other by-products of interest are that of high molecular weight tars and soot. Dependent on the product desired, tars can be seen as a valuable product, or a by-product which requires further refinement via, cracking and/or scrubbing. The production of tars can also be problematic when the product gas is utilized in power generating systems. Zhao et al [144], reported that high contents of

tars can cause increased maintenance and operating costs of industrial equipment, where, by use of adequate filters and cooling, tar levels in liquid streams can be lowered to levels of 50 mg/Nm^3.

Soot is an undesirable by-product which is formed through complex polymerization and condensation reactions during pyrolysis [141]. Soot is very similar to char in appearance; where, under a microscope soot can be identified by the agglomeration of sphere shaped solids. Unlike char this product is not regarded as catalytically active and is very high in concentration of carbon. The formation of soot represents a decrease in the effective carbon conversion potential of the system and its production is generally avoided.

Depending on the desired end product, by-products are categorized by the desired utilization and target products from the process. From an energy perspective, a process which targets the production of gaseous compounds from flash pyrolysis, electrical energy is required and heat losses throughout the system occur. However, the production of bio-char and bio-liquid from the process can be classified as an energy loss [150]. This interpretation of energy loss is simply, the energy within the biomass feed is not converted to the desired end product, albeit, what the system process is designed for. However, as documented above bio-char and bio-oil can be used for biomass drying through combustion of the species. An investigation into the trade-off of lower target product yields and added energy value for heating have not been reported in literature.

2.6.9 Prospects for Flash Pyrolysis

From the limited research which has been conducted in the process optimization, a large proportion of the experiments have been conducted with coal as the feed [140], [142], [143]. The use of flash pyrolysis for the production of synthetic gaseous hydrocarbons is relatively new. Early studies into the prospects of flash pyrolysis have illustrated the ability to produce a range of products simultaneously. Figure 2-15, shows the range of products and the possibility of both liquid fuel production and ethylene gas production [1]. Ethylene is also a desired gaseous product due to the possibility of industrial polymer production and the wide range of applications where ethylene is considered a precursor. Simulations conducted by Görling et al [150], have also proven that the production of methane products by flash pyrolysis is more efficient than that by gasification.

In the diagram below a system flowchart for the methanolysis of biomass is described, as proposed by Steinberg et al [2]. This shows the fractional yield of products which can be obtained by separating different compounds for varied final products in an industrial application. For the purpose of the flowchart, the gaseous streams produced are limited to methane, carbon monoxide and ethylene. Whilst, the liquid fraction is comprised of benzene and oils (In this case species with a molecular weight higher than benzene). Char and ash is also produced, and used as a supplementary fuel source

for drying of the biomass, as proposed by Sundaram et al [1]. From Figure 2-15, the ethylene gas is separated in a fractionator whilst other gases such as CO and CH_4 are separated, for the production of methanol and recycling to the reaction zone, respectively. Methanolysis has been proven to show no appreciable net consumption or production of methane [3]. Due to the high self-sufficiency of the system methane is recycled, and increased synergetic effects are experienced by preheating the gas through the reactor outlet heat exchanger. As described below the production of methanol as transportation fuel is suggested, however, it is likely to form a wide range of target chemicals dependent on the targeted product. Other carbonylation and hydroformylation reactions can also be conducted to produce other high value chemicals, such as; carboxylic acids and aldehydes [151].

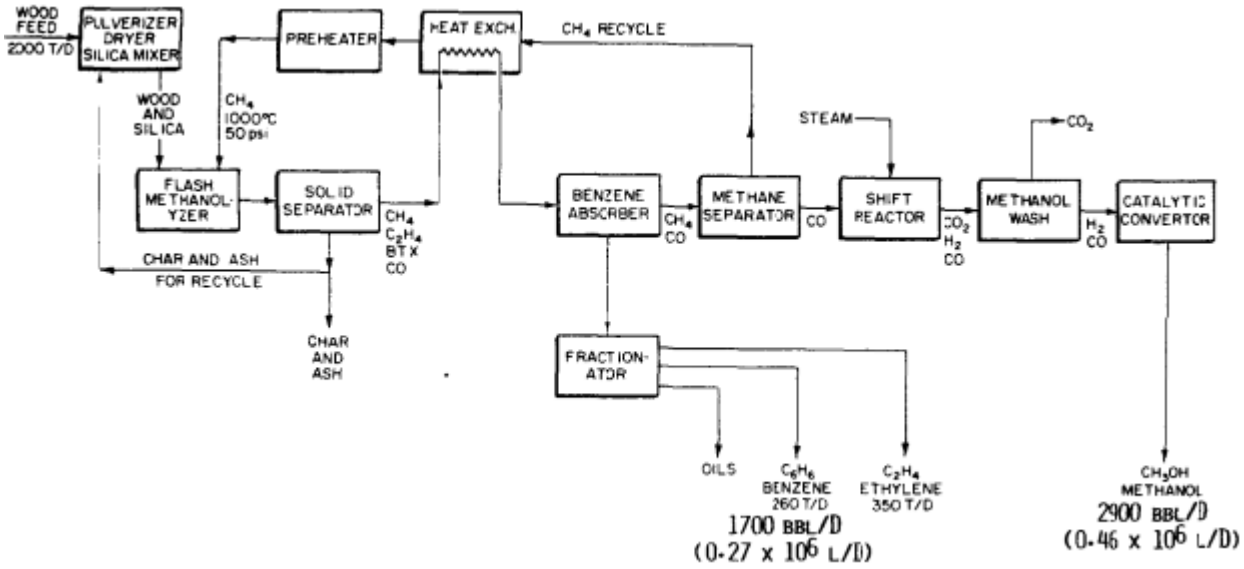

Figure 2-15: Flash methanolysis for the production of methanol, benzene and ethylene products (2000t/day feed) [2].

2.7 Flash Pyrolysis Reactors

In general, the flash pyrolysis systems consist of a preheating section, reacting section and sample collecting section. In the preheating section the gas stream is heated to an elevated temperature to reduce the overall heat requirements upon entry into the reaction zone. Following the reactor the samples are taken by quick quenching of the gas/vapours to ensure that all species are accounted for.

2.7.1 Product Condensation

Cooling agents such as ice water, Freon and liquid nitrogen have been reported as coolants used for the collection of tars in various solvent solutions [142], [148], [152]. Various different systems have been used for the collection of tars, with the application and desired products strongly influencing the system employed. For traditional pyrolysis at ~500 °C, where a mainly oil product is favoured, the

condensation of tars can be fractionated in respect to boiling temperature, through differing temperature solvents. Overall product condensation has also been observed to be improved by the use of an electrostatic precipitator (ESP), which has successfully condensed aerosol tars in product streams [132], [153], [154]. For the condensation of dilute aerosol tar streams, the use of packed cotton wool filters has proven successful, with the overall tar physically condensed on the wool which can then be subsequently dissolved using an appropriate solvent [155].Caution must be exercised in the sampling phase as low molecular weight volatile species have the tendency to escape in the vapour phase during experiments [139].

2.7.2 Drop Tube/Free Fall Reactors

Dope Tube/Free Fall reactors consist of a long cylindrical tube which is usually heated convectively from an enclosed cylindrical heater. The system can be operated as a co-current and counter current arrangement, where the gas and particles flow in the same direction or in opposite directions, respectively. The residence time of the vapours is controlled by a sweeping gas, which facilitates the removal of the produced pyrolysis volatiles. Generally the system is operated as a co-current system due to the enhanced ability to control residence time and reduce incomplete pyrolysis of the feed. For a co-current drop tube configuration, the biomass and reacting gases meet at the top of the reactor and travel through the tube under the influence of gravity. Dependent on the reactor configuration, a preheater can also be installed prior to the reactor feed, which increases inlet sweeping gas. The configuration can allow for multiple sampling points throughout the tube as modelled by a plug flow reactor. Due to the forces and distribution of particles being relatively constant the residence times of particles within the system can be readily determined by gas velocity. The reactor is usually heated by conduction with the use of electrical heaters. The reactor is popular due to the ease of construction and operation [141], [148], [156]. However, difficulties are encountered when operating in a continuous fashion or in large volumes; due to, poor heat transfer within the tube and the accumulation of char. The effect of heat transfer on the biomass depends highly on the mass flow and the pipe diameter.

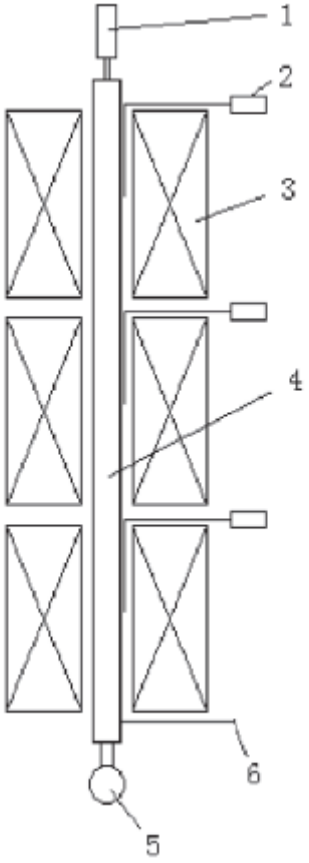

Figure 2-16: General schematic of drop tube configuration; Feeder (1), Thermocouple (2), Heating Element (3), Tube (4), Tar Trap (5), Outlet (6). [156].

2.7.3 Fluidized Bed Reactors

Fluidized and circulating fluidized bed (CFB) reactors are also common reactors used in the pyrolysis process. The reactor consists of a bed (usually sand), which is fluidized by gas which is fed from the bottom to allow for fluidization, Figure 2-17. The use of the reactor is desirable due to the high heat transfer which can be experienced when operated with a thermally stable bed material. The advantages of fluidized beds include very good mixing, simple configuration and efficient removal of char from the system. The heat transfer experienced by the biomass particles is greatly increased due to the enhanced mixing facilitating the interaction between the gas and biomass phases [36], [131]. This configuration also allows for the ease of incorporation of catalysts, as the catalyst can be added in place of the bed materials and also have enhanced heat transfer characteristics. The residence time of the vapours formed during pyrolysis within the fluidized bed is determined by the fluidizing gas flow rate. Char within the system has a tendency to remain in the bed after complete devolatilisation the biomass has occurred.

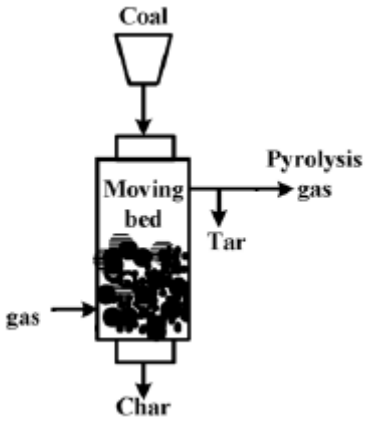

Figure 2-17: Fluidized bed system fed with coal [148].

Circulating fluidised bed (CFB) is also another common reactor system employed for pyrolysis. The system is more complicated than conventional fluidised bed systems, due to the entrainment of bed materials within the reactor system, as observed in. CFB's usually consist of a core reactor which is operated similar to a fluidised bed, however, the operating mass flowrate is sufficient to induce entrainment of the bed particles through the top of the system. The bed particles are collected in another reactor chamber where the bed materials can be heated and or conditioned depending on requirements. Advantages of the system include; ability to readily remove char from the bed, greater synergy, greater reactor wear and possibility of liquids cracking for increased gas production. However, the constructions of CFB's are generally more complicated and are not usually conducted as a lab scale apparatus. Within industry fluidized and CFB reactors are the most common with six circulating fluidized bed plants being constructed by Ensyn Technologies (Red Arrow Products Co., Inc Wisconsin) [104]. The construction of a fluidized bed was deemed the most appropriate for the experiments to be conducted, as it was believed the most accurate results for reaction characteristics could be achieved. The use of a fluidized bed also allows for easy scaling-up to the pilot plant stage.

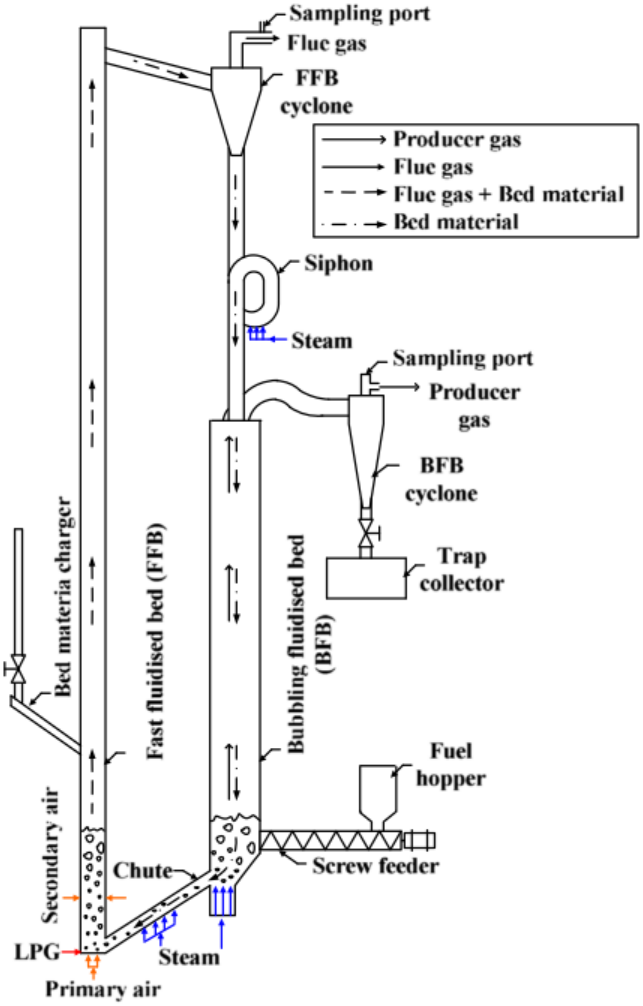

Figure 2-18: Circulating fluidised bed system used for the gasification of biomass, adapted from [157]**.**

2.8 Challenges

From the reviewed literature it was determined that the construction of a fluidized bed reactor designed for methanolysis of biomass to our knowledge, has not been attempted. The majority of reactors used are drop tube furnaces with the intentions of feeding coal. Due to the extensive use of coal in industrial activities, the behaviour of granulated coal is well documented. This in turn allows for facilitated manufacturing of feeding systems for coal based pyrolysis units. The use of biomass as a feed stock in the form of sawdust is not a conventional industrial solid; thus, requires further investigation into the mass properties. It has been reported that the cause of arching and ratholing when feeding biomass in coal designed feeders is due to the cohesion and intraparticle mechanical interference [158]. The stated characteristics of the biomass feed which must be determined for successful feeding into the system.

Other challenging aspects for the flash methanolysis of biomass are the construction of the reactor to ensure that the results are representative of the reactor conditions. This encapsulates the construction of the rig to allow for high temperature, moderate pressure and the fluidization by a reactive gas. For which, the stated characteristics have not been conducted in a fluidized bed. It is envisaged that by using a fluidized bed the mixing and intraparticle interactions are greatly increased, providing an insight into the reaction kinetics. Thus, the product selectivity of target species can be enhanced through variable operation of the reactor.

The representation of accurate reactor conditions is also very important, due to the lack of literature which has investigated single reactor condition. As observed from Steinberg et.al [1], [2], varied residence time data points have been used to investigate the reactor pressure effect. By allowing multiple reactor conditions to vary, a complete investigation into the true influence of the reaction condition cannot be accurately determined. It is proposed that in this experiment the flowrate of methane was increased, which is also another parameter is believed to be highly influential in product yield; thus, results from literature must be interpreted with caution.

2.9 References

[1] M. Steinberg, P. T. Fallon, and M. S. Sundaram, “Flash pyrolysis of biomass with reactive and non-reactive gas,” *Biomass*, vol. 9, no. 4, pp. 293–315, 1986.

[2] M. Steinberg, “Flash Pyrolsyis of Biomass with Reactive and Non-Reactive Gases,” 1984.

[3] M. Steinberg, P. T. Fallon, and M. S. Sundaram, “The Flash Pyrolysis and Methanolysis of Biomass (Wood) for Production of Ethylene, Benzene and Methanol,” 1990.

[4] F. Abnisa, W. M. A. W. Daud W.M.A. Wan, W. N. W. Husin, and J. N. Sahu, “Utilization possibilities of palm shell as a source of biomass energy in Malaysia by producing bio-oil in pyrolysis process,” *Biomass and Bioenergy*, vol. 35, no. 5, pp. 1863–1872, 2011.

[5] S. J. Kim, S. H. Jung, and J. S. Kim, “Fast pyrolysis of palm kernel shells: Influence of operation parameters on the bio-oil yield and the yield of phenol and phenolic compounds,” *Bioresour. Technol.*, vol. 101, no. 23, pp. 9294–9300, 2010.

[6] S. Li, S. Xu, S. Liu, C. Yang, and Q. Lu, “Fast pyrolysis of biomass in free-fall reactor for hydrogen-rich gas,” *Fuel Process. Technol.*, vol. 85, no. 8–10, pp. 1201–1211, 2004.

[7] S. V. Vassilev, D. Baxter, L. K. Andersen, and C. G. Vassileva, “An overview of the chemical composition of biomass,” *Fuel*, vol. 89, no. 5, pp. 913–933, 2010.

[8] U. C. S. Hukla *et al.*, “Effect of bioaccumulation of cadmium on biomass productivity, essential trace elements, chlorophyll biosynthesis, and macromolecules of wheat seedlings,” *Biol. Trace Elem. Res.*, vol. 92, no. 3, pp. 257–274, 2003.

[9] C. M. Welker, V. K. Balasubramanian, C. Petti, K. M. Rai, S. De Bolt, and V. Mendu, “Engineering plant biomass lignin content and composition for biofuels and bioproducts,” *Energies*, vol. 8, no. 8, pp. 7654–7676, 2015.

[10] M. P. Pandey and C. S. Kim, “Lignin Depolymerization and Conversion: A Review of Thermochemical Methods,” *Chem. Eng. Technol.*, vol. 34, no. 1, pp. 29–41, 2011.

[11] G. Lv and S. Wu, “Analytical pyrolysis studies of corn stalk and its three main components by TG-MS and Py-GC/MS,” *J. Anal. Appl. Pyrolysis*, vol. 97, pp. 11–18, 2012.

[12] H. Kawamoto, W. Hatanaka, and S. Saka, “Thermochemical conversion of cellulose in polar solvent (sulfolane) into levoglucosan and other low molecular-weight substances,” *J. Anal. Appl. Pyrolysis*, vol. 70, no. 2, pp. 303–313, 2003.

[13] A. K. . G. BLEDZKI, “Jochen. Composites reinforced with cellulose based fibers.,” *1999*, vol. 24, pp. 221–274, 1999.

[14] Y. Habibi, L. A. Lucia, and O. J. Rojas, “Cellulose Nanocrystals : Chemistry , Self-Assembly , and Applications,” vol. d, pp. 3479–3500, 2010.

[15] B. B. Hallac and A. J. Ragauskas, “Analyzing cellulose degree of polymerization and its relevancy to cellulosic ethanol Bassem,” *Biofuels, Bioprod. Biorefining*, vol. 5, pp. 215–225, 2011.

[16] X. Zhao, K. Cheng, and D. Liu, “Organosolv pretreatment of lignocellulosic biomass for enzymatic hydrolysis,” *Appl. Microbiol. Biotechnol.*, vol. 82, no. 5, pp. 815–827, 2009.

[17] P. R. Patwardhan, J. A. Satrio, R. C. Brown, and B. H. Shanks, “Product distribution from fast pyrolysis of glucose-based carbohydrates,” *J. Anal. Appl. Pyrolysis*, vol. 86, no. 2, pp. 323–330, 2009.

[18] X. Zhou, M. W. Nolte, H. B. Mayes, B. H. Shanks, and L. J. Broadbelt, “Experimental and mechanistic modeling of fast pyrolysis of neat glucose-based carbohydrates. 1. Experiments and development of a detailed mechanistic model,” *Ind. Eng. Chem. Res.*, vol. 53, no. 34, pp. 13274–13289, 2014.

[19] Z. Ozt and J. F. Merklin, “96/00523 Rapid pyrolysis of cellulose with reactive hydrogen gas in a single-pulse shock tube,” *Fuel Energy Abstr.*, vol. 37, no. 1, p. 31, 1996.

[20] L. Burhenne, J. Messmer, T. Aicher, and M. P. Laborie, “The effect of the biomass components lignin, cellulose and hemicellulose on TGA and fixed bed pyrolysis,” *J. Anal. Appl. Pyrolysis*, vol. 101, pp. 177–184, 2013.

[21] H. Yang, R. Yan, H. Chen, D. H. Lee, and C. Zheng, “Characteristics of hemicellulose, cellulose and lignin pyrolysis,” *Fuel*, vol. 86, no. 12–13, pp. 1781–1788, 2007.

[22] S. Wang, G. Dai, H. Yang, and Z. Luo, “Lignocellulosic biomass pyrolysis mechanism: A state-of-the-art review,” *Prog. Energy Combust. Sci.*, vol. 62, pp. 33–86, 2017.

[23] a. Demirbaş, “Mechanisms of liquefaction and pyrolysis reactions of biomass,” *Energy Convers. Manag.*, vol. 41, no. 6, pp. 633–646, 2000.

[24] C. Li, X. Zhao, A. Wang, G. W. Huber, and T. Zhang, “Catalytic Transformation of Lignin for the Production of Chemicals and Fuels,” *Chem. Rev.*, vol. 115, no. 21, pp. 11559–11624, 2015.

[25] S. Chu, A. V. Subrahmanyam, and G. W. Huber, “The pyrolysis chemistry of a β-O-4 type oligomeric lignin model compound,” *Green Chem.*, vol. 15, no. 1, pp. 125–136, 2013.

[26] F. X. Collard and J. Blin, “A review on pyrolysis of biomass constituents: Mechanisms and composition of the products obtained from the conversion of cellulose, hemicelluloses and lignin,” *Renew. Sustain. Energy Rev.*, vol. 38, pp. 594–608, 2014.

[27] J. Zhao, W. Xiuwen, J. Hu, Q. Liu, D. Shen, and R. Xiao, “Thermal degradation of softwood lignin and hardwood lignin by TG-FTIR and Py-GC/MS,” *Polym. Degrad. Stab.*, vol. 108, pp. 133–138, 2014.

[28] Q. Liu, S. Wang, Y. Zheng, Z. Luo, and K. Cen, “Mechanism study of wood lignin pyrolysis by using TG-FTIR analysis,” *J. Anal. Appl. Pyrolysis*, vol. 82, no. 1, pp. 170–177, 2008.

[29] S. D. Fernandes, N. M. Trautmann, D. G. Streets, C. A. Roden, and T. C. Bond, “Global biofuel use, 1850-2000,” *Global Biogeochem. Cycles*, vol. 21, no. 2, pp. 1–15, 2007.

[30] C. L. Sabine, M. Heiman, P. Artaxo, D. C. E. Bakker, and C. T. A. Chen, “Current status and past trends of the global carbon cycle. In ‘The Global carbon cycle: integrating humans, climate, and the natural world’.(Eds CB Field, MR Raupach) pp. 17–44.” Island Press: Washington, DC, 2004.

[31] D. O. Hall, “Biomass energy in industrialised countries—a view of the future,” *For. Ecol. Manage.*, vol. 91, no. 1, pp. 17–45, 1997.

[32] I. E. Agency, *Biofuels for transport: an international perspective*. OECD Publishing, 2004.

[33] M. Parikka, “Global biomass fuel resources,” *Biomass and Bioenergy*, vol. 27, no. 6, pp. 613–620, 2004.

[34] C. B. Field, J. E. Campbell, and D. B. Lobell, “Biomass energy: the scale of the potential resource,” *Trends Ecol. Evol.*, vol. 23, no. 2, pp. 65–72, 2008.

[35] E. I. Ohimain, “The Prospects and Challenges of Waste Wood Biomass Conversion to Bioelectricity in Nigeria,” *J. Waste Conversion, Bioprod. Biotechnol. – ISSN 2155-1804*, vol. 1, no. 1, pp. 3–8, 2012.

[36] a.V. Bridgwater, D. Meier, and D. Radlein, “An overview of fast pyrolysis of biomass,” *Org. Geochem.*, vol. 30, no. 12, pp. 1479–1493, 1999.

[37] N. Murtha *et al.*, “The State of the Paper Industry,” p. 37, 2011.

[38] J. Hill, E. Nelson, D. Tilman, S. Polasky, and D. Tiffany, “Environmental, economic, and energetic costs and benefits of biodiesel and ethanol biofuels,” *Proc. Natl. Acad. Sci.*, vol. 103, no. 30, pp. 11206–11210, 2006.

[39] F. C. Ford Robertson, *Terminology of forest science, technology, practice and products. English-language version*. Washington, DC (USA) SAF, 1971.

[40] I. R. Noble and R. Dirzo, “Forests as human-dominated ecosystems (2 copies),” *Science (80-.).*, vol. 277, no. 5325, pp. 522–525, 1997.

[41] O. M. Aina, “WOOD WASTE UTILIZATION FOR ENERGY GENERATION,” 2006.

[42] C. Rodríguez-Monroy, G. Mármol-Acitores, and G. Nilsson-Cifuentes, “Electricity generation in Chile using non-conventional renewable energy sources – A focus on biomass,” *Renew. Sustain. Energy Rev.*, vol. 81, no. June 2017, pp. 937–945, 2018.

[43] P. Norris, “The Decline of Newspapers?,” *A Virtuous Circ. Polit. Commun. Postindustrial Soc.*, no. 4, pp. 63–89, 2000.

[44] T. R. Fox, “Sustained productivity in intensively managed forest plantations,” *For. Ecol. Manage.*, vol. 138, no. 1–3, pp. 187–202, 2000.

[45] Forest Owners Association, “Facts & Figures 2015/2016,” *New Zeal. J. For.*, vol. 46, no. 2, p. 13, 2001.

[46] MPI, “National exotic forest description. As at 1 april 2016,” no. April, p. 59, 2016.

[47] Newswire, “NZ logs make an `idiotic’ round trip,” *Yahoo! Business and Finance*, 2014.

[48] P. Clarke, “Clarky’s Comment - April 2013, Prime Minister’s Trade Delegation to China,” *PF Olsen Limited*, 2013. .

[49] A. Bartley *et al.*, *Situation and Outlook for Primary Industries 2013*. 2013.

[50] C. Collins, “Forests and the Carbon Cycle: Emerging opportunties for native forest protection and afforestation in New Zealand.”

[51] D. a Norton, “Indigenous Biodiversity Conservation and Plantation Forestry : Options for the future,” *N. Z. For.*, no. August, pp. 34–39, 1998.

[52] P. Industries, *Predicting harvesting and deforestation of radiata pine forest blocks using national spatial datasets*, vol. 4, no. August. 2016.

[53] J. Arden, “Speech from the Throne,” *Speech from the Throne,Delivered by Her Excellency The Rt Hon Dame Patsy Reddy, GNZM, QSO, Governor-General of New Zealand, on the occasion of the State Opening of Parliament, Wednesday 8 November 2017.*, 2017. .

[54] New Zealand Government, “New Zealand’s Intended Nationally Determined Contribution,” no. July, p. 5, 2015.

[55] Ministry for the Environment, “New Zealand’s Greenhouse Gas Inventory 1990–2014,” no. May, pp. 1–7, 2016.

[56] Fonterra, “Sustainability Report,” 2017.

[57] M. Joy, “Polluted inheritance: New Zealand’s freshwater crisis,” 2015.

[58] T. R. Fox, “Sustained productivity in intensively managed forest plantations,” 1989.

[59] A. Dame Salmond, “Plan to revive Forestry Service not out of the woods,” *Newsroom NZ*, p. 1, 14-Dec-2017.

[60] E. A. Blekkan, R. Myrstad, O. Olsvik, and O. A. Rokstad, “Characterization of tars and coke formed during the pyrolysis of methane in a tubular reactor,” *Carbon N. Y.*, vol. 30, no. 4, pp. 665–673, 1992.

[61] D. Trommer, D. Hirsch, and A. Steinfeld, “Kinetic investigation of the thermal decomposition of CH4 by direct irradiation of a vortex-flow laden with carbon particles,” *Int. J. Hydrogen Energy*, vol. 29, no. 6, pp. 627–633, 2004.

[62] H. F. Abbas and W. M. A. Wan Daud, “Hydrogen production by methane decomposition: A review,” *Int. J. Hydrogen Energy*, vol. 35, no. 3, pp. 1160–1190, 2010.

[63] H. Gladisch, “How Huels makes acetylene by DC arc,” *Hydrocarb. Process. Pet. Refin.*, vol. 41, pp. 159–164, 1962.

[64] J. M. Holmes, “Evaluation of DuPont arc process for acetylene and vinyl chloride monomer production,” *ORNL-TM-2725*, 1969.

[65] W. M. Heffington, G. E. Parks, K. G. P. Sulzmann, and S. S. Penner, “Studies of methane-oxidation kinetics,” *Symp. Combust.*, vol. 16, no. 1, pp. 997–1011, 1977.

[66] P. Roth and T. Just, “Atom-Resonanzabsorptionsmessungen beim thermischen Zerfall von Methan hinter Stoßwellen,” *Berichte der Bunsengesellschaft für Phys. Chemie*, vol. 79, no. 8,

pp. 682–686, Aug. 1975.

[67] K. T. S.H.Bauer, “The early stages of pyrolysis and oxidation of methane,” *Combust. Flame*, vol. 34, pp. 63–83, Jan. 1979.

[68] C. K. Westbrook, F. L. Dryer, and K. P. Schug, “A comprehensive mechanism for the pyrolysis and oxidation of ethylene,” *Symp. Combust.*, vol. 19, no. 1, pp. 153–166, 1982.

[69] D. . Hucknall, “Pyrolytic reactions of hydrocarbons,” in *Chemistry of Hydrocarbon Combustion*, 1985, pp. 327–377.

[70] S. Bryen, G. H, and P. John, “Industrial Gases.”

[71] M. H. Back, “Mechanism of the Pyrolysis of Acetylene,” *Can. J. Chem.*, vol. 49, 1971.

[72] J. R. Fincke *et al.*, “Thermal Conversion of Methane to Acetylene Final Report,” Idaho, 2000.

[73] A. M. Dunker, S. Kumar, and P. A. Mulawa, “Production of hydrogen by thermal decomposition of methane in a fluidized-bed reactor - Effects of catalyst, temperature, and residence time,” *Int. J. Hydrogen Energy*, vol. 31, no. 4, pp. 473–484, 2006.

[74] R. D. Kern *et al.*, “COLLABORATIVE SHOCK TUBE STUDIES OF BENZENE PYROLYSIS,” in *Twentieth Symposium (International) on Combustion/The Combustion Institute*, 1984, pp. 789–797.

[75] K. C. Hou and H. B. Palmer, “The Kinetics of Thermal Decomposition of Benzene in a Flow System,” *J. Phys. Chem.*, vol. 69, no. 3, pp. 863–868, 1965.

[76] H. Böhm and H. Janderb, “PAH formation in acetylene–benzene pyrolysis,” *Phys. Chem. Chem. Phys.*, vol. 1, no. 16, pp. 3775–3781, 1999.

[77] H. B. Hm, H. Jander, and D. Tanke, “PAH GROWTH AND SOOT FORMATION IN THE PYROLYSIS OF ACETYLENE AND BENZENE AT HIGH TEMPERATURES AND PRESSURES: MODELING AND EXPERIMENT,” in *Twenty-Seventh Symposium (International) on Combustion/The Combustion Institute*, 1998, pp. 1605–1612.

[78] A. A. Munera Parra and D. W. Agar, “Molten metal capillary reactor for the high-temperature pyrolysis of methane,” *Int. J. Hydrogen Energy*, pp. 6–13, 2016.

[79] A. V Krestinin, “Detailed Modeling of Soot Formation in Hydrocarbon Pyrolysis,” *Combust. Flame*, vol. 121, pp. 513–524, 2000.

[80] J. Lahaye, P. Badie, and J. Ducret, “MECHANISM OF CARBON FORMATION DURING STEAMCRACKING OF HYDROCARBONS,” *Carbon N. Y.*, pp. 87–93, 1977.

[81] L. Albright and J. Marek, “Mechanistic Model for Formation of Coke in Pyrolysis Units Producing Ethylene,” *Ind. Eng. Shemistry*, vol. 27, no. 5, pp. 755–759, 1988.

[82] J. L. Pinilla, I. Suelves, M. J. Lázaro, R. Moliner, and J. M. Palacios, “Parametric study of the decomposition of methane using a NiCu/Al2O3 catalyst in a fluidized bed reactor,” *Int. J. Hydrogen Energy*, vol. 35, no. 18, pp. 9801–9809, 2010.

[83] U. P. M. Ashik, W. M. A. Wan Daud, and H. F. Abbas, “Methane decomposition kinetics and reaction rate over Ni/SiO2 nanocatalyst produced through co-precipitation cum modified StÖber method,” *Int. J. Hydrogen Energy*, vol. 42, no. 2, pp. 938–952, 2017.

[84] J. L. Pinilla, R. Moliner, I. Suelves, M. J. Lázaro, Y. Echegoyen, and J. M. Palacios, “Production of hydrogen and carbon nanofibers by thermal decomposition of methane using metal catalysts in a fluidized bed reactor,” *Int. J. Hydrogen Energy*, vol. 32, no. 18, pp. 4821–4829, 2007.

[85] C. Guéret, M. Daroux, and F. Billaud, “Methane pyrolysis: Thermodynamics,” *Chem. Eng. Sci.*, vol. 52, no. 5, pp. 815–827, 1997.

[86] M. STEINBERG, “Production of hydrogen and methanol from natural gas with reduced CO2 emission,” *Int. J. Hydrogen Energy*, vol. 23, no. 6, pp. 419–425, 1998.

[87] L. F. ALBRIGHT and C. F. McCONNELL, “Deposition and Gasification of Coke During Ethane Pyrolysis,” 1979, pp. 205–224.

[88] S. Abanades and G. Flamant, “Solar hydrogen production from the thermal splitting of methane in a high temperature solar chemical reactor,” *Sol. Energy*, vol. 80, no. 10, pp. 1321–1332, 2006.

[89] A. Holmen, A. Rokstad, and A. Solbakken, “High-Temperature Pyrolysis of Hydrocarbons. I. Methane to Acetylene,” *Ind. Chem. Eng. Process Des.*, vol. 15, no. 3, pp. 439–444, 1976.

[90] C. Guéret and F. Billaud, “Thermal coupling of methane: Influence of hydrogen at 1330°C. Experimental and simulated results,” *J. Anal. Appl. Pyrolysis*, vol. 29, no. 2, pp. 183–205, 1994.

[91] A. Holmen, O. Olsvik, and O. A. Rokstad, “Pyrolysis of natural gas: chemistry and process concepts,” *Fuel Process. Technol.*, vol. 42, no. 2–3, pp. 249–267, 1995.

[92] C.-J. CHEN, M. H. BACK, and R. A. BACK, “The themal decomposition of methane. II. Secondary reactions, aatocatalrysis and carbon formation; non-Arrhenieas behaviour in the reaction of CH3, with ethane,” *Can. J. Chem.*, vol. 54, no. 15438, pp. 956–963, 1976.

[93] H. B. Palmer, J. Lahaye, and K. C. Hou, “On the Kinetics and Mechanism of the Thermal Decomposition of Methane in a Flow System’,” *J. Phys. Chem.*, vol. 72, no. 1, pp. 348–353, 1967.

[94] J. Happel and L. Kramer, “Acetylene and Hydrogeon from the Pyrolysis of Methane,” *Ind. Eng. Chem.*, vol. 59, no. 1, pp. 39–50, 1967.

[95] T. Koike, M. Kudo, I. Maeda, and H. Yamada, “Rate Constants of CH4 + M-CH3 + H + M and CH3OH + M-CH3 + OH + M over 1400-2500 K,” *Int. J. Chem. Kinet.*, vol. 32, no. 1, pp. 1–6, 2000.

[96] W. Tsang and R. F. Hampson, “Chemical Kinetic Data Base for Combustion Chemistry. Part I. Methane and Related Compounds,” *J. Phys. Chem. Ref. Data*, vol. 15, no. 3, pp. 1087–1279, Jul. 1986.

[97] R. B. Klemm, J. W. Sutherland, M. J. Rabinowitz, P. M. Patterson, J. M. Quartemont, and W. Tao, “Shock Tube Kinetic Study of Methane Dissociation: 1726 K I T I 2134 K,” *J. Phys. Chem*, vol. 96, no. 1, 1992.

[98] D. F. Davidson, R. Di, A. Y. Chang, R. K. Hanson, and C. T. Bowman, “A SHOCK TUBE STUDY OF METHANE DECOMPOSITION USING LASER ABSORPTION BY CH3,” pp. 589–596, 1992.

[99] S. Kobayashi, M. Steinberg, “The Thermal Decomposition of Methane in a Tubular Reactor,” 1992.

[100] M.S Sundaram, M. Steinberg and P.T. Fallon, “Flash Pyrolysis of Biomass with Reactive and Non-Reactive Gases,” Richland, Washington, 1984.

[101] G. B. Skinner and R. A. Ruehrwein, “Shock Tube studies on the Pyrolysis and Oxidation of Methane,” *J. Phys. Chem.*, vol. 63, no. 10, pp. 1736–1742, 1959.

[102] A. Dean, “Detailed kinetic modeling of autocatalysis in methane pyrolysis,” *J. Phys. Chem.*, vol. 145, no. 1–2, pp. 16–37, 1990.

[103] B. M. Weckhuysen and R. A. Schoonheydt, “Alkane dehydrogenation over supported chromium oxide catalysts,” *Catal. Today1*, vol. 51, pp. 223–232, 1999.

[104] S. Czernik and A. V. Bridgwater, “Overview of applications of biomass fast pyrolysis oil,” *Energy & Fuels*, vol. 18, no. 2, pp. 590–598, 2004.

[105] A. G. W. Bradbury, Y. Sakai, and F. Shafizadeh, “A kinetic model for pyrolysis of cellulose,” *J. Appl. Polym. Sci.*, vol. 23, no. 11, pp. 3271–3280, Jun. 1979.

[106] H. Niu and N. Liu, “Thermal decomposition of pine branch: Unified kinetic model on pyrolytic reactions in pyrolysis and combustion,” *Fuel*, vol. 160, pp. 339–345, 2015.

[107] R. S. MILLER and J. BELLAN, “A Generalized Biomass Pyrolysis Model Based on Superimposed Cellulose, Hemicelluloseand Liqnin Kinetics,” *Combust. Sci. Technol.*, vol. 126, no. 1–6, pp. 97–137, 1997.

[108] J. . Diebold, “A unified, global model for the pyrolysis of cellulose,” *Biomass and Bioenergy*, vol. 7, no. 1–6, pp. 75–85, 1994.

[109] J. A. Conesa, J. A. Caballero, A. Marcilla, and R. Font, “Analysis of different kinetic models in the dynamic pyrolysis of cellulose,” *Thermochim. Acta*, vol. 254, no. C, pp. 175–192, 1995.

[110] E. Ranzi *et al.*, “Chemical Kinetics of Biomass Pyrolysis,” *Energy & Fuels*, vol. 22, no. 6, pp. 4292–4300, 2008.

[111] N. A. Slavinskaya and P. Frank, “A modelling study of aromatic soot precursors formation in laminar methane and ethene flames,” *Combust. Flame*, vol. 156, no. 9, pp. 1705–1722, 2009.

[112] K. Siegmann and K. Sattler, “Formation mechanism for polycyclic aromatic hydrocarbons in methane flames Formation mechanism for polycyclic aromatic hydrocarbons in methane flames,” vol. 698, no. 2000, 2012.

[113] H. Richter and J. B. Howard, “Formation and consumption of single-ring aromatic hydrocarbons and their precursors in premixed acetylene, ethylene and benzene flamesElectronic supplementary information (ESI) available: Thermodynamic and kinetic property data. See http://www.rsc.org/sup,” *Phys. Chem. Chem. Phys.*, vol. 4, no. 11, pp. 2038–2055, 2002.

[114] J. A. Miller, J. V. Volponi, and J. F. Pauwels, “The effect of allene addition on the structure of a rich C2H2/O2/ Ar flame,” *Combust. Flame*, vol. 105, no. 4, pp. 451–461, 1996.

[115] J. R. Appel, H. Bockhorn, and M. Frenklach, “Kinetic Modeling of Soot Formation with Detailed Chemistry and Physics: Laminar Premixed Flames of C 2 Hydrocarbons.”

[116] O. Olsvik and F. Billaud, “Thermal Coupling of Methane-A Comparison Between Kinetic-Model Data and Experimental-Data,” *Thermochim. Acta*, vol. 232, no. 1, pp. 155–169, 1994.

[117] S. Senkan and M. Castaldi, “Formation of polycyclic aromatic hydrocarbons (PAH) in methane combustion: Comparative new results from premixed flames• 1,” *Combust. Flame*, vol. 107, no. 1–2, pp. 141–150, 1996.

[118] N. M. Marinov *et al.*, “Aromatic and polycyclic aromatic hydrocarbon formation in a laminar premixed n-butane flame,” *Combust. Flame*, vol. 114, no. 1–2, pp. 192–213, 1998.

[119] L. B. Harding, S. J. Klippenstein, and Y. Georgievskii, “On the combination reactions of hydrogen atoms with resonance-stabilized hydrocarbon radicals,” *J. Phys. Chem. A*, vol. 111, no. 19, pp. 3789–3801, 2007.

[120] M. J. Castaldi *et al.*, “Experimental and Modeling Investigation of Aromatic and Polycyclic Aromatic Hydrocarbon Formation in a Premixed Ethylene Flame,” *26th Int. Symp. Comput. Naples, Italy*, vol. July 28-A, p. 31, 1996.

[121] C. S. McEnally, L. D. Pfefferle, B. Atakan, and K. Kohse-Höinghaus, “Studies of aromatic hydrocarbon formation mechanisms in flames: Progress towards closing the fuel gap,” *Prog. Energy Combust. Sci.*, vol. 32, no. 3, pp. 247–294, 2006.

[122] M. Van de Velden, J. Baeyens, A. Brems, B. Janssens, and R. Dewil, “Fundamentals, kinetics and endothermicity of the biomass pyrolysis reaction,” *Renew. Energy*, vol. 35, no. 1, pp. 232–242, 2010.

[123] M. Ringer, V. Putsche, and J. Scahill, “Large-Scale Pyrolysis Oil Production: A Technology Assessment and Economic Analysis,” *Nrel/Tp-510-37779*, no. November, pp. 1–93, 2006.

[124] C. Dupont, G. Boissonnet, J. M. Seiler, P. Gauthier, and D. Schweich, “Study about the kinetic processes of biomass steam gasification,” *Fuel*, vol. 86, no. 1–2, pp. 32–40, 2007.

[125] J. Zhang, H. Toghiani, D. Mohan, C. U. Pittman, and R. K. Toghiani, “Product Analysis and Thermodynamic Simulations from the Pyrolysis of Several Biomass Feedstocks Product Analysis and Thermodynamic Simulations from the Pyrolysis of Several Biomass Feedstocks,” *Energy*, no. 11, pp. 2373–2385, 2007.

[126] J. Lehmann and S. Joseph, “Biochar for environmental management : An introduction,” *Biochar Environ. Manag. - Sci. Technol.*, vol. 1, pp. 1–12, 2009.

[127] P. T. Williams and S. Besler, “The Influence of Temperature and Heating Rate on the Slow

Pyrolysis of Biomass," *Renew. Energy*, vol. 7, no. 3, pp. 233–250, 1996.

[128] K. Crombie and O. Mašek, "Investigating the potential for a self-sustaining slow pyrolysis system under varying operating conditions," *Bioresour. Technol.*, vol. 162, pp. 148–156, 2014.

[129] L. van Zwieten *et al.*, "Effects of biochar from slow pyrolysis of papermill waste on agronomic performance and soil fertility," *Plant Soil*, vol. 327, no. 1, pp. 235–246, 2010.

[130] D. Meier, J. Berns, and O. Faix, "Pyrolysis and Hydropyrolysis of Biomass and Lignins-Activities at the Institute of Wood Chemistry in Hamburg, Germany," *Am. Chem. Soc.*, pp. 298–303, 1995.

[131] D. Mohan, C. U. Pittman, and P. H. Steele, "Pyrolysis of wood/biomass for bio-oil: A critical review," *Energy and Fuels*, vol. 20, no. 3, pp. 848–889, 2006.

[132] N. Abdullah, H. Gerhauser, and F. Sulaiman, "Fast pyrolysis of empty fruit bunches," *Fuel*, vol. 89, no. 8, pp. 2166–2169, 2010.

[133] R. Venderbosch and W. Prins, "Fast pyrolysis technology development," *Biofuels, Bioprod. Biorefining*, vol. 4, no. 2, pp. 178–208, Mar. 2010.

[134] H. Zhang, R. Xiao, H. Huang, and G. Xiao, "Comparison of non-catalytic and catalytic fast pyrolysis of corncob in a fluidized bed reactor," *Bioresour. Technol.*, vol. 100, no. 3, pp. 1428–1434, 2009.

[135] M. Abou-zaid and I. M. Scott, "Pyrolysis Bio-Oils from Temperate Forests: Fuels, Phytochemicals and Bioproducts," *Biorefinery Co-Products Phytochem. Prim. Metab. Value-Added Biomass Process.*, pp. 311–325, 2012.

[136] T. R. Carlson, G. A. Tompsett, W. C. Conner, and G. W. Huber, "Aromatic production from catalytic fast pyrolysis of biomass-derived feedstocks," *Top. Catal.*, vol. 52, no. 3, pp. 241–252, 2009.

[137] J. Han and H. Kim, "The reduction and control technology of tar during biomass gasification/pyrolysis: An overview," *Renew. Sustain. Energy Rev.*, vol. 12, no. 2, pp. 397–416, 2008.

[138] A. Erkiaga, G. Lopez, M. Amutio, J. Bilbao, and M. Olazar, "Steam gasification of biomass in a conical spouted bed reactor with olivine and -alumina as primary catalysts," *Fuel Process. Technol.*, vol. 116, pp. 292–299, 2013.

[139] S. C. Kim, M. S. Lim, and Y. N. Chun, “Hydrogen-rich gas production from a biomass pyrolysis gas by using a plasmatron,” *Int. J. Hydrogen Energy*, vol. 38, no. 34, pp. 14458–14466, 2013.

[140] M. S. and P. T. F. Muthu S. Sundaram, “Flash Pyrolysis of Coal in Reactive and Non-Reactiv Gaseous Enviroments,” pp. 106–129, 1983.

[141] S. Septien, S. Valin, C. Dupont, M. Peyrot, and S. Salvador, “Effect of particle size and temperature on woody biomass fast pyrolysis at high temperature (1000-1400°C),” *Fuel*, vol. 97, pp. 202–210, 2012.

[142] A. Megaritis, Y. Zhuo, R. Messenbo, D. R. Dugwell, and R. Kandiyoti, “Pyrolysis and gasification in a bench-scale high-pressure fluidized-bed reactor,” *Energy and Fuels*, vol. 12, no. 15, pp. 144–151, 1998.

[143] M. S. Sundaram, M. Steinberg, and P. T. Fallon, “Enhanced Ethylene Production via Flash Methanolysis of Coal,” 1985.

[144] B. Zhao, X. Zhang, L. Chen, L. Sun, H. Si, and G. Chen, “High quality fuel gas from biomass pyrolysis with calcium oxide,” *Bioresour. Technol.*, vol. 156, pp. 78–83, 2014.

[145] R. Zanzi, K. Sjöström, and E. Björnbom, “Rapid pyrolysis of agricultural residues at high temperature,” *Biomass and Bioenergy*, vol. 23, no. 5, pp. 357–366, 2002.

[146] A. V. Bridgwater, D. Meier, and D. Radlein, “An overview of fast pyrolysis of biomass,” *Org. Geochem.*, vol. 30, no. 12, pp. 1479–1493, 1999.

[147] S. Gao, J. Wang, Z. Wang, J. Zhao, and Y. Fang, “Effect of CO on the CH4 evolution during fast pyrolysis of lignite in reductive atmospheres,” *J. Anal. Appl. Pyrolysis*, vol. 106, pp. 104–111, 2014.

[148] M. Zhong, Z. Zhang, Q. Zhou, J. Yue, S. Gao, and G. Xu, “Continuous high-temperature fluidized bed pyrolysis of coal in complex atmospheres: Product distribution and pyrolysis gas,” *J. Anal. Appl. Pyrolysis*, vol. 97, pp. 123–129, 2012.

[149] R. Zanzi, K. Sjöström, and E. Björnbom, “Rapid high-temperature pyrolysis of biomass in a free-fall reactor,” *Fuel*, vol. 75, no. 5, pp. 545–550, 1996.

[150] M. Görling, M. Larsson, and P. Alvfors, “Bio-methane via fast pyrolysis of biomass,” *Appl. Energy*, vol. 112, pp. 440–447, 2013.

[151] F. E. Paulik and J. F. Roth, “Novel catalysts for the low-pressure carbonylation of methanol to acetic acid,” *Chem. Commun.*, vol. 11, no. 24, p. 1578a, 1968.

[152] N. Zheng, J. Zhang, and J. Wang, “Parametric study of two-stage hydropyrolysis of lignocellulosic biomass for production of gaseous and light aromatic hydrocarbons,” 2017.

[153] C. J. Ellens, “Design, optimization and evaluation of a free-fall biomass fast pyrolysis reactor and its products,” pp. 1–155, 2009.

[154] S. Nakamura, S. Kitano, and K. Yoshikawa, “Biomass gasification process with the tar removal technologies utilizing bio-oil scrubber and char bed,” *Appl. Energy*, vol. 170, pp. 186–192, 2016.

[155] C. R. Tsai *et al.*, “An analytical solution for transport of oxygen in cathode gas diffusion layer of PEMFC,” *Int. J. Hydrogen Energy*, vol. 31, no. 15, pp. 2179–2192, 2006.

[156] L. Chen, C. Dupont, S. Salvador, M. Grateau, G. Boissonnet, and D. Schweich, “Experimental study on fast pyrolysis of free-falling millimetric biomass particles between 800 °C and 1000 °C,” *Fuel*, vol. 106, pp. 61–66, 2013.

[157] W. L. Saw and S. Pang, “Co-gasification of blended lignite and wood pellets in a 100 kW dual fluidised bed steam gasifier: The influence of lignite ratio on producer gas composition and tar content,” *Fuel*, vol. 112, pp. 117–124, 2013.

[158] F. Miccio, N. Silvestri, D. Barletta, and M. Poletto, “Characterization of woody biomass flowability,” *Chem. Eng. Trans.*, vol. 24, pp. 643–648, 2011.

3 Design of a Fluidised Bed Reactor for the Flash Methanolysis of Biomass

This section covers in detail; the design, construction and commissioning modifications which were conducted for the construction of the flash methanolysis system. An extensive review of the theory and the application are conducted to characterise the fluidised bed system and to determine the reactor characteristics.

3.1 Introduction

For the fast pyrolysis of biomass, fluidised bed reactors (FBR) have been the preferred system for lab scale experiments. The utilisation of fluidised bed reactors has become very popular in commercial applications as well, due to a number of reasons. Primarily, fluidised bed reactors have high heat and mass transfer rates, and uniform temperature distributions across the reaction zone. This is particularly important for the biomass feedstock as the thermal conductivity of woody biomass is low. It is important that the heat transfer from the surrounding medium to the biomass surface is not the limiting factor although the conductivity of biomass is the limiting heat transfer mechanism within the particles, which can be improved by using smaller particles. This ensures that the products from the experiments are directly related to the biomass introduced. Other advantages with the utilisation of a FBR are: ease of scalability, ease of construction and low capital cost.

FBRs have, however, disadvantages in some respects to other reactor systems, with the most common one being the observed accumulation of char in the fluidised bed during biomass pyrolysis. This characteristic could be exacerbated in a methanolysis reactor, by the accumulation of carbon from MTD. This is problematic as interaction of char or carbon with product species could disguise the true reactor kinetics and pathways. Some researchers have applied liquid metal reactors for the application as due to the difference of density, carbon/char formed collects on the top of the liquid and can be subsequently removed [1]–[3].

Another disadvantage of the reactor system is the possible interactions and influences of the reactor inner surfaces with the product gases. For the application of methanolysis of biomass, this is most apparent in the thermal degradation of methane on the inner walls of reactors. This is also undesirable as the production of carbon and interaction with carbon coated walls could significantly influence the product selectivity. To remove the uncertainty associated with solid phase interactions and heterogeneous catalysis researchers have used shock tubes [4], [5]. This is standard in understanding the kinetics and reaction pathway systems; however, the construction costs and complicated process arrangement for biomass feed have led to the systems being limited in application.

In this research group, two fluidised bed reactors have been constructed in other projects for removal of NH_3/H_2S from producer gas streams in biomass gasification and for pyrolysis of biomass (bio-oil production focussed). Both of these reactors were unable to operate under pressure and all experiments in the above fields were conducted at/or slightly above, atmospheric pressure. The reactors stated above were also unable to be operated at 1000 °C due to the integrity of material and the construction of the systems. Most importantly these systems were not specified to operate with the heating of methane above the auto-ignition point of the gas, ~600 °C [6]. Ultimately, a new reactor was designed and constructed to allow for the operating pressures of 10 bar and 1000 °C, with methane as the fluidisation gas.

3.2 Fluidised Bed Theory

This section covers the fluidised bed technology theory and the characterisation of the differing fluidisation regimes. It also covers the theory about the operation and design of a fluidised bed system. An extensive review of the theory is provided which subsequently is compared to experimental results in the following sections.

3.2.1 Fluidised Bed Hydrodynamics

Fluidised beds are defined as a bed of solid particles held in suspension due to the upward flow of a fluid. Given the descriptions in the previous sections the fluid in this study is methane gas, however, fluidised beds also exist in the application of liquid fluidisation. In the discussion below and other chapters of this thesis, the applied fluidisation fluid is strictly in the gas phase.

The random flow of particles due to the introduction of a gas stream can only occur if the upward velocity of the gas is above a certain threshold value, which is termed as the minimum fluidisation velocity, u_{mf}. Above this critical velocity the bed of particles expands and the random movement of the particles begins to occur. Below this velocity the bed is stagnant and no movement of the particles occurs.

Within the classification of fluidisation characteristics, two fluidisation conditions are normally distinguished;

- *Particulate Fluidisation:* This condition is defined primarily by the homogenous nature of the fluidisation zone. This is observed by no apparent solid-free zones or bubbling within the bed. It is found primarily in the gas phase only when the particles are very fine and accurate control of the gas flow rate allows for precise gas introduction. Operation with this condition in pyrolysis reactors is not very common.

- *Aggregative Fluidisation:* In this regime the particles fluidise freely with bubbles forming and rising free of particles. This is the most typical fluidisation scheme which is utilised in gas/solid fluidisation systems.

To initially investigate the inherent characteristics of the fluidisation particle, classifications of the fluidisation regimes have been produced to aid in the foresight of new particle/gas interaction systems. Geldart is a pioneer in the development of particle systems and has proposed a system classification method which has been widely used in the prediction of fluidisation behaviour [7]. The classification of the particles is related to the particle diameter (d_p) and relative difference of density between particles and fluidisation agent ($\rho_p - \rho_g$), as shown in Figure 3-1. It has also been concluded by Geldart that the particle size standard deviation is not of great importance if the distribution of particle sizes follows a normal distribution, [7].

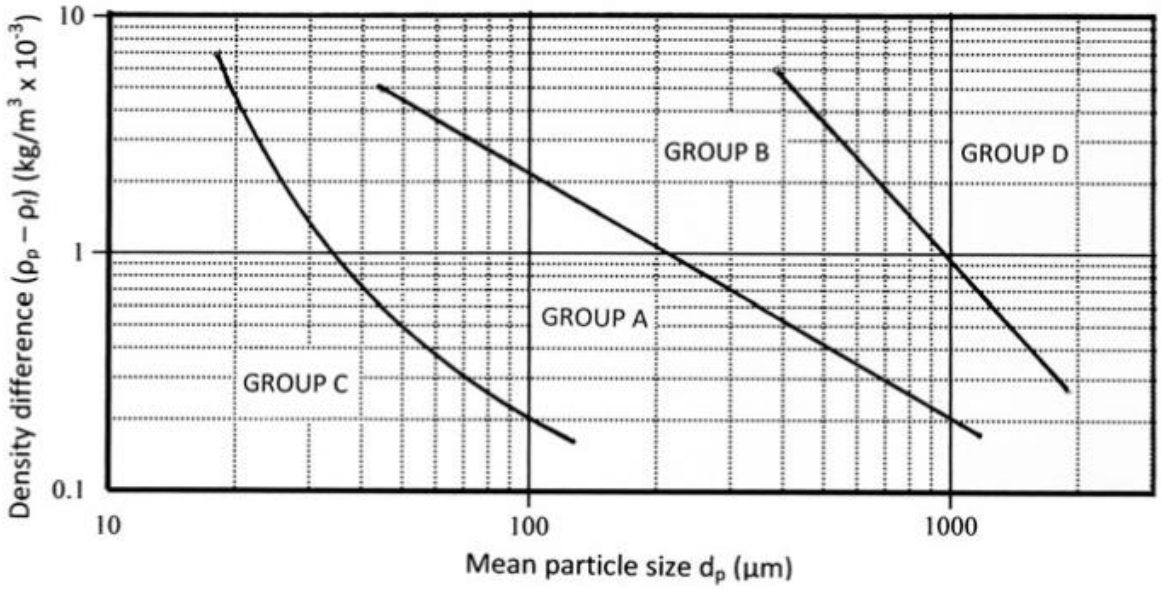

Figure 3-1: Geldart particle classification for fluidisation, retrieved from [8].

As shown in Figure 3-1, Geldart proposed four types of classifications describing the aptitude of particle fluidisation:

Class A: Easy fluidisation, particulate type fluidisation;
Class B: Easy fluidisation, aggregative type fluidisation;
Class C: Fluidisation practically impossible due to the high surface forces between grains;
Class D: Poor fluidisation.

For all fluidised bed experiments conducted in this study high purity silica sand sourced from Industrial Sands Ltd (New Zealand) was used. The sand had a typical composition of 99.3 % silica with a particle density of 2560 kg/m^3. The received sand was sieved to 300-355 µm, which under the usual conditions of the methanolysis system, would place it in Class B type particles, allowing for easy, aggregative particulate fluidisation. Due to the apparent ease of fluidisation from the classification scenario, the fundamental properties which affect the fluidization characteristics were calculated to determine the behaviour of the bed. These calculations were then compared to the experimental results extracted from the cold bed model system which was built in this project. This will be discussed in the upcoming sections.

3.2.2 Velocity and Bed Characterisation

The minimum fluidisation value is an essential parameter in the design of fluidised beds, used to determine the gas flow rates which are required within the system, or the particle size. This ultimately leads to determine the maximum velocity/mass flow rate of the system and other hydrodynamic characteristics of the system. Bed characteristics are also determined from the influence of the minimum fluidization velocity. This will be discussed in detail below with complete calculation schemes given.

3.2.2.1 Minimum Fluidisation Velocity

The characteristics of the minimum fluidization of bed particles within a fluidised bed reactor can be best described by Figure 3-2 and Equation (3.2.1) below. To achieve fluidisation of the particles, the drag force of the particles must exceed the gravitational force to unlock the intermeshed fixed bed particles; the velocity which this occurs at is the minimum fluidization velocity, u_{mf}. Once the particles are disengaged from one another, point B, they begin to move and the pressure drop reduces to the point where the drag force on the bed is balanced by the weight of the bed particles, point C. With increasing flow, the pressure increases slightly until slugging and entrainment occurs. When fluidised, the particles are suspended in the gas and have many properties of a liquid.

$$F_D - F_G = 0 \qquad (3.2.1)$$

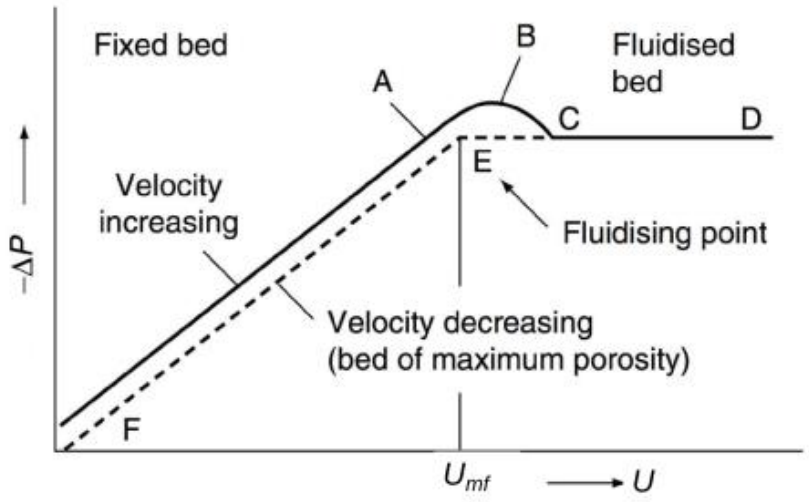

Figure 3-2: Pressure drop changes over the bed with the gas velocity for determination of the minimum fluidisation velocity.

To determine the minimum fluidisation velocity, the Ergun equation below is used to describe overall pressure drop per unit length.

$$A\frac{\varepsilon_p^2 \mu_F V_{SF}}{\left(1-\varepsilon_p\right)^3 d_p^2} + B\frac{\varepsilon_P \rho_F V_{SF}^2}{(1-\varepsilon_P)^3 d_p} = \frac{\Delta P}{L} \qquad (3.2.2)$$

The force balance, Equation (3.2.1) can be rewritten as Equation (3.2.3)

$$\frac{\Delta P}{L} = g\,(\rho_p - \rho_F)\left(1-\varepsilon_{mf}\right) \qquad (3.2.3)$$

The two expressions for pressure drop per unit length at fluidisation can then be equated and multiplied by:

$$\frac{\rho_F d_P^3}{\mu_F^2 \varepsilon_{pm}}$$

Then rearranging Equation (3.2.2), the following dimensionless expression is derived:

$$\frac{\rho_F(\rho_p-\rho_F)d_p^3 g}{\mu_F^2} = A\frac{\varepsilon_{pm}}{\left(1-\varepsilon_{pm}\right)^3}\left(\frac{d_p(V_{SF})_{mf}\rho_F}{\mu_F}\right) + B\frac{1}{\left(1-\varepsilon_{pm}\right)^3}\left(\frac{d_p(V_{SF})_{mf}\rho_F}{\mu_F}\right)^2 \quad (3.2.4)$$

Thereby with the simplification of the Reynolds number and Archimedes number the above expression can be simplified to the following equation:

$$Ar = A\frac{\varepsilon_{pm}}{\left(1-\varepsilon_{pm}\right)^3}Re_m + B\frac{1}{\left(1-\varepsilon_{pm}\right)^3}Re_{mf}^2 \quad (3.2.5)$$

Where the Archimedes and Reynolds numbers are described by the following two equations:

$$Re_{mf} = \frac{d_p(V_{SF})_{mf}\rho_F}{\mu_F} \quad (3.2.6)$$

$$Ar = \frac{\rho_F(\rho_p-\rho_F)d_p^3 g}{\mu_F^2} \quad (3.2.7)$$

Numerous researchers have taken the derivation for the Reynolds number and Archimedes number, and allocated varying constants for A and B. It is also common to see the influence of the bed expansion to be combined in the particle bed volume occupied at fluidisation. This is simplified to the form of Equation (3.2.8):

$$Ar = CRe_{mf} + DRe_{mf}^2 \quad (3.2.8)$$

Where C and D are the newly defined constants for Equation (3.2.5) and are given throughout literature from different researchers. The equation is generally factorised and given for the Reynolds number at minimum fluidisation, Equation (3.2.9):

$$Re_{mf} = \sqrt{\left(\left(\frac{C}{2D}\right)^2 + \frac{1}{D}Ar\right)} - \frac{C}{2D} \quad (3.2.9)$$

Wen and Yu state that C and D have values of 1650 and 24.5 respectively [9], therefore, the overall expressions can be expressed by Equation (3.2.10):

$$Re_{mf} = \sqrt{(33.7)^2 + 0.0408Ar} - 33.7 \qquad (3.2.10)$$

For the two extreme cases of fluidisation described by Reynolds numbers, Equation (3.2.10) can be rewritten as Equations (3.2.11) and (3.2.12):

$$Re_{mf} < 20 \qquad Re_{mf} = \frac{Ar}{1650} \qquad (V_{SF})_m = \frac{(\rho_p - \rho_F)d_p^2 g}{1650\mu_F} \qquad (3.2.11)$$

$$Re_{mf} > 1000 \quad (Re_{mf})^2 = \frac{Ar}{24.5} \quad (V_{SF})_m^2 = \frac{(\rho_p - \rho_F)d_p g}{24.5\rho_F} \qquad (3.2.12)$$

Other values for C and D in Equation (3.2.8) can be applied to render similar equations as those described above, (3.2.11) and (3.2.12), as given in Table 3-1.

Table 3-1: Values of the two constants, C and D, for derivation of the fluidisation characteristics, Equation (3.2.9).

Literature	**C**	**D**	**Ref.**
Wen and Yu	1650	24.5	*[9]*
Grace	1332	24.5	*[10]*
Chitester et al.	1162	20.2	*[11]*

For more accurate representations of the fluidisation characteristics, the values of C and D in Equation (3.2.8) can be measured from experiments. This is usually the case for unpredictable fluidised media which minimum fluidisation velocity is unavailable in literature. In this study, a number of different particle sizes for the silica sand were hypothesised for the determination of minimum fluidisation velocities.

Given that the minimum fluidisation velocity is such an important parameter for this project; a cold model reactor was constructed based on the preliminary calculations from the equations above. The aims of this cold model reactor were to verify and obtain an accurate determination of the minimum fluidisation velocity, and to understand the hydrodynamic nature of the sand bed to be analysed. Other types of sands were also envisaged for application into the cold model. A description of the cold

model will be discussed further below. For the comparisons with the cold model data, a modified Ergun equation derived from Equation (3.2.2) was utilized. For this application the derivation of the minimum fluidisation velocity could be given in terms of the voidage at minimum fluidisation and particle sphericitiy:

$$u_{mf} = \frac{\left(\Psi d_p\right)^2}{150\mu_F}\eta\frac{\varepsilon_{mf}^3}{1-\varepsilon_{mf}} \tag{3.2.13}$$

Where:

$$\eta = g(\rho_p - \rho_F) \tag{3.2.14}$$

Derived values could then be compared to equations derived by Broadhurst and Becker, Equation (3.2.15) [12] and Wen and Yu, Equation (3.2.16) [9].

$$\varepsilon_{mf} = \frac{0.586}{\Psi^{0.72}}\left[\frac{\mu^2}{\rho_g\eta d_p^3}\right]^{0.029}\left[\frac{\rho_F}{\rho_P}\right]^{0.021} \tag{3.2.15}$$

$$\varepsilon_{mf} = \frac{0.415}{\Psi^{0.33}} \tag{3.2.16}$$

3.2.2.2 Maximum Fluidisation Velocity

The maximum fluidisation velocity or the terminal velocity is the critical velocity at which particles begin to experience excessive fluidisation leading to entrainment of particles. At this point the drag force experienced by the particles exceeds the gravitational force. This parameter is important in the use of circulating fluidised bed reactors as this facilitates the circulating of bed materials. For the construction and operation of the reactor in this study, it was essential to determine this velocity, thus to prevent the bed materials from being carried out by the flowing gas. Once the gas velocity is chosen, the operating flow rate of gases and the gas residence time can be determined. For a given particle experiencing terminal velocity, the maximum velocity can be calculated by;

$$u_t = \sqrt{\frac{4d_p\left(\rho_p - \rho_F\right)g}{3\rho_G Cd}} \tag{3.2.17}$$

Where C_D is the drag coefficient, which can be calculated through a number of different empirical correlations depending on the characteristics of the particles being fluidised. Equation (3.2.18) is commonly used to determine the apparent drag coefficient [13].

$$Cd = \frac{24}{Re_P}\left(1 + (8.17e^{-4.07\Psi})Re_P^{0.096+0.557\Psi}\right) + \frac{7.69(e^{-5.075\Psi})Re_P}{Re_P + 5.378e^{6.212\Psi}} \quad (3.2.18)$$

Dependent on the Reynolds number of the particle undergoing fluidisation, terminal velocity can also be calculated by the following equations [14];

$$\begin{aligned} Re < 0.4 \quad & u_t = \frac{\eta d_p^2}{18\mu} \\ 0.4 < Re < 500 \quad & u_t = \left(\frac{1.78\eta^2}{\rho_g \mu}\right)^{\frac{1}{3}} d_p \end{aligned} \quad (3.2.19)$$

3.2.2.3 Bubble Characteristics

Another influential parameter which was calculated to better understand the flow characteristics is the bubble behaviour within the bed upon fluidisation. The velocity of bubbles within the system is complicated and can be significantly influenced by the interaction of other bubbles and the wakes produced by the movement of the bubbles throughout the system. The velocity of bubble rise can be calculated from the equation proposed by Davidson et al, [15].

$$u_b = u_0 - u_{mf} + 0.71\sqrt{g d_b} \quad (3.2.20)$$

The bubble diameter can be determined by an equation proposed by Mori and Wen [16]. This equation was derived primarily in small fluidised bed systems, with reactor diameter of 7-130 cm and for small particle sizes.

$$\frac{d_{bm} - d_b}{d_{bm} - d_{b0}} = e^{-\frac{0.3h}{d_t}} \quad (3.2.21)$$

Where d_{bm} and d_{b0} are the bubble maximum and initial diameters, respectively. Mori and Wen [16] show that these two diameters can be calculated by the following equations:

$$d_{bm} = 0.652\left(A_0\left(u_0 - u_{mf}\right)\right)^{0.4} \tag{3.2.22}$$

$$d_{b0} = 0.347\left(\frac{A_0\left(u_0 - u_{mf}\right)}{n_d}\right)^{0.4} \tag{3.2.23}$$

The fraction of the bed occupied by bubbles can then be determined by Figure 3-3.

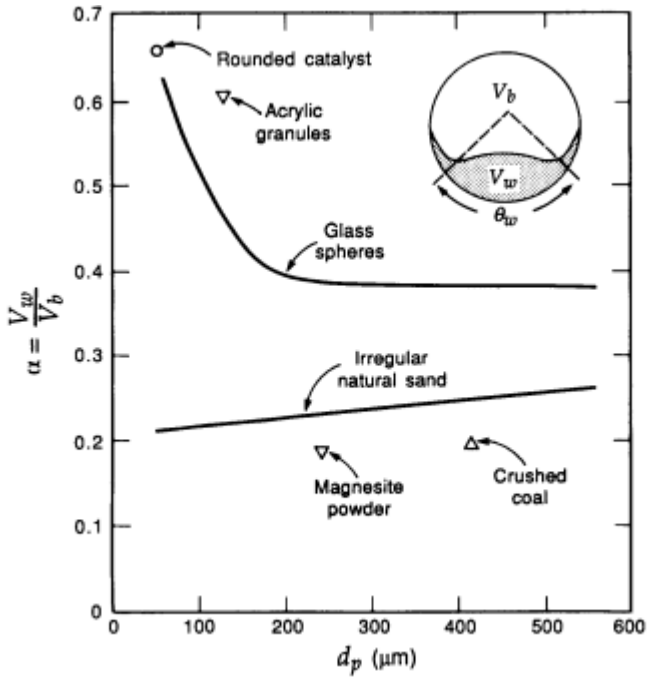

Figure 3-3: Wake angle and wake fraction of 3D bubbles at ambient conditions, evaluated from Roe and Partridge, adapted from Kunii and Levenspiel [17].

For irregular natural sand as the bed material, the wake parameter α is taken as 0.22. Applying the parameter in Equation (3.2.24), the fraction occupied by bubbles within the bed can be determined by:

$$\delta = \frac{\left(u_0 - u_{mf}\right)}{\left(u_b - u_{mf}\right)(1 + \alpha)} \tag{3.2.24}$$

When operating a fluidised bed system it is desirable to operate in a fashion which minimizes the slugging potential of the bubbles within the bed. Slugging is a phenomenon which occurs due to the growth of bubbles within the bed and the bubble diameters close to that of the reactor diameter. This occurs due to the addition of multiple bubbles which travel and collide through the bed from the sinter to the top of the bed. It is beneficial to minimize slugging effects as this phenomenon causes non-

uniform fluidisation of the bed. The bed height which slugging begins to occur can be derived by the following empirical equation (3.2.25) [14].

$$z_s = 60 d_t^{0.175} \tag{3.2.25}$$

3.2.2.4 Bed Height Determination

Another important parameter which requires characterisation for the fluidised bed design is the bed expansion upon fluidisation. Equation (3.2.25) was used to calculate the operating fluidised bed height from the operating superficial velocity. As the operational velocity increases, part of the kinematic energy input is consumed to increase the bed height on fluidisation as the drag force increases [18]. As the height of the bed would change with velocity and operating pressure, the bed height expansion value was calculated to ensure that within the experimental conditions the fluidisation of the bed maintained within acceptable limits.

$$\left(\frac{h - h_0}{h_0}\right) \rho g V_b = (\frac{u_s - u_{mf}}{V_b}) \rho g V_b \tag{3.2.26}$$

3.2.3 System Heat Transfer

Due to the high operating temperature of the reactor; radiation, conduction and convection need to be considered when deriving the system overall heat transfer rates. For an arbitrary reference temperature, the heat transfer for convection, conduction and radiation can be described by Equations (3.2.27), (3.2.28) and (3.2.29), respectively.

$$Q = UA(T_{a1} - T_{a2}) \tag{3.2.27}$$

$$Q = \frac{k}{L}(T_{a1} - T_{a2}) \tag{3.2.28}$$

$$Q = \xi \sigma (T_{a1}^4 - T_{a2}^4) \tag{3.2.29}$$

The system heat requirements could be estimated by considering the required flow rate of methane and biomass fed into the system. The cumulative heat requirement could be determined by considering the sensible heating requirements of the entering streams with the overall heat loss as described in Equation (3.2.30).

$$Q_{req} = \dot{m}_{Biomass} C_{p(Biomass)} (T_f - T_i) + \dot{m}_{CH4} C_{p(CH4)} (T_f - T_i) + \sum Q_{loss} \qquad (3.2.30)$$

To estimate the heat loss of the system, the heat loss associated with the system flanges and water cooler were modelled. The overall forced convection heat transfer could be computed by using a set of dimensionless numbers. Depending on the system conditions the Nusselt number could then be computed to determine an estimate of the heat transfer coefficient. The overall Nusselt number, Reynolds number and Prandtl number were computed by Equations (3.2.31), (3.2.32) and (3.2.33), respectively:

$$Nu = \frac{hD}{k} \qquad (3.2.31)$$

$$Re = \frac{Du\rho}{\mu} \qquad (3.2.32)$$

$$Pr = \frac{\mu C_p}{k} \qquad (3.2.33)$$

For the system employed in this study, the Nusselt number can be approximated either for constant wall temperature or for constant heat flux assuming fully developed flow, as given in Table 3-2.

Table 3-2: Nusselt number approximation for different system conditions.

System Condition	Nusselt Number
Constant Wall Temperature	3.66
Constant Heat Flux	4.36

For a laminar flow fluid systems with a Prandtl number within the region of 0.6-5.0 and a viscosity ratio such that $0.004 < \frac{\mu_b}{\mu_w} < 9.75$ the Nusselt number can be determined by Equation (3.2.34):

$$Nu_o = 1.86 \left(\frac{RePr}{\frac{L}{D}} \right)^{\frac{1}{3}} \qquad (3.2.34)$$

By assuming a constant wall temperature, the heat transfer coefficient can be corrected to account for the variation between the wall and the main stream as given by:

$$h = h_o \left(\frac{\mu_{bf}}{\mu_w}\right)^{0.14} \tag{3.2.35}$$

Conductive heat transfer resistance was assumed to be negligible for all metal surfaces; however, for the computation of heat flux about insulated regions, Equation (3.4.4) was used to determine the heat conduction through a pipe.

$$q = \frac{2\pi kL(T_1 - T_2)}{\ln(\frac{r_1}{r_2})} \tag{3.2.36}$$

Due to the reactor being supported at the top, thermal expansion (Γ) of the rector was assumed to occur longitudinally in the downward direction. The coefficient of thermal expansion of the 253 MA is reported as constant between 30-1000 °C, at 1.95×10^{-7} m/m°C [19].

$$\Delta L_{Reactor} = \Gamma L \Delta T \tag{3.2.37}$$

3.3 Fluidised Bed Cold Model Reactor Design and Build

A cold model reactor was designed and constructed to obtain an accurate determination of the minimum/maximum fluidisation velocities. The cold model reactor was also useful for understanding the extent of fluidisation at gas velocities in excess of u_{mf}. It also allowed for alternate bed materials to be investigated for their fluidisation characteristics.

3.3.1 Cold Model Construction

Prior to commencing the design of the cold model, the key characteristics of the target reactor were analysed to determine the fundamental design parameters. The major design parameters were outlined as follows.

- Surface of all heated zones must be chemically inert. All reactor inner walls and interior components should be lined with quartz to remove possible catalytic effects.
- Distribution disc should also provide adequate inactiveness with methanolysis conditions.
- The system should be able to feed biomass at a maximum flow rate that allows the methane/biomass ratio of 0.5 over the range of pressures and temperatures.
- The system should operate at temperatures of up to 1000 °C and pressures of up to 10 bar.
- The system should operate with gas velocity of at least 3 times the u_{mf}.

The cold model fluidised bed reactor was design to operate at low pressure and with a distribution disc envisaged for use in the final system. The polycarbonate tubing in the cold model reactor was sourced from Dotmar Ltd., Christchurch, New Zealand, and the quartz fritted discs were sourced from Technical Glass Products Ltd, Los Angeles. Fritted discs, (sourced from Technical Glass Products, USA) with different porosities were purchased and trialled to determine the effective influence of the distribution plate on the system.

The cold model reactor, as shown in Figure 3-4, was constructed with an inner diameter (ID) of 33.4 mm, close to the diameter of the target hot reactor. The system comprised of three sections of polycarbonate tubing of two separate diameters. The smaller diameter tubing was chosen to allow for it to slide within the larger tubing. Two metal rings with complementary recesses were fabricated to allow the placement of the fritted disc and interchange of the frits with different porosity. The two inner polycarbonate lengths were approximately the same length, with the overall length of ~10 mm shorter than the overall larger diameter tubing. This allowed for adequate positioning of the sintered disc in the system and for eye-level investigation into the fluidisation of the system, Figure 3-4. The

position of the sinter in the cold model reactor also ensured that the flow of gas was fully developed and entrance effects were minimised.

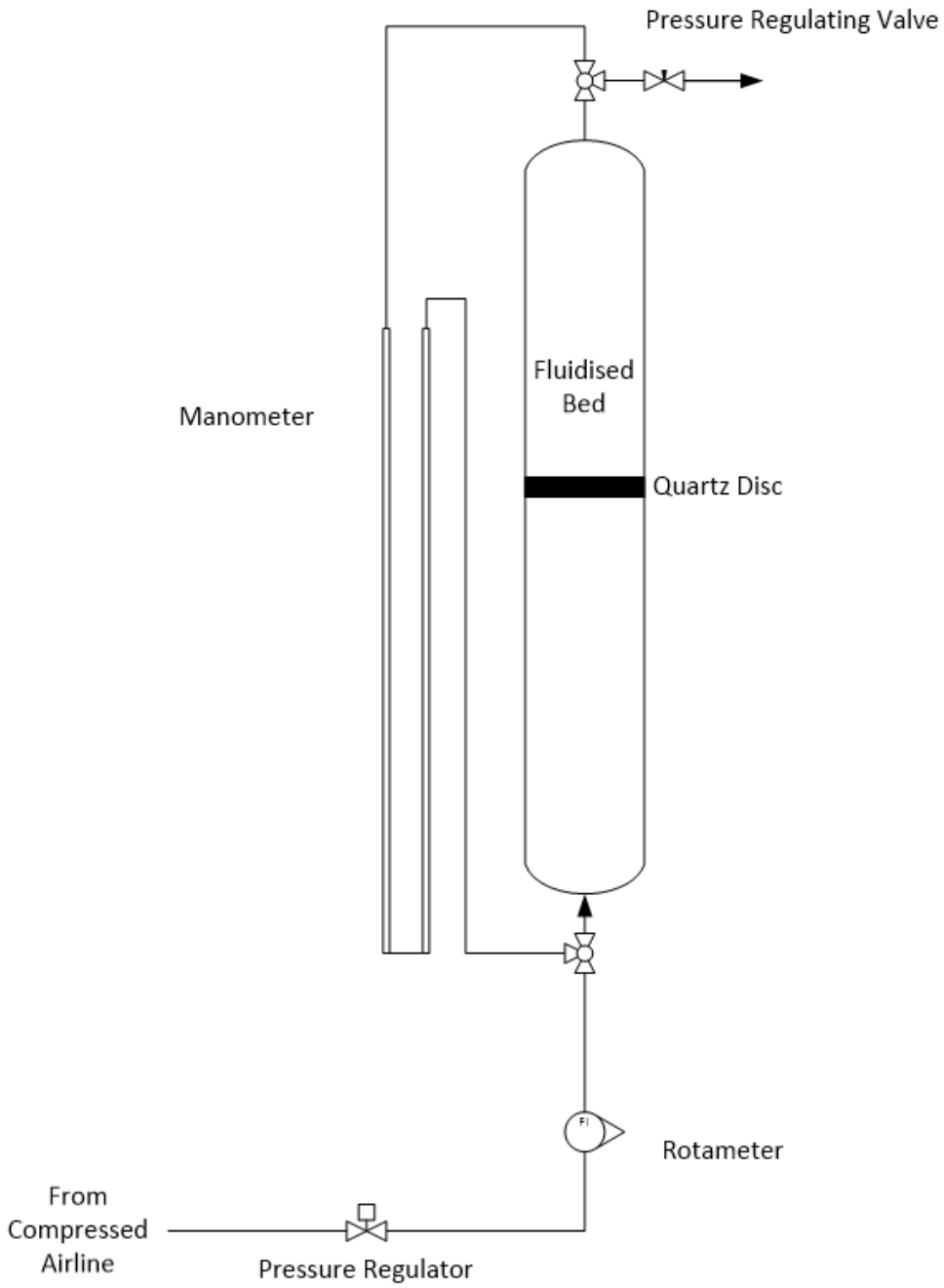

Figure 3-4: Cold model reactor configuration.

To prevent gas leaking, rubber seals and threaded rods were employed at all joints. Metal plates were used for the bottom and top of the system, with one inlet/output connection on each. To ensure adequate sealing the threaded rods were passed beside the length of the cold model and were tightening at both ends of the tubes. This also served as a system which centralized the polycarbonate

tubes. For the outlet a Swagelok ¼ turn plug valve was fitted to control the operational pressure of the system. To determine the pressure drop during operation, a water manometer was fitted in the system which was fabricated from a length of 1/4" PVC tubing. A regulator was used to control the inlet pressure, with the inlet flow controlled by a ¼" rotameter. The rotameter was calibrated against an electronic flow meter to provide accurate volumetric flows. For cold model experiments conducted at atmospheric pressure using air as the fluidisation gas, the adjusted volumetric flow rate was calculated by Equation (3.3.1) to simulate the real gas at operation conditions in the hot reactor, where the calibrated apparent gas was air at STP. All connections to and from the cold model were 7 mm PVC tubing.

$$\dot{Q}_{G(actual)} = \sqrt{\frac{PT_{Std}MW_g}{P_{Std}TMW_{Cal}}\dot{Q}_{cal}} \tag{3.3.1}$$

3.3.2 Fluidisation Characteristics and Derivation of Key Fluidisation Parameters

To determine the fluidisation characteristics of the quartz sand, various gas flow rates and sand inventories as well as sinter porosities were trialled. In these trials, air was initially used as the gaseous fluidisation agent.

To determine the minimum fluidisation velocity the flow rate of gas entering the system was altered and the bed was visibly inspected for fluidisation. This was observed by the movement of particles in the bed and the overall expansion of the bed height. Once fluidisation had occurred, the air supply would be turned off and then the trial was repeated. The value obtained was then compared to the initial minimum fluidisation velocity which was calculated to test conformity with literature. Table 3-3 shows the results of the cold model fluidisation trials in which the pressure drops were theoretically estimated based on the applied gas velocities.

Table 3-3: Minimum fluidisation velocities and estimated pressure drops from the cold model trials.

Sand Sieve Fraction	Frit Porosity	Bed Height	Experimental u_{mf}	Calculated u_{mf}	Pressure Drop	Bed Porosity at u_{mf}	Sphericitiy
(µm)	*(µm)*	*(mm)*	*(m/s)*	*(m/s)*	*(kPa)*	*(-)*	*(-)*
300-350	150-200	52	0.031	0.049	74	0.67	0.85
250-300	150-200	52	0.027	0.037	74	0.69	0.87
180-250	150-200	52	0.024	0.025	74	0.73	0.89

From the experimental results from the cold model trials, the minimum fluidisation velocity was observed to agree closely with the calculated values from theory. It was interesting to note that the variation of particle sizes seemed to be related to the discrepancy between the experimental and calculated values which is believed to be due to the difference in the sphericitiy of the particles at different fractions from the sand sieving. With the decrease in the particle size, the sphericitiy of the particles increases, the porosity at u_{mf} increases and the experimental minimum fluidisation velocity was very close to that calculated, Table 3-3.

In the first portion of experiments, the frit porosity was kept constant so that this was not an affecting factor in the trials; however, the inclusion of a smaller porosity fritted disc in the following experiments resulted in increased pressure drop. Overall the pressure drop values derived from the measured minimisation velocity were deemed not reliable due to the low values and system uncertainty. It was reasoned that the overall pressure drop over the system was more important in the hot model system than the cold model system as this had implications to the fluidisation at elevated temperatures.

Following the determination of the minimum fluidisation velocity using air as the fluidisation agent, the associated minimum fluidisation velocity for methane as the fluidisation agent was determined. In these trials, the properties of methane were taken as the extreme conditions which methanolysis would occur under, as seen in Table 3-4 with a comparison with air.

Table 3-4: Methane physical properties at the maximum operating temperature and pressure in comparison with those of air at ambient conditions.

Physical Property and Conditions	Pressure	Temperature	Viscosity	Density
	[kPa]	*[°C]*	*[Pa.s]*	*[kg/m^3]*
Air	101	25	1.83×10^{-5}	1.29
Methane	1010	1000	3.30×10^{-5}	1.50

The minimum fluidisation velocity for the methane at the highest temperature and pressure was then calculated using Equation (3.2.13), based on the particles having the same fluidisation characteristics determined in air, Table 3-3. By assuming that the bed properties were constant independent of gas a proportional relationship could be derived from the Broadhurst and Becker relationship, (3.2.15). Based on the physical properties of the gas, the influence of the gas species on the void fraction, ε_{mf}, at the minimum fluidisation velocity could be calculated:

$$\varepsilon_{mf} \propto \frac{\mu^{0.058}}{\rho_g^{0.008}} \tag{3.3.2}$$

From the values in Table 3-4 , the proportional bed voidage values were calculated by Equation (3.3.2). This resulted in a deviation of less than 4 % between calculated values, thus, justifying the assumption that the minimum fluidisation using methane at 1000 °C could be adequately simulated by air at 25 °C and 101 kPa, (as the effect of increasing density did not significantly alter the bed voidage in the operating conditions of 1-10 Bar). Given that this assumption was justified the minimum fluidisation Equation (3.2.13) could be rewritten as Equation (3.3.4), where γ is a bed physical property constant:

$$\gamma = \frac{\left(\Psi d_p\right)^2}{150}\eta\frac{\varepsilon_{mf}^3}{1-\varepsilon_{mf}} \tag{3.3.3}$$

Which could then be substituted into Equation (3.2.12):

$$u_{mf} = \frac{1}{\mu_G}\gamma \tag{3.3.4}$$

This allowed for the calculation of the minimum fluidisation velocity of the system at varied temperature and pressure. Since the viscosity of methane is not significantly influenced by pressure, the derivation of the minimum fluidisation velocity was assumed to be affected primarily by the operation temperature. At 1000 °C and 10 bar, the minimum fluidisation velocity was found to be 0.017 m/s. To ensure that there was adequate fluidisation, the chosen minimum design velocity was 3 times the minimum fluidisation velocity, e.g., 0.051 m/s for CH_4 (1000 °C and 10 bar). From the cold model trials, the bed was found to be sufficiently fluidised with the air velocity of 3 times the minimum fluidisation velocity, as also concluded from literature [20].

In practical operation of the hot reactor, only gas flow rate can be controlled thus the gas velocity was related to the gas flow rate in a range of operating conditions with an example as shown in Figure 3-5. This allowed for the operating characteristics and the system constraints to be identified. Generally, with decreasing temperature and increasing pressure the system became more confined to the system conditions. From the above analysis, a design methane mass flow rate of 1 kg/hr has been selected for the lowest operating temperature of 750 °C and an operating pressure of 10 bar. Therefore, when temperature is increased, the methane flow rate should be decreased to achieve the same gas velocity through the fluidised bed reactor. Hence, given a desirable operating methane/biomass ratio of 0.5, the maximum biomass flow rate was designed to be 2 kg/hr at 10 bar. From the parameters derived the overall heating requirements could also be derived. A summary of the operating conditions considered in the design process is given in Table 3-5.

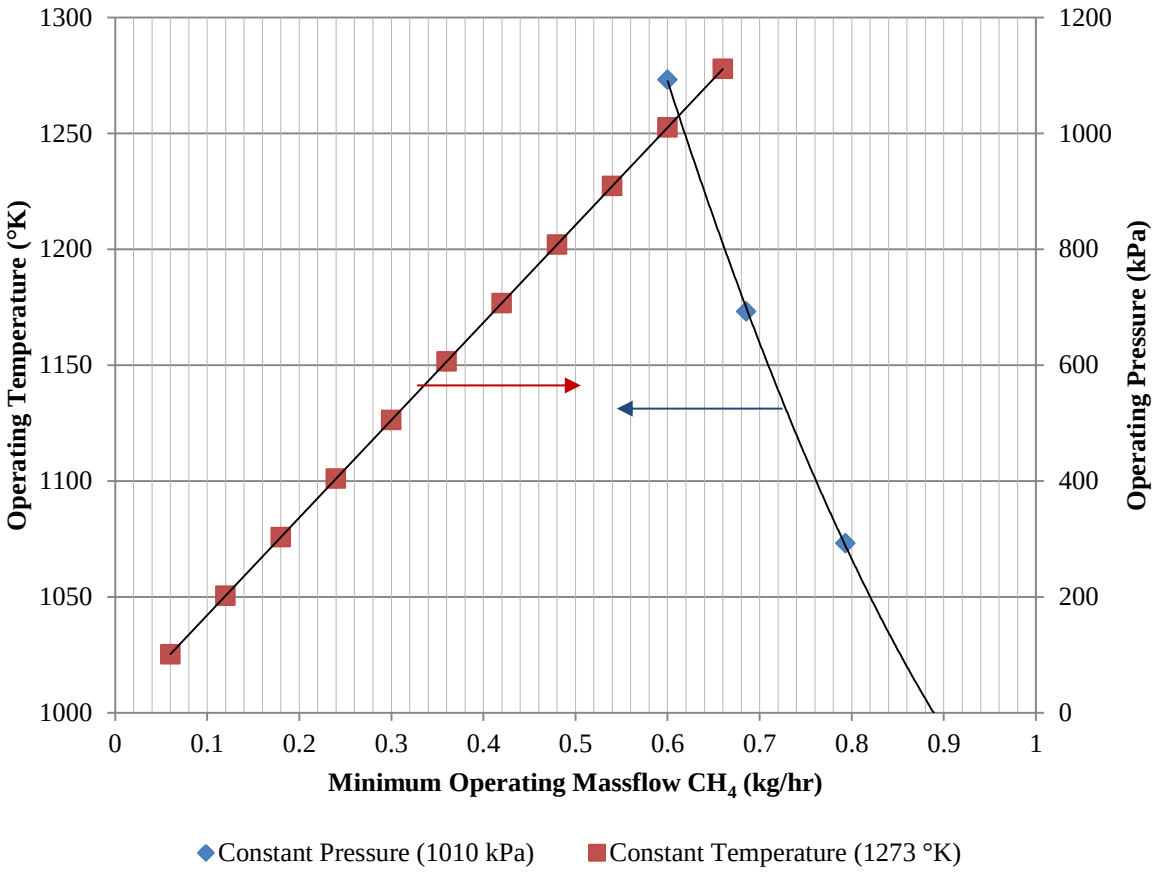

Figure 3-5: Reactor minimum mass flow rates of methane which facilitate the reactor to operate with a gas velocity of three times U_{mf} of 3.

Table 3-5: Key design parameters derived from the cold model experiments.

Parameter	Unit	Maximum	Minimum
Pressure	*[kPa]*	1010	101
Temperature	*[°C]*	1000	750[VII]
Methane Mass Flow rate	*[kg/hr]*	1	0.06
Biomass Mass Flow rate	*[kg/hr]*	2	N/A[VIII]
Heat Requirements	*[kW]*	N/A[IX]	2.4

[VII] Lower temperature operation is possible, however it is believed that this will not show significant yields of desirable products.
[VIII] The lower limit of biomass mass flow rate is not defined as the Methane/Biomass ratios above 0.5 are desirable.
[IX] A minimum heat requirement is required for the system, but for the sizing of the heater the heat requirements at the highest envisaged energy consumption are taken as the lead design value.

3.4 Flash Methanolysis Reactor System Design and Development

From the results collected from the cold model trials, the target reactor was developed and designed with minimum gas (CH_4) velocity of 0.5 m/s in the reactor at 1000 °C and 10 bar. This section will cover the complete design and construction of the target reactor system which P&ID (Piping and Instrumentation diagram) diagram is shown in

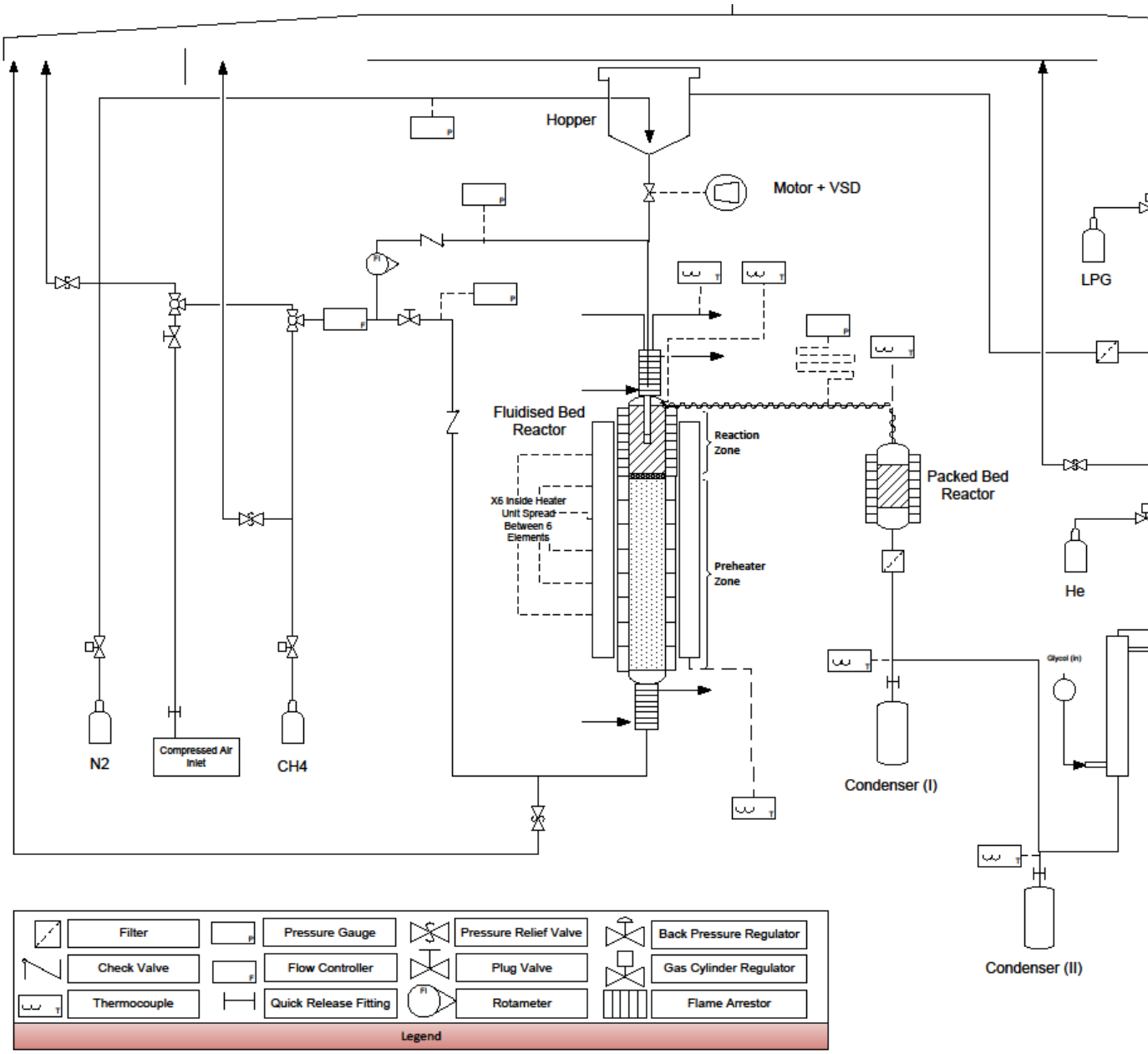

Figure 3-6. As this system design needed to comply with New Zealand pressure vessel standard, all major pressure bearing components were fabricated at Mercers Stainless Ltd., Christchurch, New Zealand. The hopper, packed bed and fluidised bed system were all designed in conjunction with leading mechanical engineers onsite. Calculations regarding the temperature-pressure rating were all conducted by the company due to the certification of the chief project engineer. The system was

mounted on a moveable frame which facilitated the movement of the reactor. This was essential as it allowed for the reactor to be moved within the campus as the University was undergoing a significant re-build.

In brief, the system consisted of a hopper which was loaded with biomass chips,

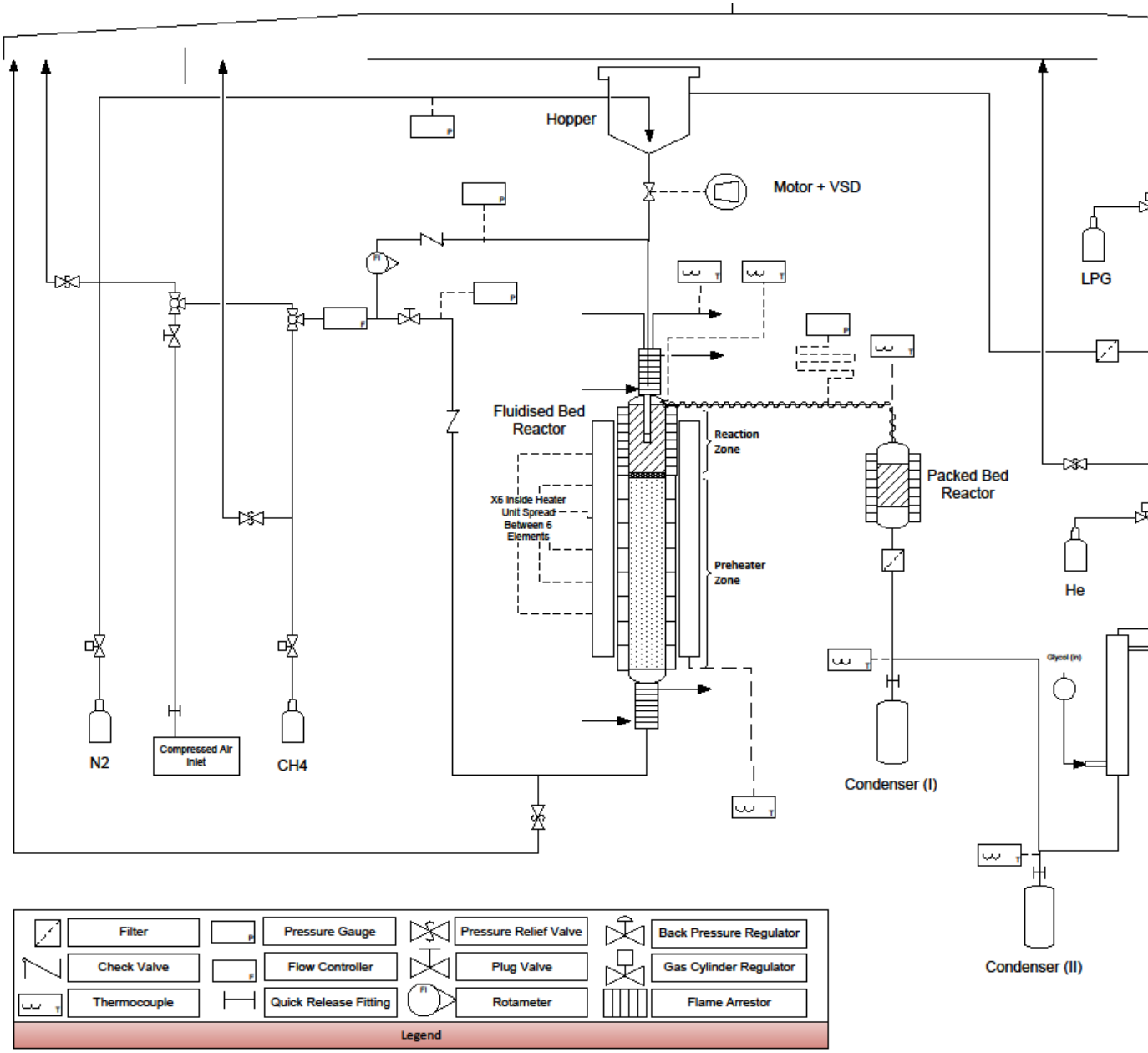

Figure 3-6. A modified rotating ball valve was used to feed the wood chip down the feeder tube into the reacting environment. The feeder tube was a section of pipe which was fitted on the top flange which facilitated the feed of biomass into the bed. The main purpose for the inclusion of the feeder tube was to cool the feeding stream using a water jacketed pipe arrangement. This was designed to reduce premature pyrolysis of biomass before the chips were able to reach the reaction zone. The hopper was pressurized with nitrogen gas to retain the required operating pressures when the reactor is

operated at the target pressure. All technical drawings can be found in Appendix C, with representative drawings given throughout the section.

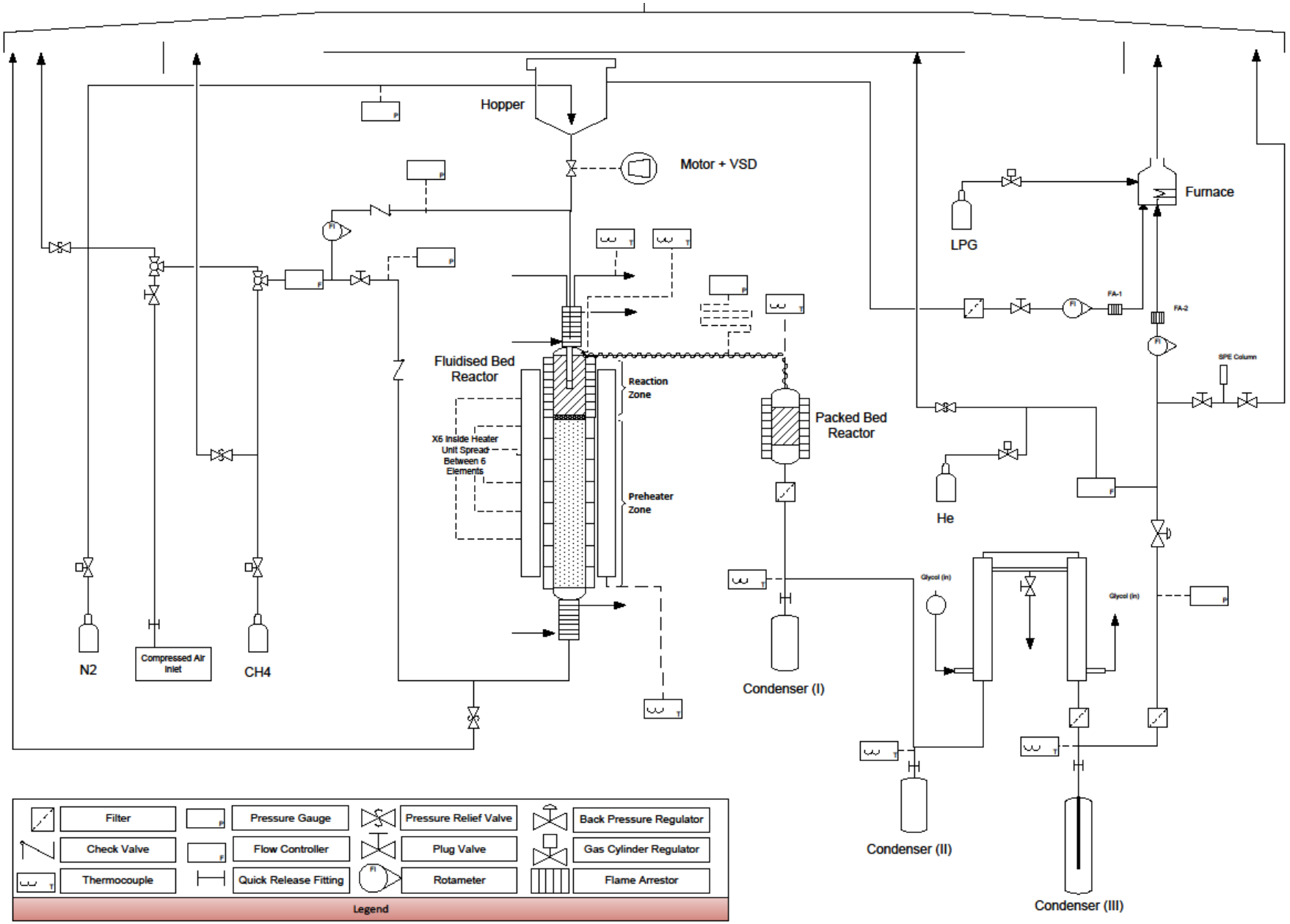

Figure 3-6: Piping and instrumentation diagram of the Flash Methanolysis Reactor.

The reactor pipe consisted of the preheater zone and reaction zone; these two zones were separated by the location of the quartz fritted disc location in the quartz liner[X]. The methane was firstly preheated in the bottom of the reactor pipe, before entering into the bottom of the fluidised bed reactor zone for reaction with the fed biomass. A small portion of the methane gas was also fed through the top of the reactor via the feeder tube which was known as the entrainment flow. This flow was introduced to aid in dilution of the nitrogen which was entrained from the hopper with the chips. This section was also designed to facilitate the flow of the particles down the feeder tube as the gas velocity was co-current with the flow of the wood. This allowed for a continuous flow of biomass to enter the fluidised bed during methanolysis.

Figure 3-7: Flash methanolysis reactor system.

[X] This volume could vary depending on the quartz fritted disc location.

The gaseous product stream from the combination of biomass and the methane feed which has entered from the preheating section and passed through the quartz frit exited in the annulus between the feeder tube and the quartz liner. It then to passed through a packed bed reactor. This was constructed in the hope of using a catalyst packed bed to perform gas cleaning functions. However, in this study, no catalyst was used and the fixed bed reactor remained empty for all experiments. Following the exit of the gas stream from the packed bed reactor the gas condensate was filtered using a 230 µm Swagelok filter and then passed through tubing which allowed the condensing of products and collection in two condensers via gravity. Following the 2nd condenser, the feed was cooled using a glycol jacket cooler, from which different boiling point tars could be collected. The gas then travelled through to a 3 mm section of perforated tubing which was immersed in solvent for tar condensation. The gas was then passed through a final filter (60 µm Swagelok filter), and through a back pressure regulator, which regulated the operating pressure of the reactor system. The outlet gas was then injected with a helium tracer gas stream which was used in the determination of the overall volumetric flow rate of the non-condensable gas stream (NCG). After sampling, the gas was eventually flared using an LPG burner. Further description of each process element is provided in subsequent sections.

3.4.1 Fluidised Bed Reactor Design

In designing the flash methanolysis reactor, a number of considerations were required in regards to the operating conditions and procedures. This section will cover the selection of materials and key dimensions to conform to the process requirements.

In the reactor design, the first parameter to be determined was the residence time which was chosen as 1 s based on the flash pyrolysis characteristics reported by Steinberg et al. [21]–[24] . This corresponds to a desired bed height of 51 mm for the target operation, allowing for bed expansion at 3 times the minimum gas velocity, u_{mf}, in the fluidised bed reactor. Once the bed height had been determined, the desired bed diameter was also determined based on bed height-diameter relationships, also obtained from literature. Satisfactory operation of fluidised bed reactors has been observed with a bed height to diameter ratio of 1; thus, an overall reactor diameter of 51 mm was targeted for the reactor construction. However, the actual diameter and the bed height have been eventually chosen by considering the availability of the pipes and materials. Further information on the sizing and specifications will be covered in the following sections.

3.4.1.1 Material Selection

When investigating the suitability of materials, it was an essential requirement that the material should be suitable for the target application including the feeding materials and the products. In addition, the material selected was also desired to have high creep strength at high temperatures as well as good resistance to isothermal cycling. With the specifications for the desired construction material, a number of different materials were considered and their properties are given in Table 3-6.

Table 3-6: Review of candidate materials for the reactor design.

Materials	Creep Rupture Strength (1000°C, 10000hrs)	Max Operating Temperature	Composition	Characteristics	Ref
	(MPa)	*(°C)*	-	-	
Sandvik 253MA	7	1150	Chromium-Nickel Steel Alloy • 21 % Cr • 11 % Ni • 1.6 % Si • 0.08 % C • 0.17 % N	• High creep strength • Very good resistance to isothermal and, particularly, cyclic oxidation • Good structural stability at high temperatures • Good weldability • Maximum operating temperature is approx. 1150°C	*[25]*
Sandvik 353MA	8	1175	Chromium Nickel Steel Alloy • 25 % Cr • 35% Ni • 1.6 % Si • 1.5% Mn • 0.07 % C • 0.16% N	• High creep strength and Good weldability • Very good resistance to isothermal and cyclic oxidation • Very good resistance to combustion gases • Very good resistance to carburization • Good resistance to nitriding gases • Good structural stability at high temperatures • Maximum operating temperature is approx. 1175°C	*[26]*
Sanicro 31HT	6.2[XI]	1100	Nickel Iron Chromium Alloy • 20.5% Cr • 30.5% Ni • 0.6% Si • 0.6% Mn • 0.5% Ti • 0.5% Al • 0.07% C	• High creep strength • Very good resistance to oxidation • Good resistance to combustion gases • Very good resistance to carburization • Good resistance to nitrogen absorption Good structural stability at high temperatures Good weldability	*[27]*

[XI] 100,000 hr average value

Table 3-6 Continued

Materials	**Creep Rupture Strength (1000°C, 10000hrs)**	**Max Operating Temperature**	**Composition**	**Characteristics**	**Ref**
	(MPa)	*(°C)*	-	-	-
SX 310	10	1035	Nickel Chromium Alloy • 25 % Cr[XII] • 20.5% Ni[XII] • 1.5 % Si[XIII] • 2 % Mn[XIII] • 0.25 % C[XIII]	• Excellent oxidation resistance • High strength at high operating temperatures • High ductility • Good weldability	*[28]*
Kanthal	3.4	1250	Iron Chromium Aluminium Alloy • 22% Cr[XII] • 5.8% Al • 0.7% Si • 0.4% Mn • 0.08% C	• Good form stability at high temperature • Excellent, non-scaling surface oxide formation • Resistive to oxidizing sulphurous and carburizing environments	*[28]*

[XII] Derived as average from stated range
[XIII] Stated maximum chemical composition

From the material review given in Table 3-6, it was concluded that Sandvik 253MA and 353MA were the most suitable materials for the reactor fabrication with required performance at high temperature and pressure. SX 310 also showed required properties; however, the application for cyclic thermal loads was a concern due to the nature of the material. As both Sandvik 253MA and 353MA were quoted as having excellent isothermal properties, it was eventually decided to select 253 MA as the main building material for the reactor system based on the purchasing price.

To ensure the chemical inertness of the reaction environment, a quartz liner was designed before the selection of core reactor material. The quartz liner was a section of high purity quartz tubing which had a quartz fritted sinter fused at an appropriate location. The glassblower from the Chemistry Department at the University of Canterbury was able to fabricate the quartz liner on site. Therefore, when required, the sinter could be placed in the exact position required for the desired bed position. Due to the relative ease of fabricating all the quartz glassware, this sleeve design allowed the reactor to take different bed configurations with the interchange of only the reactor core and, in this way, multiple configurations could be trialled and optimised.

To select the core reactor material, a number of considerations were required for the severe environment which the reactor core would be exposed to. At this point in the design the heating source was investigated. Initially it was envisaged that the system would be heated using ohmic heating principles (also known as Joule heating). However it was deemed unfeasible due to the large electrical load current required. Instead the system was heated using a conventional electric element. Although the overall efficiency of the heating regime would not be as high as that from an ohmic heating arrangement, it was significantly more straightforward. Before the heater could be sized, the material of construction was determined.

3.4.1.2 Reactor Design

Upon choosing the material of construction, 2.5” SCH40 pipe was desired for the core section of the reactor. However, it was discovered that the fabrication of 253 MA in all Schedule 2.5” pipe had been discontinued (similarly for 353 MA). Due to this it was proposed that the reactor be constructed by the boring of a solid 75 mm OD bar. The bar was line bored from both ends of the bar to an OD and ID of; 74.3 ± 0.2 mm and 59.5 ± 0.2 mm, respectively. The ends of the reactor pipe were both fitted with ANSI B16.5 Class 300 blind flanges which were machined to the corresponding ID of the reactor pipe. The overall length of the reactor was defined by the overall length of the heating system plus the additional cooling coils.

The cooling coils were necessary as this facilitated the cooling of the flanges. Due to the high temperature and pressure ratings of the system, the flanges at both ends of the reactor were rated to

650 °C. To comply with the pressure certification, a 100 mm section of the reactor pipe was fitted with 12.7 mm OD copper tubing which was coiled about the pipe and connected to a water cooling line. The flow rate of the cooling water was controlled by rotameters which were fitted on the entry of the cooling line. The copper coil was fitted in place by application of a heat transfer compound T-99 Thermon, USA. This compound was applied and cured with the coils in place to fix the coils in position, and allowed adequate heat transfer.

In order to achieve the high operating temperature, a custom made heater was imported from Thermcraft Inc NC, USA. The heater arrangement consisted of twelve separate 700 W semi-cylindrical half round heater elements (127 mm ID x 76 mm long). The heater package was housed within two separate semi-cylindrical half round insulation packages. The packages consisted of a 318 mm OD x 559 mm long housing fitted with 51 mm long vestibules at both ends with an ID of 86 mm flush with the overall external housing. The ID of the vestibule arrangement was specified as suggested by the manufacturer to facilitate heat to be removed from the inner heater system which prevented element burnout. This was specified as a 6 mm clearance about the core pipe. The elements were divided into 6 separate sections which consisted of 2 elements connected in series cylindrically. Each separate reactor section was controlled using proportional controllers. Further information into the electronical configuration of the heater system can be found in Appendix C.

From the selection of the heater arrangement and the coil length for cooling, the complete reactor pipe interior length was determined. This resulted in a pipe length of 800mm where approximately 20 mm of the pipe length was welded inside the flange sections at the ends of the reactor. The overall core reactor configuration and corresponding heater arrangement can be seen in Figure 3-8.

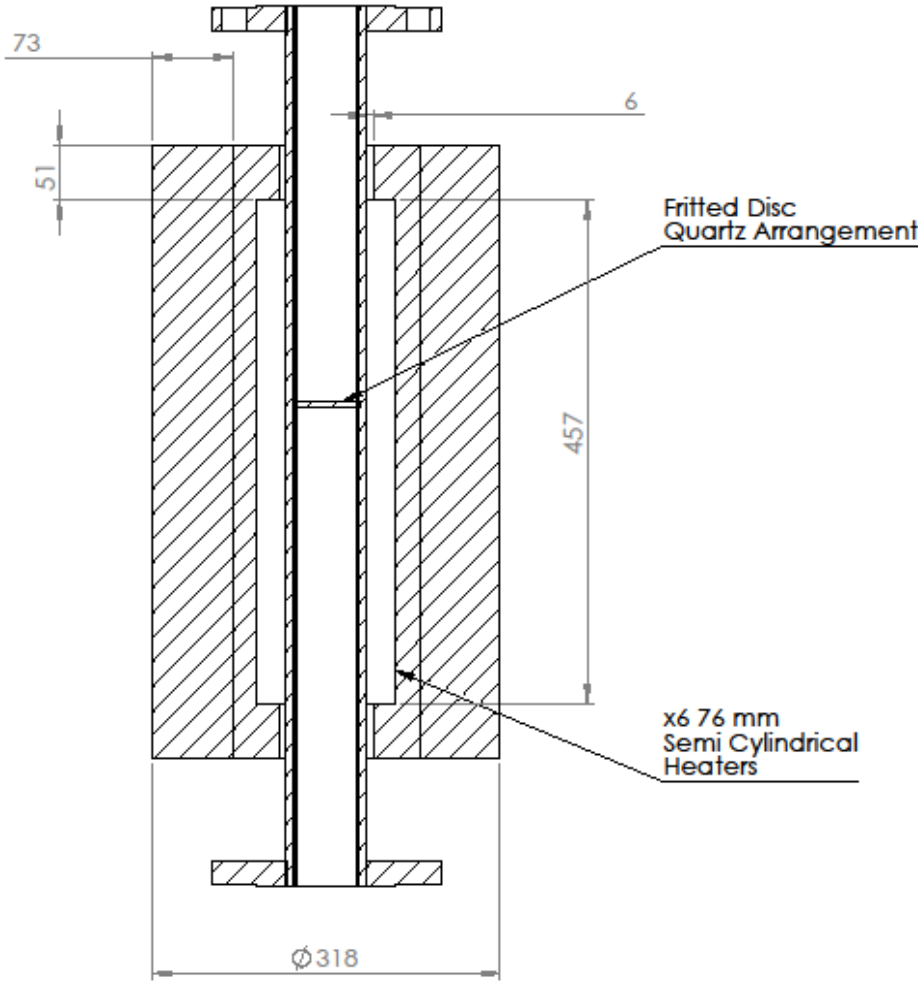

Figure 3-8: Section view of heater and fluidised reactor pipe configuration with a quartz fritted disc at 400 mm.

3.4.1.3 Quartz element design

For operation of the reactor at low residence times a quartz element was constructed. The quartz element refers to a 520 mm section of 40x46 mm quartz tubing which was evacuated and fused. The fused ends were rounded to facilitate the entrance of the gas into the system as well as the even distribution of gas below the sinter. The quartz allowed for significantly lower residence times to be obtained due to an effective volume reduction of 66 %. Subsequently, the quartz liner was modified and the quartz fritted disc was located ~5 mm above the top of the quartz element.

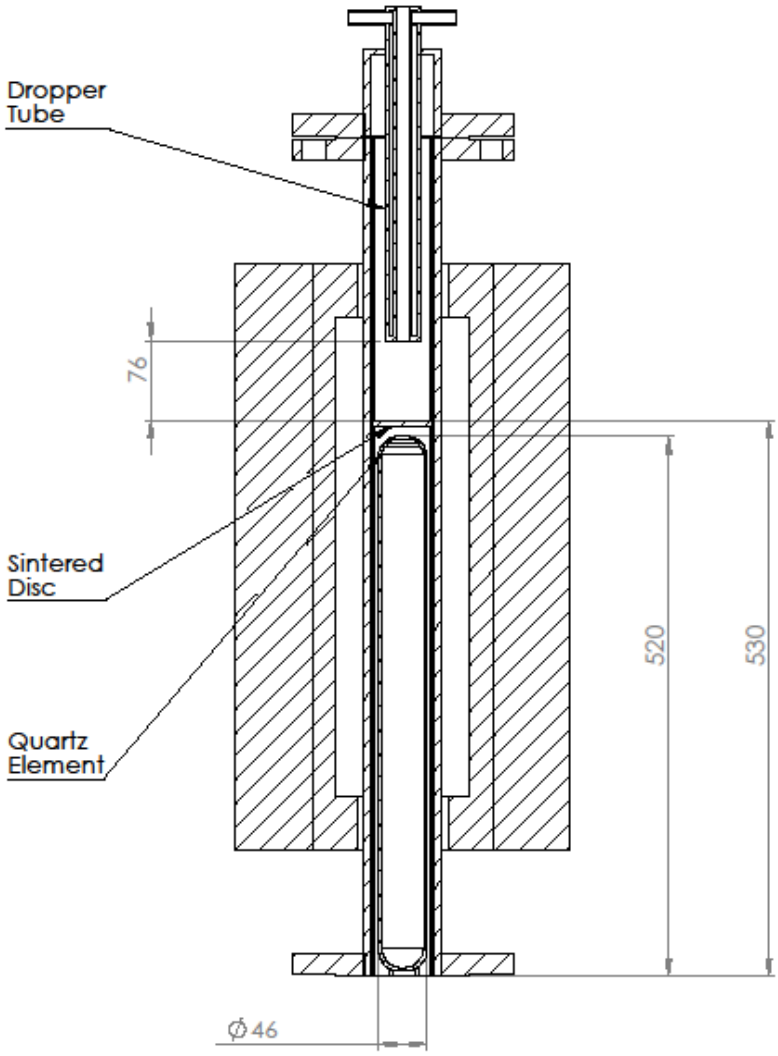

Figure 3-9: Overall interior reactor configuration with quartz element and modified quartz liner.

3.4.1.4 Quartz Liner

As discussed above the quartz liner was a section of quartz tubing which was designed to prevent the interaction of the methane gas and product stream with the reactor walls. The quartz liner also determined the position of the bed within the system, as the quartz frit behaved as a gas distribution plate within the system. A number of different quartz liner arrangements were designed to accommodate for the thermal expansion of the reactor and the expansion of the bed. As described above, the bed expansion could be calculated for the operational flow rates of the system. When conducting multiple trials with differing retention times, the bed expansion varied and the overall bed height was altered by addition/removal of bed material.

3.4.1.5 Calculation Verification

To ensure the intended operation of the fluidised bed reactor the system was comprehensively investigated and trialled to determine in situ system characteristics with calculations.

3.4.1.5.1 Minimum fluidisation velocity

To determine the minimum fluidisation velocity of the system, the overall pressure drop was measured over the reactor. By application of the pressure drop theory summarised in the prior section, pressure drop data collected can be used to determine the system minimum fluidisation (based on Figure 3-2). This system was trialled initially by visually confirming the minimum fluidisation of the sand bed. By removing the quartz liner and installing a rubber bung at the bottom with a gas inlet, the u_{mf} could be measured and compared to values of u_{mf} which were measured when the quartz liner was in the reactor. Determination of the minimum fluidisation velocity was conducted with the feeder tube unmounted from the reactor, allowing visual inspection of the bed. When using 180-250 µm quartz sand, it was discovered that the minimum fluidisation velocity was significantly higher than expected with fluidisation occurring at 0.082 m/s which was estimated based on the gas flow rate and operation conditions in comparison with the previously predicted value of 0.024 m/s. It was speculated that this was potentially due to by-pass occurring about the bottom perimeter of the quartz liner. This was confirmed by removal of the quartz and having the system sealed using a large rubber bung at the bottom, and determining the minimum fluidisation flow rate from outside the reactor pipe. To mitigate this, gasket dressing was applied about the perimeter of the quartz liner, allowing for effective sealing between the bottom flange and the quartz liner bottom. The fluidised bed minimum fluidisation velocities were re-determined with the liner in place. This allowed for the determination of the minimum fluidisation of the system subsequently without gas bypassing. Overall, a minimum fluidisation velocity of 0.029 m/s was determined for a bed height of 56 mm which is closer to the theoretical value. The sealing proved effective with good agreement between experimental values with the quartz in and out of the system as shown in Figure 3-10.

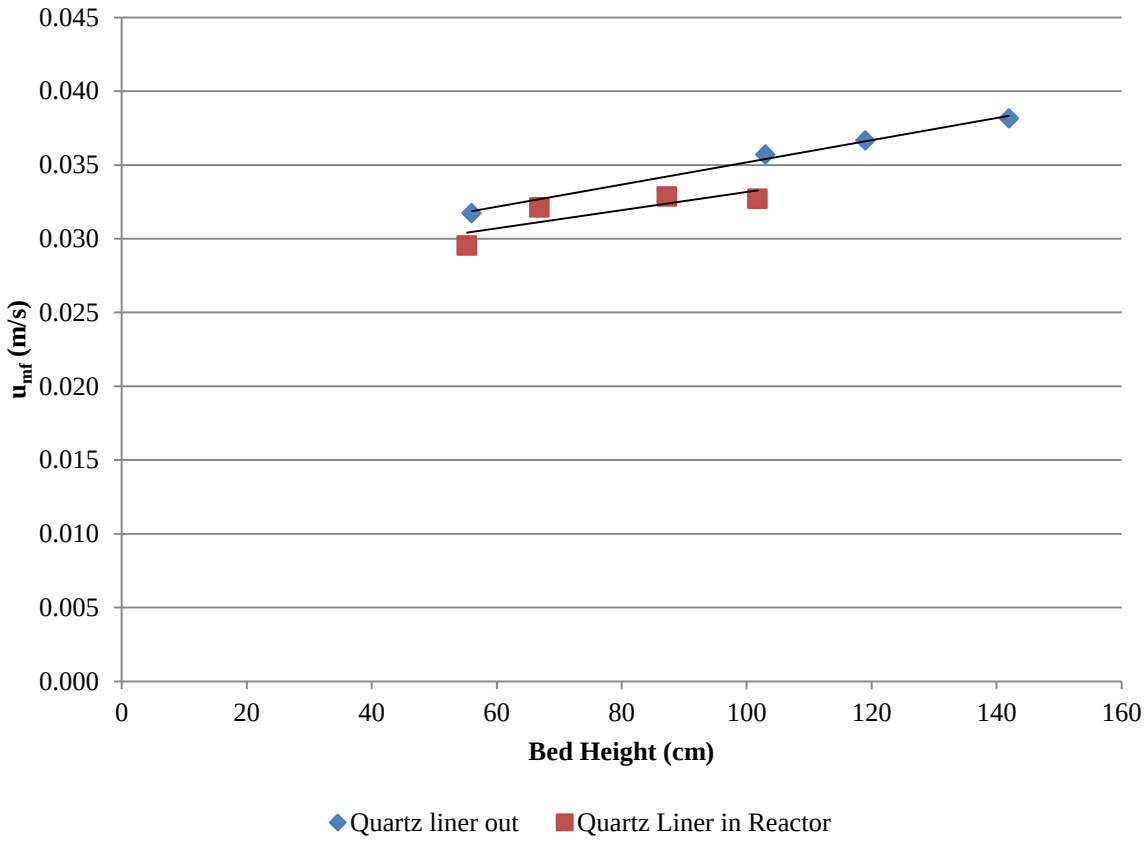

Figure 3-10: Superficial minimum fluidisation velocities determined from visual inspection of the system.

The influence of the particle size was also investigated to determine the influence which the bed particle size fraction had on the minimum fluidisation velocity with the true reactor system configuration. Overall it was found that the decrease in the particle size led to a considerable decrease in the minimum fluidisation velocity. Nitrogen and air were tested for the various particle sizes and good repeatability of the results was obtained, Figure 3-11.

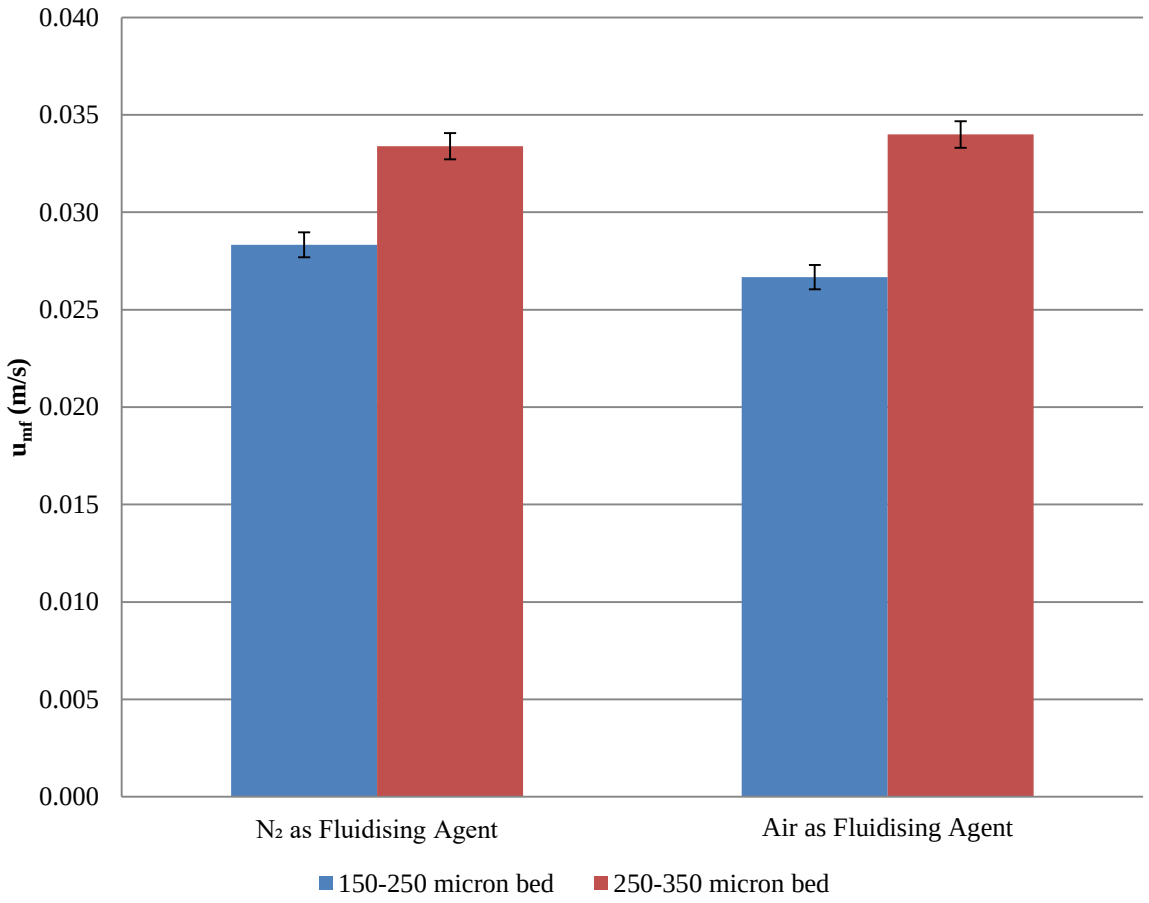

Figure 3-11: Sand bed sieve fraction minimum fluidisation effect for nitrogen and air as the fluidising fluid.

To confirm the above observed minimum fluidisation velocities with theoretical values, the system was reassembled and pressure drop measurements were taken for various mass flow rates. The theoretical minimum fluidisation velocity can be derived from the measured pressure drop, as shown in Figure 3-12, using the Ergun equation (3.2.2). If satisfactory agreement is achieved between the observed and calculated minimum fluidisation velocities, then the minimum fluidisation velocity could be predicted from the measured pressure drop for other operation conditions. To do so the system was pressure tested to ensure there were no leaks within the system. Two trials were conducted with air at 900°C and 20 °C, respectively, with a 56 mm deep bed using 250-180 μm sieved material. To determine the true pressure drop over the fluidised bed system, the process system pressure drops were required to be analysed and quantified. This was important as with increasing temperature the effective system pressure drop differed as well as the effective fluidised bed pressure drop. This then allowed for the overall pressure drop (fluidised bed and system pressure drop) to be recorded and derive the true fluidised bed pressure drop. The modification of the pressure drop was determined by recording the pressure drop of the empty system and deriving a pressure drop curve equation which could then render fluidised bed pressure drop values for the measured pressure drop of

the overall system. This was necessary to take into account the pressure drop over the sinter and the downstream associated pressure drops. Ultimately, allowing for derivation of the minimum fluidisation velocity in accordance to the Ergun equation, (3.2.2).

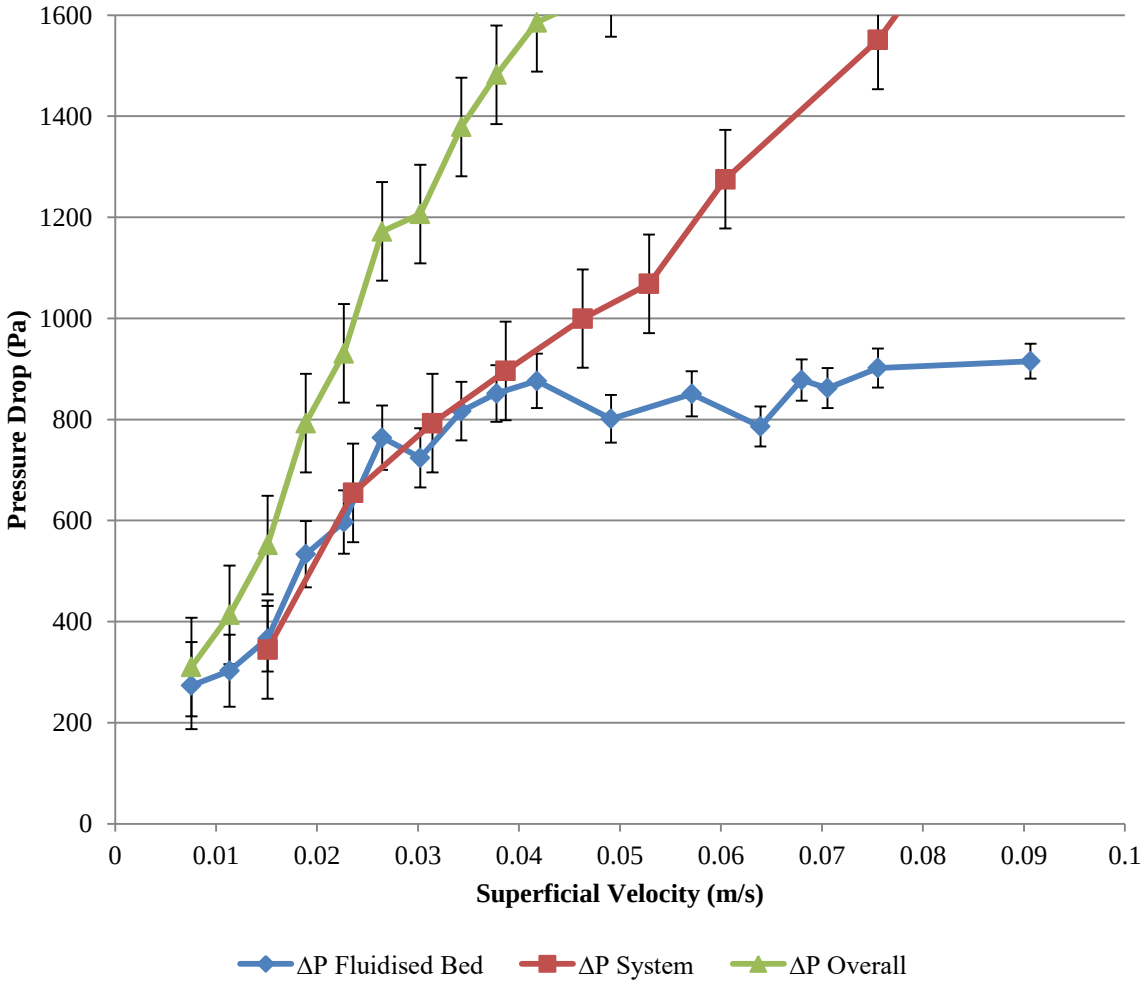

Figure 3-12: Fluidised bed pressure drop experimental results for the identification umin for the system containing a 56 mm bed (180-250 µm sieve fraction) operating at 20 °C with air as the fluidising media.

Deviation of the fluidised bed pressure drop from an upward curve suggests that fluidisation began at approximately 0.035 m/s. Using the gas physical properties in Table 3-8, the values of minimum fluidisation velocities were then calculated for the system operating at 900 °C and the same reactor configuration using values within Table 3-1 as well as the modified Ergun equation (3.3.4). The results are given in Table 3-7. This allowed for determination of the expected minimum fluidisation velocity of the system at the conditions as well as verification of the methodology for the derivation of the methane minimum fluidisation velocity.

Table 3-7: Minimum fluidisation values derived from experiments and compared with literature derived values

Relationship	Gas	Temperature	Ar	Re_{mf}	u(min)
-	-	*[°C]*	-	-	*[m/s]*
Grace	Air	25	8.59×10^{2}	0.636	0.047
Wen and Yu	Air	25	8.59×10^{2}	0.516	0.038
Experimental	Air	25	-	-	0.034
Grace	Air	900	25.1	0.019	0.016
Wen and Yu	Air	900	25.1	0.015	0.013
Modified Ergun Equation	Air	900	-	-	0.012
Grace	CH_4	900	32.5	0.024	0.026
Wen and Yu	CH_4	900	32.5	0.020	0.021
Modified Ergun Equation	CH_4	900	-	-	0.018

Table 3-8: Methane and Air physical properties for different process conditions

Gas	Temperature	Pressure	Viscosity	Density
[-]	*[°C]*	*[kPa]*	*[Pa.s]*	*[kg/m^3]*
CH_4	1000	101	3.49×10^{-5}	0.153
Air	900	101	5.55×10^{-5}	0.300
Air	25	101	1.88×10^{-5}	1.180

To validate the above calculated results, a trial was conducted with air at 900 °C and 950 °C, with a bed height of 50 mm. This allowed for comparison of the calculations with experimental data. It was observed that at 900°C the experimental minimum fluidisation velocity was approximately 0.035 m/s, as shown in Figure 3-13. This value was higher than derived from the relationships from literature, Table 3-7; however, it was suspected that the sensitivity of the equipment effected the accuracy of the derived value. It was also suspected that the higher u_{mf} value may have been an artefact of the sand bed interference with the tip of the feeder tube, effecting gas hydrodynamics which increased turbulence within the system. Nevertheless, due to the system operating much higher than the u_{mf} value, it was concluded that the relationships used to predict the system fluidisation were valid and showed reliability in the derived values. This was particularly the case for Grace relationship as the Wen and Yu relationship, and modified Ergun equation was observed to significantly underestimate the minimum fluidisation velocity from all trials, especially at elevated temperatures. Due to this the Grace correlation was determined as the best modelling equation when determining the characteristics of the reactor fluidisation. The overall expected pressure drop was calculated using equation (3.2.3) resulting in an overall pressure drop of 13000 Pa/m at 900 °C. This can be assumed to be constant between all gases due to the relatively small effect of gas on minimum fluidisation bed voidage and overall gravitational forces. By use of the 50 mm bed this related to an overall expected pressure drop of ~600 Pa.

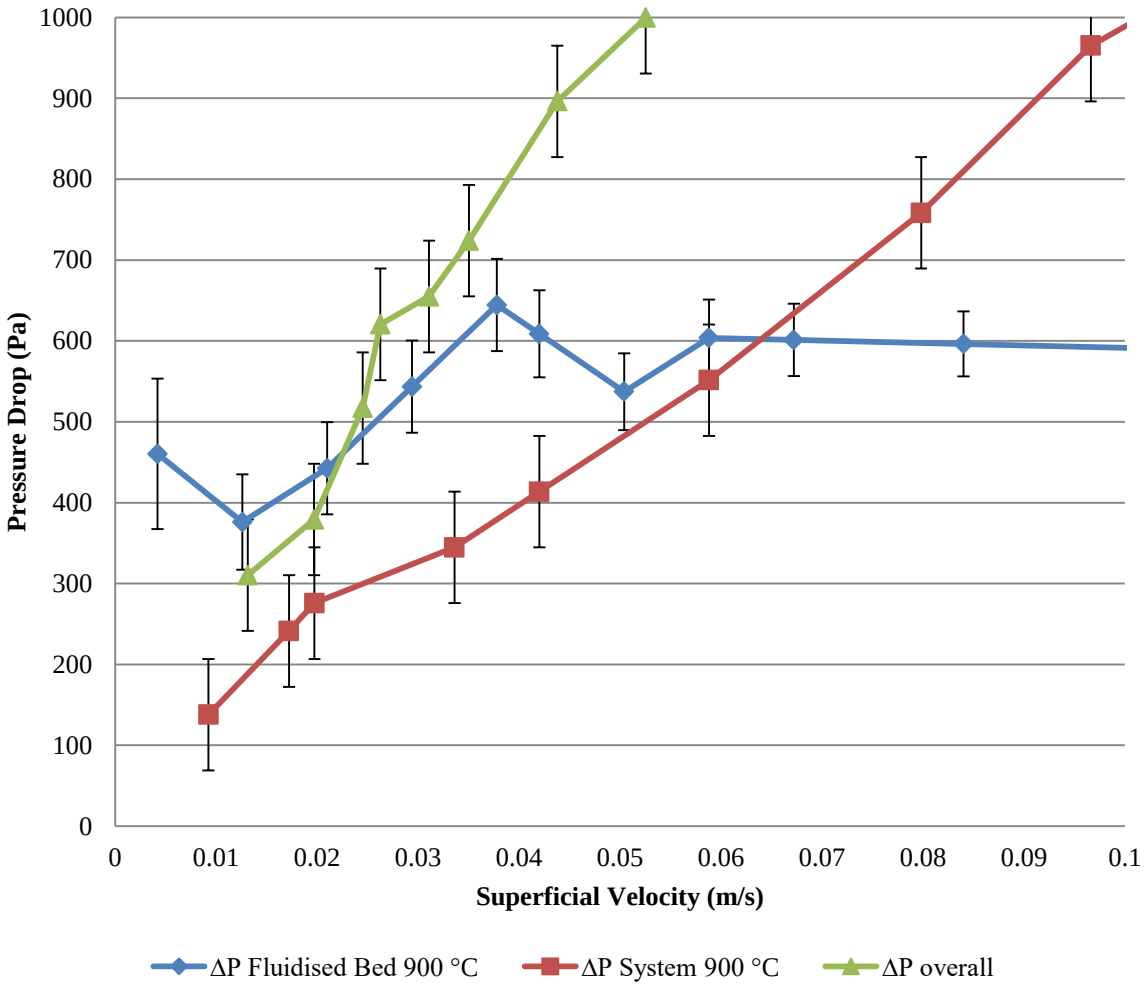

Figure 3-13: Fluidised bed pressure drop derivation and identification of minimum fluidisation velocity for the system containing a 56 mm bed (180-250 µm sieve fraction) operating at 900 °C and 950 °C with air as the fluidising media.

Although the equations were able to effectively determine the process minimum fluidisation velocities, it was observed that there was a difference between the minimum fluidisation derived from the cold model and that from within the reactor system. It was suspected that the difference in system performance may have been due to the presence of the feeder tube arrangement which was situated slightly above the bed. As the bed occupied the space directly below the feeder tube tip, it was suspected that there was some hydrodynamic disturbance which affected the overall minimum fluidisation derivation when operated with the feeder tube in the system. However, this effect was not deemed very significant as the process is operated with a flow rate which is at least three times the minimum fluidisation. It was also determined that due to the low pressure drops recorded the overall sensitivity of the pressure sensor introduced significant error in derivations. However, as concluded to above, the uncertainty was negligible due to the operation of the system well above the u_{mf}.

3.4.1.5.2 Fluidised Bed Characteristics

Table 3-9 and Table 3-10 provide an overview of the bed characteristics during fluidisation of quartz particles in the size range of 180-250 µm. The bed materials size fraction remained constant throughout the methanolysis experiments as the use of differing bed materials was not investigated. From the derivation of the system characteristics it was determined that the system could operate with a maximum operating extent of fluidisation, relating to 22 times u_{mf}. This related to the multiple choices of minimum gas velocity, u_{min}, which could be utilized in the system as long as entrainment of the particles were prevented, e.g., the gas velocity is lower than the terminal particle velocity. The slugging of the fluidised bed was not believed to be an issue as the overall bed height was significantly lower than that at which slugging sets in. For this set of conditions the maximum operating mass flow rate of methane equated 0.450 kg/hr. For the bed characteristics the influence of the gas produced during methanolysis on the fluidised bed characteristics were difficult to quantify, as the extent of gas production determined the extent of influence in the bed characteristics. To ensure the system operates below the threshold of terminal velocity, the cumulative mass flow rate of the biomass and methane did not exceed the overall maximum methane mass flow rate value which was derived. This essentially regarded all biomass fed into the system to be converted to methane and prevented entrainment of the biomass particles. Overall the highest methane mass flow rate trialled, 0.363 kg/hr, did not experience any entrainment of biomass.

To account for the expansion of the bed during fluidisation differing quartz liner arrangements could be placed in the system, as well as differing bed heights. This was important as it was desirable to have the bed fluidising below the feeder tube and preventing excess fluidisation which would cause sand particles to enter the feeder tube. By modification of the bed height and knowledge of the utilized gas velocity, overall bed heights could be estimated and the system could be reconfigured, Table 3-9. Conditions relating to the terminal velocity of the sand particles are also provided in Table 3-10.

Table 3-9: Fluidised bed bubble forming characteristics and height during fluidisation using 180-250 µm sand in fluidised bed.

Parameter	Unit	Symbol	u_{min} x3	u_{min} x6	u_{min} x12	Equation
Gas velocity	*m/s*	u	0.081	0.162	0.324	-
Reynolds number	-	$Re(p)$	7.6×10^{-2}	1.5×10^{-1}	3.0×10^{-1}	$Re(p) = \left(\frac{\rho_g d_p U}{\mu}\right)$
Velocity through annulus	*m/s*	$u_{annulus}$	0.33	0.66	1.31	$u_{annulus} = u_{inlet}\frac{A_{Reactor}}{A_{Annulus}}$
Maximum bubble diameter	*m*	d_{bm}	1.9×10^{-2}	2.6×10^{-2}	3.5×10^{-2}	$d_{bm} = 0.652\left[A_c(u_o - u_{mf})\right]^{0.4}$
Initial bubble diameter	*m*	d_{b0}	1.5×10^{-5}	7.9×10^{-5}	3.5×10^{-4}	$d_{bo} = 0.00376(u_o - u_{mf})^2$
Diameter of bubbles at top of bed	*m*	d_{b1}	4.9×10^{-3}	6.8×10^{-3}	9.4×10^{-3}	$\frac{d_{bm} - d_b}{d_{bm} - d_{b0}} = e^{-\frac{0.3h}{Dt}}$
Bed height when fluidised	*m*	h	6.7×10^{-2}	8.4×10^{-2}	1.2×10^{-1}	$\left(\frac{h - h_0}{h_0}\right)\rho g V_b = (\frac{u_s - u_{mf}}{V_b})\rho g V_b$

Table 3-10: Fluidised bed velocity profile through bed and annulus of feeding system using 180-250 µm sand in fluidised bed.

Parameter	Unit	Symbol	Value	Equation
Sphericitiy	–	Ψ	0.89	-
Porosity at u_{mf}	-	ε_{mf}	0.73	$\varepsilon_{mf} = \frac{0.586}{\Psi^{0.72}}\left[\frac{\mu^2}{\rho_g \eta d_p^3}\right]^{0.029}\left[\frac{\rho_g}{\rho_c}\right]^{0.021}$
Porosity at u_{mf}	-	ε_{mf}	0.43[XIV]	$\varepsilon_{mf} = \frac{0.415}{\Psi^{0.33}}$
Terminal velocity of sand	*m/s*	$u_{t(Bed)}$	2.8	$u_t = \left(1.78 * \frac{10^{-2}\eta^2}{\rho_g \mu}\right)^{\frac{1}{3}}(d_p)$
Terminal velocity of biomass	*m/s*	$u_{t(Biomass)}$	1.5	$u_t = \sqrt{\frac{4d_p(\rho_p - \rho_F)g}{3\rho_G Cd}}$
Annulus effective surface area	m^2	$SA_{annulus}$	5.4 x 10^{-4}	$SA_{Annulus} = \frac{1}{4}\pi({D_{ID(Reactor)}}^2 - {D_{OD(Quartz)}}^2)$
Surface area ratio	m^2	SA_{ratio}	0.25	$\frac{SA_{annulus}}{SA_{Reactor}}$
Effective terminal velocity in bed	*m/s*	$u_{t(Bed,effective)}$	0.37	$u_{t(Bed,effective)} = \frac{SA_{annulus}}{SA_{Reactor}} u_{t(Biomass)}$
Max operating extent of fluidisation	-	β	22.2	$\beta = u_{mf} u_{t(Bed,effective)}$
Max methane massflow	*kg/hr*	$\dot{m}_{CH4,Max}$	0.45	$\dot{m}_{CH4,Max} = u_{t(Bed,effective)} A_{Bed} \rho_{CH4}$
Height at which slugging sets in	*m*	z_s	0.80	$z_s = 60 d_t^{0.175}$

[XIV] Equation deemed not suitable for high sphericitiy particles.

3.4.1.5.3 Heating duty

To determine the heating requirements of the system, a model was created to determine the heating duties required throughout the system, Equation (3.2.30). To determine the specific heats of methane [29] and pine [30], the following equations were used, respectively.

$$Cp_{CH4} = 1340 + 3.15T \tag{3.4.1}$$

$$Cp_{Biomass} = 1160 + 3.87T \tag{3.4.2}$$

From the left hand side of Equation (3.2.30) and considering only the specific heats of the process inlet streams, the heat required for the reactants, $Q_{Reactants}$, has been determined by using Equation (3.4.3) assuming the constant specific heats both for the methane and biomass.

$$\dot{m}_{Biomass}C_{p(Biomass)}(T_f - T_i) + \dot{m}_{CH4}C_{p(CH4)}(T_f - T_i) = Q_{Reactants} \tag{3.4.3}$$

Equation (3.4.3) may be applicable for a small temperature change. However, the specific heats of methane and biomass vary with temperature, an integral form is more appropriate for any given temperature and flow rate within the system:

$$\int_{Ti}^{Tf} [\dot{m}_{Biomass}(1160T + \frac{3.87T^2}{2}) + \dot{m}_{CH4}(1340 + \frac{3.15T^2}{2})]dT = Q_{Reactants} \tag{3.4.4}$$

Given that the design methane mass flow rate was 1 kg/h and that for biomass was 2 kg/h, the overall maximum heat requirement was calculated to be 3.3 kW.

As from Equation (3.2.30), the overall energy balance could be established by the inclusion of the heat losses from the system. To model the heat loss a simple equilibrium heat transfer model was developed which can be separated into two sections: feeding biomass cooler and end flanges. For the model it was assumed that;

- Heat transfer between the reactor pipe above the heater vestibules were purely natural convective heat transfer and were the limiting step.
- Temperature at the midpoint of the system was taken as the average.

- Heat transfer from the product gas to the cooler sleeve was the rate determining step within the water jacketed feeder tube arrangement.
- All biomass feed was converted to gas and modelled as methane.
- All gas flow rate through heated section was modelled as methane.
- All radiative heat transferred from the reactor walls were adsorbed into the quartz sleeve.
- Quartz sleeve was at the same temperature as the reactor pipe.
- All radiation from the outer core was from the quartz sleeve.

To determine the heat transfer about the feeder tube section the system was modelled from the tip of the feeder tube to the reactor outlet, as shown in Figure 3-14 in which T_{w1} and T_{w2} represent the temperatures at the edge of the insulation on both the quartz side and water jacket side, respectively.

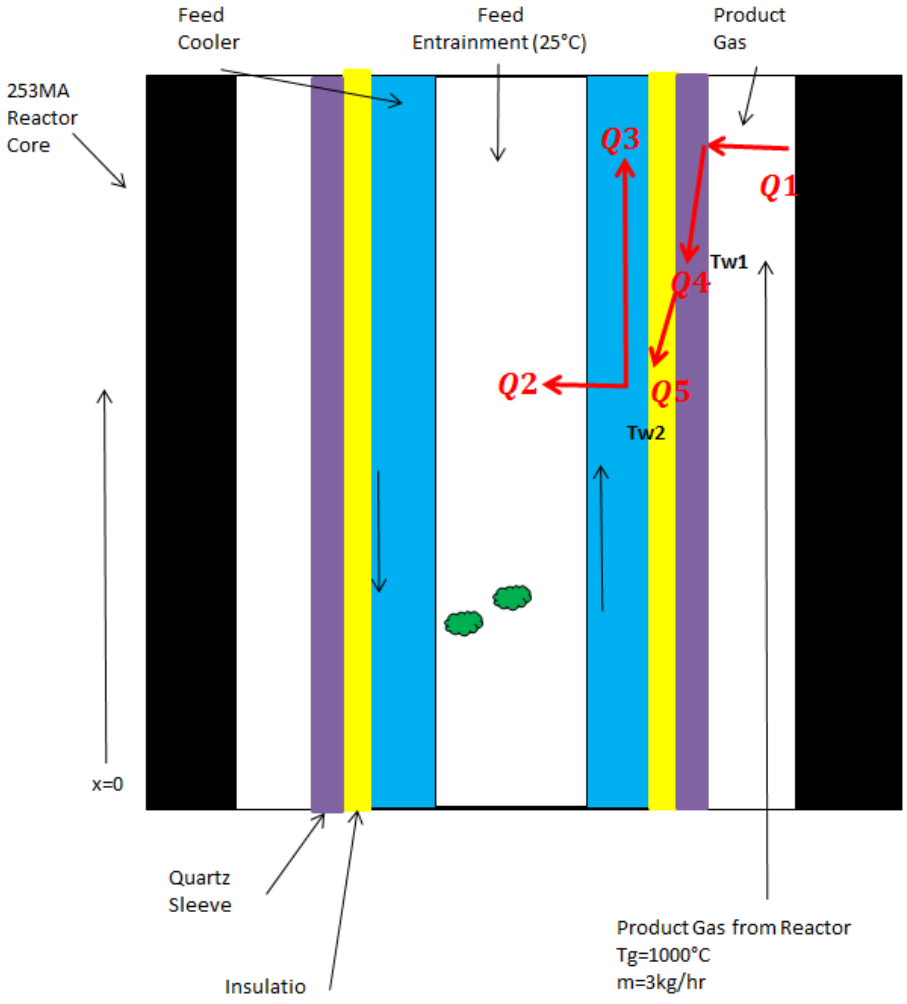

Figure 3-14: Heat transfer model figure for the heat flow throughout the feeder tube section, where Tw1 and Tw2 represent the temperature at the interfaces either side of the insulation.

Table 3-11: Heat transfer modelling derivation for the feeder tube arrangement at atmospheric pressure, as seen in Figure 3-14.

Parameter	Unit	Symbol	Value	Equation	Reference
Product Temperature	*[°C]*	$T_{Product}$	1000	-	
Cooling Water Flow	*[L/min]*	$V_{H2O\ (Cooling)}$	1.5	-	
Reactor ID	*[m]*	$D_{ID(Reactor)}$	$6.0x10^{-2}$	-	
Quartz Sleeve OD	*[m]*	$D_{OD(Quartz)}$	$4.6x10^{-2}$	-	
Quartz Sleeve ID	*[m]*	$D_{ID(Quartz)}$	$4.0x10^{-2}$	-	
Insulation Thickness	*[m]*	$\delta_{Insulation}$	$3.0x10^{-3}$	-	
Feeder Tube OD	*[m]*	$D_{Dropper}$	$3.3x10^{-2}$	-	
Feeder Tube Overall Length	*[m]*	$L_{Dropper}$	$3.0x10^{-2}$	-	
Stephen Boltzmann Constant	*[W/m^2K^4]*	σ	$5.7x10^{-8}$	-	
Heat Capacity of Water	*[J/kg.K]*	Cp_{H2O}	$4.2x10^{3}$	-	
Water Temp In	*[°C]*	$T_{H2O(in)}$	$2.0x10^{1}$	-	
Reactor Surface Area	*[m^2]*	$SA_{Reactor}$	$2.7x10^{-3}$	$\pi D_{ID(Reactor)}^2/4$	
Emissivity of Quartz	*[-]*	ε_{Quartz}	$4.1x10^{-1}$	-	[31]
Emissivity of Reactor	*[-]*	$\varepsilon_{Reactor}$	$6.5x10^{-1}$	-	[31], [32][XV]
Product Gas Density	*[kg/m^3]*	ρ_g	$1.5x10^{-1}$	-	

[XV] Where the emissivity was taken from 347 Stainless steel due to the similar chemical composition

Table 3-11: ***Continued***

Parameter	Unit	Symbol	Value	Equation	Reference
Heat capacity of Product (1000°C)	*[J/kg.K]*	Cp_{Prod}	$5.0x10^{3}$	-	
Product Viscosity (1000°C)	*[kg/m.s]*	μ_{prod}	$3.5x10^{-5}$	-	
Insulation Thermal Conductivity	*[W.m.K]*	$k_{Insulation}$	$9.9x10^{-2}$	-	[33]
Thermal Conductivity of product (1000°C)	*[W/m.K]*	k_{prod}	$2.3x10^{-1}$	-	
Quartz Thermal Conductivity	*[W.m.K]*	k_{quartz}	2.5	-	
Function Handles					
Water Flow rate	*[L/min]*	$\dot{m}_{H2O}$	1.5	-	
Water Temp Out	*[°C]*	$T_{H2O(out)}$	$2.9x10^{1}$	-	
Temperature at Wall	*[°C]*	T_{w1}	928	-	
Q1 Balance					
Product Flow	*[kg/hr]*	$\dot{m}_{prod}$	3.0	-	
Volumetric Flow	*[m^3/hr]*	$\dot{V}_{prod}$	$2.0x10^{1}$	$\dot{V}_{prod} = \rho_g/\dot{m}_{prod}$	
Flow Surface Area	*[m^2]*	SA_{Prod}	$1.1x10^{-3}$	$SA_{Prod} = 1/4\,\pi(D_{ID(Reactor)}{}^2 - D_{OD(\mathrm{Quartz})}{}^2)$	
Velocity	*[m/s]*	u_{prod}	4.9	$u_{prod} = \dot{V}_{prod}/SA_{Prod}\,(1/3600)$	
Effective Diameter	*[m]*	D_{eff}	$3.8x10^{-2}$	$D_{eff} = \sqrt{\frac{4SA_{Prod}}{\pi}}$	
Re(L)	*[-]*	Re_{prod}	$8.1x10^{2}$	$Re_{prod} = D_{\mathrm{eff}} u_{prod} \rho_g/\mu_{prod}$	

Table 3-11: ***Continued***

Parameter	Unit	Symbol	Value	Equation	Reference
Prandtl Number	*[-]*	Pr	7.8x10^{-1}	$Pr = \frac{Cp_{Prod}\mu_{prod}}{k_{prod}}$	
Entrance Effect	*[-]*	L_e	1.5x10^{1}	$Le = 0.0192Re_{prod}$	
Nusselt Number	*[-]*	Nu	8.5	$Nu = 1.86\left(\frac{Re_{prod}Pr}{L_{Dropper}/D_{Dropper}}\right)^{1/3}$	
Heat transfer coefficient	*[W/m^2.K]*	h	6.2x10^{2}	$\frac{k_{prod}Nu}{D_{eff}}$	
Heat transfer coefficient (adjusted)	*[W/m^2.K]*	h_{adj}	6.3x10^{2}	$h_{adj} = h\left(\frac{\mu_{prod}}{\mu_{wall}}\right)^{0.14}$	
Convective Heat Transfer to Quartz	*[W]*	$\boldsymbol{Q1}$	1.5x10^{3}	$\boldsymbol{Q1 = \pi D^2_{OD(Quartz)} L_{Dropper} h_{adj}(T_{Product} - T_{w1})}$	

Q2,Q3,Q4,Q5 and Q_{Rad} Balance

Temperature Drop over Quartz Sleeve	*[°C]*	ΔT_{Quartz}	6.1x10^{1}	$\Delta T_{Quartz} = \frac{Q1}{2\pi k_{quartz} L_{Dropper}} \ln\left(\frac{D_{OD(Quartz)}}{D_{ID(Quartz)}}\right)$	
Wall Temperature	*[°C]*	T_{w2}	8.7E+02	$T_{w2} = T_{w1} - \Delta T_{Quartz}$	
Quartz Heat Conduction	*[W]*	$\boldsymbol{Q2}$	-2.1x10^{3}	$\boldsymbol{Q2 = \frac{2\pi k_{quartz} L_{Dropper}(T_{w1} - T_{w2})}{\ln\left(\frac{D_{OD(Quartz)}}{D_{ID(Quartz)}}\right)}}$	

Table 3-11: ***Continued***

Parameter	Unit	Symbol	Value	Equation	Reference
Heat Transfer to Insulation	[W]	Q3	-9.4x10^2	$\boldsymbol{Q3 = \frac{2\pi k_{Quartz} L_{Dropper}(T_{w2} - T_{w3})}{\ln\left(\frac{D_{ID(Quartz)}}{D_{Dropper}}\right)}}$	
Wall Temperature at Jacket	[°C]	T_{w3}	2.9x10^1	$T_{w3} = T_{H2O(out)}$	
Heat Transfer to Water Jacket	[W]	Q4	1.0x10^3	$\boldsymbol{Q4 = \dot{m}_{H2O} Cp_{H2O}(T_{H2O(out)} - T_{H2O(in)})}$	
Heat Transfer to Feed Stream	[W]	Q5	7.9	$\boldsymbol{Q3 = Q5 + Q4}$	
Radiative Heat transfer					
Radiative Heat Transfer	[W]	$\boldsymbol{Q_{Rad}}$	1.2x10^2	$\boldsymbol{Q_{Rad} = SA_{Reactor}\sigma(\varepsilon_{Reactor} T_{Product} - \varepsilon_{Quartz} T_{w1})}$	

From the model predictions at operation temperature of 1000°C and pressure of 101 kPa, the total temperature increase of the feeding biomass through the whole length of the inner feeder tube was 9 °C at cooling water flow rate of 1.5 L/min. The model also predicted that independent on the flow rate of biomass through the feeder tube, the overall heat transfer would be from the feeding methane stream and gas product to the cooling jacket. This was due to thermal conduction being deemed negligible in the model, as the temperature difference was not suspected of being significant and the heat transfer area was high. It was determined that the feed stream was slightly elevated in temperature due to the conductive heat transfer in the hopper as well. This resulted in the biomass feed being cooled as the chip travelled through the feeder tube. This resulted in an elevated temperature of the biomass feed stream as nitrogen is known to flow through the rotary feeder system.

From the model calculations, it was also apparent that radiative heat transfer contributes ~10 % to the overall heat transfer through the system. This contribution was due to the relatively low emissivity of quartz and the high emissivity of the reactor core. From methane absorptivity of Lee and Happel [34], the methane is relatively transparent at 1000 °C with a total emissivity of < 0.2; hence, adsorption of the incident thermal radiation is unlikely. In practise it is suspected that the radiative heat transfer would in fact decrease significantly due to the surface coating which occurs throughout the system. On the other hand, with the deposition of carbon occurring within the quartz liner it is likely that with the black carbon coating which occurs on the quartz liner, the emissivity of the material increases. The emissivity of graphite and other carbon forms have a very high emissivity of 0.7-0.9 [31] which could lead to an increase in the proportion of radiative heat transfer during methanolysis.

Combining the heat losses estimated and the sensible heating required for the reaction streams the overall heat requirements were approximated at 4.6 kW. A 50 % safety factor was applied on the sizing of the heater as this allowed for the versatility of differing gases in the reaction stream and other reactor configurations. The additional heat was also able to be applied at specific areas and distributed the heating load throughout the reactor and preheater arrangement. This allowed for a versatile reactor arrangement where the temperature application could be varied, whilst, still able to access sufficient power to meet high pressure experiments (where gas mass flow rates, and thus duty requirements are highest).

3.4.1.5.4 Model Verification

To verify the model predictions, the cooling water flow rate and temperatures were recorded in trials at methane flow rates up to 0.36 kg/hr and operating temperature of 1000 °C. From the data collected it was observed that the overall heat duty was independent of the fed methane flow rate as the system at atmospheric pressure as seen from Table 3-12. It was reasoned that the outer temperature of the feeder cooler was constant and the Nusselt number could be assumed from Table 3-2. From the

experimental results it was determined that the heat duty of the jacket cooler was in fact smaller than first calculated. Approximately half of the expected heat transfer was derived from the experimental results resulting in a temperature increase of 3 °C/L of cooling water flow.

Table 3-12: Experimental heat duties of feeder tube water jacket with an operating temperature of 1000 °C at atmospheric pressure, assuming a constant water inlet temperature of 17 °C.

Methane Flow	**Water Flow rate**	**Outlet Temperature of Cooling Water**	**Water Cooling Duty**
[kg/hr]	*[LPM]*	*[°C]*	*[W]*
0.24	1.4	22.5	528
0.13	1.6	21.2	427
0.36	1.5	21.0	420

It was hypothesised that the lower than expected heat transfer to the cooling water may be due to surface effects occurring within the system due to the carbon formation on the quartz sleeve and liner section. It is believed that this increased resistance of the product gas heat transfer to the quartz sleeve has effectively decreased the value of heat transfer rate, Q1, as shown in Figure 3-14. This is due to the low thermal conductivity of carbon black, 0.2 W/m.K in the temperature range (325-425 °K), [35]. Limited data on the thermal conductivity of carbon black is available, however, it was noted from Khizhnyak et al [35], that the thermal conductivity increased slightly with temperature and decreased with particle compression.

It was also suspected that the effective area of heat transfer was significantly different than that which was modelled. As the model refers to the feeder tube directly with no convective heat loss above the vestibules of the heater, the overall heat transfer from the product gas through to the water jacket is decreased. When the model length was reduced to a constant temperature zone of 0.14 m the heat losses were similar to those which were recorded from the experimental trials. This led to the belief that the model accuracy could be improved drastically by decreasing the effective heat transfer length of the system as the convective heat transfer above the heater vestibule was significant. By decreasing the overall length of the effective feeder tube model to 0.14 m the overall heat transfer to the cooling water was decreased to 470 W, in accordance to experimental results, Table 3-12.

In conclusion it was observed that the model was effective to determine the overall heat transfer from the system to cooling water when a characteristic length of the feeder tube in the heated section was

used. This led to an overall heat transfer to the cooling water jacket which coincided with experimental results. It was also observed that the addition of quartz sleeve and kaowool insulation drastically reduced the heat transfer through the system feeder and effectively kept the feed stream cool.

3.4.2 Fluidised Bed Feeder Tube Design

The reactor pipe was sealed flanges at either end, the feeding system was constructed on the top flange to facilitate the removal of the feeding system. The feeder tube arrangement comprised of the gas product outlet, cooling jacket and entrainment flow inlet. The feeder tube refers to the complete flange arrangement and was constructed in one section to allow for the ease of access to the quartz liner and bed environment via a constructed lifting mechanism, Figure 3-15. Fully defined technical drawings can be found in of the Appendix C.

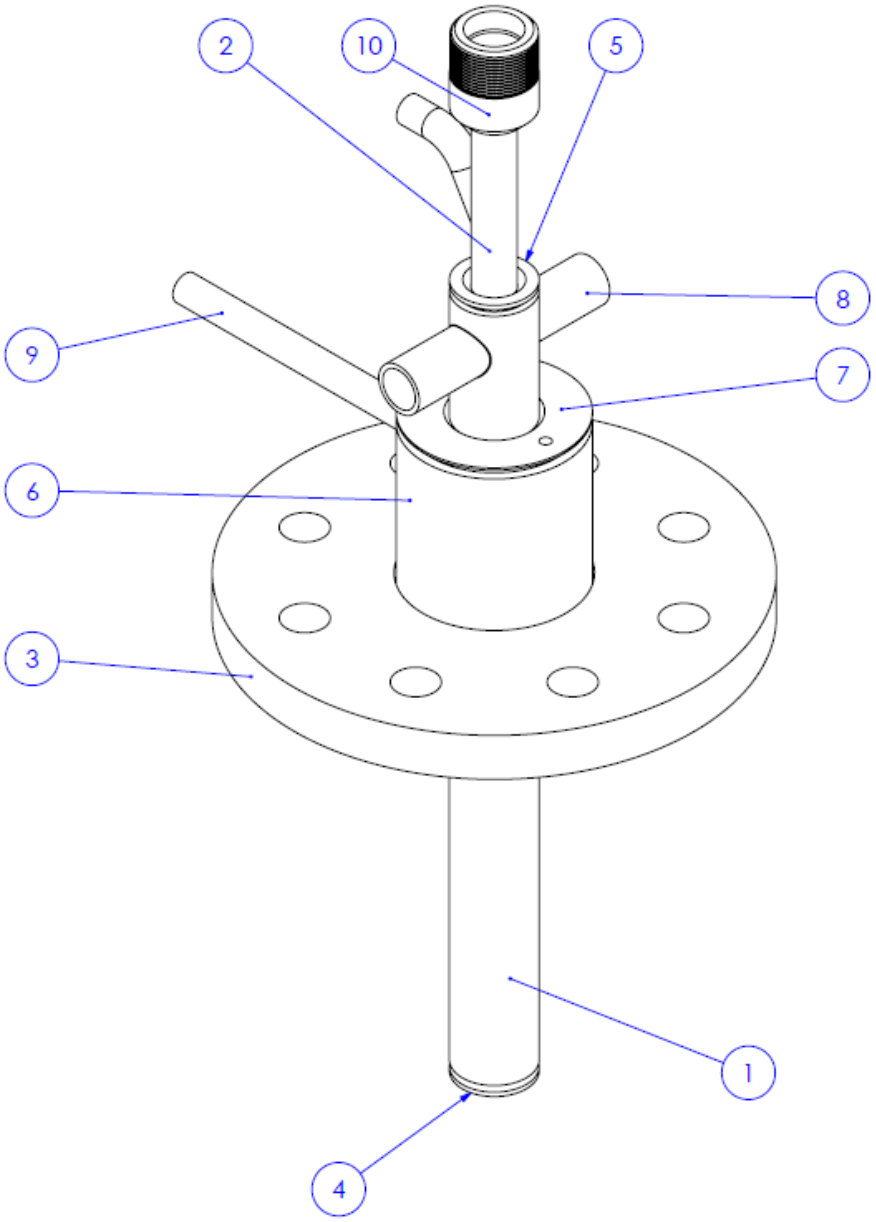

Figure 3-15: Feeder tube arrangement, with legend table below, Table 3-13.

Table 3-13: Legend for feeder tube arrangement shown in Figure 3-15.

Item #	Description	Item #	Description	Item #	Description
1	Jacket Tube	*4,5*	End Cap	*8*	Water Port
2	Feeder Tube	*6*	Pipe Flange Stub	*9*	Product Port
3	Flange	*7*	Jacket Top	*10*	Transition Cone

The water jacket arrangement consisted of two concentric stainless steel pipes which operated from the tip of the feeder tube to the entrainment flow inlet. The interior pipe was fitted with two 250 mm long 3 mm plate sections welded to the edge of the feeder tube. This plate acted as baffles within the water side of the jacket arrangement and promoted good mixing of the cooling water. The inlet flow rate of water was controlled by a rotameter. The entry and exit temperatures of the water were measured by thermocouples to determine the cooling duty of the water jacket.

The product formed during the methanolysis reaction flowed out the product port, as shown as number 9 on Figure 3-15. The gaseous product flowed about the annulus of the quartz liner and the outer of the feeder tube. The diameter of the outer jacket was designed to prevent the entrainment of particles due to the increase in velocity within the annulus. The product outlet line temperature was maintained by two glassrope® heaters (purchased from Hotwatt, U.S.A), which were helically wound about the outlet tubing. The gas outlet temperature was maintained at 400 °C to prevent excess condensation of products occurring. The product outlet and flange top section were both insulated using superwool® (Forman's, Christchurch, New Zealand). A thermocouple port was also fitted to the top section of the reactor through plate 7, Figure 3-15. This thermocouple (Inconel 600, purchased from TC Direct, Australia), allowed for measurements of the bed temperature and was installed with the thermocouple tip slightly above the sintered disc. The inlet for the entrainment flow, tube 2 in Figure 3-15, was fabricated and fitted with an entry angle of 60° facilitating the movement of feed to the fluidised bed.

The core of the feeder tube arrangement consisted of a length of 10 NB SCH10 pipe, with an overall ID of 12.5 mm. This dimension was chosen due to the performance of feeding obtained from the feeding trials, which is discussed in depth in the following sections. This section of tube was fitted with a reducing cone for the entering feed from the rotary feeder. The section was then extended by 205 mm from the bottom of the flange allowing the biomass feed to be introduced directly to the fluidised bed, whilst, reducing heat fluxes to the feeder tip. The feeding tube was water jacketed from the tip of the feeder tube to the entrance of the entrainment flow. This was essential as with the conductive and radiative heat transfer, the particles could have been subject to high temperatures. It was essential to reduce the temperature of the feeder tube as this prevented biomass from early pyrolysis reactions occurring. This was important, as elevated temperatures could cause the biomass particles to be torrified/pyrolysed before entering the system. This could lead to tar volatiles being released and causing adhesion of the particles on the side of the feeder walls, as well as varying reactor operational characteristics. The cooling of the feeder tube also provided a constant feeding temperature of the feed particles regardless of the operating temperature and mass flow rate. The characteristic of constant thermal shock was important as this reduced the likelihood of torrefaction and pyrolysis reactions at higher flow rates, where the effective cooling duty of the jacket is higher.

Throughout the design of the feeder tube it was imperative that all surfaces were smooth and no ledges were present within the system. This was due to the tendency for the biomass particles to bridge and congregate on non-vertical surfaces.

To further prevent unnecessary heat fluxes to the biomass particles, an alumina insulator disc was also fabricated. This disc was installed at the bottom of the end cap, number 4 in Figure 3-15. Two small 3 mm threaded rods were welded at the end of the feeder tube for the insulator to be affixed at the bottom of the tube using locked nuts, Figure 3-16. The arrangement was machined from Rescor 902 alumina silicate (Measure-Tech, Australia) solid bar. The ID of the insulator tip was constructed to be slightly larger than the ID of the feeder tube outlet to prevent particle congregation on the feeder tube surfaces. Overall the alumina insulator added an additional 25 mm to the overall length of the feeder tube arrangement.

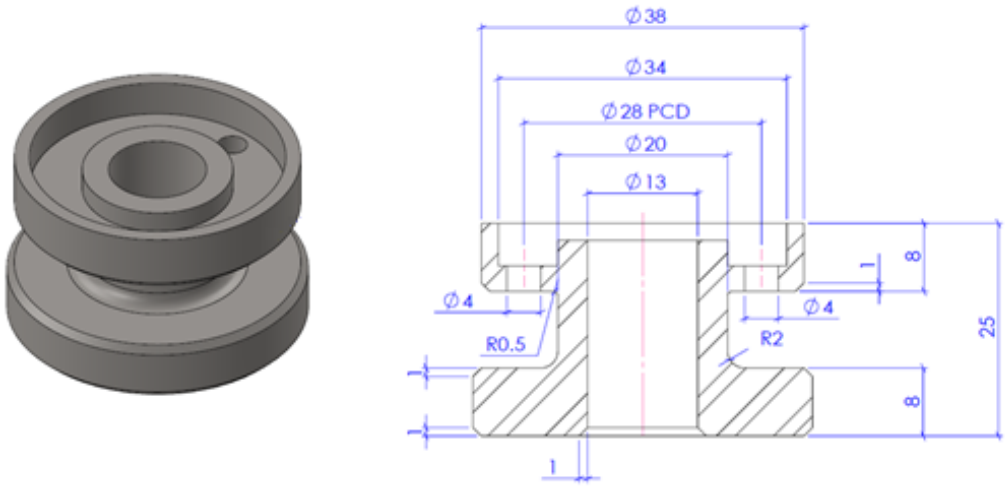

Figure 3-16: Aluminium insulator tip arrangement.

3.4.2.1 Feeder Tube Improvements

Following the commissioning trials with the system all sections of the reactor were removed and inspected. Upon removal of the feeder tube arrangement it was discovered that there was a significant build-up of tars on the length of the feeder tube arrangement close to the fluidised bed. This was observed by a soft aerated black solid build-up which was adhered to the periphery of the feeder tube, with increasing thickness towards the bottom of the pipe. It was believed that this was primarily due to the premature condensation of tars on the outer of the water jacket. To reduce the extent of tar condensation on the outer of the water jacket the system was insulated.

Initially the feeder tube system was modified with the inclusion of a 4 mm interval 304 SS wire mesh. This mesh was designed to be wrapped about the feeder tube with a corresponding blanket of 3 mm superwool about the pipe periphery. A section of the wire mesh was cut and rolled to allow for adequate contact of the superwool on the surface and still allowed for sufficient clearance between the quartz liner. This system was affixed in place with small 304 SS metallic strips, which were welded in place to form a sleeve where the superwool insulation could be exchanged.

From subsequent commissioning trials and some unexpected results, the system was deconstructed and the reactor interiors were investigated. From the dismantling of the feeder tube it was apparent that there were significant carbon deposits on the top of the pipe as well as a brown/red discolouring on the wire mesh, Figure 3-17. The discolouring was believed to be the characteristic of the oxidation of 304 SS. From the commissioning process, the extent of MTD was higher than first anticipated. It was speculated that the steel mesh was catalysing the degradation of methane, increasing the overall hydrogen production. The use of iron and aluminium catalysts has been observed in work regarding methane degradation [36], [37], water gas shift [38] and hydropyrolysis [39]; thus, it was deemed likely that the inclusion of alumina and 304 SS would catalyse the pyrolysis reaction.

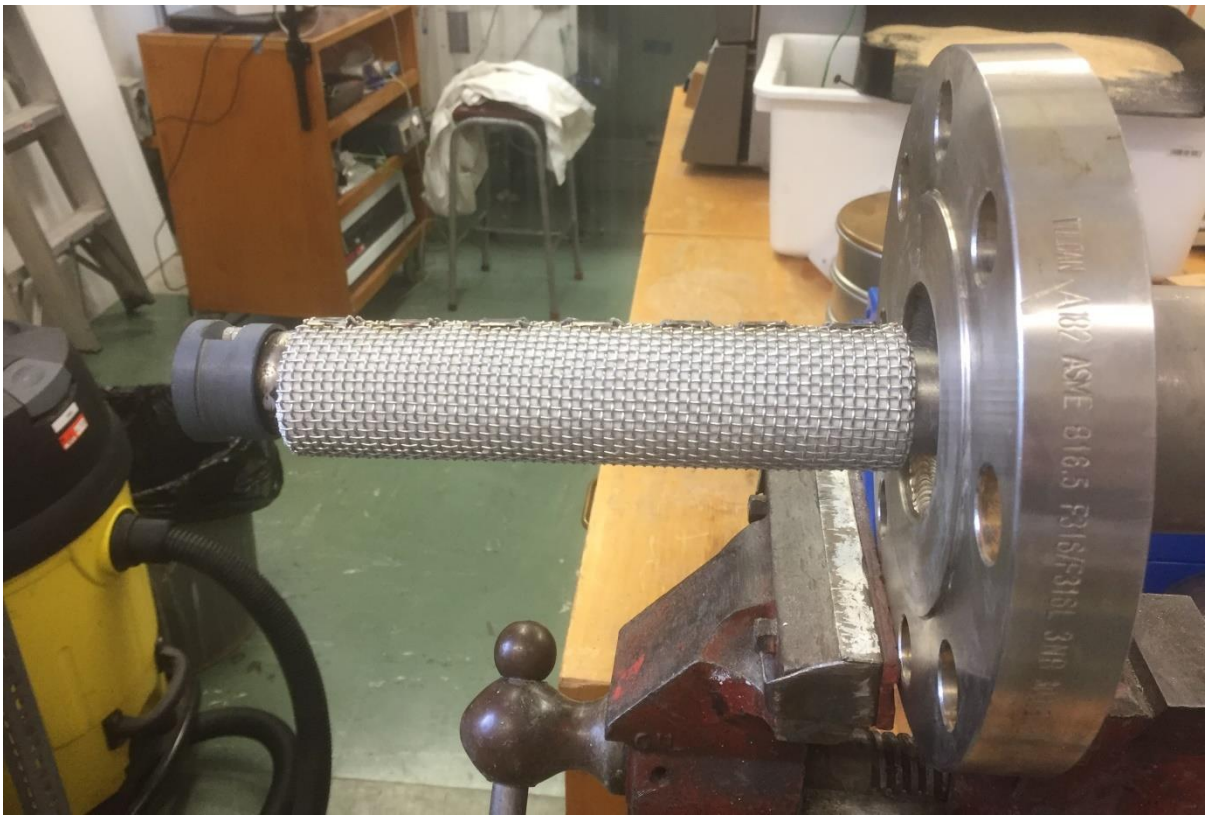

Figure 3-17: Wire mesh and alumina sinter feeder tube arrangement.

To remove the potential effect of alumina and iron inclusion in the system the feeder tube was retrofitted with a customized quartz sleeve arrangement. A complete quartz sleeve was designed as this facilitated the removal of the wire mesh and the alumina sinter as the sleeve essentially provided both functions. The sleeve was fabricated in one piece and was secured at the bottom of the feeder tube using the same lock nut arrangement. As well as the holes allowing the placement of the lock nuts, a 15 mm outlet was also cut into the bottom section. To ensure that the transition between the metal end of the feeder tube and quartz liner was smooth, a small metal packer was fabricated. This was required as welding marks at the bottom of the feeder tube which when the alumina insulator was removed, were exposed.

The overall feeder sleeve was fabricated from 46 x 40 mm quartz tubing with an overall length of 267 mm, with a fused bottom which located the product outlet and lock nuts. This length ensured that the products were shielded from the outer feeder tube pipe until the outlet of the reactor. To prevent excess heat loss, the quartz liner was also fitted with an insert of 3 mm superwool insulation which was installed in the periphery and provided insulation throughout the length. To compensate for the absence of the alumina insulator, two 3 mm superwool discs were fabricated which were placed at the bottom of the sleeve arrangement. This also prevented excess heat at the tip of the feeder tube arrangement. The arrangement could be installed by sliding the quartz over the feeder tube with all sections of the superwool insulation in place, Figure 3-18, allowing for ease of interchange when the insulation had degraded.

Figure 3-18: Quartz sleeve feeder tube arrangement.

3.4.3 Hopper Design

In designing the hopper it was important to determine the characteristics of the particles which are being fed. With proper designing and adequate consideration of the various operating conditions the hopper can be designed to accommodate a range of particle sizes of differing feeds. This is important for the system as it permits different sieve fractions of biomass be used to investigate the thermal and mass transfer characteristics of the biomass particles. During the design of the hopper system it was determined that the influence of interparticulate forces increased with decreasing particle size. The outlet diameter was 23 mm and allowed for a smooth transition to a 25 mm ball valve connection which can successfully feed the biomass particles of 355µm or larger.

It was inherently important to design the system to accommodate the smaller particles which were fed into the system. In designing the hopper for the smaller feed fraction a lower limit of 355 micron was set. Issues arose with the use of fine biomass particles as the inter-particle frictional forces increased with decreasing particle size due to cohesive properties of the chips increasing with decreasing size. This led to increased probability of bridging and arching within the hopper. Bridging and arching are common phenomena which occur with improper hopper design, Figure 3-19. The phenomena are

characterised by cohesion of particles and the linking of particles over the outlet which is able to support the cumulative force of the feed above. Another common undesirable phenomenon which occurs within hopper systems is ratholing. Ratholing is the tendency for only the inner most section of the hopper bin to be fed. This is caused by the cohesive nature of the particles which form a stable deposit of the feed beside a narrow feed outlet. The hopper system was designed to operate in a state of gravity feeding without obstruction, Figure 3-19. This allows the feed biomass to exit the hopper at a uniform and stable flow rate, as well as constant and stable discharge of the hopper following mass flow.

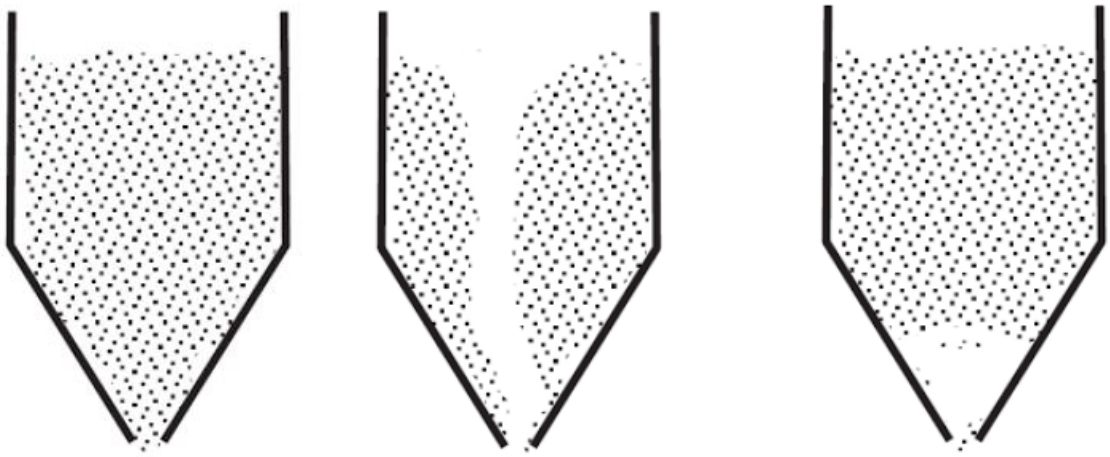

Figure 3-19: Hopper characteristics showing from left to right, Gravity flow system, ratholing and arching within a conical hopper, adapted from [40].

To accommodate for the natural variation in biomass feed, the biomass chips received were further milled to smaller size fractions and trialled in a cold model feeding system. The initial biomass used was ground using an industrial chipper and produced chips with approximate dimensions of 40 x 20 mm, with a relative thickness of 5-7 mm. The chips were prepared off site at Kinleith Mill, OJI Fibre Solutions Ltd., NZ. These chips were dried naturally in a drying room to equilibrium MC. The chips were further milled on arrival using a knife mill in the Forestry Department wood preparation lab, at Canterbury University, further information on the milling characteristics can be found below in subsequent sections.

The cold model feeding system was constructed to investigate the feeding characteristics of the rotary feeder. The arrangement consisted of an electric motor controlled by a VSD. The drive shaft of the motor had been modified and fitted with a jaw coupling which was used to rotate a modified ball valve. Further information on the ball valve arrangement is covered in subsequent sections. The motor

was controlled by a VSD which determined the overall feeding rate of the coupling arrangement, Figure 3-20.

Figure 3-20: Hopper trial model for biomass feeding.

To determine the hopper dimensions the arrangement described above was used alongside the developed conical card arrangements. As seen above in Figure 3-20 the card arrangements were affixed to the outside of the valve body and were used to analyse the required hopper angle. The feeding rate of the chips was varied to investigate the effect of flow rate on the hopper flowability characteristics. This allowed for an investigation into the flexibility of the feeding system. The bottom reducing cone was also modelled with similar geometry as the hopper to facilitate feeding below the ball valve arrangement. A conical hopper was decided upon these investigation results and the unnecessary flat ledges were removed which are known to cause blockages within hopper systems. The configuration of the hopper and the arrangement are crucial for unimpeded flow into the fluidised bed. Due to the pressure considerations, agitation of the hopper was not considered for increased

biomass particle flowability. Auger feeders were also not recommended due to the operating pressure required.

To ensure adequate biomass feeding to the reactor, wood chips were milled and sieved into separate biomass fractions; 1-2 mm, 1-0.6 mm and < 0.6 mm. The angle of repose for each of the differing sieve fractions was determined using standard loose base height and width measurements [41]. From the measurements collected and the internal friction angle of the biomass particles reported by Miccio et al. [42], the overall hopper angle could be determined by Equation (3.4.5);

$$\theta_H \leq \frac{1}{2}(180° - arccos\left(\frac{1 - sin\,\theta_{IF}}{2\,sin\,\theta_{IF}}\right) - \theta_R - arcsin(\frac{sin\,\theta_R}{sin\,\theta_{IF}}) \qquad (3.4.5)$$

The functional hopper angles were then determined by applying a discrepancy value of ± 3° for operating hopper angle and the results of derived hopper angle and angle of repose are shown in Figure 3-21.

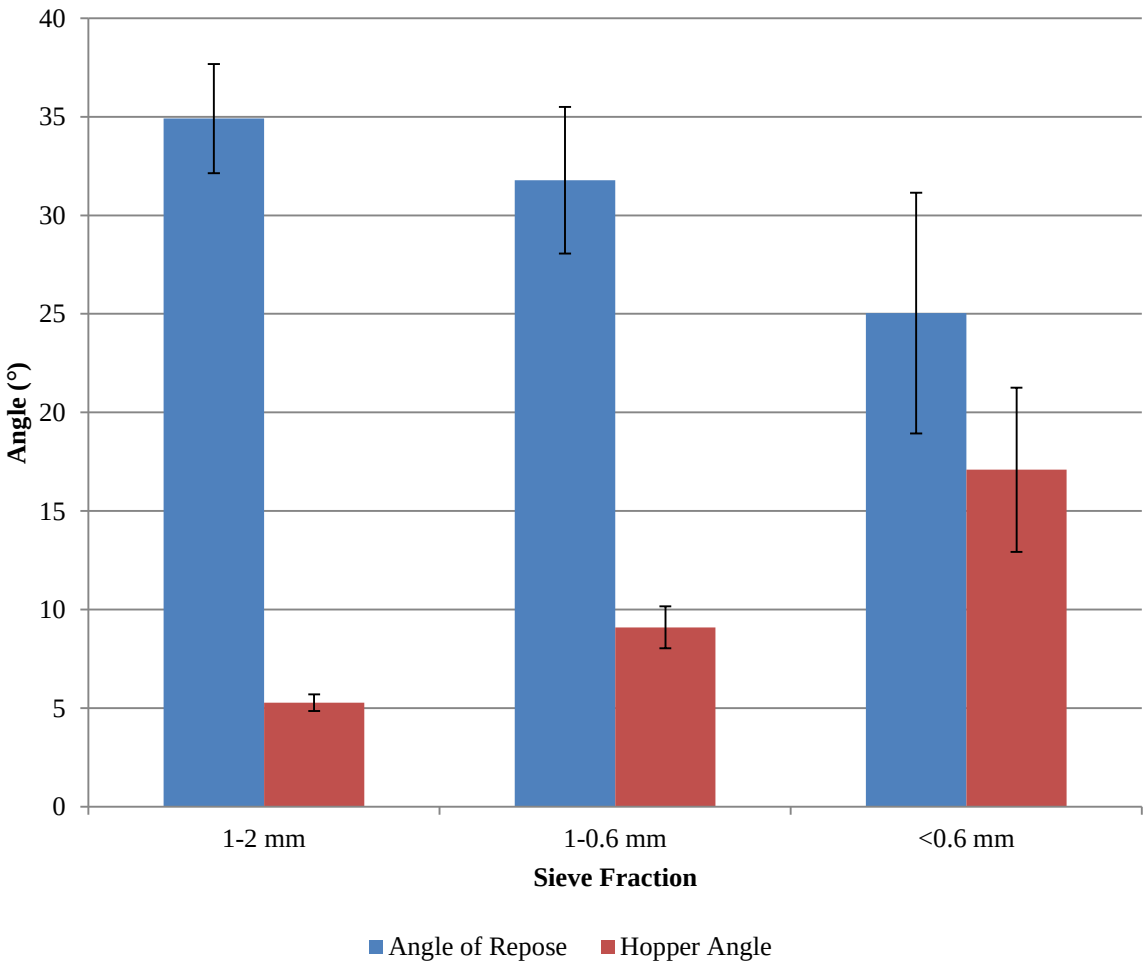

Figure 3-21: Angle of repose and derived hopper angle values.

The measured values agreed closely with those collected from the trials of the developed conical hoppers made of card. As it was desired to have a flexible system which could feed chips of < 1.4 mm, an overall hopper angle of ~5° would be required. With such an angle the overall mass of particles which could be stored in the hopper was deemed insufficient. This was due to height restrictions of the system due to the room space where the reactor would be installed. A high narrow hopper would also affect the ease of use of the system as this would lead to the requirements of scaffolding about the reactor for safe removal of the hopper and feed addition. From an in-depth investigation into the characteristics of the biomass it was found that the milling process and origin of the chips were highly influential on biomass flowability. Thus, the overall hopper design was strongly influenced by these characteristics (further information into the milling characteristics can be found in subsequent sections).

Sawdust collected from SRS Sawmill (Christchurch, New Zealand) was also utilized in a Wiley mill and showed significantly reduced angles of repose in contrast to previously trialled feed. As this characteristic was determined to have a significant influence on the cohesive properties of the biomass chip, repetitive feeding trials were conducted. A number of different hopper geometries were developed at greater angles to determine the effective angle which the feeding ceased. It was determined that the biomass would feed uniformly and under a constant mass flow regime up to a hopper angle of 35-40 °. Trials were conducted with the cold model arrangement and left for 1 hour to allow feeder repeatability and reliability to be investigated. Ultimately it was decided that a hopper angle of 30 ° was appropriate which allowed for reliable feeding through the chip size fractions trialled.

To conclude the design of the hopper a total storage volume of 15 L was desired which allowed for the hopper to store sufficient biomass to ensure 2 hour of operation at the highest flow rate (2 kg/hr assuming a bulk density of 300 kg/m^3). A gas inlet was also installed which facilitated the complete purging of the hopper before and after experiments, Figure 3-22. The outlet of the gas inlet tube was installed concentrically with the hopper biomass outlet and located 80 mm above the hopper outlet to reduce disturbance of the feeding biomass. Whilst purging the hopper, gas was able to be vented out the top of the hopper and aided in increasing the purging efficiency. The hopper could be accessed from a small blind flange which was located on the top of the main hopper flange. At the bottom of the hopper a transition cone was also fabricated allowing for a smooth transition from the hopper to the feeder system. The transition cone was fabricated with the same angle as the hopper and was threaded to allow easy interchange of the feeder arrangement if required. A 25 mm nipple section fixed the ball valve flange to the hopper system, this allowed for easy access into the feeding mechanism and interchange of the rotary feeder arrangement.

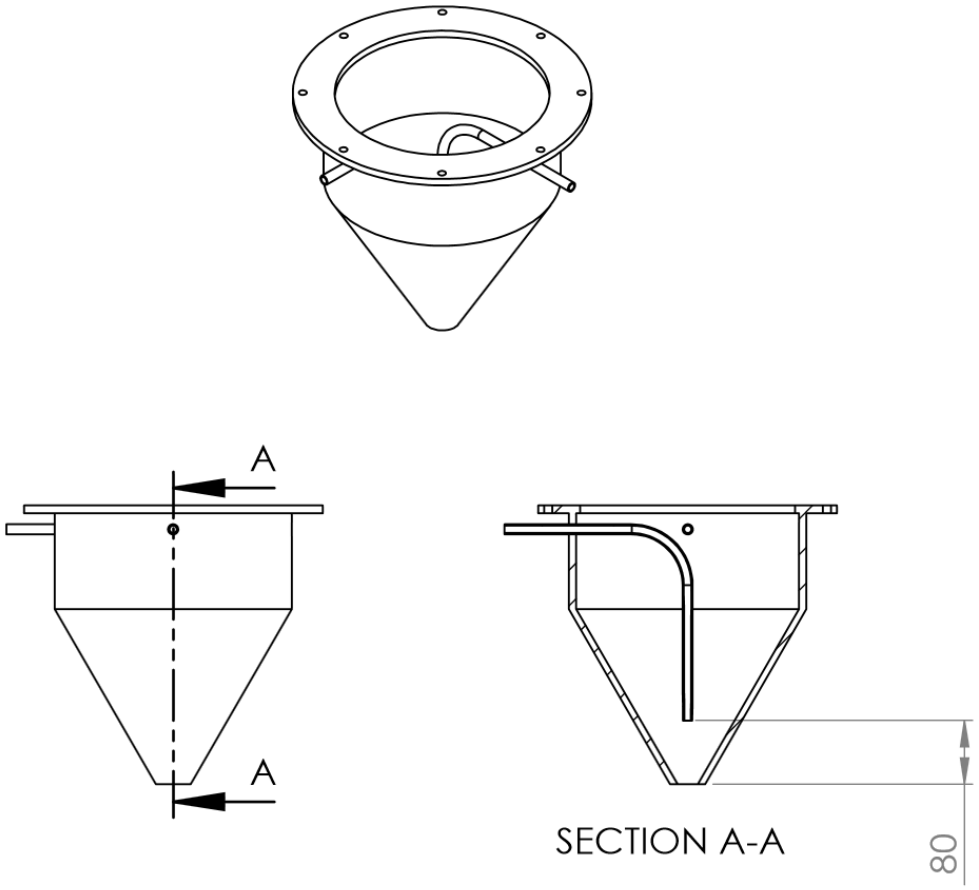

Figure 3-22: Feed hopper arrangement.

3.4.4 Feeder Design

When designing the feeding system it was that the system was able to deliver adequate flow of biomass to the fluidised bed. When determining a suitable feeding mechanism a number of key design aspects were considered;

- The feeding system should allow for continuous and constant flow of biomass into the reactor.
- System was able to produce a biomass feed flow rate up to 2 kg/hr.
- Easy removability and cleaning of the feeding elements.
- Able to operate at slightly elevated temperatures due to expected heat conduction.

3.4.4.1 Ball Valve Feeder Design

In considering the design criteria above, a number of different feeding arrangements were investigated. The feeder tube and hopper arrangements were designed in unison with the feeder arrangement. It was decided to employ a modified rotating ball valve feeder system which was

fabricated from a generic 25 mm 3- piece ball valve supplied from (MRC Global, New Zealand). The interior ball arrangement was modified by the insertion of a 4 mm plate within the rotating ball to produce a 2-cup valve arrangement. This arrangement was constructed by cool shrinking a metallic plate and inserting the rounded plate into the centre of the ball. This plate formed separate cups within the system and allowed the feed to be channelled from the hopper into the cups upon rotation of the ball. As the ball rotated further the biomass simultaneously filled the empty cup and deposited the opposing cup into the feeder tube, Figure 3-23. The ball was located by removal of the ball valve handle and affixing the driving shaft to a jaw coupling, as observed in the cold model Figure 3-20. This allowed the feeding rate to be determined by the VSD setting. The system was sealed by Teflon seals which were supplied with the valves. A number of different thicknesses of plates were inserted into different balls for the attainment of various biomass flow rates. 3-piece ball valves were chosen as this readily allowed for dismantling and exchange of the ball valve inserts.

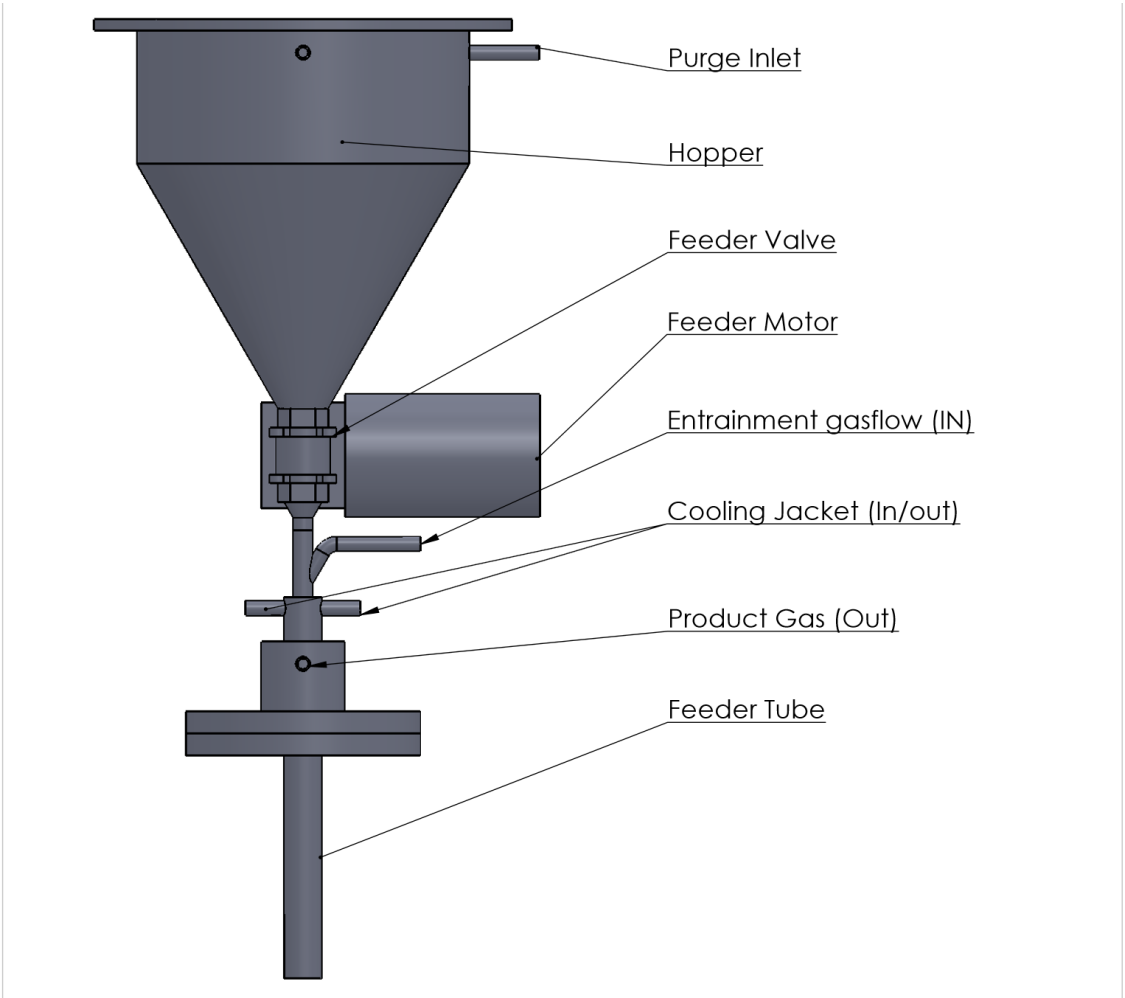

Figure 3-23: Feeding tube full arrangement with the inclusion of the rotating ball valve arrangement to show the path of biomass through the system.

During the designing phase of the hopper the cold model system was also used to observe the interactions of the ball valve and the feeding characteristics. A 2-cup rotating ball feeder was initially

designed to investigate the feeding characteristics of the designed system, Figure 3-24. After the system was constructed the feeding system was calibrated with the hopper and feeder tube in place. This allowed for observation of the feeding characteristics which would be expected in the system. It was found that for the lower flow rates the size of the cups were too great, causing the feed to flow in discrete amounts down the feeder. This caused irregular feeding as it was visible that no feed exiting the feeder tube at times. This was undesirable as it was suspected that in the hot system this would cause sudden increases in volumetric flow rate and induce fluctuating operating pressures. To decrease the intermittency of the biomass feed, the ball valve system was re-designed to allow for a multiple cup arrangement.

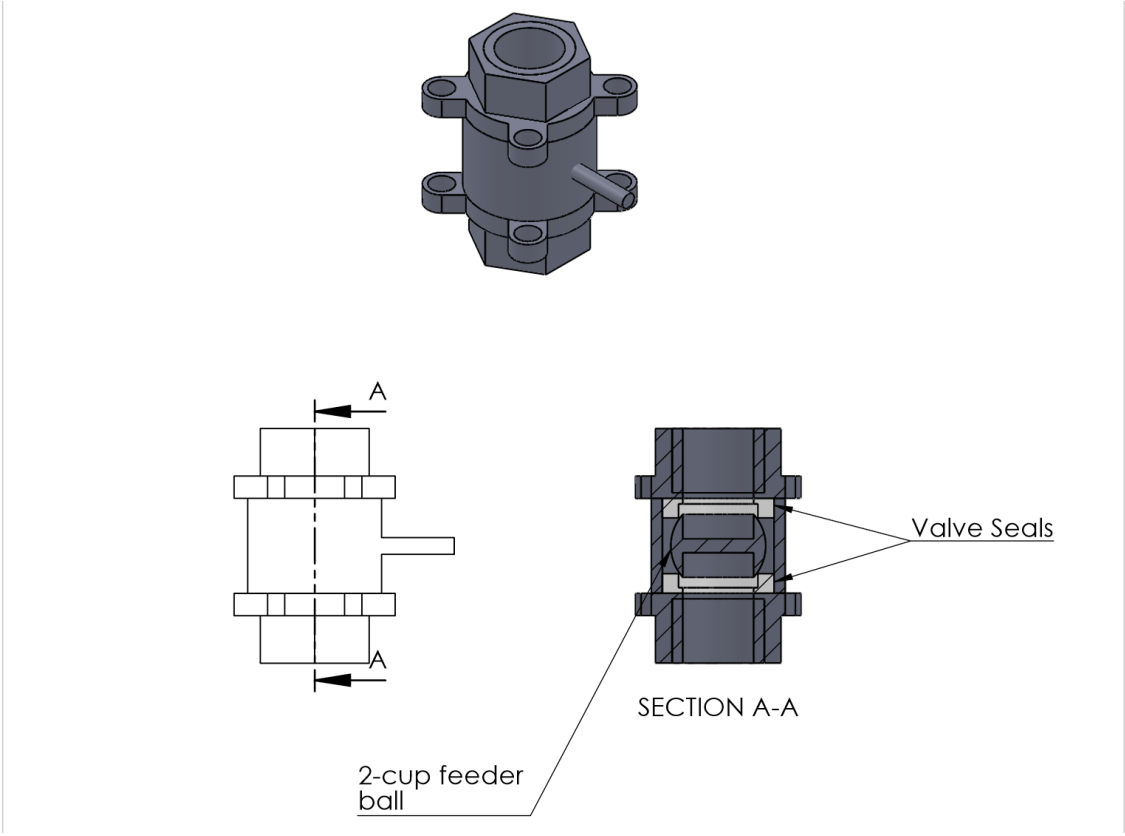

Figure 3-24: 2-cup feeder arrangement.

A multiple cup design was utilized on the periphery of the rounded edge of the ball valve insert. This allowed for the cups to be placed in a pattern about the circumference, where the pattern was determined by the cup diameter. The cups were milled using a rounded end cutter to facilitate the removal and entry of chip into the cups during rotation. The original driveshaft for the ball valve was located on a recessed slot on the rounded edge of the ball valve. This slot was milled and fabricated according to cup size for the pattern. To compensate for the removal of the driveshaft slot the interior of the ball valve insert was retrofitted with a cylindrical insert which had an overall length slightly

less than the ball depth. This allowed the existing arrangement of the motor system to be altered for the reduced drive arm length.

The system was trialled and the particle distribution during feeding greatly improved. A modification with smaller diameter cups was also fabricated to achieve the lower mass flow rate requirements. It was observed that the continuity of feed was significantly enhanced by using a smaller diameter cup insert with a high rotational frequency. This was due to a larger number of small cut portions being fed with time, hence, increasing the regularity of particles during feeding. The length which the chip required to travel to reach the tip of the feeder tube also provided natural product distribution. This allowed for continuous biomass flow which was observed to have no obvious signs of intermittent feed at the exit of the feeder tube.

It was also believed that during the operation of the feeder arrangement static electricity accumulated. This was observed as biomass particles were electrically charged to the metallic surfaces of the hopper wall, feeder tube and rotating ball. It was apparent that the particles were charged due to the dispersion of the chips when subject to a magnetic field. It was hypothesised that the chips gained charge due to the friction of the Teflon seals and the metallic ball insert during feeding. The electric charge was not observed to cause any direct influence on the flowability of the chips, however when measuring the overall remaining mass discrepancies in expected values were determined. This was due to the difficulty in removing the remaining biomass within the hopper when the experiment had finished. It was also apparent that the effective overall mass flow rate decreased due to the electrostatic charges. This was suspected to be due to the adhesion of chips on the surface of the cup which was not removed during the rotations, thus reducing the effective volume fed during each rotation.

After subsequent experiments it was discovered that the integrity of the Teflon seals decreased. Due to the biomass resting between the cups it was possible for the chip to grind against the seal during the rotating of the feeder ball. From cumulative rotations the seal became degraded and as a consequence increased the flow rate of nitrogen gas between the hopper and reactor system. The direction of the gas flow rate was dependent on the operating conditions of the system and overall pressure differential. If the pressure of the hopper was not higher than that of the reactor the effective gas flow would travel upwards to the hopper. Increases of pressure were believed to occur due to the release of volatiles and gas upon methanolysis. This was believed to be the cause of blockages which were occurring during some trials. At times trials were aborted and it was found that a significant amount of biomass was stuck in the feeder tube. When the system was taken apart, it was observed that the biomass had blocked near the exit port with a black tar like substance adhering chips to the side of the feeder tube. It was suspected that with the varying forces exhibited on the falling particles the velocity of the chips varied. If the pressure differential was sufficient it was speculated that the drag force in

fact became larger than the gravity force, and reverse particle flow occurred. With the differential pressure, hot methane gas was able to pyrolyse/torrify the feed biomass before entering the fluidised bed and it was suspected that tars were released causing the blocking of the feeder tube. Ultimately, this would cause bridging of the biomass feed and the experiment would be abandoned.

From the investigation into the feeding characteristics it was concluded that the feeding mechanism needed to prevent the flow of gas upward from the reactor environment to the hopper. A major design fault of the initial feeding mechanism was the large void space between the periphery of the rotating ball insert and the valve housing. With the wearing of the valve seals this facilitated the flow of gas throughout the feeding body, as the surface area of the seal was relatively small in comparison to the ball insert. The geometry of the insert also allowed an unobscured movement of gas at times, with an undisturbed path formed when the trough of the cup was completely over the seal, Figure 3-25.

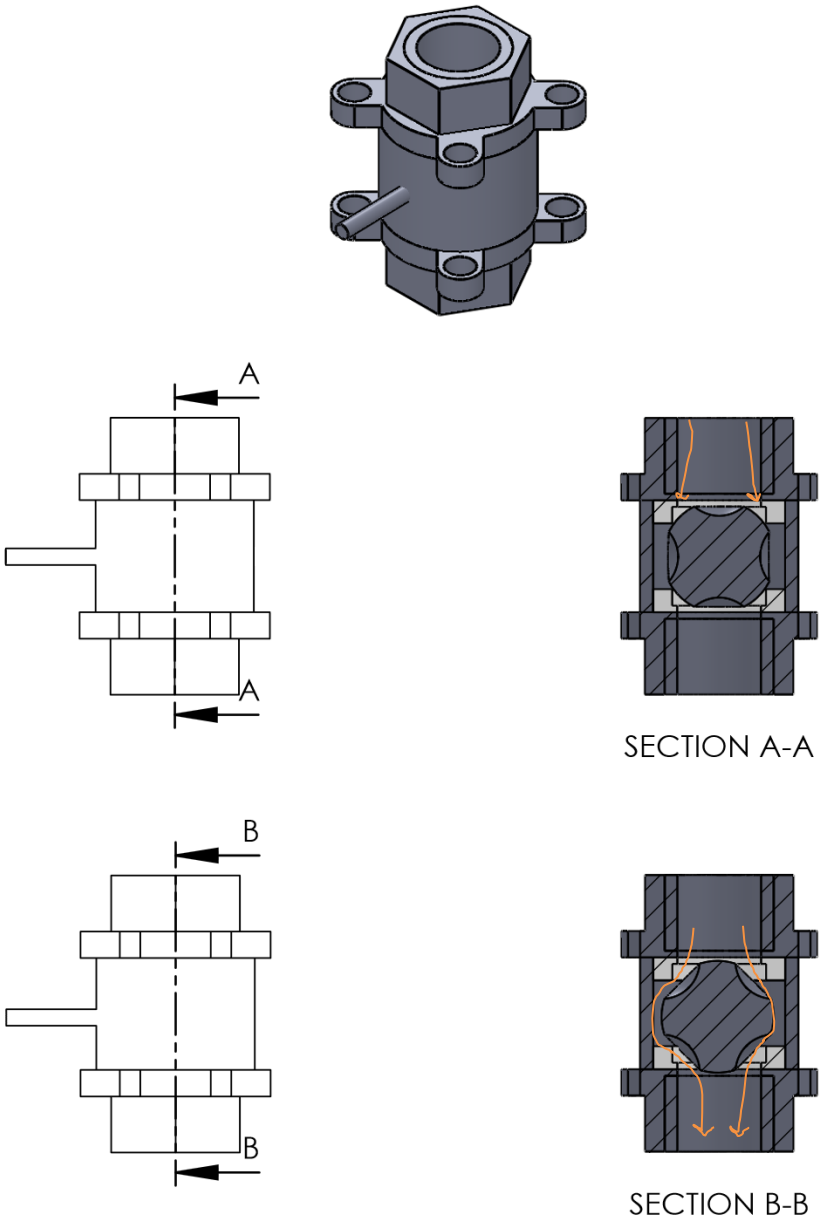

Figure 3-25: Ball feeder system and extent of gas seepage, represented in orange, over the valve in relation to the ball position.

3.4.4.2 Rotary Valve Feeder Design

From the commissioning experiments it was concluded that the movement of gas from the fluidised bed region to the hopper needed to be minimized. It was decided to remain with the feeder cup concept as previous trials had desirable particle dispersion and feeding stability. Keeping with the rotary cup system, the feeder system design was overhauled and the interior valve body was designed to increase the effective sealing area. To provide this, a brass housing was manufactured which housed small rotary inserts, Figure 3-26. The rotary inserts were installed via the side of the housing and allowed for the existing driveshaft to be used. The inserts were made to be a push fit into the brass

housing. Brass was chosen as the housing material as this allowed for an ease in milling during the conceptual stage. The housing was constructed to locate the rotary insert within the valve body and utilize the existing driveshaft system. To ensure adequate sealing about the periphery of the valve, the valve body was machined to enable a friction fit between the brass housing and the valve body. The housing design utilized the existing Teflon seals to reduce gas flow through the valve body.

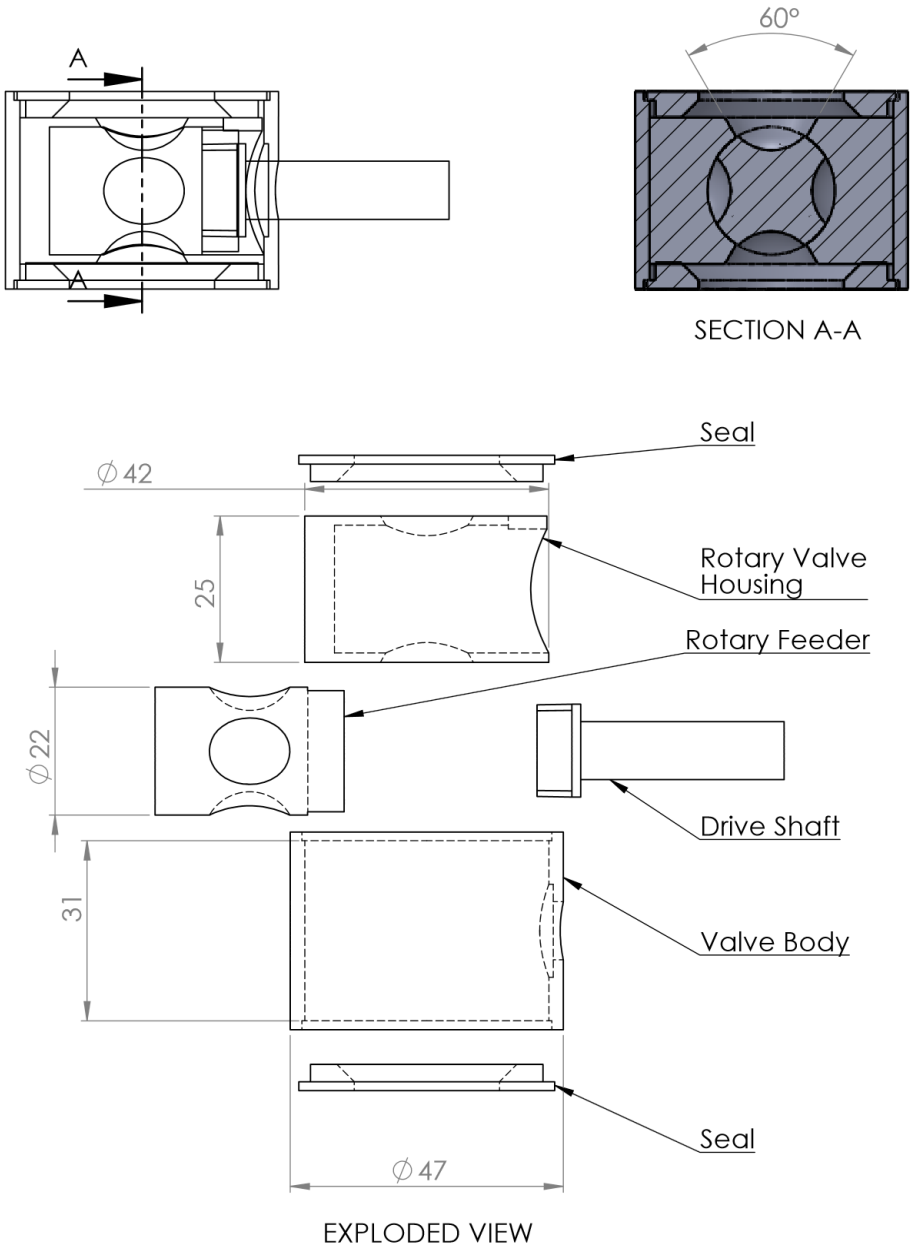

Figure 3-26: Valve, Brass housing and rotary feeder insert arrangement.

The brass housing was manufactured and a trial insert made from acetyl was utilised in the system. The feeder system arrangement was observed to feed well with good characteristic flow; however, the structural integrity of acetyl was problematic with shearing occurring at the driveshaft slot. To remedy

this inserts were fabricated from solid graphite reinforced polyether ether ketone (susta PEEK mod) sourced from Dotmar (Christchurch). Susta PEEK mod is a semi-crystalline advanced material which is exceptionally strong and temperature resistant. Susta PEEK mod is commonly used in high grade bearing manufacturing for extreme wear applications. The graphite reinforcement allowed for effective self-lubrication during rotation of the insert in the housing. This was desirable as the system was designed to inhibit gas flow through the system by inducing a larger pressure drop over the feeder system. The addition of graphite in the susta PEEK mod was also beneficial given the electrostatic charge which was exhibited in previous trials. As the graphite addition allowed the plastic to behave as a conductor it was believed that the static electricity produced would dissipate throughout the feeder arrangement.

In total three separate rotary feeder inserts were fabricated. As the majority of the experiments which were envisaged initially were at lower pressures, the cumulative range of the feeder inserts allowed for flow rates of 0.02-0.25 kg/hr, Figure 3-27. To obtain higher mass flow rates, a new rotary valve insert could be fabricated with deeper and larger cups; however, for the experiments conducted the flow rates of 0.02-0.25 kg/hr was sufficient. The three inserts were fabricated with differing depths of the cups formed with the same snub-end drill bit. This allowed for each valve insert to optimize a specific flow rate region as the biomass fed per rotation increased with increased cup depth. With decreasing cup depth the overall diameters of the cups allowed for the inserts to be fabricated with more cups overall. This ultimately led to the design of three separate valve inserts with 4, 6 and 7 cups overall. By increasing the cups available per rotation, the feed was able to be distributed more regularly. Decreased rpm of the feeder was also observed to be a factor for the feeding characteristics. It was observed that when the valve insert rpm decreased below 20 Hz the particle flow became periodic. Because of this it was implied that the rotary inserts only be used above 25 Hz, with the highest used when multiple inserts can achieve the flow rate. Overall by the use of the PEEK (Poly Ether Ethyl Ketone) rotary insert design, a flexible and easily interchangeable feeding system was developed. As the biomass flow rate demands are dependent on the experimental parameters (pressure, residence time and biomass/methane ratio) it was envisaged inserts could be fabricated in accordance to flow rate requirements.

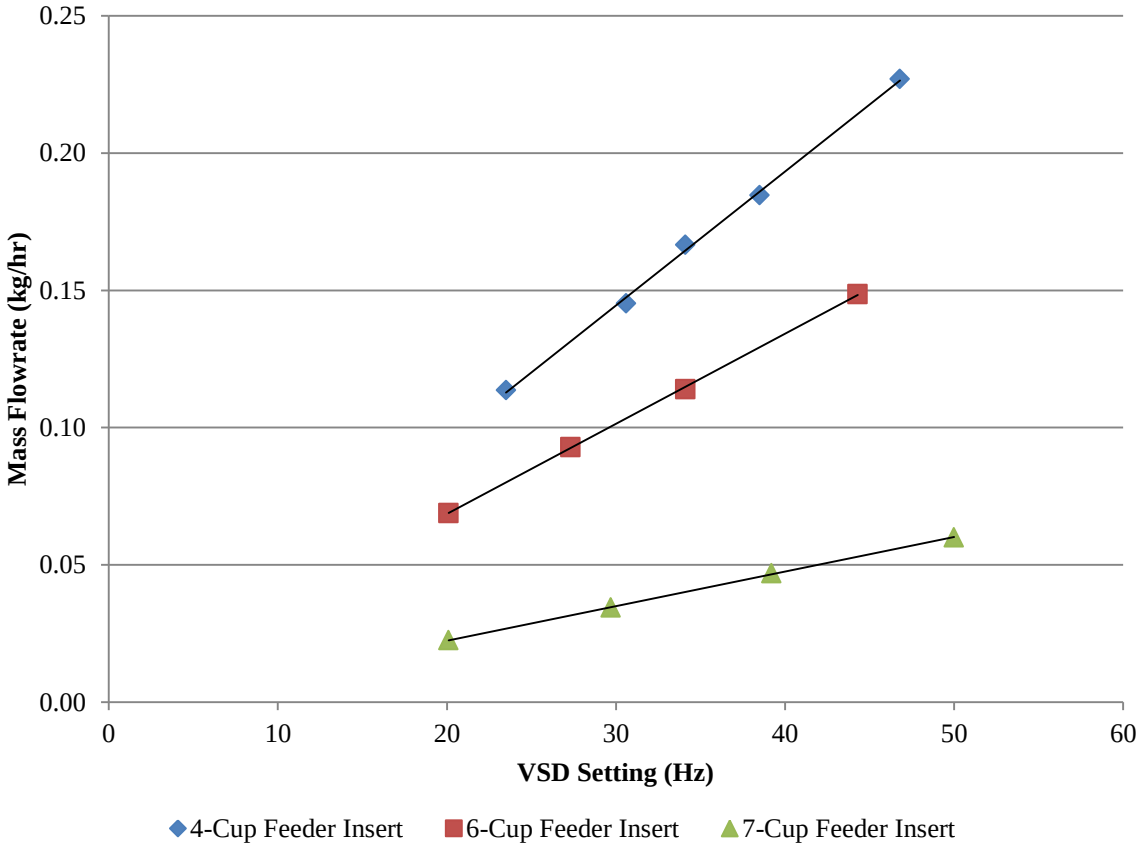

Figure 3-27: Extendable region of biomass feed flow rates obtained by the various feeder arrangements, overall obtainable mass flow rates of 0.023-0.230 kg/hr.

Following experiments with the rotary valve inserts showed good structural integrity. The feeder characteristics were also enhanced with the newly designed rotary feeder, especially at the lower flow rates achieved with the 7-cup feeder insert. As the majority of experiments were conducted at lower pressures this arrangement was the most extensively utilized throughout the experimental trials. The design was observed to effectively decrease the overall flow rate of product gas upwards toward the hopper as trials at lower pressure exhibited enhanced hydrodynamics. However, problems were still encountered with the higher pressure trials. As the operating pressure increased, induced pressure differentials were apparent due to the incorrect pressure setting of the hopper. From the movement of gas from the reactor to the hopper it was apparent that the seal formed by the susta PEEK mod insert within the brass was not sufficient at high pressure differentials. This in turn changed the operational procedure of the system. Due to this restriction between the hopper and reactor, this pressure drop was utilized by allowing a small flow rate of nitrogen to enter the hopper. This allowed the hopper to be always slightly over pressurized in comparison to the reactor. The overpressure enabled sufficient flow of gas through the feeder tube. This effectively controlled the pressure differential between the hopper and reactor, and allowed for control over the flow direction throughout the valve body.

Overall this differential pressure resulted in a small flow rate of nitrogen which was passed through the ball valve body. As the feeder tube had an additional entrainment flow of methane entering just below the reduction cone, the effective concentration of nitrogen about biomass particles could be decreased. The nitrogen flow rate was comparatively small in concentrations, typically comprising of 3-5 % in the outlet product gas. Without the feed hopper – reactor differential pressure, the concentration of nitrogen in the outlet product gas stream was slightly lower at 2-3 %, thus it was believed that the operation of the over pressure had limited influence on the gas phase reactions and gas product. The hopper could not be operated with methane present in the hopper due to the hazard classification of the vessel.

Another major issue which was identified was the creation of carbon and the deposition within the bed. This is believed to be due to the carbon accumulation within the bed and the differing densities between carbon and bed material, therefore, the carbon is believed to congregate at the top layer of the bed. This is suspected of causing the difficulties in feeding the biomass into the reactor as the experiments progressed. As the total amount of methane passing through the system increased, the overall carbon content in the bed increased, which increased the overall bed height. This is suspected of causing issues in feeding as the system bed height accounted for the fluidisation of the sand particles and not that of carbon deposition. It is believed that this was significantly influential to the feed reliability of the system.

3.4.5 Packed Bed Design

The packed bed reactor was constructed in accordance to design standards by Mercer Group Limited, (Christchurch, New Zealand). The packed bed reactor was initially designed to investigate possible catalytic gas cleaning reactions from the product outlet of the fluidised bed reactor. It was envisaged that the packed bed could provide insight into sulphur, ammonia and tar removal from the process stream. As mentioned above, the packed bed was never operated with any catalytic media in the system; however, it was constructed for future experiments. The packed bed system was fed from the outlet products of the fluidised bed reactor by an inlet tube which was heated to 400 °C. This ensured that no condensation of carbonaceous material occurred before the condensation train.

The packed bed was designed to accommodate for varied residence time through the bed, which could be controlled by the amount of catalyst added and the overall flow rate. The design was based on the operation of the system with a GHSV (gas hourly space velocity) of 1000. This resulted in an overall volume of 1.4 L. The packed bed reactor pressure and flow rate was determined by the product outlet

of the fluidised bed reactor,

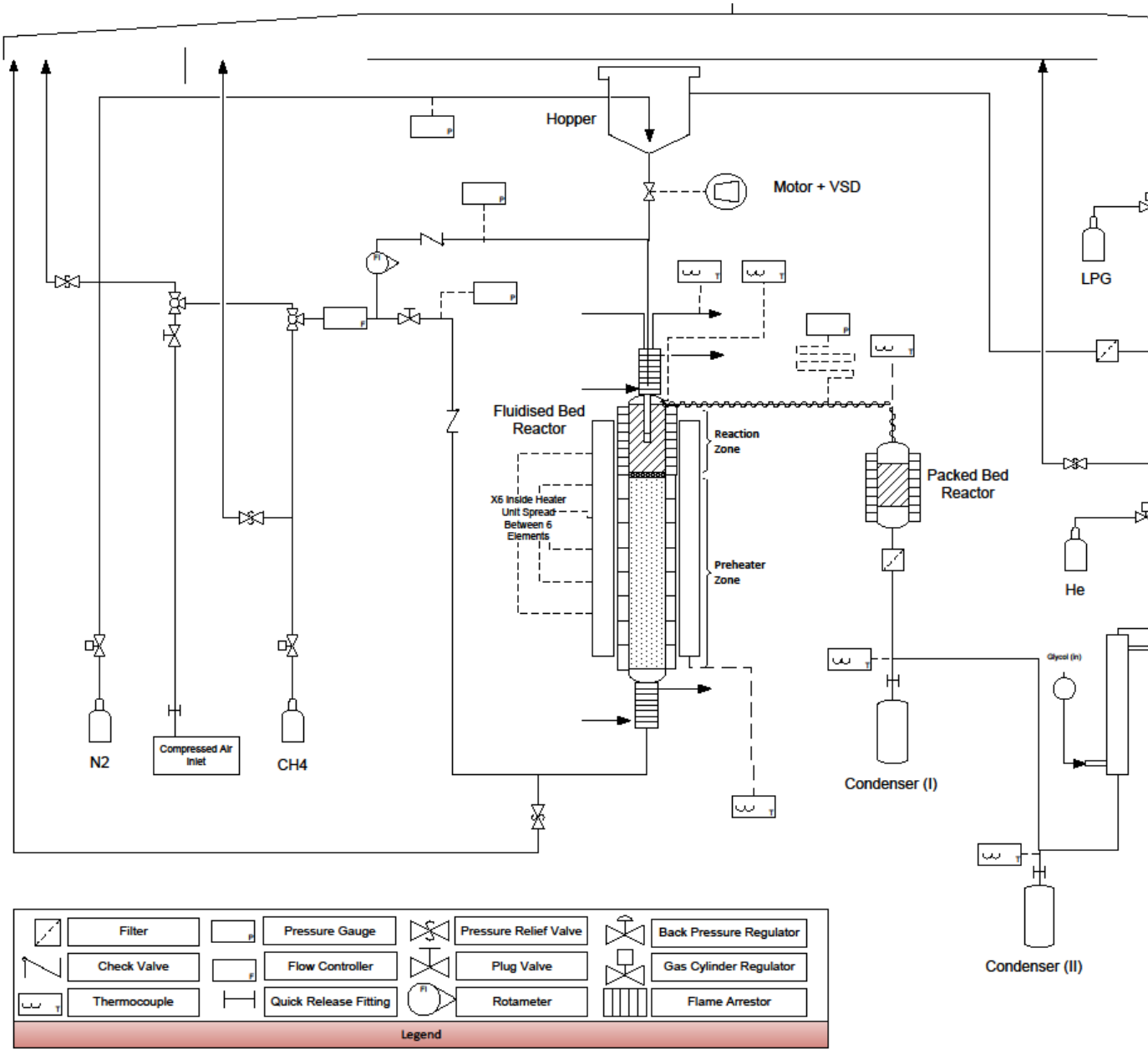

Figure 3-6. The reactor was heated using three 650 W band heaters (Watlow, USA), which allowed for a maximum operating temperature of 760 °C.

The reactor core was also constructed from 253 MA (Sandvik, Sweden), with class 300 flanges fitted on the top and bottom of the packed bed. Both flanges were fitted with a 13 mm outlet tube fitting. At the top flange the tube fitting was connected to a tee with a thermocouple fitting determining the packed bed reactor temperature. The bottom flange section was plumbed toward the remaining downstream condenser train, Figure 3-28.

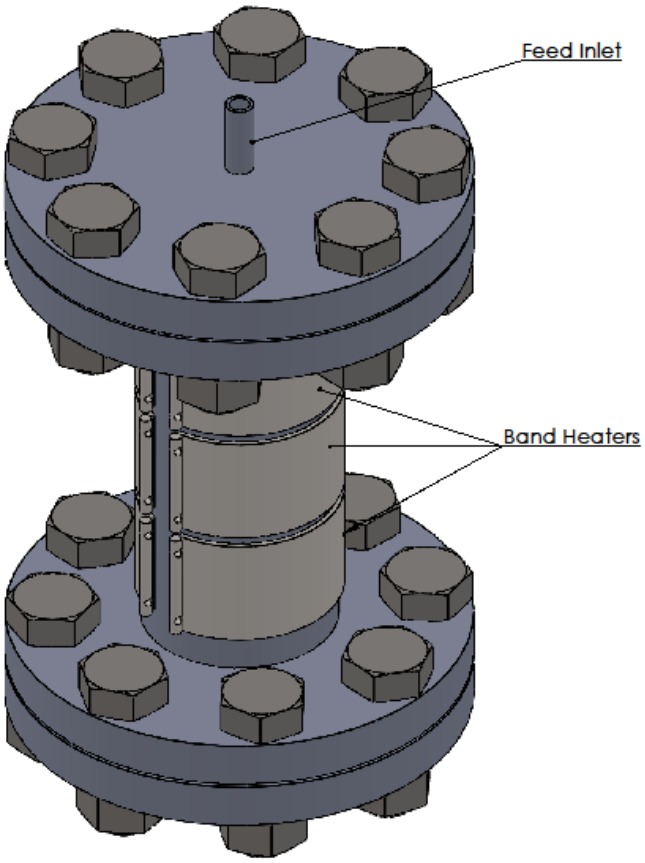

Figure 3-28: Packed bed arrangement with heaters.

No issues were observed to arise with the operation of the packed bed reactor. In usual operation the packed bed was kept at a constant temperature of 400 °C to prevent any condensation of products. When computing the mass balance for experiments it was speculated that there was deposition of char/carbon and or tars within the reactor. However, the system was opened on a number of occasions and no carbonaceous material was ever found in the system. Nor was sand from the fluidised bed ever found in the system, highlighting that it was unlikely particle entrainment of bed materials occurred.

3.4.6 Condenser Train Design

The condenser train was designed to ensure effective filtration and collection of char/carbon and tars formed from the fluidised bed reaction. The arrangement consisted of three condensers and three filters, Figure 3-29. Plumbing fittings and connections were all sourced from Swagelok, New Zealand.

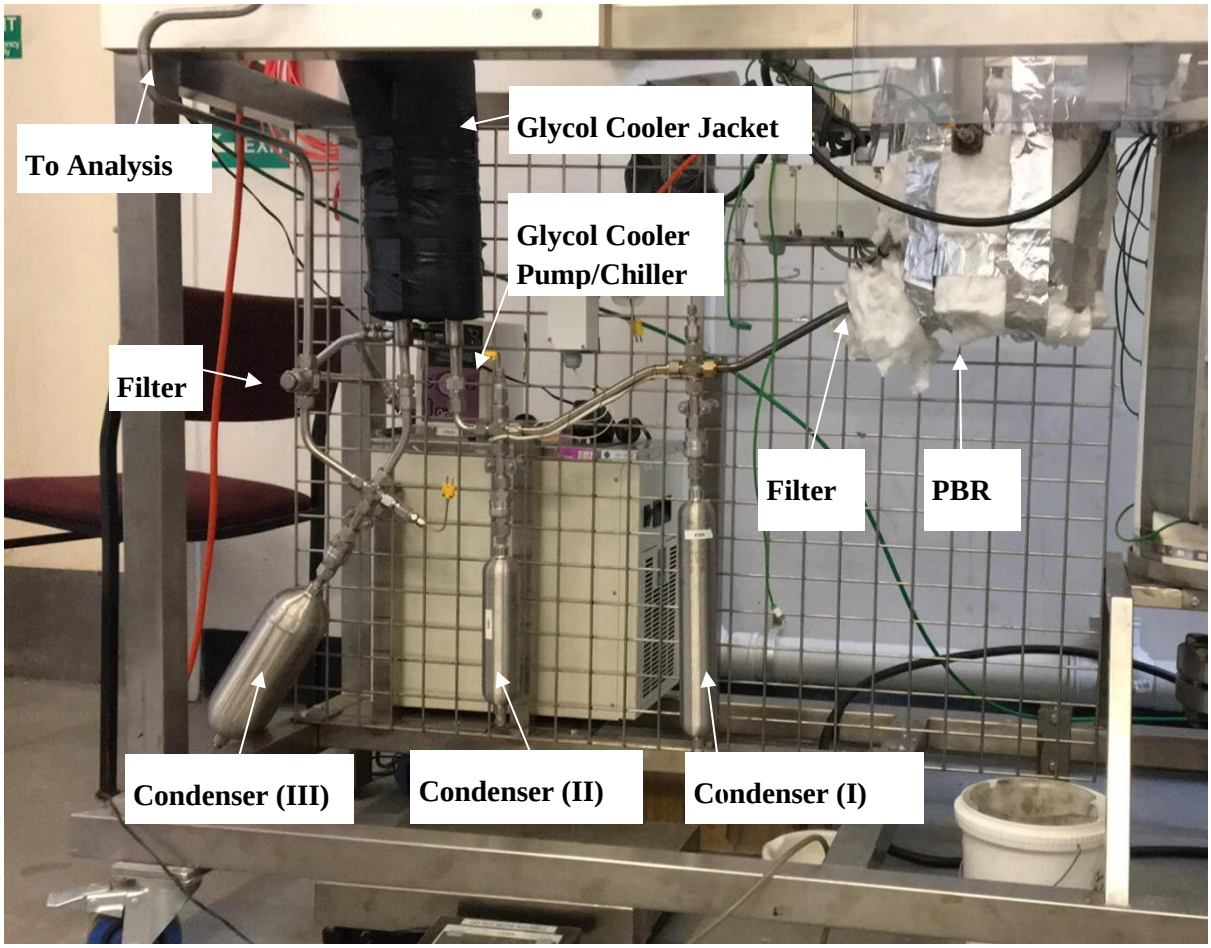

Figure 3-29: Condenser train and filter arrangement

The condenser train consisted of three Swagelok sample cylinders of different volume; 0.5, 0.3 and 1.0 L, respective, to the flow of gas. The condenser arrangement was angled between condensers to ensure that liquid condensed between the first two condensers was able to freely drain by the force of gravity. To facilitate the removal of the condensers, all condensers were fitted with Swagelok quick connect fittings. This allowed for easy removal of the product condensers and the system could be readily cleaned between trials.

As shown in Figure 3-29 two filters were placed within the system. The filters used were all 12.7 mm tee-type particulate Swagelok filters (TF-type). The filters facilitated the interchange of the filter element as the filter element housing could be removed with the filter inline. This allowed various filters to be trialled in different places throughout the condenser arrangement. Filter element sizes varied between 230-15 µm. The first filter from the outlet of the packed bed was fitted with a 230 micron and primarily collected carbon and char formed from the reactions and entrained in the product flow. The final filter was fitted with a 15 µm filter element to promote conglomeration of any fine tars which were not adsorbed in the final condenser, as well as fine solid particles in the product stream.

To facilitate the collection of the tar species, the 3rd condenser was fitted with a section of 3.2 mm tubing which was able to be inserted inside the 3rd condenser. The bottom 50 mm of tube was perforated to allow efficient dispersion of the gas stream throughout the solvent. The condensers were normally filled with ~ 500 ml of acetone which was chosen due to the similar solvent capabilities as dichloromethane, but with significantly reduced health concerns when utilising significant volumes. During trials, acetone was observed to be an effective solvent with the entrained flow of benzene, toluene and xylene recorded as < 1.5 % carbon conversion which was determined by SPE extraction. Trials were conducted over a range of operation conditions and the amount of entrained tar remained constant. Issues in reactor operation were encountered at lower residence times. This was due to the higher overall volumetric flow rate of gas through the system causing vigorous bubbling of acetone resulting in excess devolatilisation, due to the volatility of acetone. This resulted in excessive heat production from the product outlet flare, where the combustion of acetone accounted for nearly half the calorific value of the burner output. This ultimately led to the operating conditions of the reactor being constrained by the fume hood capacity, as the installed ducting of the system could not operate at temperatures > 100 °C. This was also problematic when regarding the condenser efficiency as the increasing evaporating rate led to sever decreases in the overall volume of acetone able to condense the inlet tars.

The entrainment of acetone throughout the system also caused degradation of outlet rotameters and seals as the plastics were incompatible. Due to the cumulative issues bio diesel was investigated as a possible product solvent, due to its wide use as a condensing solvent in previous studies [43]–[46] . Bio diesel proved to have much the same efficiency of product condensation with similar amounts of tars which were not captured within the acetone solvent system. The use of biodiesel removed the corrosive properties of acetone and also greatly reduced the excess heat produced by the flue gas flaring. It is noted however that a portion of the biodiesel which was added to the condenser was evaporated possibly due to the high level of agitation at higher flow rates. This was significantly lower than the acetone entrainment values as no flame could be observed when purging in N_2 when using biodiesel. The effective tar capture by the solvent was believed to be facilitated due to the high concentration of aromatic tars which do not cause condensation and solubility issues like other poly-aromatic compounds [44].

From the trials conducted with acetone and biodiesel it was observed that there was entrainment of heavier tars which were not collected in the solvent bath. This was observed by tars which had polymerised on the surface of the filter elements and blocked pores within the system. This also caused issues within the outlet rotameter system. The tars which were observed to be blocking the

system were analysed and determined to be naphthalene. This could be identified visually by the build-up of yellow crystalline deposits about the filter, Figure 3-30.

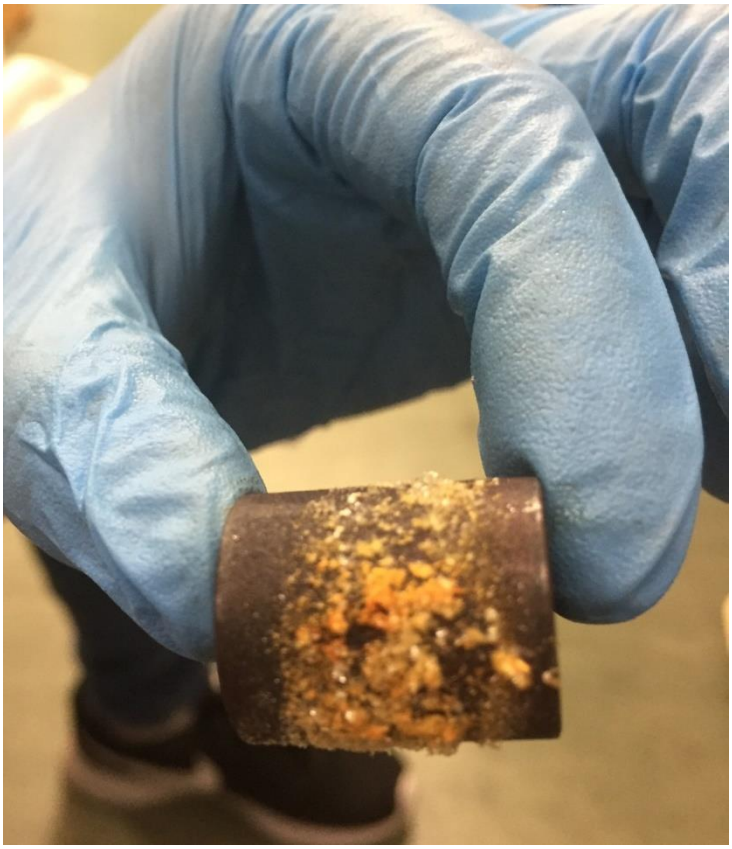

Figure 3-30: Naphthalene tar precipitate formed on outlet filter element.

To reduce the effective naphthalene entrainment throughout the system the condenser feed line was fitted with a glycol cooler. The cooler was designed to reduce the temperature of the inlet gas flow and increase the solubility of naphthalene and other poly-aromatic tar species in the biodiesel. The system was designed with a jacket type configuration with the glycol pumped through concentric pipes which surrounded the product tubing. A glycol cooler bath was fitted to the system which kept the glycol temperature constant at – 10 °C during circulation. Efficient condensation of the tars was obtained due to the decreased operating temperature of the product line, which in turn reduced the solvent temperature as well. To aid in the collection of the tars which were condensed the glycol cooler was usually ramped to 30 °C with N_2 passed through the system. This allowed for the condensed material on the wall of the cooler tubing to liquefy and flow to the condensers 2 and 3. Overall this greatly increased the product recovery from the gas stream and reduced the extent of blocking at the filters. Cumulative use of the filters did however lead to blockages occurring within the system. Due to this, all filters which were in place were removed and cleaned by use of a propane torch to combust any precipitated products within the pores. On doing so, small amounts of oil could

be observed to leach from the filter element. In an attempt to determine the composition of the tars, the system was run without the final element and the outlet gas was analysed through the SPE column. This resulted in a chemical composition of a number of differing heavy unsaturated aromatic molecules. The tars were characterised as multi-cyclic aromatics including; fluorine, phenanthrene anthracene, pyrene and fluoranthene in trace quantities. With the inclusion of the biodiesel the recordings of the stated species was unable to be conducted using the GC-FID methodology. This was due to the introduction of significant amounts of fatty acid methyl esters, which coincided with the similar boiling points of the species. This in turn masked the overall production and made GC-MS the most feasible analysis method for the production of the tars. With the overall production of the mentioned tars significantly lower than other primary tar species (> 0.01 % carbon conversion) it was concluded that the production was negligible, however periodic cleaning was required.

3.4.7 Gas Sampling System Design

Before the gas product was combusted the gas product was sampled to determine the overall entrained tar composition and non-condensable gas species. The system was designed to incorporate a helium trace gas which was introduced into the product stream by an Alicat flow controller (Alicat Scientific, U.S.A). The tracer gas allowed for the derivation of the product volumetric flow rates, and subsequent product mass flow rates. The sampling system was located after the back pressure regulator to remove hazardous pressurized operation when sampling. The sampling system consisted of utilizing a manifold where SPE columns could be mounted and the gas stream could be drawn through the column by syringe. Through a system of valves the tubing was able to be purged to ensure accurate gas sampling. The gas was then able to flow to the outlet burner then through the fume hood. Further information on the analytic operation of the system can be found in following sections.

3.4.8 System Control

To simplify process operation and allow flexibility in design all pressures and temperatures were recorded manually. The system heaters were controlled using three Love Controls Series 32B (Dwyer, U.S.A) controllers for the top 3 heaters in the fluidised bed system. The first two heaters of the fluidised bed reactor arrangement, packed bed heater and trace heater arrangement were controlled using XMT7100 PID controllers (DX, Singapore). All system temperatures were recorded using k-type thermocouples, with temperature cut out probes installed in the fluidised bed reactor and on the outside of the packed bed reactor systems. These thermocouples were installed to ensure operation did not exceed the design specifications. Although the constraining temperature for the fluidised bed reactor was about the top flange gasket, the convective cooling was sufficient to decrease the temperature well below required. Top gasket temperature would normally rest at ~200 °C when the reactor was at 1000 °C; hence the internal temperature of the reactor was chosen as a more suitable

temperature cut off measurement. The heater control was also fitted with an emergency stop button which was located on the front of the control box. As all electronics were terminated from the box, by initiating the button the complete system would stop with all heaters and biomass feeding ceased.

The inlet methane and helium gas flow rate was controlled by M-10SLPM-D/5M and M-100SLPM-D/5M Alicat flow controllers (Instrumatics, Christchurch). The entrainment flow rate into the fluidised bed was controlled by a RE Uniflux flowmeter (Dotmar, Christchurch). Pressure was controlled using a 0-100 psig Tescom back pressure regulator (Tescom, U.S.A).

3.4.9 Process Safety

Due to operation with methane above the auto ignition temperature and under pressure, safety was paramount during the system design. To prevent over pressurization of the system above the design pressure 1010 kPa, at 1000 °C, four pressure relief valves were mounted. All inlet gas cylinders were installed with a pressure relief valve to prevent over pressurization of the system directly from the gas cylinder. The remaining pressure relief valve was installed before the reactor to prevent over pressurization of the system in the case of a system blockage downstream. A standard operating procedure (SOP) checklist was produced for the operation of the system. Fundamental safety procedures included sufficient purging of the system which was checked via GC analysis. As well as, a pressure test which was conducted after any section of the system was dismantled.

The system was designed with a fume hood which was mountable on the top of the system and allowed for adequate ventilation of the heat and gas product formed. After the cooling of the methane gas the primary hazard was the presence of CO released from the system. To avoid any unforeseen exposure to any of the hazardous gases a 4 gas (LEL, CO, O2, H2S) MGC Pellistor gas monitor (Homershams, Christchurch) was carried at all time during operation. A comprehensive hazard and operability (HAZOP) study was conducted on the system which allowed for the identification and mitigation of potentially hazardous operation. Full detail of the system derivation and conclusions can be found in Appendix D.

3.5 Discussion

As described above, significant system modifications were made during the commissioning phase of the reactor system. Overall it was determined that the reactor operated reasonably well during the experiments, although operational consistency was a major issue during the operation of the system. This was experienced as numerous trials were abandoned due to early blocking of the system feeder, rendering the trial a failure. This was due to the feeding tube being blocked, when the system could not be reset and the contents required removal before the system could be operated again. This caused

long delays in operating the reactor, as the overall hazardous environment required adequate purging and pressure tests before operation could be reattempted.

It is believed that the blockages occurred within the feeding tube was due to the incorrect pressure differentials between the hopper and the reactor, as well as char/carbon accumulation in the reactor's fluidised bed. An incorrect pressure differential resulted in the hopper pressure being lower than the reactor pressure of the system, causing the biomass flow to be subjected to increased drag forces. This was observed during the trialling period as a decrease in the outlet volumetric flow, as feed was not devolatilising and the flow was similar to that of MTD. In an attempt to compensate the increasing pressure, the hopper pressure would be increased by increasing the flow of nitrogen into the hopper. However, at times this would not sufficiently compensate the pressure differential and the system feeder tube would be blocked. This was especially problematic during experiments with high biomass feed rates and/or high methane flow rates. It was suspected that this was due to the increase in pressure of the fluidised bed space during the initial volatile release from the biomass particles. This effect was exacerbated with increased biomass flow rates, as high biomass flowrates increased the overall volumetric flow rate, resulting in higher operating pressures when feed was added to the system. The methane flow rate into the system was also believed to be influential to the pressure differentials, as MTD varied during trials the overall extent of methane degraded would decrease and cause decreases in the system pressure. This was due to less hydrogen gas formed during MTD. Both these effects are believed to have induced a dynamic pressure differential which is suspected at times of causing gas flow toward the hopper.

To decrease the effect of the pressure differential the system was controlled by the back pressure regulator. By increasing the system pressure enhanced control of the system could be obtained. This allowed for the overall system pressure to remain constant and prevented excess pressure differentials within the reactor system. However, it was observed that although the back pressure regulator would regulate the overall outlet flow rate dependent of set pressure, the pressure differential was still apparent. This effect was prominent during the pressure trials in which the biomass feeding was blocked significantly during the higher pressure operation. In due course it was determined that the best control method was manual operation of the back pressure regulator. By altering operating pressure slightly during the trial, the overall pressure differential over the hopper and reaction zone could be decreased. This control system worked well and allowed for the operation at high pressures. Although, it was observed that after a certain period of time the effective control using the back pressure regulator was lost. This is suspected to be due to the build-up of deposits within the system's filters and process tubing.

Another major design issue which was apparent during the operation of the reactor was the heat deformation of the reactor's core components. The reactor's pipe was observed to deform with

operational heat cycling. This was initially determined due to difficulty in inserting the quartz liner arrangements. With subsequent trials the deformation became so severe that the quartz liner was unable to reach the bottom of the reactor arrangement. As the quartz liner OD was 57 mm and the reactor ID was 59.5 ± 0.2 mm, this related to an overall deflection of over 2 mm. It was suspected that the deflection was at the midsection of the reactor pipe, which was the meeting point of the boring which was conducted to form the pipe from the solid bar. It is likely that this is a point of weakness, as visually the boring diameters are not precisely concentric. The significance of the deformation could be observed visually when considering the vertical alignment at the middle of the reactor core, Figure 3-31. No significant work could be conducted on the pipe as this would void the pressure certification of the system. Instead, to continue operation, tapered quartz liner was fabricated which consisted of 500 mm length of 46x40 mm quartz tubing which was fused to a 270 mm length of 57x53 mm. The fusing of the quartz resulted in an overall length of 800 mm. The reduced diameter at the bottom of the liner mitigated the effects of the deflection and allowed for adequate gas flow distribution. As from the investigation into methane degradation characteristics, the smaller quartz tubing did not affect the extent of methane degradation. No noteworthy differences in the operating temperature were detected when the liner arrangement was used.

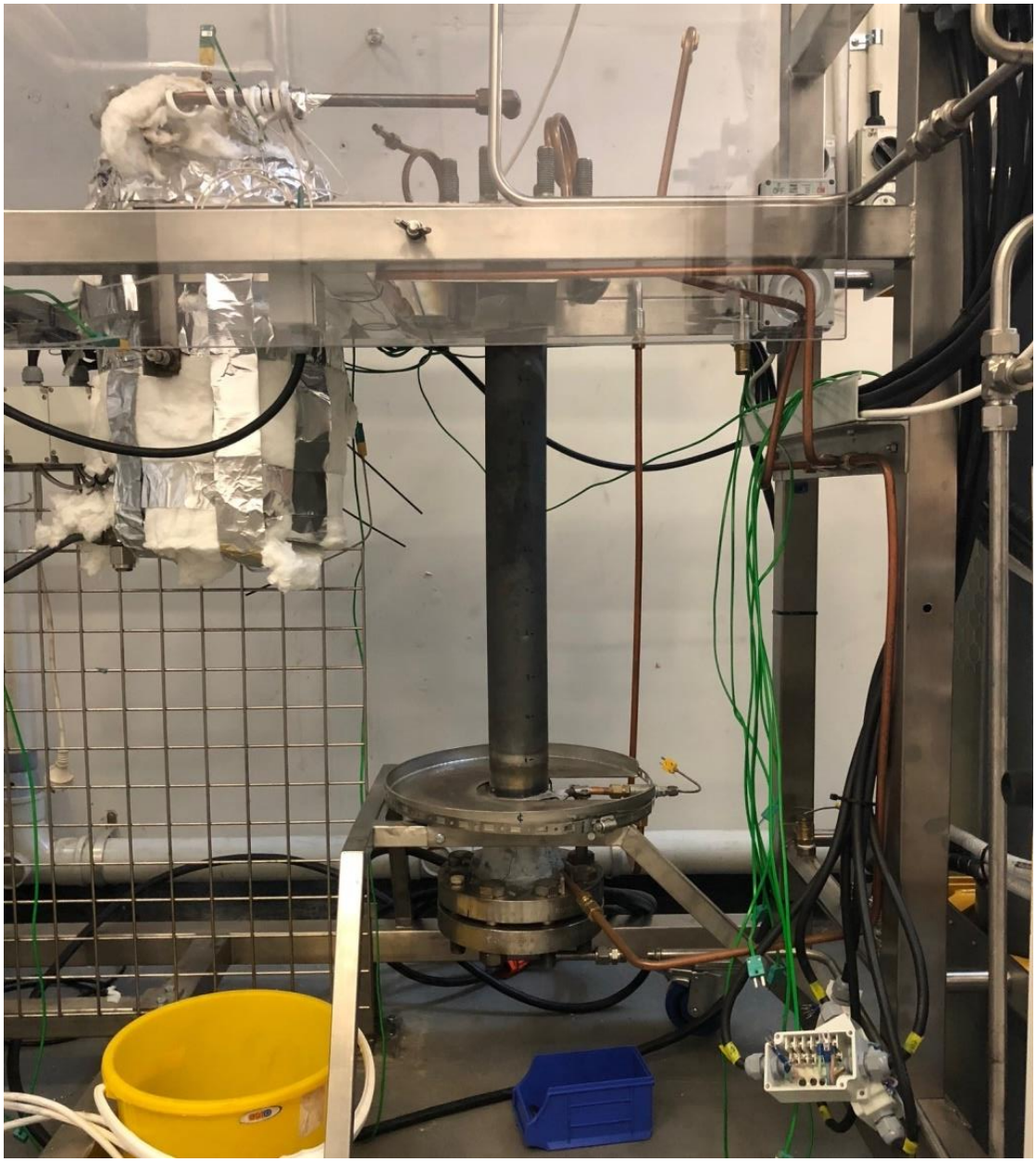

Figure 3-31: Exposed reactor pipe with heater system removed, showing the visual extent of deformation due to suspected heat cycling.

3.6 References

[1] M. Plevan *et al.*, "Thermal cracking of methane in a liquid metal bubble column reactor: Experiments and kinetic analysis," *Int. J. Hydrogen Energy*, vol. 40, no. 25, pp. 8020–8033, 2015.

[2] T. Geißler *et al.*, "Hydrogen production via methane pyrolysis in a liquid metal bubble column reactor with a packed bed," *Chem. Eng. J.*, vol. 299, pp. 192–200, 2016.

[3] A. A. Munera Parra and D. W. Agar, "Molten metal capillary reactor for the high-temperature pyrolysis of methane," *Int. J. Hydrogen Energy*, pp. 6–13, 2016.

[4] V. Kevorkian, C. E. Heath, and M. Boudart, "The Decomposition of Methane in Shock Waves," *J. Phys. Chem.*, vol. 64, no. 8, pp. 964–968, 1960.

[5] G. B. Skinner and R. A. Ruehrwein, "Shock Tube studies on the Pyrolysis and Oxidation of Methane," *J. Phys. Chem.*, vol. 63, no. 10, pp. 1736–1742, 1959.

[6] C. Robinson and D. B. Smith, "The auto-ignition temepr," *J. Hazard. Mater. Elsevier Sci. Publ. B.V*, vol. 8, pp. 199–203, 1984.

[7] D. Geldart, "Types of gas fluidization," *Powder Technol.*, vol. 7, no. 5, pp. 285–292, May 1973.

[8] J. G. Yates and P. Lettieri, *Fluidized-Bed Reactors: Processes and Operating Conditions*, vol. 26. Springer, 2016.

[9] C. Y. Wen and Y. H. Yu, "A generalized method for predicting the minimum fluidization velocity," *AIChE J.*, vol. 12, no. 3, pp. 610–612, 1966.

[10] J. R. Grace and G. Hetsroni, *Handbook of multiphase systems*, Hetsroni M. New York: Hemisphere, 1982.

[11] D. Chitester, R. Kornosky, … L. F.-C. E., and undefined 1984, "Characteristics of fluidization at high pressure," *Elsevier*.

[12] T. E. Broadhurst and H. A. Becker, "Onset of fluidization and slugging in beds of uniform particles," *AIChE J.*, vol. 21, no. 2, pp. 238–247, 1975.

[13] A. Haider and O. Levenspiel, "Drag coefficient and terminal velocity of spherical and nonspherical particles," *Powder Technol.*, vol. 58, no. 1, pp. 63–70, May 1989.

[14] D. Kunii and O. Levenspiel, *Fluidization engineering*. Butterworth-Heinemann, 1991.

[15] J. Davidson, D. Harrison, and R. Jackson, “Fluidized particles: Cambridge University Press, 1963. 155 pp. 35s,” 1964.

[16] S. Mori and C. Y. Wen, “Estimation of bubble diameter in gaseous fluidized beds,” *AIChE J.*, vol. 21, no. 1, pp. 109–115, Jan. 1975.

[17] J. Hongrapipat, “Removal of NH3 and H2S from Biomass Gasification Producer gas,” University of Canterbury, 2014.

[18] N. Menon and D. Durian, “Particle Motions in a Gas-Fluidized Bed of Sand,” *Phys. Rev. Lett.*, vol. 79, no. 18, pp. 3407–3410, 1997.

[19] Sandvik AB, “Sandvik 253 MA Tube and Pipe , Seamless,” *Http://Smt.Sandvik.Com/En/Materials-Center/Material-Datasheets/Tube-and-Pipe-Seamless/Sandvik-253-Ma/*, pp. 1–12, 2016.

[20] A. Megaritis, Y. Zhuo, R. Messenbo, D. R. Dugwell, and R. Kandiyoti, “Pyrolysis and gasification in a bench-scale high-pressure fluidized-bed reactor,” *Energy and Fuels*, vol. 12, no. 15, pp. 144–151, 1998.

[21] M. Steinberg, “Flash Pyrolsyis of Biomass with Reactive and Non-Reactive Gases,” 1984.

[22] M. Steinberg, P. T. Fallon, and M. S. Sundaram, “The Flash Pyrolysis and Methanolysis of Biomass (Wood) for Production of Ethylene, Benzene and Methanol,” 1990.

[23] M. Steinberg, P. T. Fallon, and M. S. Sundaram, “Flash pyrolysis of biomass with reactive and non-reactive gas,” *Biomass*, vol. 9, no. 4, pp. 293–315, 1986.

[24] M.S Sundaram, S. M. Steinberg and P.T. Fallon, “Flash Pyrolysis of Biomass with Reactive and Non-Reactive Gases,” Richland, Washington, 1984.

[25] Sandvik AB, “Sandvik 253 MA Tube and Pipe , Seamless,” *SANDVIK 253 MA TUBE AND PIPE, SEAMLESS DATASHEET*, 2016. .

[26] F. O. F. Supply and M. Properties, “SANDVIK 353 MA TUBE AND PIPE , SEAMLESS,” pp. 1–9.

[27] Sandvik AB, “Sanicro 31HT Tube and Pipe, Seamless,” pp. 1–10, 2010.

[28] Reimpro, “SX 310 Technical Data,” *SX 310 Techincal Data*. .

[29] J. Chase, M.W., “NIST-JANAF Themochemical Tables, Fourth Edition,” *J. Phys. Chem. Ref. Data, Monogr. 9*, pp. 1–1951, 1998.

[30] A. TenWolde, J. D. McNatt, and L. Krahn, “Thermal properties of wood and wood panel products for use in buildings.” 01-Sep-1988.

[31] M. F. (Michael F. . Modest, *Radiative heat transfer*. Academic Press, 2003.

[32] United Performance Metals, “Stainless 347,” Ohio, 1.888.282.3292.

[33] Thermal Ceramics, “Product Information Sheet Kaowool Vacuum Formed Boards,” *Kaowool Vaccum formed boards*, 2008. [Online]. Available: http://www.forman.co.nz/files/file/570/Vaccuum+Formed+Board+datasheet.pdf. [Accessed: 06-Dec-2017].

[34] R. Lee and J. Happel, “Thermal radiation of methane gas,” *Ind. Eng. Chem. …*, vol. 3, no. 2, pp. 167–176, 1964.

[35] P. E. Khizhnyak, A. V. Chechetkin, and A. P. Glybin, “Thermal Conductivity of Carbon Black,” *N. B. VargaftikandN. A. Vanicheva, Inzh.-Fiz. Zh. N. B. Vargaftik*, vol. 25, no. 3, 1973.

[36] J. L. Pinilla, I. Suelves, M. J. Lázaro, R. Moliner, and J. M. Palacios, “Parametric study of the decomposition of methane using a NiCu/Al2O3 catalyst in a fluidized bed reactor,” *Int. J. Hydrogen Energy*, vol. 35, no. 18, pp. 9801–9809, 2010.

[37] T. Zhang and M. D. Amiridis, “Hydrogen Production via the Direct Cracking of Methane over Silica-Supported Nickel Catalysts,” *Appl. Catal. A Gen.*, vol. 167, no. 2, pp. 161–172, 1998.

[38] C. Ratnasamy and J. P. Wagner, “Water Gas Shift Catalysis,” *Catal. Rev.*, vol. 51, no. 3, pp. 325–440, 2009.

[39] D. Meier, J. Berns, and O. Faix, “Pyrolysis and Hydropyrolysis of Biomass and Lignins-Activities at the Institute of Wood Chemistry in Hamburg, Germany,” *Am. Chem. Soc.*, pp. 298–303, 1995.

[40] Z. Berk, *Food process engineering and technology*. Elsevier Science, 2013.

[41] K. E. Ileleji and B. Zhou, “The angle of repose of bulk corn stover particles,” *Powder Technol.*, vol. 187, no. 2, pp. 110–118, 2008.

[42] F. Miccio, N. Silvestri, D. Barletta, and M. Poletto, “Characterization of woody biomass

flowability," *Chem. Eng. Trans.*, vol. 24, pp. 643–648, 2011.

[43] T. Phuphuakrat, T. Namioka, and K. Yoshikawa, "Absorptive removal of biomass tar using water and oily materials," *Bioresour. Technol.*, vol. 102, no. 2, pp. 543–549, 2011.

[44] S. Unyaphan, T. Tarnpradab, F. Takahashi, and K. Yoshikawa, "Improvement of tar removal performance of oil scrubber by producing syngas microbubbles," *Appl. Energy*, vol. 205, no. August, pp. 802–812, 2017.

[45] S. Nakamura, S. Kitano, and K. Yoshikawa, "Biomass gasification process with the tar removal technologies utilizing bio-oil scrubber and char bed," *Appl. Energy*, vol. 170, pp. 186–192, 2016.

[46] P. J. Woolcock and R. C. Brown, "A review of cleaning technologies for biomass-derived syngas," *Biomass and Bioenergy*, vol. 52, pp. 54–84, 2013.

4 Experimental Method and Model Development

This chapter describes the experimental method and calculating approach used to investigate the products from methanolysis. The methodology for the characterisation of the biomass and the analytical techniques used throughout this thesis are also provided. The approach taken for the derivation of the thermogravimetric analysis (TGA) model and Gibbs free energy model is also described.

4.1 Analytical Techniques

During the course of the experiments a number of different analytic techniques were utilized to characterise the products from the flash methanolysis of biomass. Characterisation of the methods will be covered in this section. All feed to the system was dried in an oven at 105 °C to remove all water. The chip was added warm into the hopper immediately after being weighed to minimize any water adsorption from atmosphere. The inclusion of water within the porous structure of the biomass was problematic and brought about uncharacterised uncertainty in derivation of species balances.

4.1.1 Uncertainty Analysis

When computing the uncertainties associated within experiments the half range rule was applied on overall data sets. Uncertainties were derived by use of Equations (4.1.1), (4.1.2) for addition/subtraction or multiplication/division, respectively:

$$(x_1 \pm \Delta x_1) +/- (x_2 \pm \Delta x_2) = (x_1 +/- x_2) \pm \sqrt{\Delta x_1^2 + \Delta x_2^2} \qquad (4.1.1)$$

$$(x_1 \pm \Delta x_1) \times/\div (x_2 \pm \Delta x_2) = (x_1 \times/\div x_2) \pm \sqrt{\left(\frac{\Delta x_1}{x_1}\right)^2 + \left(\frac{\Delta x_2}{x_2}\right)^2} \qquad (4.1.2)$$

When calculating the average of data sets the overall uncertainty was calculated by the following equation:

$$\sum_{i=0}^{n} \frac{x_i}{n} \pm \sum_{i=0}^{n} \frac{\Delta x}{\sqrt{n}} = x_{ave} \pm \Delta x_{ave} \qquad (4.1.3)$$

To compute the uncertainty associated with the tar analysis, 0.1 ml of 500 PPM dodecance internal standard was added to each sample and the external calibration value was determined (EC). The

standard samples were prepared in a similar fashion with the same standard feedstock to allow for a peak ratio analysis. Peak ratios were determined for each species (j) and were standardized against the internal standard count response, which were then graphed for derivation of the slope and intercept.

$$Peak\ Ratio(j) = \frac{Count(j)}{Count(IS)} \tag{4.1.4}$$

For each sampled species the internal calibration concentration could be determined by:

$$IC = \frac{Count\ (j)}{Count(IS)}\ x\ Peak\ Ratio(slope) + Peak\ Ratio\ (intercept) \tag{4.1.5}$$

The overall uncertainty could then be determined by:

$$\pm = \frac{EC - IC}{EC} \tag{4.1.6}$$

4.1.2 Thermogravimetric (TGA) Analysis

To determine the pyrolysis characteristics of the pine wood constituents, the decomposition rate was investigated using a thermos-gravimetric analysis (TGA). TGAs have been utilized extensively due to the rapid quantitative methods they provide for the examination of processes under non-isothermal conditions. This allows for the derivation of various decomposition reactions and estimates of the kinetic parameters.

For the trials conducted, non-isothermal pyrolysis experiments were conducted using a SDT Q600 V20 (TA Instruments, U.S.A) thermo-gravimetric analyser. The pine wood was initially milled to 710-1000 µm using the Wiley mill. The thermogravimetric analysis was undertaken using two alumina pans which had been combusted in air to prevent char carry-over between experiments. One pan was used as the reference pan for the mass measurements, whilst, the other pan was filled with ~7 mg of biomass. The analysis was conducted using nitrogen as the pyrolising agent, in total 5 heating rates were used; 1, 5, 10, 20 and 30 °C/min. It was concluded that when heating at 1 °C/min the uncertainty from the measurements were too significant and stable degradation curves could not be obtained.

4.1.3 Tar Product Analysis

Multiple techniques were used to determine the composition of the tar fraction which was collected. The use of differing solvents also altered the feasibility of the analysing method. Due to the limited literature available on the expected products formed from the flash methanolysis a number of different techniques were trialled and utilized. This allowed for investigation into the full range of possible species produced. For the tar species produced during pyrolysis, GC-MS is a common analysis technique; however it has been documented that the detection of species can be relatively low. This is due primarily to the high number of species which are formed during conventional pyrolysis, inducing peak overlapping, resulting in analytical uncertainty. As it was identified the tar distribution was relatively uniform and the majority of species produced were benzene, toluene and naphthalene GC-FID was commonly utilized. Other species were present in significantly lower concentrations, which were detected in undiluted samples.

4.1.3.1 Gas chromatography, Flame ionisation detector (GC-FID)

All tar samples were analysed using the Varian CP-3800 gas chromatograph, flame ionisation detector (GC-FID) in the department. The method utilised was developed by Saw et al. [1], and is described below. The species were separated using a 50 % phenyl and 50 % dimethylpolysiloxane fused silica capillary column of 30 m x 0.25 mm x 0.25 μm. The temperature of the injector and FID were set at 300 °C. In total 1 μL of sample was injected per run with the following temperature profile employed; 50°C hold for 1 min, 50- 180 °C at 4 °C/min, 180-245 °C at 2.5 °C/min, 245-270 °C at 2 °C/min and held for 10 min, 270-350 °C at a rate of 8 °C/min then held for 5 min. Helium was used as the carrier gas and was constant at 1 mL/min [1].

The above tar analysis method was calibrated using two different calibration mixes, Table 4-1, for identification, the standards were prepared as light and heavy tars. The light tar standard was sourced from Supelco Analytical (U.S.A) and the heavy tar standard was sourced from Restek (U.S.A.). The tar samples arrived in 2 ml vials with a concentration of 2000 ppmw for the light tar standard, and 1000 ppmw for the heavy tar standard, both standards were prepared in DCM (from the manufacturer). The standards were prepared in the same vial for a combined heavy/light tar calibration. Relative to the light tar concentration, the standards prepared were; 25, 50, 100 and 150 PPM[XVI] . Dodecance was used as the internal standard at a concentration of 50 ppm which was diluted from a 500 ppm stock prepared in DCM.

[XVI] Where the concentration of the heavy tar species was half that of the light tar concentrations.

Table 4-1: Tar calibration standard species list, listed in order of retention time on column respective to the individual tar standard.

Light Tar Std.		Heavy Tar Std.	
Benzene	o-cresol	Naphthalene	Chrysene
Toluene	m+p-cresol	2-Methylnapthalene	Benso(b)fluoranthene
Pyridine	Quinoline	1-Methylnapthalene	Benso(k)fluoranthene
p-xylene + Ethylbenzene	Isoquinoline	Acenaphthylene	Benso(a)Pyrene
m-xylene	Biphenyl	Acenapthene	Indeno(1,2,3-cd)pyrene
o-xylene		Fluorene	Benso(g,h,i)perylene
Styrene		Phenanthrene	Dibenso(a,h)anthracene
Phenol		Anthracene	Pyrene
Indene		Fluoranthene	Bens(a)anthracene

Calibrations of the tar species, Table 4-1, were prepared in both a 50/50 DCM/biodiesel solution and acetone. As the calibration tars were supplied in a solution of dichloromethane (DCM), the preparation of the calibration standards were formed in a 50/50 biodiesel/DCM dilution to analyse the condenser solutions. Two calibrations were produced to allow for the quantification of the tar species produced and also for the identification of condensed tar species on process equipment which was washed in acetone.

The biodiesel used was sourced from and was originally derived from waste canola oil. The biodiesel consisted of numerous fatty acid methyl esters (FAME) components, Table 4-2 which had various high boiling points. This in turn caused difficulty when analysing the higher molecular weight tar species due to the significantly higher concentration of FAME's above 350 °C. This overlapping of peaks in turn caused a decrease in the measureable concentrations of higher molecular weight tar species. Effectively this reduced the amount of heavy tars which could be measured and tars with a molecular weight greater than acenapthanlene Table 4-1, could not be adequately quantified. Although a significant proportion of the calibrated species had similar residence times of the FAMEs it was deemed acceptable as the majority of tars produced were light tars. This was confirmed with acetone trials which measured no tar species in the range of #19-32. The major species measured from the heavy tar standard were naphthalene, 2-methylnapthalene and 1-methylnapthalene. The

production of higher molecular weight tars was known to occur, however the thermal and corrosion issues associated with the use of acetone outweighed the analytical benefits. To confirm the presence of the higher molecular weight compounds gas chromatography mass spectrometry (GC-MS) was utilised, this will be discussed further below.

Table 4-2: Fatty acid profile and boiling temperature for biodiesel derived from Canola oil (carbon length: double bonds).

Biodiesel FAME Species	Palmitic (16:0)	Stearic (18:0)	Oleic (18:1)	Linoleic (18:2)	Linolenic (18:3)	Gadoleic (20:1)
Composition	4.7 %	1.9 %	65.4 %	19.3 %	7.3 %	1.1 %
Boiling Temp (°C)	351	361	360	390	407	403

Due to the high operating temperature, high heat rate and low residence time the tar species formed tended to be much lighter tar species. In conventional pyrolysis the distribution of tar species and average molecular weight are significantly higher [2]. This was represented by the abundance of mono-cyclic tar species, with the only abundant di-cyclic species present having the base naphthalene structure. This led to a refinement of the analytical procedure where the accurate measurements of the light tar species was the focus. To ensure accurate measurements of the tar species all condensers were removed after an experiment and the contents emptied into a 500 ml volumetric flask. The condenser was rinsed with bio-diesel 3 times and added to the volumetric flask contents. The overall flask was kept cool in a fridge until analysis. For the analysis a 0.1 ml sample was diluted x 10 in a 50/50 DCM/biodiesel mixture, with a 0.1 ml aliquot of the internal standard added (500 PPM dodecance in DCM). To accuratly determine the benzene concentration another sample was prepared and the dilution would be decreased to x2. This was required due to the significantly higher benzene concentration in comparison to other product tars in the condenser. In general, benzene would be approximately seven magnitudes higher in concentration than toluene and naphthalene. When benzene levels would increase above 10 orders of magnitude a new sample would be prepared with a suitable dilution to decrease analytical uncertainty.

4.1.3.2 Gas chromatography, Mass spectrometry (GC-MS)

All samples which were analysed by GC-FID for tar distribution were also analysed using the GC-MS (Shimadzu GCMSQP2010 Plus) to determine higher molecular weight and previously undetectable species. All samples were prepared with the same dilution methodology as described for the GC-FID. The species were separated using a Restek RTX-5MS column of 30 m x 0.25 μm. The mass spectrometer operated on scan mode from 50-700 m/z with an overall injection volume of 1 μL with a

split less injection time of 30 s. The temperature ramp program was as follows; a start point of 50 °C , held for 60 s, ramped at 5 °C/min to 180 °C, 180-210 ° at 2.5 °C/min, 210-310 at 20°C/min held for 10 minutes. The injection and interface temperature were both 300 °C, with helium operated in linear velocity mode used as the carrier gas. The GC-MS system was operated by the GC-MS Solution Version 2.70 software. The method was derived from previous analytical procedures [3], [4] where the temperature profiles were slightly altered to optimize the signal given for lighter tar species. From the samples conducted it was apparent that GC-FID analysis was sufficient for complete characterisation of the tars, as the amount of heavy tar species determined during the GC-MS analysis were insignificant.

4.1.3.3 SPE Column Extraction

Although the experimental procedure did not extensively utilise the SPE columns, the overall efficiency of the biodiesel was determined by SPE column extractions. Trials would periodically be extracted through SPE columns to detect any heavy tar products/non-soluble tar species which were produced. This was primarily conducted when significantly different system conditions were utilized, for example; high pressure, low temperature, different feed gas and differing feeds. The utilization of the SPE column extraction method essentially became redundant once biodiesel was used as the tar solvent solution. This was due to the high extraction efficiency of the biodiesel solution during the experiments.

Nevertheless it was deemed important to determine the overall fraction of tars which were not dissolved in the condensing solvent. Multiple different SPE columns were utilized to determine the efficiency of aromatic tar extraction. Supelclean ENVI (Sigma-Aldrich, U.S.A) C-18, NH_2/Si and Chrom-P SPE columns (500 mg, 3 ml solid phase) were all trialled. To determine the overall effectiveness of the columns, the effective tar removal of BTX was investigated. Following a similar method to that of Meney et al, a solution of 100 PPM BTX was prepared in methanol [5], [6]. The solution was then diluted with water to form a 50 PPM solution. The columns were conditioned with 3 ml of methanol and 3 ml of a 1% methanol in water solution passed through the column. BTX was loaded onto the column by passing through 5 ml of the 50 PPM methanol/water solution. The BTX was then extracted by the use of 5 ml DCM. All fluid was pushed through the column using a syringe with mild force. 0.1 ml of the dodecance internal standard was then added to 1.0 ml of the collected DCM solution. This solution was then analysed with the GC-FID for derivation of the BTX solutions.

From the SPE column extractions it was determined that the Chrom-P SPE columns provided superior extraction in comparison to the C-18 and NH_2/Si columns. Overall extraction efficiencies of 101 ± 2 %, 90 ± 1 % and 98 ± 1 % extraction efficiencies were obtained for benzene, toluene and xylene, respectively.

For all tar entrainment analyses, 180 ml of gas was drawn through the SPE column using a syringe. The tars were elutriated from the solid phase using 4 ml of DCM. The resulting DCM solution was collected and made to 10 ml using a volumetric flask. The tars were then analysed using the GC-FID method described above. It was stated that the maximum analyte loading on the column was 25 mg/SPE column, all SPE column extractions were below the saturation point. This reduced issues with column saturation from excess analyte loading.

4.1.4 Analysis of Water Production during Methanolysis

The uses of Karl Fisher titrations were conducted to determine the water content of the condenser using a TitraLab TIM 550 (HACH, U.S.A) radiometer. The use of Karl Fisher titrations were avoided for the use of acetone condenser solutions as the method utilized methanol in accordance to ASTM E203. As with the regular Karl Fisher titration methodology the use of methanol with a ketone leads to the production of ketals, which in turn react with bisulphites. This ultimately causes interspecies reactions which form water and causes issues in water value convergence. Issues also arose with the use of Karl Fisher titrations and the use of the biodiesel product solution. This was due to the inherent solubility of the water within biodiesel. It was apparent that there were water droplets which would form within the volumetric flask upon removal of the biodiesel from the condenser. A representative sample of the water content in the biodiesel through Karl Fisher titrations, ultimately it was decided that the water content of the condenser would be calculated via oxygen balance, Equation (4.1.7).

$$(\dot{m}(o)_{Biomass} - \dot{m}(o)_{CO} - 2\dot{m}(o)_{CO2})\left(\frac{Mw_{H2O}}{Mw_{O}}\right) = \dot{m}_{H2O} \qquad (4.1.7)$$

Where $\dot{m}(o)$ represents the mass flow rate of oxygen [kg/hr] with respect to the oxygen bearing species. As the system was completely purged and reacted with a non-oxygen bearing species it was assumed that all oxygen within the system products originated from the biomass. This allowed for the back calculation of the water content assuming that CO and CO_2 were the primary oxygenated products from the methanolysis reaction.

4.1.5 Gas Product Analysis

To determine the product distribution of the non-condensable gas phase an Agilent 3000A micron-GC gas chromatograph was used. Gas samples were manually injected by use of a 60 ml syringe which was filled with gas by drawing a sample through a SPE column. This allowed for the gas to be purged from the system and minimized contamination of the gas sample. System conditions are documented in Table 4-3, with the method devised by Bull et al [7]. To determine the overall mass flow rate of the products from the reaction a trace gas stream was introduced after the back pressure regulator. As the

experimental error associated with the trace flow was important an accurate flowmeter was utilized for the introduction of the gas stream. To decrease the uncertainty associated with the inlet gas flow an Alicat flow controller (Alicat Scientific, U.S.A) was ranged down to 0.3-3 SLPM. This reduced the effective uncertainty as the controller uncertainty is determined by 0.8 % of the reading plus 0.2 % of the full scale.

Table 4-3: Agilent Micro-GC system operating and configuration settings.

Configuration	Channel 1	Channel 2
Column	Molecular Sieve 5A plot	Plot Q
Detector	Thermal Conductivity	Thermal Conductivity
Injector	Backflush	Fixed Volume
Carrier Gas	Argon	Helium
Operating Conditions		
Inlet Temperature	95 °C	95 °C
Injector Temperature	95 °C	55 °C
Column Temperature	85 °C	60 °C
Sampling Time	15 s	15 s
Injection Time	10 ms	15 ms
Run Time	180 s	240 s
Column Pressure	207 kPa	138 kPa
Backflush time	10 s	10 s
Products Analysed	H_2, N_2, CH_4, CO, O_2, He	CO_2, C_2H_4, C_2H_6, N_2O

Initially a 50/50 He/N_2O gas was used as the gas tracer, this allowed for the derivation of the outlet mass flow rate by both channels and investigation of the uncertainty between columns. It was discovered that the helium concentration measurement was always significantly lower than the nitrous oxide. Ultimately it was discovered that matrix effects between methane and nitrous oxide led to significant variations in the nitrous oxide measurements. This caused significant uncertainty in the overall volumetric flow rate derivations. In turn, pure helium was instead used as a tracer which only allowed for effective measuring on channel 1, as channel 2 utilized helium as the carrier gas. To decrease the analytical uncertainty, the system was calibrated regularly.

4.1.6 Product Characterisation Calculations

Due to the combination of methane degradation reactions alongside those of the methanolysis reactions the overall content of solids produced was of interest. To do so the relative production of carbon and char were calculated separately. The values were calculated and not measured as this involved a lengthy cool down of the reactor and complete disassembly of the system as well as significant uncertainty in the measurements. Prior to each experiment a degradation sample was taken, which allowed for the preliminary carbon formation value. At the end of the experiment a final degradation value was also taken. The initial and final MTD samples were taken by allowing methane to flow through the system for 5 minutes to provide an adequate purge of the system. Equation (4.1.8) was used for the calculation of the relative carbon produced which could be attributed to the degradation of methane, however it is important to note that it is not believed that this value is constant during a trial.

$$\dot{m}_{(CH4,react)} - \left[\dot{m}_{(CH4,prod)} + \dot{m}_{(H2,prod)} + \dot{m}_{(C2H4,prod)} + \dot{m}_{(C2H6,prod)}\right] = \dot{m}_{(Carbon)} \quad (4.1.8)$$

From the derivation of the carbon mass flow rate the char flow rate could be determined assuming that the carbon production was constant throughout the trial. The char production was calculated relative to the biomass which was introduced for each experiment.

$$\dot{m}_{Char,prod} = ([\dot{m}_{(CH4,react)} + \dot{m}_{(Biomass,react)}] - [\dot{m}_{(CH4,prod)} + \dot{m}_{(H2,prod)} + \dot{m}_{(C2H4,prod)} + \dot{m}_{(C2H6,prod)} + \dot{m}_{(CO2,prod)} + \dot{m}_{(CO,prod)} + \dot{m}_{(H2O,prod)} + \dot{m}_{Tars,prod}])/\dot{m}_{(Biomass)} \quad (4.1.9)$$

From the stated carbon and char production flow rates described above the notation of solids flow rate was also useful to use when distinguishing between char and carbon flows. The overall solids flow rate is the accumulated carbon and char flow rates, equation (4.1.10). It was calculated through the mass balance of the system once the outlet tars, gas, water and inlet mass flow rate were determined.

$$\dot{m}_{(Char,prod)} + \dot{m}_{(Carbon)} = \dot{m}_{(Solids)} \quad (4.1.10)$$

To determine the apparent methane production during methanolysis, the methane flow rate produced during the experiment is subtracted from the methane flow rate during degradation.

$$\dot{m}_{(CH4,prod)} = \dot{m}_{(CH4,Expt)} - \dot{m}_{(CH4,Deg)} \quad (4.1.11)$$

Due to the use of methane and the relative MTD characteristics during methanolysis the effective derivation of the value of the methane production $\dot{m}_{(CH4,prod)}$ induced significant error. This is due to the variation of the methane flow rate from MTD before and after the experiments. This variation in the overall methane flow rate shows significant variations which strongly influence the overall solids production flow rate. Therefore, the overall char and carbon mass flow rates provide an indication of the carbon production characteristics during a trial.

4.1.7 Biomass Feed Characterisation

The pinus radiata feed which was sourced from Red Stag timber was fully characterised at Scion, Rotorua. An extensive analysis was conducted which determined the; % ash, elemental composition, % DCM soluble, % carbohydrates, % klason lignin, % acid-insoluble ash and % acid-soluble lignin. Four separate samples were taken for the characterisation of the chip, further information on the analytical technique and results can be found in Appendix A .The C,H,O,N,S elemental composition and main trace metals are given below in a summary.

Table 4-4: Radiata chip elemental and trace element composition.

Elemental Composition	**Carbon**	**Hydrogen**	**Oxygen**	**Nitrogen**	**Sulphur**
% o.d. Wt.	47.77	6.37	44.97	< 0.3	< 0.3
Trace Metal	**Magnesium**	**Potassium**	**Calcium**	**Iron**	**Sodium**
mg/kg	108	453	411	26.3	19.6

4.2 Free Energy Modelling

In this study the products from the methanolysis of *Pinus Radiata* were investigated. The temperature and pressure of the process is believed to have significant effects on the carbon conversion percentage, phase and composition of the results. The variation in product distribution have been briefly investigated by literature [8]–[10]. It is because of this large variance in product selectivity, Gibbs free energy modelling of methanolysis is a useful tool. Chemical modelling of such a process allows for insight into the influential process parameters to aid understanding of process trends. Ultimately, it is hoped that with the knowledge gained from the model, the methanolysis process influences can be better understood.

For the purpose of this investigation the use of a Gibbs free energy model was employed. This model is an equilibrium model as it models the process as if the reaction were to reach equilibrium (essentially if there were infinite time). The variation in the two models arises from the inputs. When using a Gibbs free energy model the equilibrium product composition is calculated by the combination of products which minimizes the Gibbs energy of the system, no reaction sets are required for this process. This model system was chosen as the number of products from pyrolysis can accumulate to over 100 different species [11]. Since there is no literature on the modelling of methanolysis of *pinus radiata* it was effectively decided that a Gibbs free energy model was most appropriate. Limitations and deviations of the products from kinetic and equilibrium modelling systems will be discussed later in the report.

4.2.1 Model Development Method

The modelling process was divided into two separate sections; 'BCE modelling' (BTX, Carbon monoxide and ethylene), and 'sulfur and nitrogen' modelling. For all of the modelling scenarios Unisim was used as the simulation reaction conditions. The models were all constructed using the *Soave–Redlich–Kwong equation (SRK) fluid package* by using a set of components which governed the formation of the products. These stated components were the species which were used by the fluid package for the Gibbs free energy reactions, a list of all the components is given in the Appendix B. Following the temperature modelling, a number of the species were altered for the pressure, molar ratio and moisture content models.

Since biomass has a very complicated structure and is not an inlet component which can be selected by Unisim, a representation of the biomass had to be produced for simulation of the species. This was conducted by producing an element balance across the biomass input. For the 'BCE modelling' the concentration of nitrogen and sulfur were deemed negligible; hence, an equivalent chemical composition formula for *pinus radiata* was given by $CH_{1.5}O_{0.8}$, this formula defined the composition of one mole of biomass. For all of the modelling the flow rate of the inlet species was calculated for a mass flow rate of 2 kg/hr of biomass by use of the equations below. As the stated formula could still not be used in the Unisim program representative species were determined by use of mass and molar balances. Matrices were produced for these stated balances and by trial and error of the inputs (A and B) the corresponding values of x, y and z could be determined, where C(A), H(A) and O(A) is the concentration of carbon, hydrogen and oxygen in species A, respectively. The definitions are identical for that of species B.

$$CH_{1.5}O_{0.8} + \mathrm{x}CH_4 \rightarrow yA + zB \qquad (4.2.1)$$

By use of the results obtained by the above equation the following chemical equation was derived:

$$CH_{1.5}O_{0.8} + 3.1CH_4 \rightarrow 2.05C_2H_6 + 0.8H_2O \quad (4.2.2)$$

By use of the above equation the biomass could now be modelled as a corresponding inlet feed. This is the advantage of using a Gibbs free energy model, as the species which comprise of the inlet are not important. This is due to the fact that the Gibbs free energy will be minimized by the outlet components which are defined.

The representative feed was altered slightly for that of the nitrogen and sulfur modelling. The equations below were utilized and the chemical equation, was derived. The inclusion of the sulfur and nitrogen element composition of the biomass, where the variables N(A) and S(A) is the nitrogen and sulfur concentration in species (A), hence:

$$CH_{1.5}O_{0.8}N_{0.0001}S_{0.0033} + uCH_4 \rightarrow \text{vA} + wB + xC + yD + zE \quad (4.2.3)$$

$$CH_{1.5}O_{0.8}N_{0.0001}S_{0.0033} + 5.08CH_4 \rightarrow 1.15H_2 + 0.62H_2O + 3.04C_2H_6 + 0.003COS + 0.00015NO_2 \quad (4.2.4)$$

For the case of the Nitrogen and sulfur trials, some sulfur and nitrogen bearing compounds were added to the component list for the Gibbs free energy balance, Appendix B. Following the development of all the representative inputs for the system models, the models were created by using the Gibbs free energy reactor in Unisim. The temperature of the system was set by the temperature of the outlet lines and the pressure was determined by the inlet stream pressures.

To allow for the investigation of the effects of excess moisture in the biomass, another stream of pure liquid water was added to the Gibbs free energy reactor. To simulate associated excess moisture all values were conducted on a weight percent basis with the formula $CH_{1.5}O_{0.8}$ (Molecular Weight = 26.3g/mol). Excess methane was calculated on a molar basis and determined from the stoichiometry of the methane. For all of the data collected from the modelling, carbon balances were conducted so that an overall carbon conversion could be calculated. This allowed for more meaningful results as the overall yields of products can be misleading as a direct figure.

4.3 References

[1] W. L. Saw and S. Pang, "Co-gasification of blended lignite and wood pellets in a 100 kW dual fluidised bed steam gasifier: The influence of lignite ratio on producer gas composition and tar content," *Fuel*, vol. 112, pp. 117–124, 2013.

[2] T. Wigley, "Improving the quality of bio-oil by fast pyrolysis of acid leached and torrefied Pinus radiata A thesis submitted in full fulfilment of the requirements for the Degree of Doctor of Philosophy in Chemical and Process Engineering at the University of Canter," 2015.

[3] M. Tariq *et al.*, "Identification, FT-IR, NMR (1H and 13C) and GC/MS studies of fatty acid methyl esters in biodiesel from rocket seed oil," *Fuel Process. Technol.*, vol. 92, no. 3, pp. 336–341, 2011.

[4] K. Eder, "Gas chromatographic analysis of fatty acid methyl esters," *J. Chromatogr. B Biomed. Sci. Appl.*, vol. 671, no. 1–2, pp. 113–131, 1995.

[5] K. M. Meney and C. M. Davidson, "Use of solid-phase extraction in the determination of benzene, toluene, ethylbenzene, xylene and cumene in spiked soil and investigation of soil spiking methods," *Analyst*, vol. 123, no. 2, pp. 195–200, 1998.

[6] M. A. MOTTALEB, M. Z. ABEDIN, and M. S. ISLAM, "Determination of Benzene, Toluene, Ethylbenzene and Xylene in River Water by Solid-Phase Extraction and Gas Chromatography," *Anal. Sci.*, vol. 19, no. 10, pp. 1365–1369, 2003.

[7] D. Bull, "Performance Improvements to a Fast Internally Circulating Fluidized Bed (FICFB) Biomass Gasifier for Combined Heat and Power Plants," pp. 1–232, 2008.

[8] M. Steinberg, P. T. Fallon, and M. S. Sundaram, "Flash pyrolysis of biomass with reactive and non-reactive gas," *Biomass*, vol. 9, no. 4, pp. 293–315, 1986.

[9] and M. S. S. M. Steinberg, P.T. Fallon, "Flash Pyrolysis of Biomass with Reactive and Non-Reactive Gases," Richland, Washington, 1984.

[10] M. Steinberg, "Flash Pyrolsyis of Biomass with Reactive and Non-Reactive Gases," 1984.

[11] a.V. Bridgwater, D. Meier, and D. Radlein, "An overview of fast pyrolysis of biomass," *Org. Geochem.*, vol. 30, no. 12, pp. 1479–1493, 1999.

5 Investigation into the Effect of Chip Preparation and Characterisation of Biomass using a Thermogravimetric Analyser

This chapter investigates the preparation and characterisation of the biomass feedstocks which were used during methanolysis. An investigation into the properties of the chip produced from various different milling devices was used and the product was investigated to determine the suitability of the chip when feeding. The pyrolysis characteristics of *Pinus Radiata* chip were also investigated to investigate the kinetics of the biomass constituents (lignin, cellulose and hemicellulose). Due to the crossover of particle sizes from the feedstock and the prepared chip, the term chip is used to describe the product and the feedstock.

5.1 Investigation into the Effect of Chip Preparation Techniques

The Wiley mill is a rotating knife mill with 4 rotating blades and 6 fixed blades, Figure 5-1. The rotating blades are fixed on a rotating block head which is centralized and shears particles which are introduced from the top via a manually operated feeding hatch. The clearance between the stationary and rotating knives are adjustable and affect the milling efficiency; the knives were set with a clearance of 0.1 mm. The mill is constrained by the size of the particles which are fed into the system, with an upper limit of 8 mm (for softwoods). Target product sizes can be obtained by changing the sieve which is located at the bottom of the mill. Due to gravity, the biomass travels to the bottom of the mill, where if the chips are of suitable dimensions will pass through and is collected. The remaining chips are collected on subsequent rotations of the milling head which further shears the biomass until passable through the sieve. A sieve screen of 2 mm was used for all experiments unless explicitly stated. The use of the Wiley mill was chosen as a sample of feedstock prepared via this milling technique produced chip with desirable feeding characteristics. From previous research, it was also apparent that Wiley milled biomass enhanced the flowability of biomass in feeding systems [1]. The Wiley mill was operated by loading a compartment with biomass and opening the hatch which releases the biomass into the milling environment. The latch is then closed again which allows particles to circulate throughout the mill, Figure 5-1. The closing of the hatch provides sealing which induces rotational motion of the chips about the rotating head. Due to the high heating rates which are desired in the reactor, small sawdust particles were targeted, < 1.4 mm. For thermochemical reactions the size of the feed sawdust particle is a very important characteristic. This is due to the fact that wood is a very poor conductor of heat, therefore when conducting thermochemical conversion reactions temperature gradients can exist due to poor heat transfer through a large particle. It has been reported that at particles sizes of 355 μm [2] , the thermochemical reaction with biomass is heat transfer limited. For the operation of the methanolysis reactor it is best to have the reaction limited by heat transfer, as this can remove experimental artefacts from results. When investigating the feeding

characteristics of the produced sawdust the biomass sieved fractions used were; 1.0-1.4 mm, 0.71-1.0mm, 0.5-0.71 mm and 0.355-0.500 mm.

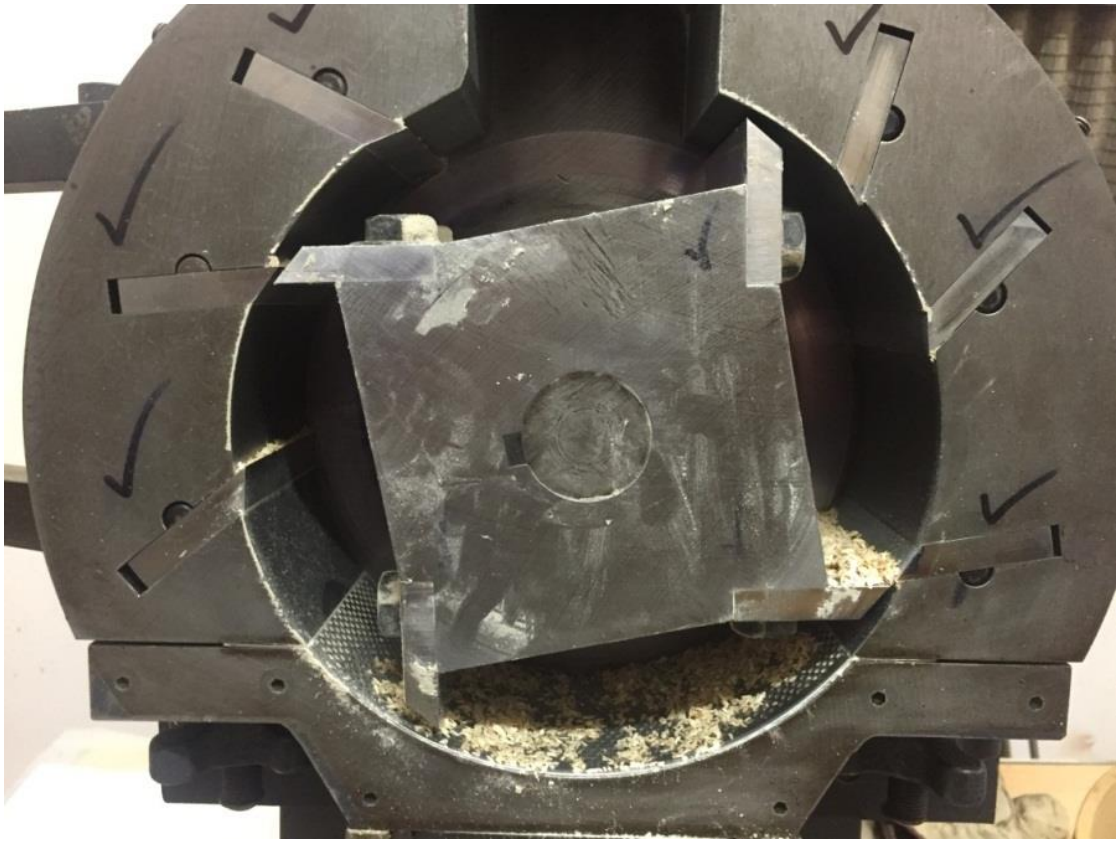

Figure 5-1: Interior of the Wiley mill with the biomass inlet shown above.

5.1.1 Investigation into the Effect of Chip Source

During the preliminary experiments to characterise the feeding mechanism, Pinus radiata was collected from two different sawmills; (RS) Red Stag Timber (Rotorua, New Zealand) and (SRS) SRS Rolleston Mill, (Christchurch, New Zealand). The chip from Red Stag was prepared by hand selecting a discrete log with minimal defects and placing the complete log through a chipper. The chips were screened using two 5 mm Williams screens placed in-between two 6 mm rod screens. The chips were then air dried at ambient conditions and bagged. The Williams screens configuration used decreased the probability of chips above the 8 mm threshold bring collected. The chip collected from SRS Rolleston was obtained from the overflow bin for the heat recovery boiler. This chip was a combination of all the drop saws used on site which cross cut logs to produce uniform sized logs in the production line. This chip was collected green from the site and oven dried at 104 °C before being placed in a humidity controlled room to keep the moisture content of the biomass at 12 %. The moisture content of the feed chip is a very important parameter as it must be kept below < 15 % to ensure effective milling from the knife mill [3].

When designing the hopper system, a sample of Wiley milled biomass was utilized in the cold model feeding trials. This sawdust was produced from chip which was sourced from SRS Rolleston. The hopper and rotating ball valve feeding system was designed from this product and tested using several different sieve fractions. Chip was subsequently prepared by OJI Fibre at the RS timber mill in Rotorua, New Zealand. After the hopper and feeding system had been constructed the prepared Red Stag timber chip was milled using the Wiley mill. It was apparent that none of the sieved chip fractions prepared using the Red Stag timber would feed through the system. The original trialled biomass which was used in the design phase was trialled and fed through uniformly for all sieved fractions. As a large amount of analysis had been conducted on the pre-prepared chips from Red Stag it was in our best interest to produce chip which would feed through the designed system.

In an attempt to utilize the Red Stag timber chip, the efficiency and effectiveness of the Wiley mill the knife spacing's between the stationary and fixed knives were varied. The chip produced was sieved into multiple fractions and the distributions of different chip fractions were recorded, Figure 5-2. The entire sieve fractions prepared, irrespective of the knife clearance, did not feed through system. This was observed by bridging and arching occurring within the hopper. From the trials it was determined that the particle size distribution was not dependent on the knife clearance settings. This was observed by the large distribution differences which occurred when trying to replicate data and determine any potential trends in the production of the chips. It was also found that although a 2 mm outlet sieve was used all chips produced were < 1.4 mm. This was in agreement with work from McCabe et al, which stated that fragments passing through a product sieve have a mean length of 60 % the diagonal opening of the sieve [4]. It is believed that the large variation in particle distribution may also be caused by the amount of sieving that is conducted in the preparation of the sieve fractions. To sieve the material, a mechanical vibrating sieve was used where the sawdust was sieved for 10 minutes with maximum magnitude and short intervals. It was observed that after the material had been sieved there were still chips which were able to pass through the sieve when agitated by hand. This was observed to be due to the blocking of the sieve pans which occurs with biomass as the feed readily became fixed within sieve pores. When the chip was collected, a large proportion of the chip was observed to be stuck within the pores of the sieve and required brushing out before sieving further material. Ultimately it is believed that this led to an over representation in the larger mass fractions in comparison to the lower size interval fractions.

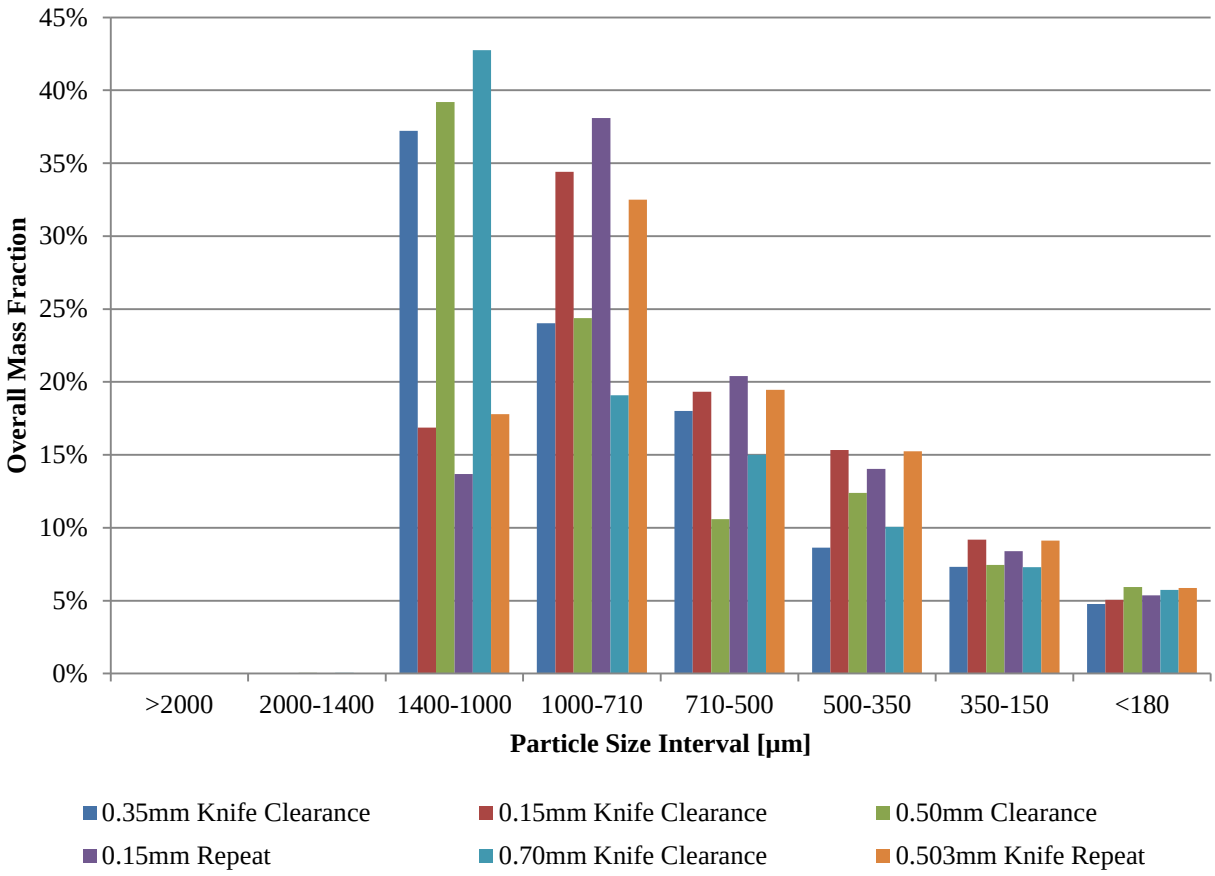

Figure 5-2: Wiley Mill sieve fraction distribution for various knife clearance dimensions, all chip sourced from Red Stag Timber conducted with a sieve size of 2 mm placed in Wiley mill.

To further investigate the leading effect of the chip preparation, the chips collected from Red Stag were chipped and oven dried. Approximately 200 g samples of the chips were oven dried at 105° for 12 hrs to ensure 0 % MC in the sample, before the chip was milled. The feeding of the produced chip was very poor and it was observed that complete drying of the chip prior to milling reduced the flowability of the biomass. It was determined that due to the absence of moisture; the particles were prone to collecting electrostatic charges which caused significant arching within the hopper.

For further chip comparison, chip from SRS Rolleston was collected to determine the differences in chip characteristics to gain insight into the chip preparation. The chip collected from SRS chip was smaller and much more irregular than the RS chip, Figure 5-3. The overall average SRS chip particle size was believed to be significantly smaller due to the cross cutting of the logs. With the Wiley mill set with a knife clearance of 0.1 mm, chip was prepared in the sieve fractions of; 1.0-1.4 mm, 0.71-1.0mm, 0.5-0.71 mm and 0.355-0.500 mm for both the RS and SRS chip. It was determined that all feed prepared from SRS chip performed well in the feeding system; whilst, all the chip fractions prepared from RS origin was unable to feed. From this finding it was believed shape of input feed to

the Wiley mill was very influential to the characteristics of the end chip product. To try and utilize the prepared and fully characterised RS chip, the chip was passed through several different mills prior to the Wiley mill. The RS chip was chipped in three different chippers; hammer mill, wood chipper and the Wiley mill configured with an 8 mm outlet sieve.

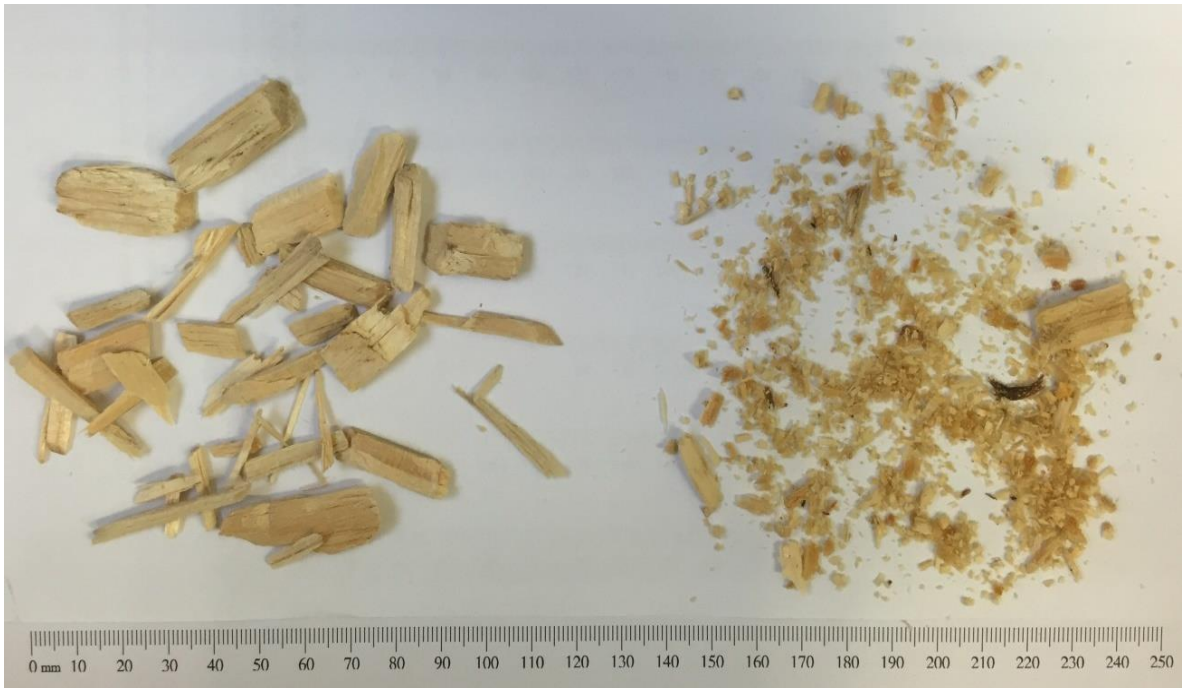

Figure 5-3: Difference in different feedstocks; Left: Red Stag Timber Chip, Right: Rolleston Sawmill.

The hammer mill comprises of a rotating interior head which shears the biomass against the casing of the mill, similar to a Wiley mill. The system has much higher tolerances between knives and was observed to form a uniform rectangular product. The product which the hammer mill formed was undesirable due to a number of long splinters like strands being formed. Overall these chips had the same length as the feed chips only narrower. This was fed into the Wiley mill and sieved into the appropriate trial fractions. It was apparent by visual inspection that the use of the hammer mill had exemplified the problems with the formation of long diamond like biomass particles predominantly formed. The entire product created in this method was unable to successfully feed through the hopper system. A second pre-treatment mill was trialled which rendered similar results. The mill was a wood chipper which had fixed blades and comprised of a rotating cutting blade within a metallic housing. The product formed was very similar to that of the hammer mill. All feed sawdust fractions prepared with this pre-treatment also did not successfully feed.

The final pre-treatment process which was investigated was using the Wiley mill at a different sieve fraction outlet size, 8 mm, and then re-feeding with a 2 mm sieve. The product from this was observed to be much more uniform in shape and particles were observed to be significantly shorter than with

the previous mills trialled. After feeding this product under the 2 mm sieve constraint, the feed was trialled and was unable to be successfully fed through the system. It was also noted that a significant amount of sawdust (< 355 µm chip) was produced in the product stream. It was determined that the product which was formed in this process was essentially the same as if the 2 mm screen was used from the onset. Hence it was concluded that the chip origin and initial preparation of the chip was more important than the subsequent milling into sawdust.

To conclude, it was determined that the Wiley mill product was very sensitive to the initial feed stock characteristics. Considering the random and arbitrary nature of the shearing which is involved between the particles large variations in product were determined between various starting chips. The combination of cross cut chips and significantly smaller particles is believed to have allowed for less cuts being performed for each biomass particle. This is believed to have reduced the overall production of rectangular shape particles and increased the average cubicity of the produced chip. This was justified by the ease of feeding within a hopper which was designed with a 30° angle and an outlet of 25.4 mm, Figure 3-23. It was determined during the course of the experiments that the RS chip caused significantly more arching of the biomass in the hopper during feeding. This could be felt when inserting a small steel rod and mixing the biomass to break the arch and keep feeding constant. Arching was the most common at the constriction of the hopper, just before the ball valve. Ratholing was also experienced but to a much lower extent and only when there was a small amount of feed before the restriction of the hopper this helped to visualise the characteristics of the blockage.

To conclude, all of the subsequent feed for the following experiments was to be sourced from the SRS Rolleston mill. Feed was collected and dried completely in large ovens to reduce the water content before placing the feed in the air conditioned room. This was conducted to ensure that the feed would not rot or degrade during the storage period as the chip had a tendency to rot due to the high water content on collection.

5.1.2 Characterisation of Milled Biomass

To better understand the feeding characteristics of the system and ensure adequate feeding throughout the trialling period an investigation into the sawdust characteristics was conducted. It was observed that the chips which were produced with the RS chip were significantly longer and thinner than the SRS chip. When the SRS chip was milled the product chip was significantly more cubic in structure. 1.0-1.4 mm, 0.71-1.0mm, 0.5-0.71 mm and 0.500-0.355 mm fractions were all used and all proved to block in less than 5 revolutions of the ball valve at the constriction of the hopper. This showed that it was not the feeding mechanism which was blocking, and that the feeding blockages were due to the chip fed into the hopper. To better understand the mechanisms that caused the blockages in the hopper, the chips were magnified x 10. As observed in Figure 5-4 and Figure 5-5, significantly more

long strands of biomass were seen to propagate off the sides of the biomass chip of RS origin. In Figure 5-5 below at point C, an example of a severe case is shown. Strands of biomass like this were apparent in many of the chips produced from the RS timber chip. This particular strand has an overall length of 0.45 mm from the 'base' of the biomass chip to the end of this protruding feature. Protruded sections like this were calculated to increase the overall dimension of the characteristic chip width by 75 %. This increase in apparent width of the chip leads the system to become susceptible to arching as the effective width of particles increases, increasing the possibility of a lattice like structure forming during feeding. Given unideal packing of the particles into the hopper, the likelihood for blockages are greatly increased as the orientation of these particles determines the hopper effectiveness. As identified by A and B in Figure 5-4, similar splinter like features are apparent from the SRS chip. However, the extent and length of these propagations are significantly smaller and decrease the likelihood of blockages during feeding is significantly reduced.

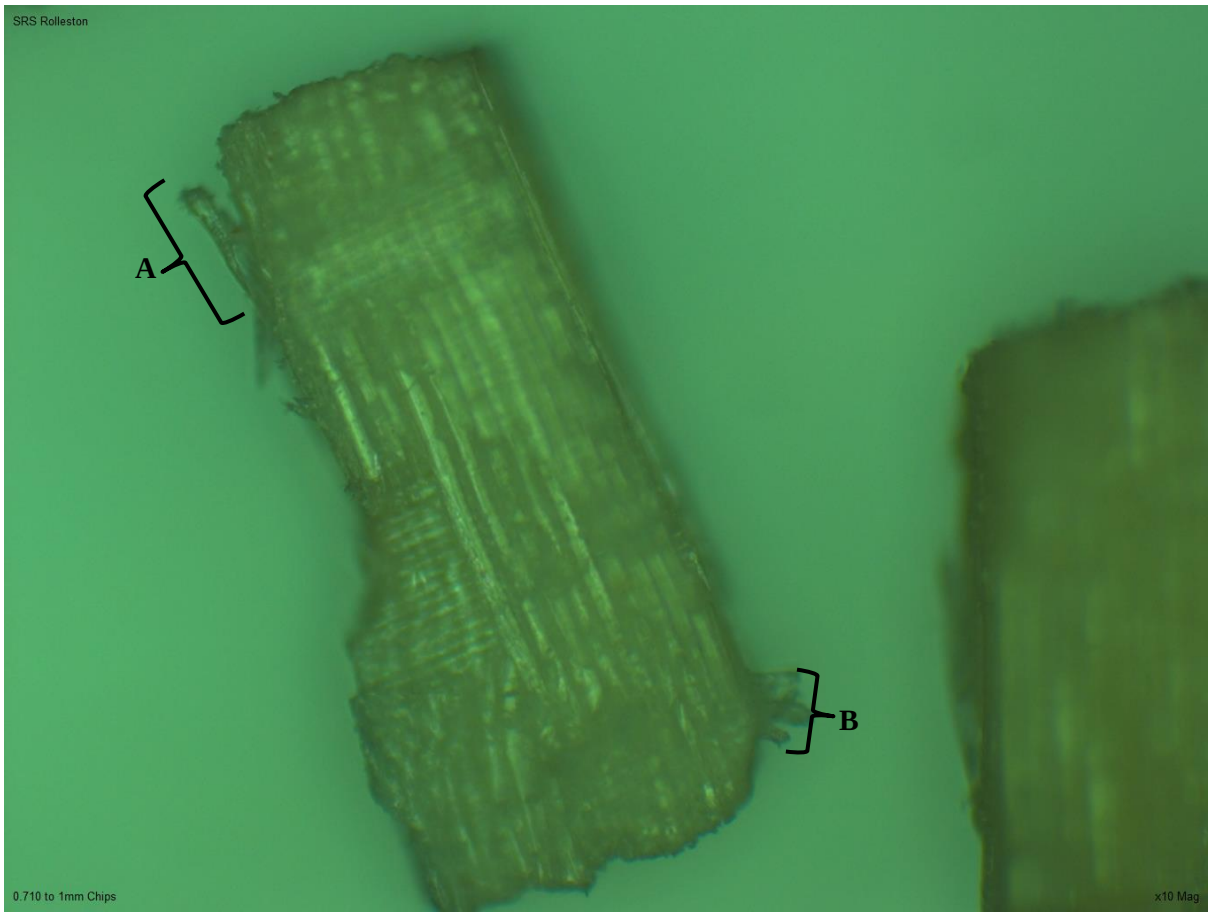

Figure 5-4: x10 Magnification of a 0.710-1.000 mm SRS chip.

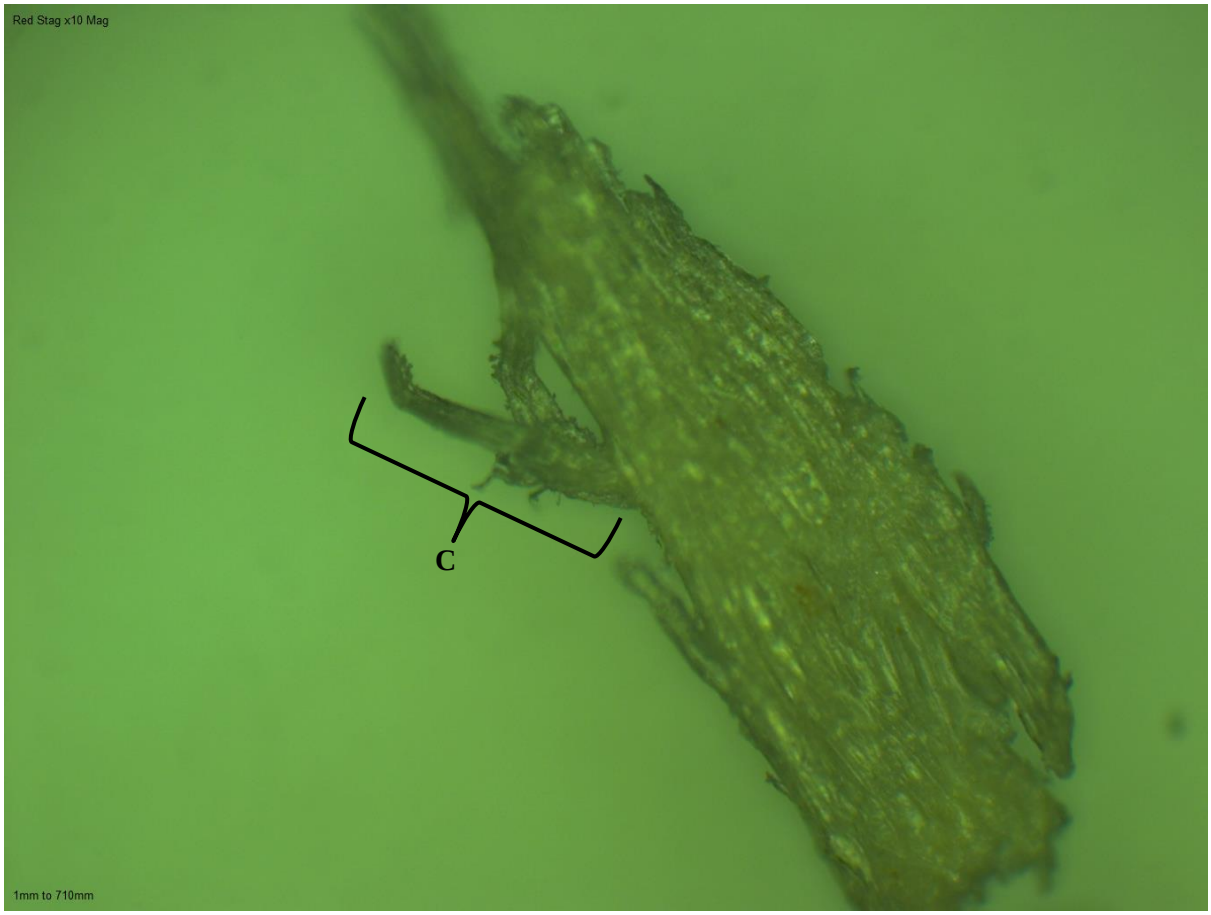

Figure 5-5 x10 Magnification of a 0.710-1.000mm RS chip.

The large splinters exhibited from the RS chip are thought to be due to the chip being much larger in the direction of the grain of the biomass. Due to the random chip orientation during milling and the increased strength of biomass perpendicular to the grain , it is believed that the chip are subject to a shearing force with the grain, or at an angle [5]. At an angle, the particles are subjected to tearing and producing particles with irregular ends which are seen to flare due to the grain structure, Figure 5-6 . If the shearing force is with the grain, this will result in long thin chip particles, which are also problematic for the feeding characteristics. It has also been reported that the energy consumption for cross-grain cuts can be up to 100 times that of parallel cuts of biomass [5]. It is suspected that during the cross-cut shearing, fractures and tearing is likely to occur between the grains if the grain structure is not perpendicular to the knives. These chips are likely to have higher length to width ratios (L/W) and tend to induce hopper blockages. When the shearing force is closest to the end of the particle, the chip may effectively bend and tear, resulting in exposing a section of the biomass, hence produce this splinter like feature, Figure 5-6. Due to the larger dimension of the RS chips in the dimension of the grain, several cuts had to be made for the chip to meet the sieving requirement. Hence, the probability of the shearing force occurring at angles increased significantly. The shearing characteristics are random and very difficult to control in such a machine which is why it is believed that the material

preparation before milling was so important. By decreasing the dimension of the feed chips in the dimension which is with the grain, it is thought that the probability and extent of these splinter like features greatly decreased. This is supported by evidence of the slinter like features in SRS chip, however significantly less abundant than that determined from RS chip.

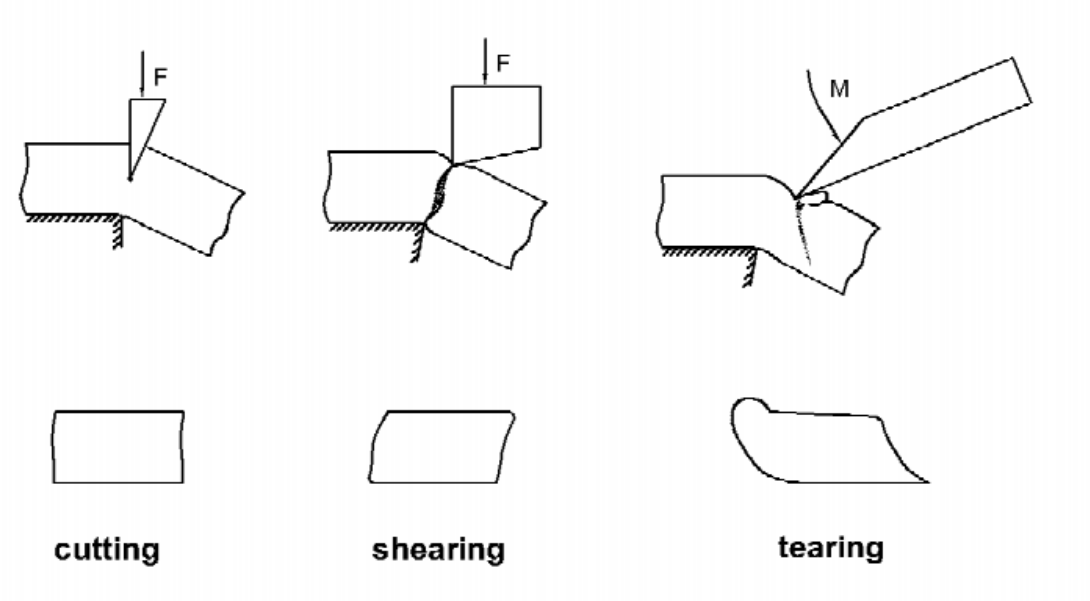

Figure 5-6: Three main size reduction phenomenon which occur during the milling process of biomass, retrieved from [6].

5.1.3 Analysis of the Chip length to width (L/W) Ratio

To rationalise this hypothesis, statistical analyses were conducted on the product chips from the two mills. In total 40 chips of each sieve fraction (1.000-0.710 mm and 0.710-0.500 mm) from each chip source were investigated under a microscope with x 5 magnification. Photos were taken of each individual chip, and the length and width of these chips were measured. The length and width of the chip were measured as the largest distance across the chip in the perpendicular axis to give the apparent maximum dimension of the chips. To aid in definition and manipulation of the data, the term 'length (L)' was given to the largest dimension and 'width (W)' described the secondary dimension, hence; L > W. The analysis was only conducted in 2 dimensions as it was assumed that the third dimension of the particle would not be any larger than the width. From the measurement of individual chips the L/W factor was calculated for the particle. This gave a value which described the geometry of the chip and allowed an average L/W to be determined. As the orientation of the chip is completely random, it is desirable to have a low L/W. This is due to the fact that a sample product with a higher

average L/W is much more prone to blocking as the chance of overlapping and bridging of particles increases.

In total 40 chips of each feed source were measured and statistical analyses were conducted to determine the correlation between the different sieve fractions as well as the same sieve fraction but of different feed source. To determine the correlation between the different sources and the homogeneity between the different sieved fractions. The correlation coefficient was calculated, using equation (5.1.1) . The CORREL feature was used on Microsoft Excel to facilitate this calculation. Along with the correlation coefficient calculations, other primary statistical information was calculated to aide in characterising the chip produced.

$$\rho(A,B) = \frac{1}{N-1}\sum_{i=1}^{N}\left(\frac{A_i - \mu_A}{\sigma_A}\right)\left(\frac{B_i - \mu_B}{\sigma_B}\right) \qquad (5.1.1)$$

It was determined that the SRS chip geometry showed less variation and had a higher degree of homogeneity in comparison to that produced from RS. Table 5-1, shows the statistical values which were calculated for the produced chip. The higher degree of homogeneity was supported from the lower 95% confidence interval between both sieve fractions in comparison to the source. This is observed when regarding the 1.00-0.71 mm sieve fraction, where; SRS and RS chip had (L/W) confidence intervals of 2.0 ± 0.3 and 3.9 ± 0.7, respectively. This shows a significant difference in L/W characteristics of the chips which are produced. This is believed to be indicative of the bridging issues which arose during feeding. This apparent doubling of the length to width ratio of chips is suspected to increase the probability of lattices forming at the hopper constriction. As L/W relates to the level of cubicity, chip samples of higher average L/W ratios have increased chances of inducing blockages.

Table 5-1: Statistical Analysis results of the different feed chips and different characteristics of L/W for the given sieved fractions.

		Rolleston Chip		Red Stag Chip	
Sieve Fraction	***[mm]***	***1.00-0.71***	***0.71-0.50***	***1.00-0.71***	***0.71-0.50***
Average (L/W)	*[-]*	1.97	2.38	3.90	2.77
Median (L/W)	*[-]*	1.80	2.00	3.50	2.30
Std Deviation (L/W)	*[-]*	0.90	0.80	2.18	1.13
Variance (L/W)	*[-]*	0.81	0.64	4.75	1.28
95% Confidence Interval (L/W)	*[±]*	0.27	0.24	0.67	0.35

The variance of the chip produced was also observed to vary significantly between feed sources. The 1.00-0.71 mm fraction of the RS chips product is observed to have a substantial variance of 4.75 mm. This leads to the fact that the variations of the chips geometry is very high, altering the feeding characteristics drastically. It is observed that the RS chip is significantly larger than that of the SRS chip initially; however, the investigation of the particle variance is believed to highlight the effect which this has. Due to the significantly higher cutting frequency, the distribution of the product varies due to increased random distribution of particles. It is believed that this is due to the significantly larger amounts of cuts which RS chip requires before passing through the Wiley mill screen. Consequently, RS chip is much more likely to undergo significantly more cuts, tears and shears than that of the product chip from Rolleston. This therefore increases the probability that the chips have been cut in an unideal fashion and subject to shearing and tearing along an angle to the grain of the wood, Figure 5-6. This effect combined with the increased cutting requirements is believed to severely decrease the feeding potential of the chips.

An interesting comparison in the chip statistical parameters is found when investigating the comparison of the chip sources sieved to 0.71-0.55 mm. From this fraction, it can be seen that the 95% confidence intervals overlap with Rolleston Chip and Red Stag chip having intervals of 2.4 ± 0.2 and 2.8 ± 0.4, respectively. Although the SRS chip L/W ratio on average is slightly lower, the RS chip was also found to have a relatively low L/W ratio. It is believed that the leading cause of bridging from this sample is due to the splintering effect of the biomass which is more pronounced in the RS chip product. As described from the visual inspection of the chips the RS timber sawdust was seen to

produce chips with significantly higher amounts of splinter flaring from the side of the chips, Figure 5-7. The belief that this biomass splintering is detrimental to the feeding characteristics is supplemented by these findings. It is believed that although the chips on average have very similar L/W ratios, the degree of splintering hinders the feeding characteristics of the biomass and induces blockages at the hopper. It is also noted that the variance is significantly higher, which is believed to also add to the increased probability of feed blockage occurring. This effect is apparent in the lower sieve fraction as it is found that the influence of these splinters is amplified at the lower particle sieved sizes. This was also observed when trying to feed < 0.50 mm particles, which blocked the system regardless of feed source.

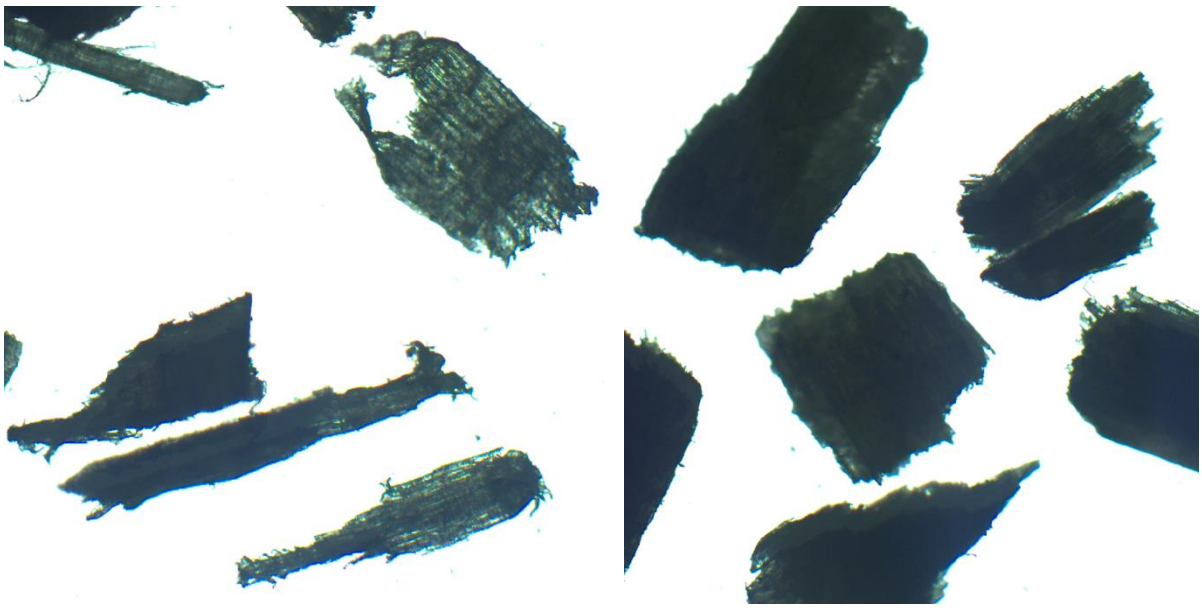

Figure 5-7: Comparison between the Red Stag Timber and SRS Rolleston Wiley milled sawdust product, Left and Right; Respectively (Sieved to 0.710-0.500 mm).

From the calculation of the correlation coefficient between the sieved fractions for the same biomass source, weak correlations were found, Table 5-2. From the analysis it was hoped that the homogeneity of the sample could be further exemplified by a correlation coefficient analysis. It was found that the correlation coefficient for the RS and SRS chip were 0.42 and 0.04, respectively.

Table 5-2: L/W correlation coefficient between the 1.00-0.71 mm and 0.71-0.50 mm sieved fractions.

Chip Source	L/W Correlation Coefficient
SRS Rolleston	0.04
Red Stag	0.42

The correlation coefficient yields a much higher value for that of the RS sawdust product compared to that of the SRS chip. Although the value is low it is speculated that there may be a correlation between the chip product geometry and the milling process. This is also believed to be due to the increased cutting requirements of RS chip. The feed from the SRS chip is also subject to other external factors. The leading factor being, some of the chips collected are already in the correct size range, hence there is a possibility that these chips do not experience a shearing force during milling. In this instance the 'effective' chip does not experience any comminution and the probability of undergoing shearing/tearing greatly decreases.

The physical and mechanical properties of *Pinus Radiata* are important characteristics to consider when investigating the size reduction processes of the biomass material. Biomass is mainly composed of non-brittle materials which mechanical behaviour can be classified between elastic-plastic and elastic-viscous at a low temperature and high stressing velocity [6]. As shown in Figure 5-8, when the stressing velocity is high and biomass temperature low, biomass is reported to exhibit elastic-viscous material behaviour [7]. When excess strain is applied to the chip, depending on the orientation the mechanisms highlighted in Figure 5-6 occur.

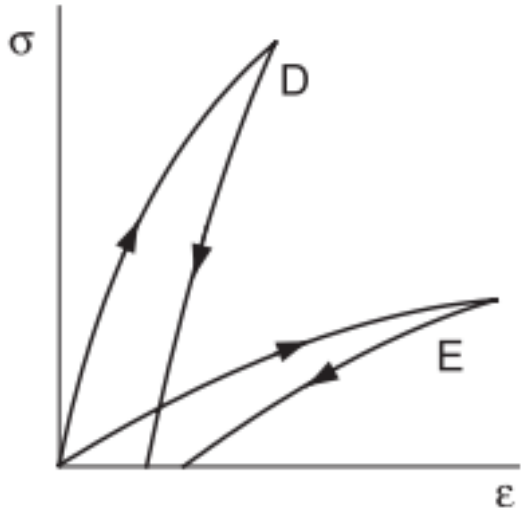

Figure 5-8: Stress-Strain curve for the elastic-viscous material behaviour which occurs at a low temperature with a high stressing velocity (Line D), low stressing velocity (Line E), Adapted from [7].

The difference in size reduction mechanism is also reported to be strongly influenced by the angle of the working tools in reference to the biomass. It has been reported that sharp knives are used for cutting to prevent shearing of the entering biomass and knives with a working angle between 75° and 90° induce shearing within the mill [6] [7]. The tearing of biomass is most apparent when the distance between the stationary and moving knives is large, this causes the particle to bend and exhibit plastic deformation. The combination of tensile stress with bending and torsion of the material is defined as 'tearing' [8]. This process is undesired in the preparation of the wood chips as this is believed to facilitate the production of these long splinter-like features off the side of the chip. From the results obtained in the sieved product yield investigation, it can be concluded that to produce chips with smoother edges it is best to reduce the knife gap. This is important in cutting the particles instead of promoting shearing. The angle of the knives was not altered as this required significant modification of the Wiley mill knives. The knife angle was constant at 40° which is within the cutting regime of mills. For all subsequent trials it is important to keep the knife clearance as low as possible and ensure that knives do not blunt.

A problematic characteristic of biomass is that the yield strength of the chips are not uniform in 2 dimensions, as if the size reduction is occurring with the grain or perpendicular to the blade, the product will differ greatly. It is hypothesised that during the milling process the product chip which is formed is a combination of the difference cuts and induces a range of different particle characteristics. To increase product uniformity between the chip particles it is recommended that the feed chip is first sieved into like fractions and then fed. It was also deemed very important to ensure that adequate sieving of the biomass was conducted. This was due to the discovery of chips below the target chip size within the chip collected. To decrease the extent of sub-sieve fraction size within the collected biomass, the chip was sieved for 30 minutes at least.

5.1.4 Preparation of Alternative Feedstocks

As it was desirable to trial other feedstocks the preparation of feed which would allow for feeding was examined. From the results which were derived from the milling samples a method was derived to ensure adequately formed biomass irrespective of the species. To do so, logs of material were taken and frozen. The log was allowed to freeze completely and was then cut with a saw to form five separate sections, four outer wood sections which completed the perimeter of the log and a central log section, Figure 5-9. These sections where then cross cut using a band saw to form sections of 2 mm plate like lengths. The sections were then broken apart to sections of 8 mm in specification of the Wiley mill. This in turn allowed for accurate control of the extent of cross cut material and induced the milling to concentrate on the commutation of the chip with the grain structure as the cross cell length was already defined by the cross cut section. This produced chip was trialled within the system and readily fed for all sieve fractions trialled; 1.4-1.0 mm, 1.0-0.71 mm, 0.71-0.50 mm and 0.500-

0.355 mm. This also allowed for the trialling between heartwood and outerwood of Douglas fir. Due to the strong difference in physical characteristics of the wood, the sections could be divided manually and chipped accordingly.

Figure 5-9: Preparation of Douglas fir wood for feeding into the methanolysis reactor. Log divided into 5 separate sections for preparation to be further milled.

5.2 Characterisation of Biomass from Thermogravimetric Analysis (TGA) and Investigation into Methane Thermal Degradation (MTD)

This section includes the results of the characterisation of the biomass kinetics during pyrolysis via thermogravimetric analysis (TGA) of the biomass at a number of heating rates. The activation energy and pre-exponential value of the overall volatisation reaction and each biomass constituent; cellulose, hemicellulose and lignin are described and discussed.

5.3 Introduction

To improve understanding of the kinetic behaviour of the biomass constituents during methanolysis, trials utilizing a TGA were conducted. It was anticipated that by characterising the feed materials, the

behaviour of the biomass during methanolysis could be improved. A model was constructed to investigate the nature of the volatisation of cellulose, hemicellulose and lignin.

Due to the high concentrations of hydrogen which were present in the commissioning experiments conducted in the constructed fluidised bed reactor, an investigation into the influence of operational parameters was conducted. An investigation into the potential catalytic activity of some of the system materials within the reaction zone was also conducted. This allowed for characterisation of the system and for improved understanding of the MTD characteristics. This was important to comprehend, as high concentrations of hydrogen in the methane stream during methanolysis was suspected of allowing reaction between hydrogen and biomass. By investigating the influential reactor parameters utilized during methanolysis, it was hoped that the influence of hydrogen produced due to MTD could be reduced.

5.4 TGA and CH_4 Degradation Analysis

In this section the characterisation of the feed biomass chemical structure is undertaken by TGA, from which the cellulose, lignin and hemicellulose portions of the biomass are modelled during the devolatilisation process. The extent of MTD is also described and discussed, with the findings during commissioning MTD experiments with the subsequent improvements conducted and comparisons with other systems.

Initially, the overall weight loss during the temperature profile was investigated, Figure 5-10. The fractional mass devolatilized was determined resulting in the mass fraction proportion remaining in the system plotted against temperature throughout the heating ramp. It was observed that with increasing heating rate the effective devolatilisation of the species occurred at higher temperatures. This was observed as a shift to the right hand side of the mass fraction proportion with increased heating rate. It was also determined that the higher heating rate resulted in lower overall extents of devolatilisation of the biomass as the mass remaining at the end of the trial increased with heating rate. It is suspected that the two phenomenon described above occurred due to the poor heat conduction of the biomass particles. Similar observations were made by Idriz et al [14], who observed similar temperature shifts and attributed this to the reduction in heat transfer to the inner portions of the particles. This phenomenon was investigated in depth by E. Biagini et al [15], who found that the extent of temperature shift with higher heating rates led to variable activation energies for the biomass devolatilisation models. It is suspected that the temperature lag in the core of the particles highlights the requirements of effective heat transfer within the methanolysis system. This is suspected to be vastly improved with the utilization of a fluidised bed system.

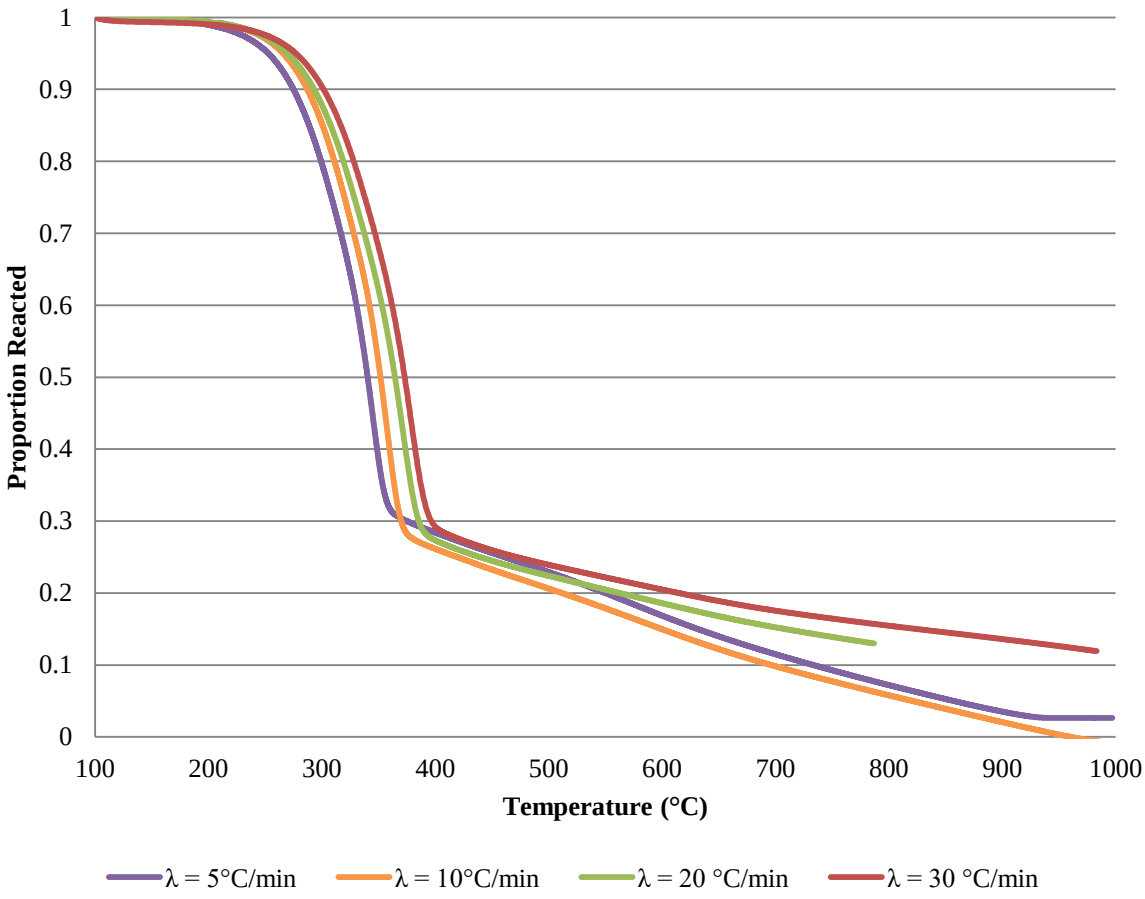

Figure 5-10: Mass fraction volatised during the pyrolysis of radiata pine biomass in nitrogen at various heating rates, (the evaporation of water has been ommited from the graph [XVII]).

To determine the activation energy and pre-exponential value of the overall biomass reaction and the constituents of the biomass, trials were conducted on the TGA. With the composition of the biomass known, the activation energy and pre-exponential value could be derived. For the investigation, 1000-710 µm pinus radiata chips were analysed using a TGA at heating rates of λ = 5, 10, 20 and 30 °C/min in order to predict the devolatilisation of the biomass particles. By the utilization of the method described in the preceding section, the overall pre-exponential factor and activation energy were derived from Figure 5-11. The conversion values were obtained from the experimental data from the TGA analysis and were interpreted by the temperature at which the overall mass loss related to the desired biomass conversion value (x). These values were obtained from the TGA profiles as shown in Figure 5-10.

[XVII] For λ=20 °C/min, data after 800 °C invalid due to negative mass values.

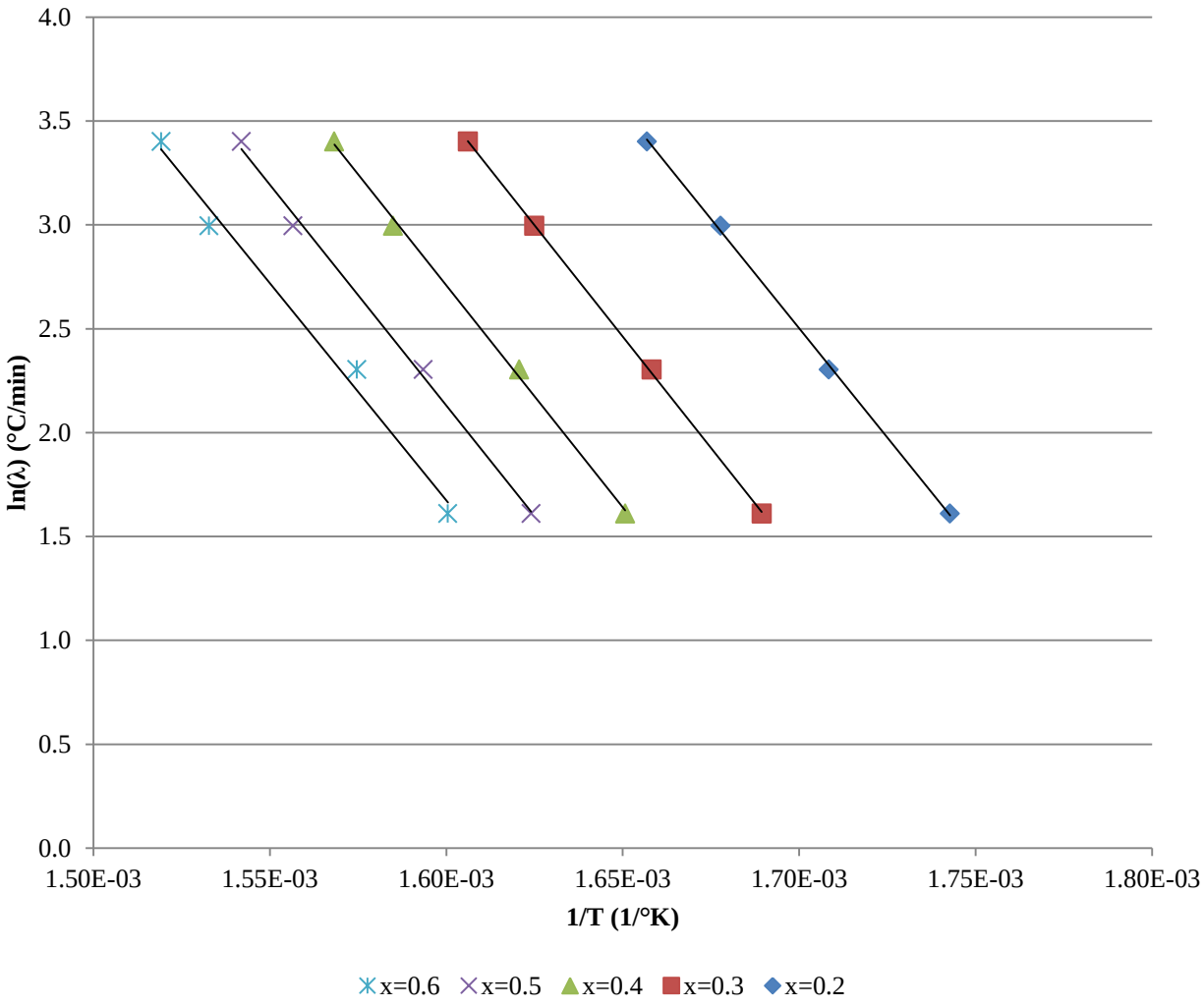

Figure 5-11: Curves of ln(λ) vs. 1/T for various biomass conversions (x).

As the heating rate was increased the temperature at which a given biomass conversion was achieved increased. This is due to the increased interactions with the volatized materials with the increased heating rate. Values of the derived activation energy and pre-exponential value were averaged for the various heating rates and compared to similar work which was conducted on biomass/coal blends, Table 5-3.

Table 5-3: Overall activation energy (E_a) and pre-exponential values (A) derrived from the TGA experiments and from literature.

	Experimental Values (Radiata Pine)		**[xviii]Seo et al. [9]**	
Conversion	E_a	A	E_a	A
-	*(kJ/mol)*	*(1/min)*	*(kJ/mol)*	*(1/min)*
20%	182	$2.7x10^{15}$	177	$3.9\ x10^{13}$
30%	182	$9.1x10^{13}$	153	$2.4x10^{11}$
40%	177	$2.5x10^{13}$	136	$7.3x10^{9}$
50%	173	$7.3x10^{13}$	114	$9.6x10^{7}$
60%	179	$1.6x10^{13}$	143	$1.6x10^{14}$
Median	178	$7.3x10^{13}$	145	$2.4x10^{11}$
Std.Dev	4	$1.2\ x10^{13}$	23	$7.0\ x10^{13}$

From Table 5-3, it was found that the activation energy and pre-exponential factor of the biomass used were significantly higher than those of biomass/coal blends. From the majority of studies on biomass, the use of a one-step reaction for the devolatilisation of the biomass renders activation energies of 60-170 kJ/mol [10]. It has been suggested that this is due to the influences of the biomass species, sample size and heating conditions [11]. It was found that close agreement for the pre-exponential value and activation energy were obtained for all conversion extents, except that of 20 %, which provided significantly larger pre-exponential values, as well as large standard deviations. This highlights the influence of the differing stage of the biomass devolatilisation processes, overall a median value of $7.3x10^{13}$ min^{-1} and 178 kJ/mol was obtained for the pre-exponential factor and activation energy, respective.

5.4.1 Biomass Constituent Kinetics

From the 3 parallel reaction mechanism proposed by Grønli et al [10], a model was created to determine the kinetic values of the biomass constituents; cellulose, hemicellulose and lignin and were

[xviii] Utilizing a biomass/coal blend.

denoted by x_i. The total volatiles released during the pyrolysis process consist of M fractions which were described by first order reaction kinetics:

$$\frac{dx_j}{dt} = A_j \exp\left(-\frac{E_j}{RT}\right)(1 - x_j) \quad M; x_j(0) = 0 \tag{5.4.1}$$

Where the overall mass loss rate can be described by the linear combination of dx_i/dt:

$$-\frac{dY^{calc}}{dt} = \sum_{i=1}^{M} c_j \frac{dx_j}{dt} \tag{5.4.2}$$

Where c_i corresponds to the amount of volatiles that are released during a given interval between t = 0 and ∞. The pre-exponential and activation energy values were determined by using the least squared method, which allowed for the best model fit which minimized the value of equation (5.4.3).

$$S = \sum_{i=1}^{M} \left(\left(\frac{dY}{dt}\right)^{obs} t - \left(\frac{dY}{dt}\right)^{calc} t \right)^2 \tag{5.4.3}$$

The error could then be computed by:

$$Error = \sum_{i=1}^{M} \left(\left(\frac{dY}{dt}\right)_j^{obs} t - \left(\frac{dY}{dt}\right)_j^{calc} t \right)^2 \tag{5.4.4}$$

The model derived the activation energy and pre-exponential factor of the biomass constituents to describe the mass loss profile of the biomass of known composition, during the heating of a sample; plots of dX/dt versus temperature are shown in Figure 5-12, Figure 5-13, Figure 5-14, and Figure 5-15 for various heating rates from 5°C/min to 30°C/min.

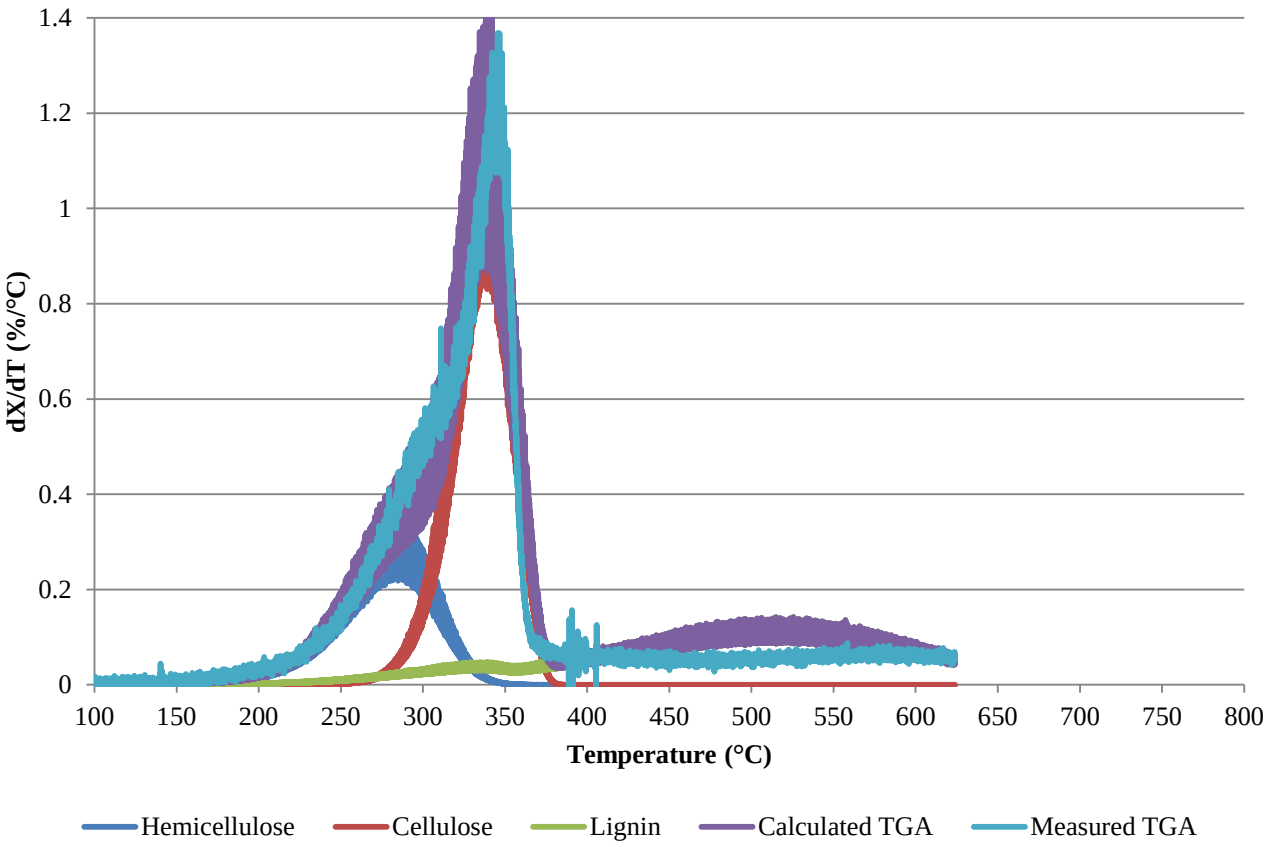

Figure 5-12: 5°C/min ramping temperature mass loss profile for radiata pine biomass, showing the relation between the modelled and measured TGA data, using a model developed by Grønli et al [10].

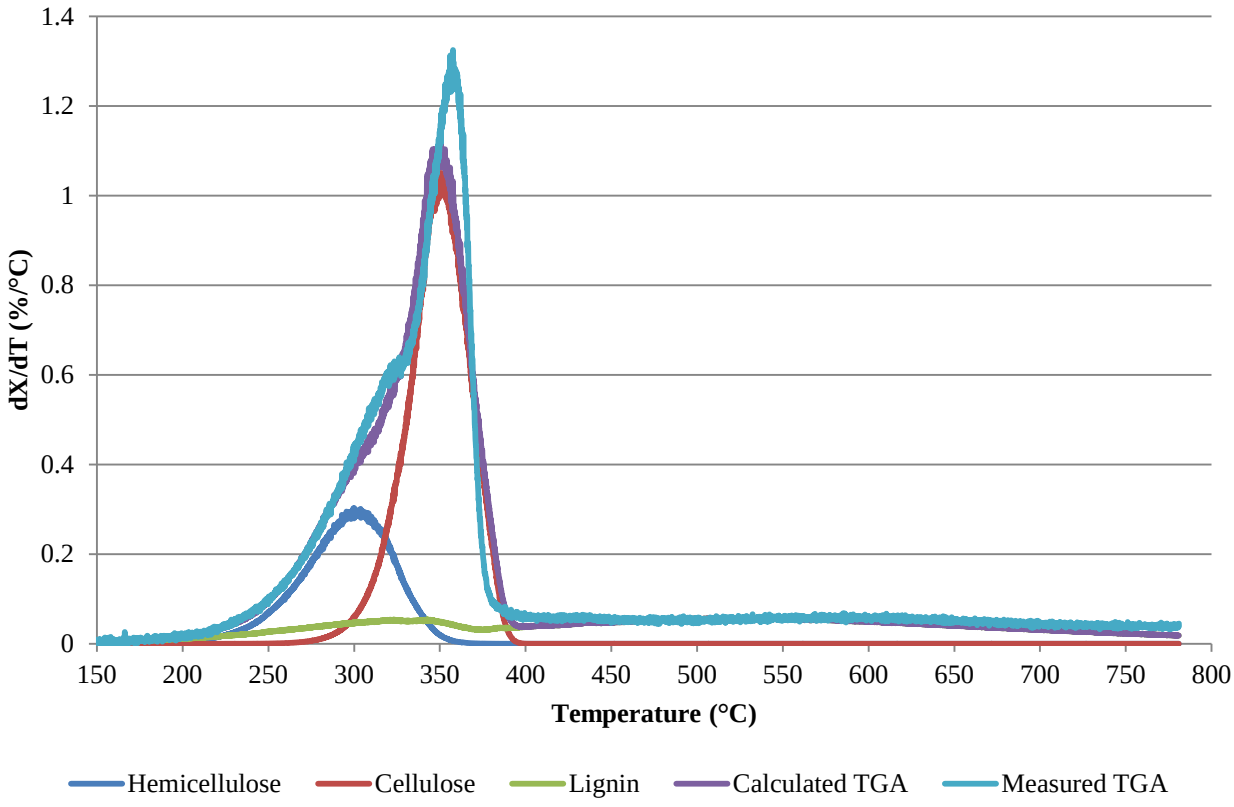

Figure 5-13: 10°C/min ramping temperature mass loss profile for radiata pine biomass, showing the relation between the modelled and measured TGA data, using a model developed by Grønli et al [10].

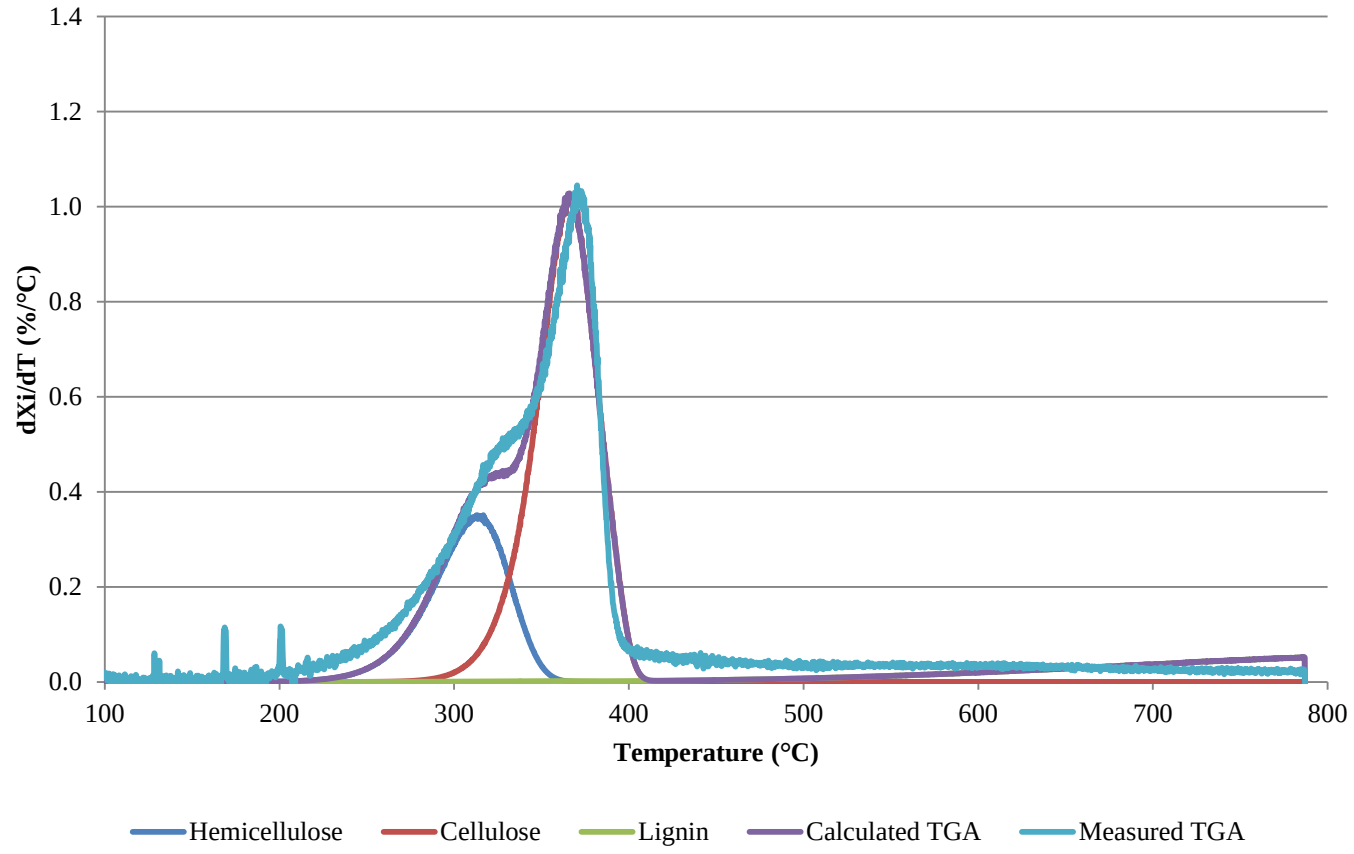

Figure 5-14: 20°C/min ramping temperature mass loss profile for radiata pine biomass, showing the relation between the modelled and measured TGA data, using a model developed by Grønli et al [10].

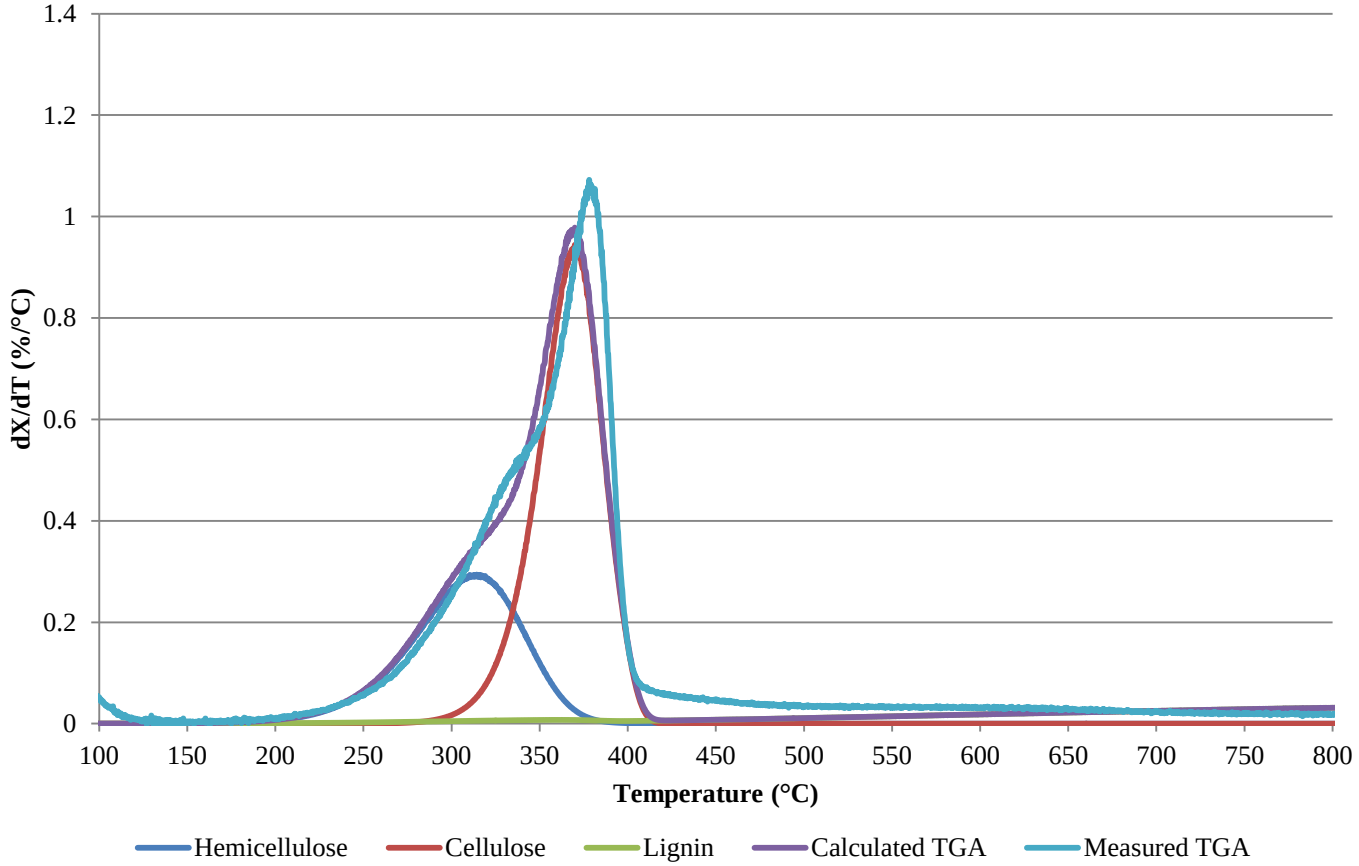

Figure 5-15: 30°C/min ramping temperature mass loss profile for radiata pine biomass, showing the relation between the modelled and measured TGA data, using a model developed by Grønli et al [10].

From the reaction kinetics models, the pre-exponential constants and activation energy values were calculated and their values are given in Table 5-4. The derived values of activation energy are 246 ± 9 kJ/mol, 119 ± 19 kJ/mol and 44 ± 21 kJ/mol, respectively, for the cellulose, hemicellulose and lignin components in the biomass. The values are in agreement with other activation energies from Grønli et al [10], which corresponding values were 236, 100 and 46 kJ/mol at temperatures above 553 ° K, for cellulose, hemicellulose and lignin. The data are also in close agreement with those of Várhegyi et al [12], who calculated an activation energy of 240 ± 10 kJ/mol for cellulose when using lignocellulosic plant samples. This validated that the constructed model, as the data for all biomass constituents was in agreement with those reported in literature. It was, however, noted that issues arose in the modelling of the lignin within the samples as at times the characteristic tail end volatisation of lignin would continue for the duration of the temperature ramp. This would result in faults when using the least square method to determine the associated error in the derivation of the kinetic values. It is suspected that this was primarily due to systematic errors from the utilization of the system, in particular the weighing pans. This was suspected due to the negative values which were derived at times during the TGA of biomass.

Table 5-4: Biomass constituent activation energies as determined by modelling of radiata pine TGA reaction profiles.

Heating Rate	**Cellulose**	**Hemicellulose**	**Lignin**	**Error**
[°C/min]	*[kJ/mol]*	*[kJ/mol]*	*[kJ/mol]*	*[-]*
5	243	105	43	21%
10	240	115	38	7.5%
20	244	143	68	3.7%
30	258	112	26	2.6%
Average	246	119	44	-
±	9	19	21	-

From literature, the pre-exponential values collected for a range of different biomass sources resulted in; cellulose, hemicellulose and lignin pre-exponential values in the vicinity of; $4x10^{17}$, $3x10^{6}$ and 40 s^{-1} [10], [13]. It was concluded that the model provided a reasonable interpretation of the pre exponential value as given in Table 5-5. Large discrepancies between the literature and the work

conducted in this study were observed in the derivation throughout all of the biomass constituents with disparities in the scale of order magnitudes. Issues with the derivation of the hemicellulose kinetics were evident with three orders of magnitude of separation at times exhibited. It was believed that this was exacerbated at the lower heating rates due to the fluctuations in weight values, which caused minimization issues using the least square approach, as seen by the overall error (λ), Table 5-5. The derivation of the lignin pre-exponential value was also subject to large uncertainties and dubious derived values. It is suspected that similar issues with the derivation of the activation energy also affected the calculation of the lignin pre-exponential value. Overall it was determined that the activation energies calculated using the models were significantly more accurate than that of the pre-exponential values. During the derivation of the pre-exponential values, Seo et al [9], also experienced variations in the order of magnitudes, indicating the potential difficulties in convergence for the pre-exponential values via this method.

Table 5-5: Pre-exponential values determined from the TGA analysis for cellulose, hemicellulose and lignin, as determined by modelling of radiata pine TGA reaction profiles.

Heating Rate	**Cellulose**	**Hemicellulose**	**Lignin**	**Error**
[°C/min]	*[s^{-1}]*	*[s^{-1}]*	*[s^{-1}]*	*[-]*
5	3.0×10^{18}	1.4×10^{07}	5.3×10^{01}	21%
10	9.0×10^{17}	1.0×10^{08}	5.7×10^{-01}	7.5%
20	1.8×10^{18}	5.5×10^{10}	1.0×10^{01}	3.7%
30	1.8×10^{19}	7.7×10^{07}	1.5×10^{-01}	2.7%
Average	2.4×10^{19}	1.4×10^{10}	2.8×10^{-01}	-
±	9×10^{18}	3×10^{10}	4.3×10^{-01}	-

In conclusion, the Grønli et al [10], model provided accurate representation of the cellulose, hemicellulose and lignin devolatilisation during pyrolysis. The model fit was observed to increase with higher heating rates as high overall error was associated with the application of 5 °C/min heating rates. The overall activation energies for the biomass constituents were determined as 236 ± 4 kJ/mol, 110 ± 11 kJ/mol and 50 ± 20 kJ/mol for the cellulose, hemicellulose and lignin components in the biomass. Pre-exponential values of; 3.6×10^{17}, 3.2×10^{6} and 39 s^{-1} were derived for cellulose, hemicellulose and lignin. These kinetic values which were determined were in close agreements with those associated with cellulose and hemicellulose. Issues arose in the modelling of the lignin volatisation due to the long tailing sections which were recorded from the analysis, these issues were

observed as high error values when completing the model. It is suspected that the model could be enhanced by utilising a different optimisation strategy as error issues arose from the utilisation of the least squared method. These issues were primarily due to the difficulty in fitting the curves within the long tail-end section of the recorded mass loss. Nonetheless, the overall values which were derived for the lignin kinetic values were within the experimental uncertainty.

5.5 References

[1] T. Wigley, "Improving the quality of bio-oil by fast pyrolysis of acid leached and torrefied Pinus radiata A thesis submitted in full fulfilment of the requirements for the Degree of Doctor of Philosophy in Chemical and Process Engineering at the University of Canter," 2015.

[2] S. Septien, S. Valin, C. Dupont, M. Peyrot, and S. Salvador, "Effect of particle size and temperature on woody biomass fast pyrolysis at high temperature (1000-1400°C)," *Fuel*, vol. 97, pp. 202–210, 2012.

[3] L. Kratky and T. Jirout, "Biomass Size Reduction Machines for Enhancing Biogas Production," *Chem. Eng. Technol.*, vol. 34, no. 3, pp. 391–399, 2011.

[4] W. L. McCabe, J. C. Smith, and P. Harriott, *Scilab Code for unit operations of chemical engineering*, vol. 5, no. October. 1993.

[5] D. N. Lanning, J. H. Dooley, and C. J. Lanning, "Shear Processing of Wood Chips into Feedstock Particles," *2012 ASABE Annu. Int. Meet.*, vol. 7004, no. 12, 2012.

[6] P. I. Miu, A. R. Woma, I. Cannayen, and S. Sokhansanj, "Analysis of Biomass Comminution and Separation Processes in Rotary Equipment. A Review," *ASABE Annu. Meet.*, vol. 300, no. 6, p. Paper number 066169, 2006.

[7] G. Schubert and S. Bernotat, "Comminution of non-brittle materials," *Int. J. Miner. Process.*, vol. 74, no. SUPPL., pp. 19–30, 2004.

[8] D. Woldt, G. Schubert, and H. G. Jäckel, "Size reduction by means of low-speed rotary shears," *Int. J. Miner. Process.*, vol. 74, no. SUPPL., pp. 405–415, 2004.

[9] D. K. Seo, S. S. Park, J. Hwang, and T. U. Yu, "Study of the pyrolysis of biomass using thermo-gravimetric analysis (TGA) and concentration measurements of the evolved species," *J. Anal. Appl. Pyrolysis*, vol. 89, no. 1, pp. 66–73, 2010.

[10] M. G. Grønli, G. Várhegyi, and C. Di Blasi, "Thermogravimetric Analysis and DevolatilizationKinetics of Wood," *Ind. Eng. Chem. Res.*, vol. 41, no. 17, pp. 4201–4208, 2002.

[11] A. F. Roberts, "A review of kinetics data for the pyrolysis of wood and related substances," *Combust. Flame*, vol. 14, pp. 261–272, 1970.

[12] G. Várhegyi, M. J. Antal, E. Jakab, and P. Szabó, "Kinetic modeling of biomass pyrolysis," *J. Anal. Appl. Pyrolysis*, vol. 42, no. 1, pp. 73–87, 1997.

[13] J. A. Conesa, J. A. Caballero, A. Marcilla, and R. Font, "Analysis of different kinetic models in the dynamic pyrolysis of cellulose," *Thermochim. Acta*, vol. 254, no. C, pp. 175–192, 1995.

[14] S. S. Idris, N. A. Rahman, K. Ismail, A. B. Alias, Z. A. Rashid, and M. J. Aris, “Investigation on thermochemical behaviour of low rank Malaysian coal, oil palm biomass and their blends during pyrolysis via thermogravimetric analysis (TGA),” *Bioresour. Technol.*, vol. 101, no. 12, pp. 4584–4592, 2010.

[15] E. Biagini, A. Fantei, and L. Tognotti, “Effect of the heating rate on the devolatilizationof biomass residues,” *Thermochim. Acta*, vol. 472, no. 1–2, pp. 55–63, 2008.

6 Investigation into Methane Thermal Degradation (MTD)

In this chapter an investigation into the influence of operational parameters on the extent of MTD is discussed, with a description of the results which motivated the retrofitting of the reactor system. Characterisation of the quartz system was also conducted against a reactor which was supposedly chemically inert, for reference on potential catalytic activity.

6.1 Investigation into the Characteristics of MTD

The pioneering work of Steinberg et al [1], established the potential for ethylene production by the reaction of methane with biomass. The formation of hydrogen due to the MTD of methane was not reported during their methanolysis investigation, whereas, later Kobayashi and Steinberg [2] investigated the potential of MTD in a very similar rig (if not the same rig), and determined that it was occurring extensively at higher pressures. In later work Steinberg et al [3], investigated the possibility of methane degradation by measuring the product gas hydrocarbon concentration at the outlet of the reactor. This approach is likely due to their use of H_2 as the carrier gas for the GC. No hydrocarbons were measured throughout their degradation investigation, whereas, during the commissioning phase, significant concentrations of hydrogen, and trace C_2 hydrocarbons, were found in the product gas using the constructed reactor. It was reasoned that the high hydrogen concentrations were due to the thermal degradation of methane.

In this part of study, the MTD was investigated by running the reactor system without feeding the biomass. The reactor was also modified to allow for different operating configurations, this allowed for an investigation into possible catalytic effects arising from the use of the reactor. This investigation focussed on the production of hydrogen, equation (6.1.1) from MTD as this major degradation product caused significant dilution of the inlet methane feed. Although hydrogen is the primary production from MTD, higher molecular weight tars and hydrocarbons are also expected. These species are formed due to the radicals that are formed during MTD, and undergo a number of propagation, saturation and aromatization reactions. Dilution of the inlet feed was thought to be undesirable as during hydropyrolysis (pyrolysis with hydrogen) experiments, Steinberg et al [1], recorded concentrations of ethylene lower than with using nitrogen and helium. At 1000 °C and 350 kPa, the hydropyrolysis conducted by Steinberg et al [1], led to 0 % carbon conversion to ethylene; where, the primary product formed was methane. It is suggested that ethylene formation is inhibited at high temperatures with hydrogen as the pyrolysing gas. The reactor type, temperature, residence time and catalytic effects will also be examined and discussed. The production of ethylene and ethane from degradation is also examined to explain MTD's effect on perceived hydrocarbon product yields.

$$CH_4 \rightarrow C + 2H_2 \quad (6.1.1)$$

6.1.1 Investigation into the Potentially Catalytically Active Reactor

During commissioning experiments in this study, unexpectedly high levels of hydrogen were measured in the product gas. The dismantling of the reactor after trials revealed significant carbon deposition on the reactor surfaces. Due to the potential for carbon to catalyse MTD [4], [5], the reactor system was cleaned by combusting the deposited carbon with air. The system burnt out by introducing air after the system had been purged following methanolysis, and the burn out generally occurred at 1000 °C, at which the temperature would increase until all material had been combusted. After the system burn out, the measurements of hydrogen production were still significant. It was supposed that MTD catalytic activity was due to:

- The metallic components surrounding the feeder tube
- The alumina silicate insulator tip at the bottom of the feeder tube, as alumina is a catalyst and support used in methane conversion technologies [6], [7].

The suspected 304 SS catalytic activity was highlighted by the characteristic orange/red iron oxide deposit on the surface of the feeder tube mesh depicted in Figure 6-1. It is suspected that the iron oxide was formed during the cooling of the rector, where during methanolysis the oxide may reduce and become catalytically active [8]. Significant carbon formation was also apparent on the mesh which was observed to have grown from the surface in the form of small carbon filaments, Figure 6-2. Similar carbon filaments have been observed in catalytic deactivation during MTD [9].

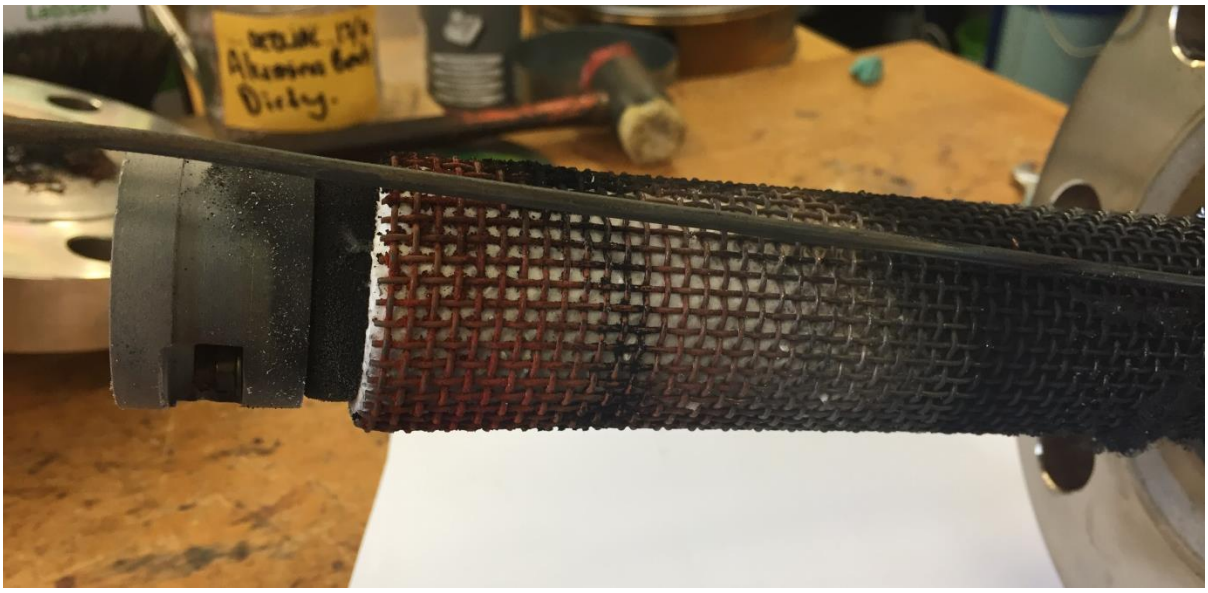

Figure 6-1: Apparent iron oxide formation on 304 SS mesh with an increase in colouring closer to the reaction zone.

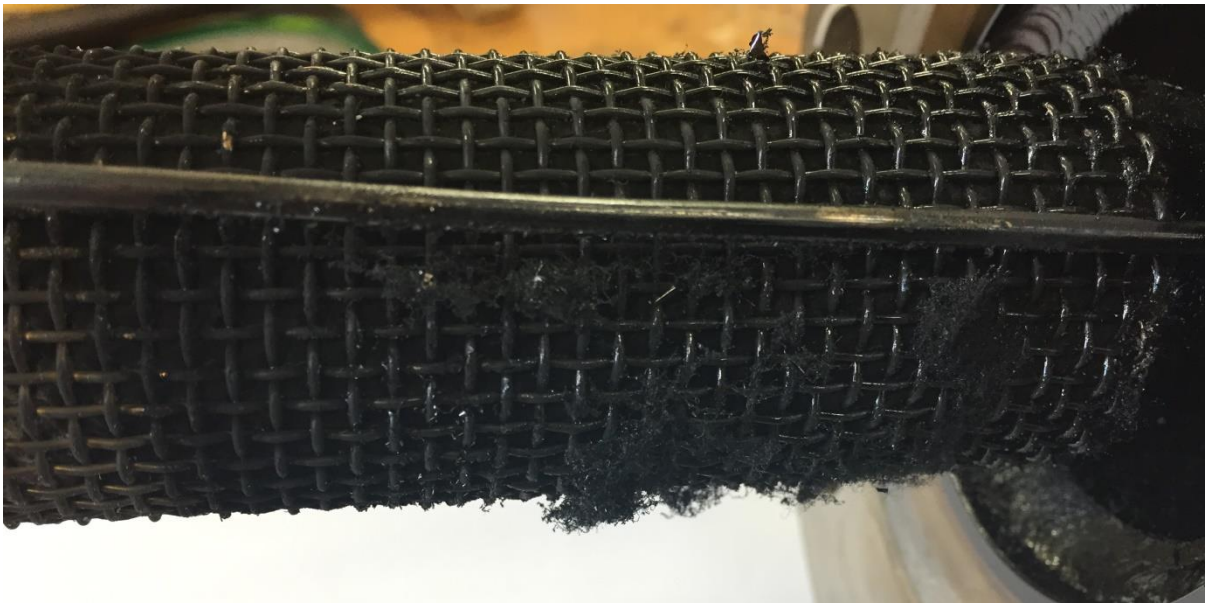

Figure 6-2: Apparent carbon filament formation which was observed close to the outlet of the gas product.

The apparent oxide and carbon filament formation was not investigated further, as, it was decided the feeder tube would be enclosed within a quartz sleeve, allowing for an overall inert reaction zone. The feeder tube was modified and the quartz arrangement was utilized for the remainder of the experiments, full detail of the modifications can be found in the previous reactor construction section on chapter 3. To determine the influence of the alumina a 90 mm high bed of 3 mm alumina balls (MTI Corporation, USA) were placed inside the reactor. It was evident that the presence of alumina significantly increased the degradation of methane within the system, Figure 6-3.

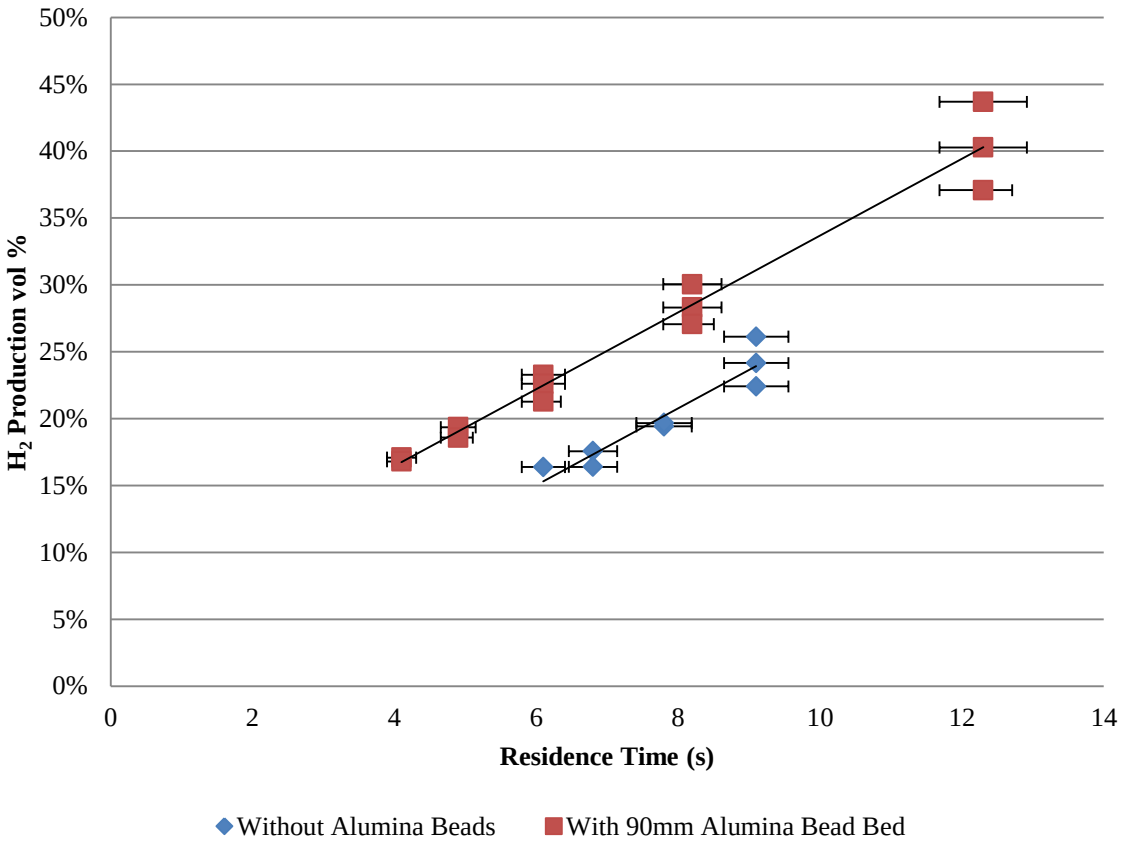

Figure 6-3: Hydrogen production influence with the incorporation of a 90 mm high bed of 3 mm spherical alumina balls. System operated at 980 °C. (N.B Feeder tube sheathed with metal mesh and with the alumina insulator tip).

Further trials were conducted to investigate factors influencing the extent of MTD, in an effort to reduce unintentional hydrogen production. Firstly the system mass flow rate was set and the system was allowed to stabilize for 10 minutes with subsequent measurements taken every 10 minutes. It was observed that the hydrogen production significantly increased with increasing elapsed time, and localised decreases were apparent during the sampling of the gas flow. A continual decrease in measured hydrogen concentration during a run at constant conditions was also observed, and was thought to be due to the system undergoing a conditioning phenomenon with carbon deposition. It was suspected that carbon formed from the process was deposited on the walls and this decreased the overall methane degradation.

With the catalytically active alumina and metal surfaces removed from the reactor to the greatest extent possible, hydrogen was still found in the product gas. In an attempt to decrease methane degradation the residence time of the gas was reduced by the inclusion of a quartz element in the preheating zone. This was centred in the preheater zone and occupied 66 % of the preheater section, hence, reducing the gas residence time. The quartz element was constructed from a 520 mm long section of 40x46 mm quartz tubing which was evacuated and sealed with four 10 mm concentric feet,

as shown in Appendix C. The ends were rounded to facilitate the distribution of gas in the preheater section and decrease the pressure drop. With the quartz element installed and quartz sleeve fitted around the feeder tube, the overall residence time of the gas decreased; however, it was apparent that the overall hydrogen production did not decrease, but increased as shown in Figure 6-4. It is suggested that the inclusion of the quartz element in the preheater section reduced the thermal gradients within the system. This was likely to have occurred, due to the inclusion of the quartz element decreasing the effective gas flow cross section area by 75 %, localising the majority of the flow closer to the heater. The reduced cross sectional surface area was thought to have increased velocities, thus, heat transfer to the process gas and reduced the possibility of a cooler gas flow at the core of the system. The reduction in cross sectional area also added more heat transfer area, as the wall of the quartz cylinder could be heated by radiating heat from the reactor above and this been then transferred to the process gas. It was suggested that due to the enhanced gas mixing, increased hydrogen production at the same residence time was measured, (Figure 6-4), likely due to the enhanced heat transfer. The extent of MTD is strongly influenced by the operating temperature; hence, enhanced heat transfer increased the average temperature of the gas, resulting in increased hydrogen production. This is indicated by the gradient of the trend lines between the trials, with, and without, the quartz element in place.

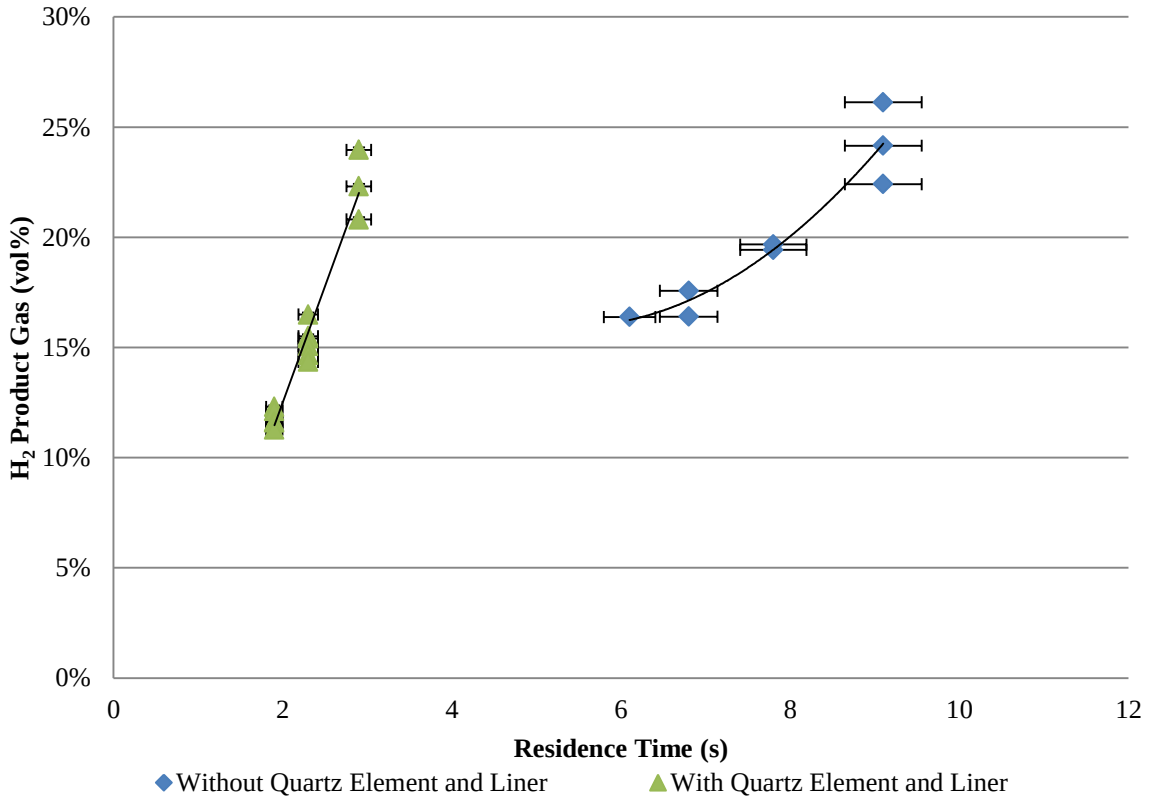

Figure 6-4: Comparison of modified system in comparison to prior assembly of the reactor internals, taken from previous reactor configuration with no quartz element and quartz liner. System operated at 980 °C, for the same mass flow rates.

To determine the possibility of quartz surfaces catalysing methane degradation, a 50 mm bed of 180-250 µm, 99 % quartz sand (Dricon, New Zealand) was added to the system. The sand was conditioned by oxidising with an air stream at 980 °C, to remove entrained moisture and volatiles. Hydrogen production was similar in the no-bed and bed trials, Figure 6-5, thus, it appears that the quartz bed and quartz reactor internals are not catalytically active. It was also suggested that the addition of the bed, indicated that the total surface area of the reactor system is influential to the extent of degradation. This could explain the increase in hydrogen production with the addition of the quartz element which provides increased surface area for carbon deposition to occur, via propagation from the surface. As carbon was observed to coat all surfaces in the reactor at the operating temperature, the surface area which was not subject to the fluidised bed sand particles increased, increasing the effective surface area for carbon deposition. It was also hypothesised that the increase may be due to a combination of the surface area effects and the heat transfer effects which were described in the previous section. However, due to the lower hydrogen concentrations being obtainable at lower mass flow rates of methane it was desirable to operate with the quartz element in place. Lower mass flow rates for corresponding low residence times were also desirable due to the decreased heat released on combustion of the flue gas. This was important as the flue gas was burned after analysis the heat released during combustion travelled through the exhaust system. The exhaust system was limited by operation at 100 °C, whereas, decreased volume allowed for lower residence time operation, with decreased heat released upon combustion.

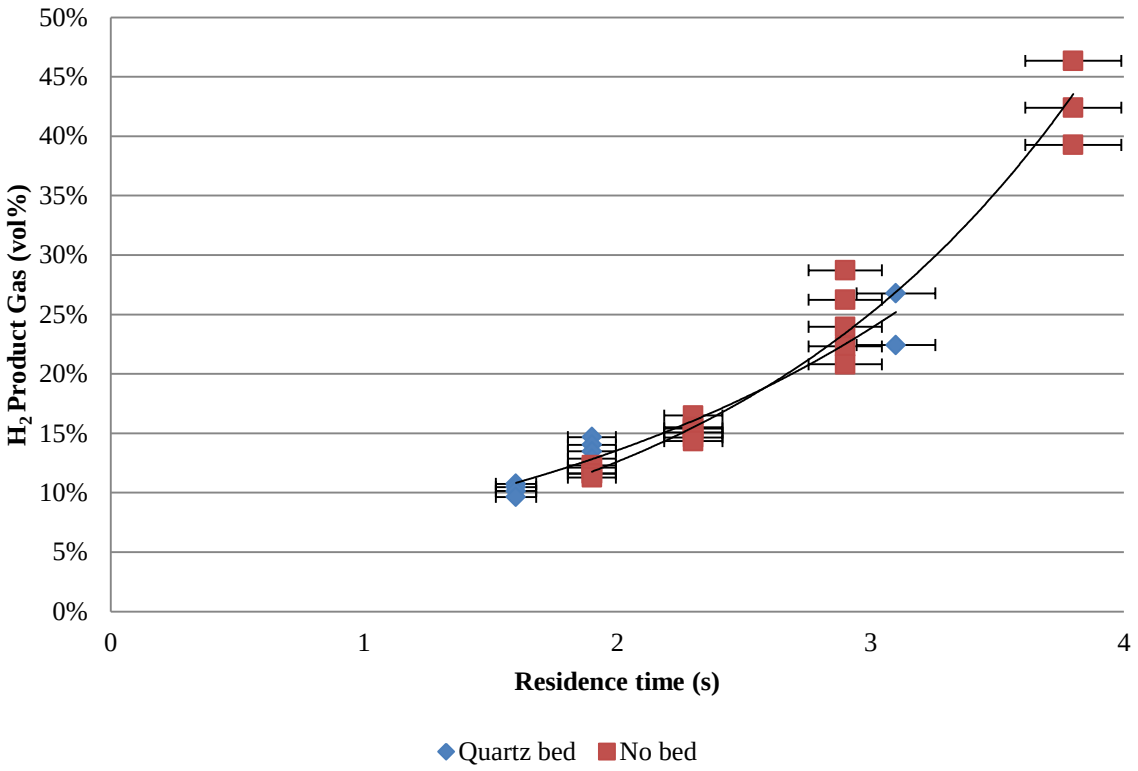

Figure 6-5: Hydrogen production for system with and without the inclusion of a 50 mm high quartz sand bed. System operated at 980 °C.

To investigate the catalytic influences within the system a trial was conducted in another fluidised bed reactor. This rig was constructed for investigating the removal of H_2S and NH_3 from gasification product streams and measured very small reductions in H_2S and NH_3 concentrations [10]. The rig was constructed with all surfaces made of quartz to provide an inert reactor arrangement. This effectively allowed for an investigation (by difference) into the catalytic activity of the bottom feeder tube nuts and thermocouple in the system.

Due to the differing sizes and constraints of the reactor, the minimum residence times attainable in the system were > 3 s with a maximum operating temperature of 940 °C. The system was operated without a bed with an identical quartz fused fritted disc arrangement. Overall it was observed that there was no significant difference between the trends observed from both reactors at the operating temperature, Figure 6-6. It is possible that with higher temperature the effect of the presence of the thermocouple and nuts may increase, however, the overall extent is not deemed significant

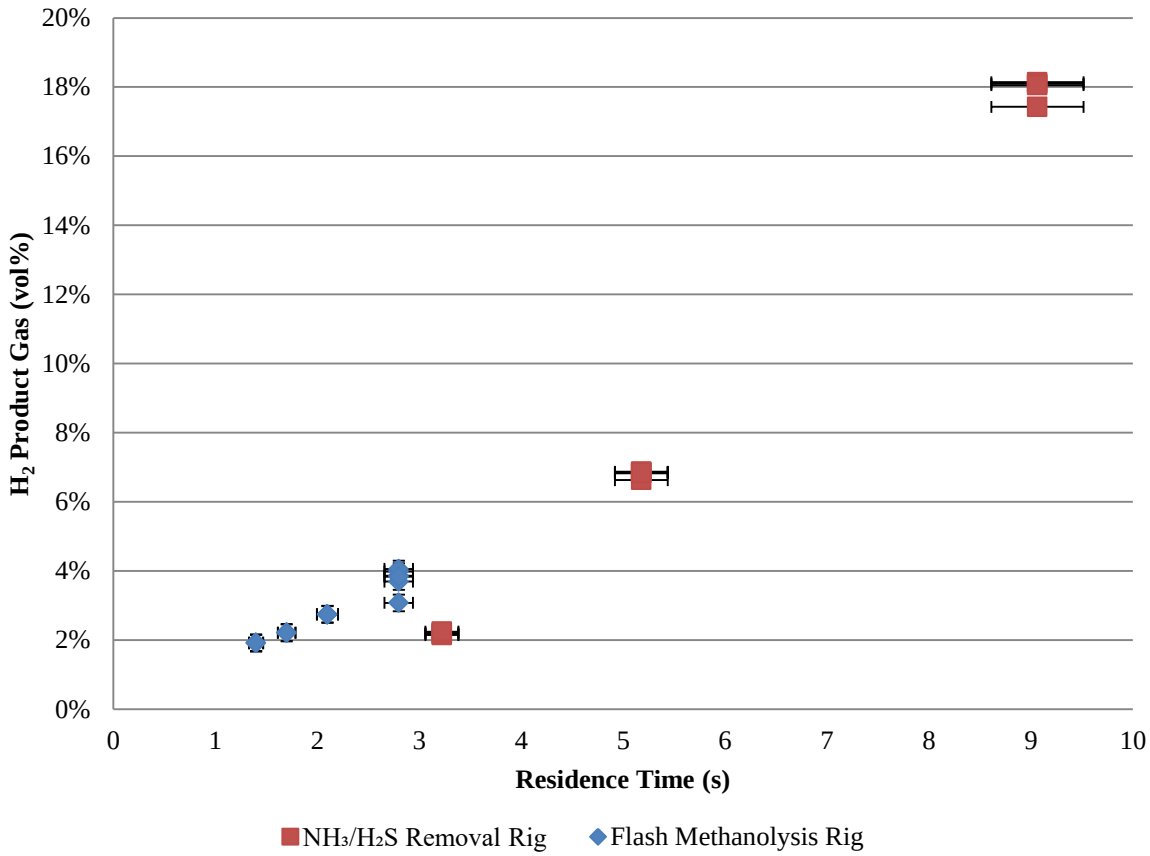

Figure 6-6: Hydrogen production from the constructed rig in comparison to the H_2S/NH_3 removal rig. Both systems operated with an average temperature of 940 °C, no bed present in both systems.

From the trial which was conducted on the H_2S/NH_3 rig it was likely that the methane degradation characteristics occurring in the flash methanolysis rig were not under any significant catalytic effect. This indicated that it was unlikely the thermocouple and feeder tube fastening nuts were catalysing the methane degradation, to a significant degree. This concluded that for the obtainable residence times the production of hydrogen in the system was inevitable and could be regulated with alterations in the temperature and flow rates through the system. Similar deactivation characteristics were observed when using the H_2S/NH_3 rig. From the trend which is observed at each flow rate, slightly lower hydrogen concentrations are recorded with increased trialling time. The decreasing hydrogen content of the product gas with operating time is suggested to be due to the thermal characteristics of the system and is discussed in depth in the following section.

6.1.2 Effect of Temperature during MTD

With sufficient chemical inertness of the reactor system established, the effect of temperature on the extent of MTD was investigated. The system was initially heated with N_2 flowing until a stable and pre-set temperature was reached. Then the system was allowed to operate for 25 minutes at the

designated methane flow rate with samples taken every 5 minutes. Figure 6-7 shows the exponential temperature dependence of hydrogen production observed between 900-1000 °C.

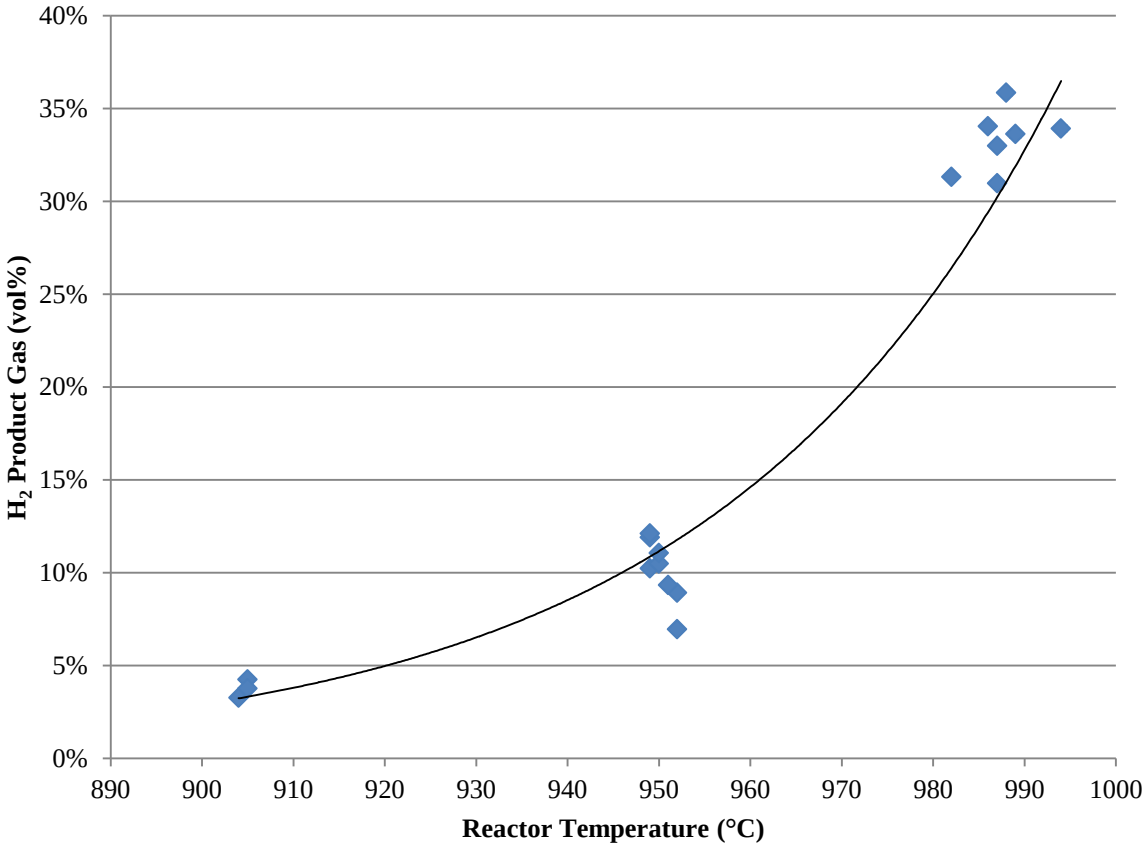

Figure 6-7: Product gas hydrogen concentrations at differing temperatures. System operated with no quartz sand in bed at a constant residence time of 2.8 s.

In order to decrease the overall hydrogen production the effect of temperature distribution about the vertical profile of the reactor was investigated. As the system was configured with six separate heating zones an approach was trialled where the heaters associated with the preheater were set at a minimum. The elements were staged in a configuration which allowed for concentrated heat in the reaction zone, which decreased the residence time of the gas at an elevated temperature, reducing the extent of MTD. For the preheater section the heaters were operated at set points as shown in Table 6-1. The temperature gradient from 730-800 °C was determined from deriving the minimum set point temperatures which would allow for 1000 °C to be reached at the top heater. It was expected that for the configuration the relative degradation in the preheater would reduce, decreasing the overall hydrogen content in the outlet gas. The trials were compared to two other trials, 50 mm bed and no bed, where 50 mm of 250-180 µm quartz sand was added for the 50 mm bed experiment, where it was removed for the no bed trials. The inclusion of the bed led to varied residence times for constant mass

flow rates, when compared to the no bed trials, however, the mass flow rate was increased so that residence time was constant between trials.

Table 6-1: Set temperatures of reactor heaters and the average operating temperatures of the associated trials. Operating temperatures taken as an average of the trial temperature.

Trial	No Bed	50 mm Bed	Staged Heating
	[°C]	*[°C]*	*[°C]*
Reactor Heater 1	940	940	730
Reactor Heater 2	1040	1040	780
Reactor Heater 3	1040	1040	800
Reactor Heater 6	1040	1040	1000

The heaters were staged with a 200 °C temperature increase about the 3-6 heaters, where heater 6 corresponded to the location of the fluidised bed. A maximum set temperature of 1000 °C was obtained for heater 6. Overall no significant decrease in hydrogen production was observed with a staged heating configuration. The overall hydrogen concentrations were in agreement with those derived from the bed trials, Figure 6-8. To decrease the electrical requirements of the individual elements, the system was operated with low temperature differences between elements.

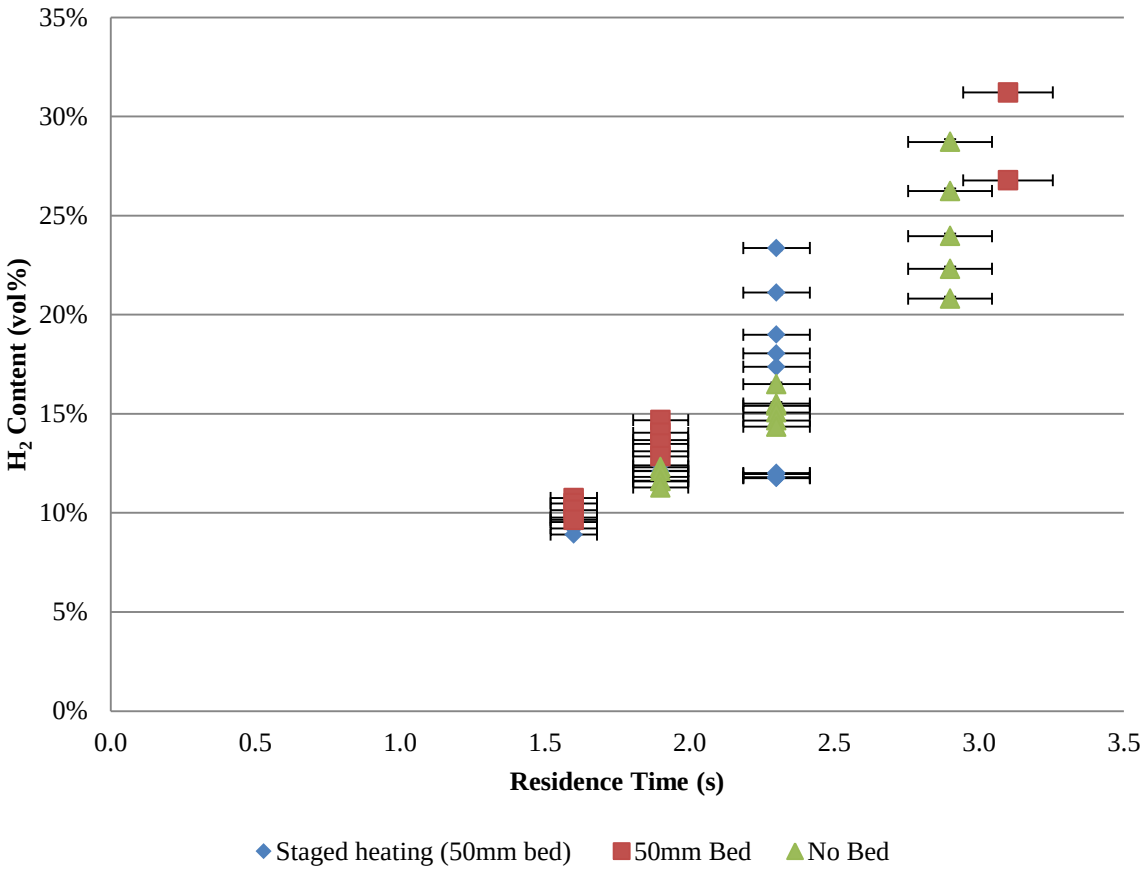

Figure 6-8: Hydrogen product gas composition for the staged heater arrangement in comparison to the 50 mm bed and no bed trials, average system temperature of 980 °C.

The hydrogen concentration increased with the residence time and was the lowest at the shortest residence time of 1.6 s, for all three cases. Although no significant decrease in the average hydrogen concentration was recorded with staged reactor heating (Figure 6-8), the trend of declining hydrogen concentration with elapsed operating time intensified. At a given residence time, the H_2 concentration decreased with elapsed operating time, as shown in Figure 6-9 for a residence time of 2.3 s. It was found that the H_2 concentration in the staged heating was reduced from 23 vol% at the start to 18 vol% over 35 minutes, whereas for the empty bed trials, the H_2 concentration decreased from 16.5 % at the start to 14.4 % in 25 minutes, Figure 6-9.

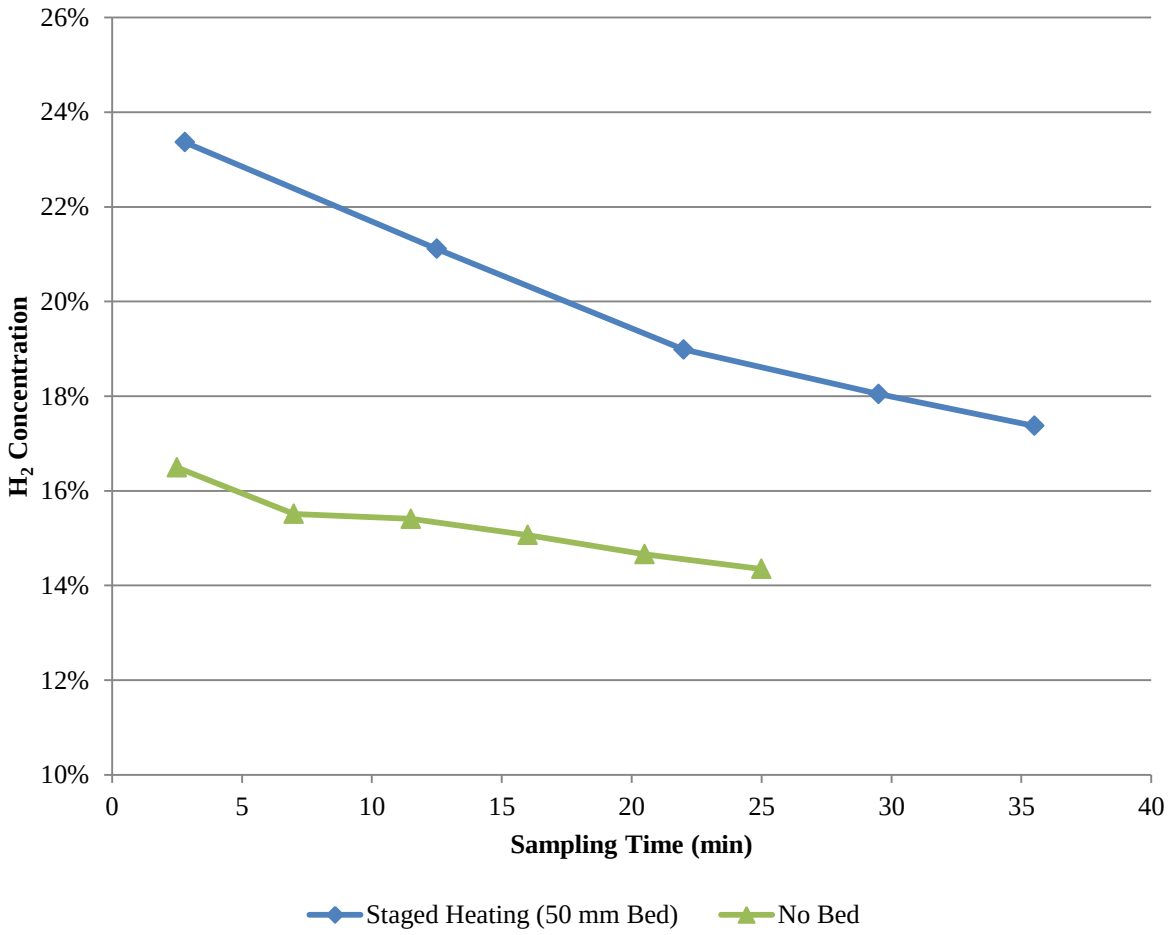

Figure 6-9: Hydrogen concentration during MTD for various methane gas flow rates, where the system was operated at 0.088 kg/hr initially then increased in gas mass flow rate, then decreased back to 0.088 kg/hr.

The data from the staged heating trial were taken and investigated to determine the trends in decreasing hydrogen which were identified. During the trial, the outlet concentration was taken over 40 minutes, approximately. The mass flow rate was then increased to the highest flow rate and then decreased to the original mass flow rate; hence, the system as operated with a residence time of 2.3 s which was then decreased to 1.9 s, then 1.6 s, and then returned to 2.3 s.

The variation in hydrogen concentration as time elapsed for a given residence time can be seen in Figure 6-10, where the hydrogen concentration decreased from 23 % to 17 % over 35 minutes of sampling at a residence time of 2.3 s. With decreased residence time, the variation in hydrogen concentration with elapsed time was reduced for the 1.9 s and 1.6 s residence time operation. In total the system was operated for another 80 minutes and then returned to the initial flow (2.3 s residence times). A further 40 minutes of sampling was repeated at this flow rate which resulted in a constant hydrogen concentration was virtually constant at 12 vol% in the last 40 min with residence time of 2.3 s which was lower than the initial 35 min results. This was suggested to be due to the increased convective heat transfer when methane passes through the system. As the temperature for the trials

were set for the system with no gas flow, following the introduction of gas, heat was transferred about the reactor increasing the overall average temperature of the system. This is likely to be facilitated by the high heat capacity of methane; effectively increasing the extent of methane degradation occurring within the reactor. With increased operational time the system could be stabilized with a constant output hydrogen concentration. This effect leads to practical difficulty in decreasing the effective methane degradation as the system requires significant time to reach equilibrium.

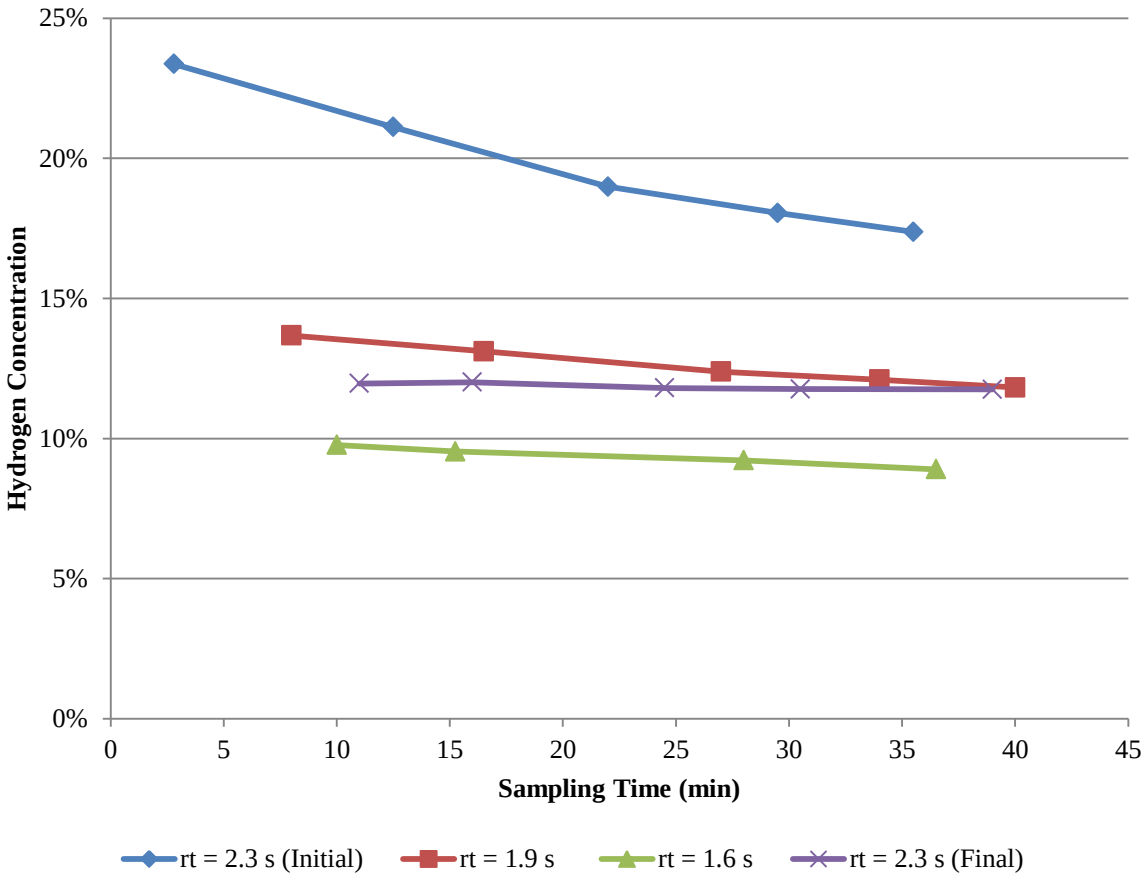

Figure 6-10: Hydrogen concentration in product gas during MTD, System operated with increasing mass flow rate, thus residence times of rt= 2.3 s (Initial), 1.9 s, 1.6 s, 2.3 s (Final).

6.1.3 Effect of Carbon Deposits during MTD

From the earlier experiments it was understood that the hydrogen and methane concentrations in the outlet gas were not constant over an extended period. Supposedly due to observed deactivation characteristics occurring within the system, therefore, an investigation of carbon deposition and the resulting effect on MTD was conducted. The system was operated post and prior to the carbon combustion with air (burn out) to determine the possible effect of previously deposited carbon on further MTD.

For the no burn out trials the system was purged with nitrogen and no oxidation step was conducted, while for the burn out trials the system as oxidised with air then purged with nitrogen. For the burn out trials, no carbon which was deposited on the surface of the interior of the reactor could influence the degradation potential. For the no-burn out trials the system was operated at a high temperature 980 °C then decreased in temperature in N2, and no intermittent combustion of the carbon formed was conducted. The results of H_2 concentrations are shown in Figure 6-11, from which it was found that the burn out of the system did not significantly reduce the overall production of hydrogen in the system throughout the temperature range 900-1000 °C. No significant change in hydrogen concentration in the outlet gas was seen after residual carbon was combusted, however, the conditioning process was likely to reoccur when operated post burn out.

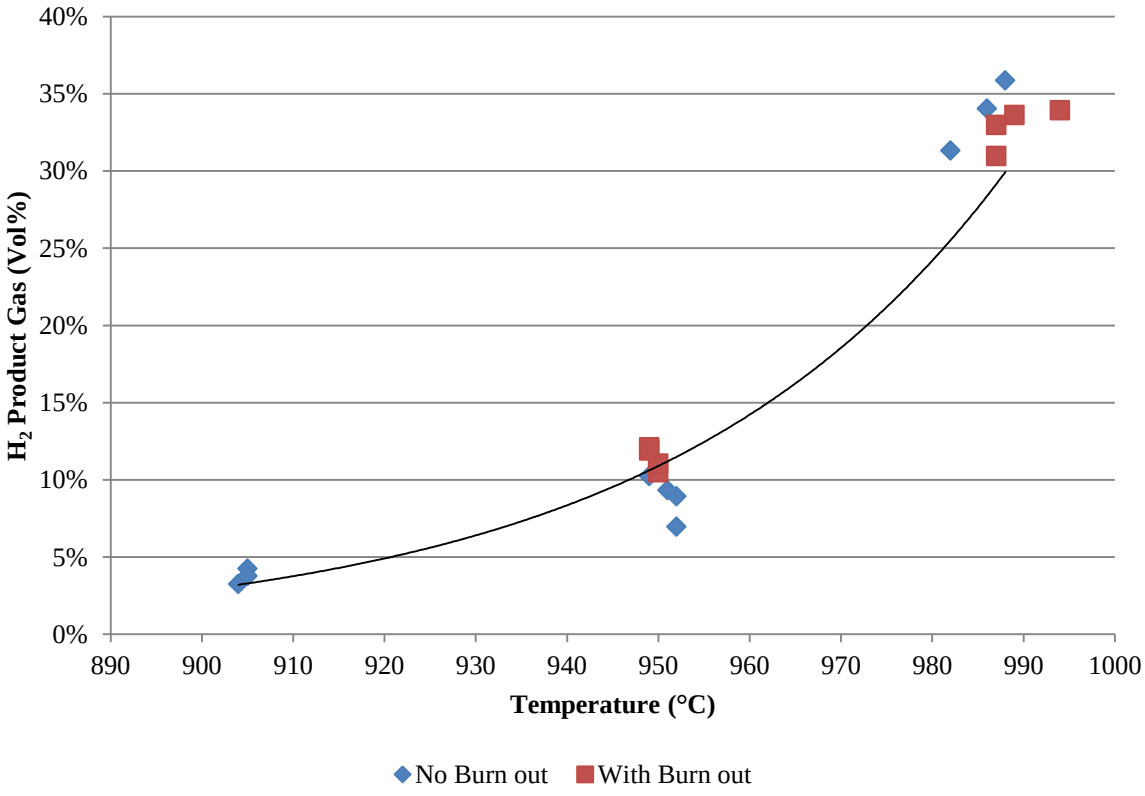

Figure 6-11: Hydrogen production with and without a burn out of the system, to determine the effect of the carbon deposition on methane degradation, at a residence time of 3 s.

From Figure 6-11, it was concluded that although carbon is a known active MTD catalyst, that deposited on the reactor walls was unlikely to significantly influence the MTD for hydrogen production. This contradicts the conclusions which were drawn from the prior MTD characterisation. It is unknown why the burn out trials did not significantly affect hydrogen production and may be due to the temperature ramping approach which was taken. This may have resulted in the system not being able to reach equilibrium during the trial, highlighting the possibility that the thermal heat transfer

effects and thermal conduction during operation were more influential on the MTD characteristics. This was suspected due to the high heat capacity of the methane and the strong increase in heat capacity with temperature. It was also likely that the carbon which was produced from the degradation was not catalytically active, possibly due to the structure of the carbon which is formed. Nevertheless, it was highly likely that the deposition of carbon effected the hydrogen production during MTD.

To investigate the carbon deposits the system was cooled in N_2 and the system internals were examined. The preheater internals showed a very thin black mirror-like coating on all heated internals exposed to methane as shown in Figure 6-12. The feeder tube was observed to have a very thin and readily removable coating of carbon for 2/3 of the feeder length with the remainder being coated with the same black-mirror type carbon as on the inter reactor at preheater location as shown in Figure 6-13. A slight build-up of carbon was also observed at the tip of the feeder tube section where the quartz liner was affixed with the locknuts. A small build up was also observed in the bed with the carbon observed to have been aerated by the nitrogen and was separated due to density.

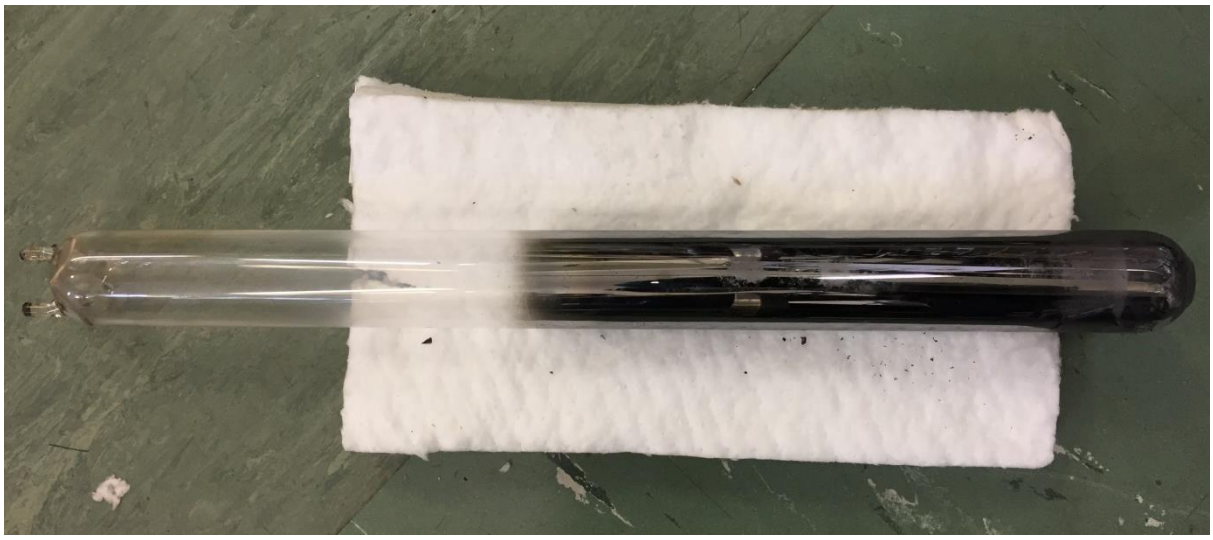

Figure 6-12: System internals where system was cooled in nitrogen gas to preserve carbon formation, quartz element from preheater section.

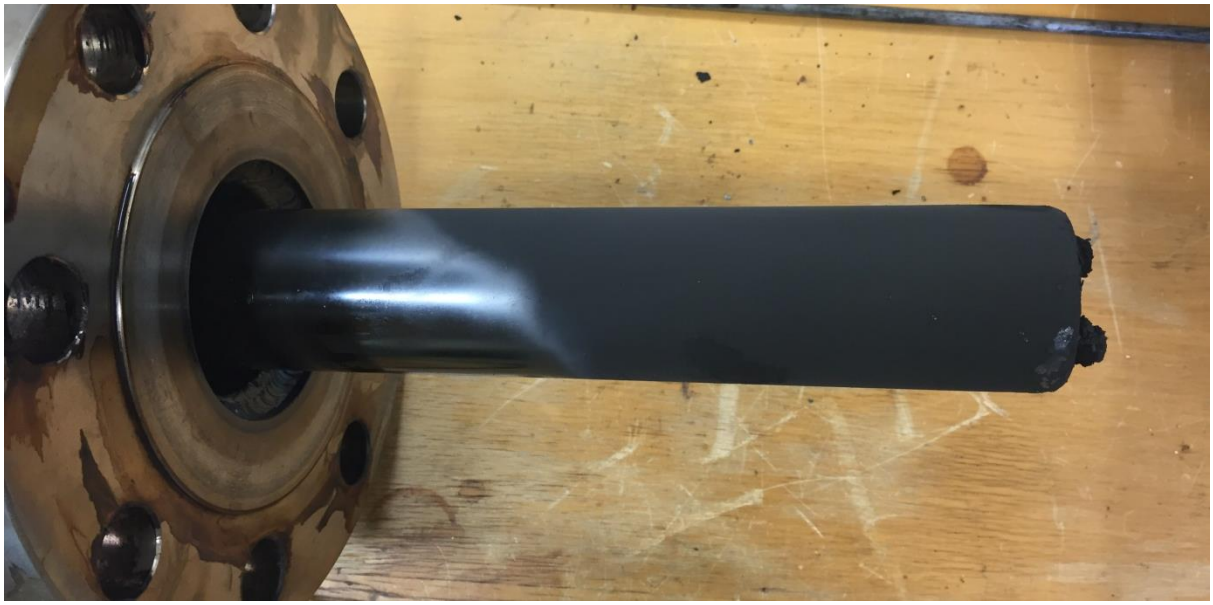

Figure 6-13: System internals where system was cooled in nitrogen gas to preserve carbon formation, feeder tube.

Below the fritted disc, the carbon formation was different as that which was observed in the bed and close to the reaction zone. The carbon formed in the preheater zone was observed to be produced in thin sheets which were rounded in a similar diameter to the quartz element/liner, Figure 6-14. This carbon was denser than that observed on the feeder tube tip, and was formed in layers similar to that of graphite. The carbon was observed to have a low porosity in comparison to the carbon formed on the feeder tube. It was unlikely that the carbon below the quartz fritted disc was a highly active catalyst.

Figure 6-14: Carbon product collected from the preheater section when the bottom flange was removed.

It was concluded that it is unlikely that the surface characteristics are influential to the methane degradation characteristics. It was determined that the black mirror-like carbon deposit was not significantly active with methane, and that the carbon deposit on the feeder tube is most likely to be active. N.Muradov determined that *glassy carbon* was characterised by no open porosity and a relatively high initial catalytic activity which was followed by quick deactivation in < 10 min [11], which agreed with trends observed during experiments. The activity of the carbon formed on the feeder tube was suspected to be higher due to the increased porosity of the carbon on the feeder tube tip. However, the carbon was observed to be too porous to significantly increase the MTD reactions, and explains why there was no apparent difference with/without a burn out of the system, Figure 6-11. Carbon which has been utilized as a catalyst in the production of hydrogen from methane are characterised by high surface areas and pore sizes, which are associated with high methane conversion [11], [12]. The high porosity carbons used are usually derived from charcoal and acquires the porous structure from the release of volatiles during the activation of the charcoal. The carbon formed is not suspected to be comparable to commercial carbon catalysts due to the much denser structure of the carbon. It is reasoned that this explains the observations from Figure 6-11, which show no reduction in hydrogen production when the system was/was not burnt out.

The carbon that was formed from the degradation of methane was assumed to accumulate in the bed. This carbon was also not likely to be catalytically active, as the hydrogen concentration decreases with time, as observed in Figure 6-8 and Figure 6-10. A reverse trend would be expected for catalytic activity as the amount of carbon in the bed increases with time, leading to increased hydrogen production. It was hypothesised that the variations in the measured hydrogen content are due to the temperature gradient above the quartz frit which decreases with increasing flow rate. This causes carbon to be deposited on additional surfaces as the system temperature increases, as increased heat transfer to colder parts of the reactor occurs. The surface area of the system at high temperature was suspected as being an influential parameter due to carbon deposition occurring readily only on sections of the system which were above a certain temperature. The temperature where carbon deposition was suspected of occurring, for residence times of approximately 1.5 s, was > 850 °C. Thus, by increasing the gas flow in the system, the amount of surface area of the quartz liner at 850 °C was increased and the deposition continues until the system stabilizes. This was characterised by a high hydrogen production initially, which subsequently decreased as the portions of the reactor surface newly at 850 °C were covered by carbon deposits. This was suggested as the characteristics which were observed in Figure 6-6 were similar for the fluidised bed reactor and the H_2S/NH_3 reactor, which also showed similar conditioning like behaviour. It was concluded that the production of hydrogen was inevitable and constant recording of the degradation extent was required to better understand the methanolysis characteristics.

Variations in the emissivity of the reactor interior were also suggested as a possible cause of the variation in the MTD characteristics. It is suggested that the deposition of the carbon may cause an increase in the adsorption of the incident thermal radiation, which causes an increase in adsorption at the bed. This may then reduce the effective radiation below the fritted disc and effectively dissipate the heat into the flow of methane. However, due to the low variations determined in the burn out trials, Figure 6-11, it is unlikely that thermal radiative heat transfer significantly varies the hydrogen production shown in Figure 6-10.

6.2 Ethylene and Ethane Production from CH_4 Degradation

During the investigation into the hydrogen production due to MTD, it was apparent that ethylene and ethane were also produced. Concentrations of these hydrocarbon gas species were low in the product gas, and accounted for < 0.5 vol% for most system conditions. It was unlikely that the interaction with the hydrocarbons and volatiles formed are significant, as the likelihood of gas phase interactions was low. However, the production of ethylene and ethane greatly influenced the overall carbon conversion analysis of biomass upon methanolysis, especially if the production via degradation is not considered. This was due to the difficulty in deriving the source of hydrocarbon formation and the high M/B ratios which are used in the experiments. This can lead to overestimated ethylene and ethane relative carbon

conversions; to better understand the ethylene and ethane formation due to methane degradation the concentrations as a function of temperature and residence time were investigated. The characteristics of the ethylene and ethane formation will be covered in this section.

6.2.1 Effect of Temperature on the Production of C_2H_4 and C_2H_6 during MTD

Although extensive studies have been published on investigating the MTD characteristics for increased hydrogen production, the pathways which have been used to describe the degradation process are very complex and the reaction pathway is not well understood. It is apparent that the majority of research concludes that MTD consists of a multitude of radical reaction pathways, which form a range of species. Ethane has been referred to as a primary product with ethylene considered secondary product due to the interactions with methyl radicals [13], [14]. Chen et al [14], suggested that the hydrocarbon production could be described in terms of the radical chain mechanism. For which further conversion of product species can undergo a plethora of competing reactions, where 242 reactions from 75 species have been utilized in the homogenous decomposition modelling attempts [15].

$$CH_4 \rightarrow CH_3 + H \tag{6.2.1}$$

$$2CH_3 \rightleftarrows C_2H_6 \tag{6.2.2}$$

$$CH_3 + C_2H_6 \rightleftarrows CH_4 + C_2H_5 \tag{6.2.3}$$

$$C_2H_5 \rightarrow C_2H_4 + H \tag{6.2.4}$$

$$CH_4 + H \rightarrow CH_3 + H_2 \tag{6.2.5}$$

The formation of hydrogen and ethane, has been described as the primary product of methane degradation, with subsequent dehydrogenation reactions production ethylene and acetylene. This reaction has been observed to exhibit non-Arrhenius behaviour and has been identified as the rate determining step [14]. The hydrocarbons formed undergo further dehydrogenation reactions to form acetylene, carbon and benzene. To determine the extent of methane conversion to the hydrocarbons the product gas stream was diluted with a small amount of accurately measured helium tracer gas. This allowed for the derivation of overall mass flows of the species, and reduced the uncertainty of dilution effects due to high H_2 content.

Gueret et al [16], described that ethylene formation is maximised at 1227 °C, with significant proportions of acetylene also formed at this temperature. Ethylene formation was observed at

temperatures of 1000 °C in the methanolysis reactor; hence, an analysis of the ethylene production was conducted between 950-1030 °C. The gas flow rate corresponded to an overall gas residence time of 2.8 s. The trials were influenced by a lack of sensitivity of the micro-GC used as the majority of gas samples contained concentrations below 1 vol%. To minimize this effect multiple readings were taken for each sample and the overall value was averaged over the sampling period. The system was recalibrated for the lower concentrations to enhance the sensitivity of the micro-GC; however, the sensitivity of the system was difficult to analyse due to suspected reactor conditioning effects, as observed with the hydrogen production. Overall a substantial increase in ethylene production due to MTD was observed from 950-1030 °C, with an overall methane conversion of 0.65 % at 1030 °C, Figure 6-15 . At temperatures below 900 °C trace formation of ethylene was measured. Ethane was observed to slightly increase over the temperature range with a final methane conversion of 0.18 %.

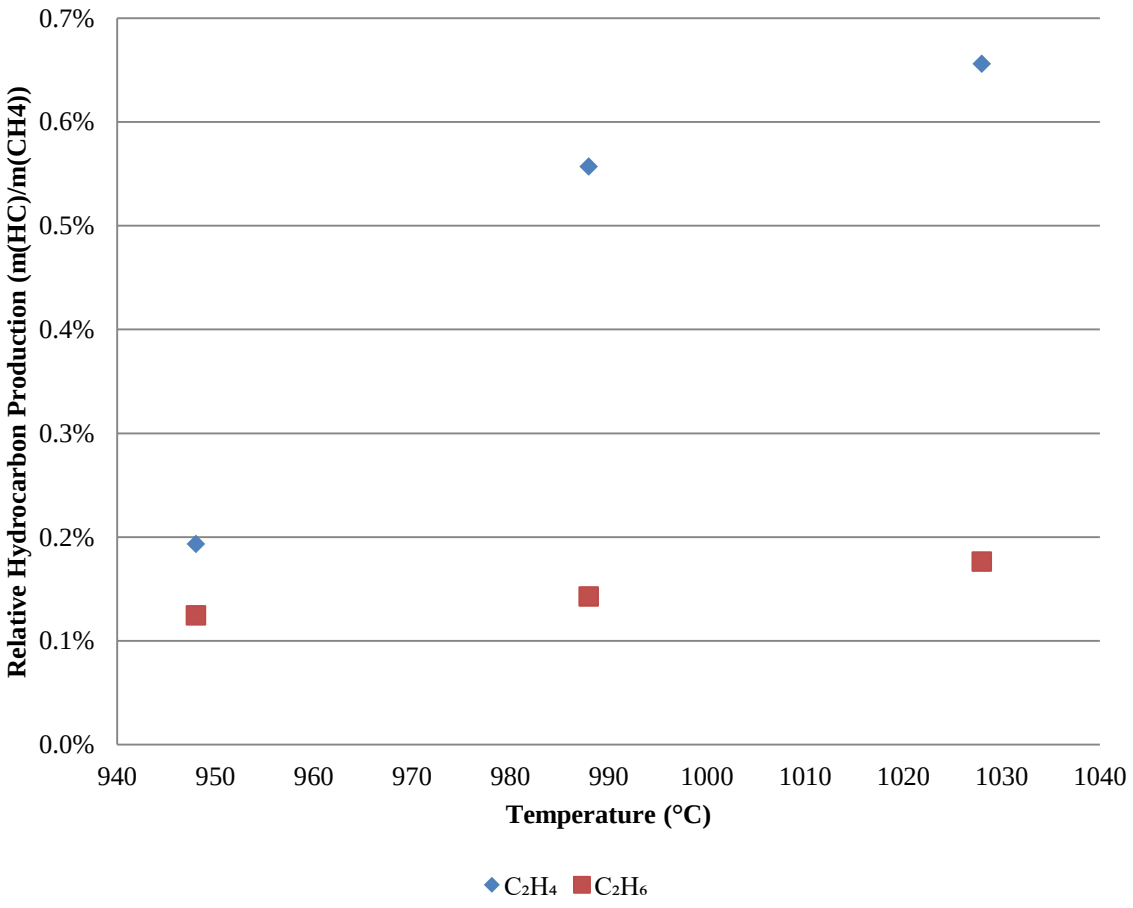

Figure 6-15: Effect of temperature for the production of ethylene and ethane from MTD. System operated with a 50 mm quartz sand bed with a constant residence time = 0.75 s.

The extent of ethylene production was in agreement with literature, where the reaction rate of Equation (6.2.2) strongly influences ethylene production [14], [17]. As the CH_3 radical readily forms ethane which decomposes to form ethylene and hydrogen, the overall production of ethylene was not

highly influenced by the rate of Equation (6.2.4). This possibly explains the low concentration of ethane in the product gas, as it was readily decomposed to form ethylene. It was also possible that the ethane production was limited by the equilibrium concentration being achieved; which potentially describes the relatively constant ethane concentrations during trials.

6.2.2 Effect of Residence Time for the Production of C_2H_4 and C_2H_6 during MTD

Due to the numerous gas phase interactions which are possible during MTD the residence time effect for ethylene and ethane production was investigated. The trial was conducted with the system at 1020 °C with a 50 mm bed in the reactor. The system was operated with increasing methane mass flow rate into the system, with a total of 5 samples taken at each flow rate. Measurements were taken over a 30 minute trialling period where the flow was increased and the system was allowed to stabilize for 10 minutes before subsequent samples were taken, Figure 6-16.

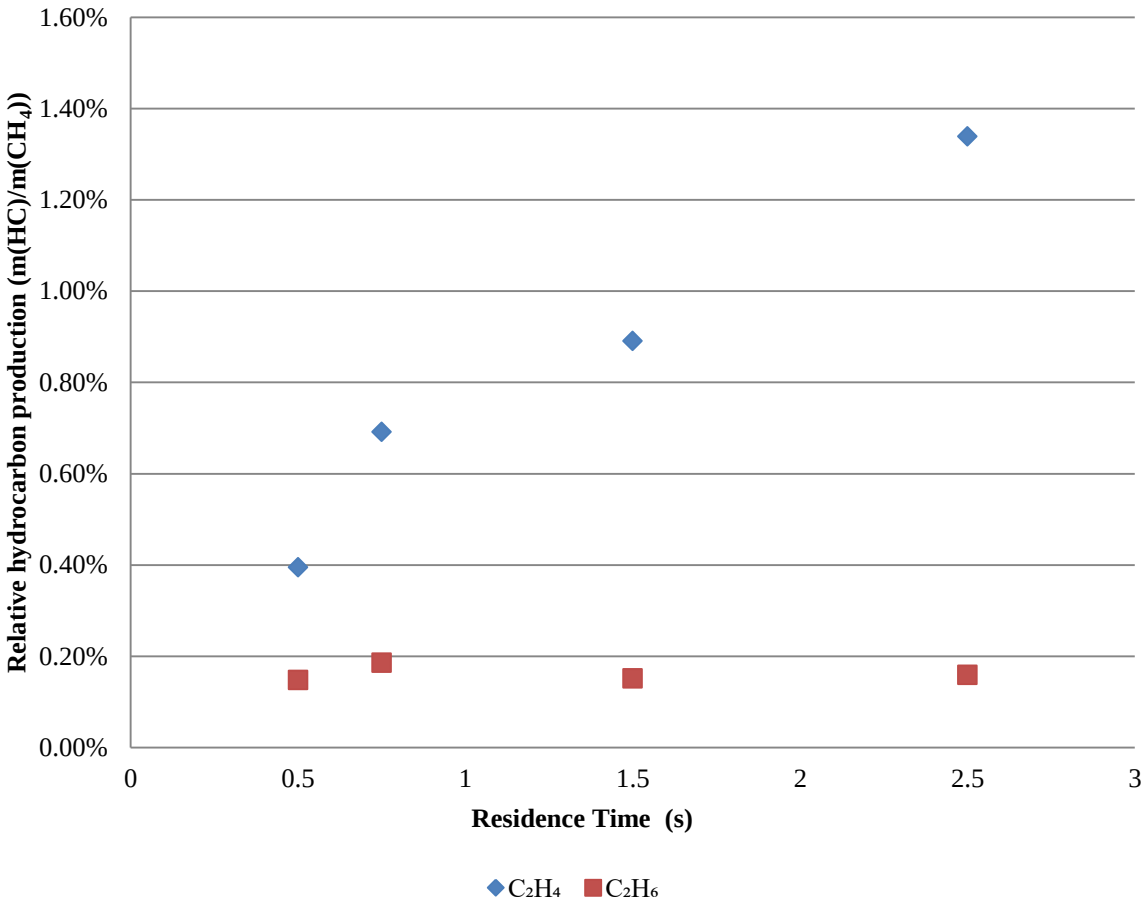

Figure 6-16: Ethylene and ethane product distribution during MTD. System operated at 1020 °C with a 50 mm bed.

Overall it was determined that the relative ethylene and ethane production increased with the increasing residence time. It is suspected that this was due to the decreased probability of methyl

radical and ethane gas species interactions with decreasing residence time. This was observed by a decrease in the ethylene concentration and not that of ethane, arising to the possibility that Equation (6.2.3) limits the overall methane conversion. The increased production of ethylene led to increased molar concentration of the outlet gas, this arises to the increased potential of ethylene interactions with the volatiles from the methanolysis of biomass at higher residence times.

6.2.3 Effect of Reactor Configuration for the Production of C_2H_4 and C_2H_6 during MTD

When conducting the bare reactor trial described in the comparison with the work from Kobayashi and Steinberg [2], an interesting trend in ethylene and ethane formation was observed, Figure 6-17. Overall ethylene concentrations were observed to decrease with increasing residence time in contradiction to that determined in the methanolysis reactor, Figure 6-16. As with previous trials, the overall ethane concentration was observed to remain constant throughout the trialling parameters.

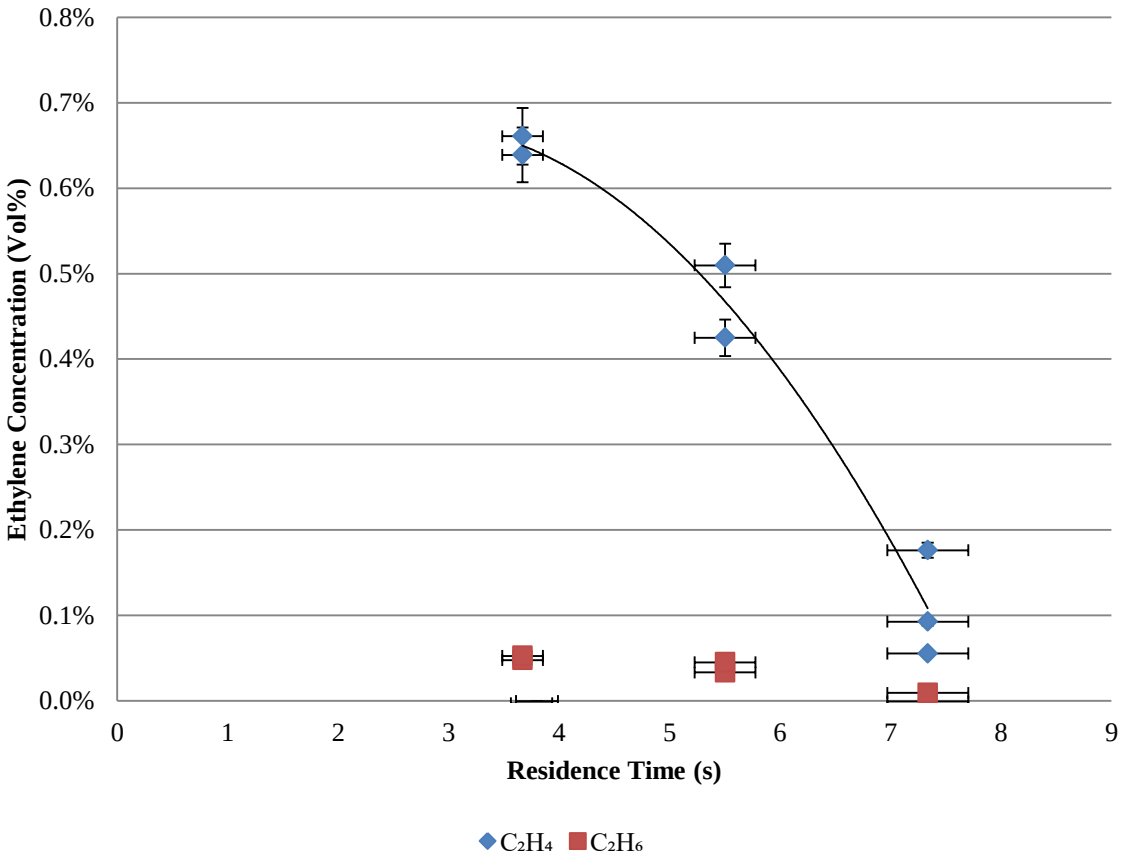

Figure 6-17: Ethylene and ethane product gas composition for various residence times. Reactor operated with no quartz liner in place at 1020 °C.

It is reasoned that the high ethylene yield was attributed to the catalytically active surface of the bare reactor surface. This is likely due to similar surface interactions which were reported during the hydrogen content analysis. It was likely that the surface catalyses the dehydrogenation reaction of

ethylene to form acetylene through the reaction pathways, Equations (6.2.6), (6.2.7), (6.2.8) and (6.2.9). Although the extent which the reactor surface catalysed the reaction rate was unknown, it was sufficient over the trialled residence time to readily decompose ethylene to acetylene as C_2H_3 radical decomposes to form C_2H_2, Equation (6.2.9).

$$C_2H_4 + H \rightarrow C_2H_3 + H_2 \quad (6.2.6)$$

$$C_2H_4 + CH_3 \rightarrow CH_4 + C_2H_3 \quad (6.2.7)$$

$$C_2H_4 \rightarrow C_2H_3 + H \quad (6.2.8)$$

$$C_2H_3 \rightarrow C_2H_2 + H \quad (6.2.9)$$

Higher concentrations of the ethylene formation with the bare reactor will give a significantly different gas composition when computing the final carbon conversion from the methanolysis process. It was postulated that this pathway may describe the high ethylene yields documented in the final work from Steinberg et al [18], [19]. From the highest ethylene conversions which were recorded from his work, it was reported that a 22.5 % ethylene carbon conversion was produced with an M/B= 4 at 1000 °C and 0.9 s. From the maximum value derived in the empty reactor, Figure 6-17, an ethylene yield of 0.6 vol% can be taken as a representative value of the ethylene production due to MTD. When taking into account the M/B ratio, assuming a carbon content of 50 % in the biomass and assuming no ethylene formed in degradation reactions, over 40 % of the overall carbon conversion to ethylene can potentially be attributed to methane degradation. Thus, careful consideration of the ethylene production is required to successfully determine the mechanisms involved in flash methanolysis.

Due to the identified catalytic possibilities discussed above the catalytic activity of the system was investigated by determining the ethylene and ethane concentration of product gas from the NH_3/H_2S reactor. From the trial it was observed that the ethylene and ethane production was in agreement with that collected from the H_2S/NH_3 reactor, Figure 6-18. Thus, confirming that the inclusion of the thermocouples in the system did not have any significant bearing on the production of C_2H_4 and C_2H_6 in the system.

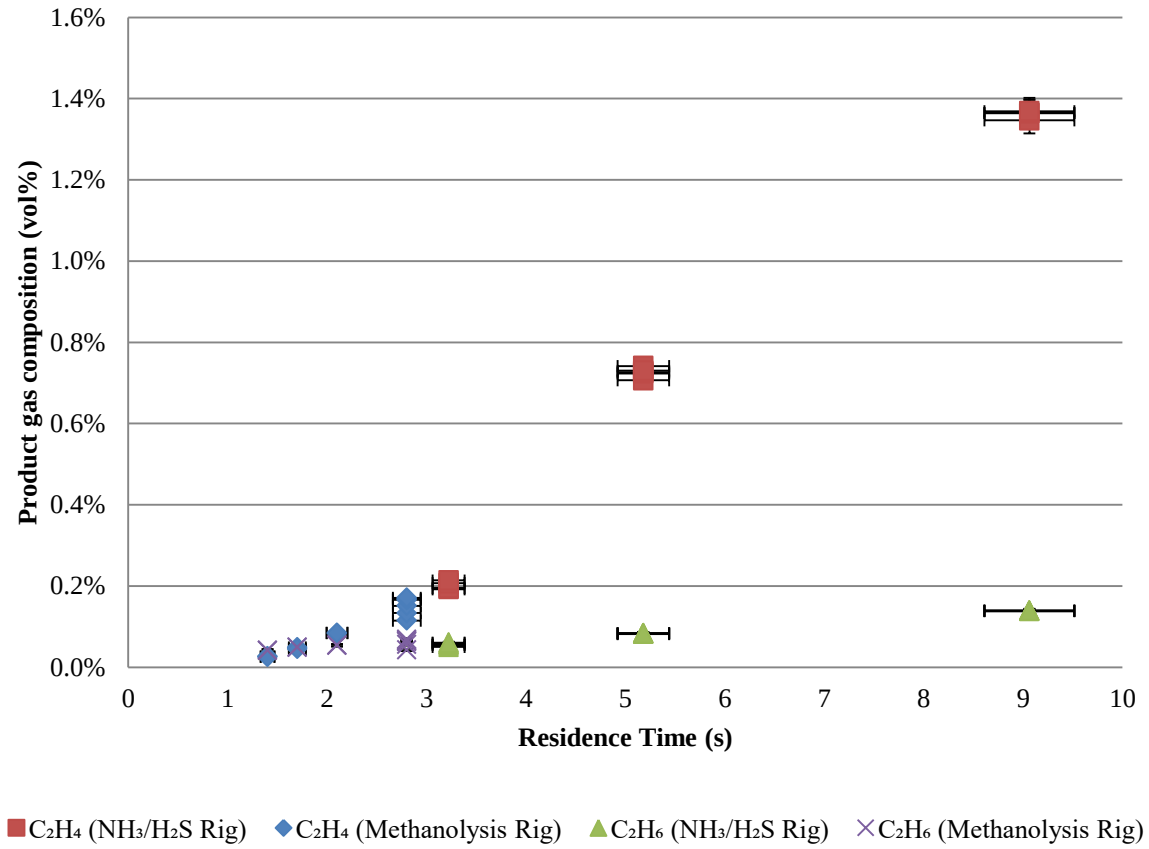

Figure 6-18: Ethylene and ethane concentrations at different residence times for different reactors. NH_3/H_2S rig average temperature 940 °C, methanolysis rig average temperature 930 °C.

6.3 Tar production from MTD

To conclude the MTD product species investigation, trials were conducted to determine the tar production during MTD. Trials were conducted with and without a bed to also determine the influence which the incorporation bed materials have in the production of hydrocarbon tar species. Trials were conducted for 30 minutes with the system held at a constant temperature of 980 °C and a residence time of ~ 9.5 s. Methane gas was passed through the system with the 3rd condenser in place and the exact times were noted to determine the effective total methane passed through the reactor. This essentially allowed for determination of the overall carbon conversion of methane to form tars. A high residence time was decided upon as from the methanolysis of biomass high tar production was observed at high residence times, which is discussed in depth in the following chapter. Overall it was determined that the production of tars was very low, with a maximum conversion to tars by 0.07 %, Table 6-2.

Table 6-2: Tar species analysis for the MTD, reactor operated at 980 °C with an overall residence time of 9.5 s.

		Packed bed	±	50 mm Bed	±
Mass Flow rate	*[kg/hr]*	0.145	±0.004	0.145	±0.004
Residence Time	*[s]*	9.4	±0.5	9.7	±0.5
Total Methane passed	*[g]*	67	±2	73	±2
Total Carbon passed	*[g]*	54	±2	50	±1
Tar Composition					
Benzene	*Carbon Conversion*	0.05 %	±0.01	0.01 %	-
Toluene	*Carbon Conversion*	0.01 %	-	0.00 %	-
Total	*Carbon Conversion*	0.07%	±0.01	0.01%	-

From the tar analysis it was concluded that the overall production of tar species was not strongly influenced by the production of tars via-MTD. This is apparent as for a hypothetical trial where M/B = 5, the overall contribution to the measured carbon conversion of biomass would be approximately ten times greater. This would result in an overall contribution of ~0.7 % carbon conversion, which was similar to the experimental error associated with the system. It was also possible that the tar species produced from MTD react with volatiles which are released during methanolysis.

6.4 Comparison with Previous Methane Thermal Degradation Studies

An investigation into the gas analysis set up in previous studies of Steinberg et al [1], [18], revealed that the use of hydrogen as the Gas Chromatograph (GC) carrier gas could not allow hydrogen concentrations in the product gas to be measured in the experiments. In these studies, CO, CO_2, CH_4, C_2H_4, C_2H_6 and C_6H_6 were stated as detectable gas species for the system, with tars collected by condensation. Later work by Kobayashi and Steinberg [2], regarded the methane degradation characteristics of what appears to be the same reactor system under similar temperatures but much higher pressures, 28 – 52 atm. By extrapolation of the work from Kobayashi and Steinberg [26], it was also suggested that MTD at low pressure would not be insignificant. Interestingly, within the designated MTD work in this study, the detection of H_2 via micro-GC was found to be significant while the previous methanolysis studies by Steinberg et al. [1], [18] suggested no MTD occurred. In

the work of Steinberg et al., and Kobayashi and Steinberg, the hydrogen concentration was not directly measured by the GC, and hydrocarbon measurements were taken as an indication of MTD occurring. Kobayashi and Steinberg, however, did conclude that degradation of ethylene within methane occurred, as indicated by a decrease in outlet ethylene concentration.

From the MTD characteristics which were determined in this methanolysis reactor, it was highly likely that significant concentrations of hydrogen were present but undetected in the product gas during experiments by Steinberg et al [1], [18]–[20]. From the work of Steinberg et al [3], no analyses were conducted before or after methanolysis, however initial measurements of the feed prior to experiments were conducted. Steinberg et al. [3], stated that the ethylene concentration within the gas was measured, this was interpreted as a quality check of the methane inlet gas, as it was stated that high purity methane was always used following the discovery that ethylene degraded in methane. Steinberg et al. [3] determined that a stream of 1.35 % ethylene in methane at 1000 °C and 350 kPa, operated at a residence time of 2 s decreased concentration by 0.33 %.

From the conclusions drawn from the methane degradation analysis of the system, it was of interest to determine the MTD characteristics with the reactor core exposed to methane. This also allowed for an investigation into the characteristics of Steinberg et al's work, as well as the extent of influence which the reactor surface may have on the extent of MTD. As previously documented, the reactor used by Steinberg for the methane pyrolysis was similar to that used by Kobayashi and Steinberg [1], [2], [18], [19], [21], and comparisons could aid in better understanding the pioneering work. Although the reactor volumes used by Kobayashi and Steinberg [21], were similar to the reactor used in this study, the overall surface area was approximately double that of the methanolysis reactor, Table 6-3. It was also noted that the preheater configuration used by Kobayashi and Steinberg was slightly different as this was a separate designated preheater, as opposed to the present system, where the preheater was essentially a zone before the fluidised bed. This varies the extent of degradation which was expected when the biomass was initially exposed to the reacting environment. It was likely that during the work of Kobayashi and Steinberg, the degradation begun shortly after the feeding of the chip and continued throughout the reactor until exit; whereas, within the constructed system, the hydrogen concentration was likely higher upon contact with the biomass.

Table 6-3: Kobayashi and Steinberg reactor and operating conditions, in comparison to this study.

		Kobayashi and Steinberg	This Study
Reactor Characteristics			
Construction Materials	*[-]*	Inconel 617	253 MA (Quartz Lined)
Reactor Type	*[-]*	Co-Current Tubular Reactor	Fluidised Bed
Designated Preheater?	*[-]*	Yes	No
Reactor Diameter (ID)	*[mm]*	25.4	53
Reactor Length	*[m]*	2.44	0.5
Surface Area	*[m^2]*	0.19	0.08
Volume	*[L]*	1.24	1.10
Operating Conditions			
Pressure	*[kPa]*	2820-5610	101-480
Temperature	*[°C]*	700-900	850-1040
Residence Time	*[s]*	5.5-103	0.5-16.3

A trial was conducted at different temperatures in order to determine the temperature influence and extent during MTD. For this trial the quartz element and quartz liner was removed to best emulate the reactor configuration from Steinberg et al [2]. Trials were conducted at temperatures similar to that of Kobayashi and Steinberg with a constant residence time of 16.3 ± 0.4 s, and the results of kinetic rate constant, k_1, are shown Figure 6-19. The decomposition was calculated using the equations stated by Kobayashi and Steinberg for the homogenous gas phase reaction rate and rate constant, Equations (6.4.1) and (6.4.2), respectively.

$$-r_{CH4} = k1\, C_{CH4}\left(1 - \frac{C_{H2}^2}{Ke\, C_{CH4}}\right) \tag{6.4.1}$$

$$t\, k1 = \frac{C_{CH4(o)} - C_{CH4(e)}}{C_{CH4(o)} + C_{CH4(e)}} \ln \frac{C_{CH4(o)}^2 - C_{CH4(e)} C_{CH4}}{C_{CH4(o)}(C_{CH4} - C_{CH4(e)})} \tag{6.4.2}$$

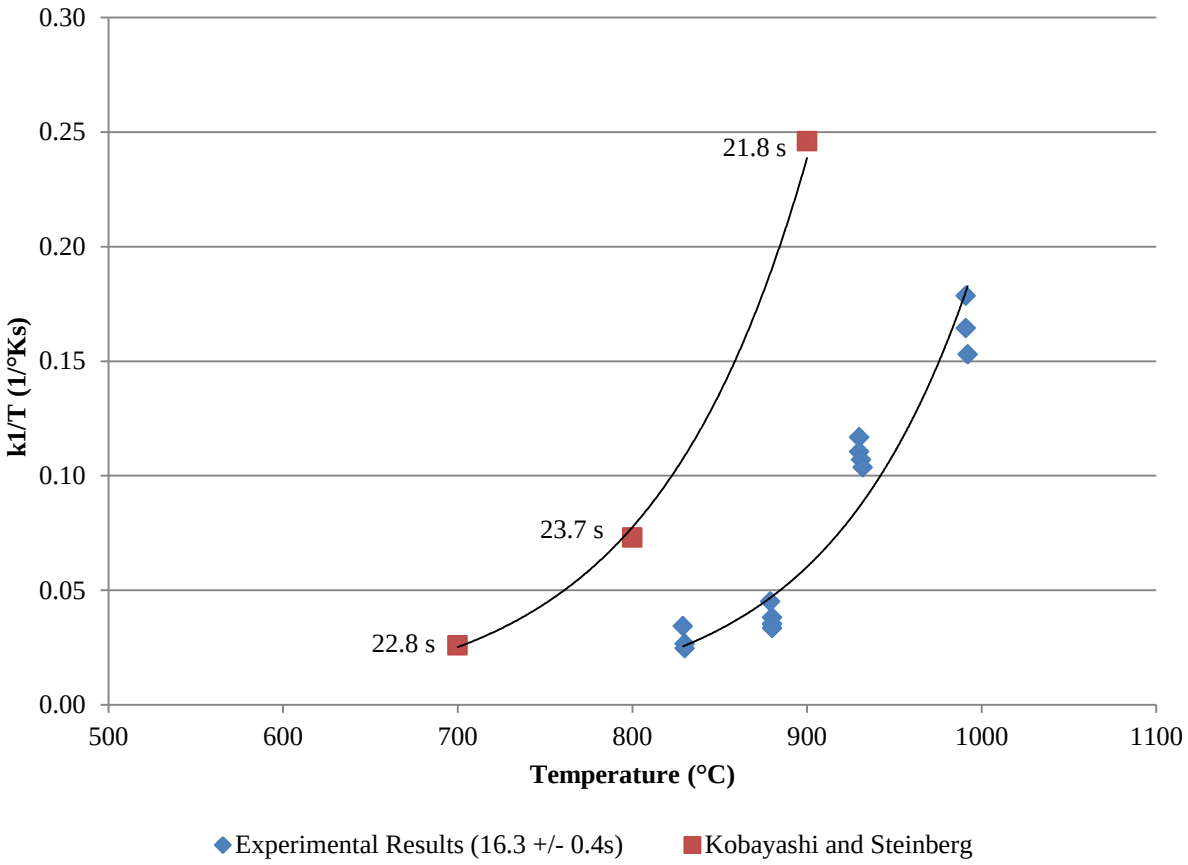

Figure 6-19: Comparison of reactor degradation rate constant between the present study without quartz liner with those in Kobayashi and Steinberg methanolysis reactor. Data point tags indicating the residence times used in the data collected from Kobayashi and Steinberg at 56.1 atm [2].

From the experiments which were conducted it was determined that the removal of the quartz element and liner significantly increased the methane degradation values. This validated the incorporation of the quartz construction within the reactor system as otherwise higher hydrogen concentrations would arise in the reacting gas. However, the results are opposite to the findings of Steinberg et al where no methane degradation was reported for the methanolysis experiments. Due to the magnitude of the degradation, it was likely that carbon was deposited during the methanolysis experiments conducted by Steinberg et al [3]. Although it has been concluded that carbon formation may not have severe methane degradation effects, subsequent cracking of product volatiles could occur. As well, it was highly likely that the reactions conducted by Steinberg et al [18], [19], were in the presence of significant hydrogen concentrations at the bottom of the drop tube reactor. This suggests a possible combined hydrogen-methane pyrolysis reaction mechanism occurring as the methane flowed through the reactor. From Figure 6-19, it was observed that the overall rate constant was not constant between reactors, and that methane degradation in the constructed rig was less than that apparently experienced by Kobayashi and Steinberg [2]. It was likely that this was due to the catalytic effect of the Inconel surface, primarily due to the increased nickel concentration which is a commonly used catalyst in

MTD [22]–[24]. It was also possible that the discrepancy of the hydrogen production could be explained by the differing residence times between the trials.

To compare the reaction kinetics of MTD between reactors the activation energy of the system was also calculated. As stated by Kobayashi and Steinberg, a recorded activation energy of 131 kJ/mol was obtained in the drop tube reactor [2]. From the same rate constant and reaction rate equations (6.4.1) and (6.4.2) it was determined that the MTD activation energy in the methanolysis reactor was 410 kJ/mol, Figure 6-20. The system was refitted with the quartz liner arrangement to prevent exposure to the outer reactor wall. The value was significantly larger than that of Kobayashi and Steinberg, and is in agreement with values determined by G. Skinner and R. Ruehrwein, and H. Palmer et al, 423 kJ/mol and 431 kJ/mol, respectively [25], [26]. This led to the conclusion that it was highly likely the extent of hydrogen production was significant during the methanolysis of Kobayashi and Steinberg; also, the MTD characteristics of the reactor used in this study were in agreement with literature indicating the unlikeliness of catalytic effects within the system. This highlights that it is likely that the work conducted by Steinberg et al, was likely influenced by the presence of unnoted hydrogen within the reacting gas stream during methanolysis.

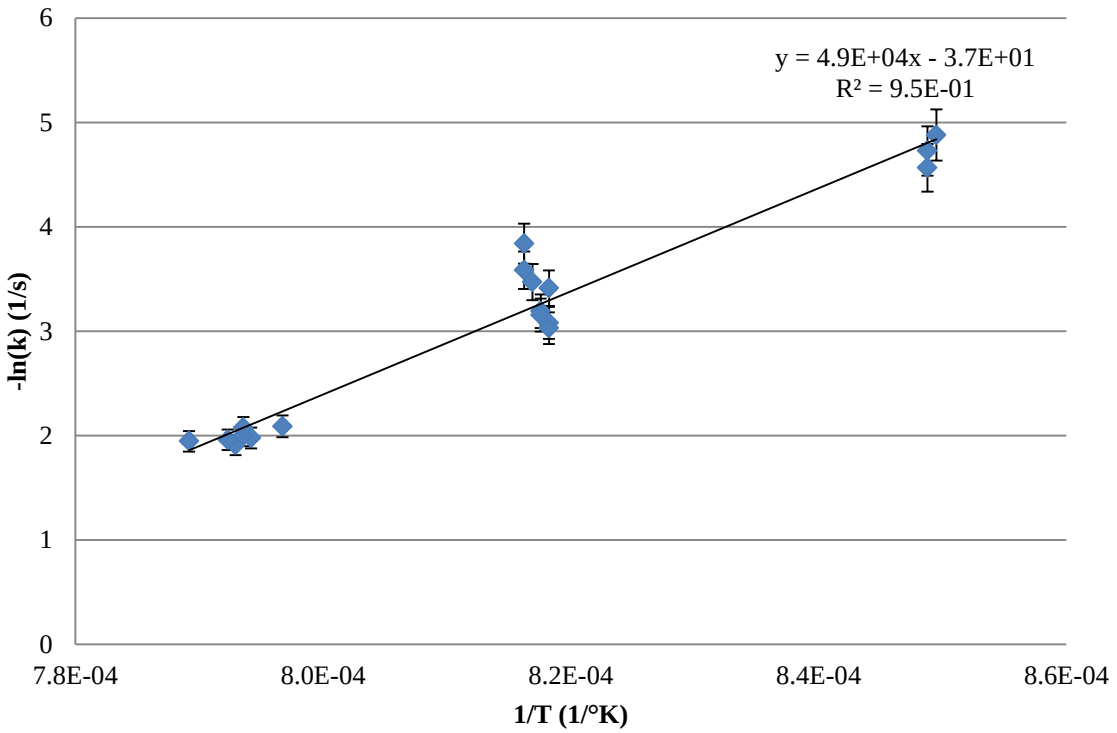

Figure 6-20: Reaction rate constant derivation for methane thermal degradation, over the trialling temperature of 900-1000 °C.

6.5 Comments on MTD in the system

To minimise methane thermal degradation (MTD), and thus decrease the production of hydrogen, the system was retrofitted with a quartz sleeve which isolated the feeder tube arrangement. This allowed for an inert reaction zone to be formed for the biomass feed with the reacting gas. Decreases in the hydrogen production were observed for the same residence time with the inclusion of quartz. As this proved to decrease the hydrogen content the modification was installed permanently. In addition, the system was modified to prevent excess hydrogen production by many possible routes. However, the extent of catalytic activity from the excluded alumina and 304 SS mesh was not investigated as the efficiency of catalysis was not of concern.

From the experiments conducted it was determined that the hydrogen production for the methanolysis reaction could be reduced by controlling the operating conditions of the system. The temperature range of 900-1000 °C was of interest for the methanolysis reactions but the operation temperature needs to be optimised to minimise MTD to reduce the extent of hydrogen interactions with biomass and devolatilisation products. Residence time was also found to affect MTD, as the H_2 concentration in the outlet gas was increased with increased residence time.

As explored in the subsequent methanolysis reactions, it was suspected that the reaction zone residence time was very influential on the end product gas distribution. As the inclusion of the quartz element decreased the overall gas residence time only, but the effective gas residence above the fritted disc was constant with any given mass flow. Although the addition of the quartz element was suspected of increasing the heat transfer to the gas in the preheater section, the majority of degradation likely occurred above the fritted disc and was dependent on the bed height. The residence time above the reaction zone could only be changed by the inclusion of a bed (which was limited by the fluidisation characteristics). This hypothesis was supported by an apparent linear correlation of hydrogen production with respect to mass flow rate. This was observed by similar hydrogen concentrations obtained at corresponding methane mass flow rates, where the effective residence time differed by a factor of 3, Figure 6-21. This alluded to the reaction zone being the primary zone of interest and also explained why the staging of the heaters did not vary the MTD characteristics. The effect of the increased heat transfer with the addition of the quartz was suspected of being more influential with increased residence time.

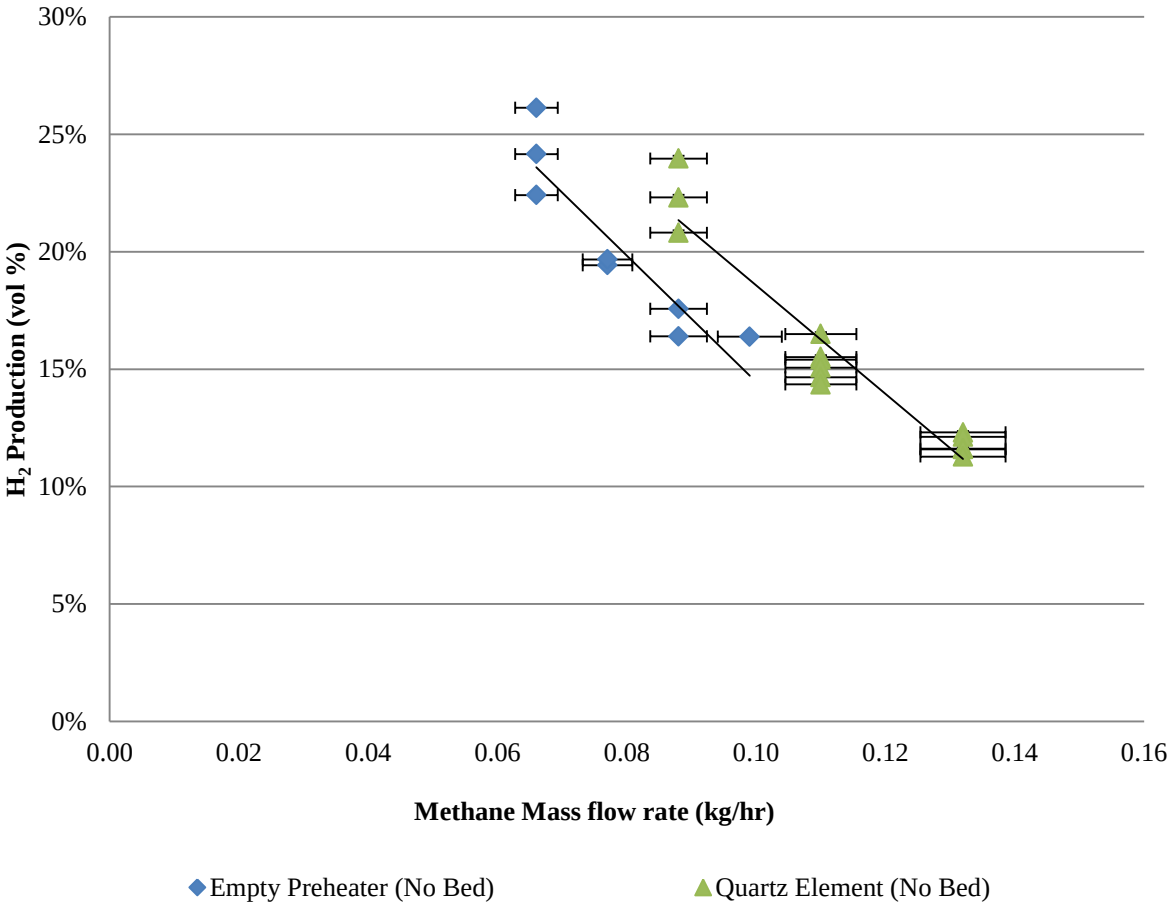

Figure 6-21: Hydrogen production by MTD for differing reactor configurations. Empty preheater (No Bed) relates to the reactor operated with no quartz element; Quartz Element (No Bed), reactor system with quartz in place (average operating temperature 985 °C).

From the trial it was also determined that ethylene and ethane were produced during MTD. This was caused by a number of side reactions which produced low concentrations of hydrocarbons. It was determined that the overall vol% of gaseous hydrocarbon production was generally < 1 vol%. The trends in the production of ethylene were similar to that of hydrogen, with increased production with increased temperature and residence time. Ethane remained relatively constant throughout the trialling period with an overall production which was significantly less than ethylene, at high residence times and temperature. It was suspected this was due to the reaction scheme which was discussed above. Although ethylene production was not significant, during the calculation of carbon conversion with regards to the inlet biomass, uncertainty in the source of the hydrocarbons can lead to errors. This was especially concerning as there was a high chance that in previous work this had not been accounted for, in which the systems are suspected to have significant ethylene production. Through back calculation this could have possibly accounted for 40 % of the ethylene production.

6.6 References

[1] M. Steinberg, P. T. Fallon, and M. S. Sundaram, "The Flash Pyrolysis and Methanolysis of Biomass (Wood) for Production of Ethylene, Benzene and Methanol," 1990.

[2] S. Kobayashi and M. Steinberg , "The Thermal Decomposition of Methane in a Tubular Reactor," 1992.

[3] M. S. Sundaram, S. M. Steinberg and P.T. Fallon, "Flash Pyrolysis of Biomass with Reactive and Non-Reactive Gases," Richland, Washington, 1984.

[4] A. M. Dunker, S. Kumar, and P. A. Mulawa, "Production of hydrogen by thermal decomposition of methane in a fluidized-bed reactor - Effects of catalyst, temperature, and residence time," *Int. J. Hydrogen Energy*, vol. 31, no. 4, pp. 473–484, 2006.

[5] N. Muradov, "Catalysis of methane decomposition over elemental carbon," *Catal. Commun.*, vol. 2, no. 3–4, pp. 89–94, 2001.

[6] N. Shah, D. Panjala, and G. P. Huffman, "Hydrogen production by catalytic decomposition of methane," *Energy and Fuels*, vol. 15, no. 6, pp. 1528–1534, 2001.

[7] T. V. Choudhary, S. Banerjee, and V. R. Choudhary, "Catalysts for combustion of methane and lower alkanes," *Appl. Catal. A Gen.*, vol. 234, no. 1–2, pp. 1–23, 2002.

[8] N. Muradov, F. Smith, C. Huang, and A. T-Raissi, "Autothermal catalytic pyrolysis of methane as a new route to hydrogen production with reduced CO2 emissions," *Catal. Today*, vol. 116, no. 3, pp. 281–288, 2006.

[9] J. Zhang *et al.*, "Hydrogen production by catalytic methane decomposition: Carbon materials as catalysts or catalyst supports," *Int. J. Hydrogen Energy*, vol. 42, no. 31, pp. 19755–19775, 2017.

[10] J. Hongrapipat, "Removal of NH3 and H2S from Biomass Gasification Producer gas," University of Canterbury, 2014.

[11] N. Muradov, F. Smith, and A. T-Raissi, "Catalytic activity of carbons for methane decomposition reaction," *Catal. Today*, vol. 102–103, pp. 225–233, 2005.

[12] M. H. Kim *et al.*, "Hydrogen production by catalytic decomposition of methane over activated carbons: Kinetic study," *Int. J. Hydrogen Energy*, vol. 29, no. 2, pp. 187–193, 2004.

[13] C. Guéret and F. Billaud, "Thermal coupling of methane: Influence of hydrogen at 1330°C. Experimental and simulated results," *J. Anal. Appl. Pyrolysis*, vol. 29, no. 2, pp. 183–205, 1994.

[14] C.-J. CHEN, M. H. BACK, and R. A. BACK, "The themal decomposition of methane. II.

Secondary reactions, autocatalysis and carbon formation; non-Arrhenias behaviour in the reaction of CH3, with ethane," *Can. J. Chem.*, vol. 54, no. 15438, pp. 956–963, 1976.

[15] M. Y. Sinaki, E. A. Matida, and F. Hamdullahpur, "Development of a reaction mechanism for predicting hydrogen production from homogeneous decomposition of methane," *Int. J. Hydrogen Energy*, vol. 36, pp. 2936–2944, 2011.

[16] C. Guéret, M. Daroux, and F. Billaud, "Methane pyrolysis: Thermodynamics," *Chem. Eng. Sci.*, vol. 52, no. 5, pp. 815–827, 1997.

[17] A. Holmen, O. Olsvik, and O. A. Rokstad, "Pyrolysis of natural gas: chemistry and process concepts," *Fuel Process. Technol.*, vol. 42, no. 2–3, pp. 249–267, 1995.

[18] M. Steinberg, "Flash Pyrolsyis of Biomass with Reactive and Non-Reactive Gases," 1984.

[19] M. Steinberg, P. T. Fallon, and M. S. Sundaram, "Flash pyrolysis of biomass with reactive and non-reactive gas," *Biomass*, vol. 9, no. 4, pp. 293–315, 1986.

[20] M. S. and P. T. F. Muthu S. Sundaram, "Flash Pyrolysis of Coal in Reactive and Non-Reactiv Gaseous Enviroments," pp. 106–129, 1983.

[21] M. STEINBERG, "Production of hydrogen and methanol from natural gas with reduced CO2 emission," *Int. J. Hydrogen Energy*, vol. 23, no. 6, pp. 419–425, 1998.

[22] J. L. Pinilla, I. Suelves, M. J. Lázaro, R. Moliner, and J. M. Palacios, "Parametric study of the decomposition of methane using a NiCu/Al2O3 catalyst in a fluidized bed reactor," *Int. J. Hydrogen Energy*, vol. 35, no. 18, pp. 9801–9809, 2010.

[23] P. Ammendola, R. Chirone, G. Ruoppolo, and G. Russo, "Production of hydrogen from thermo-catalytic decomposition of methane in a fluidized bed reactor," *Chem. Eng. J.*, vol. 154, no. 1–3, pp. 287–294, 2009.

[24] U. P. M. Ashik, W. M. A. Wan Daud, and H. F. Abbas, "Methane decomposition kinetics and reaction rate over Ni/SiO2 nanocatalyst produced through co-precipitation cum modified StÖber method," *Int. J. Hydrogen Energy*, vol. 42, no. 2, pp. 938–952, 2017.

[25] G. B. Skinner and R. A. Ruehrwein, "Shock Tube studies on the Pyrolysis and Oxidation of Methane," *J. Phys. Chem.*, vol. 63, no. 10, pp. 1736–1742, 1959.

[26] H. B. Palmer, J. Lahaye, and K. C. Hou, "On the Kinetics and Mechanism of the Thermal Decomposition of Methane in a Flow System'," *J. Phys. Chem.*, vol. 72, no. 1, pp. 348–353, 1967.

7 Investigation into the Flash Methanolysis of Biomass

This chapter includes the results and discussion of the investigation into the varying influences of the reactor parameters during the flash methanolysis of biomass. Due to the extent of degradation and differing sources of hydrogen, methane, and hydrocarbons, a definition of the terminology is provided below:

- Carbon Conversion: This is the value of the carbonaceous species produced relative to the carbon which was introduced with the biomass feed. This term is used to compare the selectivity of the produced species when feed is introduced and refers to the carbon from the biomass only (unless explicitly stated).

- Mass Balance: Refers to the complete mass balance of all species entering and exiting the system.

- Degradation Values: The value of the corresponding species which is produced during MTD measured at the beginning or end of a run.

- Methane Consumption: The overall consumption over the reactor $CH_4(Consumption) = 1 - \frac{CH_{4,out}}{CH_{4,in}}$, unless otherwise defined.

Trials were usually conducted by allowing the system to reach the operating temperature from the resting temperature of 850 °C. The biomass feed was placed in the hopper and the system was purged, Figure 7-1. Upon a successful pressure test, the hopper was pressurized with nitrogen to the desired operating pressure; the methane feed was then allowed to enter the reactor at the desired flowrate. The methane stream was fed for approximately 5 minutes then a sample was taken (MTD). The biomass feeder was then switched on to allow the methanolysis reaction to take place. Samples were taken every 4-5 minutes until the feeder was turned off. The methane was left to flow for another 5 minutes, and then another MTD sample was taken. After purging the system, the residual biomass was weighed and noted, and the 3rd condenser removed. A detailed operating procedure can be found in Appendix D.

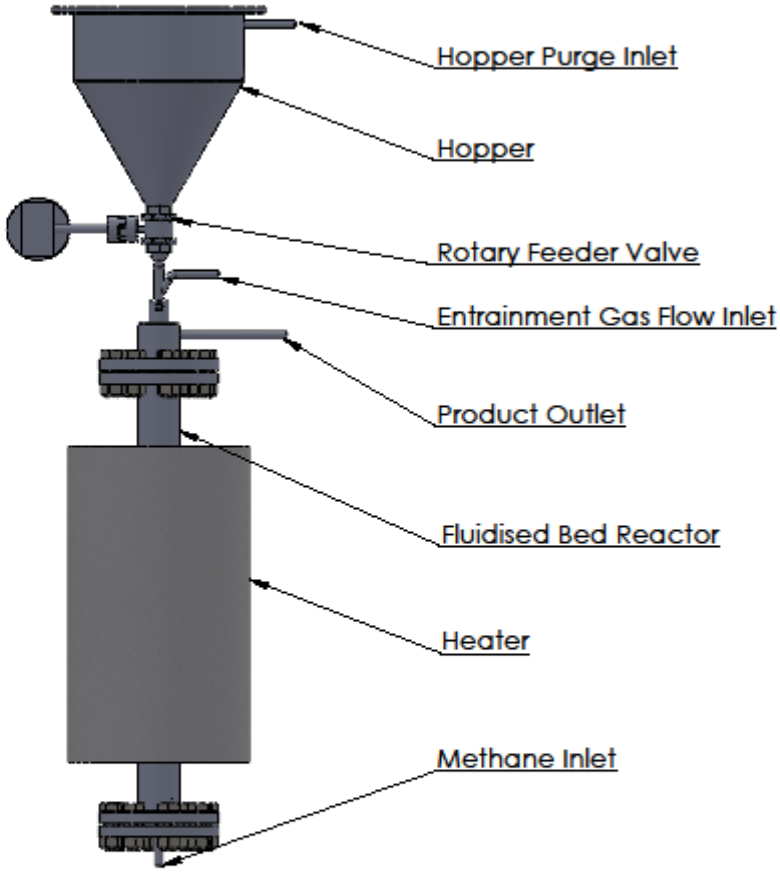

Figure 7-1: Reactor arrangement overview used for the flash methanolysis of biomass.

For the investigation into the system configuration effects during the methanolysis of biomass, the system was operated primarily in two configurations, ‘packed bed’ and ‘fluidised bed’, as shown in Figure 7-2. The major difference between the system configurations was the inclusion of the quartz sand bed, whereas, with the exclusion of the bed the quartz frit was representative of a packed bed. A full investigation of the characteristics of the system is provided in the subsequent sections.

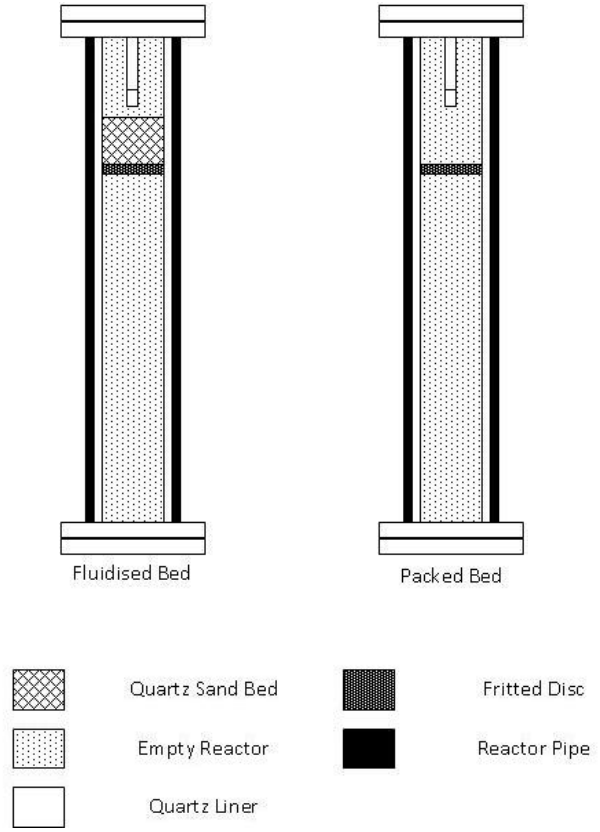

Figure 7-2: Reactor configurations utilized throughout the investigation into the effect of system parameters during the methanolysis of biomass, (no sand is placed in the packed bed arrangement).

7.1 Effect of Reaction Temperature during Methanolysis

Experiments were performed to determine the effect of temperature (948 to 1028 °C) in both the fluidised bed and fixed bed configurations. The fluidised bed was expected to improve heat transfer between the methane gas and biomass particles, and reduce horizontal temperature gradients in the reacting zone. It was found that during the packed bed reactor trials, the temperature of the system continually decreased with the feeding of biomass into the system thus, a true reaction zone temperature was difficult to accurately determine. This could possibly be caused by a number of factors;

- The endothermic nature of the reaction in the methanolysis process which decreases the temperature of the immediate region where the reaction occurs.
- Carbon depositing on the thermocouple which, once occurred, would produce an insulating layer which reduces the accuracy of the temperature measurement.
- Poor mixing, which causes localised cold/hot regions within the empty reacting zone and could affect the accuracy of the thermocouple readings

- Cold methane/nitrogen gas coming with the feed biomass.

To minimize the effect of the cold methane/nitrogen which flows down the feeder tube with the biomass, the entrainment flow and gas passing through the rotary feeder was reduced. This was controlled by decreasing the pressure drop over the feeder valve to ensure that excess gas did not flow through the valve arrangement. The endothermic nature of the reaction, carbon deposition effects and poor mixing effects are all minimized by the inclusion of a fluidised bed. Due to the larger thermal mass in the reaction zone, the temperature decreases due to the endothermic nature of the reaction was reduced. The constant motion of the bed also prevented carbon build up on the thermocouple and attrition on the surface of the thermocouple. Mixing was also greatly improved with the inclusion of a bed as the system flow rate was significantly higher than the minimum fluidisation velocity, regulating the temperature of the bed effectively. For all trials conducted the fluidisation was at least a multiple of three times the minimum fluidisation velocity, which has been observed to provide an efficient reaction environment [1]. Due to the addition of a 40 mm high bed in the system, the reaction zone residence time was decreased by a factor of 2, from 1.8 s to 0.9 s.

The experimental results from this study also show that similar trends were observed as a function of reaction temperature both in the fluidised bed and packed bed arrangements, Figure 7-3. Increasing temperature from 948 to 988 °C, the ethylene yield increased from 8 ± 1 % to 19 ± 3 %, but further increased to 1028 °C, decreased the ethylene yield to 17 ± 1 %, Figure 7-3. Following the same trend, an increase in the hydrogen production was also observed with increasing temperature. These results are consistent with the study of Steinberg et al [2] who found that the maximum ethylene yield occurred at approximately 1000 °C, and with further increase in the temperature, the ethylene yield was decreased. It is suspected that at temperatures above, 1000°C the methane degradation was significant and that the presence of significant concentrations of hydrogen strongly influences the product distribution.

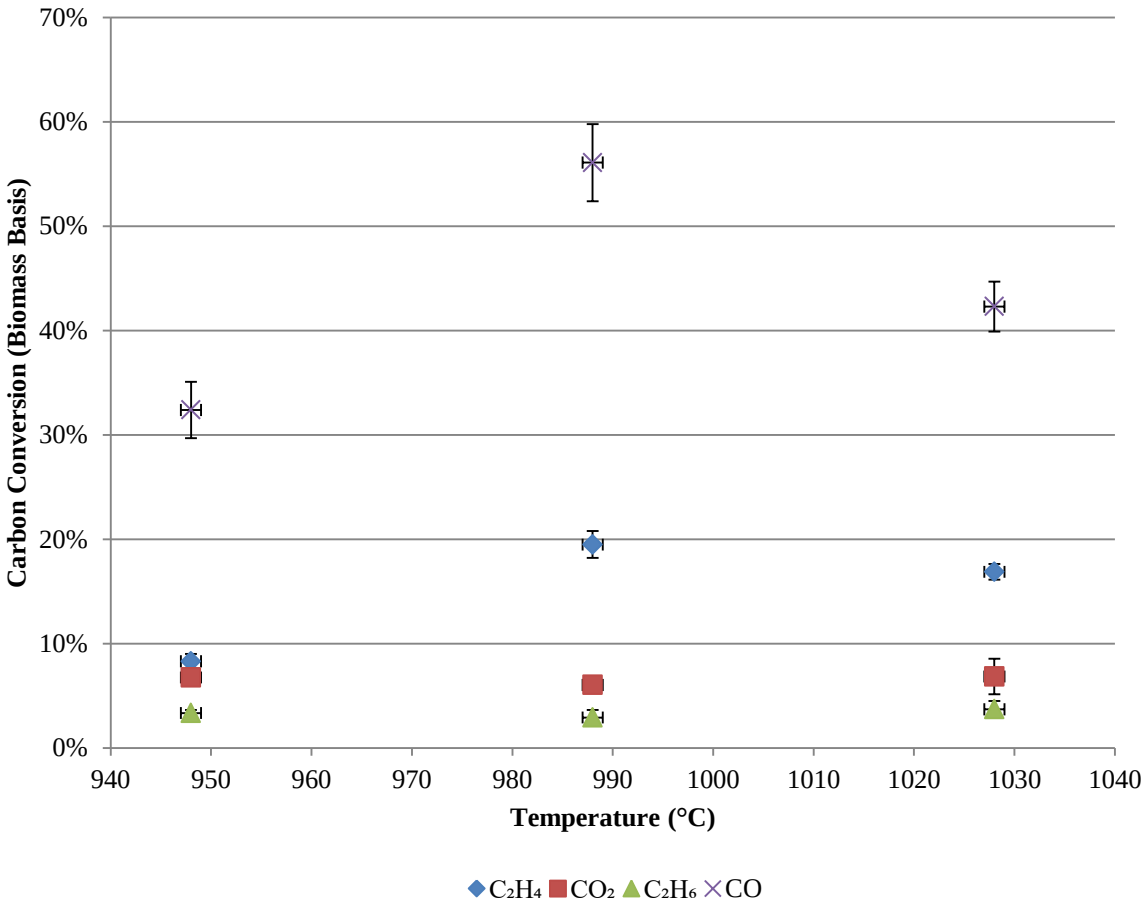

Figure 7-3: CO, Ethylene, Ethane and CO_2 production with increasing temperature. System operated with a 40 mm bed at an M/B = 5, at atmospheric pressure and a residence time of 0.75 s.

In this study, it is suggested that when the temperature was over 988 °C, ethylene dehydrogenation may be causing the decreased ethylene yield. The increasing temperature of the reactor would increase the rate of the ethylene dehydrogenation reaction, as described by Equation (7.1.1). The postulation of this pathway was supported by the increased yield in hydrogen concentration with increased temperature. This was also supported by the stabilisation in methane consumption with increasing temperature as observed in Figure 7-4. Although the methane degradation increased at temperatures above 988°C, the methane consumption was found to slightly decrease from 3.6 ± 0.2 % to 2.4 ± 0.1 %, when the temperature was increased from 988 °C to 1028 °C, Figure 7-4. The hydrogen content remained constant at 8 %, which was suspected to rise from degradation of ethylene through the pathway shown in equation (7.1.2). The hydrogen production may also rise from other gases which are not analysed. Overall if the production of hydrogen was mainly from the dehydrogenation of ethylene, increased carbon conversion would be expected. This was due to the increased acetylene formation, which is known to react very quickly at elevated temperatures.

$$C_2H_4 \rightarrow C_2H_2 + H_2 \quad (7.1.1)$$

$$2CH_4 \overset{k_1}{\rightarrow} C_2H_6 + H_2 \overset{k_2}{\rightarrow} C_2H_4 + H_2 \overset{k_3}{\rightarrow} C_2H_2 + H_2 \overset{k_4}{\rightarrow} 2C + H_2 \quad (7.1.2)$$

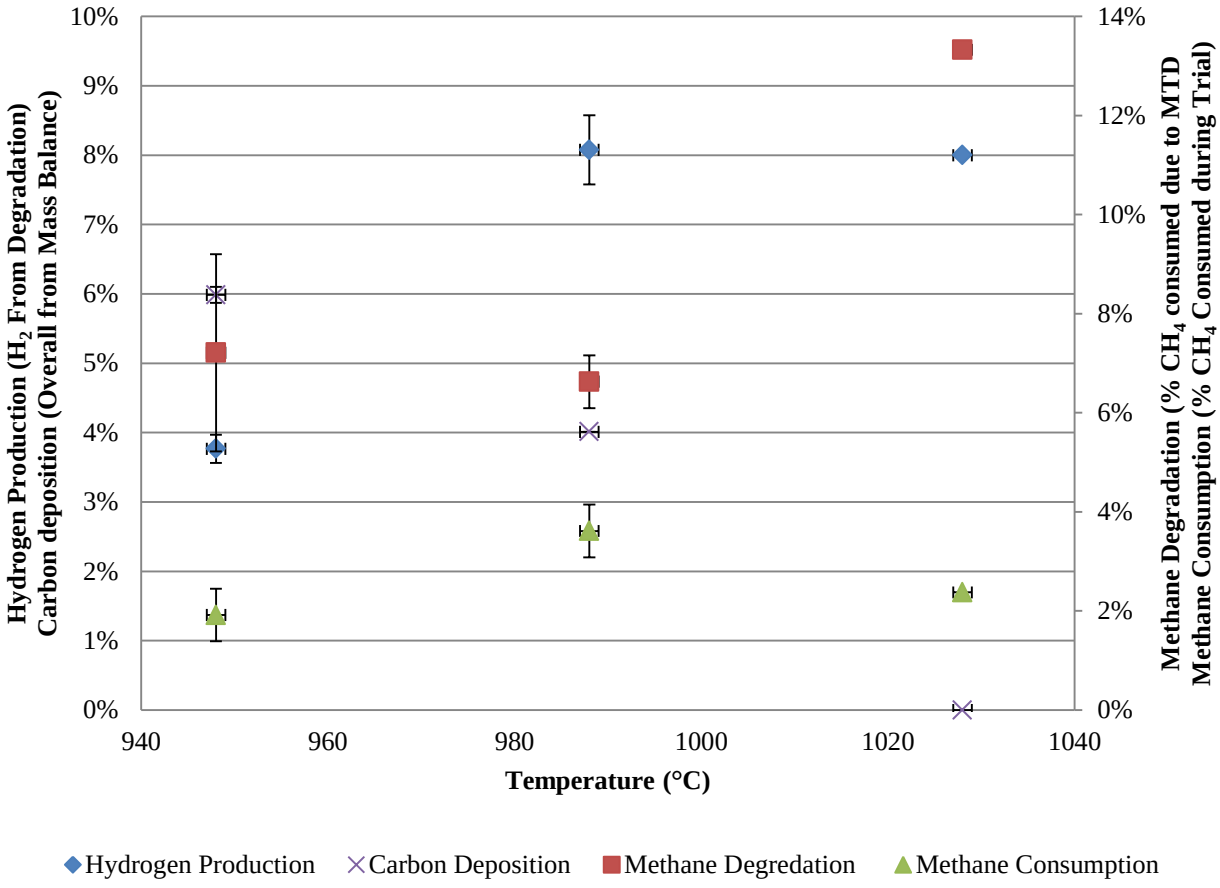

Figure 7-4: Hydrogen production, methane degradation, methane consumption and carbon deposition as a function of temperature. System was operated with a 40 mm bed at an M/B = 5, at atmospheric pressure and at 0.75 s residence time.

From the oxygen balance it was also apparent that there was a significant variation in the composition of oxygen bearing gaseous molecules (CO, CO_2 and H_2O) within the experiment, Figure 7-5. At the lower temperature of 948 °C, water was observed to be the favoured product with an overall oxygen conversion of 38 ± 4 %; however, this was decreased to 2 ± 5 % at 985 °C, Figure 7-5. This value was increased to approximately 23 % at 1028 °C. The relative oxygen conversion to CO_2 was relatively constant with values of 17-19 % oxygen conversion when the reactor temperature was changed from 948 to 1028 °C. Therefore, the composition of the CO and H_2O was essentially inversed. This would suggest that the water gas shift equation (WGS), Reaction (7.1.3), was not the dominant reaction pathway for the CO and H_2O production. This can be used to explain the variations between the trials

conducted at 988-1028 °C. However, in closing the mass balance it was found that the solid carbon deposition decreased with increasing temperatures.

$$H_2O + CO \rightleftarrows CO_2 + H_2 \quad (\Delta H = -41 \frac{kJ}{mol}) \tag{7.1.3}$$

The Boudouard reaction was also investigated as a possible pathway in the formation of CO, Reaction (7.1.4). The reaction was also exothermic and exhibits the same characteristics as the WGS reaction. The kinetics for the production of CO_2 and C increased with temperature, whilst, the overall conversion decreased at higher temperatures.

$$2CO \rightleftarrows CO_2 + C \quad (\Delta H = -173 \frac{kJ}{mol}) \tag{7.1.4}$$

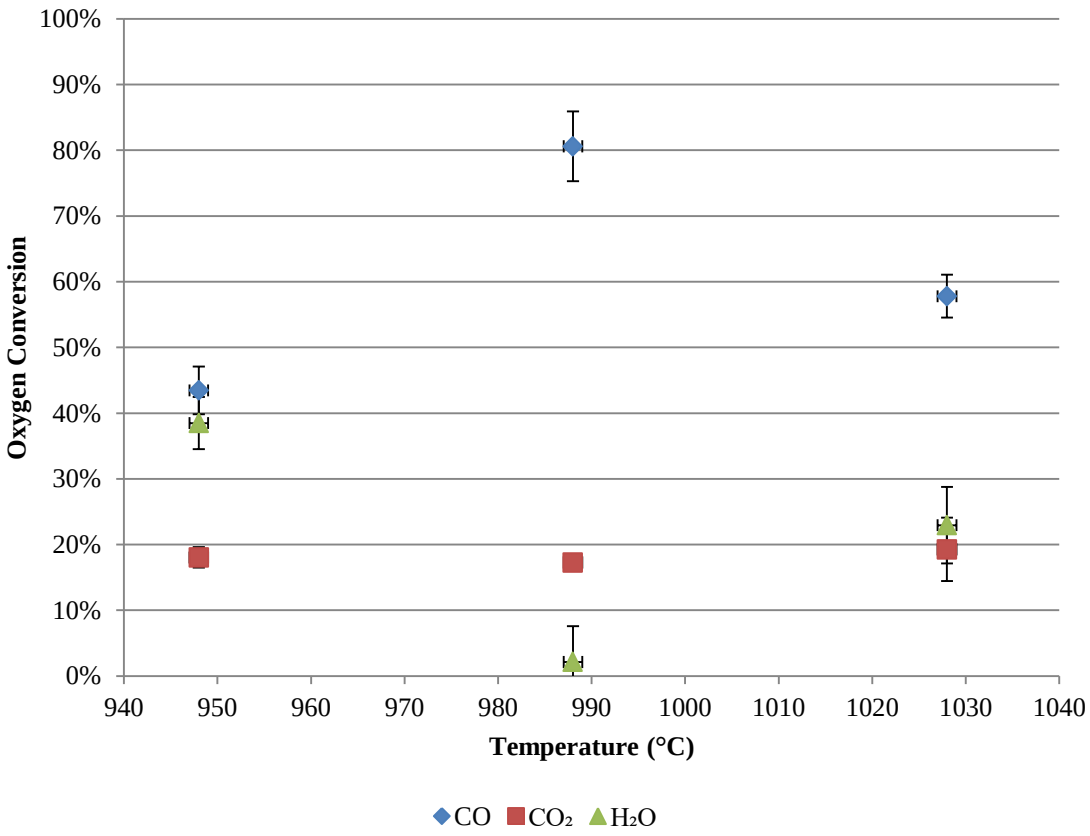

Figure 7-5: Oxygen bearing compound distribution derived from oxygen balance. System operated with a 40 mm bed at an M/B = 5, at atmospheric pressure and a residence time of 0.75 s.

For all experiments tar analyses were also conducted on the liquid products which were formed from the reactions. It was observed that generally the total amount of tar compounds produced increased with temperature, with a marked difference from 5.5 ± 0.3 % to 12.2 ± 0.9 %when the temperature

was increased from 948 to 988 °C. Above 988 °C the concentration of benzene remained and toluene yield was moderate whereas the total tar yield was increased from 12.2 ± 0.9 % to 14 ± 1 %. Notable decreases in the naphthalene yield were also apparent.

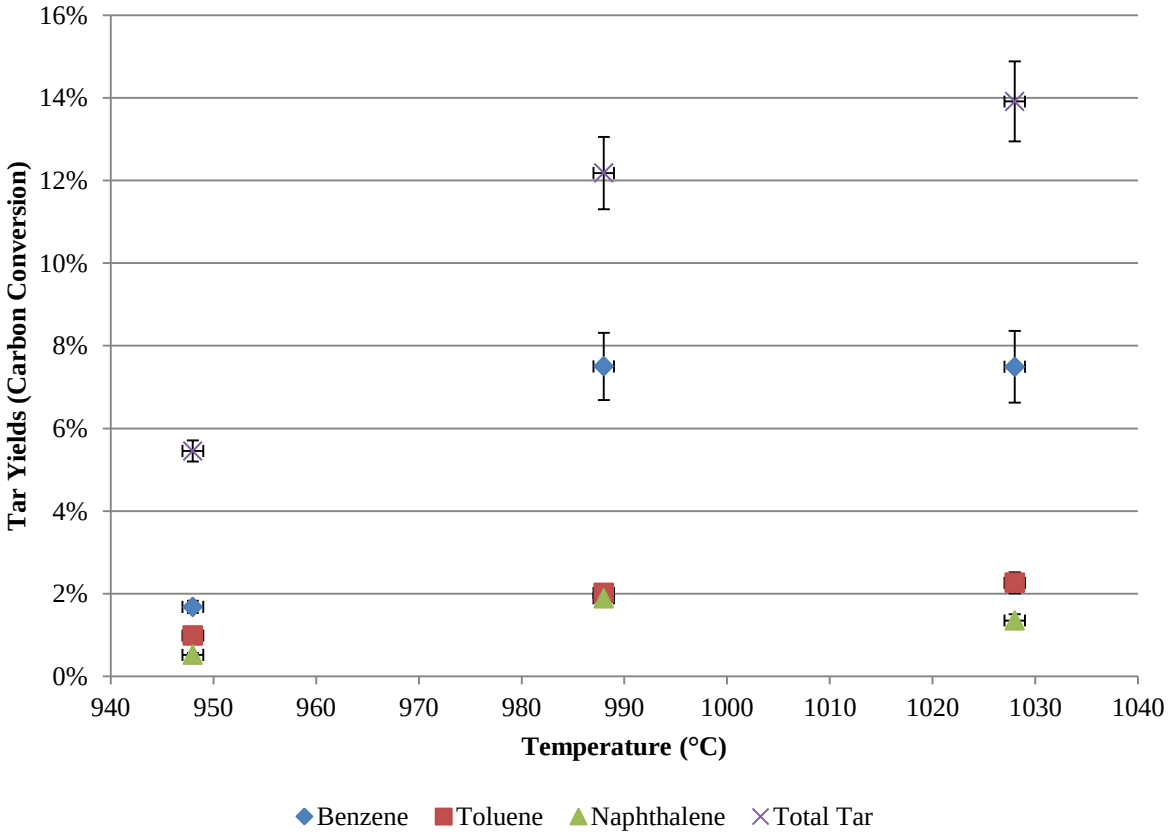

Figure 7-6: Tar analysis and total tar carbon conversion as a function of process temperature. System operated with a 40 mm bed at an M/B = 5, at atmospheric pressure and a residence time of 0.75 s.

7.1.1 Discussion on Effect of Temperature

Over the trialled temperature region the methane degradation was observed to remain constant at ~ 7% up to temperatures of 988 °C, while this was increased to 13 ± 1 % when the temperature was increased to 1028 °C. Coinciding with the increase in methane degradation, the total carbon deposition was almost zero at 1028 °C. It was highly probable that the apparent 'zero' carbon deposition was due to the carbon already being present in the system. This carbon was already present in the system due to the degradation of the methane which occurred during the stabilizing 5 minutes or so before biomass was introduced into the system. Carbon which is already in the system prior to starting the reaction had the ability to be gasified by the methanolysis products as well as methane. Ultimately this process resulted in a mass balance over 100 % and caused the apparent carbon deposition to be zero. Overall the mass balance closure was calculated to be 100 ± 1 %, indicating the possibility of no carbon being produced was within experimental error.

Overall, methane consumption increased from 4 % to ~5 % of the inlet flow rate. The hydrogen yield was observed to double from 3.77 ± 0.02% to 8.08 ± 0.04 % from 948 to 988 °C. From the stoichiometric requirements of hydrogen production from degradation, the additional hydrogen cannot be solely accounted for by methane degradation. It is suspected that the increase in temperature also increased the yield of hydrogen from the biomass. The additional hydrogen content was suspected to arise due to the increased reaction temperature, causing a decrease in larger hydrocarbon species, hence the decrease in ethylene. The additional hydrogen content which is formed may also be an artefact of the increased water produced, which potentially could be masking the direct relationship between the hydrogen and methane yields in the system. This is suspected to be due to the steam reforming of methane, which increases the overall CO production and this trend is in agreement with the increase in hydrogen observed, Equation (7.1.5).

$$H_2O + CH_4 \rightarrow CO + 3H_2 \qquad (7.1.5)$$

From the analysis on tar yield and product selectivity, the reactor temperature had a significant effect. The concentration of naphthalene in the tar products was decreased between 988 and 1028 °C. It is suggested that this is due to the cracking of larger chain hydrocarbons, which results in an increase in the mono-cyclic hydrocarbons, as shown in Figure 7-7. In the experiments the contents of toluene, styrene, phenol and indene (primarily) were increased with an increased reactor temperature from 988 °C to 1028 °C. It is worthwhile mentioning that the naphthalene cracking could generate additional hydrogen via dehydrogenation reactions which was unaccounted for from the methane degradation, Equation (7.1.6);

$$Napthalene \rightarrow (Toluene, Styrene, Phenol, Indene) + H_2 \qquad (7.1.6)$$

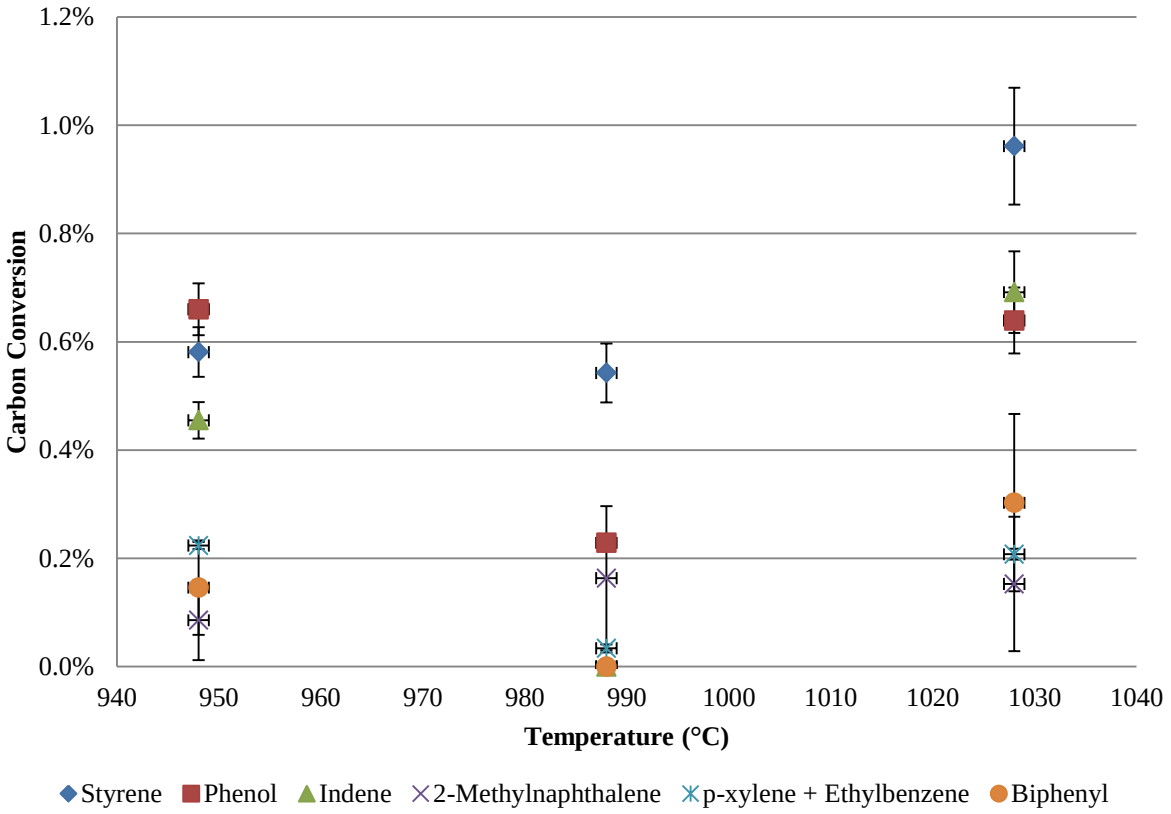

Figure 7-7: Trace tars from temperature variation trials, System operated with a 40 mm bed at an M/B = 5, at atmospheric pressure and a residence time of 0.75 s.

It is interesting to note that if the breaking of the cyclic structure was universal within the system, an increase in benzene would be likely as well. The benzene concentration between 988 and 1028 °C remained relatively constant. A possible explanation for this could be described by the low free energy of benzene which thermodynamically favours the production of benzene at 1028 °C. Branched aromatic structures such as, toluene, xylene and phenol may then undergo dealkylation due to the elevated temperature increasing the overall benzene production. It was possible that methane could be formed from the reactions and causes an apparent decrease in methane consumption (especially in the case of toluene and xylene).

Figure 7-8 shows the overall methane produced when degradation was taken into account. For this measurement, the system was allowed to run for ~5 mins with no feed entering the system and then the outlet gas composition was analysed with a stream of He to calculate the gas product flow rates. The flow rate of methane could then be back calculated to determine the product flow rates, methane consumption, production of methane and methane degradation. It was difficult to distinguish between the methane consumption and methane degradation but for simplification, it will be assumed that the degradation was constant over the trialling period. The methane which was adjusted for degradation

shows that there was a marked difference at the mid-temperature trial of 988 °C. It is suggested that this is due to the system favouring the ethylene output, where increased temperature potentially breaks the ethylene bonds and in turn formed methane and complete dehydrogenation to form carbon.

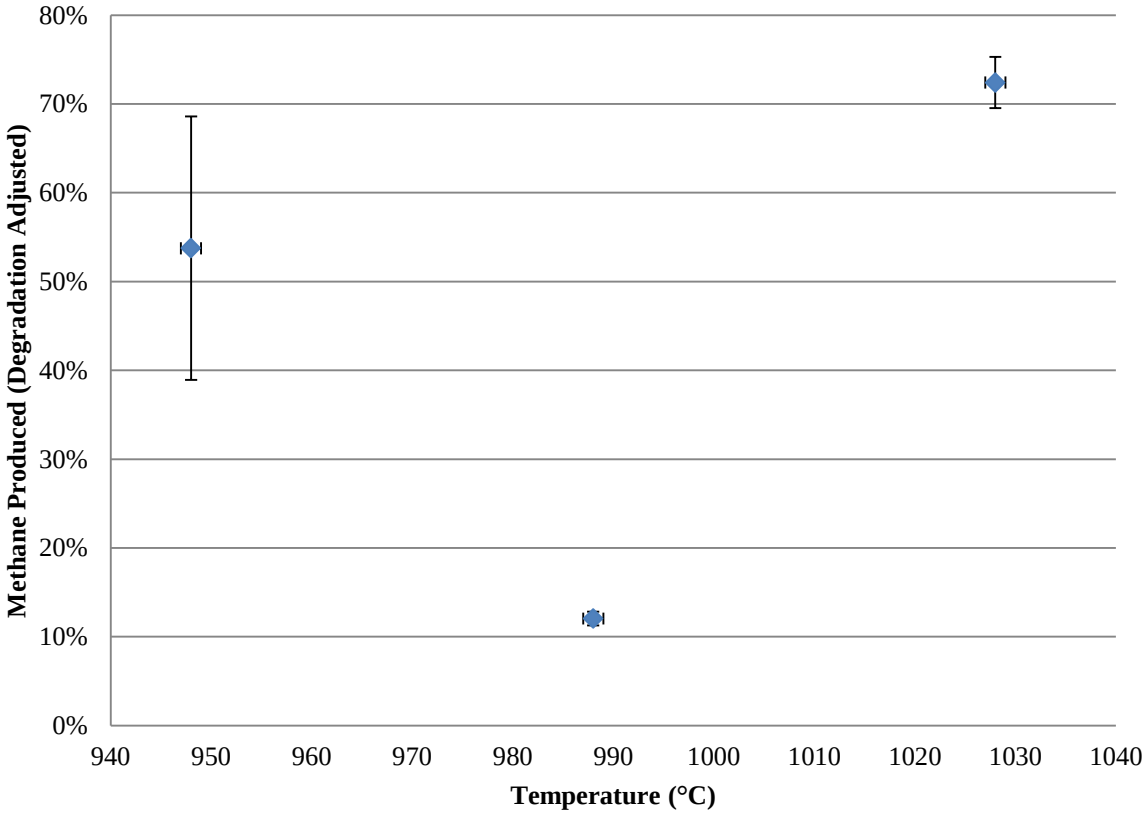

Figure 7-8: Methane production taken as the difference between the initial degradation value and that of the values for the experiments, calculated on a methane carbon conversion basis.

It is also hypothesised that thermal interactions as well as differences in the freeboard above the fluidised bed are influential on product distribution. With the inclusion of the bed, the effective freeboard area where the gases that were formed in the reactions can interact, are reduced. This may potentially be a source for a number of different reactions, where in fact the interactions between the gas molecules once the reactions have occurred are far more influential to the final product than the initial reactions between the biomass particles and methane. It is hypothesised that the amount of hydrogen which is formed in the preheater section has a significant influence on the end products in this freeboard zone.

Figure 7-9 below, shows the results from a Gibbs free energy model where M/B=5 at 100 kPa to replicate the data which was collected in the experiments. With respect to the tar species produced in the experiment, it is observed that the tar yields of benzene and naphthalene increase over the sampling period, whilst toluene decreases. Between the trials of 948 °C and 988 °C the benzene and

naphthalene follow the free energy trend, whilst the toluene is observed to increase then plateau at ~2 % carbon conversion. Similar increases are observed for the gaseous species, with the free energy modelling alluding to a decrease in CO and ethane over the sampling temperatures. In contrast acetylene and ethylene free energy indicates increases in product yield. Comparing again the temperatures of 948 °C and 988 °C the ethylene yield increases and ethane decreases in accordance with Gibbs free energy modelling. Overall carbon monoxide and ethane show opposing trends to those modelled. CO is observed to increase with temperature, nearly doubling in complete carbon conversion.

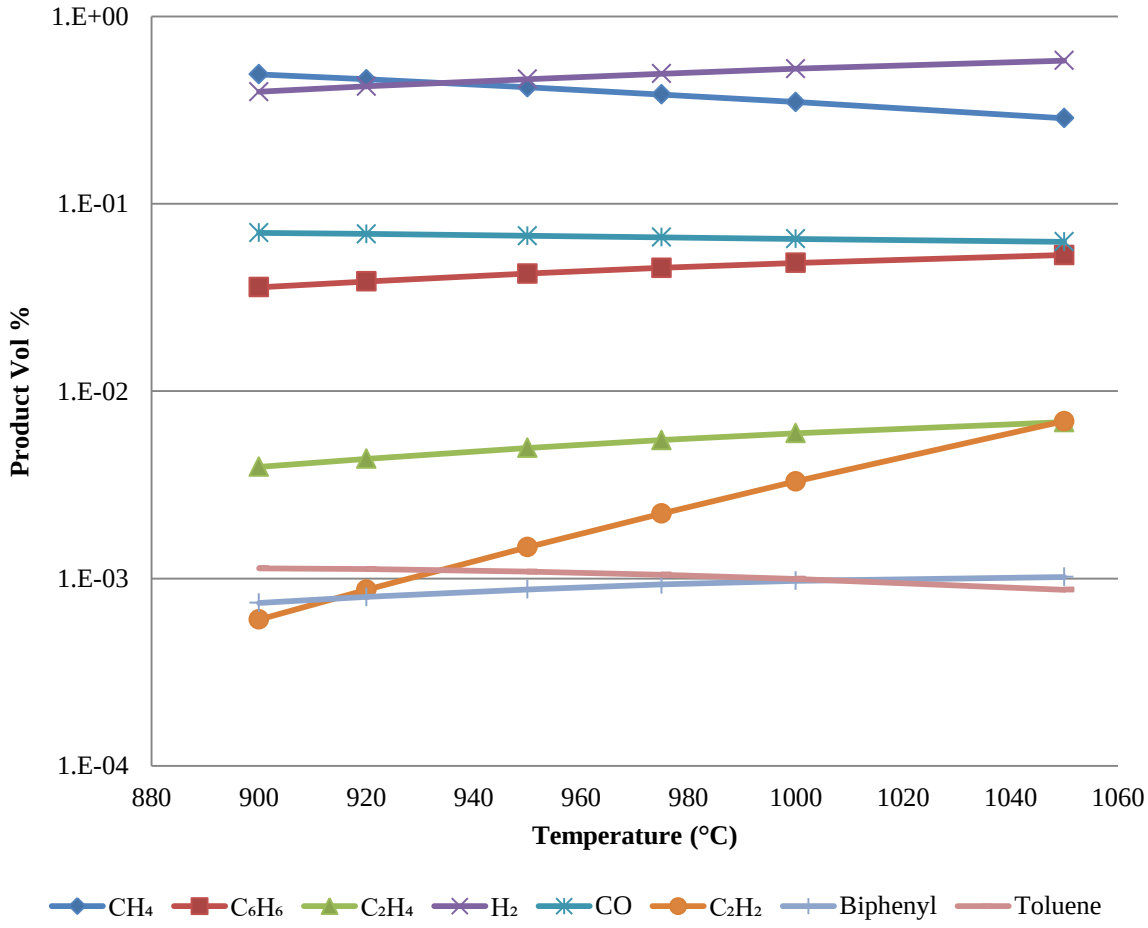

Figure 7-9: Gibbs free energy modelling for major gas and tar species at 100 kPa and M/B=5.

Over the temperature range of 948-988 °C close agreement was observed between the experimental results and those from the Gibbs energy modelling of the systems. However, in the temperature range of 988 – 1028 °C opposite trends are predicted by the model in comparison with results. This was most apparent in the ethylene, carbon monoxide and tar yields. From the Gibbs free energy modelling, it was shown that there was a considerable increase in ethylene production up to a plateau of 1200 °C. However, the ethylene yield was observed to decrease from 17-15 % over the temperature increase.

This decrease in ethylene is similar to that which Steinberg et al [3] reported, showing a plateau in production of ethylene above 1000 °C. It was also observed that over this same temperature range the production of acetylene is expected to increase.

The predicted yield of CO from the Gibbs free energy model was different from the experimental results in the temperature range of 948-988 °C, however, the experimental results agree over 988-1028 °C. In the experiments, the CO carbon conversion was found to be 32 ± 3 % at 948 °C which increased to 56 ± 4 % at 988 °C and then decreasing to 42 ± 2 % at 1028 °C. This is likely due to the carbon built up in the system which was converted during the trial. This can be explained by the Boudouard reaction, Equation (7.1.7), which shows the potential pathway. Opposing to the possibility of carbon monoxide interaction with the carbon, the free energy modelling of the system suggests that with decreasing CO formation the system is tending towards equilibrium.

$$2CO \rightleftarrows CO_2 + C \qquad (7.1.7)$$

The yields of carbonaceous tar species both from the Gibbs free energy model and the experiments have similar trends in the 948-988 °C temperature range as with the gaseous yields. The carbon conversion was observed to increase for benzene over this temperature range, while the yields of toluene and naphthalene were constant. The overall yield of tars in the experimental trials was observed to increase by over double, and tar selectivity varied significantly from 948 to 988 °C. In this temperature range, the main targeted tar species are constant with variation in carbon conversion yield observed in the trace tar species, as shown in Figure 7-7. This is suspected to be due to a combination of kinetic effects, alongside thermodynamic effects.

However, there were large differences between the fluidised bed and packed bed arrangement on the overall tar production. An additional 2 % carbon conversion to tars was recorded for the experiment at 1028 °C in comparison to 988 °C. Accounting for the increase in the overall tar production was an increase in styrene, biphenyl and indene production at elevated temperatures, which is in unison with the model predictions. Interestingly the benzene tar fraction was higher than that of naphthalene, which contradicts the free energy modelling predictions. However, this may be due to the short residence time which prevents the formation of larger polyaromatic hydrocarbons [4], [5]. The production of polyaromatic hydrocarbons is the pathway for soot formation, and it was likely that this was a strong indication that the system is operated in such a way that soot formation is prevented. For the tar analysis no hydrocarbons with more than three aromatic rings were detected, whereas, the limit of detection was pyrene[XIX] and the associated isomers.

[XIX] A four ring aromatic structure species.

It was observed that for increasing temperatures greater trace aromatic tar species were expected until approximately 1150 °C, above which the degradation of the tar species predominantly produces acetylene. Overall it was concluded that within the temperature region of 948-1028 °C, significant variations in product distributions occur, due to the strong kinetic and thermodynamic effects which vary the target species production.

7.2 Effect of Residence Time during Methanolysis

Another key parameter which was investigated was the effect of residence time which was varied in the experiment by changing the methane flow rates. By increasing the methane flow rate the residence time of the gas in the reactor was decreased. The effect of residence time is a fundamental experimental characteristic as this defines the period of time which a volume of gas is in the experimental system, thus resulting in differing reaction extents and interactions. This will also determine the use of a reactive gas which has a tendency to thermally degrade, as various hydrogen effects can occur.

Due to the construction of the system the residence time alterations cause two discrete differences in the system. Due to the preheater system and reaction vessel being constructed in the same section of pipe, the residence time affects the duration of the gas being exposed in the preheater section and in the reaction section (above the bed). This metric was important due to the fact that the increased residence time at temperatures high enough to cause MTD increase the hydrogen concentration. This inherently resulted in the composition of the gas which was reacting with the biomass varying throughout the trial. In turn, there were possible pseudo-residence time effects which are apparent in the investigation of the residence time experimental trials. This was the case as with larger residence time trials the concentration of hydrogen was increased. This led to trials with a larger residence time to be influenced by the content of hydrogen to a greater extent, than lower residence times. Given that the influences of both gas species are important, it was possible that the variation was influential on the reaction pathways.

Another key aspect of the residence time effect was the direct influence on the extent of reactions which can proceed given the period of time that the gas was in contact with the biomass particles. Adding to this, the gas had a tendency to continue reacting above the bed (freeboard area), as shown in the reactor sketch, Figure 7-10. This figure also shows the specified heating zones of the systems and the boundary of the zones with respect to the reactor system. In total two main heating zones are specified; (1) Preheater zone from the top of the bottom vestibule to the top of the fritted disc. The preheater zone dictates the amount of methane degradation which occurs in the system as only methane was present in this zone. (2) Reaction zone, which includes the fluidised bed zone and freeboard area which provide different reaction conditions for the product gas. The fluidised bed zone

was the zone where the gas was in initial contact with the biomass particles. As the heat up of the particles was very quick, the release of volatiles and reaction products from the biomass occurs in this zone. The freeboard zone was the additional area above the bed where gaseous interactions occur. This space should be minimized to ensure accurate representations for the reactor conditions.

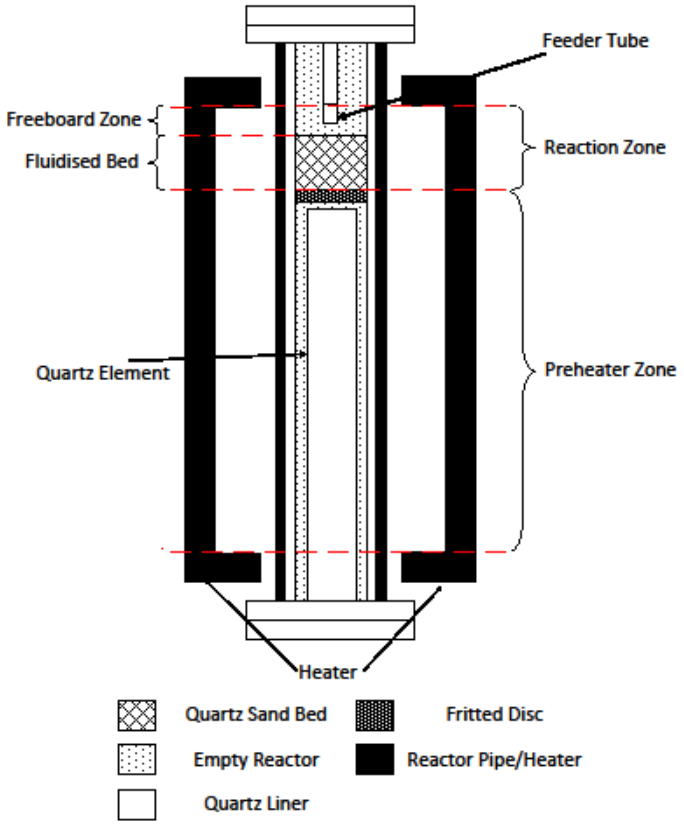

Figure 7-10: Sketch of the fluidised bed reactor which consists of two separate zones.

The characterisation of the effects which residence time has on the system was possibly one of the most complicated system characteristics to understand and control due to the multiple influences on methane degradation, initial pyrolysis reactions and secondary reactions. This was also the case given that the system was constructed with the preheater and reaction zone in one discrete pipe. This leads to a system which was inherently more difficult to control, as the methane inlet concentration to the fluidised bed and residence time are interdependent on one another. Nevertheless, the results from the residence time effects can also lead to a significantly increased understanding of the system as the effects which are observed throughout, have a tendency to resonate much more with the increase/decrease of the parameter. During operation, as the flow rate increased the gas velocity in the bed increased, reducing the residence time and enhancing fluidisation in the bed. For all the residence time trials which were conducted it was observed that the temperature of the system remained constant and that increase/decreased flow rates did not significantly affect the temperature of the bed.

In all experiments conducted, the bed temperature was constant at 1020-1025°C throughout the course of the experiment. The system fluidisation varied between 3.3-16.5 u_{mf} ensuring that the system remained in the bubbling regime.

From the investigation into the residence time effects it was observed that with increasing the residence time from 0.5 s to 2.5 s , the carbon conversion of ethylene and carbon monoxide peaked at 1.5 s, and then decreased, as shown in Figure 7-11. The CO carbon conversion at 0.5 s was 36 ± 3 % and increased to 48 ± 4 % at 1.5 s. The corresponding yields of ethylene were 13 ± 1 % and 22 ± 2 %. The CO_2 and ethane yield decreased with increasing residence time from 0.5-2.5 s, the ethane concentration decreased from 2.8 ± 0.3 % to 1.7 ± 0.2 %, CO_2 decreased from 6 ± 1 % to 5 ± 1 %.

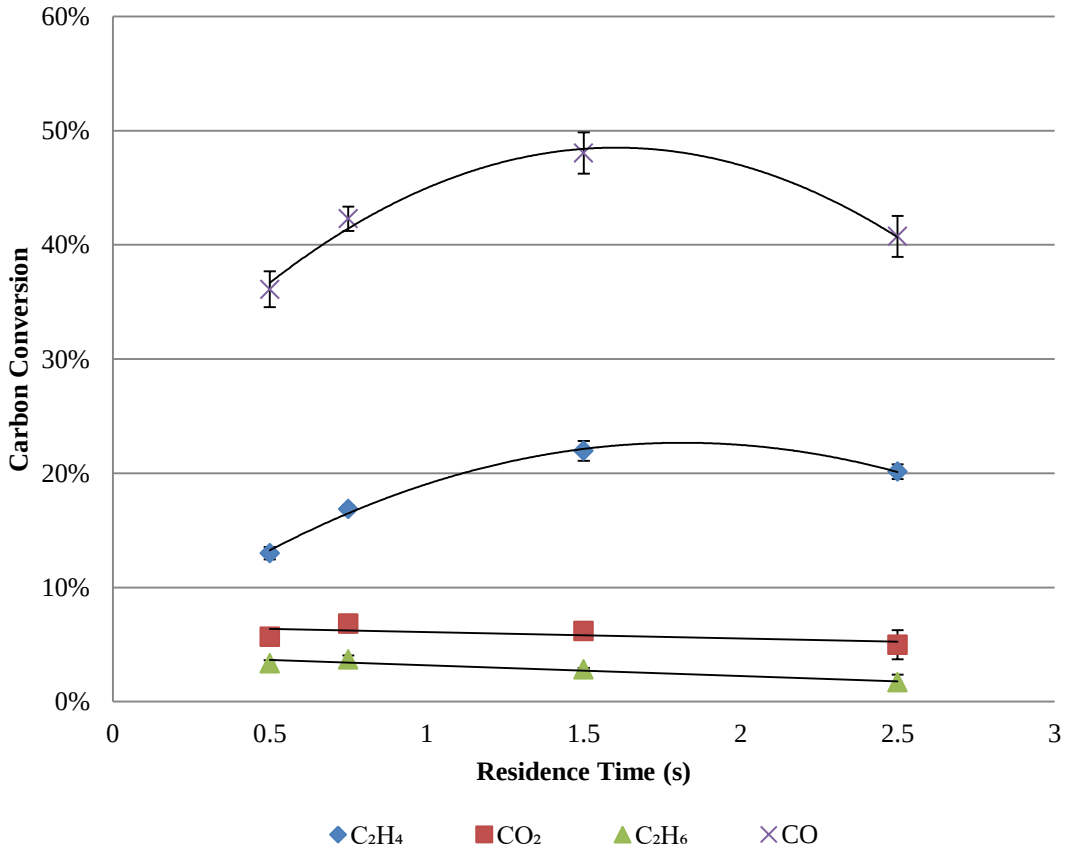

Figure 7-11: Main carbonaceous gas species concentrations with relation to the reactor residence time, reactor operated with a 40 mm bed, at atmospheric pressure, M/B =4.8 and a bed temperature of 1020 °C.

Figure 7-12 shows the distribution of the oxygen balance for all oxygen bearing species (CO, CO_2 and H_2O). It was found that the CO fraction increased initially from 49 ± 2 % at a residence time of 0.5 s to a maximum value of 68 ± 3 % at 1.5 s, further increases in residence time led to a decrease to 58 ± 3 %. Over the various residence times trialled, the CO_2 fraction remained relatively constant with an

oxygen conversion of 14-19 %. The H_2O fraction followed the opposing trend of CO, with a minima of water recorded at 1.5 s, where 14 ± 3 % oxygen conversion was recorded.

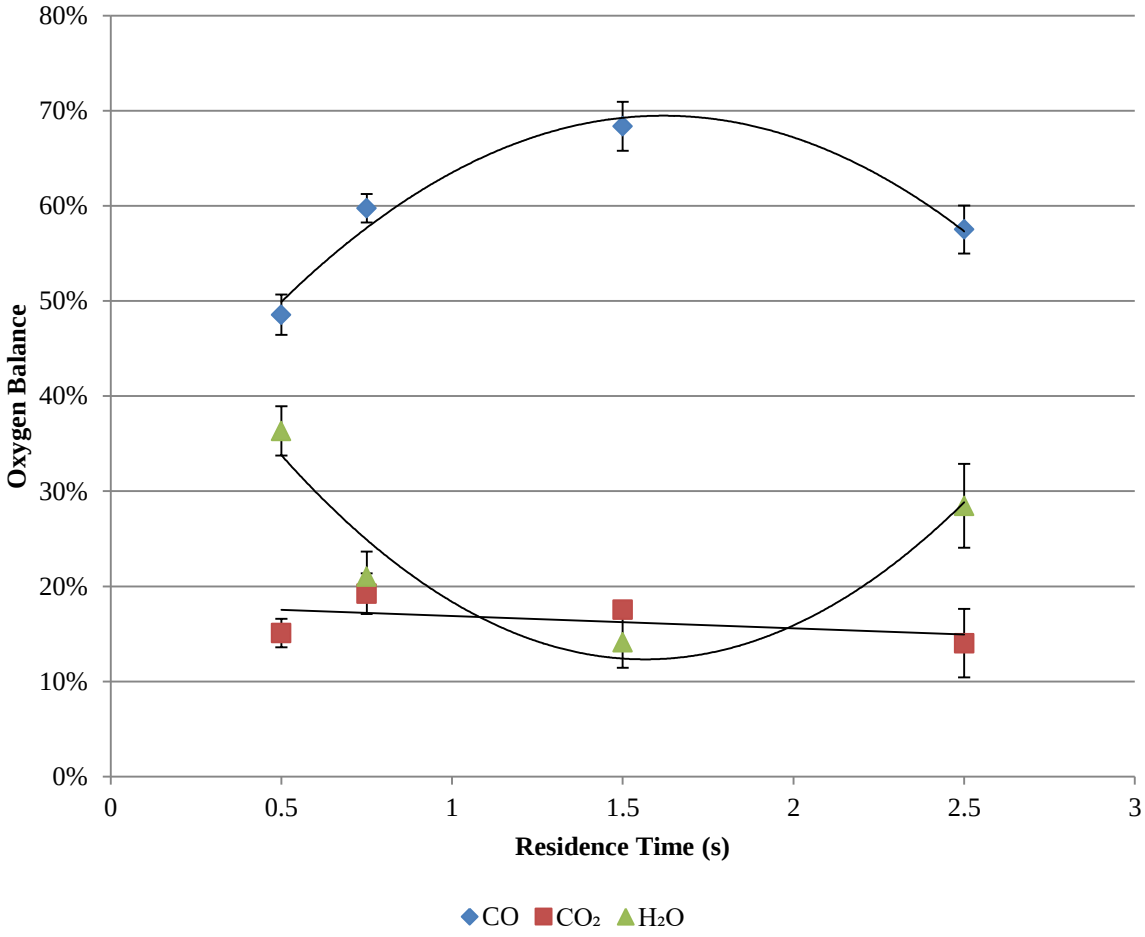

Figure 7-12: Effect of residence time on selectivity of major oxygen bearing species, reactor operated with a 40 mm bed, at atmospheric pressure, M/B =4.8 and a bed temperature of 1020 °C.

To better understand the characteristics of the ethylene formation, the ethylene formed from the degradation of methane is characterised below in Figure 7-13. From the degradation results collected prior to the experiments, it was suspected that the contribution which ethylene production from methane degradation may have significantly contributed to the final carbon conversion. In calculation, the ethylene produced from the degradation sample was used as a reference value for the ethylene production associated to degradation, then subtracted from the overall ethylene production from the experiment, as seen in Figure 7-13. From Figure 7-13, it is found that the yield of ethylene suspected to be due to MTD increased from 5 ± 1 % at a residence time of 0.5 s to 11 ± 1 % at a residence time of 2.5 s. The corresponding production of ethylene from the experiment adjusted for the production of ethylene from degradation showed an increase from 8.5 ± 0.3 % to 13.0 ± 0.8 %, with the residence

time increasing from 0.5 s to 1.5 s, respectively. The maximum overall ethylene concentration obtained was at 1.5 s with a carbon conversion of 22 ± 1 %.

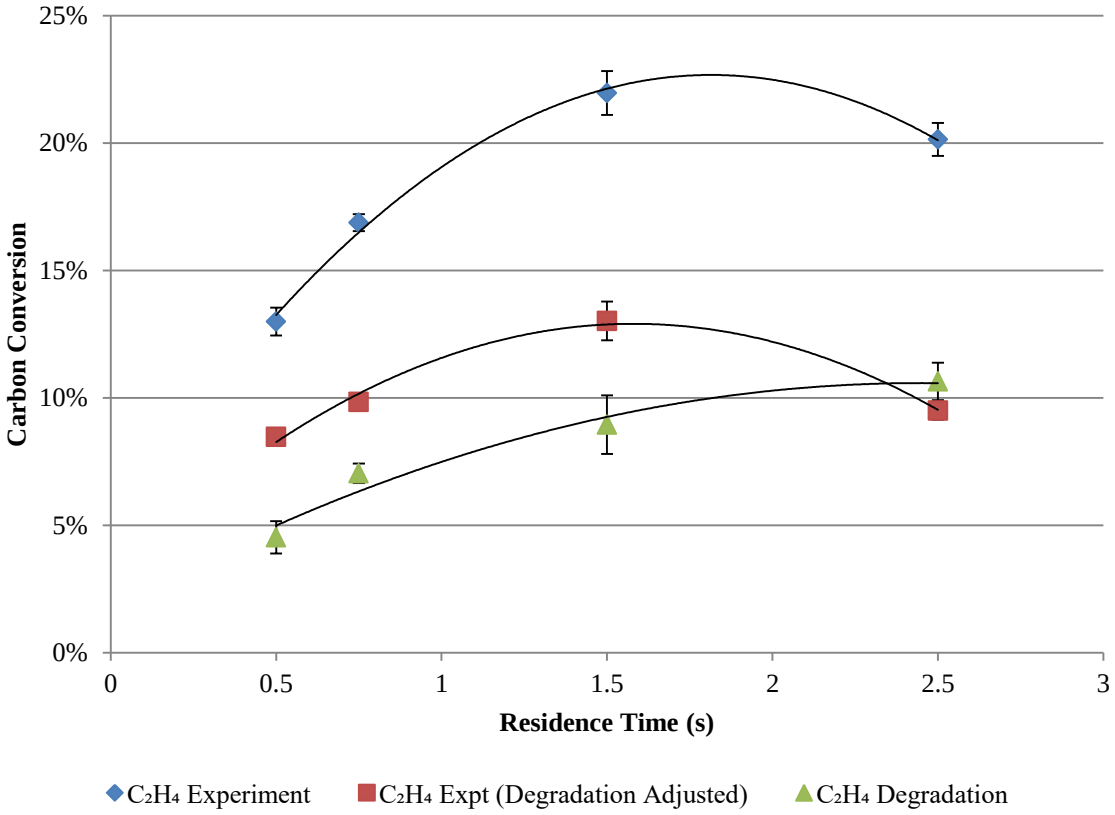

Figure 7-13: C_2H_4 degradation adjusted carbon conversions, reactor operated with a 40 mm bed, at atmospheric pressure, M/B =4.8 and a bed temperature of 1020 °C.

From the experimental results, hydrogen yield was also significantly affected by the residence time as a result of the MTD and methanolysis as shown in Figure 7-14. To determine the hydrogen production characteristics and influence during methanolysis, the hydrogen flow rate from MTD, H_2 (deg), methane inlet mass flow rate, CH_4 (feed), and hydrogen production from methanolysis of biomass, H_2 (expt), were used. To better understand the influence of the residence time, the values for the hydrogen production have been standardised as the ratios shown below. It is observed that the ratios of H_2 (expt)/CH_4 (feed) and H_2 (deg)/CH_4 (feed) increased linearly with residence time. This can be accounted for due to the general methane degradation characteristic reaction. However, at higher residence times the H_2 (Expt)/ H_2 (Deg) ratio decreases, showing that there was possibly a shift in the production of hydrogen arising from the fluidised bed and freeboard area.

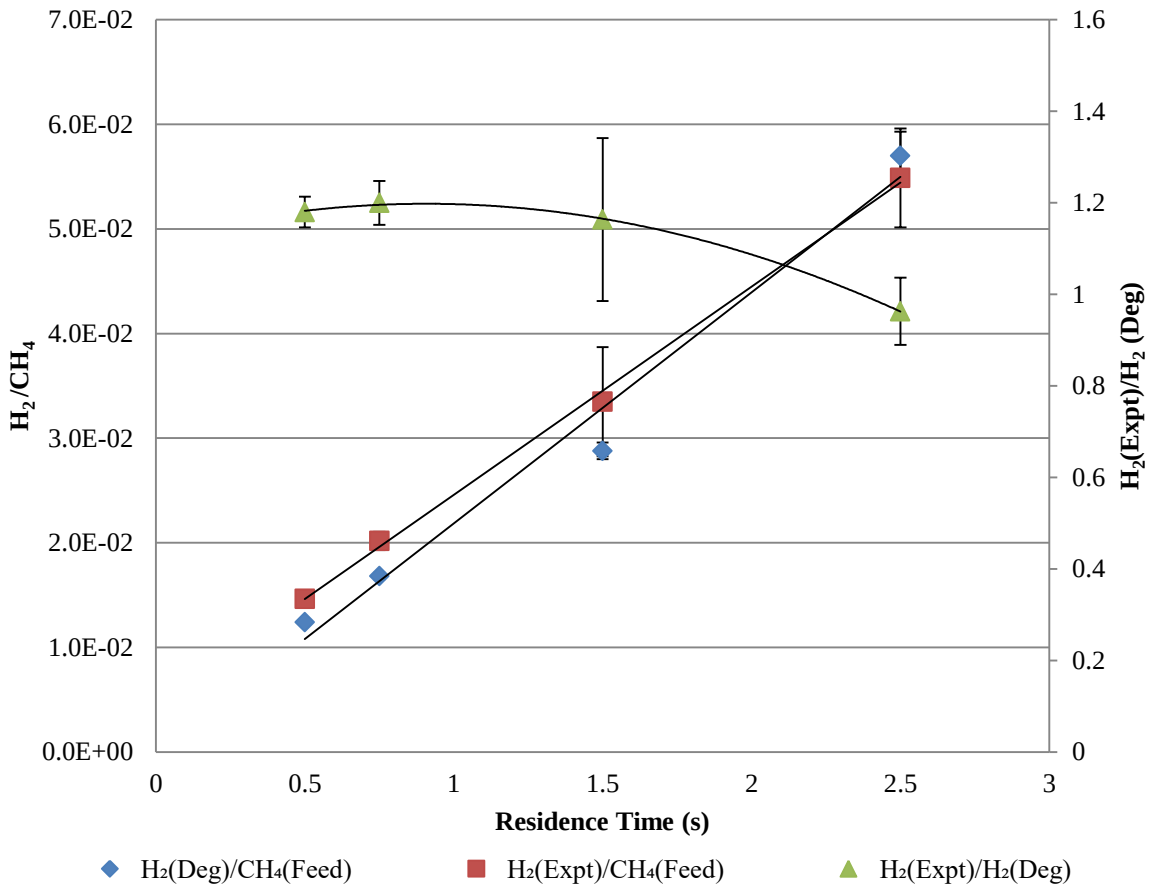

Figure 7-14: Hydrogen production from methane degradation and production from biomass methanolysis with respect to residence time, reactor operated with a 40 mm bed, at atmospheric pressure, M/B =4.8 and a bed temperature of 1020 °C.

Figure 7-15 shows the hydrogen content in the product gas in relation to the total methane consumption, relative to the residence time. When the residence time was increased from 0.5 to 1.5 s, the hydrogen concentration in the product increased linearly. While the CH_4 consumption during degradation and throughout the trial remained relatively constant at 14 % and 4 %, respectively. This was likely due to an increased production rate of methane and hydrogen during methanolysis at the lower residence times. However, at a residence time of 2.5 s, the overall methane consumption is observed to increase significantly, potentially indicating the increased favourability of MTD.

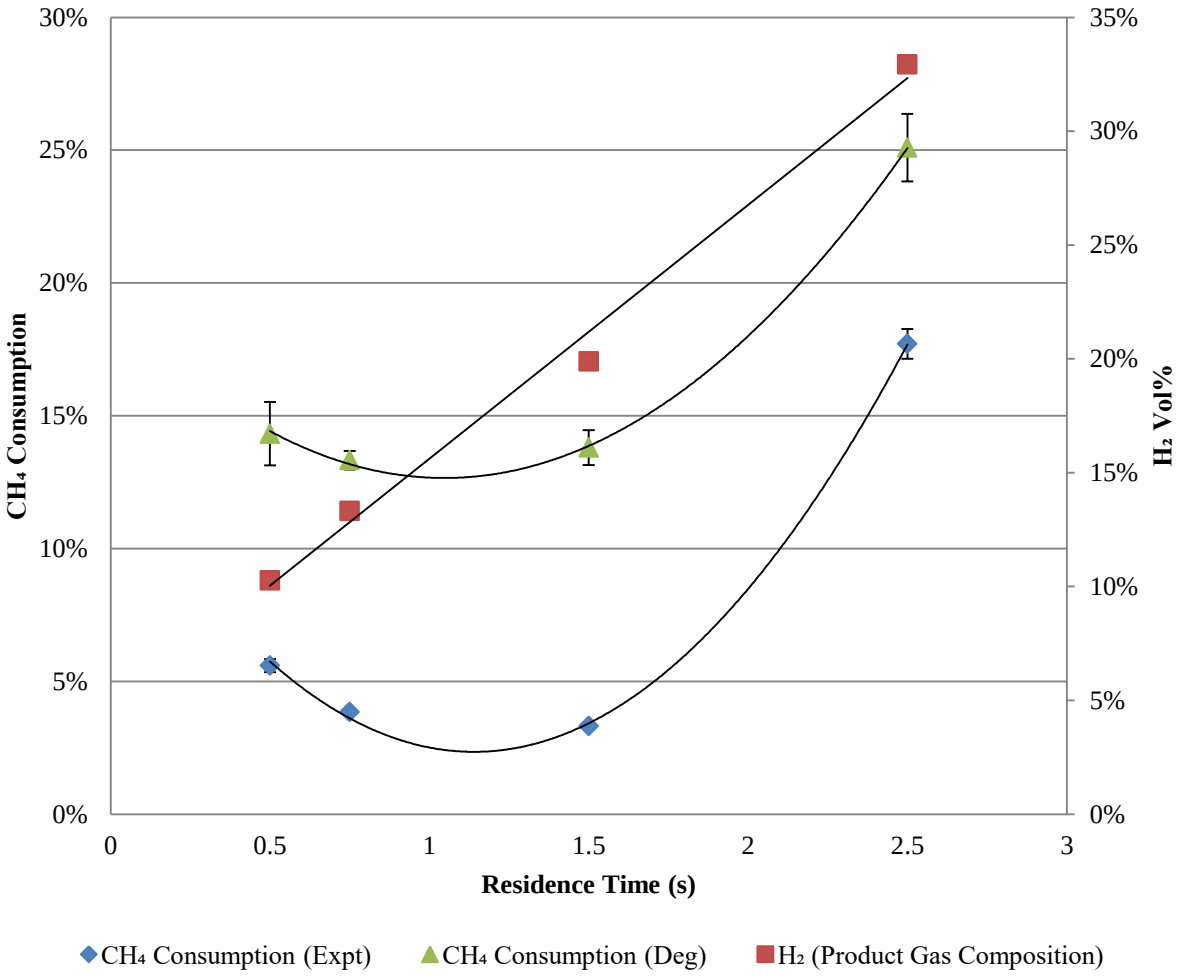

Figure 7-15: Methane consumption and hydrogen concentration in product gas, during degradation at differing residence times, operated with a 40 mm bed, at atmospheric pressure, M/B =4.8 and a bed temperature of 1020 °C.

The tar production as a function of residence time is shown in Figure 7-16, from which it is found that there was a significant increase in tar production with increasing residence time. The most apparent increase is observed as the formation of benzene with the overall benzene yield increasing from 6.0 ± 0.7 % to 21 ± 3 % with an increase in residence time from 0.5 s to 2.5 s. Total tar conversion was maximized at 28 ± 4 % at the highest residence time trialled. However, naphthalene and toluene concentrations are observed to be constant with residence time, thus, the yields of these two compounds were low.

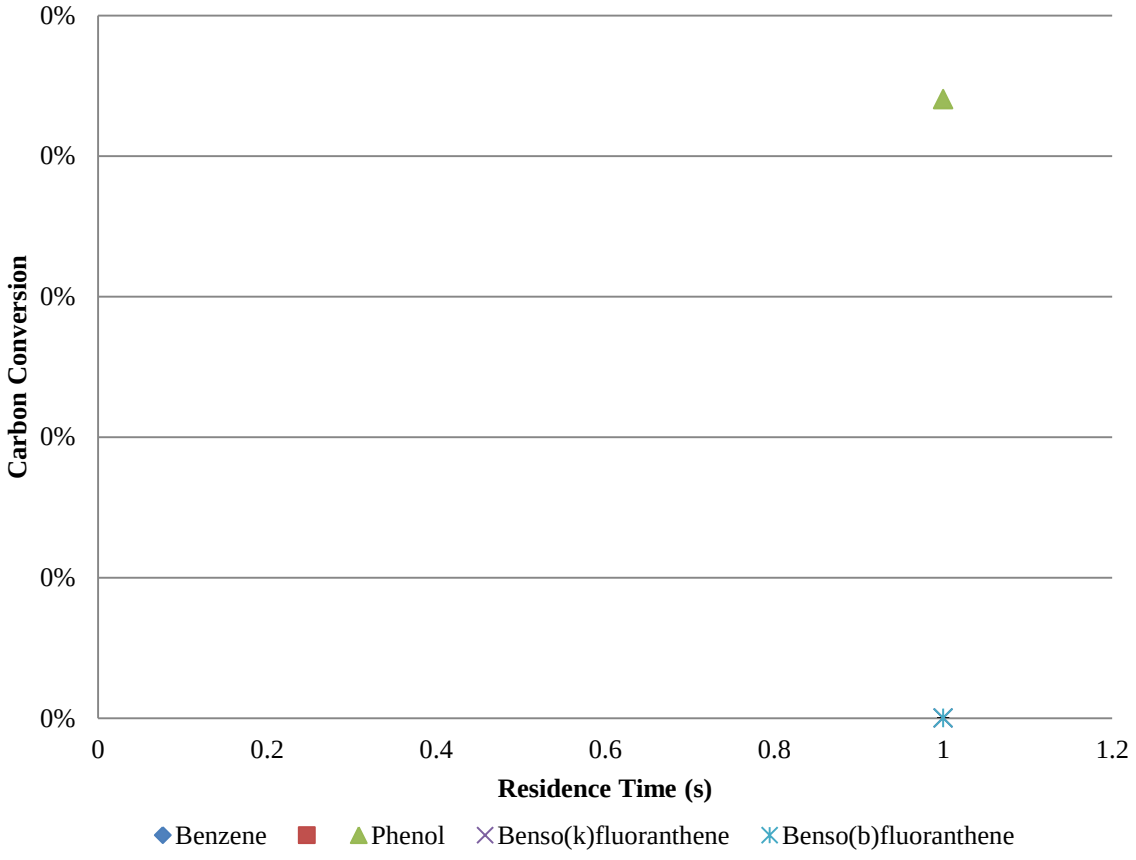

Figure 7-16: Main tar species and total tar production with respect to residence time, operated with a 40 mm bed, at atmospheric pressure, M/B =4.8 and a bed temperature of 1020 °C.

With the increase in production of tars with residence time, variation in the selectivity of lower concentration primary and secondary tars is observed, Figure 7-17. With the increasing residence time, the selectivity of primary species (excluding benzene and toluene) varies with residence time. Initially the production selectivity follows the order; styrene > phenol > indene > p-xylene + ethylbenzene>m-xylene. However, with higher residence times the order varies with selectivity becoming; Indene>biphenyl>styrene>m-xylene. Secondary tars are observed to follow a much more regimented order with selectivity of products following the order of; naphthalene >>2-methylnapthalene=1-methylnapthelene > acenapthylene, Figure 7-18.

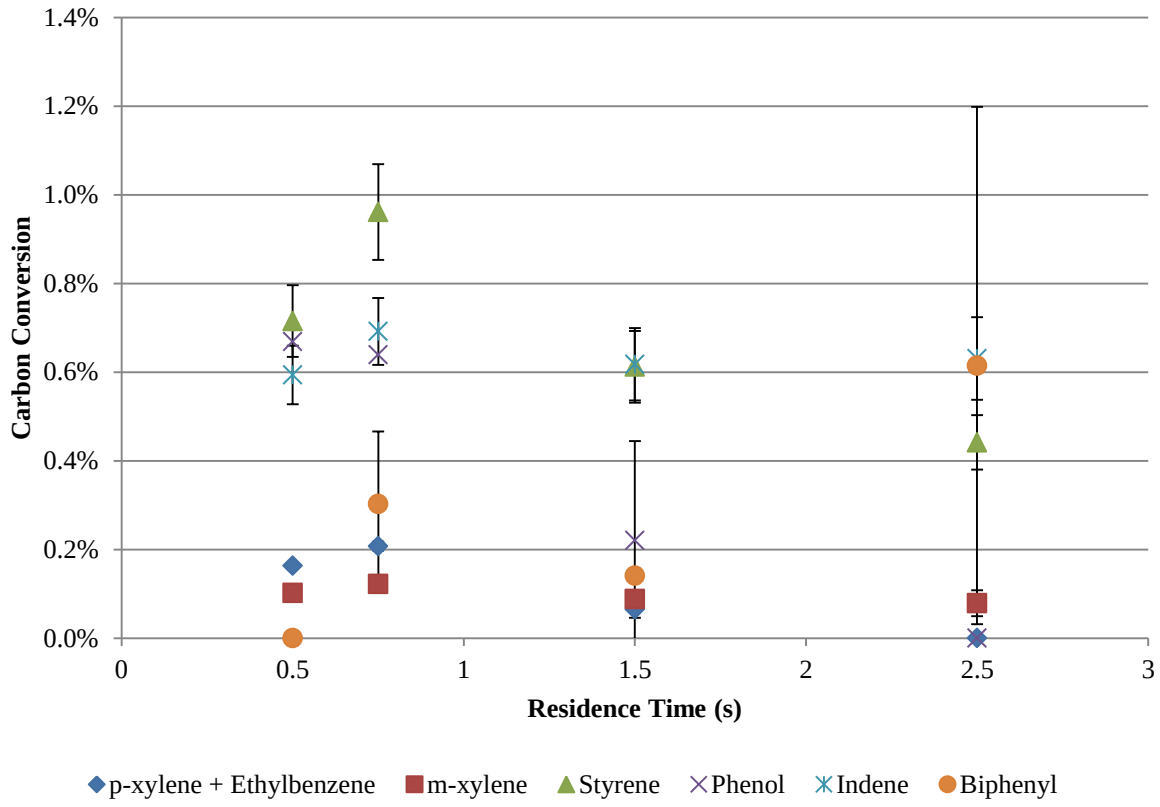

Figure 7-17: Primary tar production with respect to residence time, operated with a 40 mm bed, at atmospheric pressure, M/B =4.8 and a bed temperature of 1020 °C.

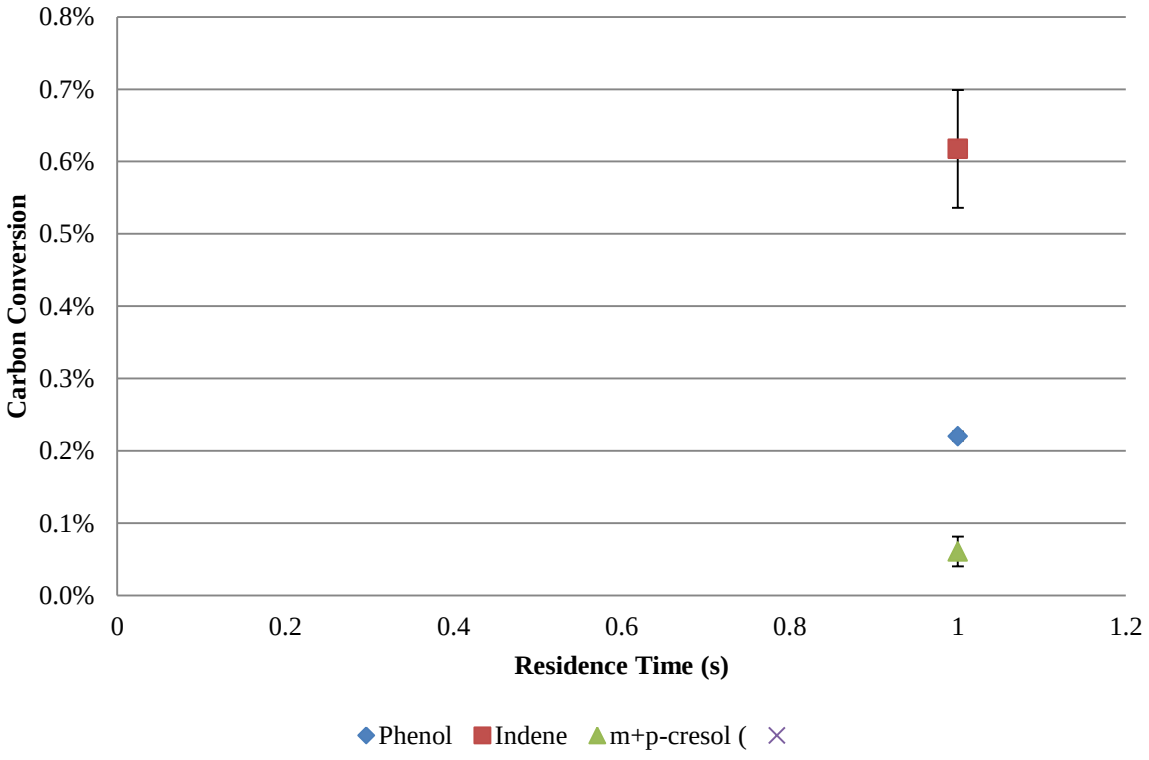

Figure 7-18: Secondary Tar production with respect to residence time, operated with a 40 mm bed, at atmospheric pressure, M/B =4.8 and a bed temperature of 1020 °C.

7.2.1 Discussion on the Effect of Residence Time

From the investigation into the residence time effect it was found that an increased in residence time from 0.5 s to 2.5 s had a significant effect on the product selectivity. At a residence time of 1.5 s a supposed optimum in system performance was observed resulting in carbon conversions of; 48%, 22% and 11% of CO, C_2H_4 and benzene, respectively, as seen in Figure 7-11. At lower residence times the total amount of gas and tar carbon conversion decreases, whilst the methane consumption increases, Figure 7-15. At lower residence time, it was also observed that there was a significant increase in oxygen conversion to water. Water production doubles at both lower and higher residence times, suggesting that water is formed initially and then reacts at residence times of 1.5 s to form CO, whereas, increased residence times of 2.5 s promote the formation of water. At higher residence times the carbon conversion to tars was significantly increased, where maximum tar yields of 28 ± 4 % were achieved at a residence time of 2.5 s. As a result of increased residence time the concentration of all recorded carbon containing gases was decreased. To encourage the production of ethylene, lower residence times are recommended as it was suspected higher residence time induced secondary reactions forming benzene due to aromatization of ethylene. It is important to consider the size of the preheater and reaction zone. The "reaction zone" includes both the fluidised bed and freeboard area, which is considered as the zone which the products from methanolysis can react prior to cooling.

The preheater section accounted for 57 % of the volume over which the overall residence time (for the methane feed) was calculated for. In turn, the actual residence time which the products from the initial pyrolysis/devolatilisation have in the reaction zone is 43 % of the overall residence time. The calculated relative residence times for the trials conducted are given in Table 7-1 the residence time of gas in the fluidised bed is very short due to the addition of sand, in this zone the high heat transfer causes the primary devolatilisation/methanolysis reactions occur. If the particles are reacted before the incoming gas is able to reach the top of the bed then the actual residence time of the products is decreased even further (overall residence time of the preheater + bed is 66 %). This in turn leads to the fact that the reacting period of the methanolysis, assumed to be freeboard area, is not adequately represented by the use of the overall residence time.

Table 7-1: Specified reaction zone residence times, where the *"reaction volume"* is a combination of the freeboard volume and fluidised bed volume.

Residence Time (s)				
TOTAL	***2.50***	***1.50***	***0.75***	***0.50***
Preheater Volume	1.43	0.86	0.43	0.29
Fluidised Volume	0.23	0.14	0.07	0.05
Freeboard Volume	0.85	0.51	0.26	0.17
Reaction Volume	1.08	0.62	0.33	0.22

Hydrogen yield was strongly related to the residence time, as expected from the methane degradation results which were collected in previous trials. From the methane degradation samples, it is observed that there were no contaminations within the system and char carry over can be neglected. However, when the reaction was allowed to proceed and biomass was introduced the amount of methane which was degraded significantly decreases. The extent of the decrease in methane consumption is stark and at times well over 50 % of the methane degradation value. As the wood enters the system, the initial pyrolysis reactions occur and a decrease of residence time can be expected due to the release of volatiles increasing the volumetric flow rate. For a constant M/B ratio the extent of influence on the residence time decreases as methane mass flow rate increases. Once the tar vapours are condensed the volumetric flow rate of the product gas is increased by the methanolysis reaction, resulting in an increased volumetric flow rate (compared to the inlet gas flows). This increase was taken as the flow of products excluding char as this has no direct effect on the residence time of the system. Direct measurements of the increased flow rates were also able to be calculated through the use of the tracer gas and were measured before each run. Table 7-2 shows the variation in product volumetric gas flow rate.

Table 7-2: Volumetric flow rate increase measured in product gas stream due to the addition of biomass and the effect on the freeboard residence time.

Residence Time (s)	Volumetric Flow rate Increase	Freeboard Residence Time Adjusted (s)
2.5	12%	0.75
1.5	22%	0.40
0.75	18%	0.21
0.5	17%	0.14

Due to the increase in volumetric flow rate above the bed, the residence time was decreased with the introduction of biomass into the system. This caused the amount of methane which was able to thermally decompose to decrease, thus decreasing the consumption of methane. It was also likely that significant amounts of methane are created throughout the processes in the freeboard area of the reactor. For the value of 1.5 s residence time the methane consumption was observed to decrease from 18 ± 1 % to 5.6 ± 0.2 % during methanolysis. On a carbon basis this corresponds to an effective carbon conversion of 77 % biomass to methane if the rate of degradation was assumed constant. It was not feasible that this was solely accounted for by the degradation, as if CO is considered the overall carbon conversion would be > 100 % from biomass. This is thought to be due to a combination of methane degradation reactions and methane forming reactions occurring with the introduction of biomass. It was evident that the methane production must be significantly lower than 77 % and the relationship between methane produced from degradation and from methanolysis is complex. It was postulated that the addition of biomass has multiple effects. The biomass is suspected of producing methane from the direct interaction of the biomass volatiles and initial pyrolytic background, as well as the reduction of residence time effect. Overall a true representation for the methane production is difficult to obtain without point source identification, as it is also possible that the production of carbon from MTD suppressed the formation of hydrogen produced.

Hydrogen production and methane consumption showed a strong relationship, as shown in Figure 7-19. At the lower residence times the overall hydrogen mass flow rate was observed to be 15-20 % higher than the initial degradation flow. However, at 2.5 s a strong decrease in the hydrogen production is observed. This explains the low volumetric flow rate increase recorded at higher residence times, Table 7-2. It is also suggested that the longer residence times facilitate recombination reactions of hydrocarbons which allow for increased tar yields, as observed by the reduction in

hydrogen production (which are investigated in depth in the following sections). The trend observed in Figure 7-19 proposes that minimal dehydrogenation reactions occur within the given residence times as in Equation (7.1.2). This was due to the increasing residence times causing a decreased hydrogen production, which, if dehydrogenation reactions were the dominant pathway would show an opposing trend. Because of this trend, it was unlikely that significant degradation of ethane/ethylene/acetylene is occurring. The adjusted residence times for the freeboard area are given in Table 7-2, which highlight the effective residence time of the product gas after reaction.

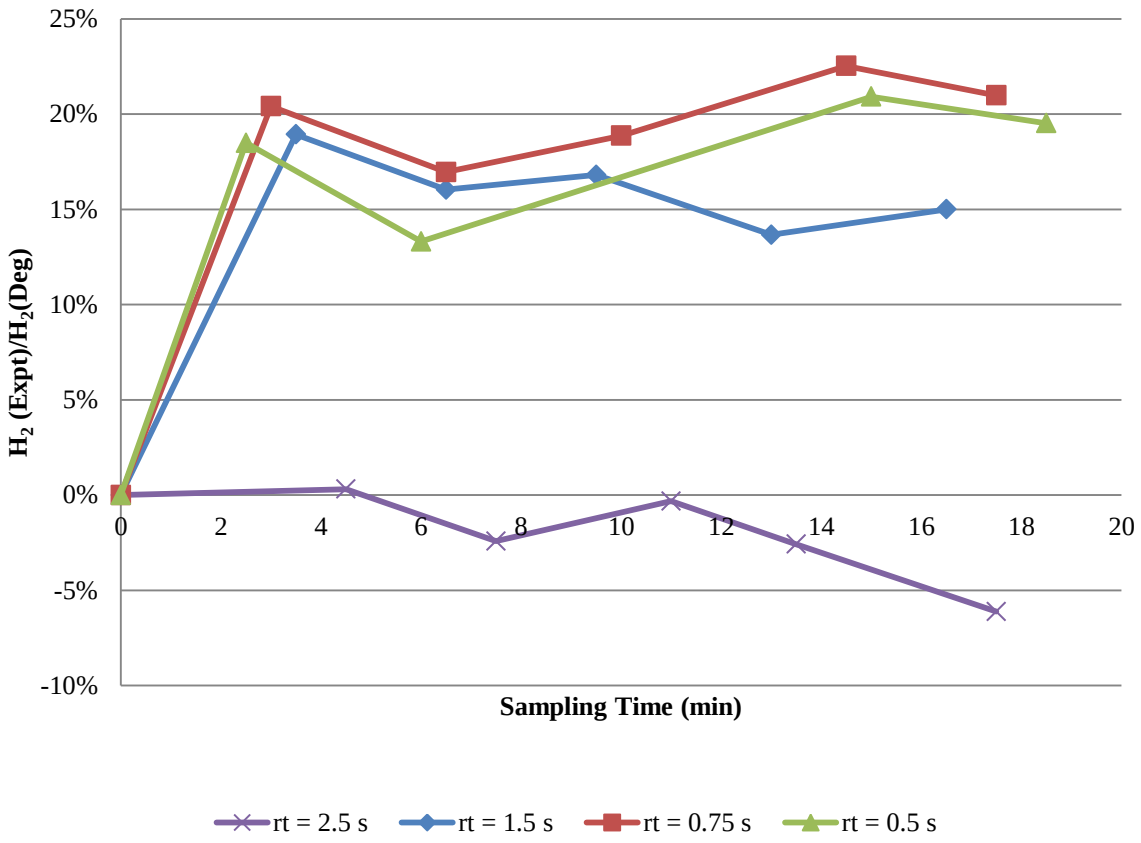

Figure 7-19: Hydrogen production attributed to methanolysis as a function of sampling time of multiple residence time trials, reactor operated with a 40 mm bed, at atmospheric pressure, M/B =4.8 and a bed temperature of 1020 °C.

It is important to note that the methane and hydrogen concentrations measured at the end of a run (the methane degradation point) are not a reflection of the gas composition in the reacting gas which meets the biomass. This was due to suspected degradation occurring within the *reaction zone* when biomass was fed into the system. To estimate the methane concentration when contacting the biomass, the measured degradation composition was interpolated from experiments conducted at lower residence times. This allowed for an estimate of the reacting gas composition which initially contacts the feeding biomass. As the degradation of methane shows a linear relationship with the residence time, Figure 6-6, it was unlikely that degradation was concentrated at a particular point in the system. For

the calculations it was assumed that the rate of degradation was directly proportional to volumetric flow and that there are no significant surface effects, as observed in the comparison of the fluidised bed and packed bed degradation comparisons. Table 7-3 shows the estimated composition of the gas which enters the reaction zone relative to the measured overall degradation value. To investigate the possibility of further degradation occurring within this zone the *concentration at the inlet to the reaction zone* was taken as the degradation value, to create a hypothetical inlet gas composition. The volumetric flow rates of both methane and hydrogen were then able to be compared to the product outlet composition. This in turn allowed for a comparison between the methane and hydrogen concentrations before and after the reacting zone. The calculation indicated that in total the H_2 concentration for an overall residence time of 2.5 s increased by 117 % in the reacting zone. This leads to the belief that approximately half of the hydrogen production occurs within the reacting zone and is likely to be attributed to the degradation of methane. This may explain the apparent zero consumption of methane which was obtained by Steinberg et al., as the biomass feed likely reacted in a completely hydrogen-free environment initially, which may reduce the extent of MTD.

Table 7-3: Overall concentration of product gas during MTD and a comparative composition when entering the reaction zone, assuming that the degradation of methane is uniform over the length of the reactor.

	Overall Measured Degradation		**Estimated Gas Composition at inlet to Reaction Zone**	
Trial Overall rt	H_2	CH_4	H_2	CH_4
(s)	*vol%*	*vol%*	*vol%*	*vol%*
2.50	37%	62%	17%	82%
1.50	21%	79%	11%	88%
0.75	13%	86%	7%	92%
0.50	10%	89%	6%	94%

From Figure 7-14 and Figure 7-19 it was observed that there was a strong reduction in hydrogen production which was observed at higher residence times. The overall production of the hydrogen varies with sampling time, and, at higher residence times the relative hydrogen production attributed to methanolysis is observed to decrease. This decrease in hydrogen production is suspected to be due to the increased production of tars within the system. With increasing residence time the tar production is observed to increase significantly, in agreement with free energy data, which shows a

tendency for high tar production, Figure 7-9. From Zhu et al [6], the hydropyrolysis of coal has shown similar tar trends with increased production of benzene with increased residence time. Of the major C_2 product gas species from the experiment, it has been identified that pyrolysis of acetylene for the formation of benzene is most likely. Benzene formation from acetylene has been speculated to form via a second-order bimolecular initiating step, of which, the kinetically favoured initiating reaction form monomeric or dimeric bi-radical species [7], Reaction (7.2.1).

$$2C_2H_2 \rightarrow \bullet CH = CH \bullet + C_2H_2 \qquad (7.2.1)$$

After subsequent addition reactions with acetylene, a tri-acetylene radical is formed and can eventually rearrange in the formation, Reaction (7.2.2)

$$[C_2H_2]_3 \rightarrow C_6H_6 \qquad (7.2.2)$$

It was also highly probable that, direct production of the single aromatic ring tar species (such as, toluene, xylene and phenol) can be attributed to the cyclic structure of lignin. It has been determined from previous biomass pyrolysis work, that the composition of benzene in the product is strongly related to the lignin content of the feed [2]. The extent of naphthalene production was also suggested to be strongly influenced by hydrogen. Chareonpanich et al [8], indicates that increased naphthalene conversion was achieved with the introduction of hydrogen at high temperatures.

Owing to the thermodynamic instability of methane, direct pyrolysis of biomass in a 100 % methane environment at elevated temperatures is very difficult. In essence the production of hydrogen before the reacting gas was in contact with the feed was inevitable unless very low residence time and temperatures are used. It was likely that the residence time is influential to product distribution owing primarily to the large increases in respective gas selctivities which are seen when hydrogen concentration varies. However, it was also concluded that the hydrogen concentration strongly influences the product distribution, with the species formed due to MTD highly likely to interact with primary pyrolysis products. The phases which are targeted in these reactions vary between the residence times and need further investigating to better understand the chemical reaction pathways.

7.3 Effect of Methane to Biomass (M/B) Ratio during Methanolysis

To investigate the interactions of the product gas and methane, the biomass ratio (M/B) was altered from 1.29 to 4.16 by increasing the biomass flow rate with a constant methane feed of 0.242 kg/hr (residence time = 1.5 s). This resulted in constant MTD until the reacting zone, however, differing residence times were expected due to increased gas production expected with the devolatilisation of higher mass flow rates of biomass. By varying the M/B ratio the product distribution effects and gas phase compositions could be explored, which were suspected to help understand the interactions which were highlighted from the residence time trials. By improved understanding of the reaction zone reaction products, it is hoped that the process configuration can be altered to target desired species.

Due to the increasing flow rate and rotary valve feeder configuration, low M/B ratios were difficult to obtain, as blockages frequently occurred below an M/B ratio of 2. This was due to the use of the 4-cup rotary feeder insert to reach the required flow rates. The 5 and 6-cup feeders were unable to reach the requirements due to the VSD (variable speed drive) speed limitation. With the 4-cup rotary feeder, the geometry allowed for larger and less frequent portions of chip to be fed. These would subsequently pyrolyse prematurely and adhere to the side of the feeding tube (a phenomenon likely due to the higher density of particles present in the feeder tube at these flow rates). Thus, the incoming feed was prevented from entering the reaction zone. Because of this, the data which was collected for the low M/B ratio of x1.29 may be unreliable as a number of assumptions were required for the computation of the mass flow rates, primarily;

- An estimation of the amount of biomass which was stuck in the feeder tube at the end of the experiment.
- The system was at equilibrium after the first sample. For the trial there were only 2 samples taken as the blockage occurred after ~7 mins of running
- Biomass which was stuck in the feeder tube was not reacting

The M/B ratio was a very important aspect to investigate in the development of the system as this is one of the most influential parameters to determine the efficiency and capital cost of the system on an industrial scale. It is desirable to have a large amount of feed entering the system and to have as low methane flow as possible. This is desirable as increased production relative to the residence time reduces equipment sizes, and ultimately increases process efficiency and economic viability. It was also noted that the construction of the feeder system somewhat restricts the ability for an adequate investigation into the M/B ratio below a ratio of 2 for a methane gas flow rate of 0.242 kg/hr. This was due to the interior diameter of the inlet feeder tube which restricted the maximum flow rate. In a

practical application, larger scale would allow for < 1 M/B ratios. By varying the M/B ratio from 1.3 to 4.2 the ethylene concentration was seen to increase from 9 ± 1% to 20 ± 1 % carbon conversion, respectively, as shown in Figure 7-20. Significant increases in the ethylene yield were observed between an M/B ratio of 1.3-2.0 and 3.5 to 4.2, Figure 7-20. However, it is suspected that the increase in the ethylene production may be due to the increased effect which the ethylene production from MTD has on the overall carbon conversion calculation. The carbon conversion of CO fluctuated significantly throughout the trial with similar increases in the carbon conversion as observed with ethylene production. CO_2 and ethane production remained stable throughout the range of M/B ratios trialled.

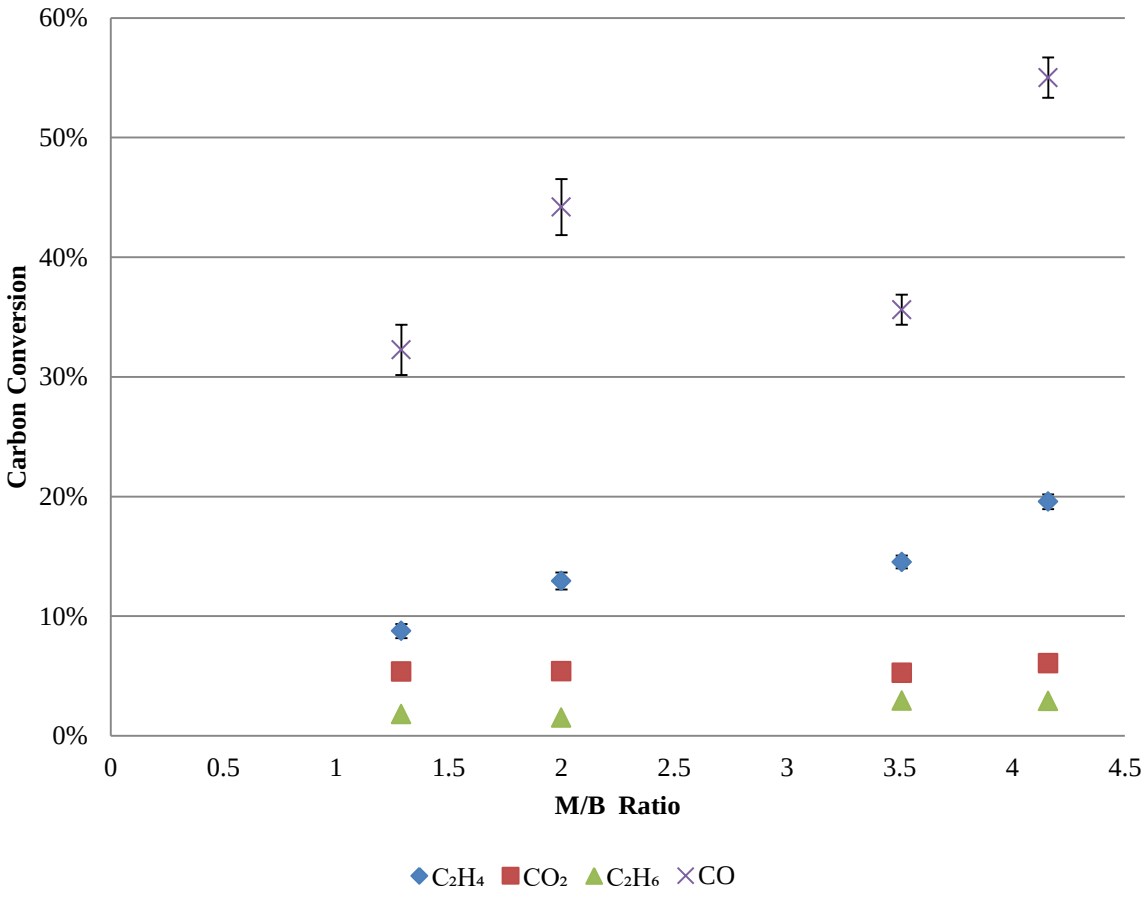

Figure 7-20: Major gas product composition distribution with varying M/B ratio, reactor operated with a 40 mm bed, at atmospheric pressure, an overall residence time of 0.75 s and bed temperature of 1020 °C.

From the oxygen balance stable production of CO, CO_2 and H_2O were observed between M/B ratios of 1.3-3.5. CO production increased from 48 % to 81 % when the M/B ratio increased from 3.5 to 4.2, whilst over the same interval the water conversion decreased from 37 % to 2 %, Figure 7-21. CO_2 is observed to remain relatively constant at approximately 14% from M/B values of 1.3-4.2.

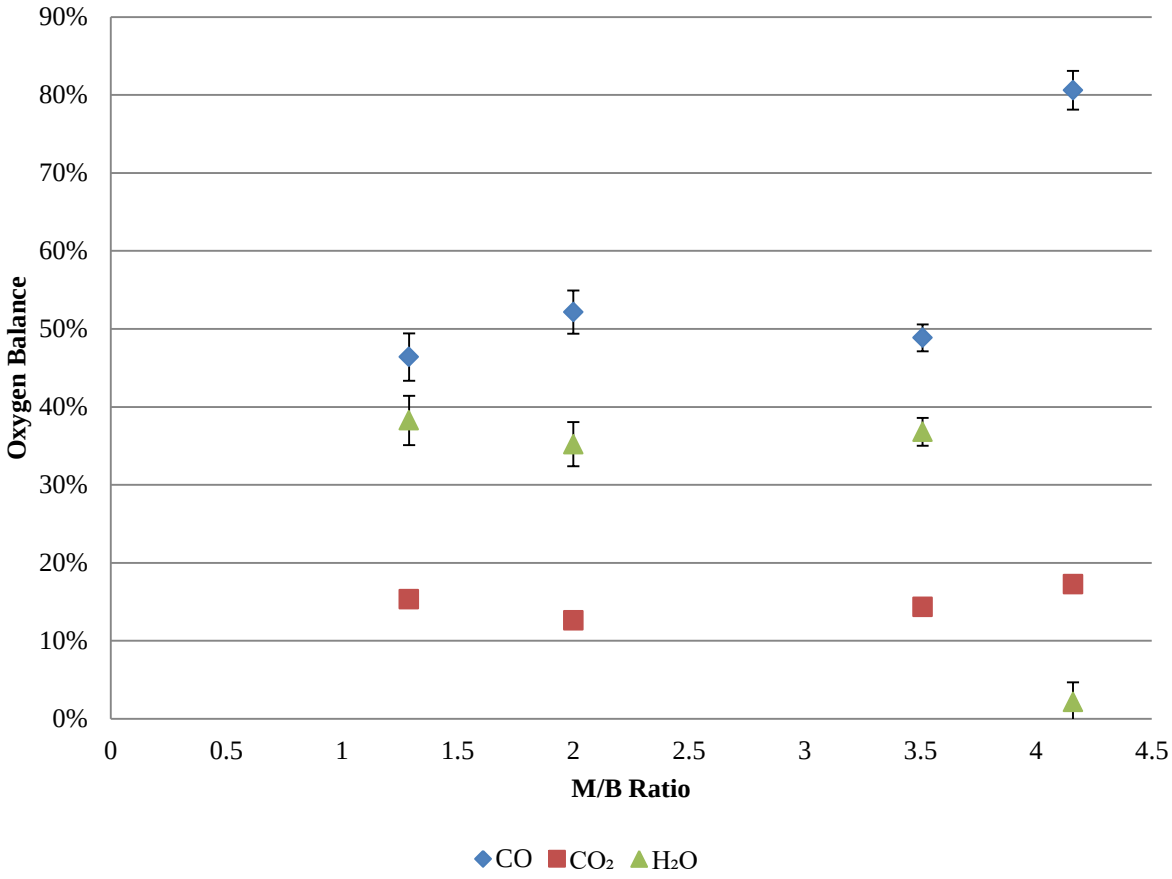

Figure 7-21: Oxygen containing species product distribution with varying M/B ratio, , reactor operated with a 40 mm bed, at atmospheric pressure, an overall residence time of 0.75 s and bed temperature of 1020 °C.

As shown in Figure 7-22, the methane consumption increased from 0.4 to 5.4 % when the M/B ratio increased from 2 to 4.2. At lower M/B ratios of 1.3 and 2 the overall consumption of methane was lower, approximately 1 %. However, the hydrogen production decreased from 14 % to 12 %, with increasing M/B ratio from 1.3 to 4.2.

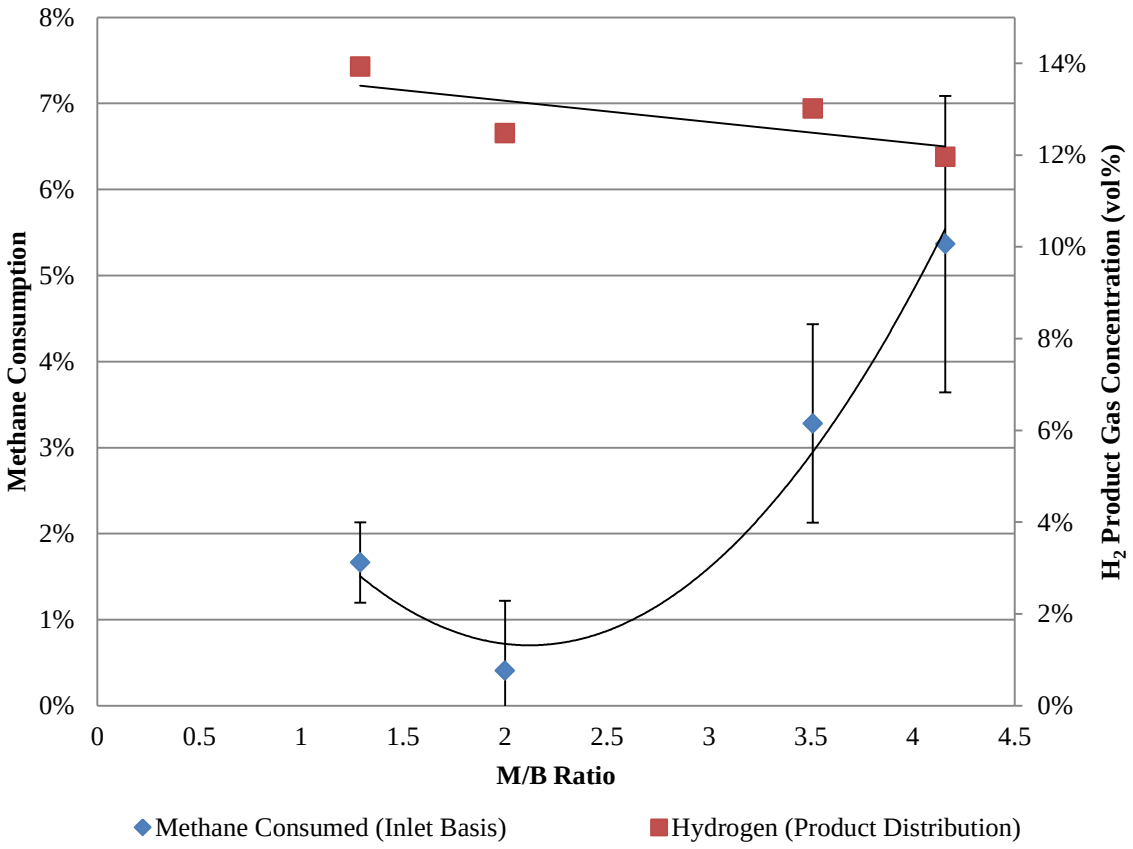

Figure 7-22: Methane consumption and hydrogen production with varying M/B ratio, reactor operated with a 40 mm bed, at atmospheric pressure, an overall residence time of 0.75 s and bed temperature of 1020 °C.

With increasing M/B ratios from 1.3 to 4.2 the tar yield of benzene, toluene and naphthalene all increased. Overall, at the highest M/B ratio of 4.2 12 ± 1% carbon conversion was recorded and benzene yield peaked at 8 ± 1 %, Figure 7-23.The yield of naphthalene and toluene remained relatively constant for M/B ratios of 1.3-4.2.

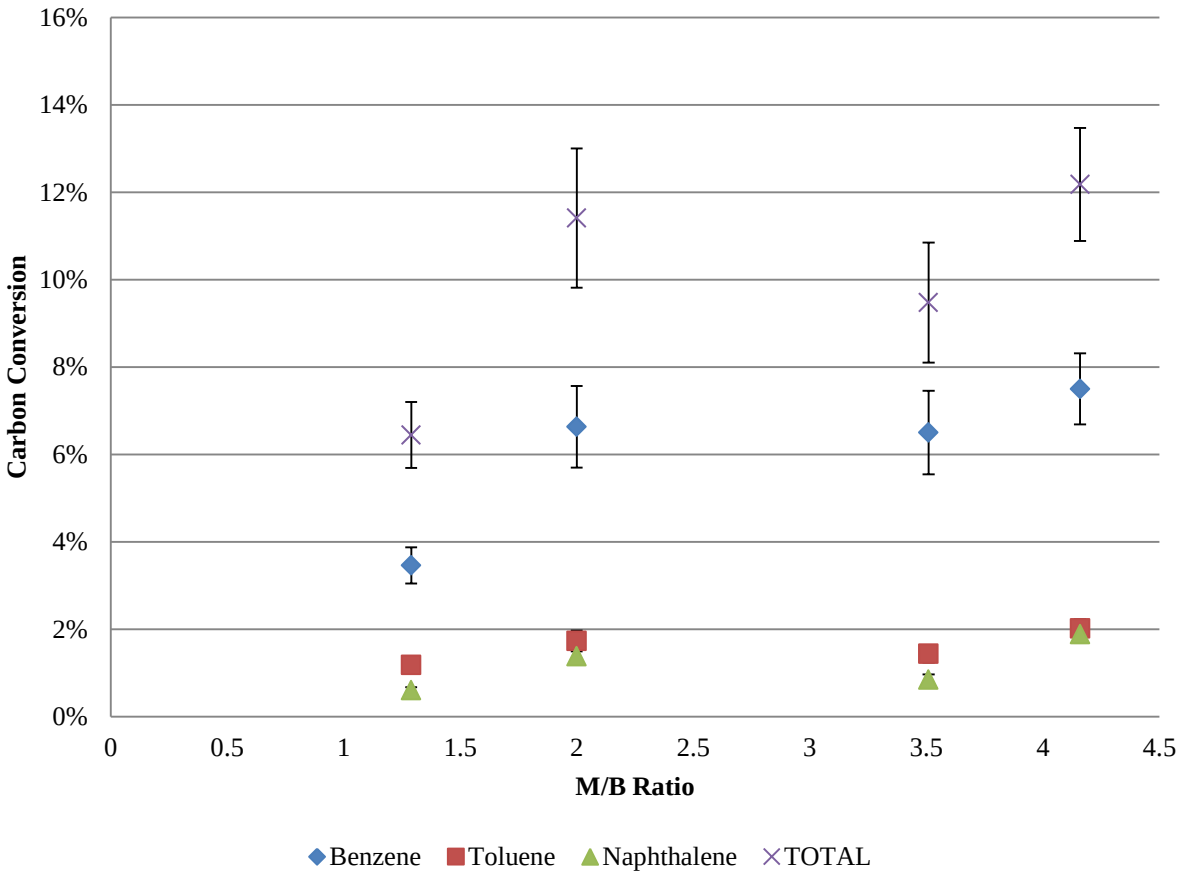

Figure 7-23: Major tar products with varying M/B ratio, reactor operated with a 40 mm bed, at atmospheric pressure, an overall residence time of 0.75 s and bed temperature of 1020 °C.

Trace tars were also observed to fluctuate significantly with varying M/B ratio. It was observed that with increasing M/B ratio, the overall contribution of trace primary tars to the overall carbon conversion decreased. Decreases in carbon conversion of biphenyl, phenol and indene were all evident with increasing M/B ratio, Figure 7-24. Low levels of secondary tars were recorded in the tar samples, primarily 1 and 2 -methylnaphthalene

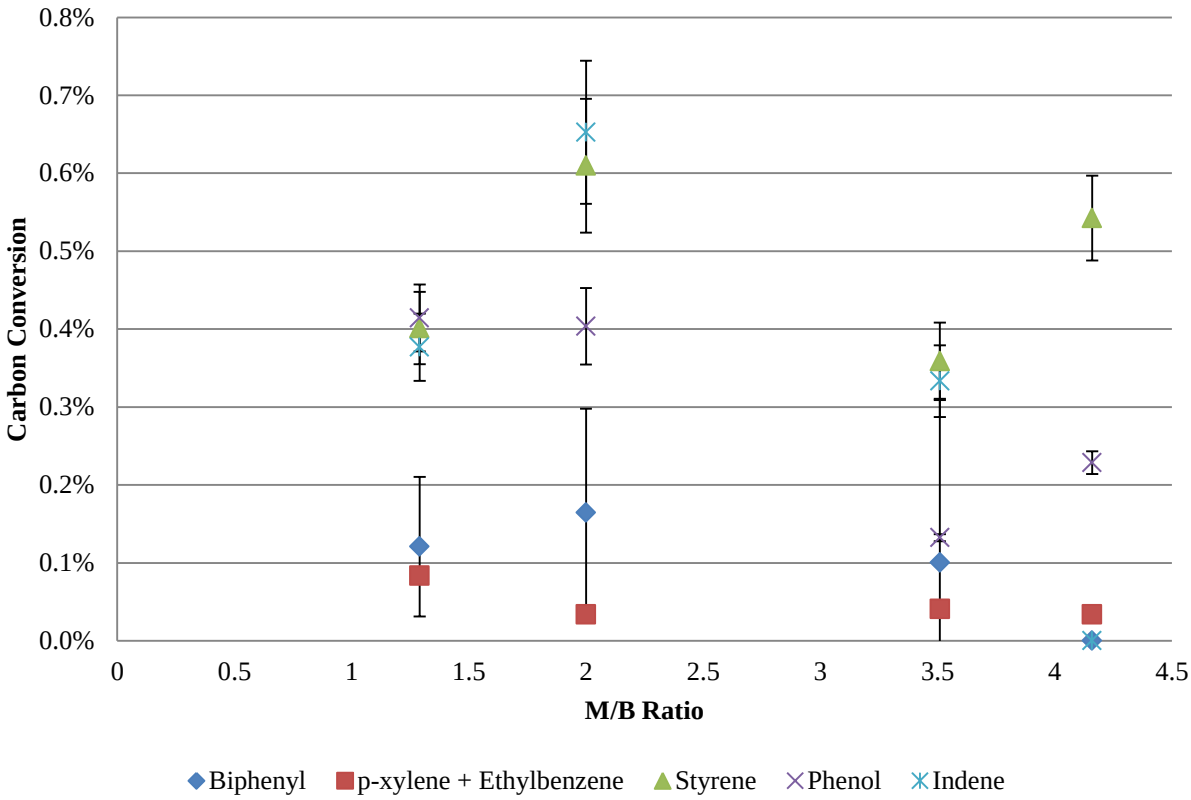

Figure 7-24: Trace primary tar composition with varying M/B ratio, reactor operated with a 40 mm bed, at atmospheric pressure, an overall residence time of 0.75 s and bed temperature of 1020 °C.

7.3.1 Discussion on the Effect of M/B Ratio

Overall it was observed that there was a stark difference in the product selectivity when the M/B was increased above 1.3. The highest ethylene, CO and benzene carbon conversion yields were obtained at the highest M/B ratio of 4.2. A discussion into the characteristics causing the variations in carbon conversion for different M/B ratios is provided below.

Due to the nature of the reaction the introduction of biomass reduces the residence time of the gas in the reacting zone, where higher M/B ratios result in larger increases in residence time. In turn, decreasing the M/B ratio causes multiple effects; where with a decreased M/B ratio the concentration of products in the outlet gas is also greater in the reaction zone. Reducing the M/B ratio also lessens the extent of secondary reactions which are also reduced at lower residence times. As shown in Table 7-4, the product gas flow rates for the various M/B ratios with overall water and gas fraction product distribution. To determine the theoretical flow rate increase, the methane degradation flow rate of 6.2 SLPM was taken as the basis for the volumetric flow rate increase. This value is constant and was averaged from all M/B ratio experiments. From this value the mass flow rate of the gas, tar and water production was calculated to determine the theoretical gas production, with respect to the inlet flow

rate of biomass. This allowed for a relative comparison between the systems, assuming that all product yield increases are from the addition of biomass.

Table 7-4: Measured product gas flow rates and the derived theoretical gas, tar and water conversions based on inlet biomass. The methane degradation flow rate of 6.2 SLPM was used for the derivation of the theoretical flows.

M/B Ratio		Product Gas Flow rate		Measured Flow rate Increase		Theoretical Flow rate Increase		Gas Product Fraction		Tar Product Fraction		Water Product Fraction	
[-]		[SLPM]		[-]		[-]		[-]		[-]		[-]	
4.2	±0.03	7.3	±0.2	17%	±0.4%	24%	±2%	72%	±5%	7%	±1%	7%	±64%
3.51	±0.02	7.4	±0.2	18%	±0.5%	28%	±0%	64%	±2%	3%	±0.3%	16%	±2.7%
2.00	±0.02	8.2	±0.2	31%	±0.8%	50%	±0%	63%	±2%	4%	±0.3%	18%	±2.0%
1.29	±0.02	8.7	±0.2	40%	±1.1%	78%	±1%	52%	±2%	2%	±0.2%	19%	±0.9%

It was observed that the feeding rate of the biomass input was highly influence by the product composition and gas phase distribution. Higher M/B ratios were observed to increase overall tar production and decrease water production. The total gas production was observed to be stable at 72 ± 5 % for an M/B ratio of 4.2, a significant decrease to 52 ± 2 % occurred when the M/B ratio was decreased to 1.29. Possibly these trends can be explained by the free energy model which shows the variation which the M/B has on the free energy of the system, Figure 7-25. The decrease in water production is likely due to the decreased mass flow rate of biomass into the system, in turn, reducing the amount of oxygen entering the system. The majority of the oxygen in the product stream was bound as CO and is the dominant oxygen bearing gaseous product at equilibrium. Overall the CO oxygen conversion was observed to increase with increasing M/B ratio, indicating that the oxygen within the feed biomass favoured the formation of CO at lower M/B ratios. It was also possible that the water production may be attributed to the decreasing residence time that was apparent with decreased M/B ratio. As observed in Figure 7-12, the residence time of the gas has a significant bearing on the oxygenated gas species. It was possible that the lower M/B ratio trials cause a lower residence time which increase water production. However, this was difficult to distinguish as the concentration of the species in the freeboard area is not constant between trials.

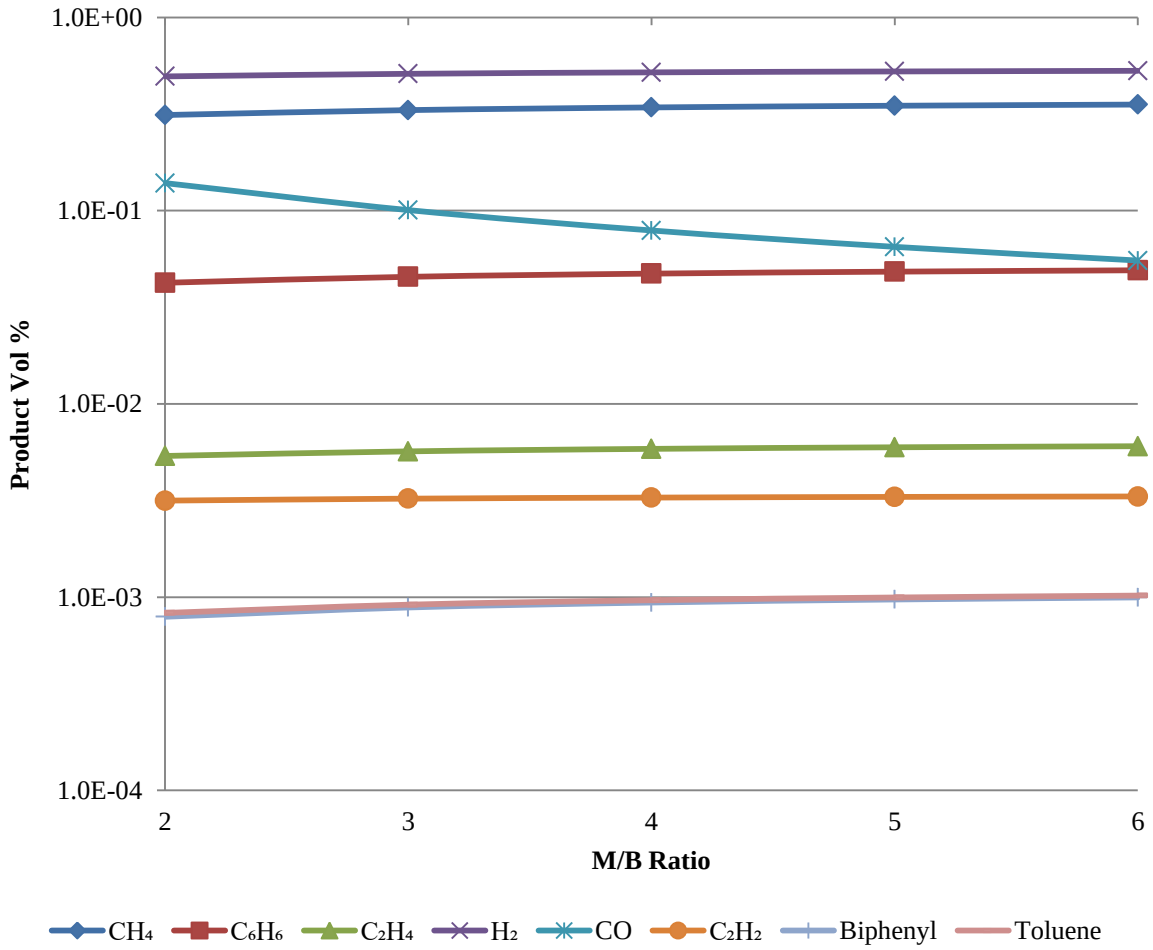

Figure 7-25: Gibbs free energy modelling for various M/B ratios at atmospheric pressure and an operating temperature of 1020 °C.

From free energy modelling, the effect of varying the M/B ratio was observed to have a subtle effect on the product distribution of all product gases bar CO. However, in comparison to the trends which were observed from the trial it is likely that the level of conformity to the free energy model is dependent on the M/B ratio. At higher M/B ratios the system was observed to behave much closer to the equilibrium data which was obtained from the modelling. Although the extent of the product distribution was not matched due to kinetic and thermodynamic limitations, the inherent trend was very similar. C_2H_4, CO, C_2H_6 and CO_2 are all observed to be stable with M/B ratios above 1.3. It was suspected that this may be caused due to the increased gas phase concentration of the product gases in the reaction zone at lower M/B ratios. This was suspected due to the effect which the kinetics of the system have as the system was further away from equilibrium. In addition to this effect, the residence time in the reaction zone was decreased in this situation, which inherently suppresses the achievement of equilibrium behaviour within the system.

Deviations in the flow rate of biomass were also apparent with varying M/B ratio, with the functionality of the reactor making measurements less accurate at lower M/B ratios. For the trials conducted above an M/B ratio of 2 feeding characteristics were greatly improved. With an M/B ratio between 2 and 4 the system was observed to have stable results with little variation across measured products. When the M/B ratio increased above 3.5, the methane consumption increased significantly from 3.2 % to 5.2 % at an M/B ratio of 4.2. It was suspected that at M/B ratios of 2-4.2 the product distribution was not greatly affected, due to the influence of the reacting composition having a greater effect than that of the ratio. However, it was suspected that because the product gas stream was diluted, the characteristics of methane consumption were altered. It was observed that with increasing M/B ratio methane consumption also increases. It was possible that this was due to the increased concentration of methane in the reacting zone, at high M/B ratios, which facilitate MTD above the bed. As the methane flow rate was constant, the methane consumption due to MTD could be assumed as stable at 12 %. The overall methane consumption varied between trials, which was possibly due to an increase in methane production at low M/B ratios.

7.4 Effect of Pressure during Methanolysis

Pressure was another important experimental parameter which was investigated to determine the influence of operating pressure on the distribution of products during the flash methanolysis of biomass. This parameter was deemed influential due to the production of multiple phased products during methanolysis. Pressure is also an important parameter in regards to the process equilibrium and kinetics of the system, as, increased partial pressure of feed gas streams can alter the reaction kinetics and competition between reaction pathways. This also allows for insight into the pressure dependency characteristics of products formed in the reaction.

Operationally, the pressure trials were difficult, due to feeding issues caused by pressure differentials between the reactor and the hopper. It was observed that with the leakage of gas which was occurring through the feeding valve, the pressure differential would at times be larger, due to the difficulty in controlling separate pressurized systems. As the hopper and the reactor were pressurized simultaneously, by two separate cylinders, best attempts were made to ensure correct pressurisation. This was evident in the higher pressure trials of 483 kPa which were conducted. Due to the high pressure, pressure differentials over the feeding system were difficult to control, resulting in flow issues due to the chip being subject to significant pressure differentials at times. This was due to the pressure in the reactor sometimes being higher than that of the hopper, resulting in gas rising through the feeder tube, severely affecting the feeding characteristics into the bed. It was suspected that due to this the chips were more likely to pyrolyse/torrify prematurely. It was because of this pressure differential that a number of trials ended in blockages of the feeding system, resulting in a number of trials being repeated.

Because of this imbalance in pressure, through back calculation it was found that feeding fluctuated significantly and at times was larger than the associated calibrated rate. This was discovered by recording the total reacted mass and comparing it to the target flow rate from calibration curves. This resulted in the M/B ratio to vary between 3.1and 4.8; however, from previous trials conducted it was suspected that the level of variation in the M/B ratio was negligible. As the pressure of the system was increased the overall methane flow rate was increased to keep residence time constant between trials. This caused limitations in what residence times were attainable, especially at higher pressures. Overall a maximum operating pressure of 483 kPa was obtained at a residence time of 2.8 s.

It was observed that pressure significantly altered the yield of CO and ethylene during methanolysis, Figure 7-26 . A minimum of 42 ± 2 % carbon conversion was obtained at 380 kPa. C_2H_4 and C_2H_6 were observed to increase significantly above 140 kPa, with maximum carbon conversions of 19 ± 3 % and 5 ± 1 % achieved at 276 kPa, respectively. CO_2 showed a slightly increasing trend with an increase from 6-8 % observed between 140- 480 kPa, Figure 7-26.

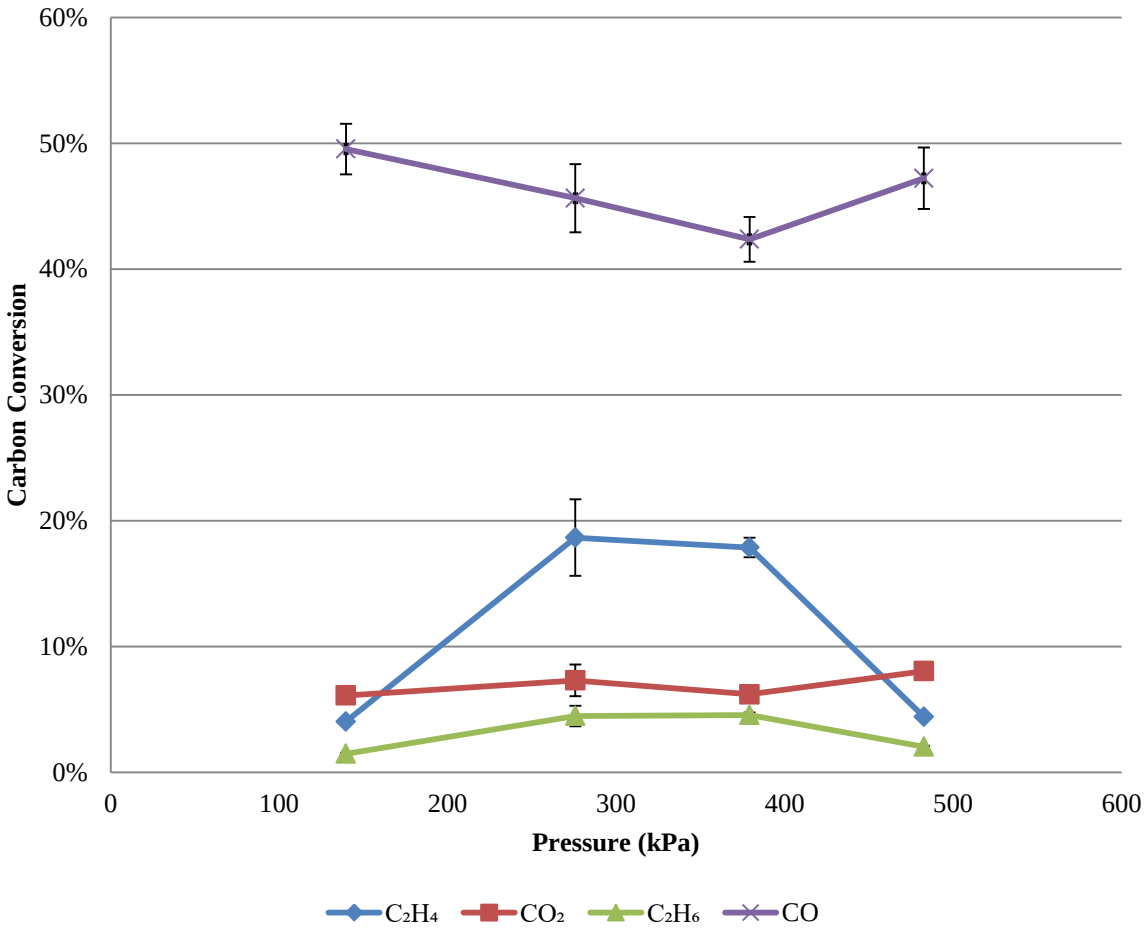

Figure 7-26: Major gas components carbon conversion with respect to pressure, reactor operated with a 40 mm bed, 1.5 s residence time, M/B = 4.8 and bed temperature of 960 °C.

Interestingly, from the oxygen conversion calculations, no significant variation in product distribution of CO, CO_2 and H_2O was observed with increasing pressure, Figure 7-27. As shown below, all product distribution was within the experimental error and CO, CO_2 and H_2O had average oxygen fraction productions of 65 ± 3 %, 19 ± 1 % and 16 ± 3 %, respectively.

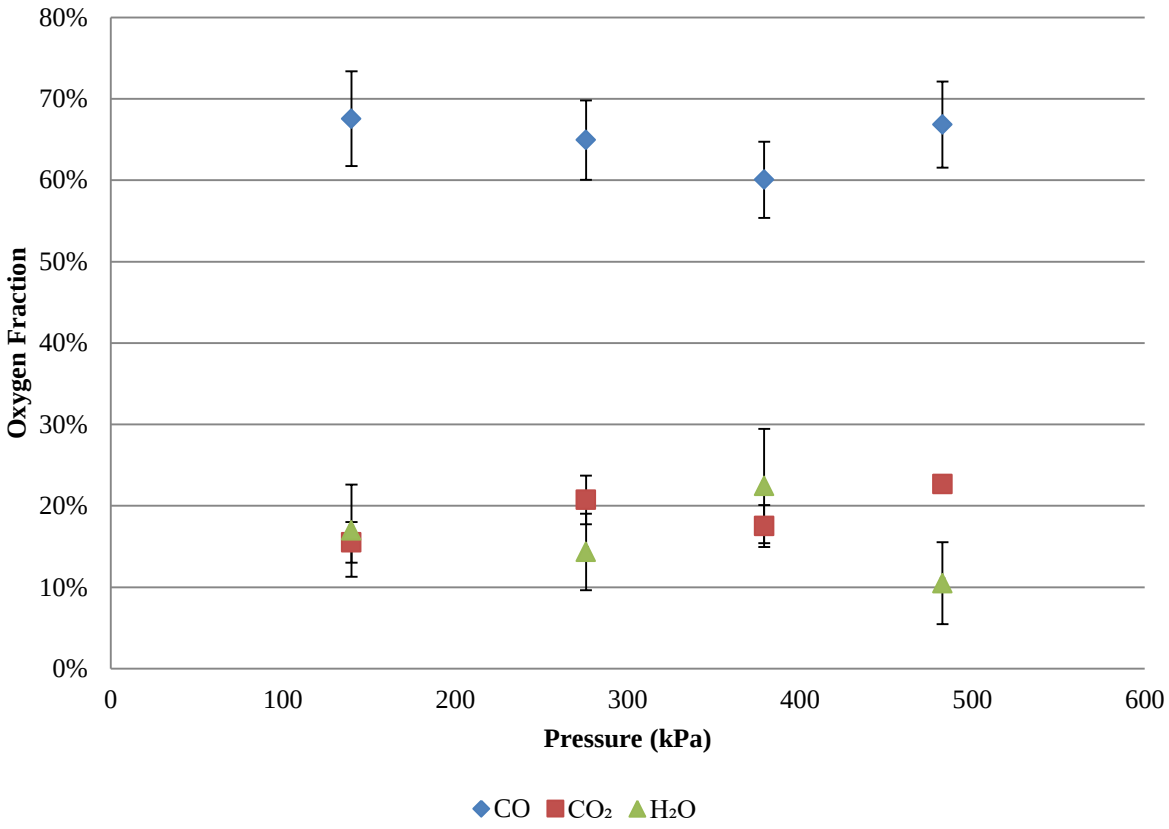

Figure 7-27: Oxygenated product species distribution in gas product, reactor operated with a 40 mm bed, 1.5 s residence time, M/B = 4.8 and bed temperature of 960 °C.

Hydrogen production was observed to plateau at pressures between 275-380 kPa with a minimum of 15 vol% detected in the product gas. Above and below the stated range, the production of hydrogen is observed to increase to 25 %. Methane consumption was stable at pressures below 380 kPa, with a significant increase from 3 % to 11 % when operated at 483 kPa, Figure 7-28.

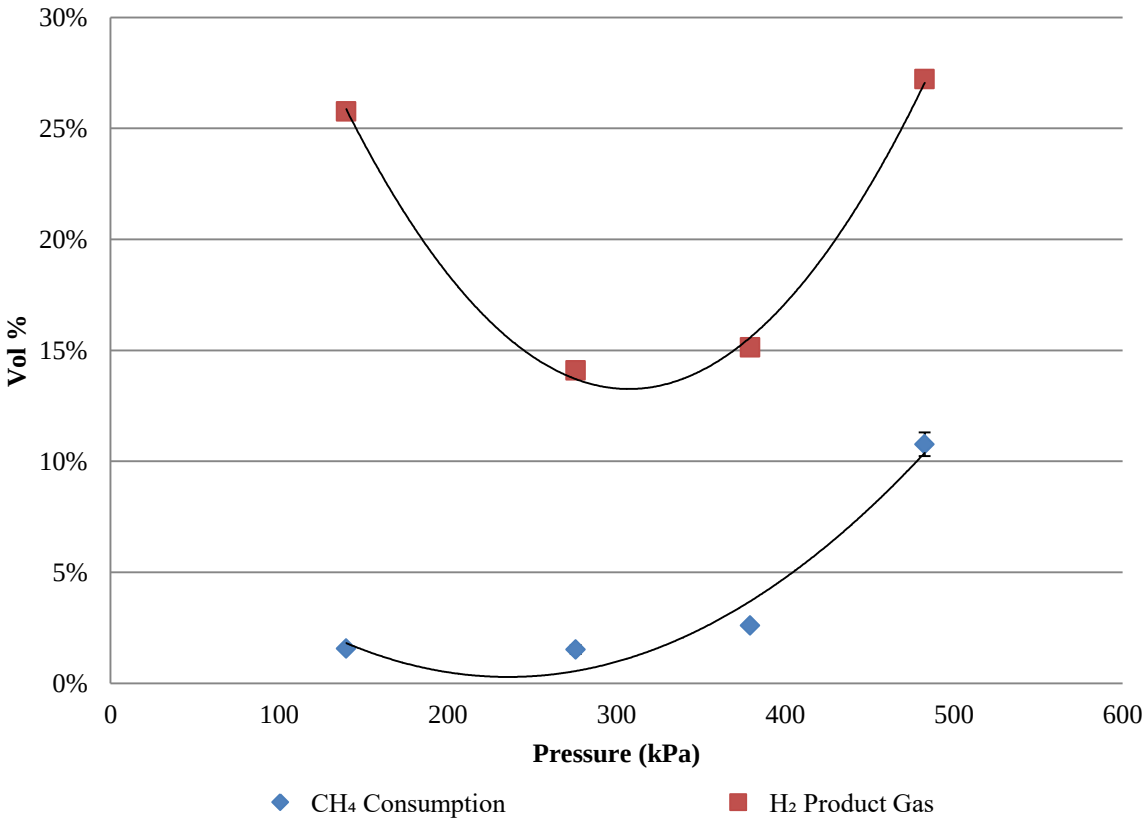

Figure 7-28: Methane consumption and hydrogen production calculated for varying pressure, reactor operated with a 40 mm bed, 1.5 s residence time, M/B = 4.8 and bed temperature of 960 °C.

Tar production was observed to significantly vary with pressure during the flash methanolysis of biomass. Overall tar productions were observed to increase from 5.4 ± 0.4 %, at 140 kPa to 26 ± 2 % at 483 kPa. Where, the majority of the tar increase accounted for due to increased benzene production, which increased from 3.0 ± 0.5 % to 16 ± 2 % carbon conversion when the pressure increased from 140 kPa to 483 kPa, Figure 7-29.

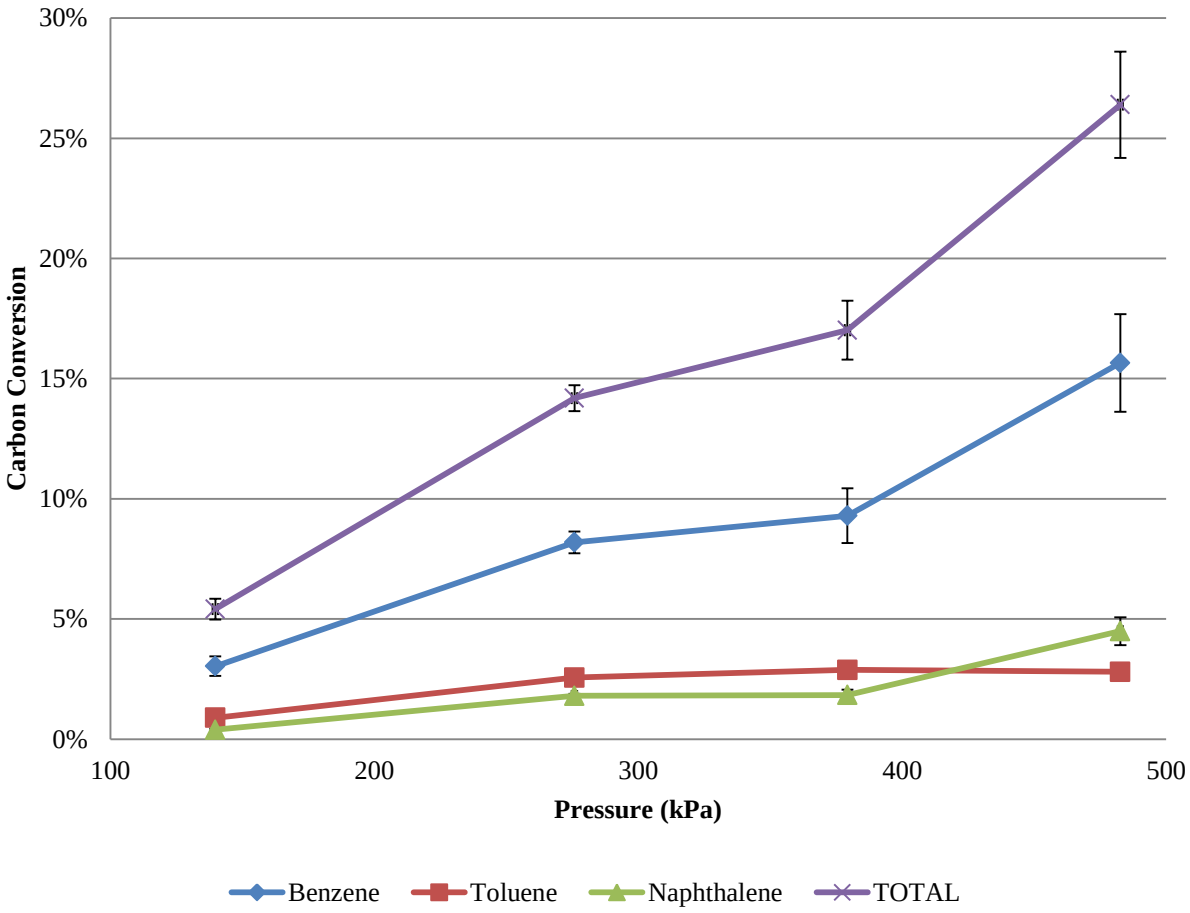

Figure 7-29: Major tar product distribution with respect to pressure, reactor operated with a 40 mm bed, 1.5 s residence time, M/B = 4.8 and bed temperature of 960 °C.

From Figure 7-30, it was observed that the composition and selectivity of the trace tar components varied significantly with pressure. The system pressure seemed to have significant effects on the yields of phenol and styrene especially, whereas, m- and o-xylene production was independent of pressure.

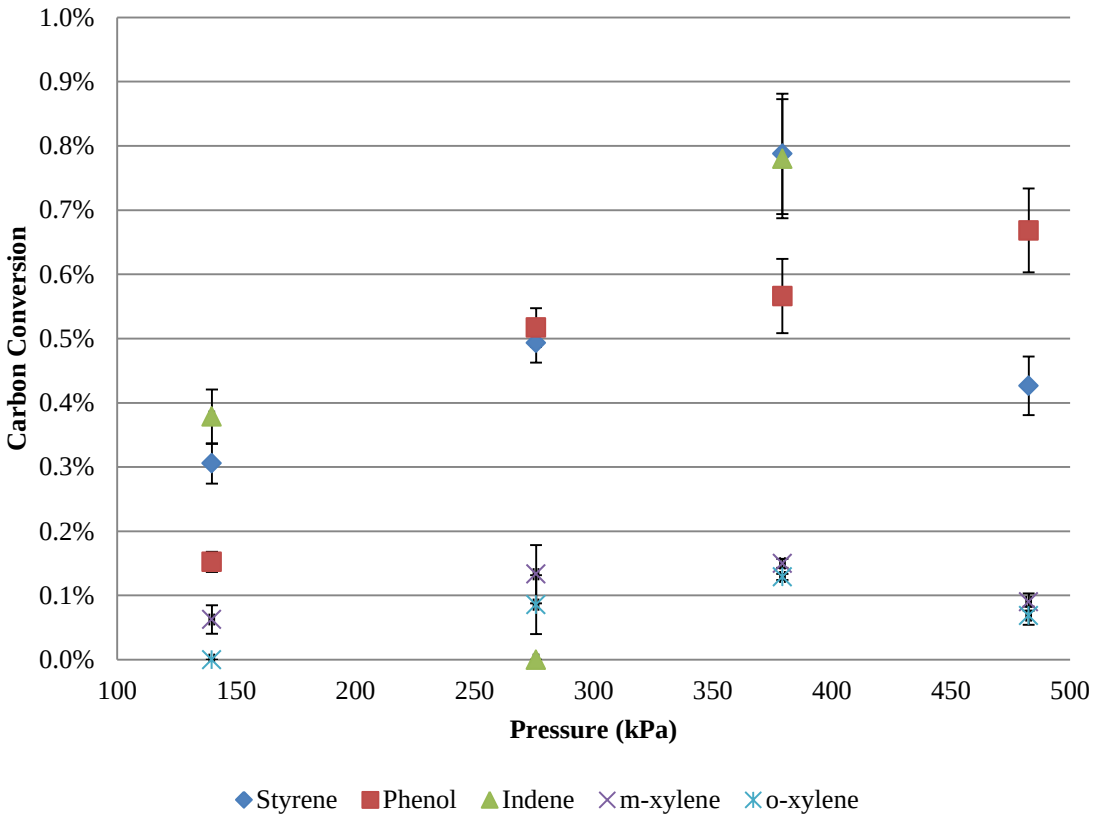

Figure 7-30: Minor tar species distribution with varying pressure, reactor operated with a 40 mm bed, 1.5 s residence time, M/B = 4.8 and bed temperature of 960 °C.

7.4.1 Discussion of the Effect of Pressure during Methanolysis

From the investigation into the effect of pressure during methanolysis, it was observed that a maximum C_2H_4 carbon conversion of 19 ± 3 % was obtained at pressures between 275-380 kPa. At higher pressures of 480 kPa, the production of ethylene decreases drastically to 4.4 ± 0.2 %. This indicated the strong influence which pressure has on the methanolysis reaction and the overall carbon conversion of biomass to ethylene. It was likely that this was primarily due to the thermodynamics of ethylene production in the system, as shown by the modelled data.

Overall, the experimental results coincided with the free energy modelling, as shown in Figure 7-31. It is observed that a local maximum in ethylene equilibrium exists between 300-450 kPa, which was suspected to predict the behaviour of ethylene formation well within the system. Significant increases in ethylene conversion are exhibited with modest increases in system pressure up until the maximum equilibrium pressure, after which the production of ethylene decreases constantly, Figure 7-31.

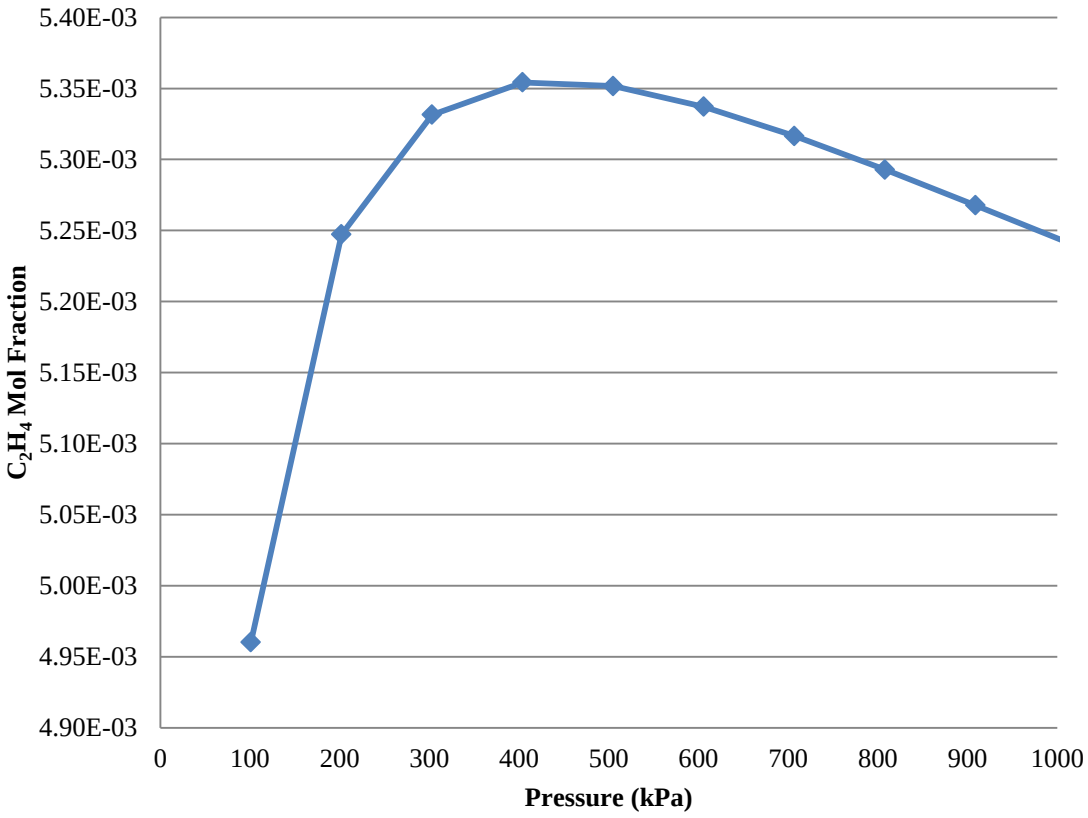

Figure 7-31: Ethylene mol fraction formation derived from free energy modelling of the system at 960 °C.

From the ethylene characteristics described above, it was observed that the ethylene yield decreases with increasing pressure due to the increased production of methane, Figure 7-32. Increases in ethane and toluene are also observed, however, the molar product distributions of the variations are several orders of magnitude smaller than that predicted by the model. Opposing trends in the methane results were obtained from the experiments conducted overall. With increasing pressure the methane degradation and methane consumption increased, Figure 7-28. It is very likely that this is attributed to the formation of carbon from MTD. The free energy modelling shows zero formation of carbon throughout the experimental pressure range. This highlights one of the weaknesses of the modelling, as it was certain that carbon deposition was occurring and was shown to have strong variations in the product distribution. Toluene production is observed to be in agreement with that described by the model, with increased yields recorded over the pressure ranges as well. Ethane showed increases with temperature but also decreased significantly at 480 kPa. Overall, the ethane formation characteristics were very similar to that of ethylene; with the maximum yield achieved at 275-380 kPa and strong decreases in yield either side.

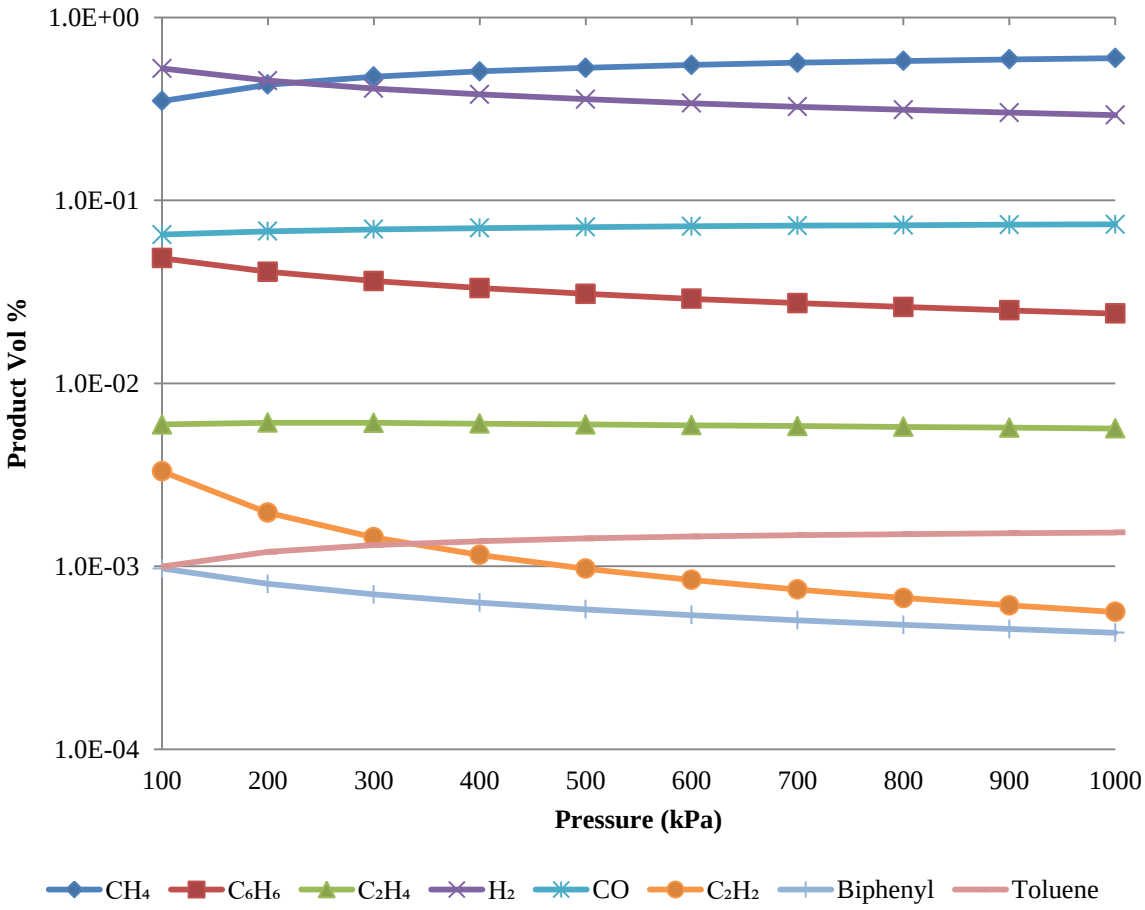

Figure 7-32: Overall system free energy equilibrium characteristics with varied process pressures. System modelled with an M/B ratio of 5 and temperatures of 1000 °C.

From the analysis it was observed that the methane consumption was minimized at pressures between 140 kPa and 380 kPa, further increases in pressure resulted in increased methane consumption. This minimum in methane consumption coincides with the maximum in ethylene yield. To determine the influence which degradation had on the ethylene production, a baseline of the degradation product before and after the experiment was taken. From the values measured, a ratio of ethylene produced from the degradation and from the experiment was derived. It was difficult to conclude if the ethylene that is formed from the experiment was due to the methanolysis reaction or MTD. It is speculated that the actual amount of ethylene produced from the experiment was larger than a simple division of degradation + experimental results. However, for comparative reasons, the ratio of degradation/experiment was useful to investigate the efficiency of the system as it allowed for a direct comparison of the ethylene sources.

Table 7-5: Relative ethylene carbon conversion in regards to the degradation ethylene formation.

Pressure (kPa)	**C_2H_4 (Deg)/C_2H_4 (Experiment)**	**±**
140	26%	*1%*
275	31%	*5%*
380	53%	*2%*
480	163%	*7%*

From Table 7-5, it was observed that there was a strong increase in ethylene yield with pressure that was due to the increased amount of MTD. This was observed to agree with the gas equilibrium constant, where the highest overall ethylene flow rate was produced at 380 kPa. It was interesting to observe that at higher pressures the ethylene yield was essentially decreased by the introduction of biomass. This is suspected to indicate that ethylene forming reactions are inhibited and/or ethylene was degraded/reacting with other gases in the product stream for this situation. The desirability of these products was unknown as the pathway for the reaction is not well understood. It was, however, hypothesised that the interactions of ethylene at higher pressures could be the pathway for the increased benzene and tar yields which are recorded, Figure 7-29. Contrary to many previous experiments the increase in naphthalene yield observed was recorded as higher than toluene with increasing pressure. A generalised reaction pathway is shown in Equation (7.4.1), with the products described in regards to apparent phase selectivity.

$$C_2H_4 + Biomass \rightarrow C_6H_6 + C_{10}H_8 + C_7H_8 \qquad (7.4.1)$$

Figure 7-29 shows the strong influence which pressure has on the overall carbon conversion to tar species. This was highlighted by the benzene yield collected at 480 kPa being higher than the overall tar yield at 275-380 kPa. Overall benzene carbon conversions of 16 ± 2 % were recorded at 480 kPa with an overall tar production of 27 ± 2 %. Free energy data leads to expected decreases in the naphthalene and benzene yield with increasing pressure, while toluene is expected to increase, Figure 7-32. Minor tar species selectivity was observed to vary with pressure, Figure 7-30, the production of phenol showed a strong increase with increasing pressure, with xylene concentrations showed similar plateau characteristics as C_2H_4 and C_2H_6. Overall, similar trends in the production of C_2H_4 were observed in the work conducted by Steinberg et al. [3], however, the tar production does not agree with previous findings. For the pressurized system, Steinberg et al [3], recorded no increase in the

production of tar species between 101 kPa and 1380 kPa. The styrene and indene yield showed random variations with pressure and it was suspected that this may be due to experimental uncertainty in measurements. Overall, the species yields are suspected to be due to the similar characteristics of benzene, toluene and naphthalene. It was suspected that the increase in pressure facilitates the production of aromatic rings, possibly through the pathway described in Equation (7.2.2). It is also postulated that the pressure may prevent the decomposition of the aromatic structures within the lignin lattice. This may explain the increase in yields of various different single aromatic ring tars, as, the C-C bonds broken in various positions can yield several different tar species, which thermodynamically favour the production of benzene.

From the trials it was also observed that CO plateaued at a minimum within the operating pressures of 275-380 kPa. This coincided with the maximum of C_2H_4 which was contrary with all other process trends observed in previous experimental investigations. Previously, the concentration maximums of C_2H_4 have coincided with CO maximums; however, with pressure variations it is observed that the opposing trend was observed with CO. In previous experiments it was likely that the CO and C_2H_4 maximums may have arisen due to increased conversion of the entering biomass and the increases in carbon conversion were mutually exclusive. With the opposing trends it was suspected that the differences in CO and ethylene production trends were related to the influence on the kinetics of the system. Overall the CO was observed to reach a minimum of 42 ± 2 % carbon conversion at pressures between 275kPa and 380 kPa, Figure 7-26. Although the increasing pressure shows strong variations of the CO carbon conversion yield, the overall oxygen conversion remains relatively stable. Overall an average of 64 %, 20 % and 16 % oxygen conversion was recorded for CO, CO_2 and H_2O during methanolysis. A slight decrease in the oxygen conversion to water was observed at higher pressures of 480 kPa, however generally the system was relatively stable. Slight variations in the product distribution of CO can be accounted for at 140 kPa, as the flow rate was slightly higher than required, thus effecting the M/B ratio. Ultimately, this causes the amount of oxygenated species to increase and decrease the overall apparent carbon conversion to CO. However, when regarding the oxygen conversion, similar conversions would be expected at the lower pressures, which suggest that the overall oxygen conversion is not highly influenced by the operational pressure.

CO_2 concentrations are observed to be relatively stable throughout the pressure range investigated. It is interesting to note that the C_2H_4 yield decreases to below the CO_2 yield at 480 kPa, which was not observed in any previous trials. This indicates that there was a strong variation in the product gas phase composition with pressure and potentially this may be due to decreased reaction completion. This was suggested due to the decrease in apparent mass balance closure, which results in a suspected increase in char/carbon in the system, Table 7-6.

Table 7-6: Mass balance closure for the experiments conducted at various pressures. The closure is calculated as the cumulative of tars, water and gas (omitting the solid phases as the composition of these is unknown).

Pressure (kPa)	Mass Balance Closure	±
140	97%	*2%*
275	100%	*5%*
380	97%	*1%*
480	93%	*2%*

7.5 Effect of Chip Size during Methanolysis

For commercial application of methanolysis the preparation of feedstock and milling are significant barriers in the utilisation of natural feedstocks as the costs associated with the preparation are generally high. To realise the commercial viability of the process it was of interest to determine the product distribution and system characteristics for varied feedstock , allowing for the benefits of comminution to be balanced upon the benefits obtained by differing product selectivity. Milling is usually conducted by electrically powered machinery in the form of rotary mills, drum mills and chippers, where milling wood to 100 µm has been deemed unattractive, due to the high relative electricity demand (0.08 $kW_e/kW_{th,\ wood}$) [9]. Great electricity savings can be obtained from torrefying the feed biomass prior to chipping, with milling costs decreasing to 0.01-0.02 $kW_e/kW_{th,\ wood}$ [9].

The particle size of the reacting biomass also has a significant effect on the physical and chemical characteristics of the vapours during pyrolysis. With increasing particle sizes the initial devolatilisation step of pyrolysis is varied, as due to greater interaction of the evolved volatiles through the particle matrix which can also interact with the outer charred portion of biomass, prior to complete conversion of the particle. The characteristic outer charring was due to the low thermal conductivity of woody biomass and occurs when the heat transfer to the biomass particle was greater than the conductance. This can be observed as a shrinking, unreacted core effect of the biomass particle which results in a greater path which the volatiles must travel through to exit the biomass matrix. This renders multiple effects within the biomass; between volatiles and the charring surface of the particle where the overall mechanism was very complicated as the charring surface was a known catalyst [10]–[12]. Hence, the larger the particle the increased extent of interaction with the outer charring surface for the volatiles released from the unreacted core.

Literature reporting the effects of biomass chip size is limited, with most pyrolysis applications focused on the investigation of chip size at low temperatures (500 °C). Septein et al. [13], operated a drop tube furnace at 1000 °C with N_2 as the carrier gas and investigated the two particle size ranges; 0.313-0.400 mm and 0.730-0.900 mm. Overall fractions of tar, char and gas were relatively stable, where only a slight increase in char observed with the use of 0.730-0.900 mm feed. Statistically significant variations in product yield were observed for the production of benzene from smaller particle sizes, which rendered higher benzene yields [13]. The object of this investigation was to better understand the interactions and influence particle size has on the product distribution and the effect of methane within the variations.

For the particle size variation trials chip was prepared in accordance to the trial preparation described in the previous sections. In total three separate chip size regions were analysed; 500-710 µm, 710-1000 µm and 1000-1400 µm. Trials were attempted with feed < 500 µm, however severe static

electricity build up and subsequent inter-particulate forces resulted in the trials being abandoned. The trials were conducted with a residence time of 0.75 s with an M/B ratio of 5 at 1000 °C. From the investigation it was observed that a significantly higher gas fraction was obtained with using the 710-1000 µm feed in comparison to the other two fractions. When using the 710-1000 µm chip, 87 ± 2 % carbon conversion to gaseous species was derived with 4 ± 2 % char and 7 ± 1 % tars, Figure 7-33. The smaller 500-710 µm particle size feed yielded carbon conversions of 68 ± 1, 3 ± 2 and 7.5 ± 0.3 for the gaseous, char and tar fractions, respectively. Whilst, the 1000-1400 µm produced an overall carbon conversion to gas of 78 ± 2 %, and producing the lowest char and tar carbon conversions of 2 ± 2 % and 3.7 ± 0.2 % , respectively.

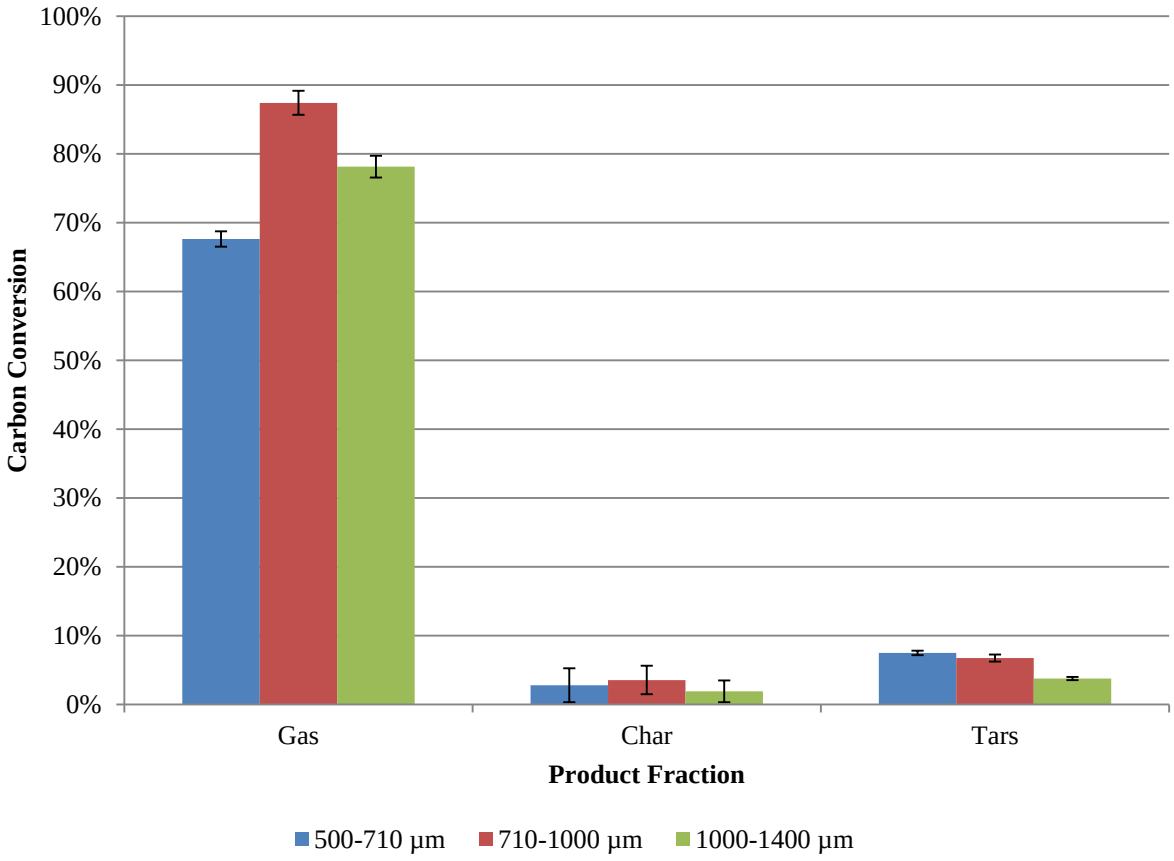

Figure 7-33: Overall product carbon conversion, system operated at 1000 °C, at atmospheric pressure, M/B = 5 and a residence time of 0.75 s.

The utilization of 710-1000 µm chip showed high gas production of CO and C_2H_4, with 54 ± 1 % and 14.0 ± 0.3 % carbon conversion recorded, respectively. The other chip fractions were observed to have a slightly lower distribution of CO, CO_2 and C_2H_6. Overall, the apparent methane production decreased with decreasing particle sizes, Figure 7-34.

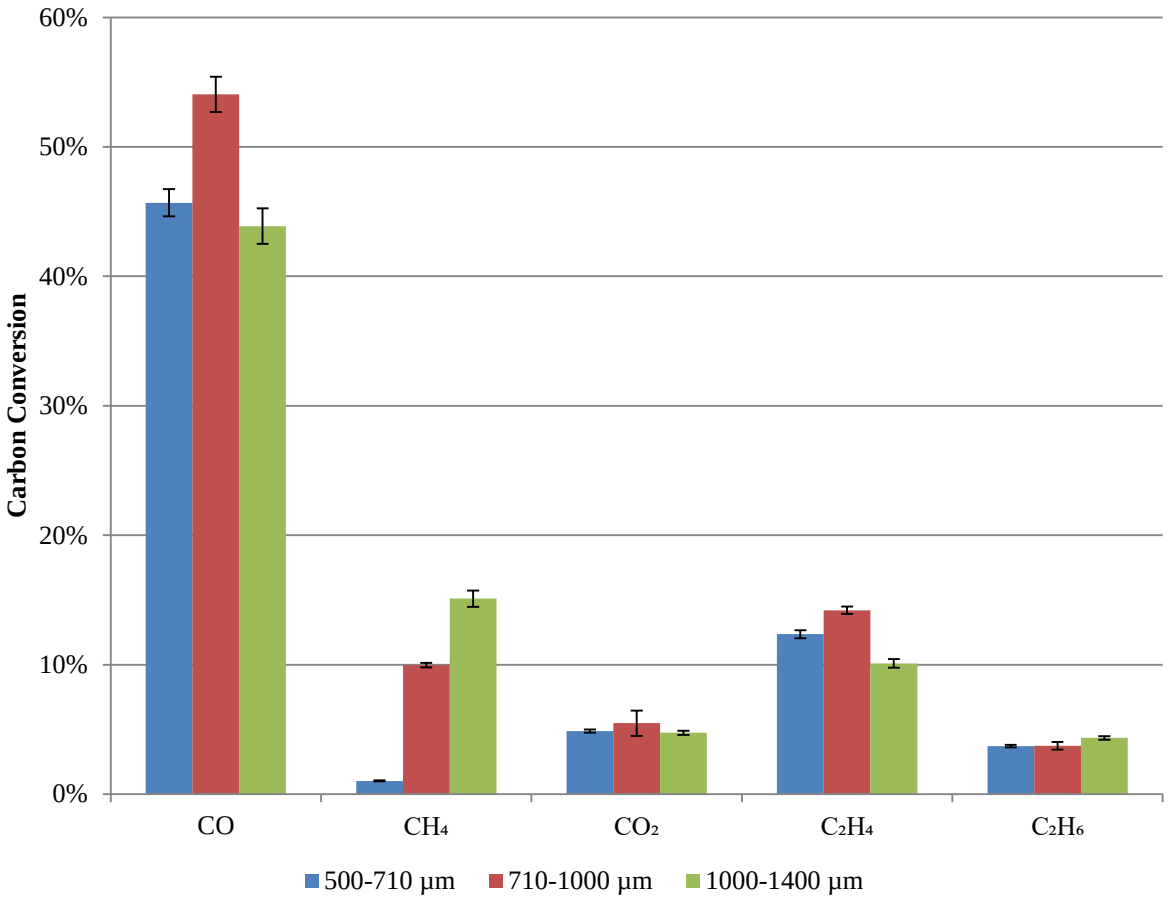

Figure 7-34: Gas phase product distribution for varied chip size intervals, system operated at 1000 °C, at atmospheric pressure, M/B = 5 and a residence time of 0.75 s.

The tar distribution profile was observed to show a marked decrease in tar production across all species for the larger biomass feed fraction of 1000-1400 µm, Figure 7-35. Tar phase selectivity was observed to be constant between the trials of 500-710 µm and 710-1000 µm with slight increases in all tars measured bar naphthalene. A maximum benzene carbon conversion yield of 3.4 ± 0.2 % was obtained with the use of 500-710 µm chips.

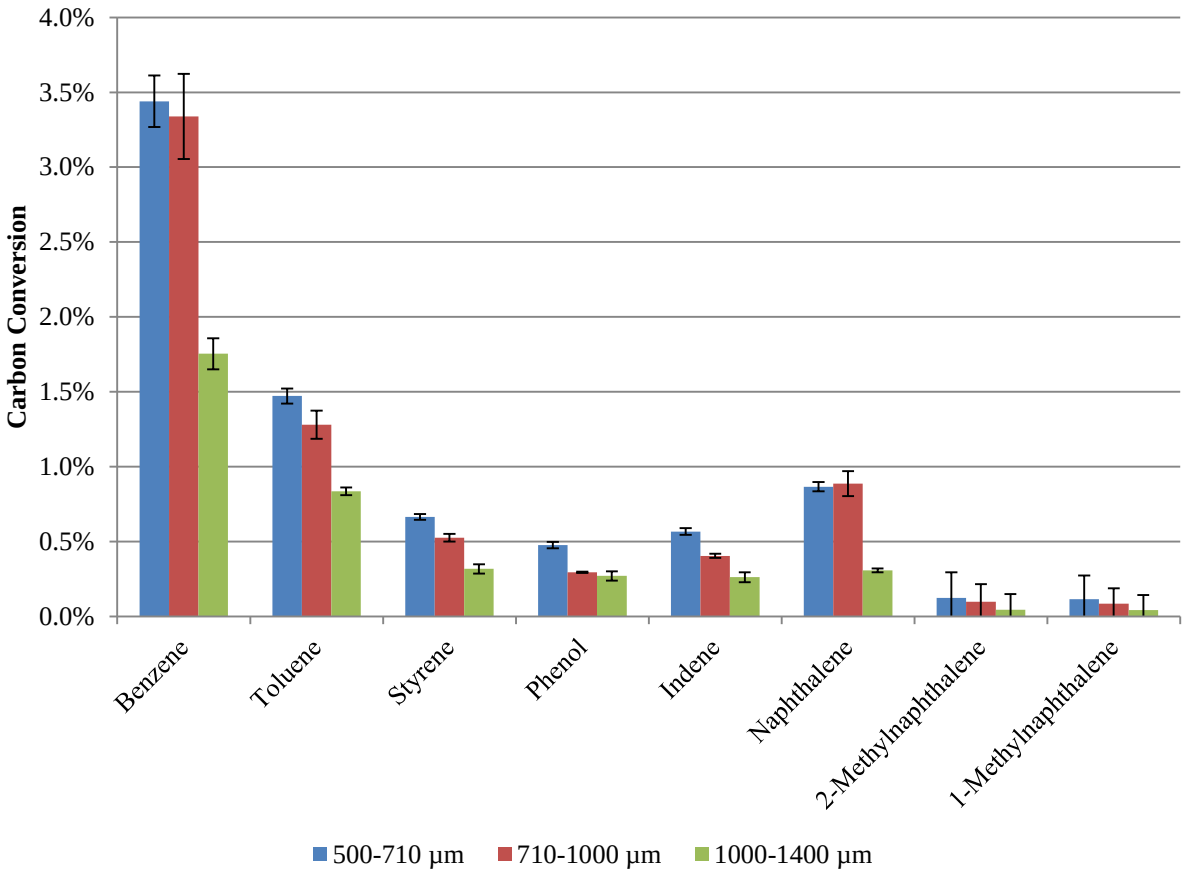

Figure 7-35: Tar species distribution for varied chip size intervals, system operated at 1000 °C, at atmospheric pressure, M/B = 5 and a residence time of 0.75 s.

An overview of the system mass balance is given in Table 7-7, which shows the various liquid, solid and gas distributions. Overall water production was observed to be minimized with the use of 710-1000 µm chip, whereas, the consumption of methane and production of solids was also the highest. The overall degradation value for the methane flow through the reactor was determined with a corresponding overall consumption of 5.8 ± 0.2 %.

Table 7-7: Various chips size fraction product distribution and mass balance.

		500-710 µm		710-1000 µm		1000-1400 µm		Degradation[xx]	
Methane In	*kg/hr*	0.290	±0.002	0.290	±0.003	0.290	±0.002	0.290	±0.002
Biomass In	*kg/hr*	0.058	±0.001	0.058	±0.002	0.046	±0.001	-	-
TOTAL	*kg/hr*	0.348	±0.002	0.348	±0.004	0.336	±0.003	0.290	±0.002
Mass Balance OUT)									
Gas Out	*kg/hr*	0.317	±0.005	0.322	±0.001	0.309	±0.001	0.275	±0.003
Water	*kg/hr*	0.014	±0.001	0.003	±0.001	0.010	±0.001	-	-
Tars	*kg/hr*	0.001	±0.000	0.002	±0.000	0.001	±0.000	-	-
TOTAL	*kg/hr*	0.332	±0.006	0.327	±0.001	0.320	±0.001	0.275	±0.003
Mass Balance	*Closure*	95%	2%	94%	±1%	95%	±1%	95%	±1%
Solids Mass flow rate	*kg/hr*	0.016	±0.006	0.021	±0.004	0.016	±0.003	0.015	±0.004
Char Production[xxi]	*kg/hr*	0.003	±0.006	0.004	±0.004	0.002	±0.003	-	-
Char Production	*Carbon Basis*	0.002	±0.003	0.002	±0.002	0.001	±0.001	-	-
Solids Fraction	-	5%	±8%	6%	±6%	5%	±8%	5%	±1%
Char	*Carbon Basis (Biomass)*	3%	±2%	4%	±2%	2%	±2%	-	-
Methane Consumption	-	-6.3%	±0.2%	-6.6%	±0.1%	-5.6%	±0.2%	5.1 %	±0.1 %

7.5.1 Effect of Chip Size Variation during Methanolysis

From the investigation it was observed that the use of 710-1000 µm chip produced the highest overall carbon conversion to gas products, with considerable ethylene and CO production. It is suspected that

[xx] Taken as an average value over the experiments conducted.
[xxi] Calculated relative to the degradation value obtained during the trial

the variation in the product distribution between the phases is due to the varied volatile characteristics, as shown in Figure 7-33. It is likely that the overall gas composition varies significantly due to the higher relative residence time which the expelled volatiles have in the reaction zone. The greater the residence times in the reaction zone, the greater the extent of secondary reactions, which are associated with tar and char production due to dehydrogenation reactions. This may explain the low gas, high tar and char product formed from the use of 500-710 µm chip. As the chip was the smallest fraction trialled, the volatile fraction which was released in the preliminary devolatilisation step of the pyrolysis pathway has the largest residence time in the reaction zone. Hence, this increases the tendency for the secondary reactions and was identified as possibly the main pathway for increased charring and tar formation. An opposing trend was observed with the utilisation of 1000-1400 µm chip, increased gas production and low tars and chars recorded. This was hypothesised due to the decreased residence time of the volatiles when released from the biomass matrix, which decreased the potential of secondary reactions occurring. Ultimately this was observed as a lower production of tars, with approximately half the amount of tars collected in comparison to using 500-710 µm chips. In accordance with the findings. Shen et al [14] reported, decreasing char and gas yields and increasing tar production with decreasing particle size when operating at 500 °C in a fluidised bed. Alternative trends were observed by Li et al [15], who determined a strong increase in the production of gas with decreasing particle size when comparing particle sizes of 0.45-0.9 mm and 0.30-0.45 mm at 800 °C in a drop tube reactor. When smaller particles were fed into the system it was observed that the gas in fact slightly decreased as well as the effective tar and solid fractions [15]. The work conducted by Septein et al. [13], shows that there were no considerable differences between product phase distribution and particle size, with ~ 80 % gas product, ~15 % tar and 5 % char reported when operated at 1000 °C. In this work it was also noted that the variation in distribution between particle sizes was apparent at lower temperatures of 800 °C.

Figure 7-34 also shows a strong increase in the apparent methane production which occurs with the utilisation of larger particle chips. When this value was compared to that of the effective methane consumption, Table 7-7, it was observed that the overall consumption of methane was the lowest of all chip fractions. It is possible that this indicates that there was effectively more methane produced through the utilisation of the larger chip. This was possible as the effective solids fraction production is significantly lower than for the other chip fractions. This showed that the increase in methane production causes less effective degradation, resulting in a larger gas phase product in comparison to 500-710 µm chip feed. Due to the difficulty in distinguishing pyrolytic methane products and feed methane it was difficult to ensure that the high methane production was not an artefact of decreased degradation. It was suspected however that methane was produced in larger quantities with the larger chip due to the chip characteristics, the residence time of the volatiles was longer through the chip, and the volatiles are suspected of undergoing cracking reactions when released from the biomass

matrix. This can be explained by the high ethylene yields which were related to higher levels of MTD due to continual dehydrogenation of the ethane formed. This would also justify the slightly higher ethane product which may not have fully reacted due to the lower residence time of the volatiles.

The tar product distributions observed in Figure 7-35 highlight the influence which increased residence time through the biomass/char matrix has on product distribution. With the smaller chip size fraction overall tar production was increased for almost all tar species measured. This was feasible due to the shorter residence times through the chip, which results in much larger tar species production. This was primarily due to the tendency of larger tar species to be further cracked into product gases and char. This suggests why the smaller chip fraction renders the lower gas and higher char fraction. It was also likely that due to the faster release of the volatised species, further secondary reactions could occur in the freeboard area due to the high temperature. This effectively explains why the char production was higher with lower particle size, in contradiction to literature [14], [15].

The utilisation of the 710-1000 µm chip was observed to reach a median between tar and char production, whilst, producing the highest proportion of gas. The effect of the chip size can also be described as a pseudo-residence time effect which arises due to the variations in residence time through the particle and consequently, the product gas residence time. The 710-1000 µm chip was observed to have a much higher overall gas product primarily due to the higher conversion of oxygen to CO rather than water. This characteristic was strongly influential on the gas product carbon conversion and was approximately 5 times lower than using the other two chip sizes. The pathway of methane steam reforming is unlikely as the hydrogen content of the 710-1000 µm trial was the lowest of all trials. The overall pathway for the production of CO and the low water content was unclear.

7.6 Experiments on Alternative Feedstocks

To conclude the experimental investigation of the flash methanolysis of biomass, trials were conducted with differing feedstocks to investigate possible feedstock composition influences on product distribution. Trials were also conducted to investigate initial feedstock conditions and the influence on the process product selectivity. Due to time constraints only one other biomass species was trialled within the system, Douglas fir, which is the 2nd most abundant forestry in New Zealand [16]. The chemical composition of Douglas fir is similar to that of Pinus Radiata with slightly lower cellulose and slightly higher hemicellulose concentrations within Douglas fir. The most apparent difference between the timber species is the lignin fraction with 5 % more lignin found within Douglas fir.

Table 7-8: Chemical structure of Douglas fir and pinus radiata feedstocks, Douglas fir data retrieved from [17].

Species	Glucose	Xylose	Galactose	Arabinose	Mannose	Lignin
Douglas fir	44 %	2.8 %	4.7 %	2.7 %	11 %	32 %
Pinus Radiata	45 %	4.6 %	2.4 %	1.2 %	11 %	27 %

Trials were also conducted with the bark of pinus radiata to determine the influence which bark may have on the product distribution. This is an important parameter as in commercial realisation of the product the debarking process can be controlled to determine the extent of bark 'contamination' within the feed. Due to the higher concentrations of tannins and polyphenolic compounds pyrolysis of bark has been observed to yield simple phenolic compounds such as phenol, catechol and furfural [18], [19]. Bark is also of interest due to the high concentration of mineral compounds present in bark, with an overall ash content of 3 % dry wt [20]. Due to the difficulty in analysing the influence of the char production and carbon formation from degradation on the overall system product selectivity, charcoal was trialled. Charcoal allowed for the simulation of char within the system to determine the distribution of products given the different chemical structure of the feed. Off the shelf charcoal was sourced from the Warehouse (Christchurch) and originated from African hardwood species as the preparation of pinus radiata generated char could not be conducted. To conclude the investigated biomass sources, a portion of 1000-710 µm pine chip was prepared and allowed to equilibrate with room moisture content, 12 % MC. The feed was then trialled as with all previous experiments to investigate the required extent of drying for the process feed.

For the analysis of Douglas fir feedstock, the outer sapwood was removed from the inner core wood and experiments were conducted on both separate portions of the tree. This was conducted as the

inner core wood of Douglas fir is known to have a much higher mineral content that the sap wood, it is also easily distinguishable on Douglas fir in comparison to pinus radiata. All trials were conducted with the reactor at the same set temperature of 900 °C with M/B =5 and an effective residence time of 1.5 s, Figure 7-36.

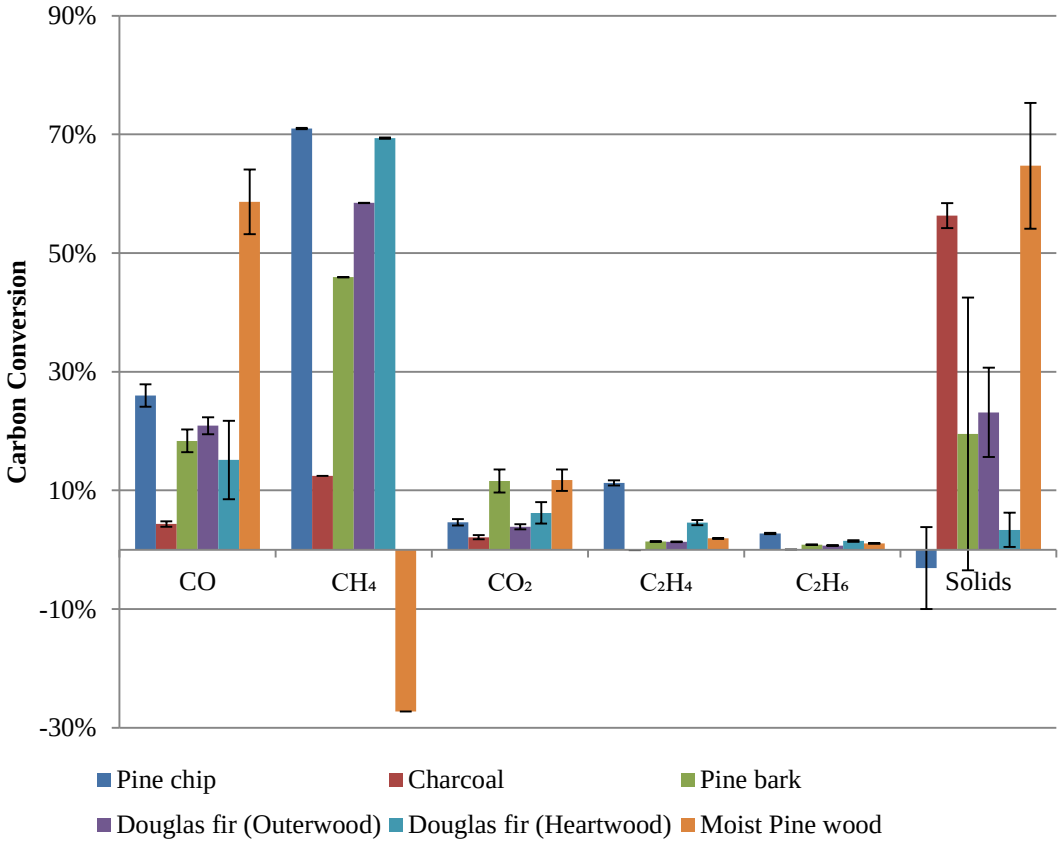

Figure 7-36: Gas species and solids fraction from trials with different feedstocks, System run with a bed temperature of 900 °C, M/B=5, atmospheric pressure and an effective residence time of 1.5 s [xxii].

It was observed that the utilization of Douglas fir resulted in increased CO and CO_2 yields in comparison to that of pine. Overall ethylene and ethane product selectivities were higher with the use of pine in comparison to that of Douglas fir. The use of moist pine resulted in high yields of solids with a high consumption of methane also noted, however, this trial resulted in the highest yields of CO. The use of charcoal also showed a high production of solids, interestingly there was no significant production of ethylene observed. Pine bark was observed to produce some of the highest CO_2 conversions recorded from the trials, with a much higher CO_2/CO ratio than all other feedstocks trialled.

[xxii] Charcoal assumed to have a carbon content of 70%.

To better understand the characteristics of the methane consumption and gas phase interactions of the product streams the hydrogen production was also monitored. The relative hydrogen production is given below in Figure 7-37, with the hydrogen production mass flow rate standardised against the degradation hydrogen mass flow.

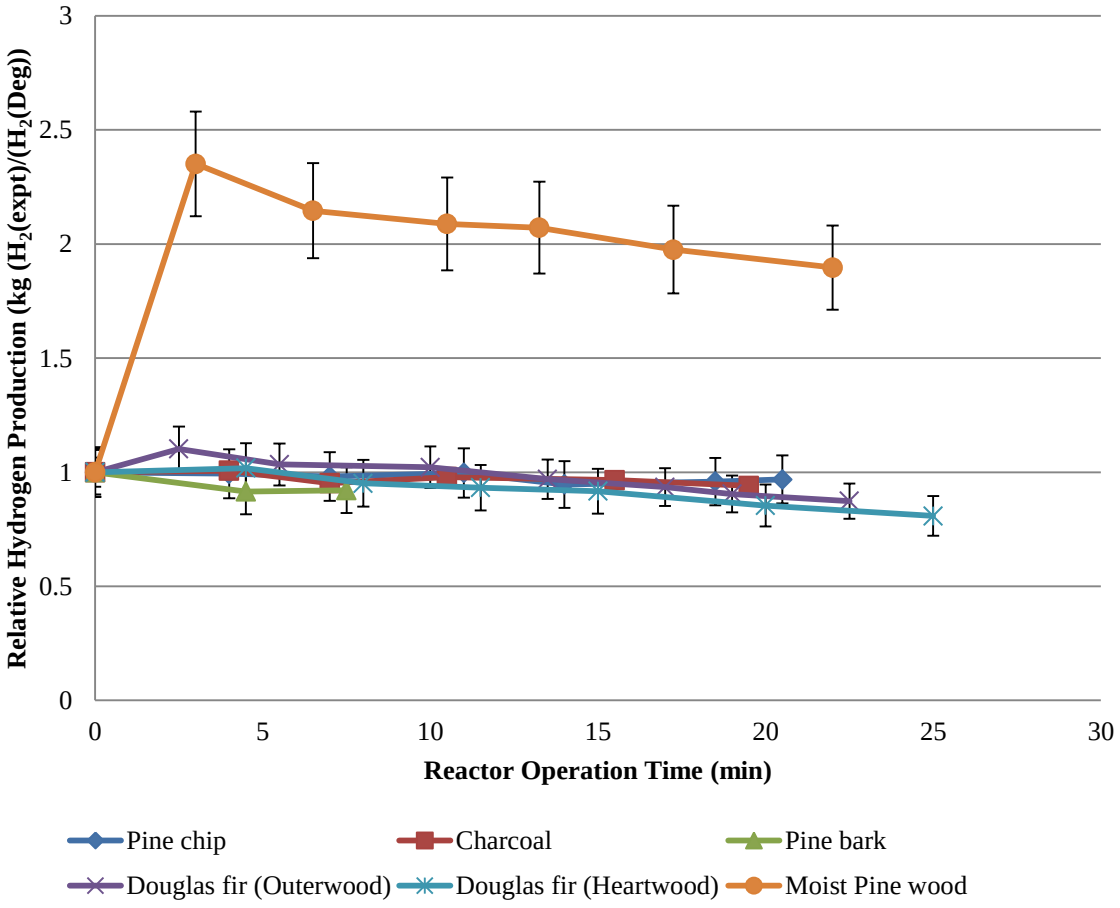

Figure 7-37: Standardized hydrogen mass flow rate ratio for alternative feeds, System run with a bed temperature of 900 °C, M/B=5, atmospheric pressure and an effective residence time of 1.5 s.

It was observed that Douglas fir outerwood and pine bark produced slightly more and slightly less hydrogen than all other feedstock other than moist pine, with overall relative hydrogen production relatively stable at a ratio of one. Moist pine was observed to increase hydrogen production significantly throughout the trialling period, with an average relative hydrogen production of ~2 throughout. Collectively for all feed materials a systematic decrease in the ratio is also observed, with an apparent relationship between hydrogen production and elapsed time, which was suspected to also be influenced by carbon deposition. This was reasoned as being due to the accumulation of carbon on the reactor surfaces, thus reducing the extent of degradation with elapsed time.

The tar fraction from the experiments was also analysed. High concentrations of benzene were recorded for the pine feedstocks with significantly more benzene, toluene and naphthalene formed from pine than any other feedstock, Figure 7-38. A blank trial was conducted with no feed to determine the extent of benzene production during degradation. It was determined that overall benzene production from methane thermal degradation did not significantly alter the proportion of benzene formed from the utilization of woody biomass. Other tar species such as phenol, o-cresol and styrene were only apparent for woody biomass feed stocks, whilst pine bark showed higher naphthalene production. Moist pine was observed to produce relatively high concentrations of both benzene and phenol during flash methanolysis of the feedstock.

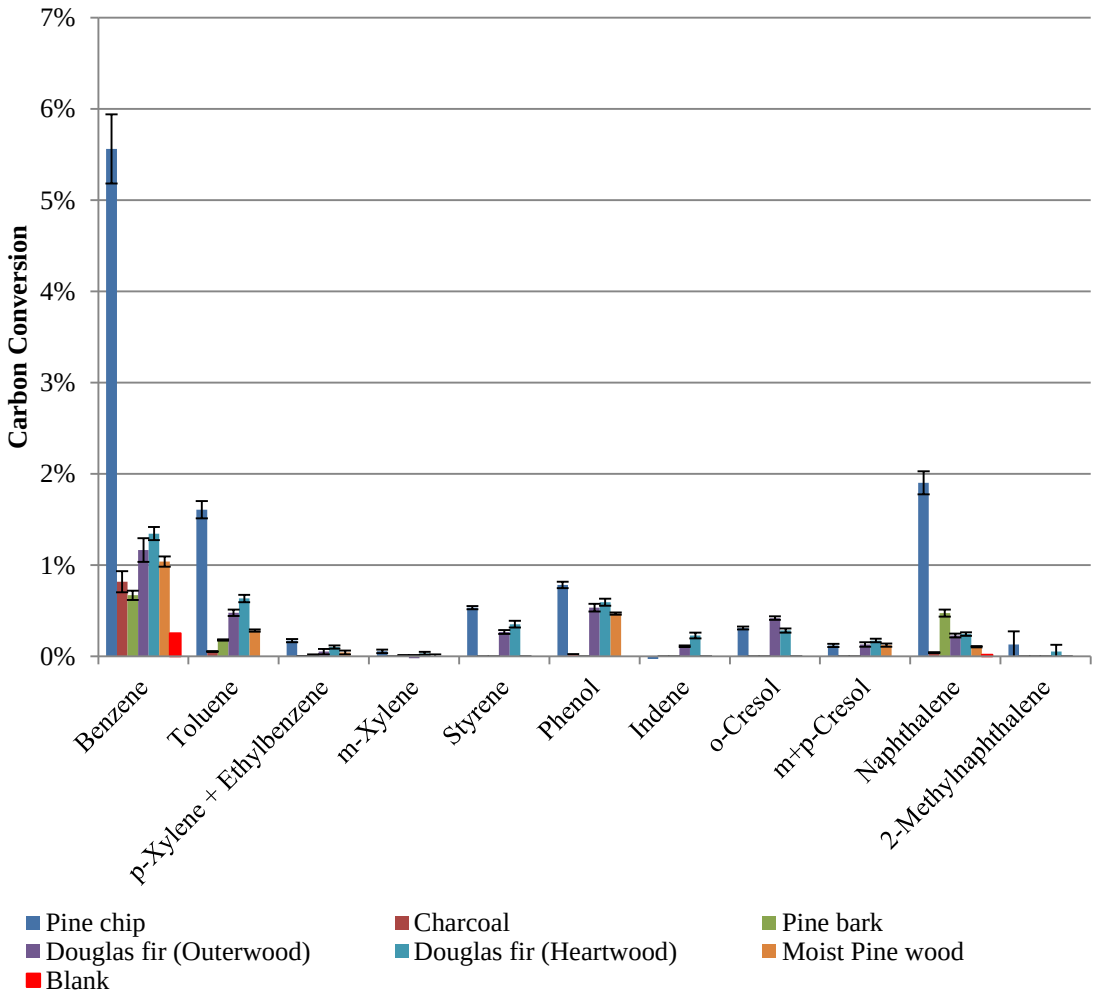

Figure 7-38: Tar fraction product distribution for alternative feeds. System run with a bed temperature of 900 °C, M/B=5, atmospheric pressure and an effective residence time of 1.5 s.

7.6.1 Alternative Feedstock Discussion

From the alternative feedstock investigation conducted it was discovered that the product selectivity varied greatly with the designated feedstock used. Overall it was determined that the use of pinus radiata rendered higher overall gas and tar production than Douglas fir. This was observed by higher yields of benzene and ethylene, CO production from Douglas fir was approximately constant between Douglas fir and pine.

Interestingly, the pine chip gave significantly higher yields of benzene than from any other feed stock, with an overall carbon conversion of 5.6 ± 0.4 %. The production of benzene from Douglas fir Outerwood and heartwood were 1.2 ± 0.1 % and 1.3 ± 0.1 %, respectively. Overall the production of toluene from pine chip was higher than the production of benzene from both Douglas fir sources. This large increase in tar production is difficult to understand as high benzene yields have been attributed to high lignin concentrations in feedstocks [21]–[24]. Possible variations in the production of benzene could be attributed to the increased extractive yields from pine chip, in comparison to that of Douglas fir. Overall tar production from pine chip accounted for 11 ± 1 % of the carbon conversion of the biomass. The overall potential for benzene production due to degradation of methane was determined as 0.30 ± 0.01 % carbon conversion on the basis of a theoretical mass flow rate of biomass. This shows that the increase in benzene is not due to degradation and is instead due to the chemical structure of the feedstock.

In highlight of the decreased benzene production from Douglas fir it is interesting to observe the relative formation of benzene from moist pine. The tar fraction collected from the moist trials indicate that benzene production decreased relative to that of the dried pine feed, but was similar to that obtained from Douglas fir. From TGA analyses it has been observed that the water fraction of the biomass is the first to devolatise from the biomass feed, resulting in the possibility for secondary reactions of biomass products with water. It is suspected that the addition of water inside the biomass matrix decreases the overall conversion of the feed due to the increase in steam reforming which occurs between H_2O and CH_4. This can be observed by the strong increase in hydrogen production, Figure 7-37, as well as the high CO production and methane consumption in Figure 7-36. Overall hydrogen production is observed to increase significantly in accordance to Equation (7.6.1), resulting in increased hydrogen concentration in the reacting gas, thus decreasing the methane-biomass reaction pathway. Overall relative hydrogen production is observed to be ~2, which regarding the stoichiometry indicates that there is potential for hydrocracking of the pine feed. From work conducted by Steinberg et al., Douglas fir was reacted with hydrogen gas at 900 °C with high conversions of biomass to methane and CO, [3]. From the study it was also observed that the CO fraction decreased with increasing pressure, whilst methane production increased strongly indicating a reversal of Equation (7.6.1). Benzene concentrations also showed decreased yields with lower

pressures and an apparent maximum at 3 Bar. It is the hydrogen which is formed from the reaction that decreases the C_2 hydrocarbon deposition due to the high concentration in the product gas facilitating the degradation of produced hydrocarbons. It is the inclusion of hydrogen in fact that increases the conversion of biomass through the mechanism described in Equation (7.6.2) and completes the subsequent degradation reaction to produce carbon. This would possibly explain the high solids content in the process as a result with the low ethylene and ethane concentrations.

$$CH_4 + H_2O \rightarrow CO + 3H_2 \quad (7.6.1)$$

$$C_2H_5 + H \rightarrow C_2H_4 + H_2 \quad (7.6.2)$$

The feeding of charcoal was characterised by large amounts of solid production during the methanolysis reactions. This is to be attributed to the poor characteristics which methane has as a gasifying agent for the residual carbon once the volatiles have been released. It is suspected this is due to the high amount of fixed carbon within the charcoal, as well as the low oxygen content of charcoal in comparison to biomass. Charcoal is observed to form a moderate amount of benzene with the reforming of the volatiles to be the main pathway for benzene production. This pathway was similar to that of the benzene production with biomass as the feed, however considerably less than pine due to the decreased volatile fraction. Overall the tar production selectivity showed a strong relationship with benzene and only small traces of toluene, phenol and naphthalene were measured. Overall carbon conversions of charcoal to gaseous species showed a low carbon conversion to methane as it was suspected that the char produced was catalysing the MTD. It is a well-known feature of char deposits with the autocatalytic nature of carbon very similar with the char-methane interactions, with the mineral content of char facilitating degradation and secondary reactions in the vapour [11], [25]–[27] From Figure 7-36 it is also observed that only trace amounts of ethylene were detected in the product gas. It was thought this indicates that char does not catalytically convert methane to ethylene (i.e. it either is devolatilized from the biomass or formed from a devolatilised species – the nitrogen trial results (below) suggests both routes are active). A slight decrease in the concentration of ethylene during the reaction of charcoal with methane indicates potential cracking of the produced ethylene formed from methane degradation. It is likely that this would occur through the C_2 cracking pathway described in Equation (7.6.3), which may also describe the low ethane concentrations as well.

$$\begin{aligned} 2CH_4 \rightarrow C_2H_6 \rightarrow C_2H_4 \rightarrow C_2H_2 \rightarrow 2C \\ + H_2 \quad + H_2 \quad + H_2 \quad + H_2 \end{aligned} \quad (7.6.3)$$

The flash methanolysis of pine bark was observed to produce relatively low conversions of all gas species bar CO_2. The pyrolysis of bark also resulted in relatively low solids production with overall residual solids less than 20 % of the inlet streams. Uncertainties arose with the utilization of bark due to the readiness of the feed to volatise and release the tannins and extractives inside the bark matrix. This resulted in a short trialling period as the feeder was more susceptible to blockage and this occurred only 10 minutes into the trial. The overall tar production from the pine bark utilization showed low conversions to benzene and toluene, with a higher respective naphthalene yield than Douglas fir and pine. The high CO_2 concentration is speculated to be due to the interactions of methane with the polyphenols extracts within the bark. As there appears to be no literature investigating the potential of the interactions between such species and methane the interactions are not well understood. The increased naphthalene may indicate that the aromatic rings are polymerised as a product of the interactions as well.

An interesting characteristic of the bark pyrolysis was the subsequent interaction of methane after the trial was conducted. Upon removal of the blocked feed and a complete burnout of the system it was apparent that the methane degradation characteristics of the system had varied greatly. It was observed that even after the system had been completely cleaned with all carbon removed with a high air volumetric flow rate significant degradation still occurred. It is that the increase in degradation of the system was due to the increased ash content of the bark feed stream. In work conducted by Lomax et al., pinus radiata bark was pyrolysed with an acetylene-air flame with an overall ash content of 3.5 % obtained, (mostly aluminium, calcium, potassium and silica) [18]. Aluminium, calcium and potassium are all proven catalytically active materials with product pyrolysis gases and tars [27]–[29]. A similar trend in degradation characteristics was observed after the feeding trials with charcoal, in which hydrogen and carbon deposition increased. The overall extent of methane degradation to hydrogen and carbon can be seen in Figure 7-39. Figure 7-39 also shows a strong increase in the overall hydrogen production and methane consumption with time, which is possibly caused by the attrition of the fluidised bed system increasing the effective surface area of the ash remaining in the system. Overall the entrainment and collection of ash within the system was identified as a significant issue, as overall methane flow into the system reacting zone was highly influenced by the presence of ash. Entrainment of the ash by increased air flow rate through the system was unsuccessful and complete removal of the bed for cleaning was observed as the only useful measure for complete removal.

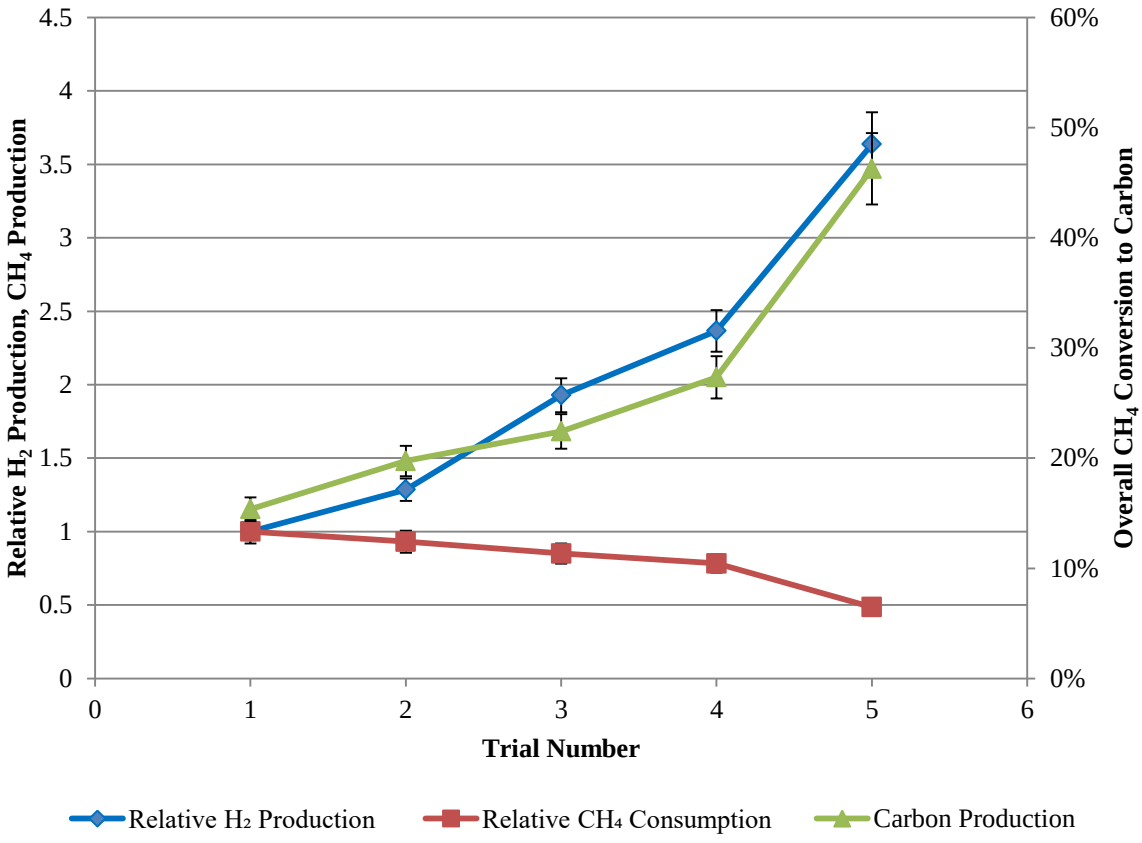

Figure 7-39: Methane degradation characteristics after the trial conducted with pine bark, where the relative mass flow rates of methane and hydrogen have been standardized against the pine chip degradation values. System at 900 °C, atmospheric pressure, residence time = 1.5 s. The trial number is given as a value corresponding to the date of which the trial was conducted after the initial bark trial.

7.7 Effect of Reactor Configuration on the Methanolysis of Biomass

To determine the reactor's effectiveness, the performance of a fluidised bed in the system was investigated and compared to other reactor configurations. This was especially important as a comparative measure for the investigation into the system characteristics with respect to previous work from Steinberg et al [2], [24], [30]. The system was investigated in three separate configurations; fluidised bed, packed bed and drop tube, Figure 7-40.

- Fluidised Bed: This reactor arrangement was identical to that which was utilized in the reactions described in the sections discussed above. To determine the influence of the bed height and the influence of constant residence time/ constant gas mass flow rate, two trials were conducted with a 40 mm bed and 53 mm bed. With the exchange of the quartz liner and use of a 40 mm bed the reactor could be operated with a constant residence time and similar mass flow rate in the reaction zone, with respect to the packed bed trial. The 53 mm bed trial was operated with the same mass flow rate, which resulted in a lower residence time. The fluidised bed arrangement was characterised by efficient heat transfer to the inflowing biomass, as well as decreasing temperature gradients axially through the reaction zone. The char and carbon formed during the reaction is likely to accumulate at the top of the fluidised bed and mix within.

- Packed Bed: The packed bed configuration refers to the use of the system without the bed present in the reactor. The quartz liner is present in the system and the quartz fritted disc provides an area where the biomass chip rests within the reactor. This in turn results in the biomass chip being subject to ideal reaction conditions as the fritted disc is located within the reaction zone. Due to this the char from the reaction is at elevated temperatures and is likely to completely devolatise during the course of the experiment.

- Drop Tube: The drop tube configuration consisted of the system operated without the quartz liner in place. The removal of the quartz liner allowed for interactions with the reactor walls and removed the collection of the biomass within the reaction zone. The system was operated in a counter-current configuration, where the feed travelled through the reactor and devolatilized as the particle passed through the reaction zone and preheater section. The char then accumulated on the bottom flange which was at a constant temperature of 100 °C.

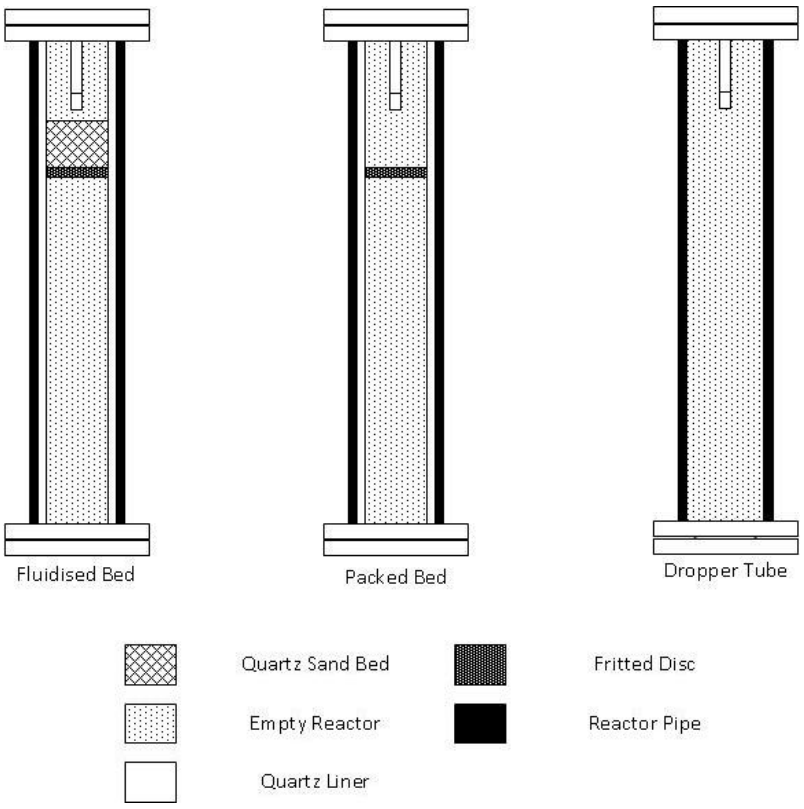

Figure 7-40: Reactor configurations of the fluidised bed rector, packed bed reactor and drop tube reactor.

7.7.1 Fluidised Bed and Packed Bed Reactor Configuration Comparison

During the design process and commissioning of the reactor a number of different quartz liner sleeve arrangements were utilized. This allowed for the system to operate with differing bed heights and preheater lengths, allowing for manipulation of gas residence time in the reactor. To determine the influence of the fluidised bed, the system was trialled with a 40 mm and 53 mm bed configuration as well as trials without a bed present. All trials were conducted with the quartz liner in place which composed of the quartz frit located at the respective position within the quartz liner. The effect of the fritted disc was also investigated with the trialling of the system without the quartz sleeve in place and the process being run similarly to a drop tube reactor. As the inclusion of the bed altered the residence time of the gas products in the reaction zone, two comparative trials were conducted. One trial allowed for a constant mass flow rate through the reaction zone 0.145 kg/hr, whilst, the other was at a constant residence time 0.58 s, Table 7-9.

Table 7-9: Product Distribution of product gases and degradation characteristics of the system at atmospheric pressure, with and without bed material at 970 °C.

		Packed Bed		**40 mm Fluidised Bed**[XXIII]		**53 mm Fluidised Bed**	
CH_4 Flow rate	*kg/hr*	0.145	± 0.004	0.121	± 0.003	0.145	± 0.004
Biomass Flow rate	*kg/hr*	0.033	± 0.001	0.027	± 0.001	0.033	± 0.001
M/B Ratio	-	4.4	-	4.5	-	4.4	-
Residence Time (Reaction Zone)	*s*	0.58	± 0.05	0.53	± 0.05	0.28	± 0.05
Gas Products							
CO	*Carbon Conversion*	34%	± 3%	49%	± 8%	41%	± 7%
CO_2	*Carbon Conversion*	5%	± 1%	6%	± 1%	5%	± 1%
C_2H_4	*Carbon Conversion*	13%	± 1%	22%	± 4%	15%	± 3%
C_2H_6	*Carbon Conversion*	3%	± 0%	3%	± 1%	4%	± 1%
TOTAL	*Carbon Conversion*	55%	± 4%	80%	± 10%	60%	± 10%
Proportional Conversions (Gas production rate/CH_4 Degradation rate)							
Residence Time (Reaction Zone)	*s*	0.58	-	0.53	-	0.28	-
H_2	*(kg/hr)/(kg/hr CH_4)*	0.104%	± 0.005%	2.9%	± 0.2%	2.0%	± 0.2%
CH_4	*(kg/hr)/(kg/hr CH_4)*	98%	± 4%	86%	± 7%	95%	± 8%
C_2H_4	*(kg/hr)/(kg/hr CH_4)*	0.180%	± 0.009%	0.9%	± 0.1%	0.18%	± 0.02%
C_2H_6	*(kg/hr)/(kg/hr CH_4)*	0.140%	± 0.008%	0.14%	± 0.01%	0.30%	± 0.03%
Carbon Formation	-	2%	± 4%	10%	± 7%	3%	± 8%
Oxygen Conversion							
CO	*Mol%*	49%	± 5%	70%	± 10%	40%	± 7%
CO_2	*Mol%*	13%	± 1%	17%	± 3%	10%	± 2%
H_20	*Mol%*	39%	± 5%	16%	± 5%	50%	± 7%

Inclusion of the bed greatly increased the overall carbon conversion of the feed biomass (Table 7-9). A 40 mm bed was utilized in a quartz liner with a slightly higher fritted disc location, this allowed for a constant residence time to be applied through the system, taken as 0.56 ± 0.07 s. The 53 mm bed trial indicated the effect of the bed for a constant mass flow rate of methane through the system of

[XXIII] Operated in different quartz liner configuration

0.145 ± 0.004 kg/hr. For a similar residence time of 0.56 ± 0.07 s the inclusion of the 40 mm bed resulted in an increase in carbon conversion to gaseous products from 55 ± 4 % to 80 ± 10 % carbon conversion, respectively. The increased conversion to gaseous products was due to the increased heat transfer with the inclusion of the bed. The entering biomass was heated by conduction by the sand particles, providing efficient and rapid heating. This in turn, reduced the proportion of feed which remained as char. At a constant flow rate of 0.145 ± 0.004 kg/hr it was observed that the inclusion of the 53 mm fluidised bed increased the overall carbon conversion to gaseous products as well. However, due to the large uncertainties in the derived values there does not seem to be an inherent carbon conversion increase with a constant residence time. From the oxygen balance, it was observed the production of CO was favoured with the inclusion of the bed (for a constant residence time). For the constant residence time of 0.56 ± 0.07 s, 70 ± 10 % of the oxygen from biomass produces CO, in comparison to an overall oxygen conversion of 49 ± 5 % obtained when the reactor was operated without a bed.

For a constant residence time, the operation of the reactor with a bed increased the overall carbon conversion to tars from 12 ± 1 % to 17 ± 2 %. However, for an equivalent mass flow rate, a significant decrease in the production of tars was observed where the tar fraction accounted for 4.3 ± 0.3 % carbon conversion of the inlet biomass, Table 7-10. It was observed that the inclusion of a bed increased the array of tar species produced for a constant residence time. However, for a constant residence time, the selectivity of benzene production remained constant at 66 % of overall tar yields for the different reactor configurations. Overall the tar productions were higher for the 40 mm bed trial and packed bed trial than the 53 mm bed trial, with an overall tar carbon conversion of; 17 ± 2 %, 12 ± 1 % and 4.3 ± 0.3 %, respectively. It was suspected that the increased production of tars was attributed to the increased residence time of the system. This is observed in previous work where the overall residence time has shown a strong relation to the production of tars. Primarily the tar production is predominantly benzene, toluene and naphthalene, suggesting that the aromatic structure of the tars is stabilized by the removal of the functional groups about the aromatic rings.

Table 7-10: Tar production and overall mass balance of system experiments with and without fluidised bed at 970 °C and atmospheric pressure.

		Packed Bed		**40 mm Fluidised Bed**		**53 mm Fluidised Bed**	
CH_4 Flow rate	*kg/hr*	0.145	± 0.004	0.121	± 0.003	0.145	± 0.004
Biomass Flow rate	*kg/hr*	0.033	± 0.001	0.027	± 0.001	0.033	± 0.001
CH_4/Biomass Ratio	-	4.4	-	4.5	-	4.4	-
rt (Reaction Zone)	*s*	0.58	± 0.05	0.53	± 0.05	0.28	± 0.05
Tars							
Benzene	*Carbon Conversion*	7.8%	± 0.7%	11%	± 2%	3.2%	± 0.3%
Toluene	*Carbon Conversion*	2.6%	± 0.2%	2.5%	± 0.3%	1.0%	± 0.0%
Styrene	*Carbon Conversion*	0.0%	± 0.0%	0.6%	± 0.1%	0.2%	± 0.1%
Phenol	*Carbon Conversion*	0.0%	± 0.0%	0.2%	± 0.0%	0.1%	± 0.1%
Indene	*Carbon Conversion*	0.1%	± 0.0%	0.6%	± 0.1%	0.0%	± 0.0%
(m+p) cresol	*Carbon Conversion*	0.0%	± 0.0%	0.1%	± 0.0%	0.0%	± 0.0%
Naphthalene	*Carbon Conversion*	1.6%	± 0.2%	1.5%	± 0.2%	0.2%	± 0.0%
2-Methylnaphthalene	*Carbon Conversion*	0.3%	± 0.3%	0.2%	± 0.1%	0.0%	± 0.1%
1-Methylnaphthalene	*Carbon Conversion*	0.2%	± 0.3%	0.2%	± 0.1%	0.0%	± 0.1%
Biphenyl	*Carbon Conversion*	0.0%	± 0.0%	0.1%	± 0.3%	0.0%	± 0.0%
Acenaphthylene	*Carbon Conversion*	0.0%	± 0.0%	0.2%	± 0.2%	0.0%	± 0.0%
Total Tars	*Carbon Conversion*	12%	± 1%	17%	± 2%	4.3%	± 0.3%
Overall Mass Balance							
Gas[xxiv]	-	90%	± 7%	100%	± 10%	90%	± 10%
Water	-	4%	± 2%	2%	± 1%	4%	± 2%
Tars	-	1%	0%	1.3%	0.4%	0%	0%
Solids	-	5%	4%	0.2%	13%	6%	12%
Relative Char	-	4%	-%	-8%	-%	5%	-%
Relative Carbon	-	2%	-%	30%	-%	1%	-%

[xxiv] Including the outlet mass flow rate of methane

From the mass balance it was determined that the overall carbon conversion to gaseous products was slightly increased for a similar residence time. The most notable increases in the selectivity of the products were the increases in carbon conversion to CO and C_2H_4. For a constant mass flow rate the overall gas, water, tar and solids production distribution remained relatively stable. Overall increases in gas production in the bed system, at a constant residence time, are thought to be due to decreased solids production in the system. The overall solids production is reported as 0.2 ± 13 % which indicates that it is likely that with the incorporation of the bed increased interactions between the formed carbon from MTD and char. For a lower residence time this effect is not observed and the overall solids production was derived as 6 ± 12 %. This is suspected to be due to the significant effect which residence time has on the interactions of the biomass volatiles with the char/carbon, which is discussed in full in Section (7.2).

7.7.2 Drop Tube Reactor Configuration Comparison

To conduct comparative trials with literature from Steinberg et al [3], [24], [30] , the reactor was also operated without the quartz liner installed which exposed the reactor surface to gases in the reactor during methanolysis, (drop tube). The bare reactor system was trialled to investigate the influence of construction material and the possibility of non-homogenous reactions occurring on the reactor surfaces. This also allowed for an indication of the influence which quartz has on the system, for example whether quartz reactor surfaces were inert. The trials differed in regards to the motion of the particles within the system between the trials. For the bare reactor trials the feeding characteristics were different than that of the packed bed reactor configuration. This was due to the removal of the quartz liner, removing the fused sinter disc, thus the particles travel through the reactor and rest at the bottom flange which is significantly cooler ~100 °C. For the bare reactor trials the reactor effectively operated as a counter current drop tube reactor. As the system was not designed to run in such a manner it is likely that during the pyrolysis process the char which formed was recirculated at the bottom of the reactor as the methane entered. To counter this effect a low mass flow rate was chosen which related to three times the minimum fluidisation of the sand bed. This minimised possible re-entrainment of the char into the high temperature reaction zone. It was assumed that there was no influence on the methane degradation from the char collecting at bottom.

A notable difference between the operation of the bare reactor configuration and that of the quartz liner without the bed was inclusion of the quartz frit within the system. This effectively allowed the char to ‘rest’ within the optimal zone for interaction with both the products of pyrolysis and the reacting methane gas. The presence of char being known to both catalyse the degradation of methane [10] as well as the conversion of biomass pyrolysis product gases [31]. Due to the differing orientations of the process the quantification of the effective time in the reaction zone is difficult and becomes subject to large uncertainties. This is due to the likelihood of gaseous compounds and tars

being released as the biomass particles descend. It is possible that this is due to the effective residence time of the tar species varying, depending on the position of the vapour release in the reactor. This effect is also compounded in the use of a counter flow arrangement, causing the released tars to interact with incoming particles as well as released volatiles during the particle pyrolysis. It is however assumed that the significant proportions of species released are within the reaction zone. Figure 7-41 shows the distribution of gas species from the trials conducted with the drop tube and packed bed configuration.

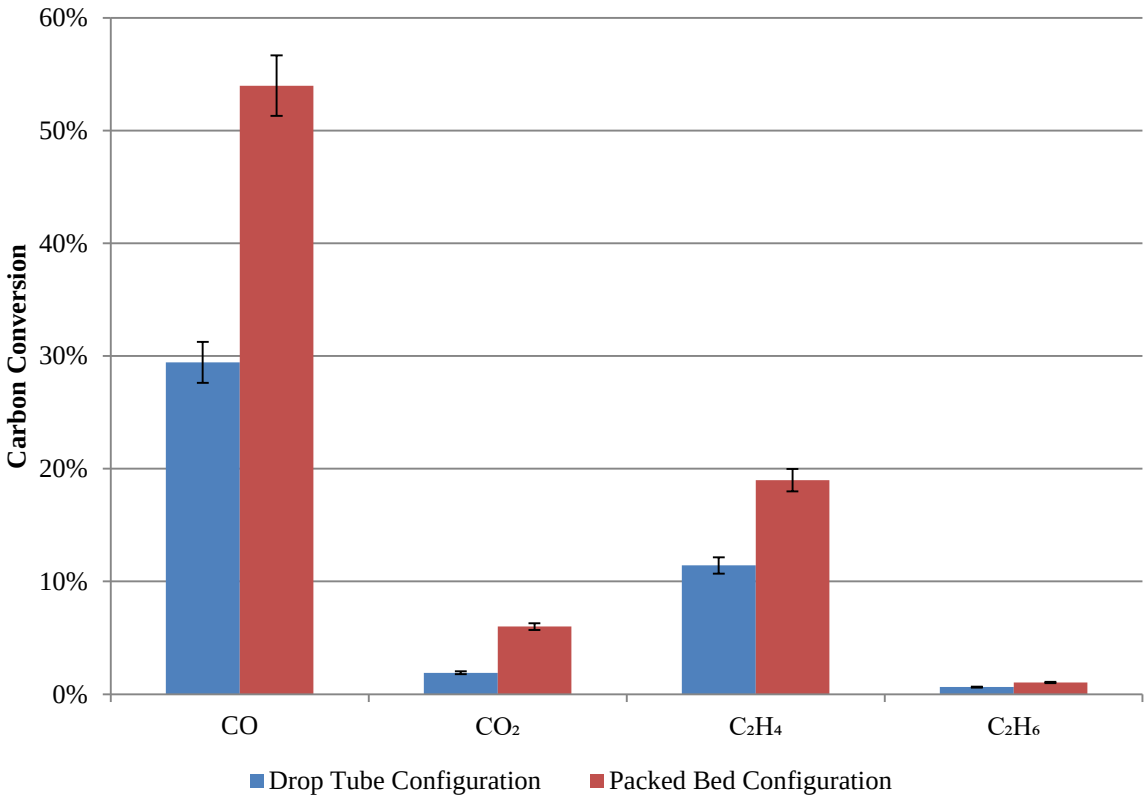

Figure 7-41: Carbon conversion of biomass gas fraction selectivity, system run at 970 °C, at atmospheric pressure, 4.5 M/B ratio with an effective residence time of 1.32 s in the reaction zone.

The overall gas production of the system is increased with the addition of the packed bed quartz configuration, Figure 7-41. This is suspected to be due to the decreased catalytic activity of the quartz sleeve, as well as the increased overall conversion of the biomass particle. CO and C_2H_4 carbon conversions increase from 29 ± 2 % and 11 ± 1 % to 54 ± 3 % and 19 ± 1 %, respectively. The overall ethane concentration is observed to remain relatively low independent of the reactor system. A large variation in the CO_2 is observed with 6.0 ± 0.3 % carbon conversion recorded for the packed bed system, in contrast to 1.9 ± 0.1 % from the bare reactor trial. Overall tar conversions were also analysed within the system and are tabulated below, Table 7-11.

Table 7-11: Tar distribution with differing reactor configurations.

		Drop Tube Reactor		Packed Bed Reactor	
Benzene	*Carbon Conversion*	13.8%	± 0.4%	9.6%	± 0.8%
Toluene	*Carbon Conversion*	1.5%	± 0.1%	0.6%	± 0.1%
p-xylene + Ethylbenzene	*Carbon Conversion*	0.0%	± 0.0%	0.2%	± 0.0%
m-xylene	*Carbon Conversion*	0.0%	± 0.0%	0.1%	± 0.0%
o-xylene	*Carbon Conversion*	0.0%	± 0.0%	0.1%	± 0.0%
Styrene	*Carbon Conversion*	0.0%	± 0.0%	0.1%	± 0.0%
Indene	*Carbon Conversion*	0.0%	± 0.0%	0.1%	± 0.0%
Naphthalene	*Carbon Conversion*	0.0%	± 0.0%	0.2%	± 0.2%
TOTAL	*Carbon Conversion*	15.3%	± 0.5%	11%	± 1%

From the tar analysis it is evident that the overall yield of tar decreased with the use of the quartz liner configuration. Overall the tar fraction was observed to decrease from 15.3 ± 0.5 % to 11 ± 1 % with the inclusion of the quartz liner. Benzene was the primary product of the process, with the use of the bare reactor producing a very uniform tar sample, whilst the quartz configuration rendered a number of different tar species. Toluene production also increased with the use of the drop tube arrangement, whilst, naphthalene production decreased and was undetectable. This is possibly due to the catalytic influence of the reactor walls promoting the formation of mono-cyclic aromatic species.

7.7.3 Discussion on the Effect of Reactor Configuration during Methanolysis

When investigating the effect of the addition of bed material to the reactor it was observed that the overall carbon conversion of the biomass feed varied. The additional bed material altered the residence time of the gas in the reaction zone, so a trial was conducted where the gas mass flow rate was decreased to provide a constant residence time (40 mm bed trial). Another configuration was trialled which allowed for a comparison of the system at constant mass flow rate with a 50 mm quartz sand bed. It was observed that the inclusion of the bed increases the efficiency of the biomass conversion which is possibly due to the increased heat transfer rate during fluidisation and enhanced methane/biomass mixing. The production of gaseous species CO and C_2H_4 sharply increased with the inclusion of bed material which led to overall productions of 49 ± 8 % CO and 22 ± 4 % C_2H_4 at a residence time of 0.53 s. The high CO yield indicates a low conversion of oxygen to form water, so

the water gas shift reaction was probably not the dominant reaction mechanism in the production of CO. This is suggested due to the low equilibrium constant for the WGS reaction, where K_{WGS} = 0.69 for the production of CO and H_2O at 1243 °K[XXV]. Therefore, with the increased residence time and inclusion of a bed, the interaction of the water produced increases the conversion to CO.

A decrease in carbon formation from the degradation of the methane with the inclusion of the bed materials is observed as the solids fraction reduces, Table 7-9. With the inclusion of the bed, overall solids production was observed to decrease as the overall proportion of gas produced increased. When regarding the constant mass flow rate of the 53 mm bed configuration the overall solids fraction remained unchanged. The carbon produced was suspected of increasing the degradation of the inlet methane as it has been reported that carbon has a tendency to catalyse MTD increasing hydrogen production [32]. The inclusion of the fluidised bed is expected to facilitate the complete conversion of the carbon which accumulates in the bed. Due to the increased heat and mass transfer which was achieved with the addition of a bed, in comparison to the empty bed. In regards to the char production, the overall solids production was lower than the initial degradation value for carbon deposition. This suggested that there were interactions with the devolatilized species from biomass and the carbon which was adhered to the reactor interior surfaces. The mechanisms of the interactions between the degradation products and that between the pyrolytic products are very complicated with a large assortment of possible pathways. In work regarding the deactivation of ammonia forming, carbon black catalysts, it has been noted that the interaction of methane with carbon black at temperatures above 340 °C have led to the formation of H_2, CO and CO_2 [33]. This is akin to the interactions which are suspected with the carbon/char interactions, where oxygen-bearing gaseous products are formed from interaction with oxygenated carbon material. It is suspected that this is far more influential in the production of the char and the interactions of the char with the incoming fluidising gas. This effect is also increased by the catalytic tendency of trace elements which accumulate in the biomass char structure and ash [34], [35]. Methane production has also been observed at operating temperatures of 500 °C with an observed mass decrease in carbon black in the presence of hydrogen gas. It is unclear how other product species such as; ethylene, ethane and benzene interact with the carbon black which is formed during MTD. Literature is scarce on the interaction of the noted species with carbon black, with the most notable interactions being between methane and carbon black species [36]–[38]. It was suggested that other species in the vapour phase are likely to interact with the carbon which was deposited within the reactor due to the relative ease of methane to interact with the surface of commercial carbon surfaces [38]. The main vapour phase chemical reaction pathways are suggested to be those described in Figure 7-42. It is hypothesised that the hydrogen from the degradation and methanolysis of biomass facilitates dehydrogenation reactions in the reaction scheme. The reaction

[XXV] From: $K_2 = exp(\frac{4400}{T} - 4.036)$, for: $CO + H_2O = CO_2 + H_2$

pathways of the oxygenated gas species are unknown and the overall conversion of CO and CO_2 interchangeably is not expected to be significant.

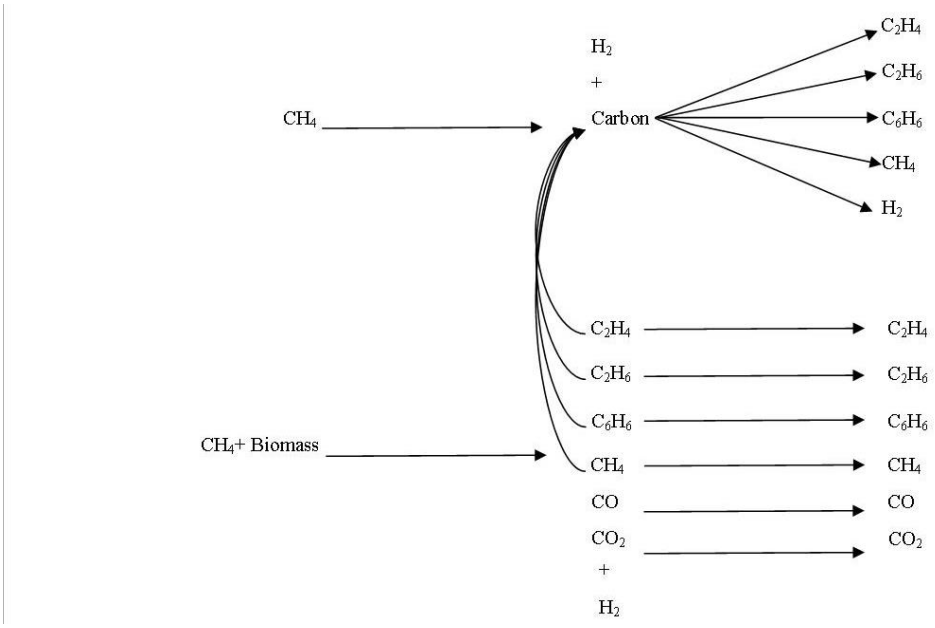

Figure 7-42: Schematic of the gas species interactions with carbon formed from the thermal degradation of methane.

Overall tar production was observed to increase with the addition of the fluidised bed within the system. Decreases in the overall yield of the tar fraction at constant mass flow rates are likely due to the residence time effect and not directly from the bed inclusion. The effect of residence time on product distribution will be discussed in more detail in the following sections. An increase in the overall tar production was observed between the packed bed and 40 mm bed reactor configuration, indicating the increase in efficiency of tar production with increased heat transfer and decreased temperature gradients within the reaction zone. Due to the increased uniformity in temperature across the reaction zone, the tar production increased with an increase in average temperature, which will be discussed further in the following sections. From Figure 7-41 it is observed that the overall gas production was decreased when using the bare reactor configuration in comparison to the packed bed configuration. This was due to the incomplete pyrolysis of the feed chip which resulted in overall poor carbon conversion of inlet biomass. In comparison, the packed bed configuration allowed for extended exposure of the biomass chip at the reaction conditions. Reliable values of hydrogen formation during degradation were difficult to obtain during the trials due to the high residence times of the gas in the system. This resulted in a long period of conditioning before reliable data could be sourced. Replicate data was obtained through subsequent trials and showed hydrogen concentrations of 39-34 ± 0.2 % H_2 for both data sets. The overall hydrogen production mass flow rate was significantly higher for the packed bed reactor configuration in comparison to the bare reactor trial, as seen in Table 7-12.

Table 7-12: Degradation and relative hydrogen production, where the relative hydrogen production is standardised to the methane inlet mass flow rate (0.066 kg/hr).

		Drop Tube Reactor		**Packed Bed Reactor**	
Relative Hydrogen Production	$H_2/CH_4(in)$	5.0%	± 0.7%	7%	± 1%
Degradation gas outlet concentration	*vol%*	34.0%	± 0.2%	39.0%	± 0.2%

Overall decreases in the hydrogen production for the bare reactor trial are suspected to be due to the interactions of the hydrogen formed from degradation and biomass. It is likely that the hydrogen reacts with the primary products from the flash methanolysis of the biomass, in particular, the methanolysis products from the lignin component. Lignin has been attributed to the production of the aromatic tar production during methanolysis [3], due to the cyclic structures within the lignin lattice. This is suspected due to the potential of the reactor surface catalysing the aromatic tar constituents to undergo dealkylation reactions to form stable benzene aromatic structures. It has also been noted that Mo and Zn oxide catalysts were active in producing benzene from direct thermal degradation of methane [39], [40]. Solymosi et al. [40], have reported overall selectivity of 54.2 % benzene when using $MoO3/SiO_2$ catalysts at 923 °K. Wang et al. [39], also suggested that the production of ethylene and hydrogen were active in the aromatization of methane when using a ZSM-5 catalyst incorporated with molybdenum, where, both species were identified at operating temperatures above 970 °K which was the same temperature at which benzene was evolved. [39].

7.8 Experiments with Nitrogen as Fluidising Gas

In literature, most studies of biomass pyrolysis have used inert gases such as nitrogen as the fluidising agent. This study used both nitrogen and methane in the experiments for a comparison of the behaviour and product selectivity between methane and nitrogen. When nitrogen is used the gas behaves as a stream to entrain the pyrolysis products and vary the extent of secondary reactions. As opposed to the use of methane as the fluidising agent, which also affects the extent of reaction, but also provides a reactive species which can influence the end product selectivity and distribution. The use of inert gases can also cause shifts in the chemical equilibria within systems, affecting product selectivity. Other common inert gases used in the pyrolysis of biomass include argon and helium which, due to the difference in heat capacity and diffusivity of the gas, have been found to vary product distribution. These gases can alter the heat and mass transfer properties of the product vapours which are released from the biomass particle. The utilisation of reactive gases such as methane provides the system with a reactive medium which is involved within the reaction pathway. Methane is also of interest due to the varying physical chemistry of the gas with significant differences in heat capacity, offering enhanced heat transfer to the particle as localised cooling is significantly reduced.

The use of methane also provides the economic opportunity for production of valuable product gases through the process of methanolysis in comparison to pyrolysis conducted with inert gas. Although methane is more expensive, abundant natural gas sources exist and can readily be applied given that the production of target species is greater with use of the gas. This is due to the higher costs of methane in comparison to nitrogen. As described by Steinberg et al. [3], methane is an attractive fluidisation medium as it is a product gas from pyrolysis and has been suggested to exhibit no net consumption. In the same report it was also suggested that the consumption/production of methane was unclear within the system, which enhanced the commercial viability. However, it is apparent that consideration of methane degradation during methanolysis may change this perspective.

Experiments were conducted to investigate the characteristics of methane and nitrogen flash pyrolysis in the reactor system with a packed bed reactor arrangement at 970 °C, Table 7-13. Comparative trials were also conducted with a constant molar gas flow/biomass ratio of 0.001 which allowed for a constant concentration of reacting gas to biomass. Overall the gas carbon conversion fraction is observed to increase significantly for the use of methane where the overall carbon conversion to gaseous molecules can account for 100 ± 11 % of the total carbon conversion at 0.142 kg/hr methane. Overall tar production was also observed to increase and vary with the use of methane gas. Benzene production was seen to increase to 11 ± 2 % carbon conversion with the use of 0.142 kg/hr methane. Benzene production decreased significantly with the use of nitrogen as the gas fluidising agent. This also resulted in also a lower overall carbon conversion to tars, whilst the nitrogen experiments showed

significantly higher char formation. The volumetric proportion of hydrogen in the product gas was significantly higher with the use of methane than nitrogen, which is highly likely due to the degradation of methane.

Table 7-13: Product distribution and system characteristics for pyrolysis conducted with N_2 and CH_4 as the process gas. System operated as a packed bed at 970 °C and at atmospheric pressure.

Feed Gas		**N_2**				**CH_4**			
Molar Flow/Biomass	***(Mol/hr)/(kg/hr)***	**0.0014**		**0.0010**		**0.0008**		**0.0010**	
Volumetric Flow rate	*SLPM*	2.50	± 0.02	2.50	± 0.02	4.80	± 0.02	3.60	± 0.02
Molar Flow rate	*mol/hr*	89	± 1	89	± 1	171.0	± 0.4	129	± 1
Gas Mass Flow rate	*kg/hr*	0.171	± 0.001	0.171	± 0.000	0.189	± 0.000	0.142	± 0.001
Biomass Flow rate	*kg/hr*	0.13	± 0.01	0.09	± 0.01	0.14	± 0.01	0.12	± 0.01
Carbon From Biomass	*kg/hr*	0.062	± 0.005	0.041	± 0.005	0.069	± 0.002	0.059	± 0.005
Overall Carbon Input	*kg/hr*	0.062	± 0.005	0.041	± 0.005	0.21	± 0.01	0.16	± 0.01
Molar Flow/Biomass	*(Mol/hr)/(kg/hr)*	0.0014	-	0.0010	-	0.0008	-	0.0010	-
H_2 Content Prod Gas	*vol%*	8.4%	± 0.2%	5.0%	± 0.1%	12.6%	± 0.4%	15.9%	± 0.4%
Gas Carbon Conversion									
CO	-	37%	± 2%	26%	± 2%	53%	± 3%	56%	± 3%
CH_4	-	18%	± 1%	14%	± 1%	43%	± 2%	17%	± 1%
CO_2	-	7%	± 0%	5%	± 0%	7%	± 0%	8%	± 0%
C_2H_4	-	8%	± 0%	5%	± 0%	15%	± 1%	16%	± 1%
C_2H_6	-	0%	± 0%	0%	± 0%	1%	± 0%	3%	± 0%
Total	-	71%	± 8%	50%	± 9%	118%	± 15%	100%	± 11%
Tar Carbon Conversion									
Benzene	*%*	5.4%	± 0.3%	7%	± 1%	8%	± 1%	11%	± 2%
Toluene	*%*	0.7%	± 0.01%	0.3%	± 0.0%	1.6%	± 0.0%	0.0%	± 0.0%
Styrene	*%*	0.2%	± 0.00%	0.2%	± 0.0%	0.3%	± 0.0%	0.0%	± 0.0%
Indene	*%*	0.3%	± 0.05%	0.2%	± 0.0%	0.3%	0.0%	0.0%	0.0%
Naphthalene	*%*	0.8%	± 0.04%	0.8%	± 0.1%	1.0%	0.1%	0.0%	0.0%
TOTAL	*%*	8%	± 0.4%	9%	± 1%	12%	2%	11%	2%

Carbon conversion to ethylene, CO and benzene were higher with the use of methane in comparison to nitrogen as reactor feed gas. When comparing the trials it is likely that the comparison of similar

molar flow/biomass trials represent the true influence of process gas. This is due to the similar molar flow of gas with biomass and removes the effect of differing relative molar compositions in the comparison, which were discussed in depth in the preceding sections. The high carbon conversion to CO is suspected to be a result of the interactions of the fed methane with the oxygen which is present within the biomass and embedded in the volatiles formed. It is suspected that there is a strong interaction of the methane with the oxygen bearing volatiles which are formed at 1243 °K. This is confirmed by the resulting oxygen balance which shows an increased proportion of water with the use of nitrogen, Table 7-14. It was unlikely that the increase of CO is attributed to the WGS reaction as this would be observed by increased water production. This is in agreements as the overall CO_2 oxygen balance proportion was constant throughout the trials. Consequently, it was suspected that the CO production arose from interactions of methane with water formed during devolatilisation, which subsequently undertakes the reforming of methane. This pathway would explain the high CO values, as well as the high H_2 increases, which although MTD is occurring, is significantly higher than that of nitrogen.

Table 7-14: Oxygen balance for system operating with nitrogen and methane as process gas. System operated as a packed bed at 970 °C and at atmospheric pressure.

Oxygen Balance		**N_2**				**CH_4**			
Molar Flow/Biomass	***(Mol/hr)/(kg/hr)***	**0.0014**		**0.0010**		**0.0008**		**0.0010**	
Volumetric Flow	*SLPM*	2.50	0.02	2.50	0.02	4.80	0.02	3.60	0.02
Gas Mass flow rate	*kg/hr*	0.171	± 0.001	0.171	± 0.001	0.189	± 0.001	0.142	± 0.001
CO	-	55%	± 4%	38%	± 3%	75%	± 5%	80%	± 6%
CO_2	-	19%	± 1%	15%	± 1%	20%	± 1%	20%	± 1%
H_2O	-	25%	± 2%	47%	± 3%	5%	± 0%	0%	± 0%

It is also possible that a portion of the CO production can be accounted for by the interactions of methane with the hydroxyl groups of cellulose and lignin, forming CO and H_2, equation (7.8.1). It is also possible that when nitrogen is used the oxygen within the biomass has a tendency to remain in the resulting char. This was observed by Septein et al. [13], where char products with up to 10 % oxygen content were produced when pyrolising beech wood at 1000 °C in N_2.

$$CH_4 + Biomass \rightarrow CO + 2H_2 \qquad (7.8.1)$$

Tar production is also suspected to be affected by the interactions of methane with the oxygenated branches of cellulose and lignin. The effective hydroxyl removal can stabilise the aromatic ring structure which is hypothesized to be the cause for the increased conversion to benzene with methane. The variation in tar distribution between reactor gases showed less variation than the gas and char distributions. It is supposed that methane interacts with the aromatic tar vapours and stabilizes the aromatic ring structure; whilst nitrogen gas, is suspected to increase carbon deposition through dehydrogenation reactions. It is noted, however, that the production of tars between nitrogen and methane was marred by the varying volumetric flow rates between trials, which allowed for a constant molar flow/biomass application to the system reacting zone. From the study of Steinberg et al [3], the carbon conversion for BTX (8 %) can be interpolated for the system operated at 970 °C and 345 kPa. This is in accordance with the values documented in Table 7-13, with tar production between 345-100 kPa relatively constant for BTX.

Another significant difference observed between the use of nitrogen and methane is the carbon conversion to ethylene. For corresponding molar flow/biomass trials the use of methane increases the overall ethylene production by a factor of three. A similar increase in ethylene production was observed from Steinberg et al. [3], with ethylene production using N_2 approximately half that of when methane is used as the process gas. From Steinberg et al. [3], it was suggested that the ethylene production was co-produced with benzene, and suggested the following radical pathway for hydrocarbon production, Equation (7.8.2).

$$HC\ free\ radicals + CH_4 \rightarrow\ C_2H_4 +\ C_6H_6 \qquad (7.8.2)$$

Therefore, the high ethylene concentration could be a combination of ethylene formed from degradation along with specific methane-biomass interactions, which were described in the previous sections.

7.9 Discussion of the Effects during Methanolysis

Throughout the experimental programme difficulties were encountered when determining trends between trials, due primarily to MTD. As well as the hydrogen production which resulted in mixed hydrogen/methane pyrolysis, degradation characteristics varied during the trials with significant differences observed between initial and final MTD values. Data on this effect was limited due to time constraints, once the effect had been identified; nevertheless, a representation of the extent of the degradation is shown below in Figure 7-43. The effective change in the product distribution was calculated by:

$$\Delta vol\% = vol\%_{\,Final} - vol\%_{initial} \tag{7.9.1}$$

This allowed for the relative decrease in methane consumption to be calculated, which was observed to decrease exponentially with increasing mass flow rate. It was observed that at flow rates below 0.182 kg/hr, the reduction in the amount of methane degraded increased before and after the trials.

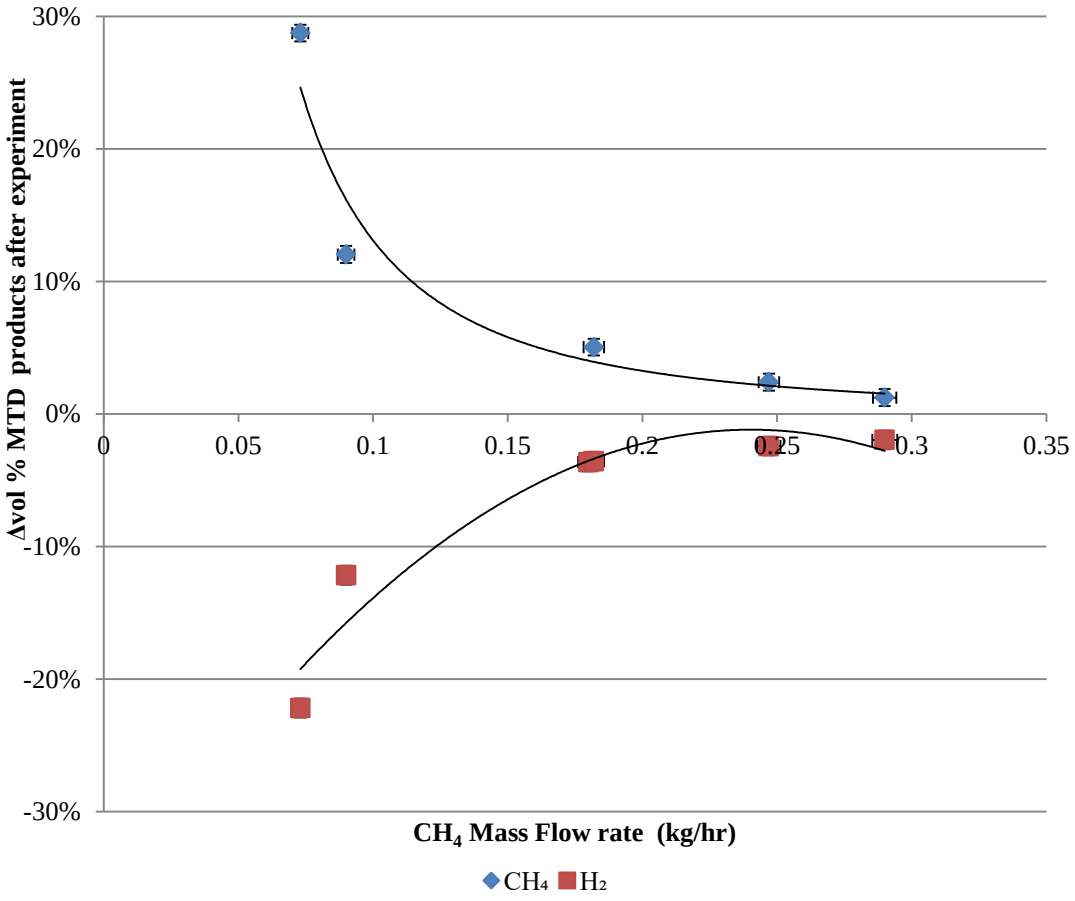

Figure 7-43: Change in product distribution of MTD products after methanolysis.

The data shown in Figure 7-43 was collaborated from various trials, and it was discovered that the correlation between the variations in degradation was proportional to the mass flow rate. Full detail of the operating conditions of the methane and hydrogen data can be found in Table 7-15. Interestingly, it was observed that the relative methane and hydrogen variation between trials was independent of the operating pressure and residence time. It was supposed that this indicated that the process of system conditioning was directly influenced by the operational mass flow rate of methane into the system. Hence, an overall cumulative amount of methane was required to render stable MTD values. This was important due to the apparent deactivation which was occurring, which proposed that the deposition of carbon formed from MTD prevented further degradation from occurring. This indicated that the MTD characteristics of the system were most probably dynamic during the operation of the reactor, which is likely to have affected the interactions of the methanolysis volatiles with the inlet gas. Nevertheless, as shown in Figure 7-43, the overall extent of this influence is more prominent with the lower flow rates < 0.180 kg/hr CH_4, where the variation in hydrogen and methane production can be expected to exceed 5 % during methanolysis. This allowed for the relative decrease in methane consumption to be calculated, which was observed to decrease exponentially with increasing mass flow rate. It was observed that at flow rates below 0.182 kg/hr, the change in the amount of methane degraded before and after the trials increased the most.

Table 7-15: System operating conditions for the relative methane and hydrogen variations before and after methanolysis as shown in Figure 7-43. All trials conducted at 960- 980 °C with M/B ~4.5-5.5.

Reaction Zone (rt)	**Pressure**	**CH_4 Inlet Flow rate**		**CH_4 Deg**	
[s]	*[kPa]*	*[kg/hr]*		-	
[XXVII]0.46	101	7.3 x10^{-2}	±2.9 x10^{-3}	61 %	14 %
0.87	135	9.0 x10^{-2}	±3.1 x10^{-3}	24 %	7 %
0.44	135	1.8 x10^{-1}	±3.8 x10^{-3}	17 %	0 %
0.87	270	1.8 x10^{-1}	±3.8 x10^{-3}	10 %	3 %
0.87	370	2.5 x10^{-1}	±4.3 x10^{-3}	18 %	1 %
[XXVI]0.14	101	2.9 x10^{-1}	±4.7 x10^{-3}	16 %	1 %

To determine the characteristics of carbon formation, a mass balance was conducted on two trials which had the degradation characteristics quantified. By measurement with the tracer helium gas, mass flow rate of the product species could be determined during MTD, effectively allowing for the derivation of the initial and final mass flow rates from a series of trials, Table 7-16. The carbon which

is produced during MTD is referred to as solids, due to the identification of hydrogen possibly bonded within the solids produced from MTD. It was determined that the solids production decreased from 79 ± 5 % to 30 ± 5 % between the final and initial MTD samples, respectively, when 0.073 kg/hr CH_4 was fed. With an increase in methane flow rate to 0.290 kg/hr, the overall solids produced were 6 ± 4 % initially, with a final value of 4 ± 4 %. It was also apparent that the solids produced were on average 96 wt% carbons and 4 wt% hydrogen.

Table 7-16: MTD product gases and composition of produced solids formed.

CH_4 Mass Flow rate		**0.290 kg/hr** [XXVI]				**0.073 kg/hr** [XXVII]			
		Initial		**Final**		**Initial**		**Final**	
H_2	*[kg/hr]*	$4.4x10^{-3}$	$\pm2x10^{-4}$	$3.6x10^{-3}$	$\pm1x10^{-4}$	$1.4x10^{-2}$	$\pm6x10^{-4}$	$7.3x10^{-3}$	$\pm3x10^{-4}$
CH_4	*[kg/hr]*	$2.7x10^{-1}$	$\pm1x10^{-2}$	$2.7x10^{-1}$	$\pm1x10^{-2}$	$1.3x10^{-2}$	$\pm5x10^{-5}$	$4.4x10^{-2}$	$\pm2x10^{-3}$
C_2H_2	*[kg/hr]*	$9.0x10^{-4}$	$\pm4x10^{-5}$	$1.3x10^{-3}$	$\pm6x10^{-5}$	$2.4x10^{-4}$	$\pm1x10^{-5}$	$1.8x10^{-4}$	$\pm8x10^{-6}$
C_2H_6	*[kg/hr]*	$5.1x10^{-4}$	$\pm2x10^{-5}$	$7.2x10^{-4}$	$\pm4x10^{-5}$	$9.8x10^{-5}$	$\pm5x10^{-6}$	$1.3x10^{-4}$	$\pm6x10^{-6}$
Total Gas Flow	*[kg/hr]*	$2.7x10^{-1}$	$\pm1x10^{-2}$	$2.8x10^{-1}$	$\pm1x10^{-2}$	$1.6x10^{-2}$	$\pm6x10^{-4}$	$5.1x10^{-2}$	$\pm2x10^{-3}$
Carbon Deposited	*[kg/hr]*	$1.7x10^{-2}$	$\pm1x10^{-2}$	$1.3x10^{-2}$	$\pm1x10^{-2}$	$5.7x10^{-2}$	$\pm3x10^{-3}$	$2.2x10^{-2}$	$\pm3x10^{-3}$
Solids Conversion	*[kg/hr]*	6%	±4%	4%	±4%	79%	±5%	30%	±5%
Hydrogen and Carbon Balance									
%C in Solids [XXVIII]	-	94%	±82%	95%	±111%	93%	±6%	100%	±20%
%H in Solids [XXVIII]	-	7%	±10%	6%	±13%	7%	±2%	0%	±4%
TOTAL	-	100%	±0%	100%	±0%	100%	±6%	100%	±20%
C/H Ratio of Solids	-	14	-	16	-	13	-	1958	-

Considering the MTD characteristics with an inlet methane flow rate of 0.073 kg/hr, the production of solids was observed to vary significantly, with the composition of the solid relatively stable. It was unlikely that the production of tar was significant during the MTD trials, as it was observed that for a mass flow rate of 0.145 kg/hr, with similar operating conditions, the overall tar carbon conversion accounted for <0.001 %. However, it was apparent that the solids composition derived agree with

[XXVI] Same Trials
[XXVII] Same Trials
[XXVIII] Measured from mass balance

carbon analyses which were conducted on a sample of carbon which was collected from a different trial, Table 7-17. The carbon which was analysed was collected during cleaning of the reactor when the deposition was first discovered. However, the composition of the analysed solids fraction was in agreement with the derivation of the composition taken from the MTD analysis. Nevertheless, the carbon and hydrogen concentrations are within the values which were derived which indicate that a portion of hydrogen within the system is bound within the MTD solids produced.

Table 7-17: MTD solids composition.

Species	Concentration
[-]	*[wt%]*
Carbon	94.2
Hydrogen	1.28
Nitrogen	0.23
Oxygen	2.4
Nitrogen	0.23
Sulphur	<0.01
Ash	0.03

It was also interesting to note the concentration of oxygen within the solids. It was likely that this may have arisen from the collection of char with the MTD solids when the sample was prepared; this was due to the difficulty in isolating the separate species, which at times were an amalgamated mixture of the two species. Due to the oxygen content of the MTD solids species produced, it was likely that the water content calculated from the mass balances were over estimates. This was due to the mass balance approach, which assumed that all oxygen which was not bound to CO and CO_2 was present as H_2O. This conclusion was supported by the modelling of the methanolysis process through, temperature, M/B ratio and pressure variations, as shown in Figure 7-9, Figure 7-25 and Figure 7-32, respectively. From the model it was proposed that the thermodynamics of the system tend to favour the production of CO, with very low concentrations of water at equilibrium expected. However, it was suspected that water is produced from the experiment and in turn, undertakes reforming of the inlet

methane to form hydrogen and CO. This was apparent from the utilization of moist biomass, which showed a large increase in CO and relative hydrogen production.

It was also established that the production of carbon highlighted a weakness of the model. As the model did not produce any carbon during the simulations of the reactor conditions, high concentrations of naphthalene were modelled. The extent of which, predicted the outlet product to be dominated by naphthalene production, resulting in very low methane concentrations to be suspected. The high naphthalene conversions are due to this species being thermodynamically favoured. However, it was suspected that the kinetics were too slow to proceed to the expected conversions. It is likely that the production of naphthalene however is a precursor, as Frenklach et al [41] proposed that the production of solids from aromatics underwent a H abstraction C_2H_2 reaction pathway (HACA). Böhm et al [5], also utilized this pathway and determined that the formation of solids through this pathway were limited by the kinetics of the formation of the outer rings, which included the formation of naphthalene, anthracene and pyrene. It was suspected that this route through the MTD is unlikely, and that the production was due to the dehydrogenation of ethane produced from the degradation. Nevertheless, due to this weakness in modelling, the system was modelled without naphthalene, resulting in benzene production being favoured, which was in agreement with the values determined experimentally. When considering the model for the MTD it was determined that the benzene production increased from 4.1 % to 5.4 % with an increase from 900 °C to 1000 °C, respectively. Increases over the same temperature region were also recorded for ethylene and acetylene as shown in Figure 7-44.

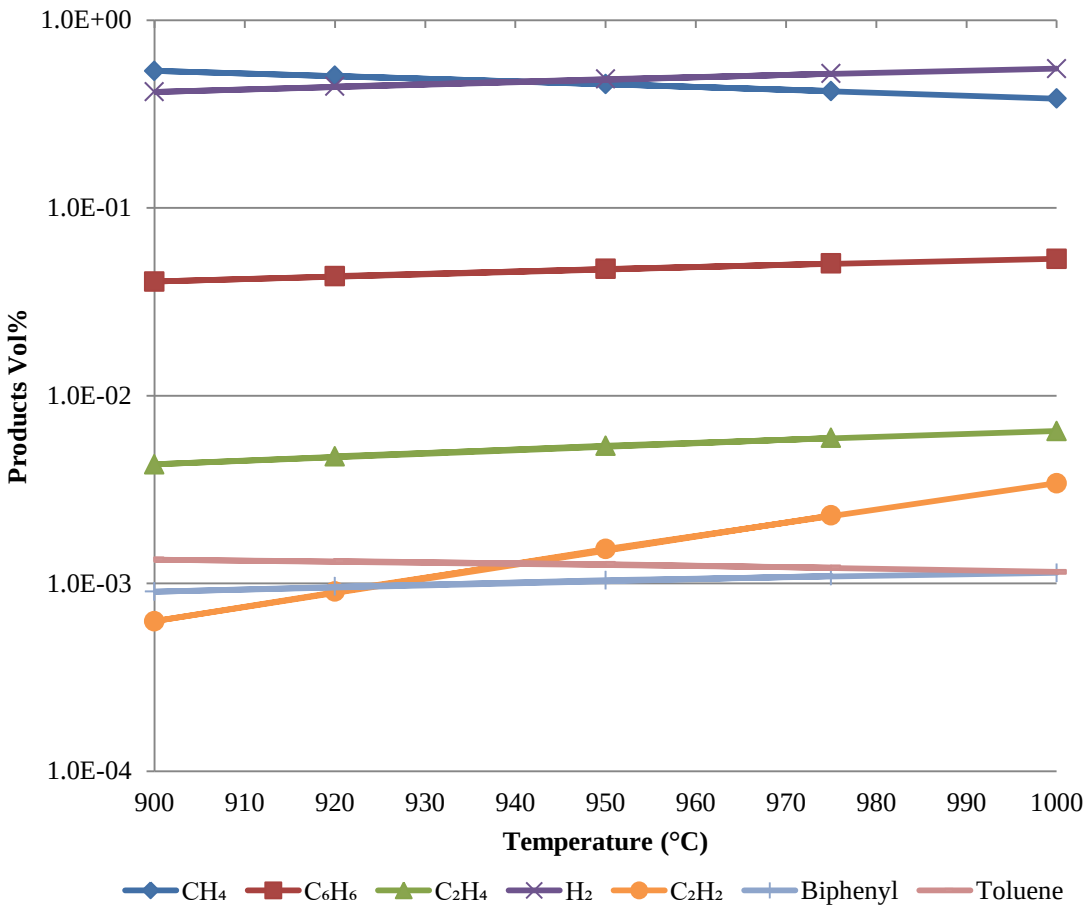

Figure 7-44: MTD modelling for various temperatures at atmospheric pressure.

Contrary to the HACA reaction pathway, Melius et al. [42], suggests that the production of PAHs originates from the interactions of cyclopentadienyl radicals undergoing a series of ring closures and openings to form naphthalene, Equation (7.9.2). Melius et al. [42], suggested that the primary source of cyclopentadienyl radicals are formed from the oxidation of benzene. It was not likely that benzene was oxidised during methanolysis, as increased phenol concentrations would be expected. The cyclopentadienyl pathway for naphthalene was not regarded as a leading pathway as the production of biphenyl was expected to be more abundant as well, due to the lower enthalpy in comparison to naphthalene, $\Delta^0_{f(298)} = 357$ and $\Delta^0_{f(298)} = 366$, respectively [42], [43]. It is believed that the naphthalene production is a consequence of fragmentation reactions from lignin and the HACA pathway described above

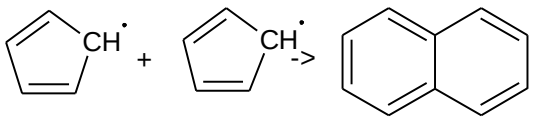

(7.9.2)

To investigate the effect of MTD during methanolysis, dual models were constructed to determine the effective selectivity of the species when MTD was accounted for, Figure 7-45. It was observed that the inclusion of biomass within the system increased the overall thermodynamic favourability of the formation of benzene. This was in agreement with the results from the investigation into the temperature effect, which showed an increase in the production of tar species, primarily benzene, with increasing temperature between 948 and 988 °C. This possibly explains the increased production of tars with the increasing residence time, where the increased residence time leads to the system becoming closer to the thermodynamically preferred state.

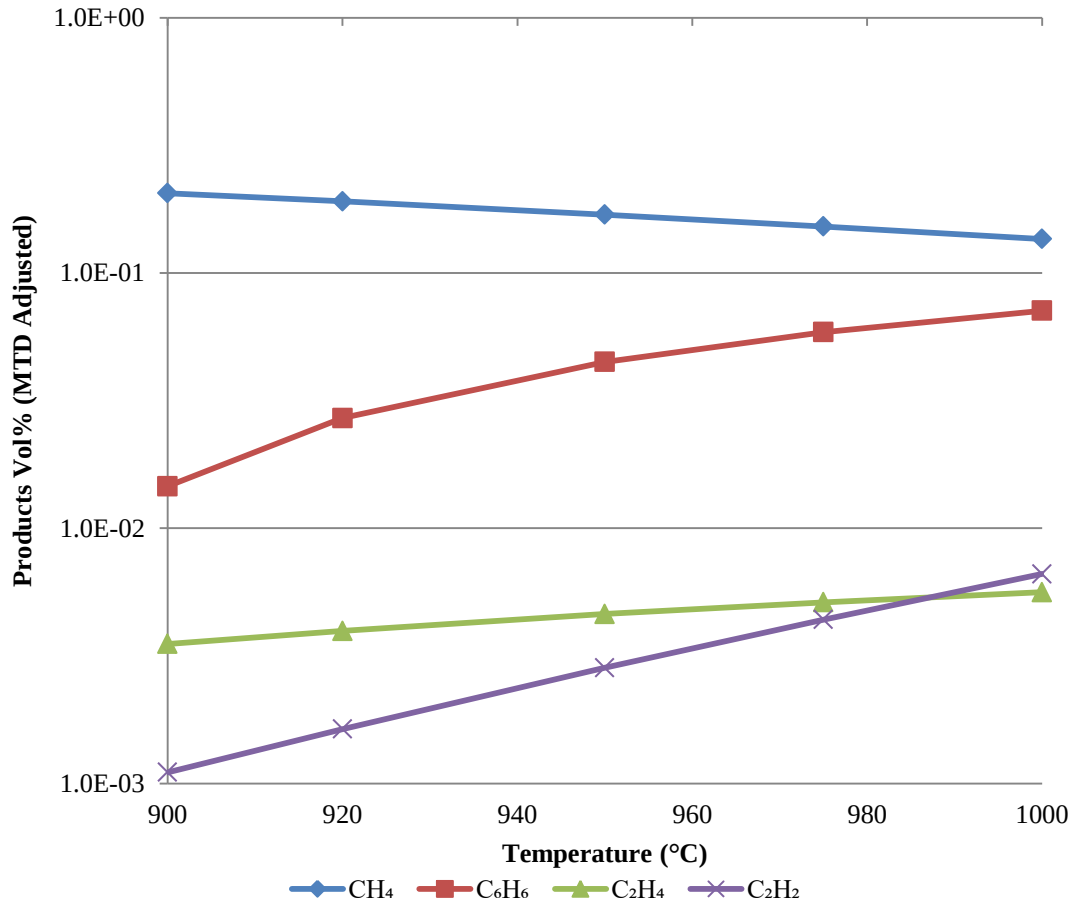

Figure 7-45: MTD adjusted modelled product distribution during methanolysis.

It was suspected that the increase in benzene produced can be attributed to the interactions of toluene with the hydrogen produced from degradation. Jess [44], proposed that at temperatures of 1000 °C, and residence times of 1 s, conversion of toluene in the presence of hydrogen produced benzene and methane reached nearly 100 %. It was possible that this was a leading pathway for the production of benzene from aromatic fragments which are cracked from the lignin structure during methanolysis. It was highly likely that similar pathways also existed for the production of benzene from xylene, styrene and ethylbenzene. This pathway was supported by the modelling of toluene, xylene and

ethylbenzene, during methanolysis to show very low concentrations in the product gas due to the unfavourable thermodynamic characteristics of the species. The extent of which the reactions contribute on the overall distribution of the product was unknown, and is a region which requires further investigation.

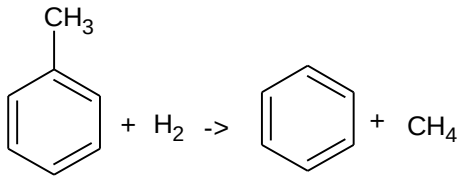

(7.9.3)

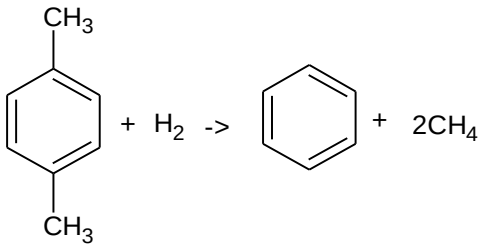

(7.9.4)

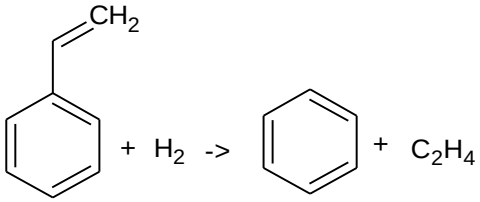

(7.9.5)

Another possible pathway for the production of benzene is via production and stabilization of propargyl radicals as proposed by Miller et al [45]. The proposed reaction scheme suggested the production of phenyl + H, which could then be stabilized by hydrogen addition to form benzene. This pathway was also identified as the main pathway from:

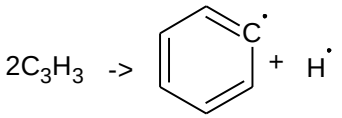

(7.9.6)

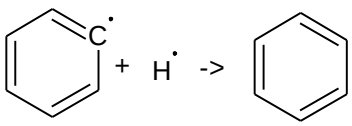

(7.9.7)

This has generally been regarded as the pathway for the production of benzene for a number of hydrocarbon ($C_2H_2/O_2/Ar$) flame product investigations. Miller et al. [45], highlighted a number of pathways for the production for the propargyl, however, suggested that the reaction between acetylene and CH_2 was the dominant pathway, Equation (7.9.8). It is plausible that the production of propargyl radicals during methanolysis arise from the products of the degradation of methane as CH_2 has a

tendency to form and it is highly likely acetylene is formed. From this it was possible that the formation of benzene can proceed as:

$$CH_2 + C_2H_2 \leftrightarrow C_3H_3 + H \qquad (7.9.8)$$

As observed from the comparison of fluidisation gases, it was highly likely that methane was produced during methanolysis. This effectively reduces the apparent methane consumption during methanolysis, and explains why the concentration of hydrogen cannot be attributed directly to the methane consumption during the reaction. It is also suspected that production of methane increases with increasing residence, which was also reported by Conesa et al [46], whom investigated the pyrolysis of HDPE (which produces very similar hydrocarbon products). Conesa et al. [46], determined that the increase in residence time increased the methane, benzene and toluene species, due to the cracking of the C_2-C_5 species. The increasing formation of methane and benzene is in agreement with the Conesa et al, with high increases in benzene production with increased residence time from 0.5 to 2.5 s. However, it is likely that the toluene which is formed undergoes hydrogen addition to form benzene (7.9.3), given that the methane concentration between a residence time of 1.5 s and 2.5 s decreases significantly. It is suspected that the degradation values increase significantly, masking the methane production. The hydrogen produced is likely to facilitate the hydrogenation of toluene.

It was also observed during the temperature investigation into methanolysis that it was highly likely that the methane which is produced/not degraded also undergoes steam reforming extensively, which also varies the methane to hydrogen ratio of the product gas. This was suspected due to the thermodynamic favourability at 1000°C, which had an equilibrium constant of 8.42 x 10^7 kPa^2 [XXIX] . This also provides an explanation for the decrease in CO production which was observed with increasing pressure.

It was suspected that the ethylene formation during the methanolysis of biomass was strongly influenced by the production of ethylene through MTD. This was significant as throughout the calculation of the effective carbon conversion, all ethylene was assumed to arise from methanolysis. As observed in Figure 7-13, with increasing residence time the proportion of ethylene, which could be attributed to methane degradation, increased. This effect was also suspected of being enhanced by the varying degradation characteristics which occurred during methanolysis. Opposed to the effective decreasing methane variation with increased residence time Figure 7-46, the proportional increase in ethylene from degradation was shown to increase with higher mass flow rates of methane.

[XXIX] Calculated $1.198\ x\ 10^{17} \exp\left(-\frac{26830}{T}\right)$, [51]

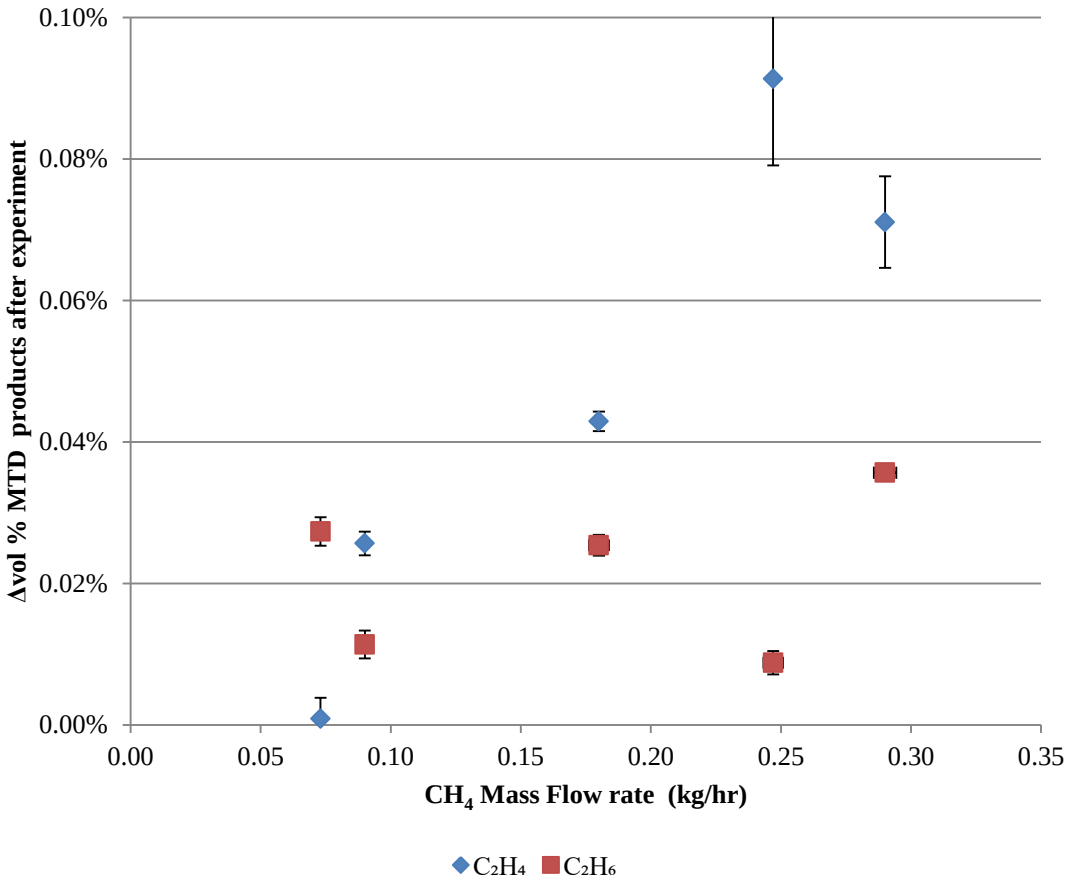

Figure 7-46: Varying extent of ethylene and ethane production during methanolysis.

Nevertheless, significant increases in ethylene production in the pressure region of 276-380 kPa were observed. This was suspected to be due to the increased equilibrium constant of the ethylene, resulting in favored production. The formation of ethylene from radicals is suggested as the primary formation pathway, where ethane is the primary product and undergoes dehydrogenation reactions. This would suggest that, the concentration of ethane and ethylene was close to equilibrium, and subject to the hydrogen concentration (which is largely due to MTD).

At 1000 °C, the kinetics of the dehydrogenation of ethane was likely to be much higher than that of ethylene. Whereas, increased operating temperature showed a decrease in the ethylene production due to the kinetics of ethylene dehydrogenation increasing. Thus, the concentration of acetylene in the product gas likely increased unless the species interacted/degraded quickly at the high temperature, depositing carbon. It was also suggested that the residence time variation also affected the proposed pathway, as at lower residence time a decrease in ethylene production was apparent. This is likely due to the decreased production of ethane during methanolysis, which reduces the overall ethylene production. Conversely, increased residence time allows for the extent of ethylene dehydrogenation to increase which results in expected increases in the acetylene formation.

The increase in production of ethylene was observed up to 988 °C, at higher temperature the ethylene yield was observed to decrease. It is commonly regarded that the production of ethylene is predominantly from the pyrolysis of cellulose [24], [47]–[49], through an extensive multi-step reaction mechanism. Evans and Milne [49], observed increased selectivity to ethylene production from cellulose when the temperature was increased 500 to 950 °C, at which the primary product was ethylene at max temperature. The extent of production of other species was significantly reduced, with the only detectable named species in the range 0-300 m/z [49]. At 950 °C, the production of ethylene from the hemicellulose fraction, xylan, also increased, with the primary product identified as ethylene, where selectivity increased with temperature. This is expected to explain the increased yields of ethylene with temperature, where the increasing temperature > 988 °, led to the degradation of the ethylene product. The pathway through the degradation of methane is also a likely source of ethylene production; however, the differentiation between ethylene produced via MTD and through cellulose/lignin/hemicellulose based pathways needs further investigation. It was suspected that a synergy with the radicals formed during MTD with the products of the initial volatisation from pyrolysis produce the combined ethylene concentration.

Char production throughout the trials was difficult to estimate due to the contribution of carbon deposition via MTD, and no system in place to readily determine the solids production in the bed. This issue was even more pronounced with the reduction in effective degradation throughout the trials, which was suspected to be significantly higher in extent than that of the apparent char production. Nevertheless, the overall char production was suspected to be low throughout the trials, with accumulation of the char in the fluidized bed, char in the packed bed and downstream filter was never observed. The presence of char was suspected of catalytic activity, as discussed above, inducing cracking of hydrocarbon molecules during pyrolysis. Given that the separation of the char and sand in the fluidized bed was effective, the residence time of the gas through the char was not expected to be long. However, it was suspected that the formation of char had a larger impact on hydrocarbon formation due to MTD. As shown in Figure 7-46, the apparent production of ethylene and ethane during MTD increased throughout the trials, hence, it was suspected that char catalyzed this formation to a higher extent than the volatiles from biomass pyrolysis. It is likely that the char production increased with increasing biomass size, lower residence times, and lower reaction temperatures; where, decreased particle size of the chip increased the char reactivity [50].

The varying formation in trace tars was likely due to the cracking of the lignin structure. This was likely as the model predicted very low extents of, and at times zero, formation for the branched aromatic tar species throughout the operational configurations. The most common minor tar species, phenol, styrene, indene and xylene all showed varied extents of production throughout methanolysis. As mentioned above, it was likely that these species undergo subsequent benzene formation, which

results in the production of methane, ethylene and ethane. Phenol was observed to increase with pressure and increased to slightly below 1 % carbon conversion at 483 kPa. This was in conjunction with the increase in overall tar production at higher pressure, which suggests that at higher pressures the extent of lignin cracking increases, and the methanolysis product selectivity was influenced by the biomass structure. From the trial conducted with moist pine it was also observed that the phenol produced was in agreement with dried pine, indicating that the oxidation of benzene is an unlikely pathway for phenol production.

7.10 References

[1] A. Megaritis, Y. Zhuo, R. Messenbo, D. R. Dugwell, and R. Kandiyoti, "Pyrolysis and gasification in a bench-scale high-pressure fluidized-bed reactor," *Energy and Fuels*, vol. 12, no. 15, pp. 144–151, 1998.

[2] M. Steinberg, "Flash Pyrolsyis of Biomass with Reactive and Non-Reactive Gases," 1984.

[3] M. Steinberg, P. T. Fallon, and M. S. Sundaram, "Flash pyrolysis of biomass with reactive and non-reactive gas," *Biomass*, vol. 9, no. 4, pp. 293–315, 1986.

[4] H. B. Hm, H. Jander, and D. Tanke, "PAH GROWTH AND SOOT FORMATION IN THE PYROLYSIS OF ACETYLENE AND BENZENE AT HIGH TEMPERATURES AND PRESSURES: MODELING AND EXPERIMENT," in *Twenty-Seventh Symposium (International) on Combustion/The Combustion Institute*, 1998, pp. 1605–1612.

[5] H. Böhm and H. Janderb, "PAH formation in acetylene–benzene pyrolysis," *Phys. Chem. Chem. Phys.*, vol. 1, no. 16, pp. 3775–3781, 1999.

[6] Z. Zhu, Z. Ma, C. Zhang, H. Jin, and X. Wang, "Flash hydropyrolysis of northern Chinese coal," *Fuel*, vol. 75, no. 12, pp. 1429–1433, 1996.

[7] C. F. Cullis, G. J. Minkoff, and M. A. Nettleton, "Infra-red Spectrometric Study of the Pyrolysis of Acetylene Part 1 .-The Homogeneous Reaction."

[8] M. Chareonpanich, T. Boonfueng, and J. Limtrakul, "Production of aromatic hydrocarbons from mae-moh lignite," *Fuel Process. Technol.*, vol. 79, no. 2, pp. 171–179, 2002.

[9] A. Van der Drift, H. Boerrigter, and B. Coda, "Entrained flow gasification of biomass.," *ECN - Energy Cent. Netherlands*, no. April, p. 58, 2004.

[10] L. Wei, M. Zhu, Y. Ma, Z. Zhang, and D. Zhang, "Hydrogen production by methane cracking over Xiaolongtan lignite chars: The role of mineral matter," *Fuel*, vol. 183, pp. 345–350, 2016.

[11] M. L. Boroson, J. B. Howard, J. P. Longwell, and W. A. Peters, "Heterogeneous Cracking of Wood Pyrolysis Tars over Fresh Wood Char Surfaces," *Energy and Fuels*, vol. 3, no. 6, pp. 735–740, 1989.

[12] S. Liu, Y. Wang, R. Wu, X. Zeng, S. Gao, and G. Xu, "Fundamentals of catalytic tar removal over in situ and ex situ chars in two-stage gasification of coal," *Energy and Fuels*, vol. 28, no. 1, pp. 58–66, 2014.

[13] S. Septien, S. Valin, C. Dupont, M. Peyrot, and S. Salvador, "Effect of particle size and temperature on woody biomass fast pyrolysis at high temperature (1000-1400°C)," *Fuel*, vol. 97, pp. 202–210, 2012.

[14] J. Shen, X.-S. Wang, M. Garcia-Perez, D. Mourant, M. J. Rhodes, and C.-Z. Li, “Effects of particle size on the fast pyrolysis of oil mallee woody biomass,” *Fuel*, vol. 88, no. 10, pp. 1810–1817, 2009.

[15] S. Li, S. Xu, S. Liu, C. Yang, and Q. Lu, “Fast pyrolysis of biomass in free-fall reactor for hydrogen-rich gas,” *Fuel Process. Technol.*, vol. 85, no. 8–10, pp. 1201–1211, 2004.

[16] M. O. Kimberley, R. B. McKinley, D. J. Cown, and J. R. Moore, “Modelling the variation in wood density of New Zealand-grown Douglas-fir,” *New Zeal. J. For. Sci.*, vol. 47, no. 1, pp. 0–15, 2017.

[17] R. C. PETTERSEN, “The Chemical Composition of Wood,” pp. 57–126, 1984.

[18] T. D. Lomax, R. A. Franich, and H. Kroese, “Note - Pyrolysis products of Pinus radiata bark,” *New Zeal. J. For. Sci.*, vol. 21, no. 1, pp. 111–115, 1991.

[19] R. Sands, “Radiata pine bark - aspects of morphology, anatomy and chemistry,” *New Zeal. J. For. Sci.*, vol. 5, no. 1, pp. 74–86, 1975.

[20] D. M. Updegraff and W. D. Grant, “Microbial utilization of Pinusbasmati rice radiata bark.,” *Appl. Microbiol.*, vol. 30, no. 5, pp. 722–6, 1975.

[21] C. A. Mullen and A. A. Boateng, “Catalytic pyrolysis-GC/MS of lignin from several sources,” *Fuel Process. Technol.*, vol. 91, no. 11, pp. 1446–1458, 2010.

[22] T. R. Carlson, G. A. Tompsett, W. C. Conner, and G. W. Huber, “Aromatic production from catalytic fast pyrolysis of biomass-derived feedstocks,” *Top. Catal.*, vol. 52, no. 3, pp. 241–252, 2009.

[23] J. Zakzeski, P. C. A. Bruijnincx, A. L. Jongerius, and B. M. Weckhuysen, “The catalytic valorization of lignin for the production of renewable chemicals,” *Chem. Rev.*, vol. 110, no. 6, pp. 3552–3599, 2010.

[24] M. Steinberg, P. T. Fallon, and M. S. Sundaram, “The Flash Pyrolysis and Methanolysis of Biomass (Wood) for Production of Ethylene, Benzene and Methanol,” 1990.

[25] A. V. Bridgwater, “Principles and practice of biomass fast pyrolysis processes for liquids,” *J. Anal. Appl. Pyrolysis*, vol. 51, no. 1, pp. 3–22, 1999.

[26] A. Dufour, A. Celzard, B. Ouartassi, F. Broust, V. Fierro, and A. Zoulalian, “Effect of micropores diffusion on kinetics of CH4 decomposition over a wood-derived carbon catalyst,” *Appl. Catal. A Gen.*, vol. 360, no. 2, pp. 120–125, 2009.

[27] J. Han and H. Kim, “The reduction and control technology of tar during biomass gasification/pyrolysis: An overview,” *Renew. Sustain. Energy Rev.*, vol. 12, no. 2, pp. 397–416, 2008.

[28] A. Demirbaş, “Mechanisms of liquefaction and pyrolysis reactions of biomass,” *Energy Convers. Manag.*, vol. 41, no. 6, pp. 633–646, 2000.

[29] B. M. Weckhuysen and R. A. Schoonheydt, “Alkane dehydrogenation over supported chromium oxide catalysts,” *Catal. Today1*, vol. 51, pp. 223–232, 1999.

[30] M. S. Sundaram, S. M. Steinberg, P.T. Fallon, “Flash Pyrolysis of Biomass with Reactive and Non-Reactive Gases,” Richland, Washington, 1984.

[31] H. Zhang, S. Shao, Y. Jiang, T. Vitidsant, P. Reubroycharoen, and R. Xiao, “Improving hydrocarbon yield by two-step pyrolysis of pinewood in a fluidized-bed reactor,” *Fuel Process. Technol.*, vol. 159, pp. 19–26, 2017.

[32] A. M. Dunker, S. Kumar, and P. A. Mulawa, “Production of hydrogen by thermal decomposition of methane in a fluidized-bed reactor - Effects of catalyst, temperature, and residence time,” *Int. J. Hydrogen Energy*, vol. 31, no. 4, pp. 473–484, 2006.

[33] B. Lin *et al.*, “Deactivation study of carbon-supported ruthenium catalyst with potassium promoter,” *Appl. Catal. A Gen.*, vol. 541, no. March, pp. 1–7, 2017.

[34] F. A. Agblevor and S. Besler, “Inorganic compounds in biomass feedstocks. 1. Effect on the quality of fast pyrolysis oils,” *Energy and Fuels*, vol. 10, no. 2, pp. 293–298, 1996.

[35] V. Kirubakaran, V. Sivaramakrishnan, R. Nalini, T. Sekar, M. Premalatha, and P. Subramanian, “A review on gasification of biomass,” *Renew. Sustain. Energy Rev.*, vol. 13, no. 1, pp. 179–186, 2009.

[36] J. L. Pinilla, R. Moliner, I. Suelves, M. J. Lázaro, Y. Echegoyen, and J. M. Palacios, “Production of hydrogen and carbon nanofibers by thermal decomposition of methane using metal catalysts in a fluidized bed reactor,” *Int. J. Hydrogen Energy*, vol. 32, no. 18, pp. 4821–4829, 2007.

[37] T. Zhang and M. D. Amiridis, “Hydrogen Production via the Direct Cracking of Methane over Silica-Supported Nickel Catalysts,” *Appl. Catal. A Gen.*, vol. 167, no. 2, pp. 161–172, 1998.

[38] M. J. Lázaro, J. L. Pinilla, I. Suelves, and R. Moliner, “Study of the deactivation mechanism of carbon blacks used in methane decomposition,” *Int. J. Hydrogen Energy*, vol. 33, no. 15, pp. 4104–4111, 2008.

[39] L. Wang, L. Tao, M. Xie, G. Xu, J. Huang, and Y. Xu, “Dehydrogenation and aromatization of methane under non-oxidizing conditions,” *Catal. Letters*, vol. 21, no. 1–2, pp. 35–41, 1993.

[40] F. Solymosi, A. Erdöhelyi, and A. Szöke, “Dehydrogenation of methane on supported molybdenum oxides. Formation of benzene from methane,” *Catal. Letters*, vol. 32, no. 1–2, pp. 43–53, 1995.

[41] M. Frenklach, H. Wang, and O. Process, “Aromatics Growth Beyond the First Ring and the Nucleation of Soot Particles,” *202nd ACS Natl. Meet.*, vol. 36, no. 4, p. 1509, 1991.

[42] C. F. Melius, M. E. Colvin, N. M. Marinov, W. J. Pit, and S. M. Senkan, “Reaction mechanisms in aromatic hydrocarbon formation involving the C5H5 cyclopentadienyl moiety,” *Symp. Combust.*, vol. 26, no. 1, pp. 685–692, 1996.

[43] D. Wang, A. Violi, D. H. Kim, and J. A. Mullholland, “Formation of naphthalene, indene, and benzene from cyclopentadiene pyrolysis: A DFT study,” *J. Phys. Chem. A*, vol. 110, no. 14, pp. 4719–4725, 2006.

[44] A. Jess, “Mechanisms and kinetics of thermal reactions of aromatic hydrocarbons from pyrolysis of solid fuels,” *Fuel*, vol. 75, no. 12, pp. 1441–1448, 1996.

[45] J. A. Miller, J. V. Volponi, and J. F. Pauwels, “The effect of allene addition on the structure of a rich C2H2/O2/ Ar flame,” *Combust. Flame*, vol. 105, no. 4, pp. 451–461, 1996.

[46] J. A. Conesa, R. Font, A. Martilla, and A. N. Garcia, “Pyrolysis of Polyethylene in a Fluidized Bed Reactor,” *Energy and Fuels*, vol. 8, no. 6, pp. 1238–1246, 1994.

[47] D. H. Lee, H. Yang, R. Yan, and D. T. Liang, “Prediction of gaseous products from biomass pyrolysis through combined kinetic and thermodynamic simulations,” *Fuel*, vol. 86, no. 3, pp. 410–417, 2007.

[48] H. Yang, R. Yan, H. Chen, D. H. Lee, and C. Zheng, “Characteristics of hemicellulose, cellulose and lignin pyrolysis,” *Fuel*, vol. 86, no. 12–13, pp. 1781–1788, 2007.

[49] R. J. Evans and T. A. Milne, “Molecular characterization of the pyrolysis of biomass,” *Energy & Fuels*, vol. 1, no. 2, pp. 123–137, 1987.

[50] R. Zanzi, K. Sjöström, and E. Björnbom, “Rapid high-temperature pyrolysis of biomass in a free-fall reactor,” *Fuel*, vol. 75, no. 5, pp. 545–550, 1996.

[51] K. Hou and R. Hughes, “The kinetics of methane steam reforming over a Ni/α-Al2O catalyst,” *Chem. Eng. J.*, vol. 82, no. 1–3, pp. 311–328, 2001.

8 Conclusions and Recommendations

8.1 Conclusions

To investigate the methanolysis of biomass, a fluidised bed reactor system was designed, constructed, commissioned and operated up to temperatures of 1000 °C and 1010 kPa. During the operation of the system, the optimization of CO, ethylene and benzene were targeted as a potential source of renewable chemicals for a range of industries. The reactor was fabricated to investigate the product distribution using a fluidised bed reactor, and to better understand the product selectivity during operation, as methanolysis of biomass was an area of research which had not received significant attention. In turn, a modular and portable reactor system was constructed, which allowed for numerous experiments to be conducted.

Methane Degradation

After system commissioning it was found that significant issues arose from the thermal degradation of methane. MTD was problematic for the experimental investigation due to the high hydrogen concentration entering into the reaction zone, causing H_2 as well as CH_4 reactions. The extent of degradation was significantly decreased by the removal of suspected catalytic surfaces and subsequent retrofitting with quartz fabrications. The carbon production from the MTD reactions was suspected of causing issues whilst feeding as well, with the overall bed height increasing as experiments progressed. This was a likely cause of feeder tube blockages during feeding, as well as pressure differentials which existed between the hopper and the fluidised bed reactor. The reactor degradation characteristics were compared with an all quartz reactor to show that there was no significant additional catalysis occurring arising from the small amount of non-quartz reactor components.

Subsequent experiments showed that MTD increased with increasing temperature and residence time, this was suspected to be due to the increased kinetics of the system and probability of species interaction. When comparing different reactor configurations it was indicated that it was very likely that the majority of the degradation occurred primarily within the reaction zone. This led to overall hydrogen production being dependent on gas mass flow which is related to the residence time.

For the succeeding methanolysis experiments it was determined that a complete reduction in hydrogen was not possible and that it was important to analyse hydrogen production throughout. This was imperative as the overall ethylene and ethane production value may include those from MTD and thus may lead to possible errors in calculations of biomass carbon conversion. However, the production of ethylene and ethane was observed to be low (< 1 vol %); hence, no significant interaction of the

species with biomass is expected during methanolysis. It was also found that significant tar production was unlikely from MTD.

From the MTD characteristics which were determined in the methanolysis reactor, it is highly likely that hydrogen was abundant in the work from Steinberg et al. [1]–[4], with ethylene concentrations possibly below detectable limits (which were not stated). However, due to differing reactor configurations, the hydrogen concentration throughout the reaction zone was different than that of the methanolysis reactor, resulting in differing hydrogen gradients through the reactor in comparison.

Reactor Construction

With the inclusion of the modifications which were required to the system, the effective maximum methane mass flow rate operatable within the system was below 1 kg/hr. This was due to the inclusion of the quartz sleeve decreasing the effective surface area for flow. In turn, by use of smaller sand particles and/or increasing the reactor diameter the required system configuration can be operated for a mass flow rate of 1 kg/hr. The reactor diameter was altered throughout the experimental period, due to the cyclic thermal stresses the reactor was exposed to. It was evident that the cycling thermal stresses were not accounted for during the design and fabrication of the core reactor pipe as significant warping of the reactor eventually prevented the insertion of the quartz liner. After necessary modifications and improvements, the developed methanolysis reactor system operated reasonably well and a series of experiments have been successfully conducted.

The ethylene and CO carbon conversion yields were observed to increase by the use of a fluidised bed, in comparison to a packed bed like configuration and drop tube reactor. By operating the system as a fluidised bed, the ethylene and CO carbon conversion increased from 13 ± 1 % and 34 ± 3 %, to 22 ± 4 % and 49 ± 8 %, respectively, in comparison to packed bed operation. However, higher tar production was observed in the drop tube configuration, as opposed to the packed bed reactor. The overall methane consumption was seen to increase with the use of the fluidised bed. It was suspected that the increase in methane consumption and production of ethylene and CO was due to enhanced heat transfer to the gas from the fluidising sand. This was suspected of increasing the MTD reactions, as well as increasing the interactions with the volatiles from pyrolysis with the gas. The higher benzene production during operation as a dropper tube type reactor are likely to be due to the catalytic surface effects of the reactor when the quartz liner is removed.

Biomass Preparation

The preparation of the feedstock before milling was determined to significantly alter the feeding potential of the biomass into the system. This was observed by the strong influence which cutting direction had on the overall product of the Wiley milled biomass. Significant increases in the

flowability of the Wiley milled biomass were apparent with cross cut biomass chip, as opposed to longitudinal chipping which is more likely to occur during the use of a chipper. A new methodology for the preparation of feedstocks from logs was devised and was shown to perform well, allowing for adequate gravity feeding performance in a 30° hopper system.

Flash Methanolysis of Biomass

From the investigation into the flash methanolysis of biomass the operating temperature of the system was observed to significantly increase ethylene and benzene production. This was most pronounced at temperatures of 948 and 988 °C, which resulted in an increase of ethylene and benzene carbon conversion, from 8 ± 1% and 1.7 ± 0.2 % to 19 ± 1 % and 8 ± 1 %. At a higher temperature of 1028 °C, decreased ethylene yields and stable benzene production was observed. It was suspected that with increasing temperature the dehydrogenation of ethylene occurred, resulting in possible increases in acetylene production. It was also likely that at higher temperatures the MTD reactions to form ethylene were enhanced and a greater proportion of ethylene could be accounted for by MTD.

The effect of residence time during methanolysis was difficult to quantify, due to the effect of MTD and the relative residence time influences within the reaction zone. As highlighted from the MTD analysis, the residence time through the reaction zone was indicative of the product distribution, as observed during methanolysis. The reaction zone residence time accounted for ~44 % of the total reactor residence time in total, whereas, the remainder was the preheating of methane. At a reactor residence time of 1.5 s the CO and C_2H_4 reached a maximum carbon conversion of 48 ± 2 % and 22 ± 1 %, respectively. With increasing residence time the benzene yield increased significantly, with the carbon conversion increasing from 11 ± 2 % to 21 ± 3 % for residence times of 1.5 s and 2.5 s, respectively. The increase in total tar production could essentially be attributed to the production of benzene, which was reasoned to be due to the HACA (H abstraction C_2H_2 reaction pathway) aromatic reaction pathway, which effectively reduced the ethylene yield, due to possible acetylene formation. This was also supported by indications that at a residence time of 2.5 s, the hydrogen production was lower than the respective MTD hydrogen yield, indicating high hydrogen consumption at higher residence times. For a residence time of 0.5 s, 0.75 s and 1.5 s, the increase in hydrogen production relative to the degradation production was constant at ~ 17%.

The methane to biomass ratio during experiments (M/B ratio), showed significant influence on the gas phase interactions of methane and the initial pyrolysis products. The production of CO, C_2H_4 and benzene all increased with increasing M/B ratio. By increasing the M/B ratio from 1.29 to 4.16, the ethylene and CO carbon conversion increased from 9 ± 1 % and 32 ± 2 %, to 20 ± 1% and 55 ± 2 %, respectively. The production of benzene increased from 3.5 ± 0.4% to 7 ± 1% carbon conversion, when the M/B ratio increased from 1.29 to 2; however, further increases in the M/B ratio did not

affect the benzene production significantly. It was determined that with decreasing M/B ratio the production of water increased which reduced the CO yield. The effective methane consumption increased with increasing M/B ratio, indicating it was possible that the decreased biomass feed resulted in higher extents of degradation. This could have caused increases in the MTD production of ethylene and ethane, which since the M/B ratio is high, has a significant effect on the derivation of the carbon conversion value. Quantification of the decreasing effective reaction zone residence time with decreasing M/B ratio was also challenging as variations in the M/B ratio changed the solids, tar and gas distribution. Therefore, control of the residence time decrease in the zone was difficult to determine.

Variations in operating pressure significantly increased the ethylene selectivity. With an increase in pressure from 140 kPa to 275 kPa the ethylene carbon conversion increased from 4.1 ± 0.2 % to 19 ± 3 %, respectively. The ethylene yield remained constant with further increases to 380 kPa, whilst, at 480 kPa a significant decrease in ethylene yield was observed, with an overall carbon conversion of 4.4 ± 0.2 % obtained. The CO yield remained constant throughout the pressure range of 140-480 kPa, with an average carbon conversion of 45%. Significant increases in the production of tars was observed when the operating pressure increased from 140 kPa to 480 kPa, where the benzene carbon conversion increased from 3.0 ± 0.4 % to 16 ± 2 %, respectively. Significant increases in naphthalene and toluene were also observed with increasing pressure, resulting in a total tar production of 26 ± 2 % carbon conversion. It was understood that the high ethylene production at pressure of 275 kPa to 380 kPa were due to the increased stability of ethylene, as a local maximum equilibrium exists between 300 and 450 kPa, as identified by the Gibbs energy modelling. Interestingly, a comparison of the ethylene produced from MTD and from methanolysis revealed that with increasing pressure the relative production of ethylene from methanolysis decreased. This was exemplified at higher pressures, whereas, at 480 kPa the percentage of ethylene formed from MTD was higher than during methanolysis. The influence of MTD ethylene formation decreased with decreasing pressure. It was proposed that the increase in tar production was due to an increase in reaction kinetics for the HACA aromatic production pathway, which could subsequently form toluene and naphthalene.

Of all the chip size fractions utilized, the use of 500-710 µm chips resulted in the lowest gas product yield obtained, 68 ± 1 % carbon conversion; whilst, the tar production was the highest, at 7.5 ± 0.3 % carbon conversion. With increasing particle size to 710-1000 µm, the production of gas increased to 87 ± 2 %; whilst 1000-1400 µm chips produced an overall gas phase product yield of 78 ± 2 %. The ethylene and CO yields were enhanced by the use of 710-1000 µm chip, resulting in a carbon conversion of 14.2 ± 0.3 % and 54 ± 1 %, respectively. The extent of methane degradation increased with decreasing chip size, demonstrating that with decreased particle size, the interaction of methane with volatised products in the reaction zone was enhanced. This was thought to result in the higher tar

production, as with increased interactions with the gas the production of tars was observed. Difficulties in determining the remaining char were apparent with the overall carbon production from MTD suspected of significantly affecting the derived char values.

The use of Douglas fir and pine bark was observed to produce significantly lower ethylene and benzene yields in comparison to pine wood, as well as higher solids production. The difference in product distribution of the pine wood in comparison to the Douglas fir wood was reasoned to be due to the higher mineral content in Douglas fir heartwood, which likely increases cracking of the hydrocarbons formed during methanolysis. A build-up of ash in the system was suggested as a possible cause for the increasing degradation between trials, after the bark trial, the solids production was observed to increase from 15 % to 46 %. The use of charcoal revealed that the interactions of char with methane is not likely to form ethylene and that the accumulation of the char can cause issues when feeding. The use of moist pine resulted in high H_2 and CO concentrations, and large methane consumption which was supposedly due to steam reforming occurring, highlighting the importance of biomass drying.

Comparative trials with nitrogen indicated that the overall ethylene, CO and benzene production increased significantly with the use of methane. For similar molar flow rate trials, it was determined that with the use of methane the ethylene, CO and benzene increased from 5 %, 26 ± 2 % and 7 ± 1 % to 16 ± 1 %, 56 ± 3% and 11 ± 2 %, when compared to nitrogen, respectively. This was suggested to be due to the significant influence of the methyl radical production during methanolysis, which through a very complex reaction pathway produces increases production of ethylene, CO and benzene. The production of methyl radicals during methanolysis was suspected of increasing ethylene production during methanolysis, due to the combination reactions which produce ethane which was subsequently dehydrogenated. It was also reasoned that cyclopentadienyl and propargyl radicals are important in the production of benzene from the HACA reaction pathways which describe the aromatization reactions during the combustion of methane.

Other potential pathways for the production of aromatic species from methanolysis are the cracking of lignin to form a number of aromatic fragments. Due to the high concentration of hydrogen within the reacting environment it was suspected that hydrogenation of the fragments occurs, which leads to the favoured production of benzene. This was suspected of explaining the production of the tar species which were evident throughout the experiments, where, when Douglas fir was utilized similar concentrations as pine wood were observed.

Due to the MTD characteristics during methanolysis quantification of the true hydrocarbon and hydrogen production was difficult. This was due to the observed production of ethylene and ethane during MTD, as well as the high hydrogen production, in turn, resulting in varying composition of the

methane feed before it was able to reach the reaction zone. This was likely to vary the influence of methane during the residence time investigations. Characterisation of the degradation characteristics was difficult due variation in MTD behaviour throughout methanolysis. It was very likely that a conditioning phenomenon was occurring within the system during operation, which effectively reduced the extent of MTD, but, in some cases, increased the ethylene production which could be attributed to MTD. The conditioning of the system was likely dependent on the mass flow rate of the methane and was characterised by a thin black mirror like layer of carbon which would coat surfaces at high temperature.

8.2 Recommendations

The interactions of the product species from methanolysis with methane is suspected of being very complex. It is recommended that further investigation into characterising the influence of species interactions originating from methane and from biomass be investigated to determine associated contributions. Using carbon isotope measurements of the product species could be useful for the identification of the origins of carbonaceous products. The use of chloroform/DCM as the fluidising gas could provide information on the reaction pathways during methanolysis as identification of chlorinated branched products is relatively straight forward. Investigations into the use of a TGA under a methane environment are also suggested as a possible route for further characterisation of the pyrolysis volatiles and methane during methanolysis.

Extensive distinguishing of the MTD products for various operating conditions is also suggested as significant variations in MTD products were experienced. If hydrogen production can be suppressed the understanding of pyrolysis volatiles and methane interactions can be enhanced. It is likely that the hydrogen which was produced via MTD induces significant hydrogenation reactions of the initial methanolysis products. The balance and influence of the hydrogen concentration is an interesting area of research which requires further investigation.

As it was hypothesised that a significant amount of the interactions may possibly be occurring between radicals and initial methanolysis products, an investigation into radical production is proposed. This would highlight key pathways which have been suspected of influencing the species distribution. Of particular interest is the production of methyl, propargyl and cyclopentadienyl radicals from methane. Another interesting avenue for the production of radicals could originate from the fragmentation of biomass and interactions with methane.

Improvements in the feeding characterises of the system are also highly recommended. The suspected pressure differentials which varied throughout the trials were likely causes of numerous blockages which occurred during trials. The effect of char and carbon build up on the dynamics of the feeding system is not completely understood, and is recommended for further trials. The constructed system is suitable for lower pressure trials; however, at higher pressures the magnitude of the issue seems to increase.

Further optimization of the yields of ethylene, CO and benzene are also recommended. It is highly likely that the optimization of the species all require different operating conditions. Higher pressure trials are suggested to yield increased benzene production, whilst, ethylene and CO production can possibly increase by operation at pressures of approximately 300 kPa. Characterisation of the system at elevated pressures was not conducted due to the time constraints, however, further experiments based on this operating pressure are recommended.

Appendix A System Characterisation

A.1. Feeder Calibration

To determine the overall mass flowrate of biomass which entered the reactor, the feeder valve was calibrated throughout the experiments conducted.

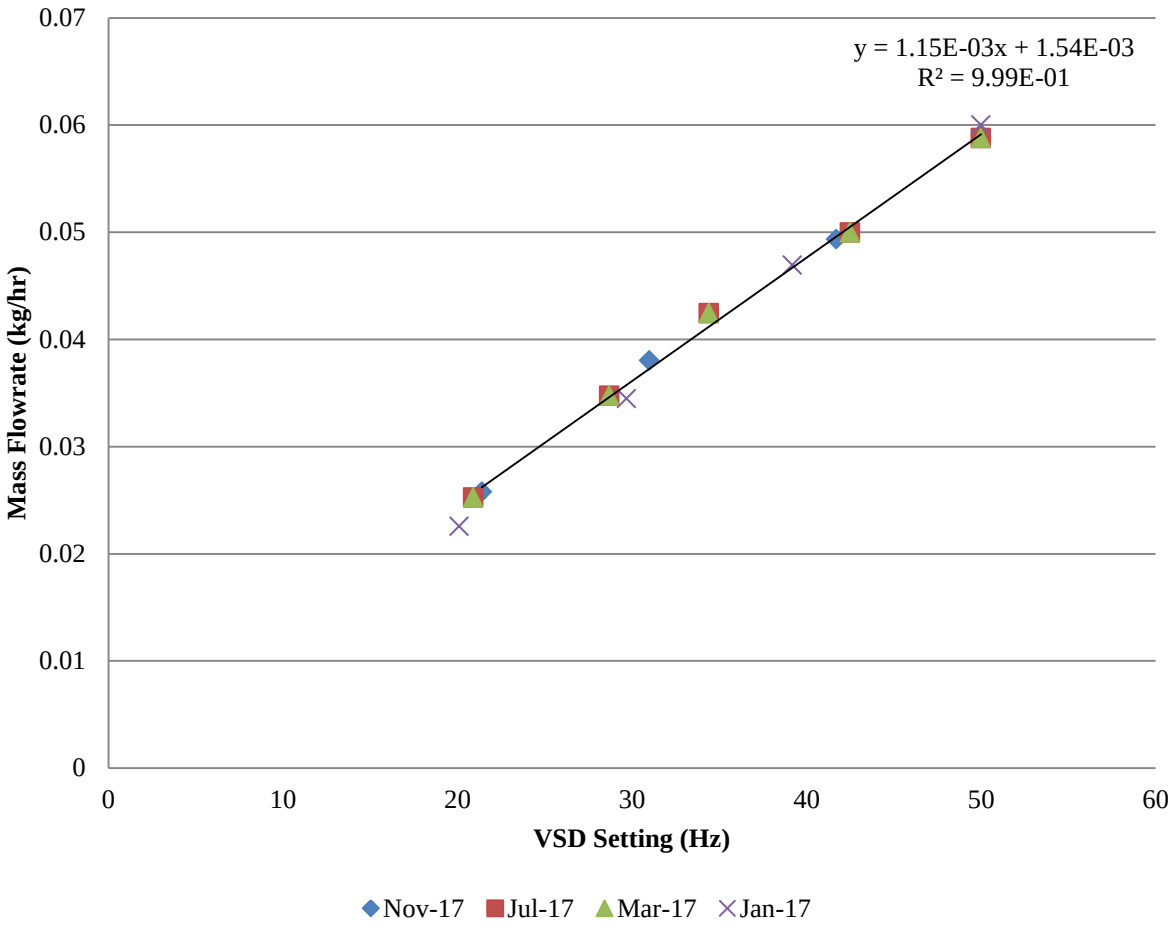

Figure A: Cup peek rotary valve feeder calibration.

To determine the uncertainty associated with the feeding system the standard error was calculated and the calculated error was determined for the feed rate for varied VSD settings. The overall calculated error was graphed and a third order polynomial was fitted for ease of computing the error given the VSD setting, Figure. An overall residual plot was also produced which suggested it was unlikely that the uncertainty was systematic.

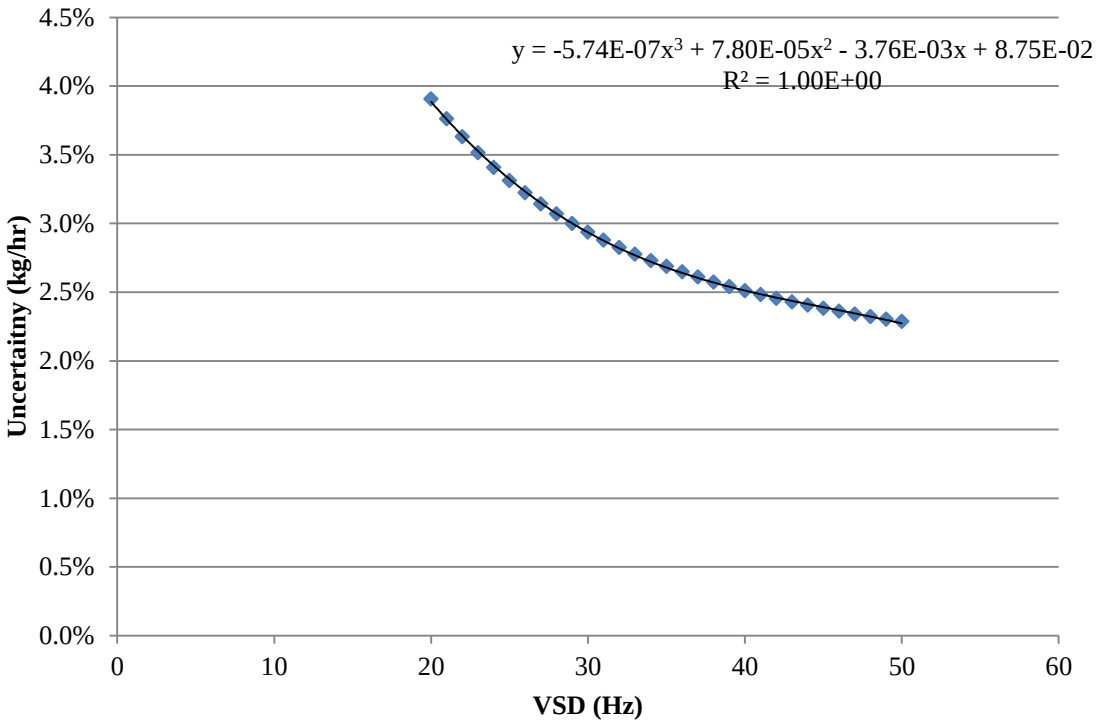

Figure B: Graph for computation of feeder uncertainty.

Micro GC Calibration

Concentration residual plots were produced to determine the uncertainty of the micro-GC utilized from a regression analysis. It was in turn determined that the random error of the machine was greater than the preparation of the samples for the calibration. This was also observed to increase/decrease depending on the concentration range for different species. Overall for consideration of the micro GC samples varying uncertainties were determined for each process gas in the concentration range of interest; an example for C_2H_4 is given below.

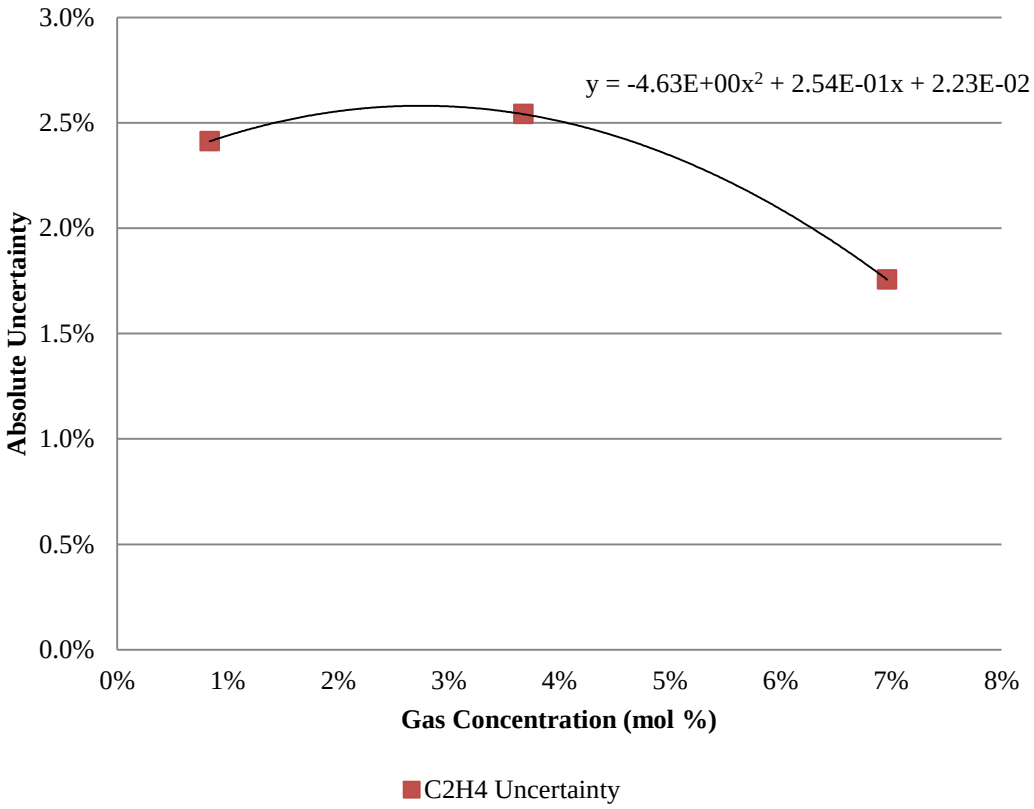

Figure C: Ethylene uncertainty from overall product gas composition.

A.2. Chip Characterisation

The following tables are derived from the results collected from the biomass characterisation report prepared by Scion, Rotorua.

Methods:

Moisture content:	Drying in oven at 104-105°C
% Extractives	Extraction with dichloromethane (DCM) following Tappi method T204 cm-97. Mean of duplicate analyses reported.
% Ash	Loss on ignition at 525°C following Tappi method T211 om-02. Mean of duplicate analyses reported.
% Acid-insoluble ash:	Amount of ash (chip weight basis) when residue after sulphuric acid hydrolysis is ashed at 575°C.
Elemental composition	Digestion with ICP-MS
% Carbohydrates	Sulphuric acid hydrolysis followed by sugar quantification by ion exchange chromatography. Mean of duplicate analyses reported.
% Klason lignin	Sulphuric acid hydrolysis/filtration (residue minus acid insoluble ash). Mean of duplicate analyses reported.
% Acid-soluble lignin	Transmission ultraviolet spectroscopy on the acid hydrolysate. The absorbance at 205 nm and an absorptivity of 110 L/g. Mean of duplicate analyses reported
% CHNS	Determined by Campbell Analytical Laboratory, university of Otago (Samples dried at 70°C under vacuum before analysis). Mean of duplicate analyses reported
% O	100 – [C+H+N+ash+S]

A.3. Residence Time Derivation

Due to the characteristics of the methane degradation and methanolysis products distribution the derivation of accurate residence times was essential. For the derivation of the effective value, the distance of the cold portions of the reactor were determined. This was assumed to be the 215 mm as this was the length until the pipe was exposed to a bare heater element. The derivation of this value was supported by the height of the black mirror carbon deposits which were on the quartz element, which related to a cool section of 215 mm. The overall volumes were dependent on the configuration of the reactor, where significant variations in residence times were obtained with the removal/addition of materials within the reactor system. A relationship was formed for the variations which allowed the bed height, frit location, quartz element dimensions, and gas flowrate and gas temperature to be function handles. For the residence time calculations, it was assumed that the temperature of the gas was constant throughout, and the value reduction in residence time, due to devolatisation during methanolysis, could be derived from the analysis. For MTD it was assumed that the residence time as not varied due to hydrogen release, although this is unlikely, the composition of the carbon and gas stream were usually in a constant ratio, which avoided any significant variations. The values used for the definition of the residence times are shown below in Table A,

Table A: Methanolysis reactor system constants utilized for the derivation of the residence time, where the cells highlighted in orange show the values that varied significantly with reactor configuration (All values when the system is at set temperature, 1000 °C for this example).

Constant	Value	Units
Quartz liner ID	53	*mm*
Quartz liner length	800	*mm*
Dropper Tube OD	46	*mm*
Dropper Tube Length	174	*mm*
Bed height	**53**	***mm***
Quartz frit location (From Top)	**260**	***mm***
Preheater Length	540	*mm*
Quartz frit thickness	5	*mm*
Bottom/Top length (Cold)	215	*mm*
Quartz element length	**520**	***mm***
Quartz element OD	**46**	***mm***
Flange Thickness	28.5	*mm*
Length of Dropper in heated Zone	36.5	*mm*
Free Board Area above bed to dropper	10	*mm*

From the values of the reactor configuration, similar to the example in Table B, the overall volumes of the separate sections could be deduced, as shown in Table B.

Table B: Volume derivations for the separate sections of the reactor.

Constant	Value	Unit
Preheater volume	3.3E-04	m^3
Volume below Frit	1.9E-04	m^3
Volume below frit + bed	2.3E-04	m^3
Including freeboard volume	3.9E-04	m^3
Volume above dropper tip	2.0E-05	m^3
Total volume	7.3E-04	m^3

Form which the overall residence time for the section of interest could be determined using Table C.

Table C: Reactor residence time variations, calculated from the volumes derived in Table B, cells in orange indicate variables which were modified throughout the derivation of residence time.

Constant	**Value**	Unit
Gas flowrate	**0.145**	kg/hr
Gas Temperature (Atmospheric Pressure)	**1000**	°C
Gas Density	0.15	kg/m^3
Volumetric Flowrate	9.5E-01	m^3/hr
Volumetric Flowrate	2.6E-04	m^3/s
rt (Overall)	2.8	s
Residence Time in Freeboard Area[xxx]	2.8E-01	s

[xxx] Where the residence time in the freeboard area is the volume above the frit to the end of the heated zone.

Appendix B Modelling Description

B.1. TGA Modelling Constraints

Table D: Constraint settings used for the modelling of cellulose, hemicellouse and lignin during pyrolysis.

Variable	Constriction	Constraint Value
$Ea_{Cellulose}$	<=	300 kJ/mol
$Ea_{Cellulose}$	>=	200 kJ/mol
$Ea_{Hemicellulose}$	<=	150 kJ/mol
$Ea_{Hemicellulose}$	>=	75 kJ/mol
Ea_{Lignin}	<=	100 kJ/mol
Ea_{Lignin}	>=	10 kJ/mol
$k_{Cellulose}$	<=	$9x10^{19}$ s^{-1}
$k_{Cellulose}$	>=	$1x10^{16}$ s^{-1}
$k_{Hemicellulose}$	<=	$9x10^{10}$ s^{-1}
$k_{Hemicellulose}$	>=	$1x10^{6}$ s^{-1}
k_{Lignin}	<=	450 s^{-1}
k_{Lignin}	>=	0.1 s^{-1}

The solver function was used to minimize the error associated with the least squared method. The Solver function on Microsoft Excel was used; the solving method used was GRG Nonlinear, where the constraint precision was 0.01. The convergence level of the GRG Nonlinear method was also set to 0.01, with a forward derivative approach used.

B.2. Gibbs Energy Modelling

The Gibbs energy modelling was conducted on UNISIM R440. The model comprised of three separate feeds; ethane (Biomass Model), Methane Excess and Water (Biomass Model). The modelling was conducted using the SRK fluid package with Lee Kesler equation of state relationships. The three streams were combined using a mixer and were then compressed to the desired pressure, as water was in the stream an error would arise (as shown by the yellow outline), which could be overridden and it was assumed that the water was still liquid when it arrived at the Gibbs reactor. The pressurized feed then entered the Gibbs reactor which was operated via minimization of the identified components, as listed below, with respect to the feed. The bottoms and tops products were at the operating temperature, with the tops products cooled with a hypothetical cooler. The reactor temperature was kept constant with a hypothetical electricity stream Note: no product was ever modelled to be removed via the bottoms product stream. A screenshot of the process application from Unisim is provided below in **Error! Reference source not found.**.

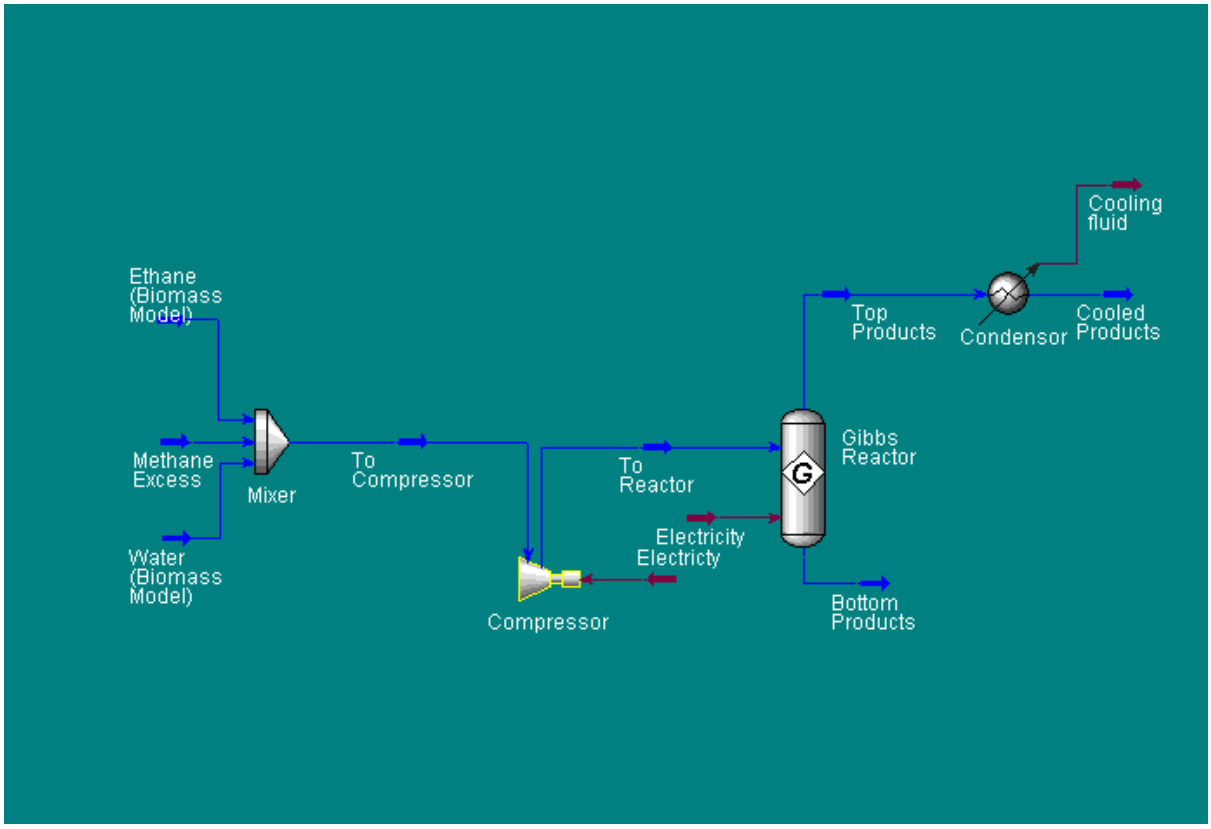

Figure D: Unit operations and feedlines utilized in Gibbs energy modelling.

In total 17 species were utilized in the model, as additional species rendered issues as outlined in the results chapter. Note: The presence of naphthalene varied during the modelling scenarios. The species employed in the model were:

- CH_4
- C_2H_4
- C_2H_2
- C_2H_6
- CO_2
- Toluene
- Benzene
- Carbon
- H_2O
- H_2
- CO
- Biphenyl
- Propadiene
- Phenol
- Styrene
- Indene
- Naphthalene

To determine the flowrate of methane for various M/B ratios, the species were adjusted to determine the flowrate of the 'excess methane'. Equation A.1(A.1), provided the stoichiometry for the equation and allowed for the representative values of ethane (named: Ethane Biomass Model) and water (named: Water Biomass Model) to be determined. The additional methane was added respective to the M.B ratio.

$$CH_{1.5}O_{0.8} + 3.1CH_4 \rightarrow 2.05C_2H_6 + 0.8H_2O \qquad \text{(A.1)}$$

Appendix C Flash Methanolysis apparatus Drawings

C.1. Reactor System Drawings

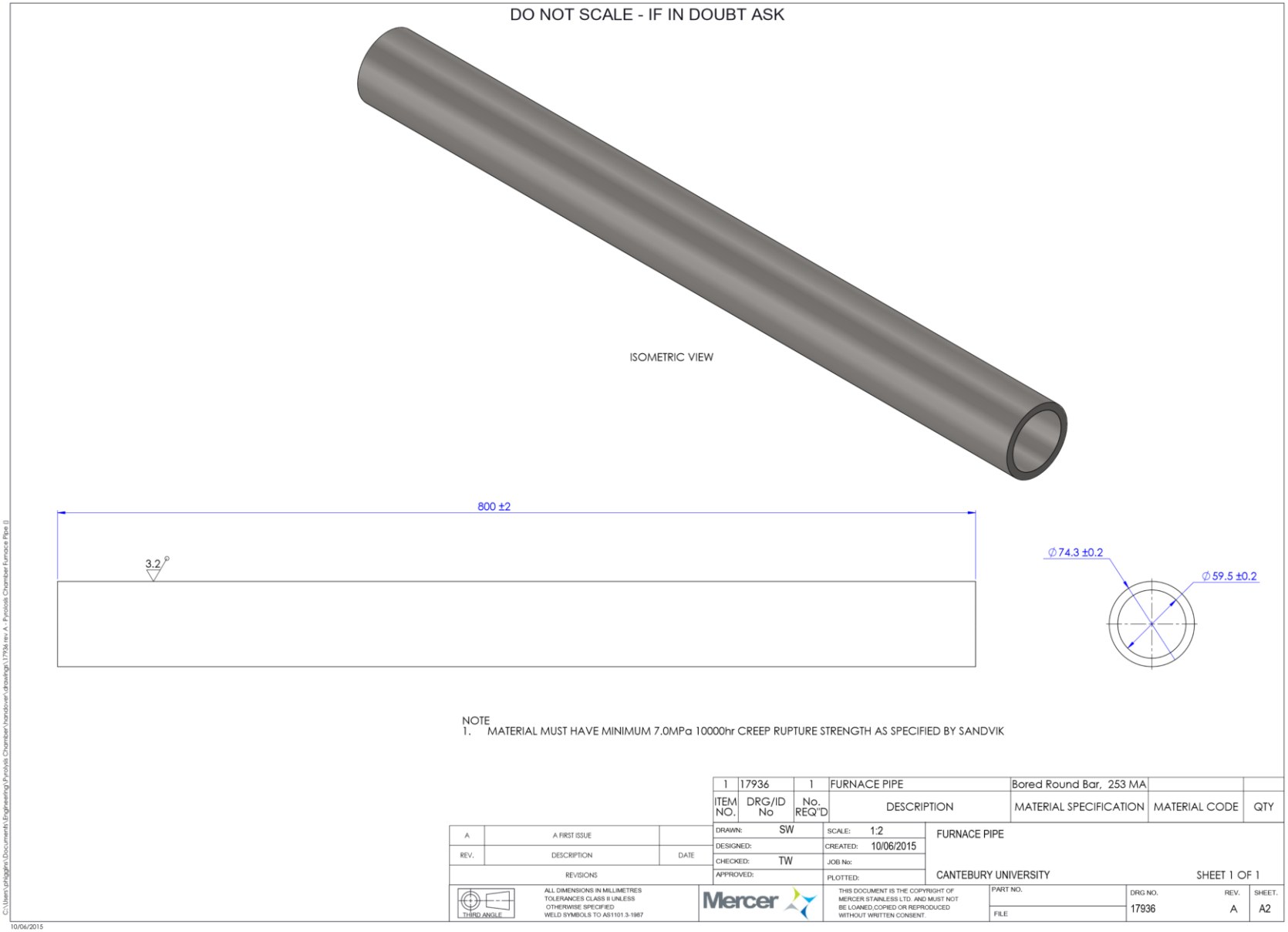

Figure E: Reactor fluidised bed pipe boring.

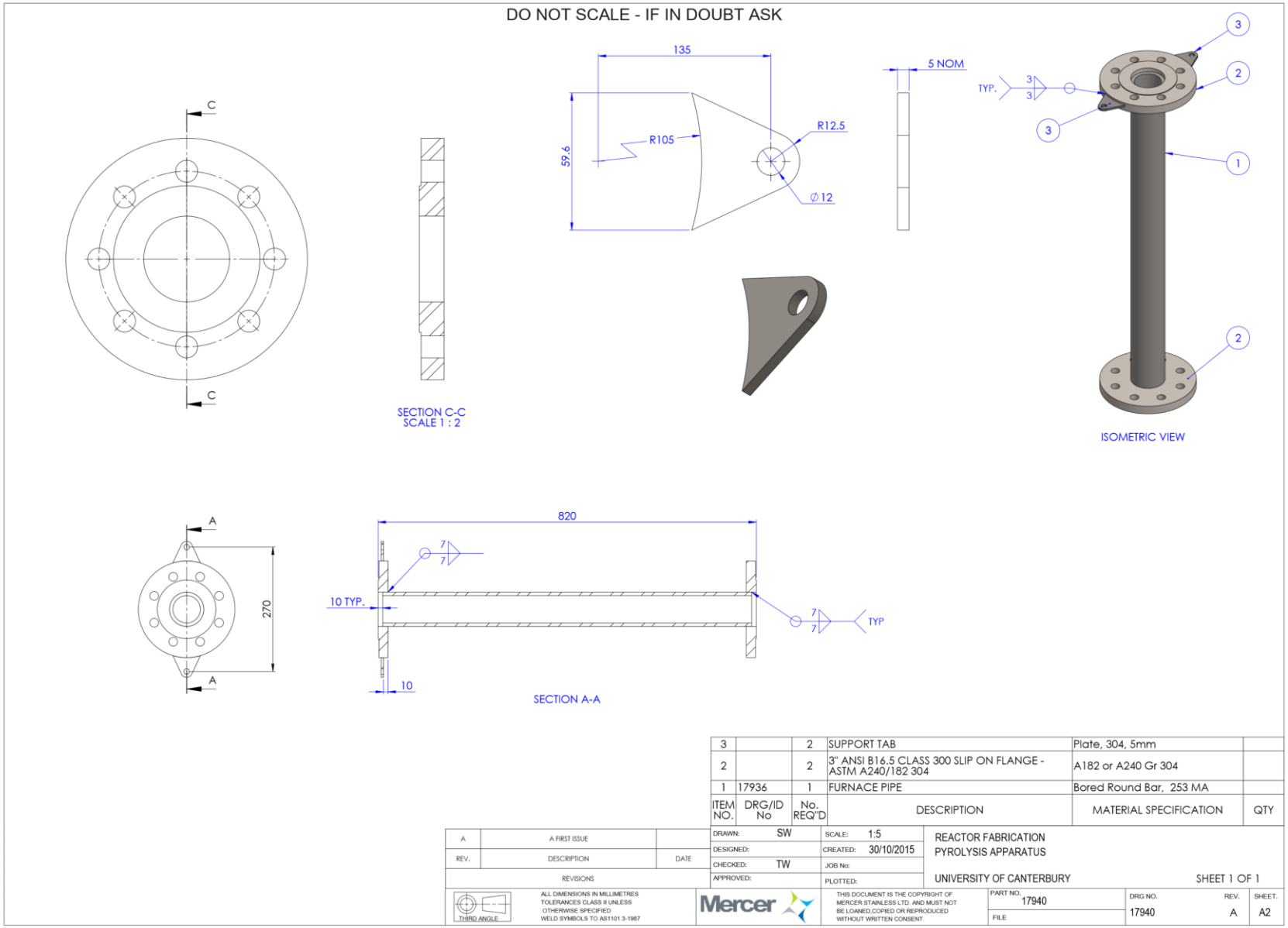

Figure F: Fluidised bed reactor pipe arrangement.

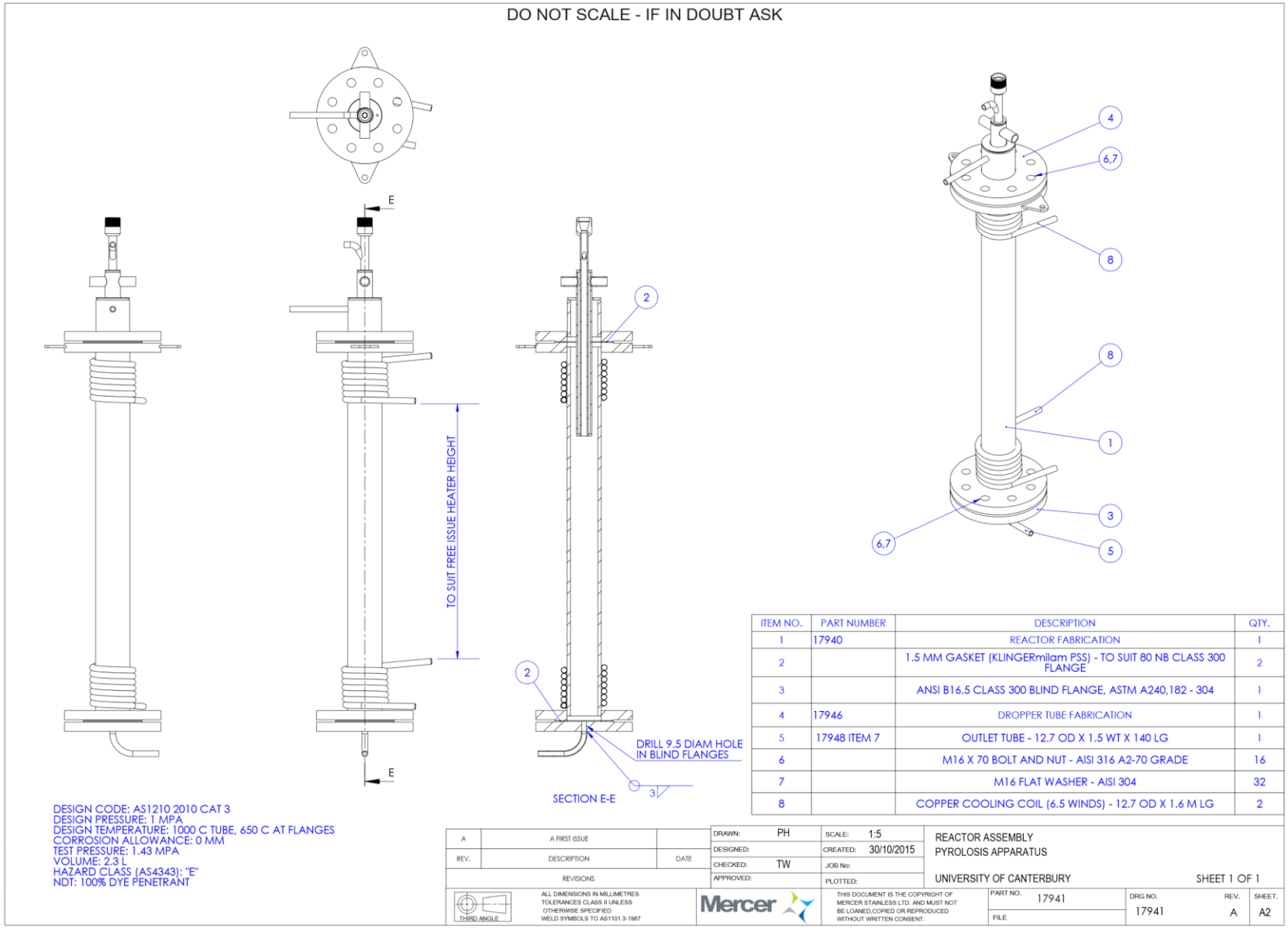

Figure G: Fluidised bed reactor pipe arrangement (continued).

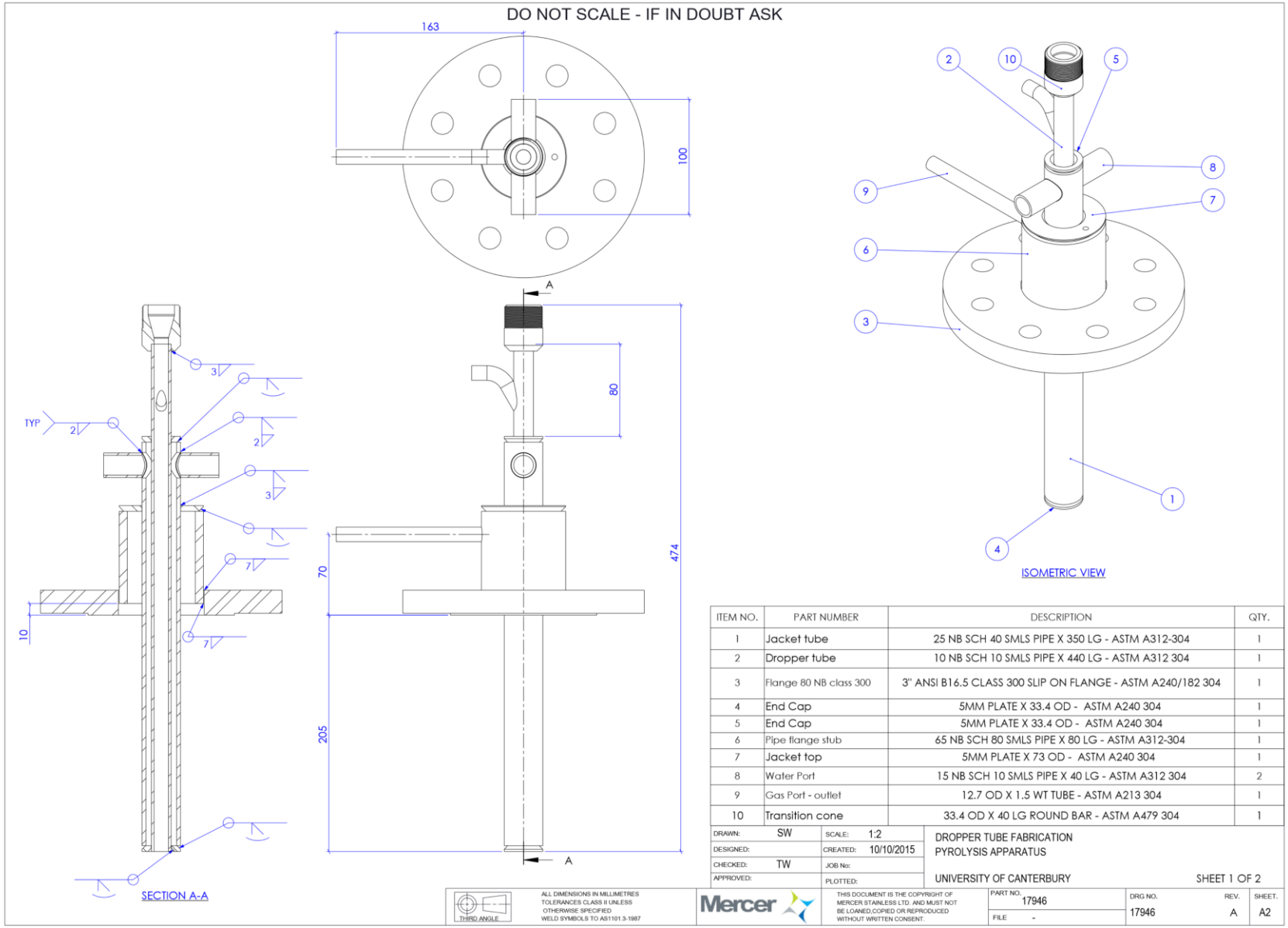

Figure H: Reactor dropper tube arrangement.

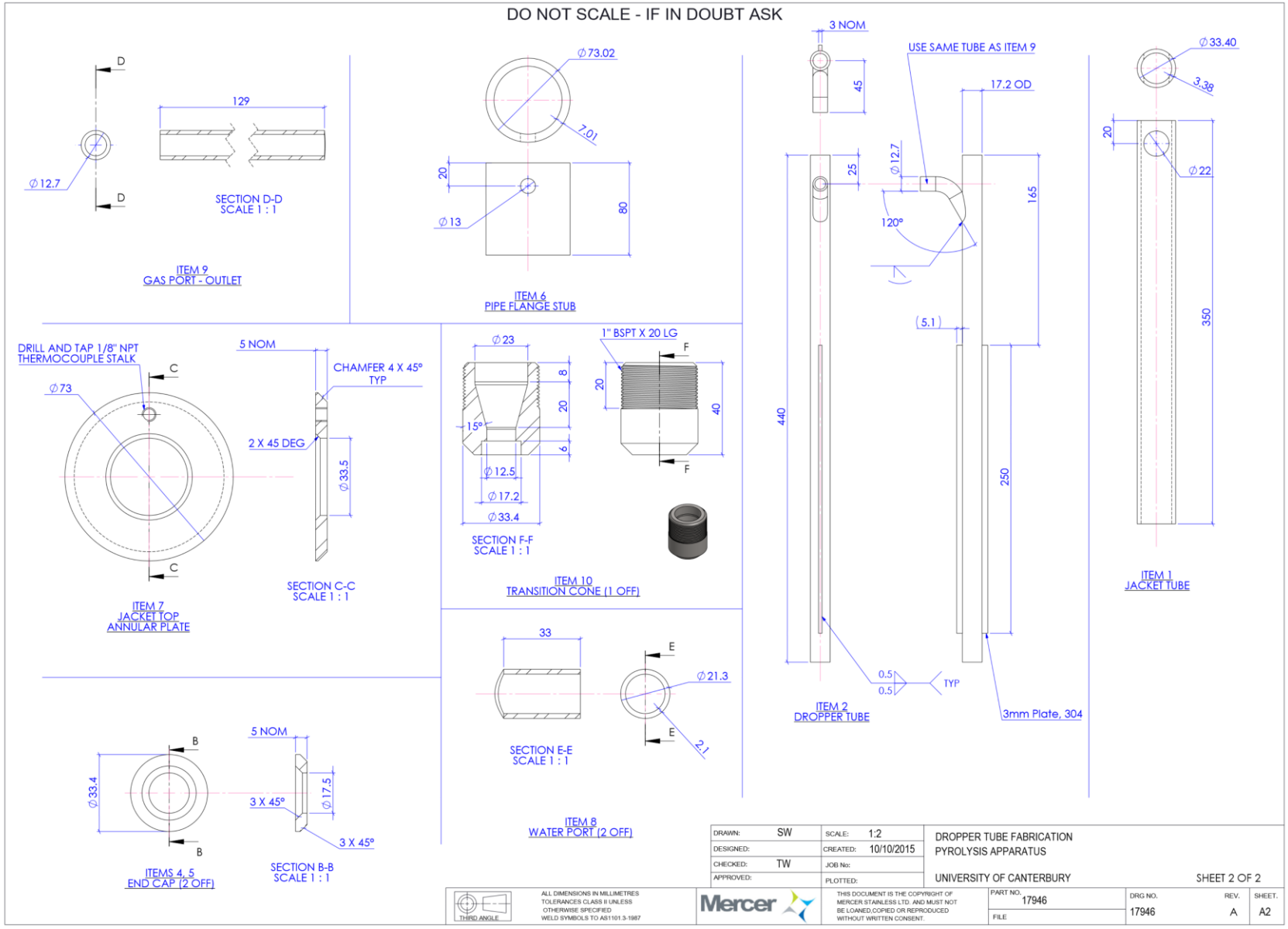

Figure I: Reactor dropper tube arrangement (continued).

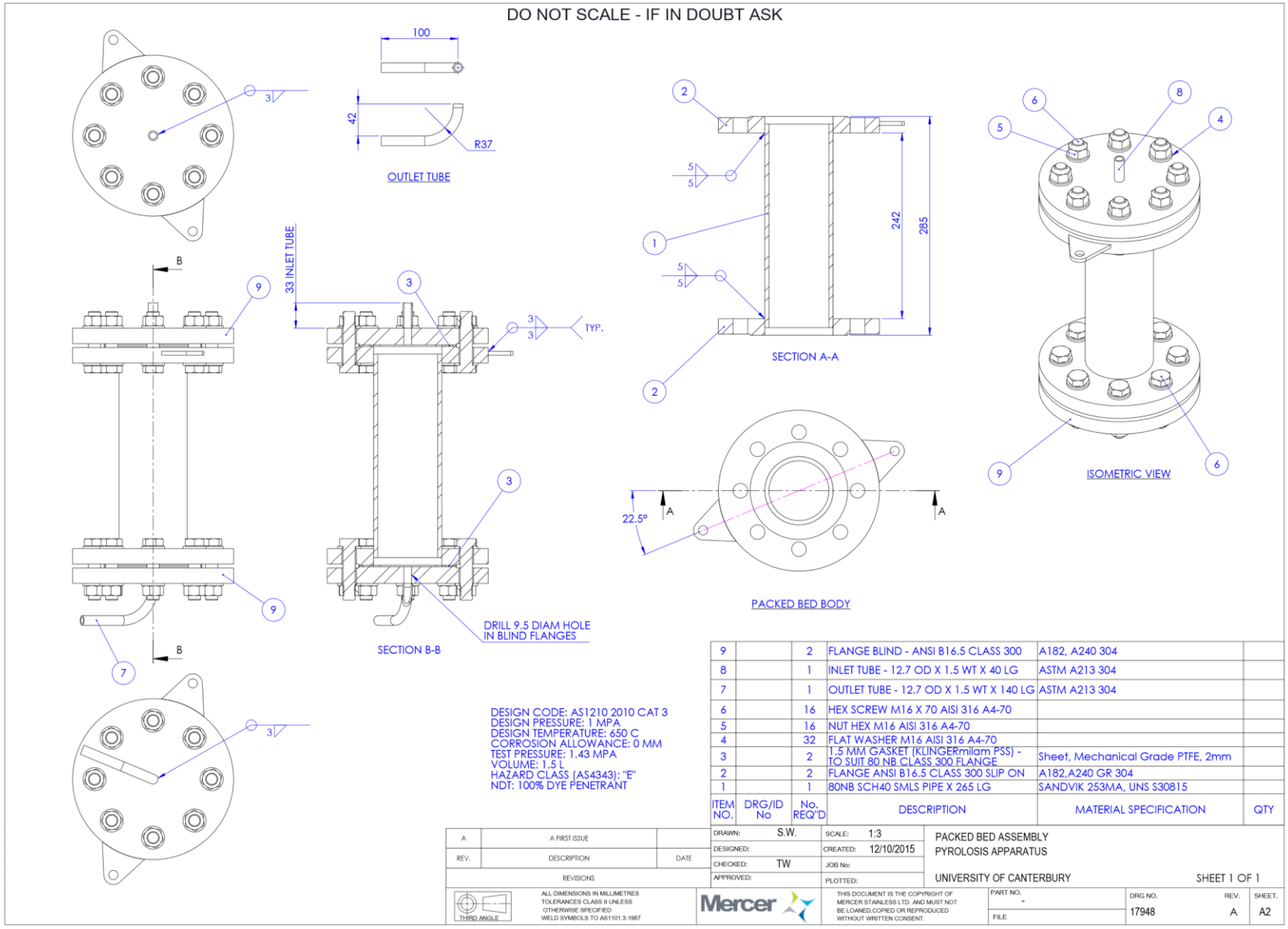

Figure J: Packed bed reactor.

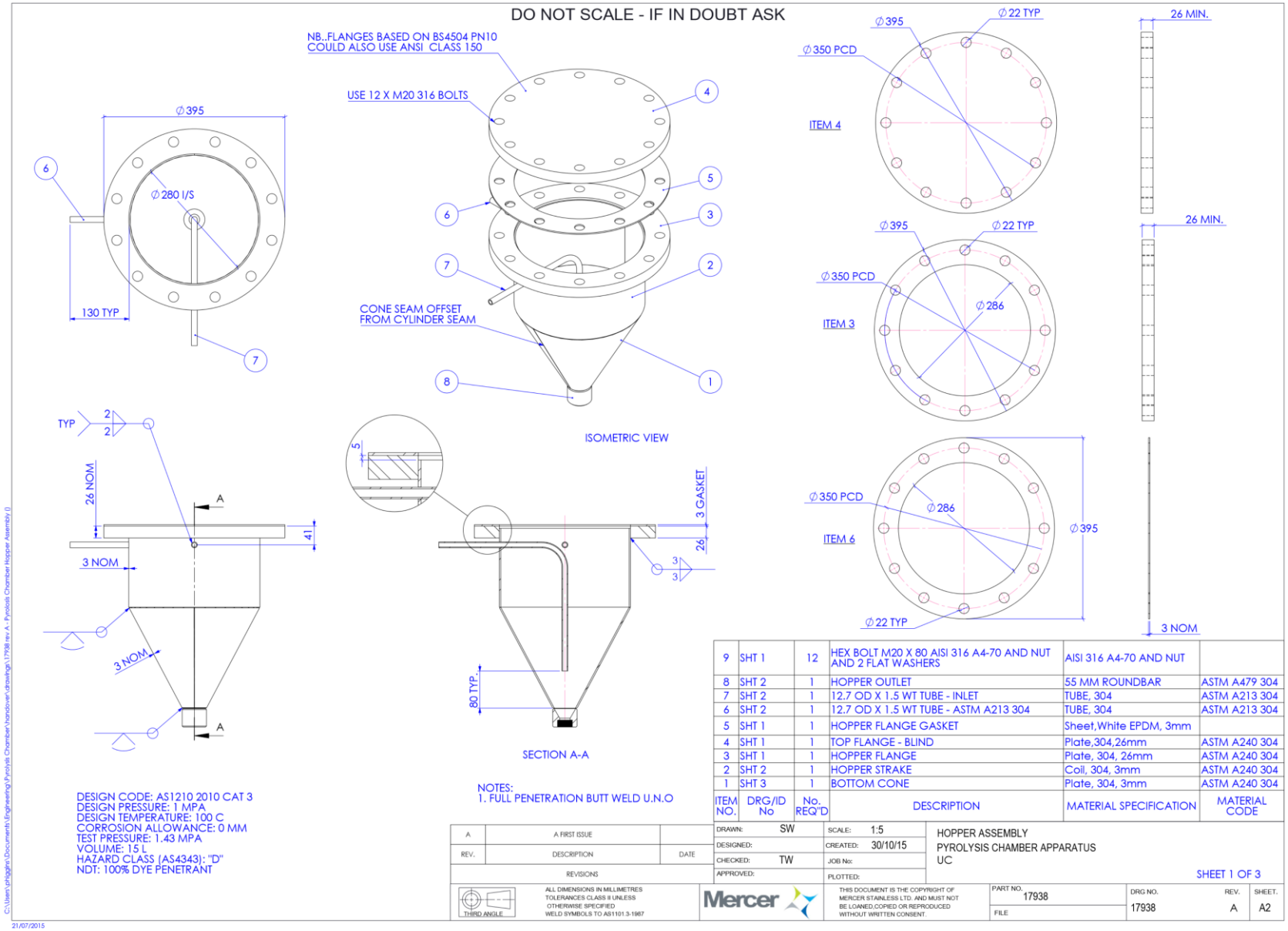

ITEM NO.	DRG/ID No	No. REQ'D	DESCRIPTION	MATERIAL SPECIFICATION	MATERIAL CODE
9	SHT 1	12	HEX BOLT M20 X 80 AISI 316 A4-70 AND NUT AND 2 FLAT WASHERS	AISI 316 A4-70 AND NUT	
8	SHT 2	1	HOPPER OUTLET	55 MM ROUNDBAR	ASTM A479 304
7	SHT 2	1	12.7 OD X 1.5 WT TUBE - INLET	TUBE, 304	ASTM A213 304
6	SHT 2	1	12.7 OD X 1.5 WT TUBE - ASTM A213 304	TUBE, 304	ASTM A213 304
5	SHT 1	1	HOPPER FLANGE GASKET	Sheet,White EPDM, 3mm	
4	SHT 1	1	TOP FLANGE - BLIND	Plate,304,26mm	ASTM A240 304
3	SHT 1	1	HOPPER FLANGE	Plate, 304, 26mm	ASTM A240 304
2	SHT 2	1	HOPPER STRAKE	Coil, 304, 3mm	ASTM A240 304
1	SHT 3	1	BOTTOM CONE	Plate, 304, 3mm	ASTM A240 304

REV.	DESCRIPTION	DATE
A	A FIRST ISSUE	

REVISIONS

DRAWN: SW | SCALE: 1:5
DESIGNED: | CREATED: 30/10/15
CHECKED: TW | JOB No:
APPROVED: | PLOTTED:

ALL DIMENSIONS IN MILLIMETRES
TOLERANCES CLASS II UNLESS
OTHERWISE SPECIFIED
WELD SYMBOLS TO AS1101.3-1987

THIRD ANGLE

PART NO. 17938 | FILE
DRG NO. 17938 | REV. A | SHEET. A2

C:\Users\phiggins\Documents\Engineering\Pyrolysis Chamber\Handover\drawings\17938 rev A - Pyrolysis Chamber Hopper Assembly (

21/07/2015

Figure K: Hopper construction.

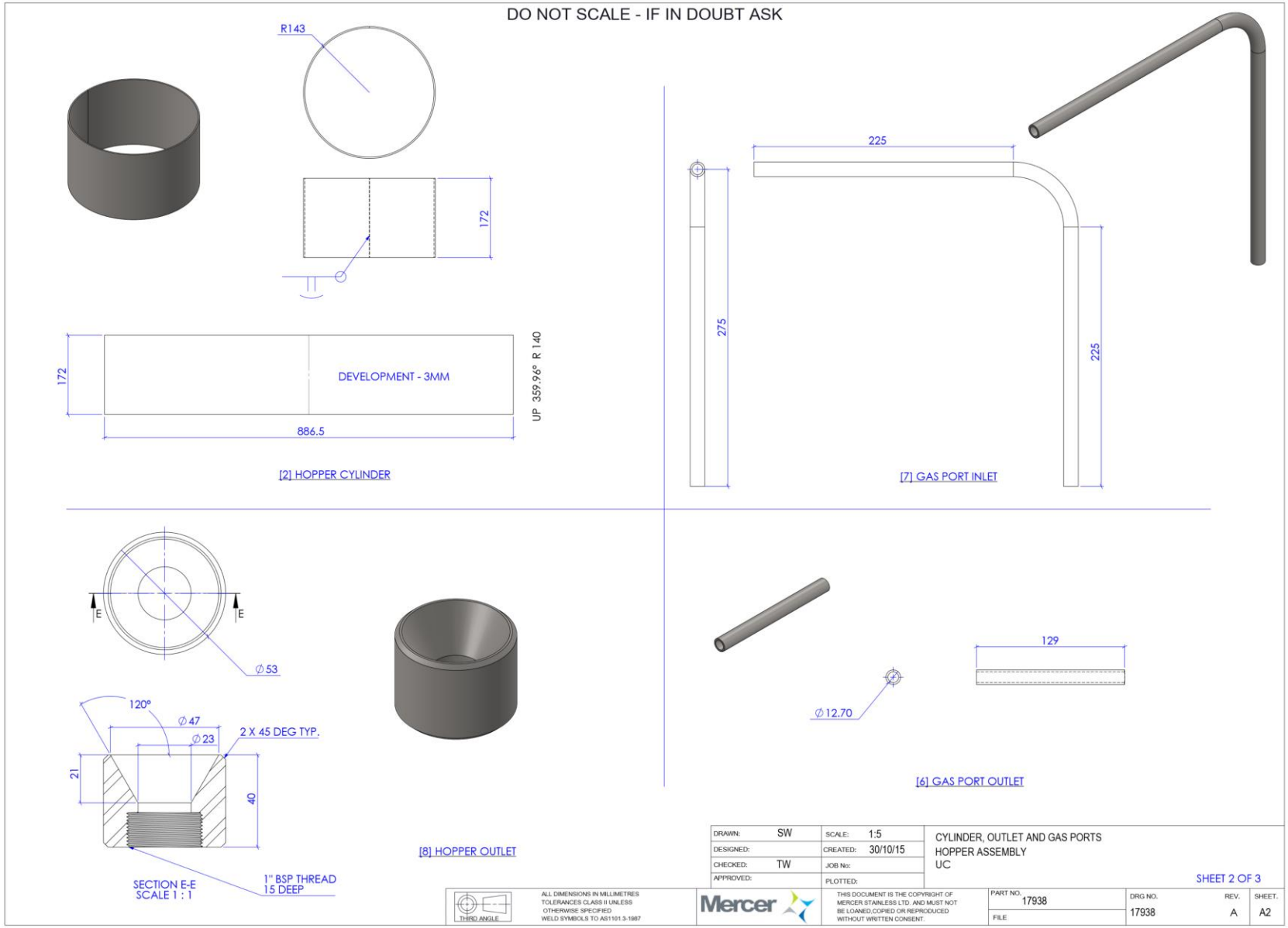

Figure L: Hopper construction (continued).

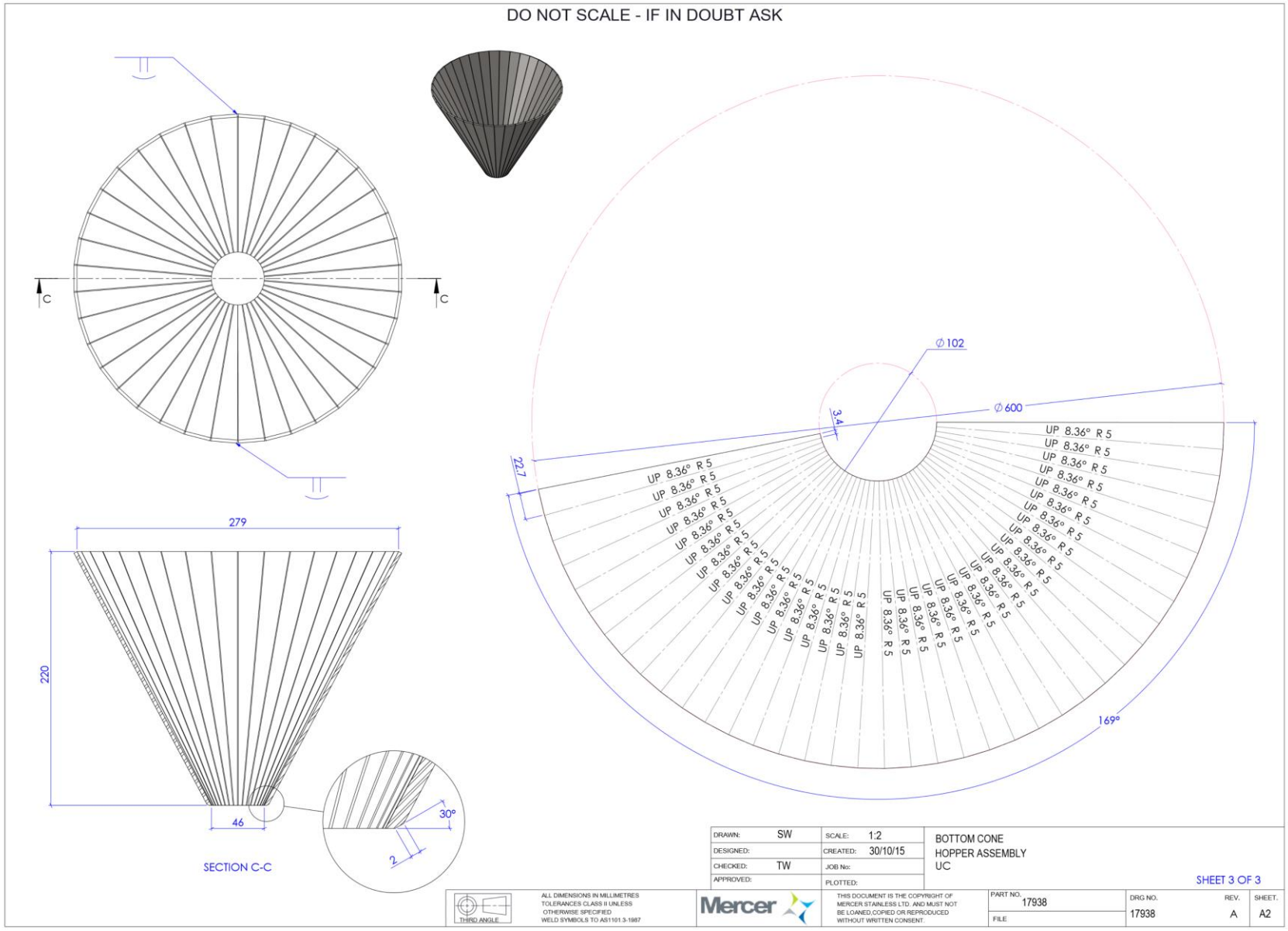

Figure M: Hopper construction (continued).

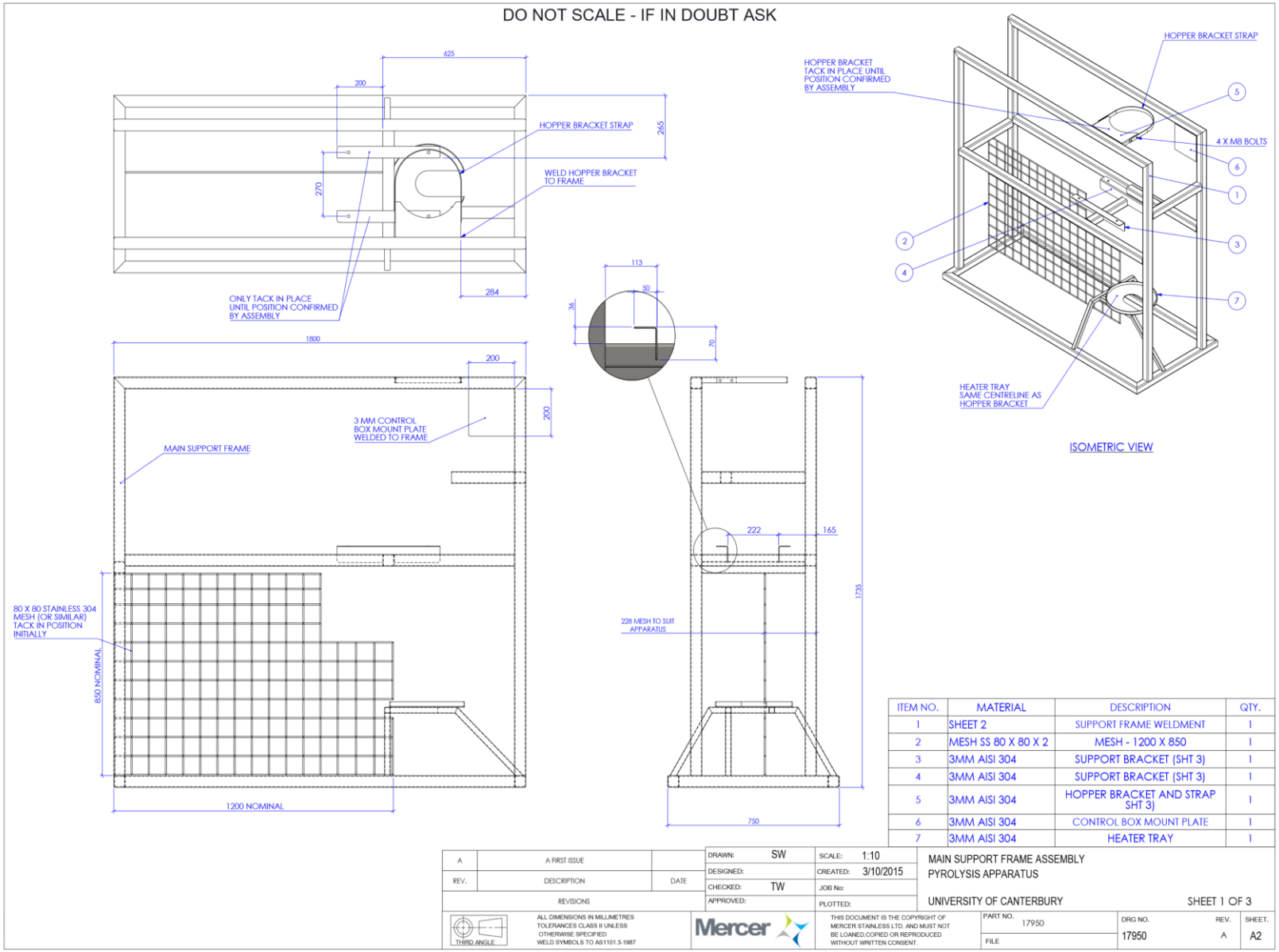

Figure N: Reactor apparatus frame.

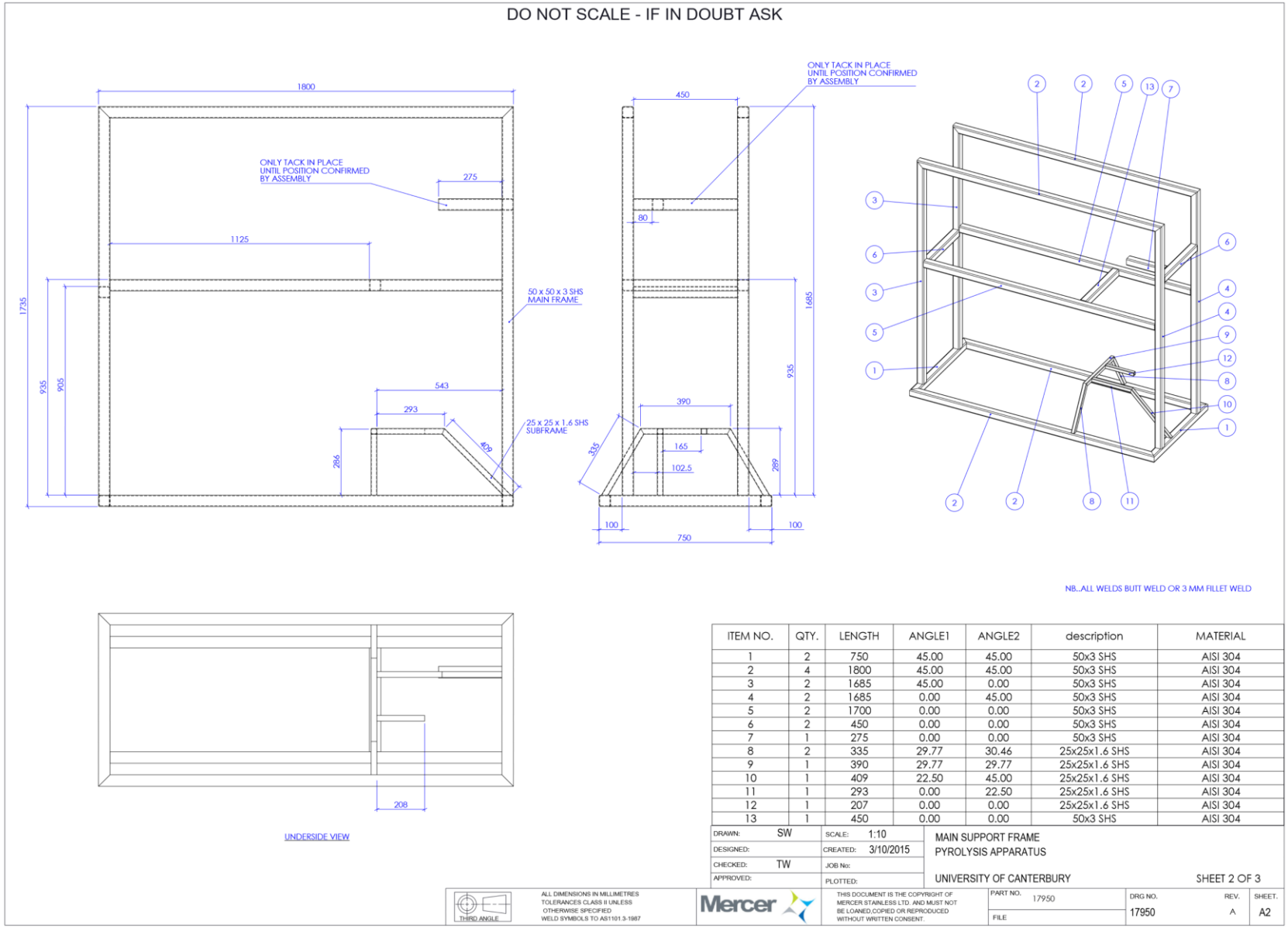

ITEM NO.	QTY.	LENGTH	ANGLE1	ANGLE2	description	MATERIAL
1	2	750	45.00	45.00	50x3 SHS	AISI 304
2	4	1800	45.00	45.00	50x3 SHS	AISI 304
3	2	1685	45.00	0.00	50x3 SHS	AISI 304
4	2	1685	0.00	45.00	50x3 SHS	AISI 304
5	2	1700	0.00	0.00	50x3 SHS	AISI 304
6	2	450	0.00	0.00	50x3 SHS	AISI 304
7	1	275	0.00	0.00	50x3 SHS	AISI 304
8	2	335	29.77	30.46	25x25x1.6 SHS	AISI 304
9	1	390	29.77	29.77	25x25x1.6 SHS	AISI 304
10	1	409	22.50	45.00	25x25x1.6 SHS	AISI 304
11	1	293	0.00	22.50	25x25x1.6 SHS	AISI 304
12	1	207	0.00	0.00	25x25x1.6 SHS	AISI 304
13	1	450	0.00	0.00	50x3 SHS	AISI 304

DRAWN: SW	SCALE: 1:10	PART NO. 17950	DRG NO. 17950
DESIGNED:	CREATED: 3/10/2015	FILE	REV. A
CHECKED: TW	JOB No:		SHEET. A2
APPROVED:	PLOTTED:		

Figure O: Reactor apparatus frame (continued).

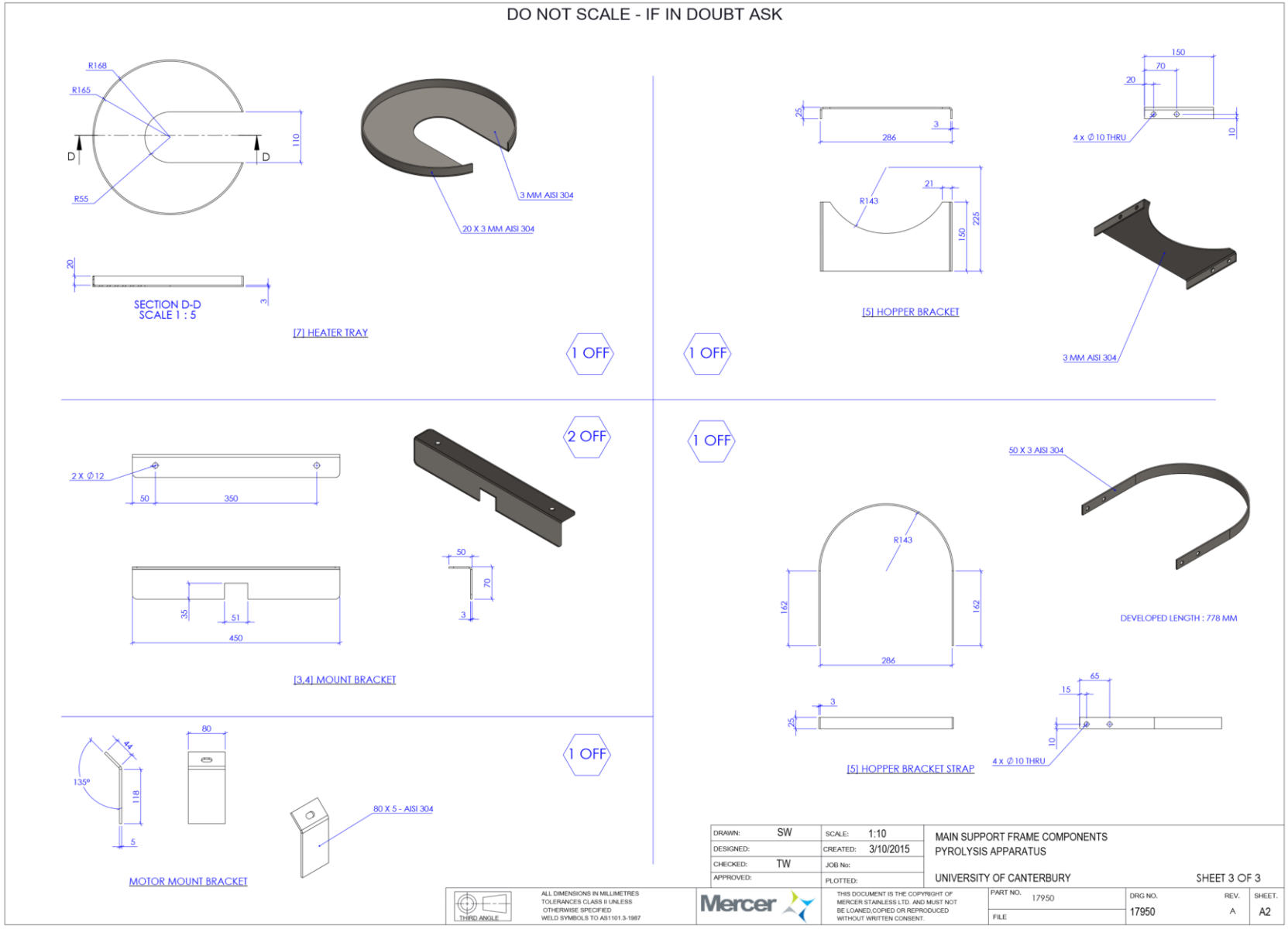

Figure P: Reactor apparatus frame (continued).

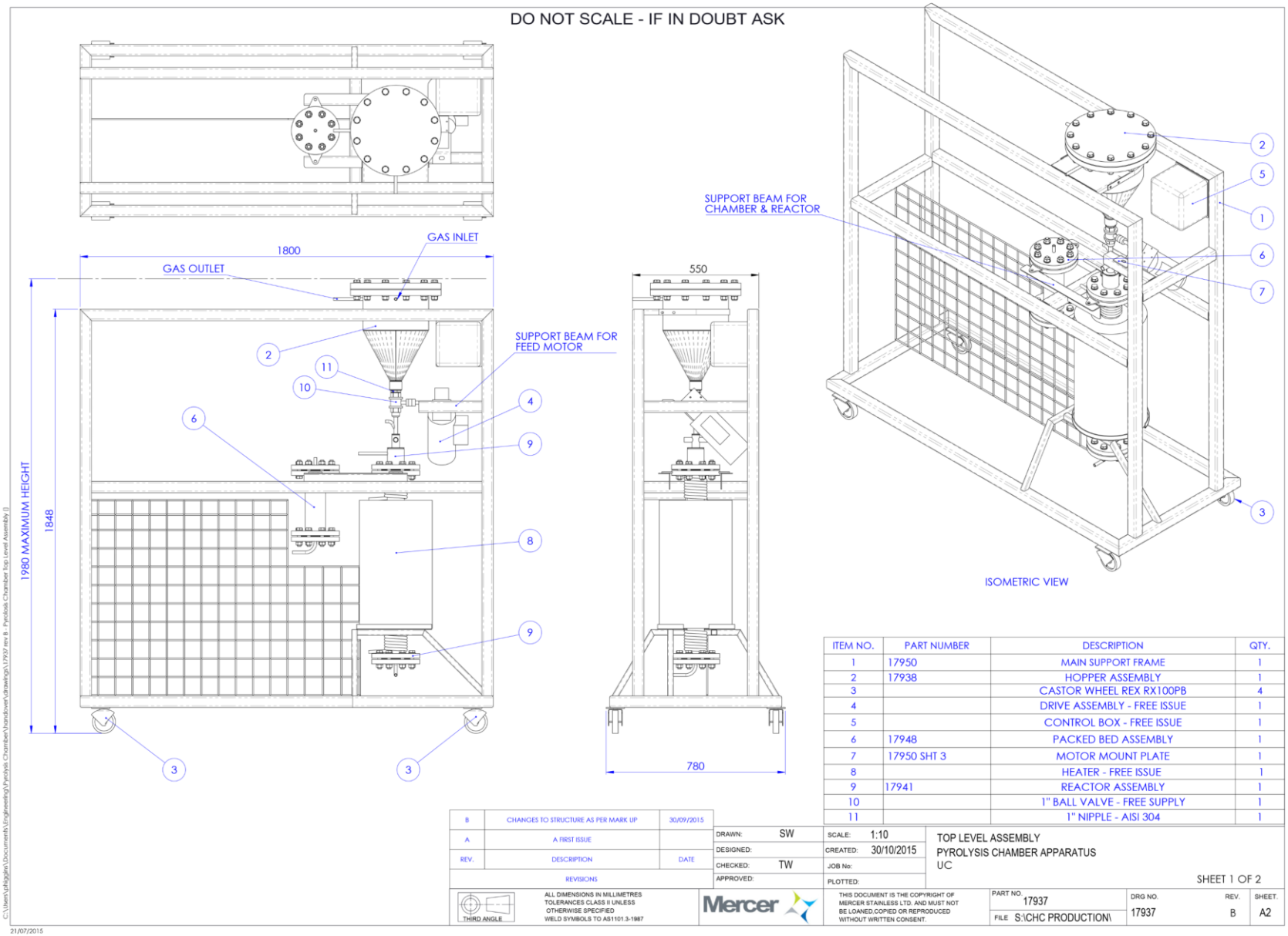

Figure Q: Reactor apparatus complete arrangement.

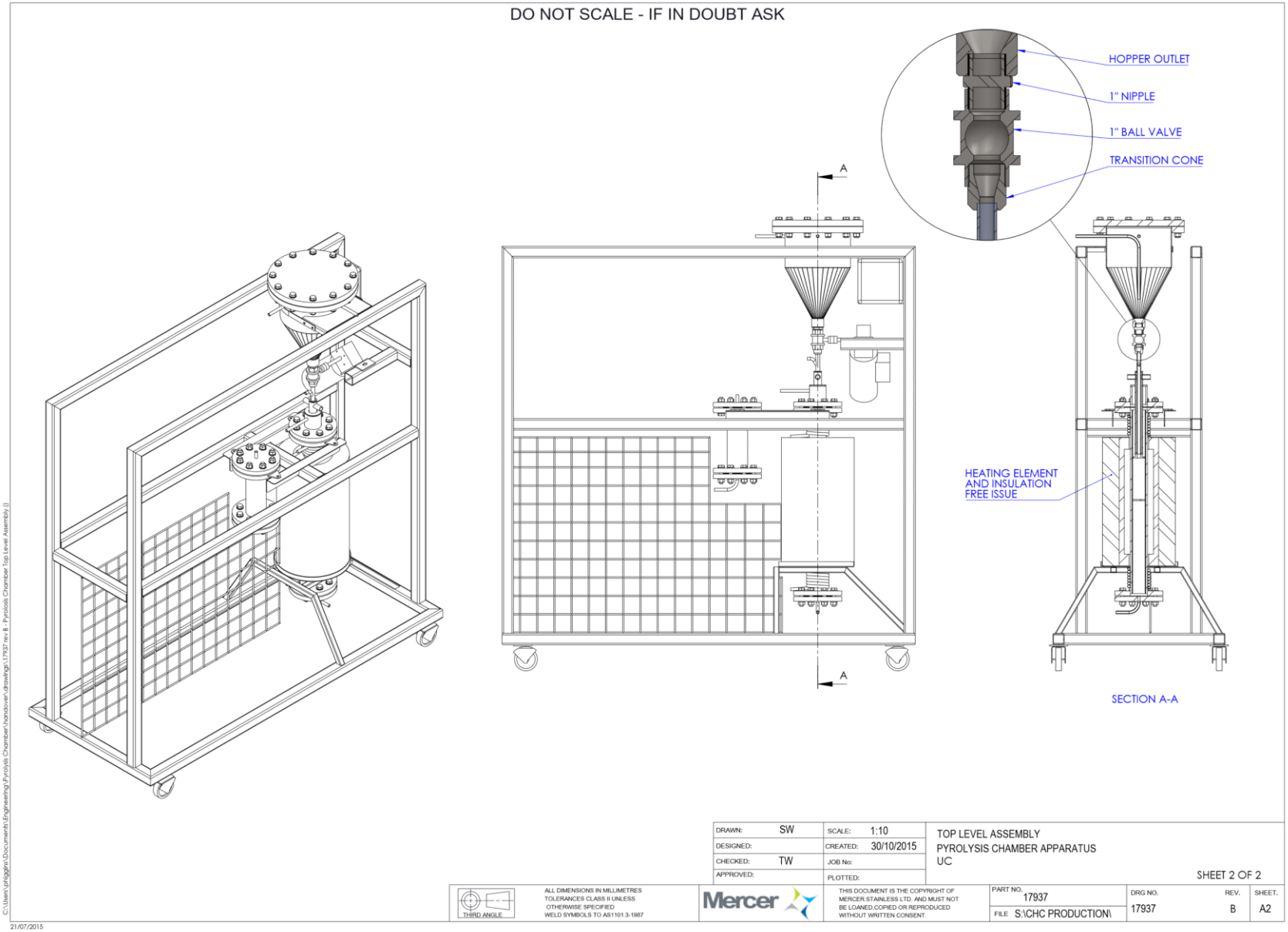

Figure R: Reactor apparatus complete arrangement (continued).

C.2. Quartz Liner Diagrams

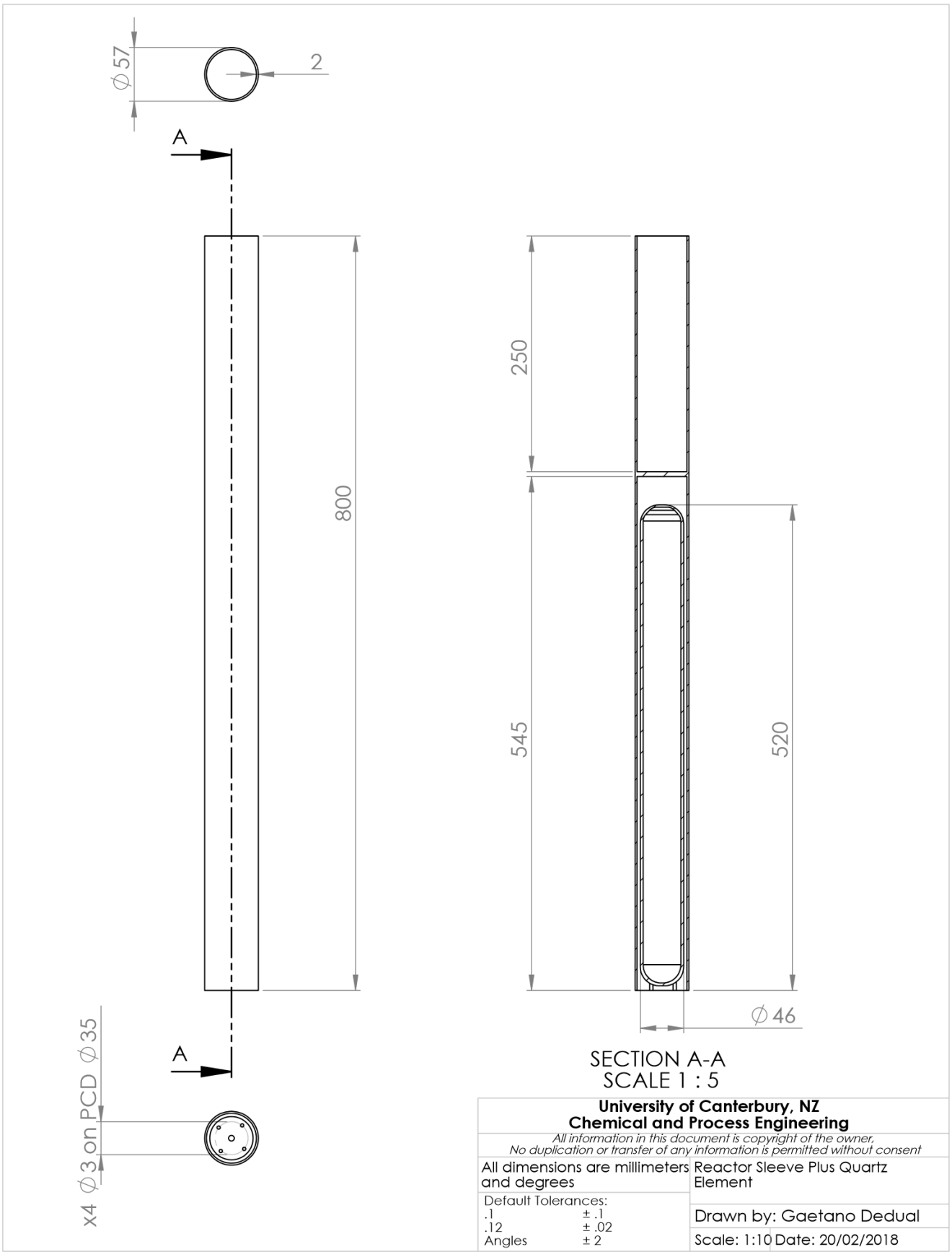

Figure S: Quartz liner arrangement (I), with fabricated quartz element.

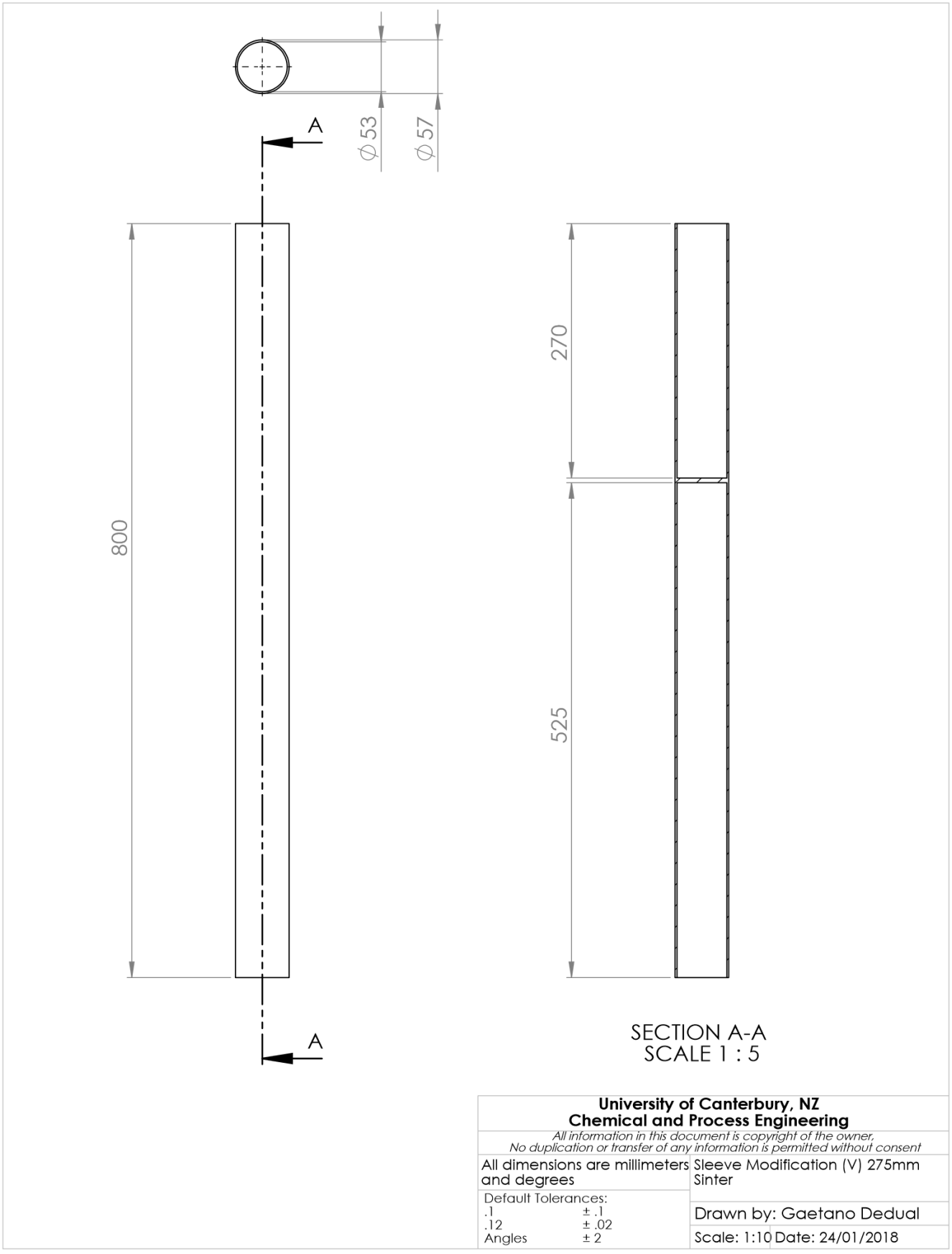

Figure T: Quartz liner arrangement (II).

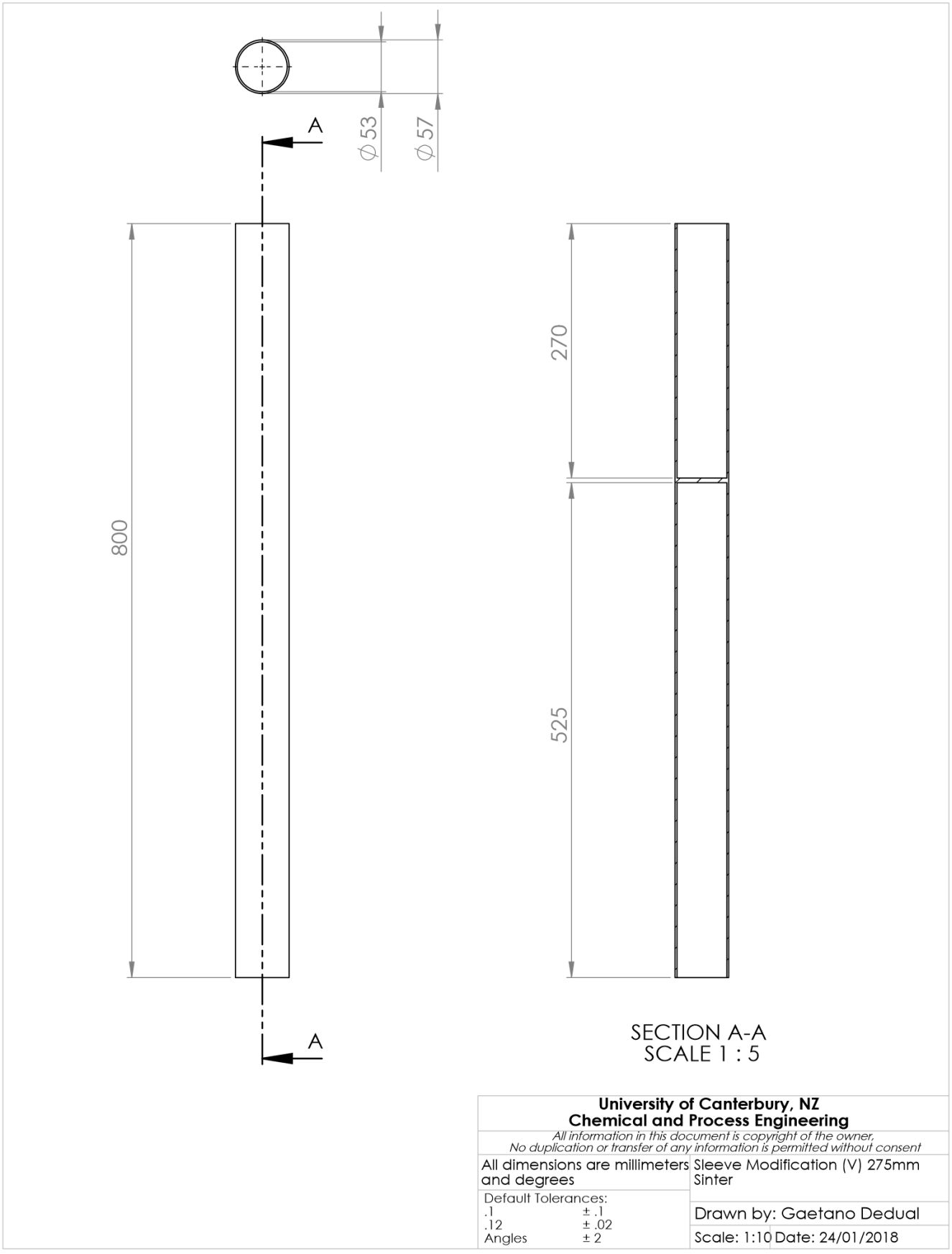

Figure U: Quartz liner arrangement (III).

C.3. Rotary Feeder Drawings

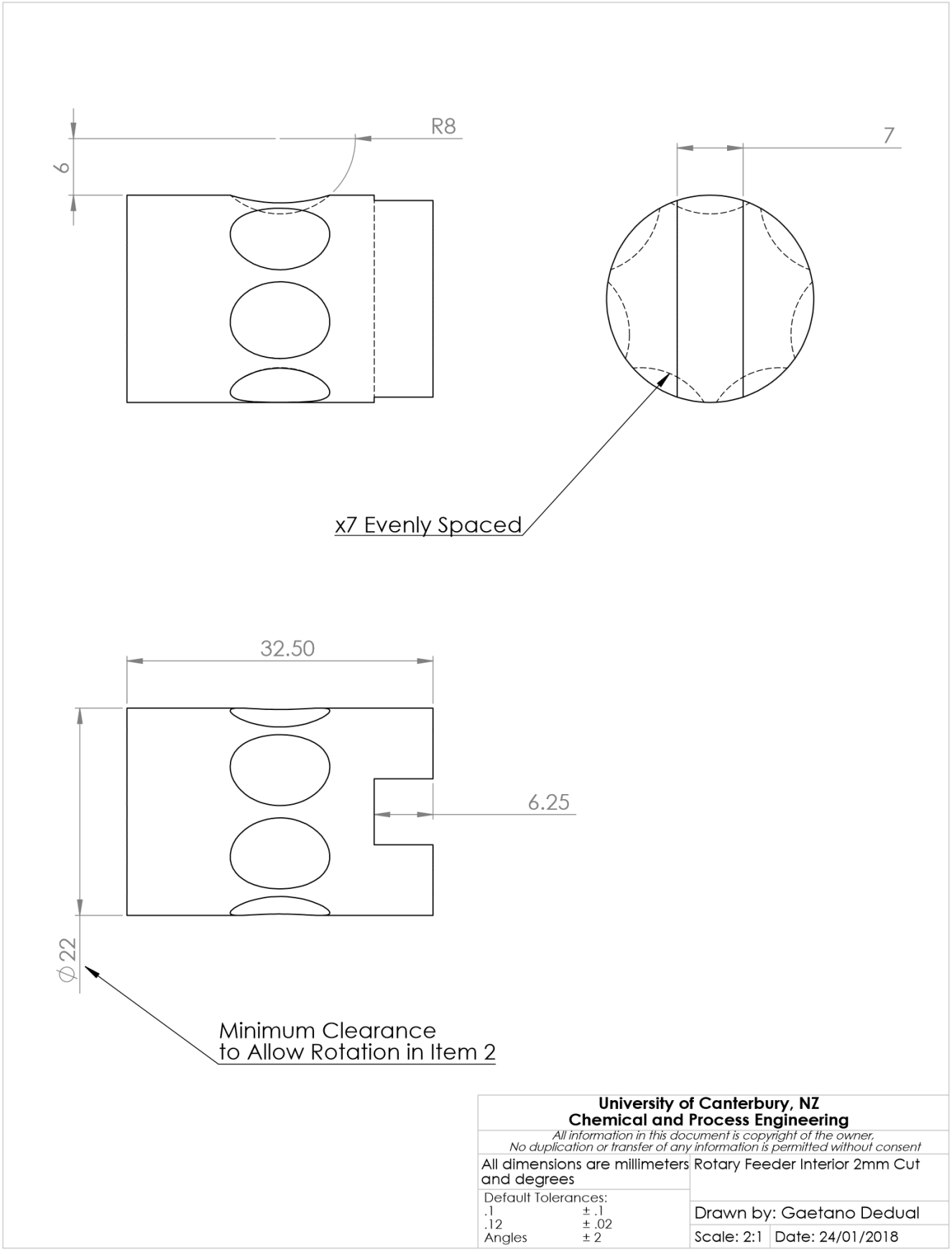

Figure V: 7-cup rotary feeder insert.

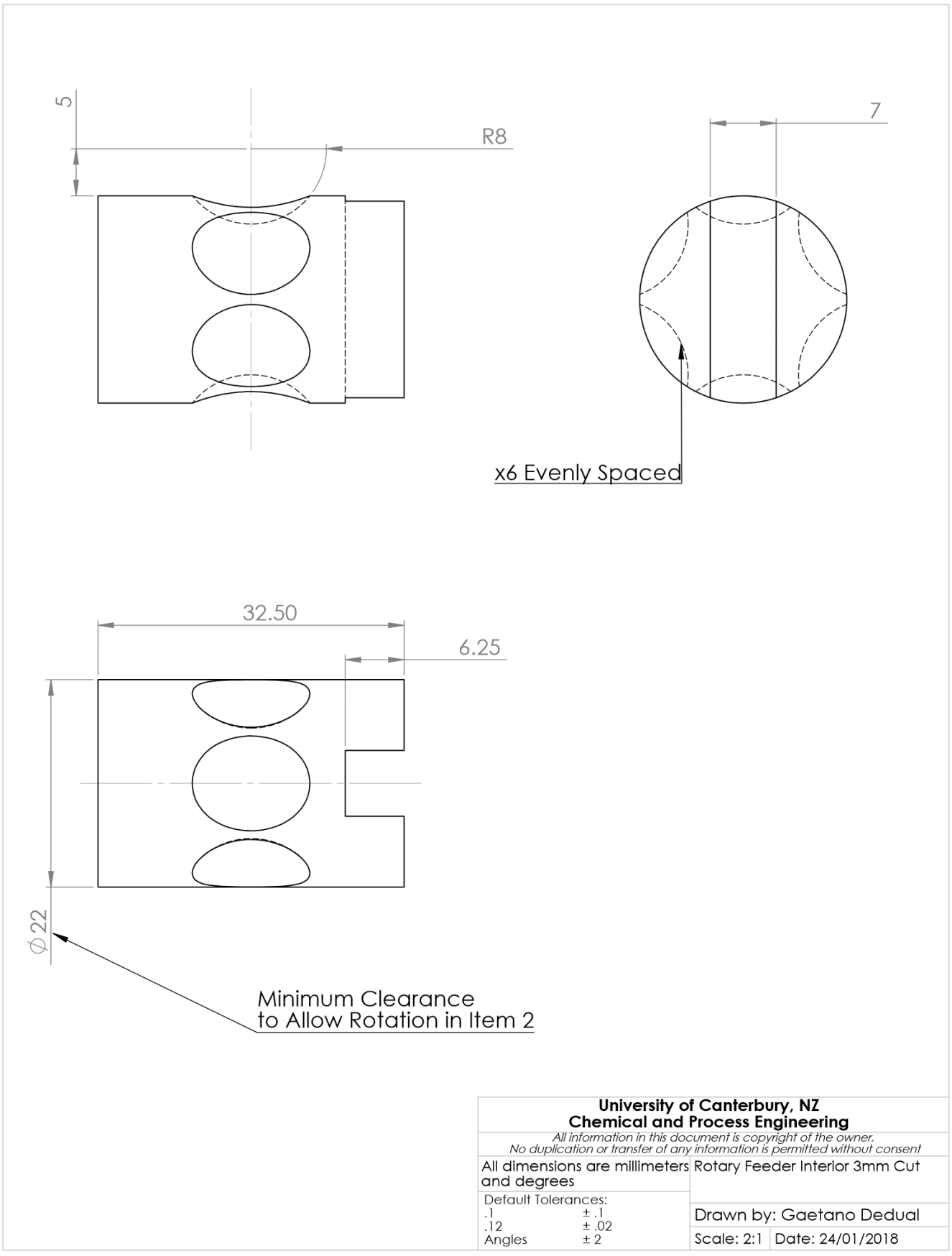

Figure W: 6-cup rotary feeder.

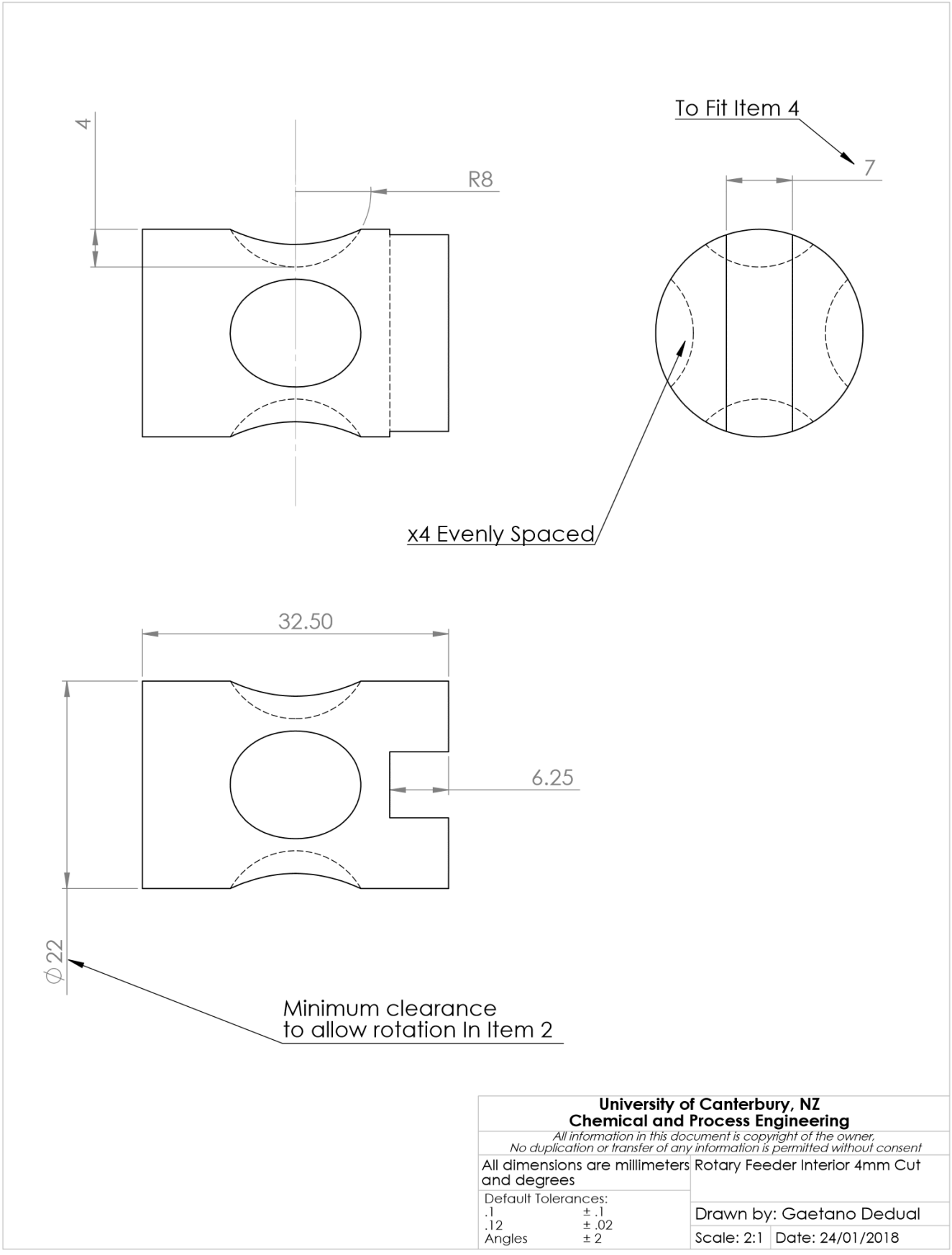

Figure X: 4-cup rotary feeder insert.

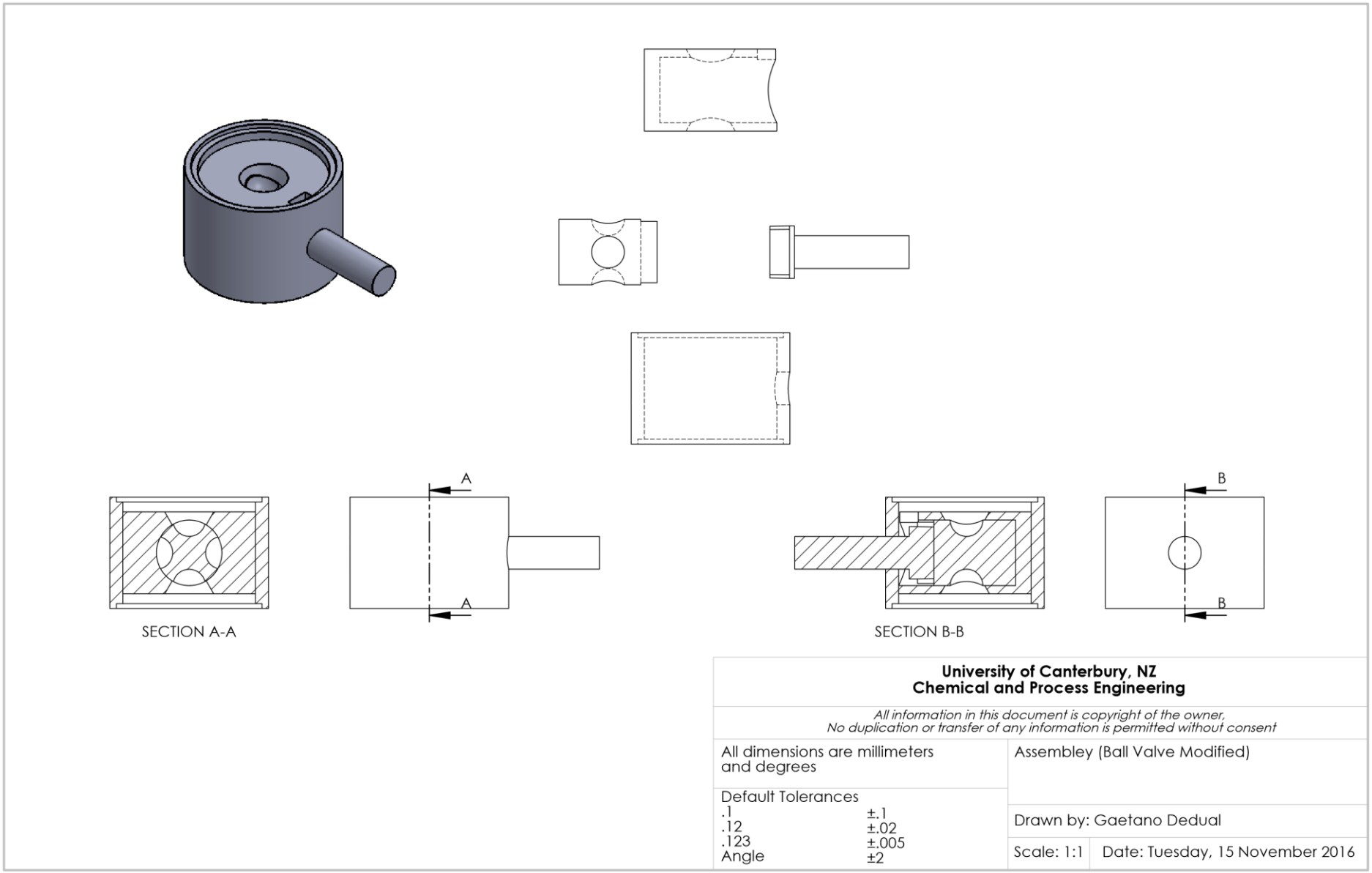

Figure Y: Rotary feeder arrangement.

C.4. Electric Wiring Configuration

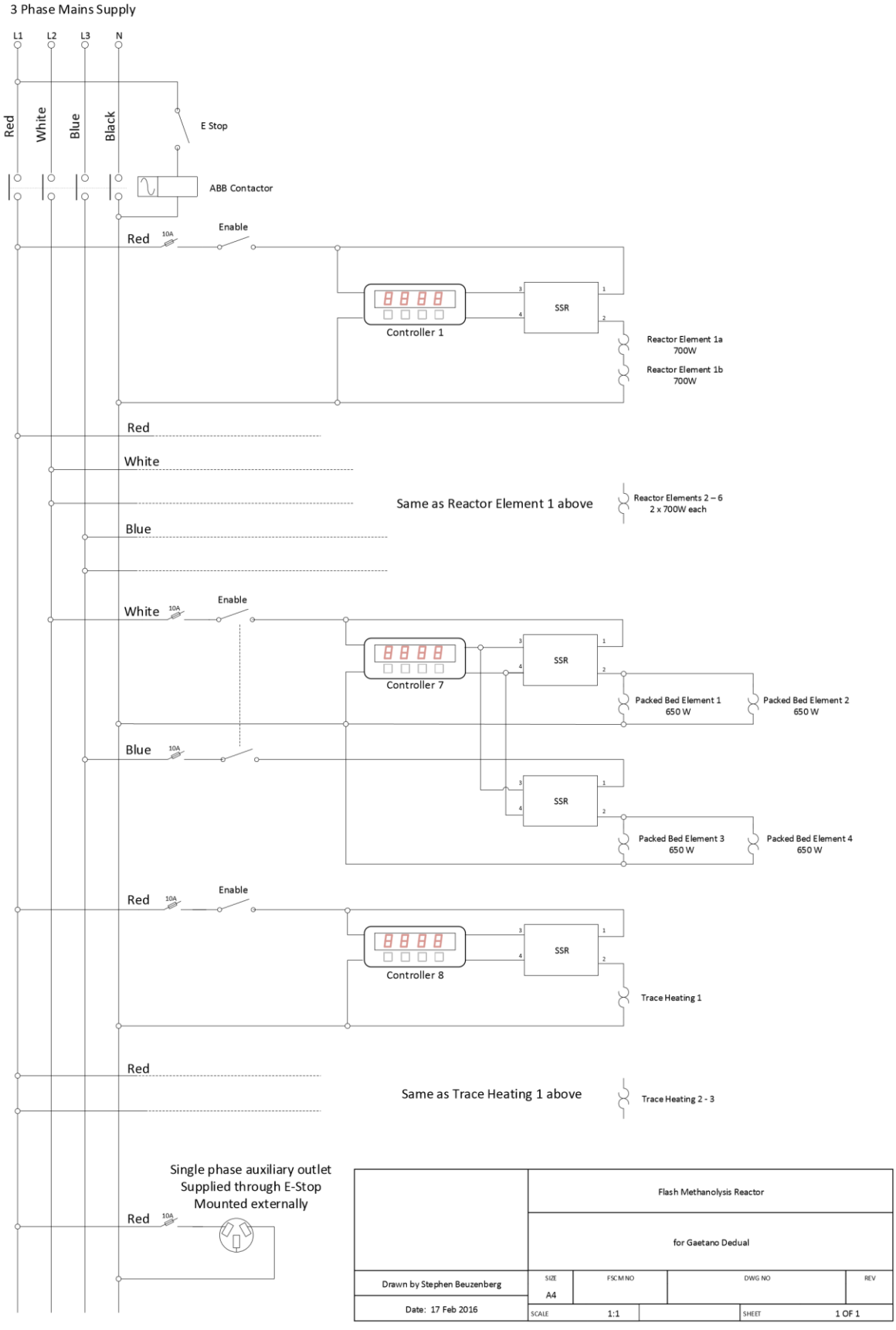

Figure Z: Electrical wiring diagram.

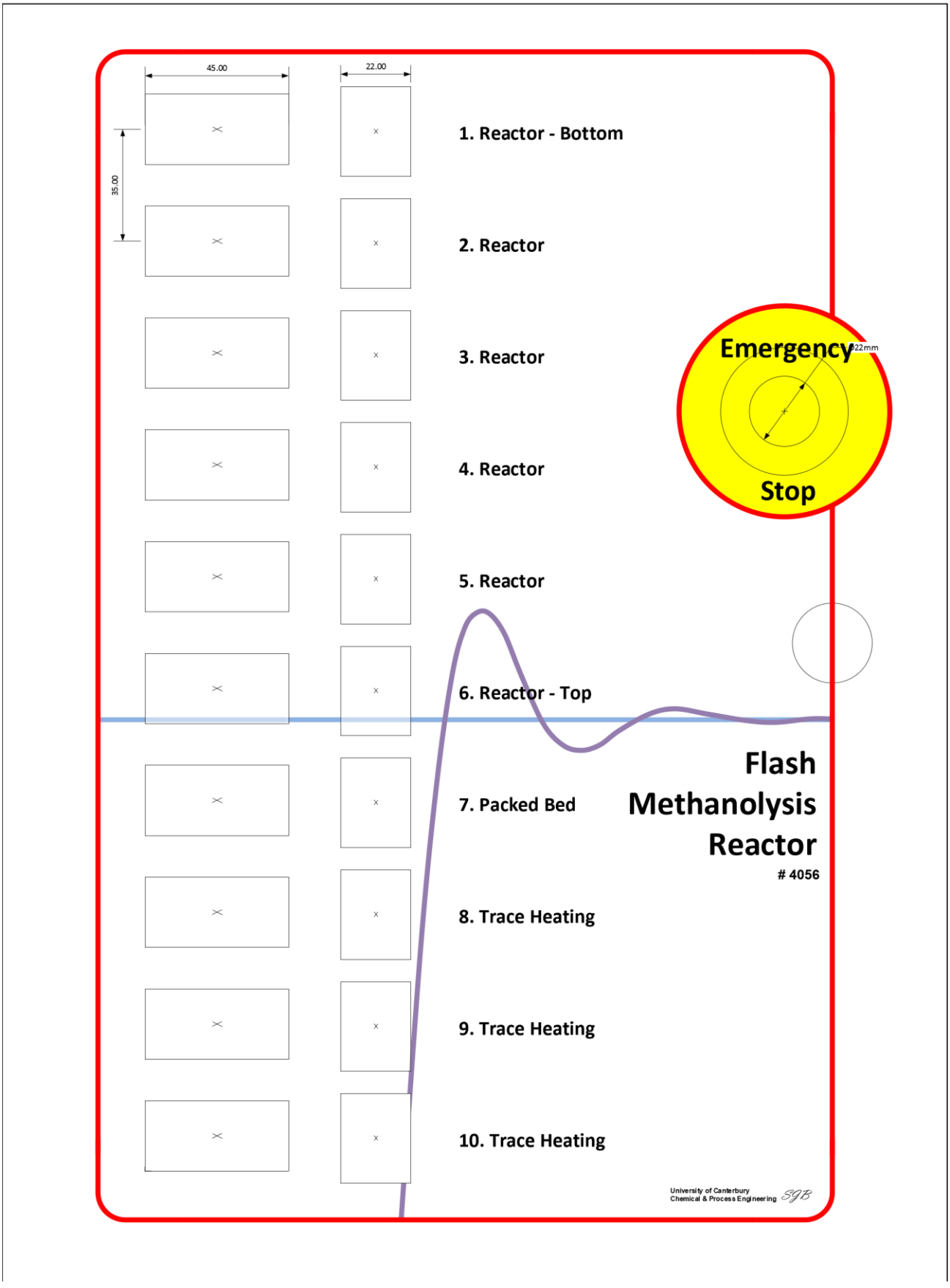

Figure AA: Electrical control manifold.

C.5. Supplementary Drawings

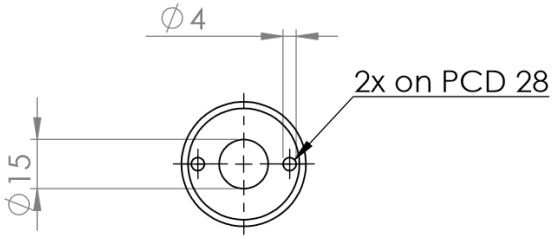

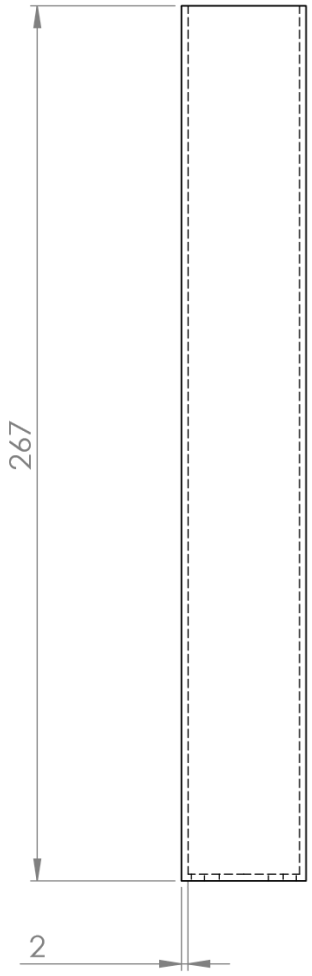

University of Canterbury, NZ
Chemical and Process Engineering

All dimensions are millimeters and degrees	Dropper Tube Sleeve
Default Tolerances: .1 ± .1 .12 ± .02 Angles ± 2	Drawn by: Gaetano Dedual
	Scale: 1:2 Date: 14/02/2017

Figure BB: Quartz sleeve fabrication.

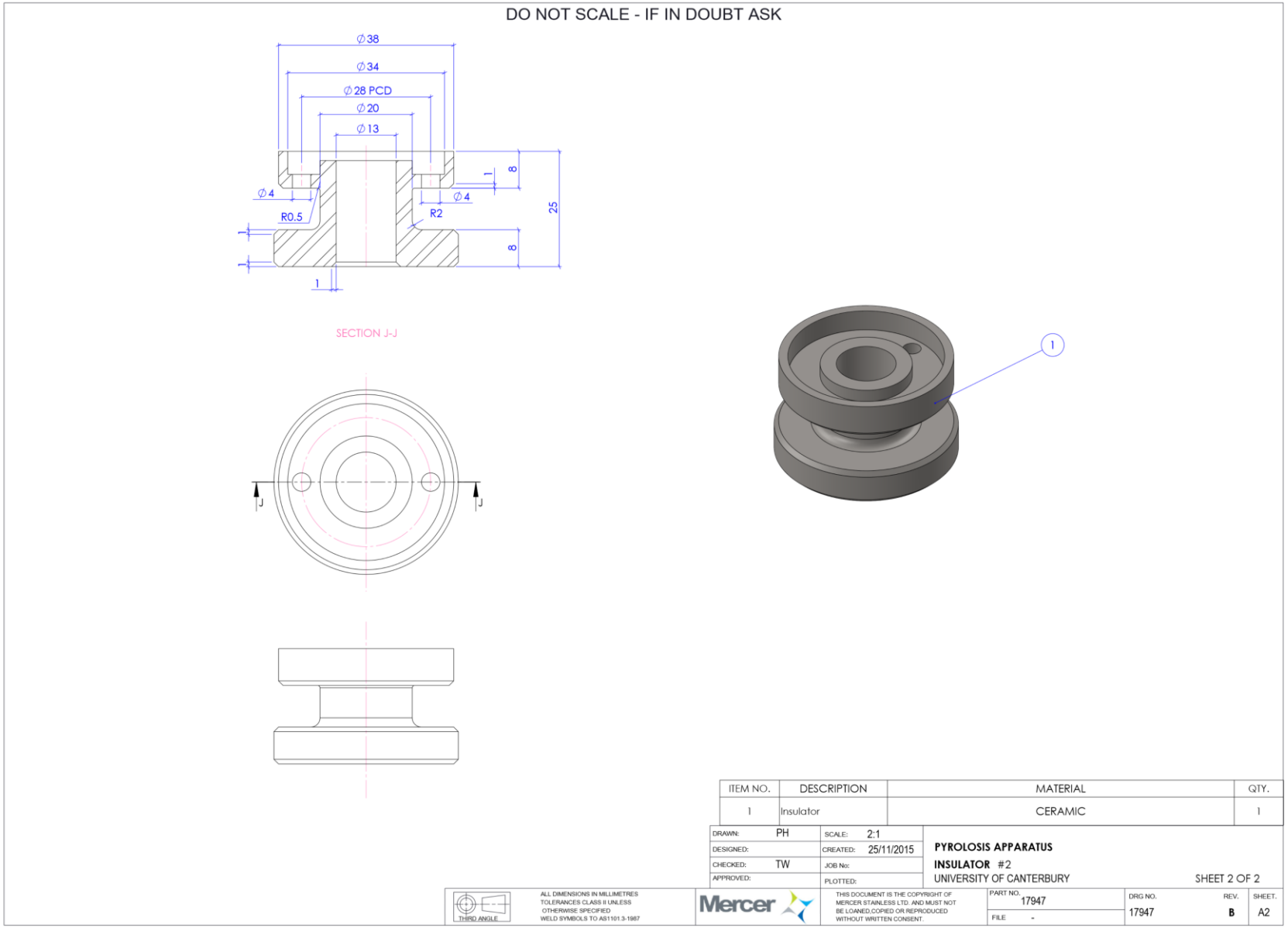

Figure CC: Alumina feeder tube tip insulator.

Appendix D Hazard and Operability Study Description (HAZOP)

D.1. Introduction

For the design of the system and consideration of the hazards, two hazard and operability studies (HAZOP) studies were conducted. This section covers the final HAZOP which was conducted as this is most representative of the final system. Conclusions and Minutes from both HAZOPs are summarized in the final section. A complete review of the HAZOP and all materials associated with the description and scope are provided in this section. The standard operating procedure is provided below:

D.1.1 Standard Operating Procedure (Numbered Items Refer to PID)

Last Updated: 15th March 2017

Gaetano Dedual

Set temperature of the heaters should be ~850 °C. Otherwise, if the reactor is cold, turn on desired water jacket flows and increase temperature up to 850°C slowly. It is suggested that the temperature of the heater be held at 100°C for 2 hrs initially to evaporate any condensed water; then follow the REACTION PROCEDURE. The system should be left with the polycarbonate shield upright whenever heaters are on, displaying that the system is hot and the reactor is in use. The fumehood should also be checked to ensure that there is adequate ventilation for the system. Anytime that the heaters are on, air should also be supplied to the outside of the electrical connections to ensure cooling. This airline is left ON when the heaters are ON

It is suggested that the ball valve not be changed when the system is hot. The hopper can be opened at 850 °C by careful application of the below process.. This can lead to biomass entering the reacting zone upon removal, producing ash in the bed. Caution to avoid excess dropping of biomass into the system should be practised here. To remove the ball it is suggested that the bolts are undone for the ball valve, then raise the hopper slightly to allow a piece of paper to slide between the mid-section and the end section of the ball valve. Wrap the piece of paper around the bottom of the hopper creating a seal adequate to prevent excess biomass dropping down into the reactor. Pull out the ball valve body and place a catch container to empty the contents of the hopper.

Whenever operating the reactor it is imperative that a CO/CH_4 gas monitor is worn at all times.

Reactor Procedure

- Check system and ensure that all of the outlet valves are open and that the system is completely depressurized.
- Check LPG scales to ensure enough LPG for the run
- Check for any abnormalities from leaving the system idling at 850 °C overnight
- If required open ball valve and change ball. Ensure that the orientation of the ball valve allows for a 'seal' between reactor and hopper. NOTE: after a run with new seals, it is assumed that there is no seal between the hopper and the reactor, purging one will effectively purge the others
- If required open hopper (Unit-1) and fill with biomass
- Ensure glycol pump is on (Unit-25) and fluid is circulating
- Ensure cooling water flowrates are suitable and set
- Switch Valve-27 Closed for AIR and turned on for NITROGEN. A low flow of 0.5-1 LPM is suggested through the reactor system.
- Ramp heaters slowly to minimize thermal stresses Wait for system to reach desired temperature
- Close I-18 and ensure no flow
- Purge hopper with Approximately 75L of Nitrogen (15L/min for 5mins). Ensuring that Valve-4 is open and visual confirmation of a successful purge is obtained through I-13.
- Close Valve-4.
- Open I-18 and set flow controller to suitable flowrate (suggested 5 L/min)
- Purge system completely with Approx 35 L of Nitrogen. Where 10 L is passed through the top entrainment flow, by closing Valve-15. The remaining 25 L of Nitrogen is purged through the reactor bottom entry by closing rotameter I-10.
- Once the purges have completed ensure that there is a successful purge by holding gas monitor at the gas outlet ensuring that no CO and CH4 are detected.
- If CO and/or CH4 is detected pass gas through hopper and reactor (as in previous steps) until recorded level becomes 0.
- Once purged , pressurize the system at the operating pressure and hold.
- Perform 30 minute leak test.
- If system fails to hold pressure, inspect joints and all other areas which have been recently disconnected.
- Repeat leak test until satisfied.
- When leak test passes, allow the system to depressurize and wait for the system to achieve the set temperature once again.
- Remove required condenser and fit with 'blank' end

- Fill condenser with required amount of Bio-diesel, then return to system and ensure quick release fitting is adequately connected.
- Turn on Valve-10 and set I-15 to a suitable flow of He/N2O for the experiment (~10% flow of inlet)
- Open Valve-23 and light the Flare ensuring that there is sufficient LPG for the run
- Purge system with Nitrogen for 2-3 minutes, snoop leak detect the condenser fitting
- Check that the purge has been successful by analysing the gas on the Micro-GC
- Close Valve-22 NITROGEN and open for METHANE
- Bring the pressure of the reactor and the hopper to similar values (hopper slightly larger than reactor) by altering Valve-9 and Valve-3.
- Once the system is at the operating pressure the system is ready for the experiment.
- Once the outlet flow stream is steady the system is ready for operation
- Allow Valve-1 to open via operating Unit-3

Allow Expt to take place, Following the analytical techniques checklist

Analytical Procedure

- Once the system has reached steady state, insert a fresh SPE column into the manifold.
- Insert the syringe manifold into the groove and connect the tubing.
- Open Valve-21 and throttle Valve-8 and allow the system to purge for a few seconds.
- When purge is sufficient, close Valve-8 and draw sample through the SPE Column opening the valve on the syringe and pulling through
- Ensure that Valve-21 and the valve on the syringe is closed before removing the SPE column
- Analyse gas with GC and store SPE column for DCM extraction after expt.
- If required repeat steps for different SPE columns.
- Purge the system by opening Valve-8 between extractions to ensure there is no carry over when the new SPE column is used.

Once the experiment has run for the designated time period and/or analyses are complete carry on to the cleaning method.

Clean up

- When the experiment has ended close Valve-1 by turning off Unit 3.
- Purge the system, by opening Valve-22 for NITROGEN and closing METHANE.
- Purge hopper with 75L of Nitrogen (15L/min for 5mins). Ensuring that Valve-4 is open and visual confirmation of a successful purge is obtained through I-13.
- Close Valve-4.
- Open I-18 and set flow controller to suitable flowrate (suggested 5 L/min)

- Purge system completely with 35 L of Nitrogen. Where 10 L is passed through the top entrainment flow, by closing Valve-15. The remaining 25 L of Nitrogen is purged through the reactor bottom entry by closing rotameter I-10.
- Extinguish flare
- Turn off Valve-10 and set I-15 to a suitable flow of He/N2O for the experiment (~10% flow of inlet) Check that the purge has been successful by using the gas monitor to check for CO and CH4 concentration.
- If level of CO and/or CH4 is detectable on the monitor continue with purge, ensuring that the flare is relit.
- Once purge has been completed, allow the system to depressurize by decreasing the outlet pressure of Valve-9
- As the system depressurizes allow Valve-4 to open and depressurize at the same rate.
- Once the system has reached ambient pressure, remove the condenser units and take away for analysis
- Block the outlet of the condenser train with the dummies and ensure fittings are securely in place.
- Turn off glycol pump, Unit-25
- Allow air to enter by opening Valve-27 for AIR and closing Valve-27 for NITROGEN.
- Allow air to pass through and remove all condensable materials within the lines

Increase the temperature of the heat tapes and packed bed reactor if necessary.***If conducting another experiment continue with checklist, elsewise skip to the next section (COOL DOWN)***

Follow-up Experiment

- Ensure that condensers are in place and all dummies have been removed
- Once the cleaning process is completed close Valve-27 for AIR and open Valve-27 for NITROGEN
- If required open unit-1 and fill with biomass, ensure that there is no CO in the hopper by locating the gas sensor close to the hopper flange..
- Close I-18 and ensure no flow
- Hopper purged with 75L of Nitrogen (15L/min for 5mins). Ensuring that Valve-4 is open and visual confirmation of a successful purge is obtained through I-13
- Once complete close Valve-4.
- Open I-18 and set flow controller to suitable flowrate (suggested 5 L/min)
- Purge system completely with 35L of Nitrogen. Where 10L is passed through the top entrainment flow, by closing Valve-15. The remaining 25L of Nitrogen is purged through the reactor bottom entry by closing rotameter I-10.

- Pressurize the system at the operating pressure and hold.
- Perform 30 minute leak test.
- If system fails to hold pressure inspect joints and all other areas which have been recently disconnected.
- Repeat leak test once satisfied.
- When leak test passes, allow the system to depressurize and wait for the system to achieve the set temperature once again.
- Close Valve-22 NITROGEN and open for METHANE
- Bring the pressure of the reactor and the hopper to similar values (hopper slightly larger than reactor) by altering Valve-9 and Valve-3.
- Once the system is at the operating pressure the system is ready for the experiment.
- Allow Valve-1 to open via operating Unit-3

Once experiment is finished follow the CLEAN Up procedure

Cool Down

- With a steady stream of air passing through the system, bring the temperature of the fluidised bed reactor heater down to 850 °C
- Allow the packed bed heaters and trace heaters to come to rest at a low temperature as well.
- Ensure that the flare for the furnace has been extinguished and Valve-23 has been turned off.

Solving common Issues

Filter Blockages (Applicable for Units 20,24 and 16)

- Depressurize system by opening valve-4
- Leave system to depressurize and check pressures between alicats (Units I-15 and I-18), ensuing atmospheric pressure before opening the system.
- Once depressurization has been successful squirt snoop around the edges of the filter element and slightly loosen the filter body.
- Ensure that the gas flow out is not excessive
- If gas flow is large, close the filter body and allow to depressurize for longer.
- Ensure that an extraction line is in place to extract any potentially harmful gas from exiting the system.
- Once fully depressurized remove the filter body and remove the sintered elements inside.
- Close and tighten the filter body and ensure that flow is now not restricted (confirming the blockage was at the filter).

- Burn build up on filters using propane torch
- If suspected filter blockage is at Unit-20 increase temperature of heat tape to 850 °C and pass through 1 LPM of Air to aide combustion.

Feeder Tube Blockages

- Purge system through hopper and reactor and ensure that there is no remaining CO and/or CH4 in the system.
- Allow system to cool to 850 °C.
- Run air through the reactor for ~10 minutes
- Bring over an extraction hose for the fumes/smoke
- Remove valve body mid-section and vacuum/brush excess biomass into the fluidised bed.

D.2. Volumetric Purge Considerations

Overall purge volume was determined by the overall volume of the system condensers reactors and process tubing.

Condensers

Condenser 1	500	*mL*
Condenser 2	1000	*mL*
Condenser 3	300	*mL*
Volume Total	1.8	*L*
Fluidized Bed Reactor		
Diameter	70	*mm*
Length	900	*mm*
Volume	3.5	*L*
Process Tubing		
ID	10	*mm*
Length	5	*m*
Overall Volume	0.4	*L*
Packed Bed Reactor		
Diameter	70	*mm*
Length	300	*mm*
Volume	1.2	*L*
TOTAL	6.8	*L*
Safety Factor	5	-
Volume	35	*L*

D.3. HAZOP Description

Hazard and Operability Study (HAZOP)	One of the risk assessment tools for examination of the process and engineering intentions of new or existing Facilities to identify and assess potential hazards, consequential effects, and protective and corrective actions.
Hazard	Potential source of harm. Deviations from design or operational intent may constitute or produce a hazard. Hazards are the focus of HAZOP studies, and it should be noted that a single hazard could potentially lead to multiple forms of harm.
Harm	Physical injury or damage to the health of people or damage to property or the environment. Harm is the consequence of a hazard occurring and may take many forms: patient or user safety, employee safety, business risks, regulatory risks, environmental risks, etc.
Risk	Combination of probability of occurrence of harm and the severity of that harm. In a strict sense, "risk" is not always explicitly identified in HAZOP studies since the core methodology does not require identification (also referred to as rating) of the probability or severity of harm. However, risk assessment teams may choose to rate these factors in order to further quantify and prioritize risks if needed
Deviation	A departure from the design and operating intentions
Guide Words	Key supporting elements used to identify deviations from the design and operating intentions in which they guide and stimulate creative thinking towards appropriate deviations.
Score O	Score rated for probability of **O**ccurrence
Score E	Score rated for **E**nvironmental impact
Score P	Score rated for impact on **P**eople
Score SG	Score rated for probability of **S**afe**g**uard Failure
Risk rating score	Final score rated for risk assessment which is calculated from Score O + Score E + Score P - Score SG

D.4. HAZOP Methodology

The HAZOP analysis process is divided into four phases as illustrated below (Product Quality Research Institute, 2011):

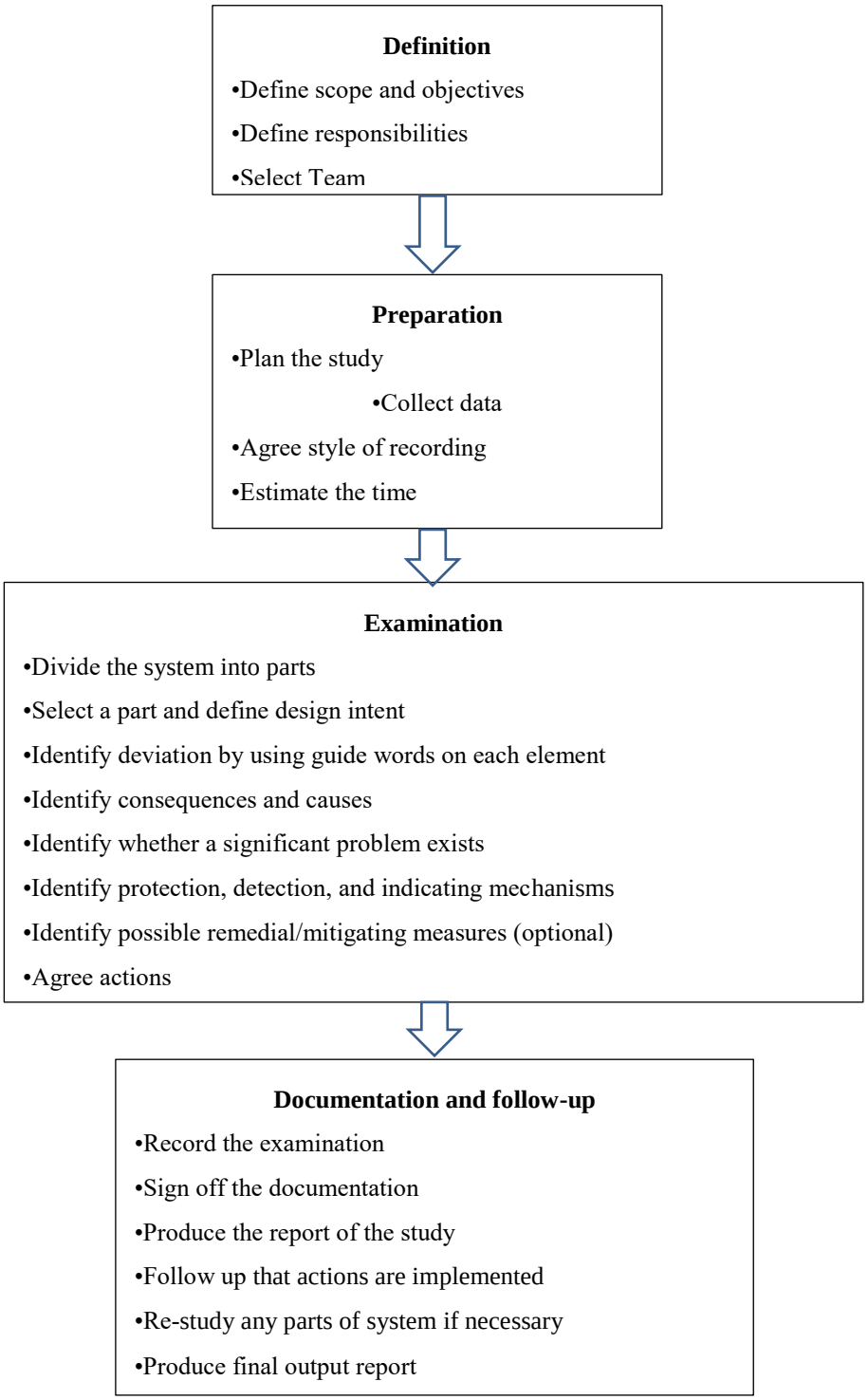

Figure DD: Diagram of HAZOP methodology

Hazop Team Members

Supervisor	Professor Shusheng Pang
Associate Supervisor	Dr. Brendon Miller
Ph.D Student	Gaetano Dedual
Hazop Team:	Michael Sandridge
	Frank Weerts
	Stephen Beuzenberg
	Tim Moore

Hazop System Boundaries

This HAZOP study covers a review of a lab-scale reactor for the production of chemical feedstocks (ethylene, benzene and CO), all equipment and operations of the reactor in order to identify possible deviations from normal operating conditions which could lead to potential hazards and operational problems. Causes, consequences, and safeguards of the possible deviations are determined. Consequently, probability and impact of the possible deviations as well as probability of safeguard failure are rated to quantify and prioritize the risks. Finally, risk control measures and additional protective measures are arranged if necessary.

Description of Lab-Scale Reactor

In the reactor, small particles of *Pinus radiata* are to be flash pyrolysed with the reactive gas methane at elevated temperature (from 700 to 1000°C) and pressures up to10 bar). The experiments will be conducted using a fluidized bed reactor, where the reacting gas is the fluidizing agent and the bed material is silica sand. The range of products created from the reaction is vast and is expected to be in three states, solid, liquid and gaseous. The effects of operation temperature and pressure on the characteristics of the products will be investigated for the above mentioned ranges. The other operation conditions and feedstock properties which will be investigated are the particle size, retention time and excess methane flowrate. Flash pyrolysis is characterized by high heating rates of carbonaceous materials in an oxygen free environment. The effect of catalysts may also be explored in the system by adding catalysts directly into the sand bed.

Expected gas products from the reactions are CO, CO_2, H_2, CH_4, C_2H_2, C_2H_4, and C2H6. Other species which are expected to form in the reactions are ‘tars’, (In pyrolysis the term ‘tars’ is often given to chemicals with a molecular weight higher than benzene). This terminology is useful due to the wide range of species which exist in the liquid phase. It has been reported that the amount of

liquid species can be over 200 which makes characterising the liquid product very difficult. The liquid product is often very viscous, low in pH, and at times has been modelled/reported as a benzene/naphthenic solution.

The reactor and preheater sections of the experiment apparatus are to be constructed from a section of quartz tube with quartz sintered discussed between the sections. This configuration is then then to be placed inside a section of high specification alloy pipe; thus decreasing the possibilities of methane leakage. The preheater section will contain small silica balls which are included in the apparatus to increase the heat transfer to the gas. The reactor will be heated by electrical elements from a 3 phase power supply. All of the reactor and preheater system will be pressurized at the same pressure as that of the biomass feeder; Figure 1 shows the reaction setup.

The biomass hopper is filled with biomass chips during trials and is fed into the process with a small entraining flow of methane. The biomass is allowed to react with the fluidizing gas in the reactor section for a very short periods of time (<2 s), and then the products are passed into condensing units. From here the excess gas products (after a sample is taken), are burnt in a furnace and passed into a fume hood.

Methane Characteristics:

Design Conditions (MAX):

Condition	Value	Units
Methane Flow	1	kg/hr
Biomass Flow	2	kg/hr
Operating Temperature	1273	°K
Operating Pressure	10	Bar
Volumetric Flow	2	m^3/hr

At the highest operating temperature and pressure, (1273.5°K, 10 bar, respectively), the reactor contains approximately 1.75g of methane.

Methane Characteristics:

Characteristics	Value	Unit
Lower Explosion Limit (LEL)	5%	% (Volume in air at 25°C)
Upper Explosion Limit (UEL)	15%	% (Volume in air at 25°C)
Automatic Ignition Temperature (AIT)	~580	°C
Methane Density	0.656	kg/m^3 (STP)

Methane Flowrates:

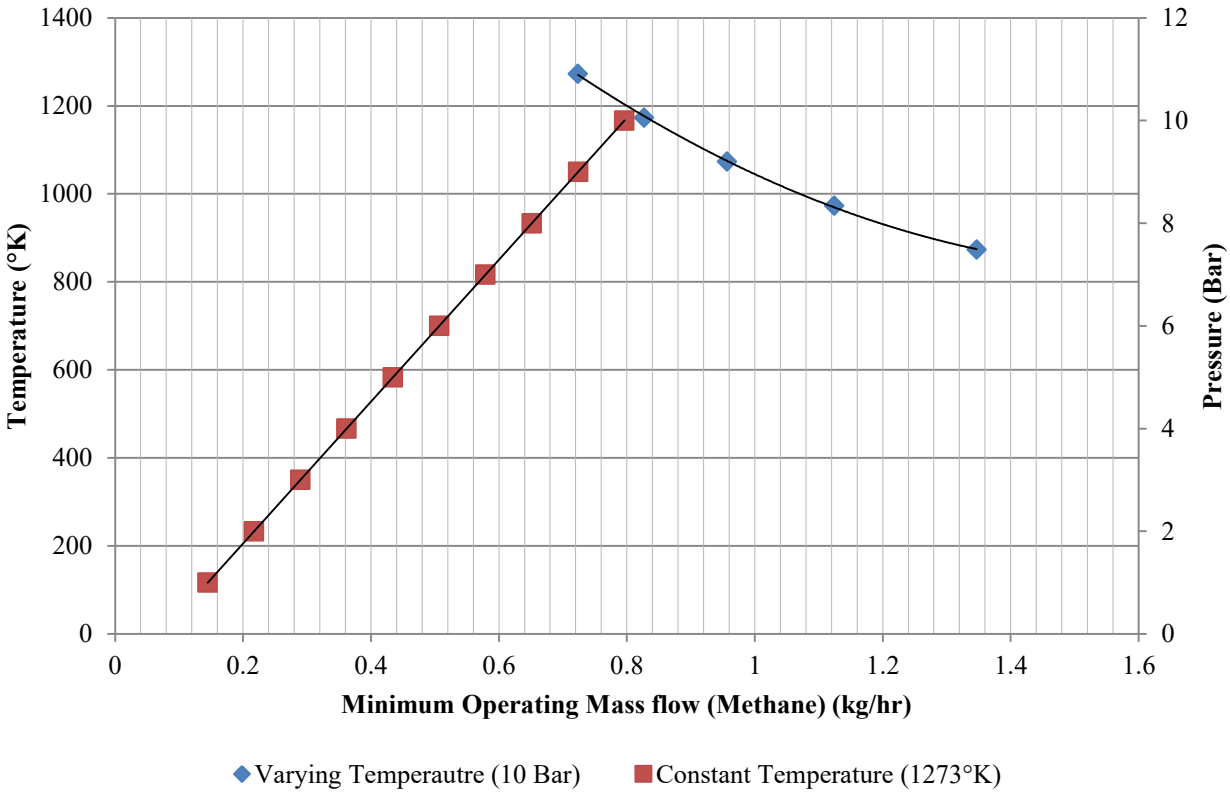

Operational Notes:

- Fume hood is always on in the room
- Cooling water always on when heater is on
- Airline in directly to the terminal box of the heater
- Hopper Purge Volume: 75L

- Reactor System Purge Volume: 35L

Heater Operation:

- To avoid excess cyclic stresses, the heater will be reduced from operation temperature to 500°C after experiments have been concluded. The heater will be operated for weeks on end, until removal of the interiors of the reactor are required.

- The cooling water for the reactor feed and top and bottom will also be allowed to run continuously, this is to avoid thermal shock to the system, as these flows are required at 1000°C and need to be on during the heat up/Cool down period.

- The condenser units can be successfully removed when the heater is at 500°C as the heat conduction to this section is very low and the condensers are effectively at ambient temperature. Attention will need to be drawn to the trace heating elements as these will need to be turned off, as well as the packed bed heating section. The cyclic thermal stresses on these heaters are significantly lower due to the lower operating temperature.

- When the heater is idling at 500°C air will be introduced to the system in a steady stream.

Analyses

Due to the wide range of species in the pyrolysis products of liquid and gases, various analysis techniques will be utilized. The inline gas samples are to be taken by use of a needle inserted directly into the gas line whilst the reactor is operating. The sampling port will consist of a tee with the port which is perpendicular to the other two being sealed with a rubber septum. The gas will be analysed using a micro--GC which will provide near real-time analyses of the species in the gas phase, the sampling/analyses will be in a semi-batch operation. The gases which will be analysed by the micro-GC include; CO, CO_2, H_2, C_2H_4, C_2H_6, H_2S, CH_4 The gas will be analysed by inserting a stream of N2O/He to determine the concentration and provide a quality check for the micro GC. This is incorporated into the system for the hopes of increasing the analysis accuracy and for total flowrate measurements.

The liquid phase will be analysed by use of an H-NMR. This will allow for a determination of the functional species in the liquid. This analysis will be conducted by the Chemistry Department at The University of Canterbury. The liquid used in these analyses will be collected from the condensers in Swagelok bombs and will need to be cleaned of any entrained particles. CHN analyses of the liquid and solid samples will also be conducted by SCION; this analysis will be periodic and will not be conducted on every run unless required later in the experimental section. Liquid samples of the tars collected in the process will be sent to Lincoln University for GC-MS analysis if required. Samples

will also periodically be sent to Lincoln University for ICP-OES analyses of the ‘raw wood’ to determine the inorganic constituents.

The level of complexity of the analysis is highly dependent on the products which are produced from the experiments. If the tars show a relatively high concentration of BTX (Benzene, Toluene and Xylene), in comparison to other tars, simple GC analyses will be conducted on the liquid. This will help increase turnover of the analyses as this analysis can be conducted at the University of Canterbury.

Construction Considerations

All of the piping to be used in the system is 316 SS. This material is chosen due to the high resistance against hydrogen gas and low concentrations of hydrogen sulphide and ammonia. To prevent any leaking of methane at high temperatures (~1000°C in the reactor environment), the preheater section and the reactor section follow one another within a high specification alloy pipe. For all construction queries please consult drawings

Equipment List

Table E: Equipment list for Pyrolysis Reactor.

No.	Description	Dimension/Size/ Characteristic	Intended Operating Condition	Total Number
1	Pure Nitrogen gas cylinder	Size G	Maximum of 10 bar after the regulator Flowrate: (2-4 kg/hr)	1
2	Pure Methane gas Cylinder	Size G	Maximum of 10 bar after the regulator Flowrate: (1kg/hr Max)	1
3	Regulator For Methane	Outlet of 10 Bar Max (Room Temperature)	No higher than 10 bar	1
4	Nitrogen Regulator	Outlet of 10 Bar Max (Room temperature)	No Higher than 10 bar	1
5	Methane Rotameter	0- 2 m^3 Rotameter with Charts for varying pressures	0-2 m^3 flowrate of methane. Temperature and pressure (25°C and 10 bar Maximum)	2
6	Nitrogen Rotameter	0-0.5 m^3 Rotameter	0-0.5 m^3 to allow for adequate flushing of the apparatus	1

Table E: Equipment list for Pyrolysis Reactor *Continued.*

No.	Description	Dimension/Size/ Characteristic	Intended Operating Condition	Total Number
7	One way valve/ Check Valve	1/2” in size. Cracking pressure 0.03 Bar	Pressures higher than 0.03 bar, up to a maximum of 10 bar, Room temperature	2
8	Pressure Control Valve (Needle Valve)	1/2” in Size	Pressures up to 10 bar and room temperature	2
9	Pressure Relief Valve	1/2” in size	Pressure Relief valves set at 11 bar	2
10	Ball Valve	1” Ball valve with Partition	10 bar maximum, Room temperature. Rotating at <25 rpm	1
11	Motor with gear box and VSD	240V Motor	Room Temperature, Atmospheric Conditions	1
12	Pressurized Hopper	~0.25m^3	10 bar, Room Temperature	1
13	Preheater Section	2.5” Diameter Sandvik 253MA	1000°C 10 bar	1
14	Fritted Disc	33mm diameter with various porosities (250-100µm)		1
15	Reactor with Quartz sand	2.5” Diameter		1
16	Biomass Cooler	300 mm 25NB Sch40 316 SS Pipe	<100°C, Atmospheric Pressure	1
17	Char Trap	¾” Tube, 100mm length	~700°C	1
18	Needle Valve for sampling	1/2”	~500°C, 10 bar Pressure Swagelok tee fitted with rubber septum	2
19	Wet gas flowmeter	1/2” in size	~500°C, 10 bar pressure	2

Table E: Equipment list for Pyrolysis Reactor *Continued.*

No.	Description	Dimension/Size/ Characteristic	Intended Operating Condition	Total Number
20	Tar Recovery Unit (I)	1/2" Tee, 500cm^3 cylinder	~150°C, 10 bar Pressure (Use of heat tape for thermal conservation)	1
21	Tar Recovery Unit (II)	1/2" Tee, 500cm^3 cylinder	~25°C, 10 bar Pressure (Water Jacketed if required)	1
22	Globe Ball Valve	1/2" Valve	Room temperature, 10 bar (Samples taken at atmospheric pressure)	2
23	Flue Gas Burner	Maximum of 5 m^3/hr (Atmospheric Pressure), 22kW	10 bar, High temp	1
24	Methane Detector	Methane analysis Detector	10 bar Pressure, Recording for the LEL of methane (5% volume air)	1
25	Fume Hood	Laboratory Scale	Atmospheric pressure slightly elevated temperature	1
26	Packed Bed Reactor	1.2L packed bed	Up to 650°C (Design Considerations), 10 Bar	1
27	N2O/He Gas mixture cylinder (50/50 v/v)	Size D gas bottle, used for analytical considerations in GC	Slightly above atmospheric pressure, low flowrate, ~10% of inlet CH4 flow	1
28	SPE Columns	500 microgram SPE columns, varying composition	Slightly above atmospheric using a syringe to draw sample	1-2 used each Expt

HAZOP Study

Details of parameters, guide words, score O, score E, score P, score SG, and final risk rating and prioritization are shown in Table 2-7. The HAZOP analysis of all nodes or streams as assigned in Figure 2 is shown in Table 8.

Table F: Parameters and guide words used in the HAZOP.

Parameter	Guide words
Flow rate	Zero, Too High, Too Low, Reverse, Other than
Temperature	Too high, Too low
Pressure	Too high, Too low
Level	Zero, Too High, Too Low
Start-up/Shut-down	Too fast, Too slow, Other than =Actions missed
Reaction	Zero, Too fast, Too slow, Other than = unwanted reaction
Utility failure (power)	Failure

Table G: Probability of occurrence score (Score O).

Score	Order of magnitude Frequency or Likelihood	Qualitative
+1	About once per month (10^{1})	Expected to occur frequently or regularly
0	Once per month (10^{0})	Likely to occur occasionally/several times during plant lifetime
-1	10% chance per year (10^{-1}) (once every 10 years)	Probably will happen more than once during plant lifetime
-2	1% chance per year (10^{-2}) (once every 100 years) (100 plant, once/year)	Not expected to occur but could occur during plant lifetime
-3	1 in 1,000 chance per year (10^{-3})	Would be very surprising if happened during plant lifetime
-4	1 in 10,000 chance per year (10^{-4})	Extremely remote, or not expected to be possible

Table H: Environnemental impact score (Score E).

Score	Effects expected to occur exclusively On-Site	Effects expected to occur Off-site
6		• Catastrophic release to environment • Long term effects • Substantial fines/penalties expected
5	• Catastrophic release to facility • Long term effects • Substantial fines/penalties expected	• Major release to environment • Long term impact likely • Fines/penalties likely
4	• Major release to facility • Long term impact likely • Fines/penalties likely	• Minor release to facility/outside help needed • Short term impact likely • Legal/public relation consequences
3	• Minor release to facility/outside help needed • Short term impact likely • Legal/public relation consequences	• Major release handled with internal resources • No legal/public relation consequences
2	• Major release handled with internal resources • No legal/public relation consequences	• Minor release handled with internal resources • No legal/public relation consequences
1	• Minor release handled with internal resources • No legal/public relation consequences	• Environmental impact unlikely
0	• Environmental impact unlikely	none

Table I: Impact on people score (Score P)

Score	Unlikely but might affect one person On-site (10% of time)	Likely to affect 1-2 people On-site	Likely to affect 5-20 people On-site or Off-site
6	-	-	Fatality
5	-	Fatality	Immediate impairment, Permanent health effects
4	Fatality	Immediate impairment, Permanent health effects	Severe injury, Lost time
3	Immediate impairment, Permanent health effects	Severe injury, Lost time	Injury requiring medical treatment
2	Severe injury, Lost time	Injury requiring medical treatment	Minor injury
1	Injury requiring medical treatment	Minor injury	Probably none
0	Minor injury	Probably none	None

Table J: Probability of safeguard failure score (Score SG).

Score	Probability of safeguard failure	Example
0	100%	• No safeguards • Operator in difficult position
1	10%	• Single operator with adequate time (> 5 min) fails to do correct thing 1 out of 10 times
2	1%	• Single set of hardware, functionally tested • Automatic shutdown procedure
3	0.1%	• Passive protection (explosion disk) • Combination of Score 1 & 2
4	0.01%	• Two independent sets of hardware

Table K: Risk rating and prioritization.

Risk level	Risk rating score	Descriptions
1	-4 to -1	Low risk, existing safeguards are adequate
2	0 to 3	Low risk, but risk control measures are required
3	4 to 8	High risk, risk control measures and additional protective measures are needed
4	9 to 13	Very high risk, this part or process cannot be operated unless risk control measures and additional protective measures have been conducted to reduce the risk and hazard

The P&ID used for the Hazop is provided in Figure EE: HAZOP PID used for HAZOP study with identified nodes colour coded. *Note: A number of small components were added after the final HAZOP which did not require recompletion of the HAZOP study.* And the associated HAZOP table is provided below.

D.5. Hazard and Operability Study (HAZOP)

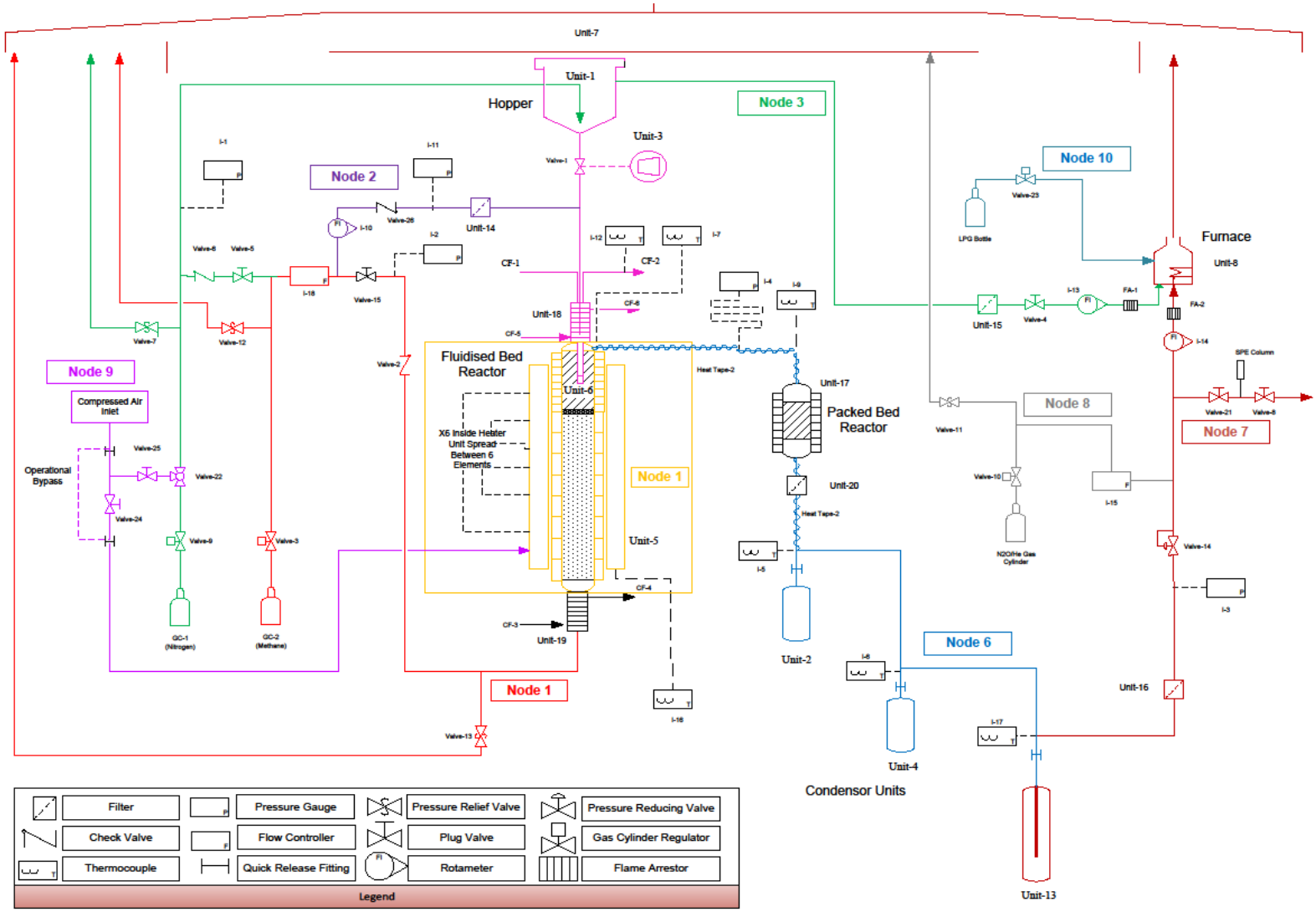

Figure EE: HAZOP PID used for HAZOP study with identified nodes colour coded. ***Note: A number of small components were added after the final HAZOP which did not require recompletion of the HAZOP study.***

Table L: Hazard and Operability Table (HAZOP)

Node/ Stream	Parameter	Guide word	Deviation	Causes	Score O	Consequences	Score E	Score P	Safeguards	Score SG	Comments	Risk Rating	Risk level	Actions
1. Methane Reactive Gas Flow	1.1 Flow rate	Zero	No Flow	Empty Gas Cylinder (GC-2)	-1	No Fluidizing Gas Flow	0	0	Have Checklist to ensure that the pressure of the gas cylinder is sufficient before each run	1	Other than when the system is being flushed with Nitrogen, the passing gas will be Methane. Methane is an extremely flammable gas. HSNO New Zealand, identifies Methane as a high hazard gas with class 2.1	-2	1	
				Regulator Fail (Valve-4)	-1	No Fluidizing Gas Flow	0	0	Test Regulator before each run	1		-2	1	
				Regulator is Closed (Valve-4)	-1	No Fluidizing Gas Flow	0	0	Have Checklist ensure regulator is opened	1		-2	1	
				Rotameter Blocked (I-5)	-2	No Fluidizing Gas Flow	0	0	Test Flowmeter before run	1		-3	1	
				Feeding Tube Rupture	-1	No Fluidizing Gas Flow	1	0	Test tubes by filling system with nitrogen and measuring the pressure of the system for 20 minutes	1		-1	1	
				Unit -19 no Water flow CF-3		No consequence, excess heat loss								

Table L: Hazard and Operability Table (HAZOP) *Continued*

Node/ Stream	Parameter	Guide word	Deviation	Causes	Score O	Consequences	Score E	Score P	Safeguards	Score SG	Comments	Risk Rating	Risk level	Actions
1. Methane Reactive Gas Flow	1.1 Flow rate	High	Fluidizing gas flow rate is too high	Regulator Fail (Valve-4)	-1	Gas flowrate to the reactor is too high and may cause excess fluidization of quartz sand bed, ultimately causing entrainment of the sand.	0	0	Test Regulator before each run	1		-2	1	Rotameter moved form after the rotameter to after the tee section of methane reactive gas flow and entrainment flow
				Rotameter failure (Valve-4)	-1		0	0	Check Rotameter before every run	1		-2	1	
				Blockage in Tube	-1	Slight increase in flowrate, Flowrate to Tube-5 <10% of flowrate feeding to the reactor, results are VOID	0	0	Entrained Gas flow	1	Flow through I-6 very small compared to fluidizing gas flow	-2	1	
				GC-1 and GC-2 Opened	-1	Gas flowrate to the reactor is too high and may cause excess fluidization of quartz sand bed, ultimately causing entrainment of the sand.	0	0	Checklist to ensure that only one bottle is opened as there is no application when both are required to run simultaneously	1	Nitrogen is chemically inert and will not react with methane if fed simultaneously	-2	1	
				Rotameter Blocked (I-6)	-1	Slight increase in flowrate, Flowrate to Tube-5 <10% of flowrate feeding to the reactor, results are not justified. Pressure imbalance over the reactor, causing product gases to flow through biomass feed line	0	0		1		-2	1	

Table L: Hazard and Operability Table (HAZOP) *Continued*

Node/ Stream	Parameter	Guide word	Deviation	Causes	Score O	Consequences	Score E	Score P	Safeguards	Score SG	Comments	Risk Rating	Risk level	Actions
1. Methane Reactive Gas Flow	1.1 Flow rate	Low	Fluidizing gas flow too low	Regulator Failure (Valve-4)	-1	Low flow to reactor, bed acts as a packed bed	0	0	Check Regulator before each run	1		-2	1	
				Rotameter (I-6,I-5) blockage	-2		0	0	Check Rotameter before each run	1		-3	1	
				Regulator Blockage (I-5)	-2		0	0	Check Regulator before each run	1		-3	1	
				Rotameter (I-6) Failure	-1		0	0	Check Rotameter before each run	1		-2	1	
		Reverse	Gas flow occurs in Opposite direction	Opening Valve 7		Methane To flare						0	2	
		Other Than	N2			No problems								
			Air Stream								See Node 9			
	1.2 Temperature	High	Not a Concern		-1		0	0		1	Gas enters at room temperature	-2	1	
		Low	Not a Concern		-1		0	0		1		-2	1	
	1.3 Pressure	High	Fluidizing gas which is entering the reactor is at a high pressure	Regulator Failure (Valve-5)	-1	High pressure gas enters the reactor, possibility of causing excess fluidization of the bed and possibility of entrainment of particles further down the process line	0	0	Check Regulator before each run	2		-3	1	Pressure Relief Valve moved to after the regulator to safeguard further upstream equipment
				Rotameter Blockage (I-6)	-1		0	0	Check Rotameter before each run	2		-3	1	

Table L: Hazard and Operability Table (HAZOP) *Continued*

Node/ Stream	Parameter	Guide word	Deviation	Causes	Score O	Consequences	Score E	Score P	Safeguards	Score SG	Comments	Risk Rating	Risk level	Actions
1. Methane Reactive Gas Flow	1.3 Pressure	Low	Fluidizing gas which is entering the reactor is at a lower pressure	Regulator Failure (Valve-5)	-1	Poor fluidization if any, Experiment Void			Check Regulator before each run	1		-2	1	
				Rotameter Malfunction (I-6)	-1		0	0	Check Rotameter before each run	1		-2	1	
				I-6 Rotameter malfunction	-1	Excess gas enters the biomass feed line, too much methane entering the tubing cannot be cooled before entry, results are void	0	0	Check Rotameter Before each trial	1		-2	1	
				I-6 Flowmeter Malfunction	-1		0	0	Check Rotameter Before each trial	1		-2	1	
				Regulator Malfunction (Valve-5)	-1		0	0	Check regulator before each trial	1		-2	1	
		Low	Flowrate Entering Valve-3 too low	Blockage of rotameter I-6	-1	Insufficient gas enters into the reactor, possibility of causing more entrainment which results in void results	0	0	Check Rotameter Before each trial	1		-2	1	
				Blockage of rotameter I-5	-1		0	0	Check Rotameter Before each trial	1		-2	1	
				Regulator malfunction	-1	Poor entrainment of particles (if any)	0	0	Check regulator before each trial	1		-2	1	

Table L: Hazard and Operability Table (HAZOP) *Continued*

Node/ Stream	Parameter	Guide word	Deviation	Causes	Score O	Consequences	Score E	Score P	Safeguards	Score SG	Comments	Risk Rating	Risk level	Actions
1. Methane Reactive Gas Flow	1.3 Pressure	No	No gas flow entering Valve-4	Blockage of Rotameter I-6	-1	Excess flowrate entering into the reactor, void results. The feed line of biomass will not be pressurized causing the gases from the reactor to entering into the tube line	0	0	pressure relief valve and a check valve with a cracking pressure of 0.03 Bar	2	High temperature and pressure check valves with cracking pressure 0.03 Bar	-3	1	
				Blockage of I-6	-1	No gas flow entering the feed line, Void Results	0	0	Check Rotameter before experiments	1		-2	1	
				Gas Bottle Empty (GC-2)	-1		0	0	Check gas bottle before experiments	1		-2	1	
				Regulator (Valve-5) Failure	-1		0	0	Check rotameter before experiments	1		-2	1	
				Valve-2 Closed	-1		0	0	No entrainment flow, pressure imbalance over feeding ball valve (valve-1)	1		-2	1	
		Reverse	Flow reversal from the reactor	Blockage of I-6 Rotameter causing a pressure imbalance over the reactor.	-1	Product gases from the reactor entering the tubing lines 14 and 6.	0	0	pressure relief valve and a check valve with a cracking pressure of 0.03 Bar	2		-3	1	

Table L: Hazard and Operability Table (HAZOP) *Continued*

Node/ Stream	Parameter	Guide word	Deviation	Causes	Score O	Consequences	Score E	Score P	Safeguards	Score SG	Comments	Risk Rating	Risk level	Actions
2. Methane Entrainment Flow	2.1 Flow	No Flow	Rotameter I-6 closed	Human Error	-1	Blocking at Unit-7, No real hazard, see 5.1	0	0	-	1		-2	1	
		High Flow	Excess methane flow through the entrainment flow tube line	Incorrect Setting of rotameter I-6	-1	No Problems	0	0		1		-2	1	Movement of I-5 for after the tee, looking at the regulation of the feed stream in
		Low Flow	Insufficient methane flow through the entrainment flow tube line	Incorrect Setting of rotameter I-6	-1	No Problems	0	0		1		-2	1	
		Reverse Flow	No flow through entrainment line	Pressure differential over the top and bottom of the reactor, blockage of the filter	-1	Void results and blockage of feed as flow is reversed	0	0	Filter Unit-15	1		-2	1	Addition of a filter into Tube 6, Removal of Valve 3 as it is believed that it has no use where it is at the moment

Table L: Hazard and Operability Table (HAZOP) *Continued*

Node/ Stream	Parameter	Guide word	Deviation	Causes	Score O	Consequences	Score E	Score P	Safeguards	Score SG	Comments	Risk Rating	Risk level	Actions
2. Methane Entrainment Flow	2.2 Pressure	High	Excess pressure >10 Bar entering	Regulator malfunction (valve-5)	-1	Excess pressure entering feeding line, Void results	0	0	Pressure relief valve, Check regulator before experiment	2	Tubing max operating pressure 220 Bar,	-3	1	movements of the pressure relief valve, pressure relief on the bottle for the blockage due to biomass
				Rotameter I-6 malfunction	-1		0	0	Pressure relief valve, Check rotameter before experiment	2		-3	1	
		Low	Low gas pressure entering system	Regulator failure (Valve-5)	-1	Low Pressure resulting in void results, possibility of no particle entrainment and blocking of the line, No over pressure for the feed section. Reverse flow of gas experienced, Methane feed is passed through the reactor and up towards hopper	0	0	Check regulator before each experiment	1		-2	1	Addition of a pressure gauge on the inlet tubing, used to ensure that an over pressure exists
				Rotameter I-6 Malfunction	-1		0	0	Check rotameter before each experiment	1		-2	1	
				Rotameter I-6 Malfunction	-1		0	0		1		-2	1	
				Valve-7 Open	-1		0	0	Ensure all pressure relief valves are not open after they have been activated	1		-2	1	
				Valve-6 Open	-1		0	0		1		-2	1	
				Gas bottle Near empty	-1		0	0	Check gas bottle before experiments (Checklist)	1		-2	1	

Table L: Hazard and Operability Table (HAZOP) ***Continued***

Node/ Stream	Parameter	Guide word	Deviation	Causes	Score O	Consequences	Score E	Score P	Safeguards	Score SG	Comments	Risk Rating	Risk level	Actions
2.Methane Entrainment Flow	2.3 Temperature	High	Not a Concern		-1		0	0	Gases enter at room temperature	1		-2	1	
		Low	Not a Concern		-1		0	0	Gases enter at room temperature	1		-2	1	
3. Nitrogen Pressurization/Purge line	3.1 Flow	Zero	No flow during reaction	Regulator closed	-1	No problem	0	0		1	There should be no flow during experiments	-2	1	
		Too High	High Nitrogen flow during reaction	Valve-11 open	-1	No problem	0	0		1	There should be no flow during experiments	-2	1	
			High nitrogen flow during purging	Regulator malfunction (valve-12)	-1	Entrainment of particles into the outlet line that feeds the furnace	0	0	System checklist/Addition of Unit-16	1		-2	1	Addition of filter on outlet of the pressurized hopper. Outlet tubing for hopper placed to prevent entrainment
			High nitrogen flow during purging	Incorrect rotameter setting I-18	-1		0	0		1		-2	1	
		Too Low	Low Nitrogen flow during reaction	Valve-11 open	-1	No problem	0	0		1	no flow during experiments	-2	1	
		Reverse	Methane entering the hopper system and nitrogen purging stream	Valve 10 open	-1	Methane entering hopper system and purge line	0	0	Check Valve	2		-3	1	Addition of a check valve before valve-10, used to prevent against reverse flow

Table L: Hazard and Operability Table (HAZOP) *Continued*

Node/ Stream	Parameter	Guide word	Deviation	Causes	Score O	Consequences	Score E	Score P	Safeguards	Score SG	Comments	Risk Rating	Risk level	Actions
3. Nitrogen Pressurization/Purge	3.2 Temperature	High	High Nitrogen Temperature		-4		0	0	All gases at room temperature feeding to hopper	1	Feed at Room Temperature	-5	1	
		Low	Low Nitrogen Temperature		-4		0	0		1	Feed at Room Temperature	-5	1	
	3.3 Pressure	High	High pressure in line	Regulator malfunction Valve-12	-1	Excess pressure in pressurization line	0	0	Pressure relief valve located after the regulator, set at design pressure of 10 Bar	2		-3	1	Addition of pressure relief valve after the regulator
		Low	Low Pressure in line	I-1 malfunction	-1	Reverse pressure differential, i.e. hopper pressure lower than that of reactor.	0	0	Checklist	1	Talked about in more depth at Node 5	-2	1	Checklist addition to start-up scenario
				Upstream leak	-1		0	0		1		-2	1	
				Valve-12 failure	-1		0	0		1		-2	1	
				Valve-11 open	-1		0	0		1		-2	1	
	3.4 Start-up/Shut down	Other:	Actions Missed	Improper purging of system	0	Methane still exists in the hopper system	0	0	100L of nitrogen used to purge system (5x the hopper volume) [start-up protocol]	2		-2	1	Entry point for the nitrogen purge is placed at the bottom/middle of the hopper to ensure adequate purging of the system
				Poor purging of system and methane remains in the system after start-up	0		0	0		2		-2	1	
				Poor purging and oxygen is in the system	0	No hazard unless methane enters the environment at high temperature, very unlikely	0	0		2		-2	1	

Table L: Hazard and Operability Table (HAZOP) ***Continued***

Node/ Stream	Parameter	Guide word	Deviation	Causes	Score O	Consequences	Score E	Score P	Safeguards	Score SG	Comments	Risk Rating	Risk level	Actions
4. Methanolysis Reactor	4.1 Flowrate	High	High fluidizing gas flowrate	Regulator Malfunction (valve-5)	-1	Excess fluidization and the possibility of particle entrainment, Temperature of the reactor decreases due to insufficient heating capabilities. Void results	0	0	Check regulator prior to experiments	1		-2	1	
				Rotameter Failure (I-5)	-1		0	0	Check rotameter before experiment	1		-2	1	
				Blockage of Rotameter I-6	-1		0	0	Check rotameter before experiment	1		-2	1	
				Valve-3 Cracked	-1		0	0	Check Valve-3 before experiment	1		-2	1	
			Biomass Feed	human error	-1	Increased flow of chips into the reactor	0	0		0	Reaction is endothermic	-1	1	
		Low	Low Fluidizing Gas flow	Rotameter blockage (I-5)	-1	Low flowrate entering into reactor, Experiment is void, Slight increase in reactor temperature	0	0	Check rotameter before experiment	1		-2	1	
				Unit 4 blockage	-1	Void Results from experiment	0	0		0	No Hazard	-1	1	
				Quartz rupture	-2	Void Results from experiment	0	0		0	No Hazard	-2	1	
				Regulator Malfunction (I-5)	-1	Low flowrate entering into reactor, Experiment is void, Slight increase in reactor temperature	0	0	Check regulator prior to experiments	1		-2	1	

Table L: Hazard and Operability Table (HAZOP) *Continued*

Node/ Stream	Parameter	Guide word	Deviation	Causes	Score O	Consequences	Score E	Score P	Safeguards	Score SG	Comments	Risk Rating	Risk level	Actions
4. Methanolysis Reactor	4.1 Flowrate	Low	Low Fluidizing Gas flow	Gas bottle Near empty (GC-2)	-1	Low flowrate entering into reactor, Experiment is void, Slight increase in reactor temperature	0	0	Check gas bottles before experiment	1		-2	1	
				Valve-7 open	-2	Low flowrate entering into reactor, Experiment is void. Methane release to outlet of PRV, slight increase in wear of the reactor	0	0	Check Valves before experiment	1		-3	1	
			Biomass Feed	human error	-1	Decreased flow of chips into the reactor	0	0		1	Reaction is endothermic	-2	1	
		No	No fluidizing Gas flow	Valve-4 Cracked	-1	No Gas entering, Experiment is Void	0	0	Check valves before experiments	1	No immediate Danger as Heater max temperature 1100°C	-2	1	
				Gas Bottle Empty (GC-2)	-1		0	0	Check gas bottles before experiment	1		-2	1	
				Rotameter I-5 Blocked	-1		0	0	Check rotameter before experiment	1		-2	1	
				Regulator Malfunction	-1		0	0	Check regulator prior to experiments	1		-2	1	

Table L: Hazard and Operability Table (HAZOP) *Continued*

Node/ Stream	Parameter	Guide word	Deviation	Causes	Score O	Consequences	Score E	Score P	Safeguards	Score SG	Comments	Risk Rating	Risk level	Actions
4. Methanolysis Reactor	4.1 Flowrate	Reverse	Reverse flow of gases in the reactor	Upstream Rupture	-3	Product gases and methane flow throughout the system to the source of the rupture, Pressure is lost in the system throughout.	2	1		1		-1	1	
				Tube-15 Blockage	-1	Reactor Wear, possibility of rupture occurring at the outlet and inlet sections of the reactor, Void results from the experiment	0	0	pressure Relief valves and check valves placed on both inlet streams to the reactor	2		-3	1	
	4.2 Pressure	Low	Low reactor pressure	Regulator malfunction (Valve-5)	-1	Poor fluidization if any, experiment is void	0	0	Check regulator before experiments	1		-2	1	
				Rotameter Blockage (I-5)	-1	pressure imbalance over the reactor, causing an increase in flow to the feed tubing preventing entrainment of biomass, experiment void	0	0	Check Valve	2		-3	1	
				Rotameter Blockage (I-5)	-1	Poor fluidization if any, experiment is void	0	0	Check Rotameters before an experiment	1		-2	1	
				Gas bottle Near empty	-1		0	0	Check gas bottle before each experiment	1		-2	1	

Table L: Hazard and Operability Table (HAZOP) *Continued*

Node/ Stream	Parameter	Guide word	Deviation	Causes	Score O	Consequences	Score E	Score P	Safeguards	Score SG	Comments	Risk Rating	Risk level	Actions
4. Methanolysis Reactor	4.1 Flowrate	High	High reactor Pressure	Regulator malfunction (Valve-5)	-1	Excess reactor pressure, void results	0	0	pressure relief valve	2		-3	1	pressure relief valve, moved to below the reactor system, at the methane reactive gas inlet
			Sudden Pressure Build-up	Spontaneous Blockage of system	-2	Reactor rupture at weak point of system (most probably welds and other inlets/outlets of reactor)	1	2	Pressure Relief valve, Rupture disc	2		-1	1	pressure relief valve, moved to below the reactor system, at the methane reactive gas inlet
	4.3 Temperature	High	High Reactor Temperature	No fluidizing gas flow	-1	Temperature of the reactor increases and the reactions become void	0	0	Check regulators, rotameters and gas bottles and ensure there is flow before the experiment	1	The heater unit for the reactor is expected to be <3kW with a max temperature of 1100°C, hence only a slight increase in temperature is expected. Nitrogen has a lower heat capacity	-2	1	temperature relay of the measurement of the system, independent temperature cut out\
				Wrong gas fed into system (Nitrogen instead of Methane)	0		0	0		1		-1	1	
				Low fluidizing gas flow	-1		0	0		1		-2	1	

Table L: Hazard and Operability Table (HAZOP) ***Continued***

Node/ Stream	Parameter	Guide word	Deviation	Causes	Score O	Consequences	Score E	Score P	Safeguards	Score SG	Comments	Risk Rating	Risk level	Actions
4. Methanolysis Reactor	4.3 Temperature	Low	Low Reactor Temperature	Failure of heating elements for Unit-6	-1	No Reaction occurs and the experimental analyses are void	0	0	Check that heating element is working before experiment	1	No Hazard, wasted methane	-2	1	
				Heating Elements for Unit-6 Not Turned on	-1	No Reaction occurs and the experimental analyses are void	0	0	Check that heating element is working before experiment	1	No Hazard, wasted methane	-2	1	
	4.4 Start Up	Other Than	System not purged	System is not purged with nitrogen before methane is added	-1	Potential for leakage of methane	0	1	Checklist for Nitrogen purging and holding for detection of leaks		Leak testing done by nitrogen	0	2	
	4.5 Shut Down	Other Than	Previous trial products remain	Human error	-1	Incorrect shutdown methodology	0	0	Checklist	1	Void Results, Dirty Reactor	-2	1	
			System left pressurized with Methane	Human error	-1	Potential for methane release when changing parts without expecting methane to be present	0	1	Checklist and protocol, Methane sensor in the room	2	Include in a checklist which is conducted before and after every experiment	-2	1	
	4.6 Reaction	No	No reaction occurs	Temperature of reactor too low	-1	If temperature is too low methane does not react	0	0	Checklist/Protocol	1	Nitrogen Fed initially, then methane is added	-2	1	

Table L: Hazard and Operability Table (HAZOP) *Continued*

Node/ Stream	Parameter	Guide word	Deviation	Causes	Score O	Consequences	Score E	Score P	Safeguards	Score SG	Comments	Risk Rating	Risk level	Actions
4. Methanolysis Reactor	4.6 Reaction	No	No reaction occurs	No Biomass fed to system blockage	-1	Pure Methane exits the reactor	0	0	Ensure biomass feed operation before experiment	1		-2	1	
				No fluidizing gas flow	-2	Wood is effectively combusted in the reactor, cleaning of system required	0	0	Checklist for gas flow	1	Combustion products CO2, CO and H2O expected	-3	1	
		Fast	Biomass pyrolysis too fast	High temperature and long retention times	-1	increase in tertiary reactions which have the possibility of producing significantly more oils and tars	0	0		1	Reaction is Endothermic	-2	1	
		Slow	Biomass Pyrolysis Reactions too slow	Low temperature	-1	Deviation in expected products, cleaning of system	0	0		1		-2		
	4.7 Utility	Failure	Power Cut	Disturbance in electrical grid and/or power cut and/or other natural disasters	-2	Experiment Void	0	0	Methane interlock	1		-3	1	Purge until the electricity comes back on , no real hazard with methane interlock system
	4.8 Composition	Other	Nitrogen added as fluidizing gas	Human error	-1	Experiment Void	0	0	Checklist	1	All initial experiments will be conducted with nitrogen	-2	1	

Table L: Hazard and Operability Table (HAZOP) ***Continued***

Node/ Stream	Parameter	Guide word	Deviation	Causes	Score O	Consequences	Score E	Score P	Safeguards	Score SG	Comments	Risk Rating	Risk level	Actions
4. Methanolysis Reactor	4.8 Composition	Other	Nitrogen added as fluidizing gas	Blockage of Rotameter I-6	-1	Excess fluidization and the possibility of particle entrainment, Temperature of the reactor decreases due to insufficient heating capabilities. Void results	0	0	Check rotameter before experiment	1		-2	1	
				Unit-3 Malfunction	-1	Increase in biomass feed, causing an increase in product gases	0	0	Checklist to ensure that the Unit is operating consistently before experiments	1		-2	1	
		Low	Low Flowrate Entering Char trap	Lower than expected flowrate entering reactor upstream	-1	Slight increase in temperature, Void experiment	0	0	Checklist for all upstream applications, regulators rotameters etc.	1		-2	1	
				Blockage in Tube-15 from char agglomeration	-1	Tubing blocking from the production of char which may cause blocking	0	0	Clean tubing after every trial, (Burn off residue)	1		-2	1	

Table L: Hazard and Operability Table (HAZOP) ***Continued***

Node/ Stream	Parameter	Guide word	Deviation	Causes	Score O	Consequences	Score E	Score P	Safeguards	Score SG	Comments	Risk Rating	Risk level	Actions
4. Methanolysis Reactor	4.8 Composition	Low		Pressure differential over the reactor	-1	Methane gas enters into biomass feed loop, no reaction	0	0	Check valve, pressure regulating loop	2		-3	1	
		No	No gas entering Char trap	No hazard								0	2	
		Reverse	Flow reversal through char trap	Downstream Pressure build-up	-1	Reversal of product gases back through the char trap	0	0	Check valves (Valve-3 Valve-4) Pressure relief Valves (6&7)	3		-4	1	
	4.9 Level	Other	Incorrect amounts of alumina balls and sand in reactor system	human error	-1	Sand entrainment	0	0	Checklist	1	Operational problem with the incorrect level of packing materials sand and the balls etc.	-2	1	Addition into checklist, no blockage expected to occur, more than likely reactor will need to be opened and completely cleared out
5. Biomass Feed system	5.1 Flowrate	High	Excess Biomass fed	Malfunction of Motor (Unit-3)	-1	Excess feed into Tube-6, Causing blockages of tubes, Possibility of combustion at Unit-7 as insufficient cooling for the flow, charring of cooler feed tube	0	0	Check Valve preventing excess pressure	1	Any increase in flowrate will only be <2.3kg/hr as the VSD does not allow for a higher flowrate	-2	1	

Table L: Hazard and Operability Table (HAZOP) *Continued*

Node/ Stream	Parameter	Guide word	Deviation	Causes	Score O	Consequences	Score E	Score P	Safeguards	Score SG	Comments	Risk Rating	Risk level	Actions
5. Biomass Feed system	5.1 Flowrate	Low	Low Biomass feed	Malfunction of Motor (Unit-3)	-1	Void Results	0	0		1	No hazard with low feed	-2	1	
			Gas flow	I-6 malfunction	-1	Poor entrainment of particles, chance for a blockage of feed	0	0	Checklist to ensure that all units etc. are clear	1	Low flow/blockage/charring of feed is deemed no to be a hazard	-2	1	Charring of feed in the biomass cooler is not believed to be a hazard
				Unit-15 blocked	-1		0	0		1		-2	1	
		No/Zero	No Biomass Flow	Power Cut	-2	Void Results	0	0		1		-3	1	
				Gearbox malfunction	-1	Void Results	0	0		1		-2	1	
			Nitrogen Flow during purging	Valve-12 failure		Entry of methane to the hopper, if Valve-1 seals fail	0	0		1	Movement of I-16 above the tee where valve-10 is placed	-1	1	Rotameter I-18 added above tee section to ensure that when purging the system the flow can be observed
		Reverse	Methane flow to hopper	Rotating ball valve seal failure/leaking	0	Hazardous environment in the hopper unit-1. Void results as the pressure differential causes product to flow through the unit	0	0	expected to happen, checklist and purging protocol used to ensure no methane in the system	2	indication of the extent of methane leaked can be observed from the flare	-2	1	Altering of shutdown procedure and modifications of nitrogen tubing to prevent any nitrogen by-pass

Table L: Hazard and Operability Table (HAZOP) ***Continued***

Node/ Stream	Parameter	Guide word	Deviation	Causes	Score O	Consequences	Score E	Score P	Safeguards	Score SG	Comments	Risk Rating	Risk level	Actions
5. Biomass Feed system	5.2 Start-up/shut down	Low	Low nitrogen flow	Incorrect start-up procedure	0	No purge occurring/ very poor	0	0		1	Movements of the inlet for the nitrogen to the hopper	-1	1	Rotameter I-18 added above tee section to ensure that when purging the system the flow can be observed
		Zero	Cooling fluid into biomass cooler	Operator forgets to turn on cooling fluid to biomass feed cooler	-1	Charring of the feeding tube and blockage of system occurs.	0	0	Temperature indicator	1	Included in Checklist	-2	1	Temperature probe placed on the outlet of the cooler system to indicate the extent of cooling/if any is occurring
		Reverse	Gas Flow	Valve-1 Malfunction	-1	Product gases in pressurization line	0	0	Check valves and nitrogen slight overpressure	1		-2	1	
	5.3 Temperature	High	See 4.2											
		Low	Not a Concern								The biomass feed is purposely cooled			
	5.4 Pressure	High	High pressure in the hopper	Regulator Malfunction (Valve-12)	-1	Possibility of the vessel to rupture if in significant excess	0	0	Pressure Relief Valve	2	High pressures assumed to be >>10 bar	-3	1	

Table L: Hazard and Operability Table (HAZOP) *Continued*

Node/ Stream	Parameter	Guide word	Deviation	Causes	Score O	Consequences	Score E	Score P	Safeguards	Score SG	Comments	Risk Rating	Risk level	Actions
5. Biomass Feed system	5.4 Pressure	High	High pressure in feeding line	Blockage	-1	Explosion	1	2	Pressure Relief Valve-7 and rupture disc, also pressure relief valve and	3	Rupture disc installed in system, Movements of valve-6 to below the reactor where valve-7 was situated	-1	1	rupture disc inclusion at the bottom of the reactor, Pressure relief valve removed from the top of the reactor and placed on the methane feed stream
		Low	Low pressure in feed line	Valve-5 malfunction	-1	Reverse flow of the system, poor entrainment	0	0			Void Results			
			Low pressure in the hopper	Regulator Malfunction (Valve-12)	-1	Void Results	0	0		1	Some experiments will be conducted at low pressures	-2	1	
				Valve-10 Open	-1	Nitrogen and methane gas mix. Constant pressure differential over the hopper, Void results	0	0	Checklist	1		-2	1	
				Valve-1 Malfunction	-1		0	0		1		-2	1	
				I-1 Malfunction	-1	Gas reverse flow	0	0	Check valve	1		-2	1	
				Valve-13 Cracked open	-1	Hopper not pressurized, Nitrogen passes to gas hood	0	0		1		-2	1	
			Reverse flow from low pressure	See 5.1										

Table L: Hazard and Operability Table (HAZOP) *Continued*

Node/ Stream	Parameter	Guide word	Deviation	Causes	Score O	Consequences	Score E	Score P	Safeguards	Score SG	Comments	Risk Rating	Risk level	Actions
5. Biomass Feed system	5.5 Utility failure	Power Cut	Cooling fluid in Unit-7 remains in the unit	Power cut, no fluid flow	-1	Steam production possible	0	0	Temperature indicator on outlet stream of feed cooler fluid					Allow the cooler fluid to flow to atmosphere
6. Reactor Products	6.1 Flow	Zero	Zero flow of products from reaction	No methane flow	-1	No Problem	0	0	Checklist	0		-1	1	
			Zero flow of products from reaction	Packed Bed Blocked	-1	No Problem	0	0		1		-2	1	
			Zero flow of products from reaction	Filter Block	-1	No Problem	0	0		1		-2	1	
		Low	Low flow of products from reaction	Low biomass/methane feed	-1	No Problem	0	0		0	Will cause premature condensation likely to block Unit-4 and collect in Unit-2, void results	-1	1	
		High	Higher than expected liquid product flow	Reaction parameters induce liquid production	-2	Excess liquid, Units 2 and 5 become full	0	0	Unit-14 large Volume	1	Sizing of Unit-14 conducted to ensure that overflow is not possible	-3	1	Extra knock-out pot added to increase the condensation of entrained condensable. Sized accordingly to a 100% liquid yield at highest flowrate of biomass

Table L: Hazard and Operability Table (HAZOP) ***Continued***

Node/ Stream	Parameter	Guide word	Deviation	Causes	Score O	Consequences	Score E	Score P	Safeguards	Score SG	Comments	Risk Rating	Risk level	Actions
6. Reactor Products	6.1 Flow	High	Higher Backpressure	Same as Node 4										
	6.2 Temperature	High	Increased flow of oils past the unit-5	High gas flow	-1	Improper separation of products if the cooling is insufficient	0	0	Addition of filter to prevent upstream damage	1		-2	1	Filter placed after Unit-17 to ensure that any condensable cannot condense in the valve bodies
			Exceed design temperature	Heater Malfunction	-1	excess temperature, above the design constraint of the heater	0	1	Inclusion of electrical trip which allows the heaters to turn off if there is a malfunction	1	See Safeguard, put into action after HAZOP (2016)	-1	1	
		Low	Blockage of the ash trap	Low gas flow	-1	Increased pressure drop over the system, poor condensation	0	0		0	Void Results	-1	1	
	6.3 Pressure	High	High entering pressure	Methane regulator failure	-1	increased pressure in the system	0	0	PRV Valve-7	0		-1	1	
		Low	Low product pressure	Downstream disturbances	-1		0	0		0		-1	1	
	6.4 Start-up/shut down	Incorrect	No cleaning of the filters and the condensers	Human Error	-1	Possibility for overflow of all of the units 2,5,14	0	0	Large condenser volumes	0	Will need to be a significant amount of liquid as volumes are large, hazard is very small	-1	1	

Table L: Hazard and Operability Table (HAZOP) *Continued*

Node/ Stream	Parameter	Guide word	Deviation	Causes	Score O	Consequences	Score E	Score P	Safeguards	Score SG	Comments	Risk Rating	Risk level	Actions
6. Reactor Products	6.4 Start-up/shut down	Oxygen leak	breaking and re-joining joints at the condensers and ash trap not securing the fittings	Removing samples of the liquid products collected from the experiments	0	Oxygen present in the product collection system. Possibility for explosion if any reverse flow is experienced	0	1	inclusion of a pressure holding test for 30 minutes before the reaction is able to take place, also a 20L purge of the line	2	inclusion of a pressure holding test for 30 minutes before the reaction is able to take place, also a 20L purge of the line	-1	1	inclusion of a pressure holding test for 30 minutes before the reaction is able to take place, also a 20L purge of the line
	Utility	Failure	Checking that LPG is sufficient for the run	No more LPG in bottle	-1	Flare is extinguished and release of methane through fume hood	0	0	Checklist to ensure sufficient LPG, weighing of bottle to determine how much is left suggested	1		-2	1	Add to checklist
7. Sampling and Flue gas Line	7.1 Flowrate	High	High flowrate passing sampling tee	Elevated temperature of Unit-5, Poor condensation	-1	Vapour fractions in the gas flow, poor analyses potential damage to GC	0	0	Cooling jacket added if required, heat loss to environment believed to be sufficient to bring products to room temperature by this point	1		-2	1	
				Increased production of gas/vapour from reactor	-1	No hazard	0	0		1		-2	1	

Table L: Hazard and Operability Table (HAZOP) *Continued*

Node/ Stream	Parameter	Guide word	Deviation	Causes	Score O	Consequences	Score E	Score P	Safeguards	Score SG	Comments	Risk Rating	Risk level	Actions
7. Sampling and Flue gas Line	7.1 Flowrate	Low	Low flowrate passing sampling tee	Rupture in upstream tubing and/or units	-2	Release of Vapour/gas to atmosphere (at the point of the rupture)	0	0	Adequate design for temperature and pressure applications	1		-3	1	
		No	No flow pass the tee	No hazard	-1	Experiment Void	0	0		1		-2	1	
			Flow to flare	no methane flow	-1		0	0		1	no hazard	-2	1	
		Reverse	Flow reversal	No hazard					Not possible		Not possible			
	7.1 Temperature	High	High product temperature	High Flowrates	-1	See 7.1	0	0		1		-2	1	
		Low	Lower Temperature than expected	No Hazard	-1		0	0		1	External convective cooling expected to approximately the same as the cooling jacket	-2	1	
	7.3 Pressure	High	inlet gas/vapour stream at elevated Pressures	Upstream disturbances	-1	Release of rubber septum in the tee, Possible release of product gases	0	0	Check valves high upstream of the unit, pressures no higher than 10 Bar design considering	1	Design to allow pressures up to 10 Bar	-2	1	
				Downstream blockage	-1		0	0		1		-2	1	
		Low	Low Pressure of inlet gas/vapour stream	Pipe rupture/leak upstream/downstream of unit	-1	No hazard at Node	0	0	Over spec materials with respect to the characteristics of the gas flows	1	Design against ruptures and leaks	-2	1	system placed under a fume hood to ensure adequate ventilation

Table L: Hazard and Operability Table (HAZOP) ***Continued***

Node/ Stream	Parameter	Guide word	Deviation	Causes	Score O	Consequences	Score E	Score P	Safeguards	Score SG	Comments	Risk Rating	Risk level	Actions
7. Sampling and Flue gas Line	7.4 Level	High	High level in Unit-14	operator forgot to remove liquid from Unit-14	-1	excess condensation and chances for overflow	0	0	Checklist, large volume of condenser	1	Designed well over expected volume of liquid expected	-2	1	
8.N2O/He Analysis Gas stream	8.1 Flow rate	High	High flowrate of He/N2O	I-15 Failure	-1	Loss of ignition of	0	0	Checklist Procedure	0	Check that the nitrogen and the He/N2O flow of gas is suitable for the flare to not extinguish	-1	1	
		Low	Low He/N2O flow	Low Pressure feed	-1	No Consequence	0	0		0		-1	1	
		No Flow	I-15 Closed		-1	Experimental problems	0	0		0		-1	1	
		Reverse	Sample as low flow		-1		0	0		0		-1	1	
	8.2 Temperature	High			-1		0	0		0	No source of temperature	-1	1	
		Low			-1		0	0		0	No Source of temperature	-1	1	
	8.3 Pressure	High			-1	Pressure releases from Valve-11	0	0		0		-1	1	
		Low			-1	No vacuum possible, limited to atmospheric	0	0		0		-1	1	
	8.4 Procedure	Incorrect	Alicat turned on too late after reaction has started		-1		0	0		0		-1	1	

Table L: Hazard and Operability Table (HAZOP) ***Continued***

Node/ Stream	Parameter	Guide word	Deviation	Causes	Score O	Consequences	Score E	Score P	Safeguards	Score SG	Comments	Risk Rating	Risk level	Actions
9. Compressed Air inlet	9.1 Flow rate	High												
		Low												
		No Flow												
		Reverse												
	9.2 Temperature	High												
		Low												
	9.3 Pressure	High												
		Low												
10. LPG Burner Stream	10.1 Flow rate	High	high LPG Flow	Regulator Malfunction	-1	flame out, part of the operation protocol	0	0		0	part of the operation protocol	-1	1	
		Low	Low LPG Flow	Regulator Malfunction	-1	flame out, part of the operation protocol	0	0		0		-1	1	
		No Flow		No gas in bottle	-1	abandon experiment shift to nitrogen	0	0		-1	Scale to weigh LPG Cylinder	-2	1	
		Reverse			-1						Unlikely	-1	1	
	10.2 Temperature	High			-2						Unlikely	-2	1	
		Low			-2						Unlikely	-2	1	
	10.3 Pressure	High	See High Flow		-1							-1	1	
		Low	See Low Flow		-1							-1	1	

D.6. HAZOP Minutes

HAZOP Meeting (I)

Flash Methanolysis of Pine Wood

Meeting:	HAZOP Meeting
Location:	E547B, University of Canterbury
Date/Time:	9:00am-2:30pm, 3rd February 2015

Present	**Email**
Gaetano Dedual	gaetano.dedual@pg.canterbury.ac.nz
Shusheng Pang	shusheng.pang@canterbury.ac.nz
Brendon Miller	Brendon.miller@jembec.com
Frank Weerts	frank.weerts@canterbury.ac.nz
Stephen Beuzenberg	stephen.beuzenberg@canterbury.ac.nz
Tim Moore	tim.moore@canterbury.ac.nz
Michael Sandridge	michael.sandridge@canterbury.ac.nz

Minutes:

- Deemed a requirement to have adequate ventilation over the whole system. Believe on having a system which is on wheels and can be moved under a fume hood when reactions are required to take place.
- Carbon monoxide and flammable gas sensors required in the designated room of operation
- Very strong probability that the reactor will be placed in the SP labs, this provides inbuilt interlocks for power failures, gas releases and ventilation with a more than adequate fan
- Safety conclusion: addition of a rupture plate into the bottom of the reactor, if the heat of the reactor will allow for this. Due to the possibility of high heat the burst pressure of a designed rupture disc can be affected.
- Removal of the pressure relief valve on the biomass feed tubing

- Allow the feed cooler fluid to exit to atmosphere, i.e. running tap that is then routed to a sink. Addition of a thermocouple on the exit line of this apparatus.
- Large concerns were encountered with the possibility of the hopper to fill with methane. This could be caused by damage to the ball valve seals, which are not designed for the rotation which we are planning to place them under. Strong emphasis put on an accurate checklist before any experiments.
- Checklist to ensure that 5 times the hopper/reactor volume has been purged to ensure that all of the methane and/or oxygen are removed from the system.
- Total removal of methane/oxygen from the system will be conducted in three sections. I.e. hopper pressurization line, methane entrainment line and reactor feed line. To ensure that the purge was successful the flowmeter I-7 will be recorded.
- Stephen suggested a pressure differential interlock over the methane entrainment and reacting gas feeds. This will allow for a slight over-pressure to be present in the system, although was believed to be more complicated than required for the system.\
- Charring of the feed cooler system was deemed not a safety issue, caused by the cooling water not being activated. It is more than likely that this would simply result in a void run and blockage of the rotating ball valve.
- All pressure relief valves to be set at the design pressure of 10 bar
- Revision of the purge protocol in the checklist needs to be revisited to ensure that the correct set of steps is taken during purging. High possibility for nitrogen to by-pass sections of the equipment which need to be purged; hence, purging to be conducted in separate sections to ensure effectiveness.
- Temperature relay for the measurement of the reactor temperature, with an independent temperature cut out system.
- Ensure that checklist entitles what to do after a utility failure (complete purge of system)
- Discussions about whether valve-10 should be a solenoid valve or not., however believed to over complicate the system
- Addition of a fail closed valve on the methane
- Requirement that the operator of the reactor must be present for the duration of the reaction
- Heating of the ash trap is more than likely required due to the low flowrates and the excess heat loss which will be experienced.
- Staged heating over Units 4 and 2, required for the desired temperature to be held constant to ensure that the correct boiling point species are condensed from the product stream. Prior experience led to the thought that the heat loss would be far in excess and external heating would be required. This implication will be applied if need-be, initial reactions with inert N2 will help to show the heating requirements in these sections.

- The possibility of having a hot sampling section was discussed and was more likely to be extracted by a syringe with a filtering system. However, for simplicity this was not implied in the system and will be something that will be looked at once the overall system is built and running, as per the PID.
- Filter added onto the inlet stream of the methane entrainment flow, Unit-15. This will prevent any biomass chips entering the entrainment feed in the case of backflow/reverse flow.
- Filter added onto the outlet of Unit-14. This was added to ensure that the valves do not contain any uncondensed tars which have a tendency to clog and block such sections of equipment. This also helps to keep the flowmeter clean (wet gas flowmeter). This will also help to show the effectiveness of the downstream knock-out pots, as filter clogging is a sign of poor downstream condensation.
- Addition of an extra knock-out pot. This knockout pot is designed for two reasons; contain a high liquid yield reaction (theoretically 100% conversion to liquid) and to ensure that the downstream knockout pots were effective.
- Filter added on the hopper purge stream, after the hopper unit. This ensures that no biomass is fed into the flare system.
- LPG blow torch configuration suggested instead of camp stove arrangement. This will be met with a pilot flame, where the torch is directed at an upwards angle. This will allow for a reliable flame system that can with stand two separate feed streams.
- Feed cut-out and heater cut-out system put in place for the case of ventilation failure. An interlock system is required for the reactor system. Can be easily applied at the SP labs.
- Creation of a feed tube that nearly reaches the bottom of Unit-14. As this unit is added to the system, by feeding the product gas at the bottom the maximum potential for condensation occurs.
- Need to check to ensure that the fan dilution for the ventilation system is sufficient for any expected methane leaks. Also applicable to the temperature of the gas and the heat which is given off by the flaring of the gas.
- Sampling needle valve to have a very small Cv, so that if it is left open a small release of methane/product gas is released to the environment of the reactor.
- Sampling valve placed after the pressure regulating system, so that the pressure is significantly less and the chances for a gas bag rupture are nearly eliminated.
- Movement of the purge ling into the flare system, but not in the same line as the product burner. This configuration was put in place to burn any methane which passes into the hopper by reverse flow.
- Auto shut-off system for the fume hood if the system fails and the ventilation system is tripped off.

- Isolation valves recommended for the system around the reactor however deemed to be not necessary.
- Exit line for the hopper to be placed as far as possible up the hopper, with the entry to the hopper to be placed relatively deep into the system. The addition of this tubing is not expected to have effects on the flow of biomass.
- Moving pressure relief valves before the rotameters for both nitrogen and methane as this allows for quicker response if the regulator fails and safeguards rotameters.
- Pressure indication placed on the methane entrainment line, used to ensure that there is a pressure differential over the reactor for feeding.
- Most likely to have heating tape from the reactor all the way to Unit-2, preliminary experiments will help to confirm this once the reactor is built.

HAZOP Meeting (II)

Flash Pyrolysis of Biomass

Meeting:	HAZOP Meeting
Location:	Law 112, Commerce and Law Building, UoC
Date/Time:	10:00am-3:00pm, 8th August 2016

Present	**Email**
Gaetano Dedual	gaetano.dedual@pg.canterbury.ac.nz
Brendon Miller	Brendon.miller@jembec.com
Frank Weerts	frank.weerts@canterbury.ac.nz
Stephen Beuzenberg	stephen.beuzenberg@canterbury.ac.nz
Michael Sandridge	michael.sandridge@canterbury.ac.nz

Minutes:

- Require the inclusion of a thermocouple on the top flange, location and method of affixing the thermocouple to be confirmed. The main issue was identified as if the temperature of the system becomes higher than the 650°C design temperature at the flange.

- Identified the requirement to introduce a safety interlock for the heating systems used on the packed bed and fluidised bed reactors, Unit-17 and Unit-6, respectively. This is required due to the high excess heating power which the heaters possess (especially the fluidised bed, where as a faulty temperature probe or controller could lead to significant excess heating.
- During the operating procedure, it is paramount that the pressure reducing valve is set and left at the desired outlet pressure. When getting ready for an experiment the system is pressurized with nitrogen at the experiment pressure and temperature. The pressure should be slightly less than that of nitrogen due to the slightly higher pressure in the hopper system. From here a three-way valve is used to replace valve-5 at the tee between the methane and nitrogen line. This allows for the methane introduction to occur simultaneously.
- Check valve-26 accepted into the process, where check valve-6 has been used as the inclusion of a three way valve replacing valve-5 renders this valve useless. Straight swap for the check valves
- The possibility of reverse flow occurring over Valve-14 was explored (pressure reducing valve) as the outlet side of this valve has a possibility of reaching 3 bars before the pressure relief is encountered.
- Rotameters I-14 and I-13 require the valve capabilities to be removed, to ensure that there is no possibility that an increase in pressure can occur over Node 7, as there is no pressure release on this side of the system. It will also act as a safeguard for the alicats within the system.
- Dummy ends for all condensers (Units -4 -13 -2) all require connections which allow the ends of these quick release fittings to be capped off when the system is being cleaned, as there is risk for CO formation.
- Questions rose about the integrity of the process tubing which is between the fluidised bed reactor and the packed bed reactor.
- LPG bottle which is used in the furnace arrangement to be placed on a set of scales to ensure that there is significant gas for the run, as there is no visual guide for the level of the bottle.